University of Silesia in Katowice

Faculty of Natural Sciences

Institute of Earth Sciences

Dorota Staneczek, MSc

Paleoenvironmental conditions and evolution of the Central Carpathian Paleogene Basin and the Tatra Mts. based on geochemical and magnetic methods

Paleośrodowisko i ewolucja Centralnokarpackiego Basenu Paleogeńskiego i Tatr w oparciu o metody geochemiczne i magnetyczne

PhD Dissertation

Supervisor: Prof. Dr. hab. Leszek Marynowski

Assistant supervisor: Dr. hab. Rafał Junosza-Szaniawski, Prof. PAS

Sosnowiec, 2025

Table of contents

Articles included in the PhD dissertation

Article 1

Staneczek Dorota, Więcław Dariusz, Marynowski Leszek, 2024. Depositional conditions, wildfires, maturity, and hydrocarbon potential evaluation of Central Carpathian Paleogene Basin based on integrative approach from Orava Basin. International Journal of Coal Geology 285, 104490. https://doi.org/10.1016/j.coal.2024.104490

IF: 5.6

Journals and publications scored by the Ministry of Science and Higher Education: 140 pts

Article 2

Staneczek Dorota, Szaniawski Rafał., Chadima Martin, Marynowski Leszek, 2024. Multi-stage tectonic evolution of the Tatra Mts recorded in the para- and ferromagnetic fabrics. Tectonophysics 880, 230338. https://doi.org/10.1016/j.tecto.2024.230338

IF: 2.7

Journals and publications scored by the Ministry of Science and Higher Education: 140 pts

Article 3

Staneczek Dorota, Marynowski Leszek, 2025. Application of biomarker and non-biomarker parameters to assess maturity using the Central Carpathian Paleogene Basin as a case study. Organic Geochemistry 201, 104933. https://doi.org/10.1016/j.orggeochem.2025.104933

IF: 2.6

Journals and publications scored by the Ministry of Science and Higher Education: 100 pts

Manuscripts included in the PhD dissertation

Manuscript 1

Staneczek Dorota, Szaniawski Rafał, Marynowski Leszek. Under review. Burial impact on the Tatra Mts from a rock magnetic and magnetic fabric perspective. Tectonics.

Other articles by the PhD student

1. Satolli Sara, Robustelli Test Claudio, **Staneczek Dorota,** Zanella Elena, Calamita Fernando, Tema Evdokia, 2020. Magnetic fabric in carbonatic rocks from thrust shear zones: A study from the Northern Apennines (Italy). Tectonophysics 791, 228573.

IF: 2.7

Journals and publications scored by the Ministry of Science and Higher Education: 140 pts

2. **Staneczek Dorota**, Szaniawski Rafał, Szczygieł Jacek, 2022. Transpression-driven deformations of the Chočské vrchy Mountains (Western Carpathians): insights from magnetic fabric. Geologica Carpathica 73.

IF: 1.0

Journals and publications scored by the Ministry of Science and Higher Education: 70 pts

Summary of the PhD dissertation in Polish

Centralnokarpacki Basen Paleogeński (CBP) znajduje się w północnej Słowacji, a częściowo także w południowej Polsce. Nazwa odnosi się do jednostki geologicznej obejmującej skały osadowe zdeponowane w basenie morskim utworzonym na obszarze Karpat Środkowych w eocenie. Podłoże, na którym powstał basen, składało się z mezozoicznych skał płaszczowinowych. W turonie wspomniane płaszczowiny zostały nasunięte na krystalinik i paraautochtoniczną pokrywę osadową masywów Karpat Wewnętrznych (np. Tatry, Mała Fatra, Góry Strażowskie). CBP i Tatry były obiektem zainteresowania naukowców przez ponad dwa stulecia. Jednak mimo szeroko zakrojonych badań niektóre zagadnienia wciąż pozostają bez rozwiązania. Obecnie rozwój metodyki badawczej może przyczynić się do rozwikłania części z nierozwiązanych kwestii. Badania prowadzone w ramach tej rozprawy doktorskiej koncentrują się na rekonstrukcji ewolucji CBP i Tatr od kredy do neogenu. Szczególny nacisk położono na charakterystykę warunków sedymentacyjnych w CBP, oligoceńsko-mioceńskie pogrzebanie Karpat Wewnętrznych przez utwory kenozoiczne oraz ewolucję tektoniczną CBP i Tatr.

Aby rozwikłać te kwestie zdecydowano się na wykorzystanie zróżnicowanych metod badawczych, które obejmują geochemię organiczną (np. chromatografię gazową sprzężoną ze spektrometrią mas, pomiary całkowitego węgla organicznego, analizę Rock-Eval), petrografię (np. refleksyjność witrynitu, pomiary pirytów framboidalnych) oraz rock magnetyzm i analizę tekstur magnetycznych. Do badań wybrano następujące jednostki: dolnokredowe margle, wapienie margliste i wapienie formacji Mraznica, która należy do płaszczowiny kriżniańskiej, oraz skały klastyczne wraz z węglami formacji Huty, Zuberec i Biely Potok, które należą do CBP.

Analiza biomarkerów udokumentowała zmienne warunki sedymentacyjne w CBP. W oligocenie dominował otwarty basen morski, a sedymentacja przebiegała w warunkach od dysoksycznych do euksynicznych. Charakter materii organicznej był mieszany, morsko-lądowy. Obecność izorenieratanu i jego pochodnych oraz przewaga drobnych pirytów framboidalnych wskazuje na występowanie warunków euksynicznych w strefie fotycznej. Z czasem morfologia basenu uległa zmianie, co w znacznym stopniu wpłynęło na warunki sedymentacyjne. W późnym oligocenie i wczesnym miocenie sedymentacja przebiegała w estuarium. Warunki w kolumnie wody były tlenowe, a jeśli występowały warunki dysoksyczne, to wyłącznie w osadzie. Materia organiczna typu lądowego przeważała nad typem morskim, odzwierciedlając stopniowe spłycanie basenu. Różnorodność związków pochodzących z roślin okrytozalążkowych, nagozalążkowych oraz grzybów potwierdza intensywną dostawę materii lądowej do zbiornika poprzez erozję gleb spowodowaną pożarami udokumentowanymi w jednostkach późnego oligocenu i miocenu.

Relatywnie intensywna sedymentacja skał CBP oraz sybsydencja w strefach przyuskokowych basenu doprowadziła do pogrzebania badanego obszaru i osiągnęła maksimum w późnym oligocenie-wczesnym miocenie. Wpływ i skala pogrzebania zostały udokumentowane przez trend paleotemperaturowy. Obszar Spiszu charakteryzuje się najwyższą dojrzałością termiczną wskazaną przez parametry oparte na biomarkerach oraz wskaźnik T_{max} (parametr analizy Rock-Eval). Najmniej przeobrażone rejony to północna część Orawy oraz obszar Szarysza. Wartości paleotemperatur wahają się od poniżej 60°C do 200°C. Co więcej, trend termiczny w paśmie Gór Choczańskich i Tatr ściśle odzwierciedla trend obecny w skałach CBP. Wpływ paleogeńskiego pogrzebania jest największy w Tatrach Bielskich i powoli maleje w kierunku zachodnim. Intensywność pogrzebania jest również odzwierciedlona w mineralogii magnetycznej i charakteryzuje się rosnącą zawartością minerałów ferromagnetycznych (*sensu lato*) wraz z przeobrażeniem termicznym skał. Podobieństwo trendów paleotemperaturowych w skałach płaszczowinowych i skałach paleogeńskich sugeruje, że te pierwsze doświadczyły wyższych temperatur w późnym oligocenie-wczesnym miocenie, a nie w turonie.

Tekstury magnetyczne formacji Mraznica i Huty odzwierciedlają różne etapy ewolucji Tatr i ich przedpola. Głównymi minerałami wpływającymi na tekstury magnetyczne są glinokrzemiany i/lub tlenki żelaza. Wszystkie tekstury charakteryzują się mieszanką cech sedymentacyjnych (foliacje magnetyczna spowodowana kompakcją) i tektonicznych (lineacje magnetyczne powstające pod wpływem naprężeń tektonicznych). W formacji Mraznica anizotropia podatności magnetycznej zapisała kierunki kompresji związanej z turońskim nasuwaniem się płaszczowin, podczas gdy na teksturę skał formacji Huty największy wpływ miała kompresja podczas mioceńskiego wypiętrzenia i wychylenia Tatr. Tekstury ferromagnetyczne, takie jak anizotropia urojonej składowej podatności magnetycznej i anizotropia bezhisterezowej pozostałości magnetycznej, zapisały tekstury związane z oligoceńsko-mioceńskim pogrzebaniem. W formacji Huty, ekstensja podczas tworzenia się CBP wpłynęła na wykształcenie się specyficznej lineacji magnetycznej. Pogrzebanie spowodowało również przyspieszoną krystalizację magnetytu uwarunkowaną matrycą glinokrzemianową. Tekstury ferromagnetyczne obecne w skałach formacji Mraznica z Tatr Zachodnich i Wysokich wskazują na transpresję podczas wypiętrzania.

Podsumowując, badania prowadzone w ramach tej rozprawy doktorskiej ukazały ewolucję geologiczną CBP i Tatr w nowym świetle. Wartością dodaną jest charakterystyka warunków sedymentacyjnych i paleotemperatur w CBP i w Tatrach. Połączenie zróżnicowanych metod badawczych okazało się skutecznym podejściem w badaniu basenów sedymentacyjnych na przykładzie CPB i Tatr.

Summary of the PhD dissertation in English

Central Carpathian Paleogene Basin (CCPB) is located in northern Slovakia, and partly also in southern Poland. This geological unit comprises sedimentary rocks deposited in a sea basin formed in the Central Carpathian area in the Eocene. The basement on which the basin was developed consisted of Mesozoic rocks belonging to allochthonous thrust sheets. During the Turonian, these nappes were thrust onto the Central Carpathian massifs (e.g., Tatra Mts., Malá Fatra Mts., Strážov Mts.), over their crystalline basements with their paraautochthonous sedimentary cover. The CCPB and the Tatra Mts. were the subject of a broad range of studies for over two centuries. However, several questions still remain unanswered. Contemporary advances in diverse research methods provide excellent tools to revisit some of the unresolved issues. In general, this research focuses on reconstructing the evolution of the CCPB and Tatra Mts from the Cretaceous to the Neogene. The emphasis was placed on the following topics: the sedimentary conditions in the CCPB rocks, the Oligocene-Miocene burial event in the Central Carpathians, and the tectonic evolution of the Cretaceous and Paleogene rock sequences.

A complex, multi-faceted approach was adopted to shed new light on these issues. The methods comprise organic geochemistry (e.g., gas chromatography-mass spectrometry, total organic carbon measurements, Rock-Eval analysis), petrography (e.g., vitrinite reflectance, pyrite framboid diameter measurements) and rock magnetism coupled with magnetic fabric analyses. The units chosen for this study are as follows: the Lower Cretaceous marls, marly limestones, and limestones of the Mraznica Fm., which is a member of the thrust nappe system, and the clastic rocks along with coaly layers of the Huty, Zuberec, and Biely Potok Fms. which belong to the CCPB.

Biomarker analysis revealed a changing depositional environment during the sedimentation of the CCPB rocks. In the early Oligocene, an open-marine basin prevailed, and the sedimentation proceeded under dysoxic to euxinic conditions. Mixed marine and terrestrial organic matter with abundant organic compounds associated with dinoflagellates, suggests open marine conditions with terrestrial input from the land. The presence of isorenieratane and its derivatives, along with tiny pyrite framboids documents the occurrence of photic zone euxinia. Over time, the morphology of the basin has changed, largely remodeling the sedimentary conditions. In the Late Oligocene, the sedimentation proceeded in an estuarine-type basin. The conditions in the water column were predominantly oxic, while disoxic conditions occurred only intermittently in the sediment. The terrestrial type of organic matter prevailed over the marine type, reflecting the gradual shallowing of the basin. Abundant angio-

10

and gymnosperm biomarkers along with fungi-related compounds point toward an intense supply of terrigenous organic matter. Moreover, intense erosion resulting in terrestrial run-offs to the basin could be facilitated by wildfire episodes documented in the Late Oligocene units.

The sedimentation of the CCPB rocks led to the subsequent burial of the study area and reached their maximum in the Late Oligocene-Early Miocene. The impact and intensity of the burial are recorded by a changing paleotemperature pattern in the studied area. Biomarker-based parameters and Rock-Eval-derived T_{max} document the highest thermal maturity in the Spiš Basin, whereas the least thermally affected areas comprise the northern part of the Orava Basin, and the Šariš Upland. The calculated paleotemperatures span from <60°C in the least mature regions, to 200°C in the highly altered CCPB parts. Moreover, this trend is closely reflected by the paleotemperature pattern documented in the nappe rocks of the Choč-Tatra Belt by organic and rock magnetic methods. The burial impact is the highest in the Belianske Tatra Mts., and slowly decreases towards the west. Its impact is reflected in the magnetic mineralogy, and is characterized by an increasing content of ferromagnetic (*sensu lato*) minerals. This similarity suggests that the Oligocene-Miocene burial had a larger impact on the nappe rocks than the Turonian one.

Magnetic fabrics of the Mraznica and Huty Fms. recorded different evolution stages of the Tatra Mts and their foreland. The main minerals controlling the fabrics are phyllosilicates and/or iron oxides. All fabrics are characterized by a mixture of sedimentary and tectonic features, mainly a compactional magnetic foliation and a strain-related magnetic lineation. In the Mraznica Fm., the anisotropy of in-phase magnetic susceptibility (ipAMS) documented the shortening direction linked with Turonian thrusting, whereas the Huty Fm. rocks recorded the compression during the Miocene uplift and tilting of the Tatra Mts. Ferromagnetic-driven fabrics, such as anisotropy of out-of-phase magnetic susceptibility (opAMS) and anisotropy of anhysteretic remanent magnetization (AARM), revealed burial-related fabrics. In the Huty Fm., extension during the opening of the CCPB was documented in the majority of studied sites. The burial resulted in the formation of magnetite on the phyllosilicate matrix, resulting in opAMS and AARM fabrics mirroring the ipAMS fabrics in some sites. Moreover, the ferromagnetic fabrics in Mraznica Fm. rocks from the Western and High Tatra Mts., recorded an impact of transpression during uplift.

In conclusion, this thesis sheds new light on the geological evolution of the CCPB and Tatra Mts. Furthermore, it provides novel data on the sedimentary conditions and paleotemperature patterns in the CCPB. Moreover, combining different methods proved to be a good approach to investigating sedimentary basins.

1. Introduction

This PhD dissertation focuses on applying complementary organic geochemistry, rock magnetic, and magnetic fabric methods to shed new light on the evolution of the Central Carpathian Paleogene Basin (CCPB) and the Tatra Mts. from the Cretaceous to the Neogene. The geological evolution of mountain belts, involves a complex interplay of processes that shape their structure. Some of these processes, such as initial strain, are subtle and challenging to detect, while others, like metamorphism, have a major impact on the rocks. Tatra Mts. and the surrounding areas have been researched for over two centuries (e.g., Grabowski, 1997; Hrouda and Kahan, 1991; Kázmér et al., 2003; Kotański, 1971; Kováč et al., 1994; Králiková et al., 2016; Madzin et al., 2021; Passendorfer, 1952; Plašienka et al., 1997; Sokołowski, 1959; Środoń et al., 2006; Staszic, 1815; Szaniawski et al., 2012; Uhlig, 1897). However, even though extensive studies were performed, several problems remained unresolved. Some issues, especially the paleotemperature distribution study in the CCPB area, initiated by Środoń et al. (2006), and the impact of the Oligocene-Miocene burial on the Tatra nappe units need a more in-depth investigation. So far, the majority of studies performed in the Tatra Mts. and the CCPB region applied only one methodology to investigate sometimes very complex processes. In this dissertation, different research methods were applied, in order to have an extensive understanding of the geological background of tectonic processes in the Late Mesozoic to Cenozoic. Organic geochemistry methods, namely the biomarker analysis, are commonly used to investigate the depositional environment of sedimentary rocks (Peters et al., 2005), yet they also shed light on the factors controlling the formation of magnetic minerals. Furthermore, investigation of magnetic fabrics without a thorough paleotemperature analysis may lead to an erroneous interpretation of their origins. The region chosen for this study was proven suitable for applying rock magnetic, magnetic fabric, and organic geochemistry methods in previous studies performed by the PhD student (Staneczek et al., 2022) and other authors (e.g., Marynowski et al., 2006; Środoń et al., 2006; Szaniawski et al. 2020). Finally, the characterization and reconstruction of the tectonic evolution, as well as other processes affecting rocks in the geological past, is extremely relevant for the study of the uplift of massifs (including the Tatra Mts.). Moreover, the research contributes to a better understanding of the general model of orogenic evolution.

2. Main research objectives

The main goals of this PhD dissertation include:

- Reconstruction of the tectonic evolution of the Tatra Mts. and the CCPB from the Cretaceous to the Neogene.
- Characteristics of the sedimentary conditions in the CCPB and their changes with time, the type of organic matter deposited in the basin, the hydrocarbon potential, and other processes that may potentially affect sedimentation in the basin (e.g., wildfires).
- Investigation of the thermal maturity of CCPB and the allochthonous Tatra rocks complemented by a study of the thermal maturity of Chochołów PIG-1 and Bukowina Tatrzańska PIG-1/GN boreholes.
- Recognition of the possible causes of the paleotemperature distribution and the impact of the Oligocene-Miocene burial on the Cretaceous and Paleogene rocks.
- Analysis of the magnetic mineralogy of the Cretaceous and Oligocene units (Mraznica and Huty Fms., respectively).
- Tracing the impact of evelated temperatures on the magnetic mineralogy of Mraznica and Huty Fms.
- Comparison of the intensity of the Late Cretaceous burial and the Oligocene-Miocene burial and their impact on nappe rocks.
- Identification of different magnetic fabrics in rocks and interpreting their origin in relation to tectonic processes.

3. Geological setting of the study area

The Central Carpathian Paleogene Basin and the Tatra Mts. are located in the Central Western Carpathians (CWC; Fig. 1). The geological evolution of this region is complex and includes several stages ranging from the Late Paleozoic to the Pliocene (Anczkiewicz et al., 2015; Catlos et al., 2022; Gawęda et al., 2016; Jurewicz, 2007; Králiková et al., 2014a, 2016; Kováč et al., 1994; Passendorfer, 1952; Plašienka et al., 1997). The oldest recorded processes are the Variscan magmatic and metamorphic events that formed the Tatra crystalline basement (e.g., Burchart, 1972; Kohút et al., 1999; Král, 1977; Petrík and Kohút, 1997; Plašienka et al., 1997). In the Triassic, the dominating rifting-related extensional regime resulted in the opening of oceanic domains and the onset of predominantly carbonate sedimentation which continued

in the Jurassic (Csontos and Vörös, 2004; Plašienka et al., 1997). The Cretaceous is characterized by a change in the tectonic regime to a compressional due to the collision of the North European Platform with Adria- and Europe-derived units (Castelluccio et al., 2016; Csontos and Vörös, 2004; Kováč et al., 2018; Plašienka, 2018; Plašienka et al., 1997). This resulted in basin inversion, large-scale folding, and the formation of a nappe system (Fatric-Hronic system[1]; Plašienka, 2018). In the Late Turonian, the nappe system represented here by the Krížna-Choč nappes was thrust onto the Tatra crystalline basement with its para-autochthonous cover (Prokešová et al. 2012). The following minor uplift resulted in a partial erosion and karstification of the nappe sediments (Činčura 1990, 2002; Danišík et al. 2010; Králiková et al., 2014ab, 2016; Kováč et al. 1994, 2016; Plašienka, 1997; Vojtko et al. 2016). In the Late Eocene-Early Oligocene, the CCPB was opened in the CWC area on a basement consisting of Mesozoic nappes (Kováč et al., 2016; Soták et al., 2001).
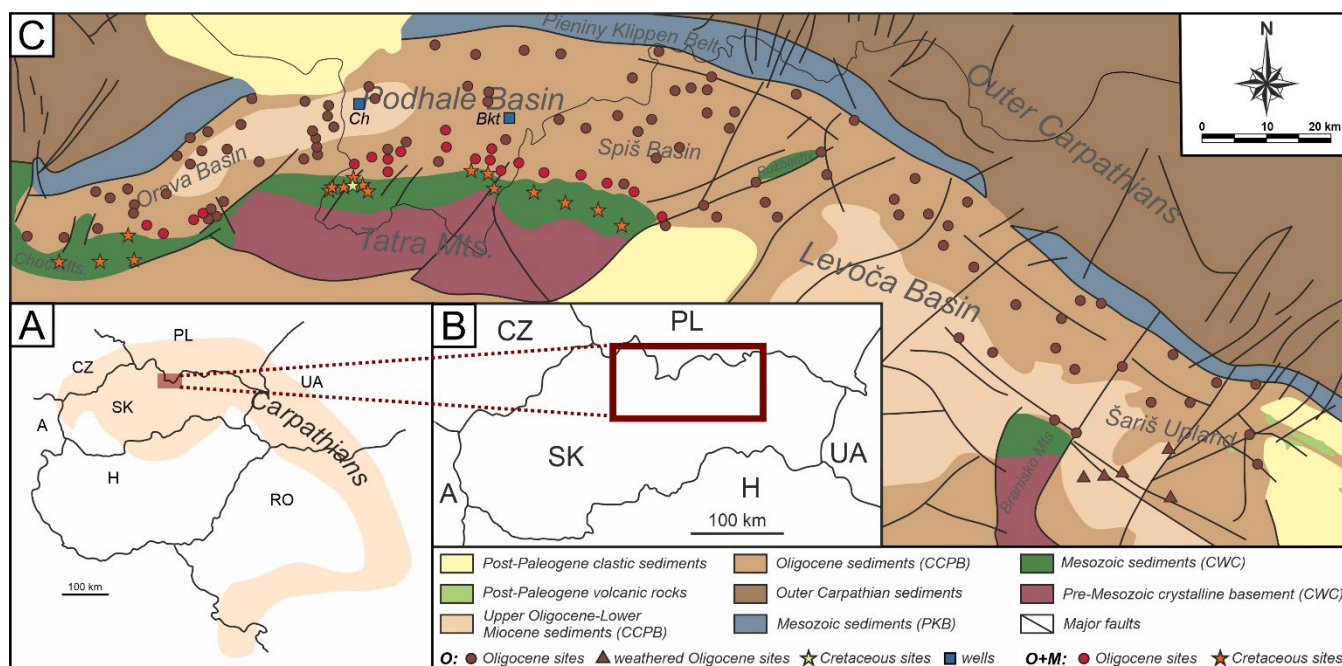
Fig. 1 Simplified geological map of the study area (modified after Gross et al., 1993a, 1999; Nemčok et al., 1993a) and adjacent areas with marked sampling localities. Ch = Chochołów PIG-1 well, Bkt = Bukowina Tatrzańska PIG-1/GN well.

The beginning of sedimentation was marked by basal transgressive facies (mainly carbonates) followed by fine-grained clastic rocks reflecting the deepening of the basin (Fig. 2; Gross et al., 1984, 1993b; Soták et al., 2001). In the Early Miocene, the sedimentation in the CCPB ceased due to the onset of the uplift-related compression in the CWC massifs (Garecka,

---

[1] The names of different units and formations are derived from the Slovak terminology.

2005; Soták et al., 2001). The uplift and exhumation of the Tatra Mts. accelerated in the Middle Miocene and was accompanied by a northward tilting of the Tatra block (Jurewicz, 2005; Rubinkiewicz and Ludwiniak, 2005; Sperner et al., 2002; Szaniawski et al., 2012). Subsequently, the CCPB sediments were partially eroded and underwent mostly brittle deformations (Pešková et al., 2009). However, the exhumation of the Choč-Tatra horsts resulted also in ductile deformations such as the asymmetrical folding of the Orava and Podhale Basins (Pešková et al., 2009).

4. Samples and methods

a. Sample description

The sampling region covers the pre-Cenozoic massifs of the CWC: the Tatra Mts., and partly also the Choč Mts. with their surrounding depressions, namely the Orava, Podhale, Spiš, Levoča, and Šariš regions (Fig. 1; Appendix 1). Altogether, 146 sites (21 from the Mraznica Fm., 73 from the Huty Fm., 44 from the Zuberec Fm., and 8 from the Biely Potok Fm.) and 482 samples (141 from the Mraznica Fm., 247 from the Huty Fm., 81 from the Zuberec Fm., and 13 from the Biely Potok Fm.) were taken from fresh outcrops in the streams, rivers and valleys. The surface samples were complemented with 53 samples from Bukowina Tatrzańska PIG-1/GN (17 samples), Chochołów PIG-1 (29 samples) , Furmanowa PIG-1 wells (4 samples), Bańska IG-1 well (1 sample), Biały Dunajec PAN 1 well (1 sample), and Zakopane IG-1 well (1 sample).

The oldest sampled unit is the Lower Cretaceous Mraznica Fm. which is a part of the Krížna nappe (Prokešová et al., 2012). Outcrops of this unit are located on the northern slopes of the Tatra Mts. and Choč Mts. (Fig. 1; Appendix 1). The lithology of the Mraznica Fm. comprises mainly marly limestones, marls, and limestones (Fig. 2; Kędzierski and Uchman, 1997; Lefeld, 1974; Lefeld et al., 1985). Here, three units from the post-Cenozoic cover of the CWC (the CCPB) were investigated: the Late Eocene-Oligocene Huty Fm., Oligocene Zuberec Fm., and Oligocene-Early Miocene Biely Potok Fm. (Fig., 2; e.g., Gross et al., 1984, 1993ab). The sampled units consist mainly of clastic sediments, such as mudstones, shales, and sandstones. More details on the sampled units are provided in the publications.
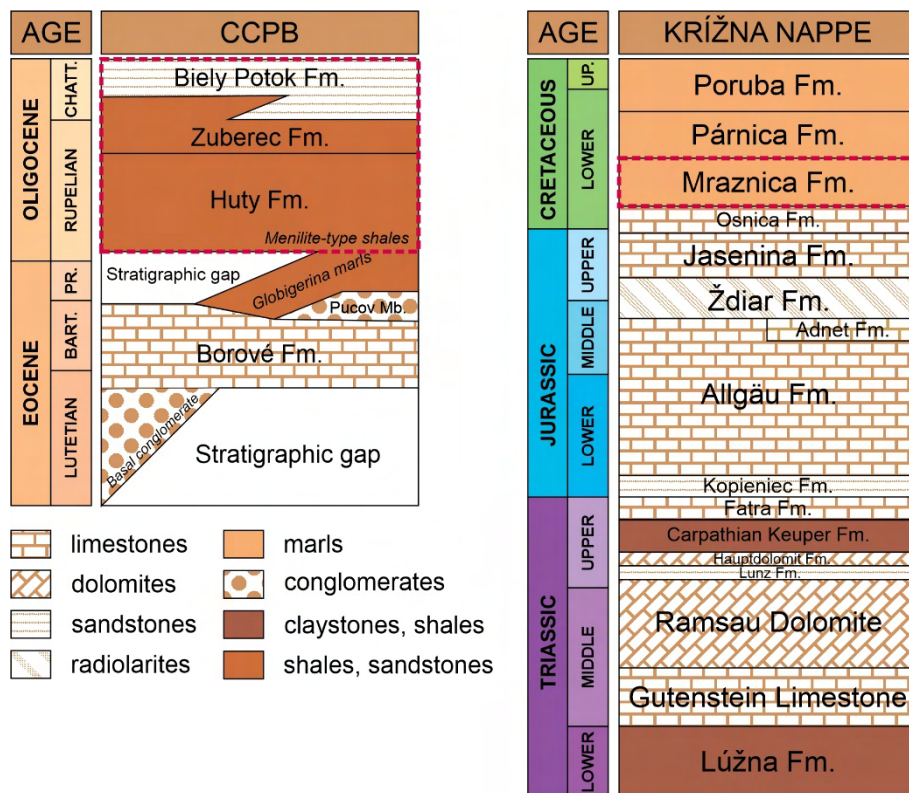
Fig. 2 Lithostratigraphy of the Central Carpathian Paleogene Basin units and the Krížna nappe modified after Gross et al. (1984), Starek (2001), and Lexa et al. (2000).

b. Methodology

To achieve reliable and high-quality results essential for a comprehensive study of the CCPB and the Tatra Mts., an interdisciplinary approach was adopted. The study incorporated four primary methodological frameworks: rock magnetic and magnetic fabric analyses, organic geochemistry, petrographic examinations, and inorganic geochemical analyses (Tab. 1). The methods were carefully chosen to investigate the evolution of these units starting from the depositional paleoenvironment, and diagenesis to tectonic processes. For more details on the methodology, the reader is referred to the publications.

Tab. 1 Methodology used in the PhD dissertation.

No.	Equipment/process	Sample unit	Main goal	Laboratory
1	Washing with distilled water, drying, removing weathered layers, crushing and grinding	Mraznica Fm., Huty Fm., Zuberec Fm., Biely Potok Fm.	preparation of samples for further organic and inorganic geochemistry analyses	Laboratory for Organic Geochemistry, Institute of Earth Sciences, University of Silesia in Katowice
2	Eltra CS-500 IR-analyzer equipped with a TIC module	Mraznica Fm., Huty Fm., Zuberec Fm., Biely Potok Fm.	Total Organic Carbon, Total Sulfur measurements	Laboratory for Organic Geochemistry, Institute of Earth Sciences, University of Silesia in Katowice
3	Zeiss Axio Imager.A2m	Mraznica Fm., Huty Fm., Zuberec Fm., Biely Potok Fm.	vitrinite and fusinite reflectance measurements in immersion oil and reflected light	Laboratory for Organic Geochemistry, Institute of Earth Sciences, University of Silesia in Katowice
4	Environmental scanning electron microscope Philips XL30 ESEM/TMP in backscattered electron mode (BSE)	Huty Fm., Zuberec Fm., Biely Potok Fm.	pyrite framboid diameter analysis	Laboratory for Organic Geochemistry, Institute of Earth Sciences, University of Silesia in Katowice
5	Vinci Technologies Rock-Eval 6 Turbo apparatus	Huty Fm., Zuberec Fm., Biely Potok Fm.	Rock-Eval pyrolysis	Faculty of Geology, Geophysics, and Environmental Protection at AGH University of Krakow; the Oil and Gas Institute - National Research Institute, Krakow and the Polish Geological Institute - National Research Institute, Warszawa.
6	Optical Emission Spectroscopy (OES) and Inductively Coupled Plasma Mass Spectrometry (ICP-MS)	Huty Fm., Zuberec Fm., Biely Potok Fm.	analysis of the content of 37 elements (Mo, Cu, Pb, Zn, Ag, Ni, Co, Mn, Fe, As, U, Au, Th, Sr, Cd, Sb, Bi, V, Ca, P, La, Cr, Mg, Ba, Ti, B, Al, Na, K, W, Sc, Tl, S, Hg, Se, Te, and Ga)	AcmeLabs, Vancouver, Canada

7	Thermo Scientific Dionex ASE 350 solvent extractor; column chromatography; derivatization using N,O-bis-(trimethylsilyl)trifluoroacetamide (BSTFA)	Mraznica Fm., Huty Fm., Zuberec Fm., Biely Potok Fm.	extraction of organic matter, fractionation into the aliphatic, aromatic and polar hydrocarbons and derivatization of the polar fraction in the less mature samples	Laboratory for Organic Geochemistry, Institute of Earth Sciences, University of Silesia in Katowice
8	Gas chromatograph (GC) and an Agilent 5975C Network mass spectrometer with Triple-Axis Detector (MSD)	Mraznica Fm., Huty Fm., Zuberec Fm., Biely Potok Fm.	detection of organic compounds, biomarker analysis	Laboratory for Organic Geochemistry, Institute of Earth Sciences, University of Silesia in Katowice
9	Drilling of cylindric specimens from oriented hand samples	Mraznica Fm., Huty Fm.	preparation of samples for further magnetic analyses	Laboratory for Paleomagnetism and Environmental Studies, Institute of Geophysics, Polish Academy of Sciences, Warszawa
10	MFK1-FA Kappabridge	Mraznica Fm., Huty Fm.	in- and out-of-phase magnetic susceptibility measurements	Laboratory for Paleomagnetism and Environmental Studies, Institute of Geophysics, Polish Academy of Sciences, Warszawa
11	KLY-5A Kappabridge with heating and cooling units (CS-4/CS-L)	Mraznica Fm., Huty Fm.	Anisotropy of in-phase and out-of-phase Magnetic Susceptibility, in- and out-of-phase temperature dependent magnetic susceptibility measurements	Laboratory for Paleomagnetism and Environmental Studies, Institute of Geophysics, Polish Academy of Sciences, Warszawa
12	JR6a automated dual speed spinner magnetometer; LDA5/PAM1 Alternating Field Demagnetizer/ Anhysteretic and Pulse Magnetizer	Mraznica Fm., Huty Fm.	Anisotropy of Anhysteretic Remanent Magnetization measurements	Laboratory for Paleomagnetism and Environmental Studies, Institute of Geophysics, Polish Academy of Sciences, Warszawa
13	PAM1 Pulse Magnetizer, MMPM10 pulse magnetiser, 755–1.65 2G Enterprises cryogenic magnetometer DC SQUID with AF degausser	Mraznica Fm., Huty Fm.	Isothermal Remanent Magnetization (IRM) acquisition	Laboratory for Paleomagnetism and Environmental Studies, Institute of Geophysics, Polish Academy of Sciences, Warszawa

14	755–1.65 2G Enterprises cryogenic magnetometer DC SQUID with AF degausser, MMTDSC - Nonmagnetic furnace for thermal demagnetization	Mraznica Fm., Huty Fm.	thermal demagnetization of the three-component IRM experiment	Laboratory for Paleomagnetism and Environmental Studies, Institute of Geophysics, Polish Academy of Sciences, Warszawa
15	Micromag AGFM 2900-02 Alternating gradient force magnetometer	Mraznica Fm., Huty Fm.	hysteresis curves and IRM back-field measurements	Laboratory for Paleomagnetism and Environmental Studies, Institute of Geophysics, Polish Academy of Sciences, Warszawa

5.   Results and discussion

   a.   Paleoenvironment of the CCPB sedimentary rocks (Staneczek et al., 2024a)

      i.   Sedimentary conditions

Biomarker- and non-biomarker methods document a complex evolution of the CCPB characterized mainly by differences in the sedimentary environment. The sedimentary environment study was performed in the Orava Basin, which shows the lowest thermal maturity in the whole basin, and where all of the investigated units can be sampled.

In the Late Eocene, the deposition of the Huty Fm. rocks began (Gross et al., 1984; Starek, 2001). Based on the C_{27}, C_{28}, and C_{29} regular steranes distribution (see Fig. 7 in Staneczek et al., 2024a), the CCPB at that time reached its maximum depth and was characterized by an open-marine environment (Fig. 3). In the Huty Fm. the highest concentrations of dinosteroids are found (Tab. S6 in Staneczek et al., 2024a), which given the origin of these compounds (presumably from dinoflagellates; Kokinos et al., 1998) confirms the marine setting. Basic parameters such as pristane/phytane ratio within the ranges of 1-5.5, relatively low TOC (~1%), and hopane distribution with the domination of C_{31} 22S and 22R epimers point towards aerobic conditions during the organic matter sedimentation (see Tab. S1 in Staneczek et al., 2024a; Didyk et al., 1978; Huang and Meinschein, 1979; Peters et al., 2005). This is further supported by the Th/U, Ni/Co, and V/Cr ratio values which suggest an oxygen-rich sedimentary environment (Figs. 12 in Staneczek et al., 2024a; Hartkopf-Fröder et al., 2007). However, there are indications that the conditions changed commonly to suboxic and locally to even anoxic/euxinic (Fig. 3). In some samples, aryl isoprenoids, isorenieratane decomposition derivatives, and gammacerane occur. The presence of these compounds is linked with photic zone euxinia (PZE; Grice et al., 1996, 2005; Koopmans et al., 1996; Summons and Powell, 1987) in the water column. Such intermittent euxinia is also documented by the relatively high percentage (>50%) of small pyrites (<5 μm) in some Huty Fm. samples (see Tab. S4 in Staneczek et al., 2024a). Unstable sedimentary conditions, when the oxic water column was disrupted by events of suboxic-anoxic conditions are indicated by the Mo enrichment to U (Tab. S7 in Staneczek et al., 2024a; Algeo and Tribovillard, 2009; Ai et al., 2021) and by scattered TOC/P values.
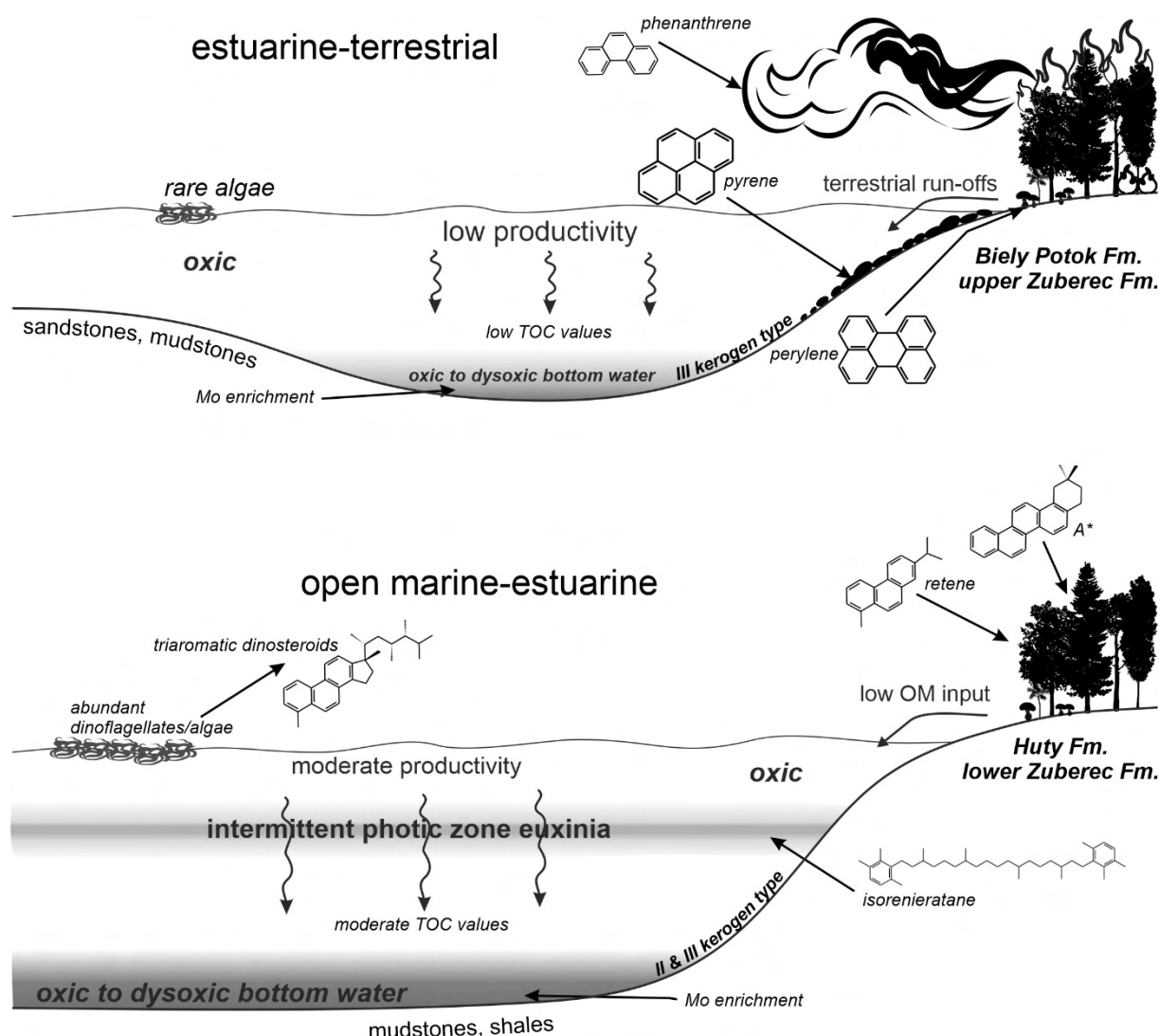
Fig. 3 Depositional conditions and their changes over time in the CCPB sedimentary rocks. Parts of the figure derived from rawpixel.com, pch.vector, Freepik.

A paleoenvironment characterized by aerobic conditions with localized PZE prevailed in the Oligocene during the sedimentation of the lower part of Zuberec Fm. The sterane distribution ternary diagram shows the Zuberec Fm. samples mainly in the estuarine and terrestrial sectors (see Fig. 7 in Staneczek et al., 2024a). Since at least some of the analyzed samples display features very similar to those of the Huty Fm. samples, the estuarine setting was likely sporadic and occurred mainly during the Huty-Zuberec transition. Common dinosteranes also suggest an open marine type of the basin (Fig. S4 in Staneczek et al., 2024a). During the longest period, the basin was surrounded by land and inflowing rivers. Gradual shallowing led to the formation of fragmented more restrictive subbasins and/or bays, where the conditions enabled the formation of PZE. Such basin features are suggested by the occurrence of aryl isoprenoids (and even isorenieratane) and gammacerane in more samples than in the Huty Fm (see Fig. 10 in Staneczek et al., 2024a). Periodic euxinia is also documented

by the small (<5 μm) diameter of pyrite framboids, which in ten out of twenty-four samples constitute at least 50% of the population (see Fig. 14 and Tab. S4 in Staneczek et al., 2024a). In comparison, the age-corresponding Menilite shales from the Outer Carpathians were deposited under more restrictive conditions since the content of tiny framboids in these rocks is usually higher than 80% (Wendorff-Belon et al., 2021). Anoxic or euxinic conditions were interrupted by the influx of oxygenated waters along with terrestrial organic matter. Interestingly, some Zuberec Fm. samples (presumably the upper Zuberec Fm.) contain fusinite which indicates the presence of wildfires on the land (Fig. S1 and Tab. S3 in Staneczek et al., 2024a). The oxic pulses and generally unstable sedimentary environment are recorded by inorganic ratios (Mo enrichment, particulate shuttle, see Fig. 13 in Staneczek et al., 2024a), similar to the Huty Fm.

The gradual transition to the shallow-water Biely Potok Fm. is marked mainly by the distribution of steranes which generally fall into the terrestrial type (Fig. 3; Fig. 7 in Staneczek et al., 2024a). Algal biomarkers are found in the lowest concentrations in comparison to other units (Tab. S6 in Staneczek et al., 2024a). The prevalent terrestrial input is indicated by the presence of high amounts of 18α + 18β-oleananes, norlupanes, and bisnorlupanes and also common fusinite (Fig. 6 and S1 in Staneczek et al., 2024a). Basic parameters, such as TOC, Pr/Ph ratio, and the homohopane distribution (Tab. S1 in Staneczek et al., 2024a) indicate oxic conditions that could be sporadically interrupted by dysoxic bottom waters as suggested by the Mo enrichment (Fig. 3; Ai et al., 2021) found in some samples. The oxygenated water column was also documented by the generally large pyrite framboids (Fig. 14 and Tab. S4 in Staneczek et al., 2024a).

ii. Terrestrial organic matter

The input of the terrestrial organic matter varies between the studied formations, which is reflected by the relative amount of algae-derived biomarkers and the diversity of the land-derived compounds. However, in the case of the Orava Basin, it should be noted, that due to the high maturity levels of some samples, the proper identification of the rates of terrestrial input can be erroneous since some compounds disappear or are degraded above certain paleotemperatures. The Rock-Eval pyrolysis documented the domination of the type III kerogen, or type III with an elevated share of type II kerogen in the Orava Basin samples (Fig. 5 in Staneczek et al., 2024a). Some Huty and Zuberec Fms. samples show the prevalence of the type II kerogen. The origin of the mentioned kerogen types corresponds well with the

22

paleoenvironment changes discussed in the previous paragraph. The kerogen type II is associated with planktonic organic matter and generally indicates deeper marine conditions, while type III is derived from terrestrial organic matter, mainly from higher plants, and is found in shallow marine or deltaic settings (Vandenbroucke and Largeau, 2007). Type II is the only type of kerogen found in a few Huty and Zuberec Fms. samples. Generally, the majority of samples from these units show mixing of the II and III kerogen types. On the contrary, "pure" type III kerogen is found in a few Zuberec Fm. samples and all Biely Potok Fm. samples. It is therefore reasonable to assume, that the input of terrestrial organic matter increased with the shallowing of the basin and with age.

Three main types of terrestrial organic matter were identified in the samples. The first type is associated with angiosperms (Tab. S8 in Staneczek et al., 2024a). The flowering plant-derived compounds were detected in both aliphatic and aromatic fractions. The main compounds include oleananes, lupanes, picenes and α- and β-amyrin derivatives (Fig. 6 in Staneczek et al., 2024a). Their variety is larger in Biely Potok and upper Zuberec Fms. than in lower Zuberec and Huty Fms. rocks, most likely due to their lower thermal maturity and thus, better preservation of these compounds. However, a higher enrichment in terrestrial organic matter of the upper Zuberec and Biely Potok Fms cannot be ruled out. The second type of terrestrial organic matter is derived from gymnosperms (Fig. 8 and 9 in Staneczek et al., 2024a). Aliphatic compound groups associated with conifers include among others bi-, tri-, and tetracyclic diterpenoids, including labdane, fichtelite and kaurane, which were found mainly in the less mature samples. Similarly, the aromatic dehydroabietane and simonellite were also found only in the thermally unaltered rocks. Other aromatic gymnosperm representatives are cadalene, retene, 6-isopropyl-1-isohexyl-2-methylnaphthalene (iPiHMN), or methyl derivatives of retene and simonellite. In addition, conifer-related compounds were identified in the polar fraction (dehydroabietic acid; Tab. 2 in Staneczek et al., 2024a; Otto and Simoneit, 2001). The presence of resinous plants is also confirmed by the discovery of amber in the Podhale Basin (Kojsówka village; Kotulová et al., 2019). Lastly, the third organic matter type, most likely fungal, is documented by perylene (Fig. S3 in Staneczek et al., 2024a; e.g., Grice et al., 2009; Li et al., 2022; Marynowski et al., 2013; Oskay et al., 2019). This compound is present only in Biely Potok and upper Zuberec Fms. It is known to disappear above 0.7% Ro (Marynowski et al., 2015), which is in good agreement with its occurrence in the CCPB units. In the least mature samples, perylene sometimes dominates the aromatic fraction. Such a high quantity of this compound may suggest a humid climate, where organic matter decays faster

due to thriving fungi (Hossain et al., 2013). However, perylene could also be potentially related to wildfire-induced soil erosion and runoffs from surrounding lands.

One may be tempted to quantify the percentage contribution of the gymnosperm versus the angiosperm compounds in the studied units. However, even though such calculations are possible, they may give erroneous results due to differences in the thermal maturity of the units. Not all compounds are equally resistant to increasing paleotemperatures. Yet, it can be concluded, that gymnosperm and angiosperm higher plants were abundant during the CCPB sedimentation and contributed to the kerogen formation.

iii.   Wildfires in the CCPB

The first evidence of wildfires in the CCPB are macerals from the inertinite group (here mainly fusinite and semifusinite) frequently found in the Biely Potok and upper Zuberec Fm. samples (Fig. S1 and Tab. S3 in Staneczek et al., 2024a). It is known, that the measured vitrinite reflectance can be converted into the approximate fire temperature (Belcher et al., 2018; Jones et al., 1991), enabling the assessment of the wildfire type (Scott, 2000, 2010). In the case of the studied units, the average temperatures ranged from 382 to 734°C, with the highest being recorded in the Zuberec samples (Tab. S3 in Staneczek et al., 2024a). Such temperatures correspond with surface (low-temperature) and crown (high-temperature) fires. Wildfires can also be indicated by a significant contribution of the polycyclic aromatic hydrocarbons (PAHs) in marine sedimentary rocks and coal seams (Killops and Massoud, 1992). The most common fire-related compounds found in these samples are anthracene and methylanthracenes, 4Hcyclopenta[*def*]phenanthrene, benzo[*ghi*]fluoranthene, benz[*a*]anthracene and benzo[*a*]pyrene (Fig. S2 in Staneczek et al., 2024a). Coronene, a compound linked with high fire temperatures (Kaiho et al., 2023), was identified in all fusinite-rich samples, except those where the calculated temperatures were low. Other potentially wildfire-related compounds such as retene (Ramdahl, 1983) were excluded from further analysis as they were present in all samples regardless of PAH levels. Another investigated aspect was the smoke or residue PAH origin. The low-molecular-weight PAHs to total PAHs ratio (LMW/Total; Tab. 3 in Staneczek et al., 2024a; Karp et al., 2020; Vachula et al., 2020) investigates the relationship between the smoke migrating PAHs (LMW PAHs: phenanthrene, anthracene, fluoranthene, and pyrene) and residue-related high-molecular-weight PAHs found commonly in charcoals. In the case of the CCPB, the ratio values were higher (0.7-0.8) in Zuberec Fm. samples suggesting a mixed PAH

origin. In contrast, the Biely Potok Fm. samples displayed lower values associated with residue-related PAHs. Interestingly, the change from a partial smoke contribution to residue-related PAH origin corresponds well with the shallowing of the sedimentary basin. Moreover, it indicates, that during the deposition of Zuberec Fm. and especially the Biely Potok Fm., wildfires could accelerate land degradation and soil erosion, leading to intense run-offs (Fig. 3; Boudinot and Sepúlveda, 2020; Synnott et al., 2021) and nutrient input into the basin (Kaiho et al., 2016). Yet, these processes must have been sporadic since the TOC values in the majority of the Zuberec and Biely Potok Fms. are rather low.

A thorough study of other PAHs, such as dimethylphenanthrenes may also shed light on the type of burned vegetation (Kappenberg et al., 2019; Karp et al., 2020; Zhao et al., 2023). Here, the ratio values (Fig. 15 in Staneczek et al., 2024a) indicate, that herbaceous plants like grasses were the main burned biomass. However, the importance of this type of plant was low before the Miocene (Sage, 2004; Karp et al., 2018). Moreover, some less stable dimethylphenanthrenes could partly disappear during diagenesis (Zheng et al., 2023), and therefore affect the ratio values. Given the angio- and gymnosperm biomarkers present in the Zuberec and Biely Potok Fms., the dimethylphenanthrenes could be derived from both soft- and hardwoods. Such mixture was documented in the Thrace Basin during the Late Oligocene (Çelik et al., 2017), where conifers and angiosperms, including *Ulmus*, *Carya*, and *Zelkova* were present. In general, Oligocene wildfires were commonly reported from both European (e.g., Neuwid Basin, Westerwald in Rhineland-Palatinate; Uhl et al., 2020, 2022) and other areas (e.g., northern South China Sea, North Pacific Ocean, Bengal Basin; Jia et al., 2003; Herring, 1985; Hossain et al., 2013).

b. Thermal maturity and paleotemperatures in the CCPB and Tatra area (Staneczek et al., 2024ab; Staneczek and Marynowski, 2025; Staneczek et al., under review)

i. Biomarker maturity indicators

The presence of organic compounds in samples can be used as a maturity level indicator, due to their different thermodynamic stability. Typical processes indicating elevated paleotemperatures include the aromatization of cyclic organic compounds or the isomerization of less stable biomarkers into more thermally stable ones (Peters et al., 2005; Radke et al., 1997). Based on the occurrence of some compounds or compound groups several ratios were

proposed which give comparable results. The two groups most often studied are aliphatic and aromatic hydrocarbons. In this study, various organic compounds and Rock-Eval-derived T_{max} were applied to characterize the maturity of the CCPB and the Tatra Mts. The maturity changes were also investigated in Chochołów PIG-1 and Bukowina Tatrzańska PIG-1/GN wells, for data comparison and better interpretation of the results. Moreover, the thermal characteristics of a region usually shed light on the possibility of future hydrocarbon exploration. The most important maturity indicators are discussed below.

Aliphatic ratios applied in this study only to the CCPB rocks and wells include the distribution of homohopanes (C$_{31}$S/(S+R); Seifert and Moldowan, 1980), steranes (C$_{29}$-$\alpha\alpha\alpha$ 20S/(S+R); Mackenzie and McKenzie, 1983), and three groups of immature compounds (oleananes, lupenes, and C$_{30}\beta\beta$ hopanes; Tab. S.3 and S.4 in Staneczek and Marynowski, 2025). Hopanes and steranes are present in the majority of the CCPB, except the eastern Podhale and Spiš Basins. Both ratios show the lowest values in the northern Orava, northern Levoča, and eastern Šariš (Fig. 4 in Staneczek and Marynowski, 2025). The hopane-based parameter shows no virtual trend in the spatial distribution. Conversely, the sterane ratio values seem to increase towards the Podhale Basin and from Šariš Upland to the central Levoča Basin (Fig. 4 in Staneczek and Marynowski, 2025). Hopanes and steranes are found only in the Chochołów PIG-1 well, and the corresponding ratio values increase with depth to 2410 m and 2264 m, respectively, and to ~0.75% Rc (Fig. 3, Tab. S.4 in Staneczek and Marynowski, 2025). The immature compounds are, however, found only in three isolated areas, which are also marked by the lowest values of the previous parameters: northern Orava, northern Levoča and eastern Šariš (Fig. 4 in Staneczek and Marynowski, 2025). Moreover, these compounds are not present in the well samples.

Several parameters based on the presence of different aromatic compounds were used to investigate both CCPB and Choč-Tatra sedimentary rocks. Phenanthrene- and methylphenanthrene-derived MPI1 and MPI3 ratios (methylphenanthrene index 1 and 3, respectively; Radke and Welte, 1983) can be calculated for the whole studied area. Both ratios show their highest values in the Spiš Basin and the Belianske Tatra Mts., and then slowly decrease towards the Orava Basin and Šariš Upland (Fig. S3 and Tab. S3 in Staneczek and Marynowski, 2025). In wells, MPI1 and MPI3 increase gradually with depth, showing the highest values in the Bukowina Tatrzańska PIG-1/GN bottom samples (Fig. 3, Tab. S4 in Staneczek and Marynowski, 2025). Moreover, the MPI1 parameter can be further converted into theoretical vitrinite reflectance (Rc; Radke, 1987), which, in some rock types, can be compared with the measured vitrinite reflectance. The spatial distribution of Rc shows similar

features to those documented by MPI1 and MPI3. The minimum values (~0.5%, Tab.S3 in Staneczek and Marynowski, 2025) are recorded in the Orava and western Podhale Basins, and some parts of Levoča Basin, whereas the highest (~3.0% Rc) are documented close to the Ružbachy-Tatra junction. In wells, the lowest values are calculated for the top of the Chochołów PIG-1 well (~0.5% Rc), and the highest at the bottom of Bukowina Tatrzańska PIG-1/GN (2.68% Rc; Fig. 3 and Tab. S4 in Staneczek and Marynowski, 2025). In the Cretaceous Tatra rocks (Mraznica Fm.), a weak increasing trend can be observed from the Western to Belianske Tatra Mts. (Tab. S1 in Staneczek et al., under review). However, for rocks with marine organic matter, this parameter is not recommended and may give erroneous results (Radke et al., 1986). The same, yet more coherent trend in the Tatra Mts. is displayed by the phenylphenanthrene-based ratio (Rospondek et al., 2009; Fig. 4 and Tab. S1 in Staneczek et al. under review). Both in surface and well samples, this parameter follows the same pattern as the previously described aromatic parameters. The next ratio likewise based on PAH compounds is the benzo[*e*]pyrene (B*e*P), benzo[*a*]pyrene (B*a*P), and perylene (Pe) parameter (Figs. 3, 5 and Tab. S3, S4 in Staneczek and Marynowski, 2025). Due to the high stability of BeP, the ratio could be applied in the whole CCPB region. The least mature regions are indicated by the presence of perylene, and, similarly to aliphatic ratios, include northern Orava Basin, northern Levoča Basin, and eastern Šariš Upland. However, the majority of the CCPB shows very high values between 0.9-1.0.

Finally, the two last parameters are characterized by the distribution of three gymnosperm biomarkers: retene, simonellite, and dehydroabietane which all have different thermal stability (Fig. 5 and Tab. S3, S4 in Staneczek and Marynowski, 2025). The less stable simonellite and dehydroabietane are present in limited areas only, while the most stable retene is not detected in the Spiš Basin, eastern Podhale Basin, the bottom of the Chochołów PIG-1 borehole, and in all Bukowina Tatrzańska PIG-1/GN samples. The surface distribution of the ratio values is strongly related to the presence (and quantity) of simonellite. Therefore, the least mature regions highlighted by this parameter include northern Orava and western Podhale Basins, Šariš Upland, and northern/central Levoča. A second ratio based on retene coupled with 3-methylphenanthrene could be applied in the borehole samples (only in Chochołów PIG-1), where it documented a constant decrease with depth up to 2264 m, below which retene disappears (Fig. S4 in Staneczek and Marynowski, 2025). However, the spatial distribution of this parameter is more scattered than the first retene-based ratio (Fig. 5 in Staneczek and Marynowski, 2025).

27

ii. Rock-Eval parameter and hydrocarbon potential

Rock-Eval analysis provides valuable insight into the thermal maturity of the studied area. An important parameter is the T_{max} which changes with increasing paleotemperatures. First, the Chochołów PIG-1 and Bukowina Tatrzańska PIG-1/GN borehole samples were subjected to this analysis. The T_{max} values show a rather consistent trend of rising temperatures starting from ~430°C in the upper Chochołów PIG-1 borehole and reaching ~465°C at the bottom, to ~445°C in the upper Bukowina Tatrzańska PIG-1/GN borehole to over 500°C measured in the deepest samples (Tab. S2 in Staneczek and Marynowski, 2025). In the surface samples, the distribution of the T_{max} values follows a very similar trend to those recorded by biomarker maturity parameters. The highest values (~600°C; Fig. S2 and Tab. S1 in Staneczek and Marynowski, 2025) are documented in the Belianske Tatra Mts. foreland and close to the Tatra-Ružbachy junction. T_{max} decreases slowly and coherently towards the east and west. Moreover, a northward decrease of the T_{max} values from the Mesozoic units of the CWC to the Pieniny Klippen Belt is also documented (Fig. S2 in Staneczek and Marynowski, 2025). The lowest values (<430°C) were measured in the samples from the northern Orava Basin and Šariš Upland (Fig. S2 and Tab. S1 in Staneczek and Marynowski, 2025).

The CCPB rocks are characterized by the domination of the gas-prone type-III kerogen. Some samples also display the oil-prone type-II kerogen or a mixture of these two types (Fig. 5 in Staneczek et al., 2024a; Staneczek and Marynowski, 2025). When applying the criteria of Peters and Cassa (1994), the generative potential of the CCPB rocks spans from poor to excellent. The Zuberec Fm. samples show the best source rock potential, while the majority of the samples from Huty and Biely Potok Fms. are rather poor source rocks (Fig. 4 in Staneczek et al., 2024a). However, some levels of the Huty Fm. show excellent hydrocarbon potential levels (Fig. 4 in Staneczek et al., 2024a). Correlation of two sterane indicators ($C_{29}20S/(S+R)$ vs. $C_{29}\alpha\alpha/(\alpha\alpha+\beta\beta)$; Fig. 7 in Staneczek and Marynowski, 2025) locates the majority of samples in the early mature or mature fields proving their ability to generate hydrocarbons. Only a few surface samples and none of the well samples show immature features. In the CCPB area, contrary to the Outer Carpathians, liquid hydrocarbons are very rare and were found only in the Levoča Basin (Soták et al., 2001). Hydrocarbon migration was recorded in the Tatra Mts. and the Podhale Basin, but their source rocks were the underlying Mesozoic rocks (Marynowski et al., 2001, 2006). In general, even though some levels in the CCPB seem to be promising for hydrocarbon generation/exploration, further research needs to be performed to confirm this hypothesis.

iii.   The measured vitrinite reflectance and its applicability in the study area

In the CCPB, the vitrinite reflectance (Rr) was measured mainly for the Orava Basin rocks. Additionally, for magnetic studies, the Rr for the Mraznica Fm. in the Choč-Tatra Mts. (Fig. 4). and the adjacent Huty Fm. was investigated. In the case of the Mraznica Fm., contrary to the majority of biomarker-derived parameters, the Rr values are very consistent and document a slow increase from ~0.80% Rr in the Choč Mts. to a maximum of 1.70% Rr in the Belianske Tatra Mts. (Fig. 4; Fig. S1 in Staneczek and Marynowski, 2025; Fig. 2 and Tab. S1 in Staneczek et al., under review). Such a coherent maturity trend is also observed in the overlying Huty Fm. rocks (from ~0.40% Rr in the Orava Basin to ~1.50% Rr in the Belianske Tatra Mts. foreland; Fig. S1 in Staneczek and Marynowski, 2025; Tab. S1 in Staneczek et al., under review). Some sites in the Orava Basin and Šariš Upland show even lower values (<0.40% Rr). Notably, there is a significant discrepancy between the measured vitrinite reflectance and the calculated vitrinite reflectance (Rc) in both CCPB and Cretaceous units. The difference for the Paleogene units in the Spiš Basin can reach even 0.50%. In the Orava Basin, the studied samples were characterized by the occurrence of both dark hydrogen-rich vitrinite grains (documented also in the Outer Carpathians; Waliczek and Więcław, 2012; Waliczek et al., 2019) and reworked vitrinites (Fig. S1 in Staneczek et al., 2024a; Marynowski et al., 2006) which cause reflectance suppression (Petersen and Vosgerau, 1999) or disorders. The vitrinite reflectance measured on such grains can show values even 0.4% lower than the real values (Goodarzi et al., 1994). The calculated vitrinite reflectance is not affected by this phenomenon, and thus more suitable for paleotemperature investigations.

In the Mraznica Fm., the Rr values reflect better the maturity trend than the Rc by showing less scattered values. However, considering the high Rc obtained for the overlying Huty Fm., the Rr values for Mraznica Fm. should be at least 0.3-0.5% Rr higher. A possible cause of this underestimation is the size of vitrinite in the Mraznica Fm., which commonly forms elongated yet thin (<10μm; Fig. S1 in Staneczek et al., under review) grains. Measuring the reflectance of such small grains may result in slightly lower values obtained. However, for the purpose of this study, the Rr is generally a good and one of the few indicators that can be used for the Mraznica Fm. maturity estimations.
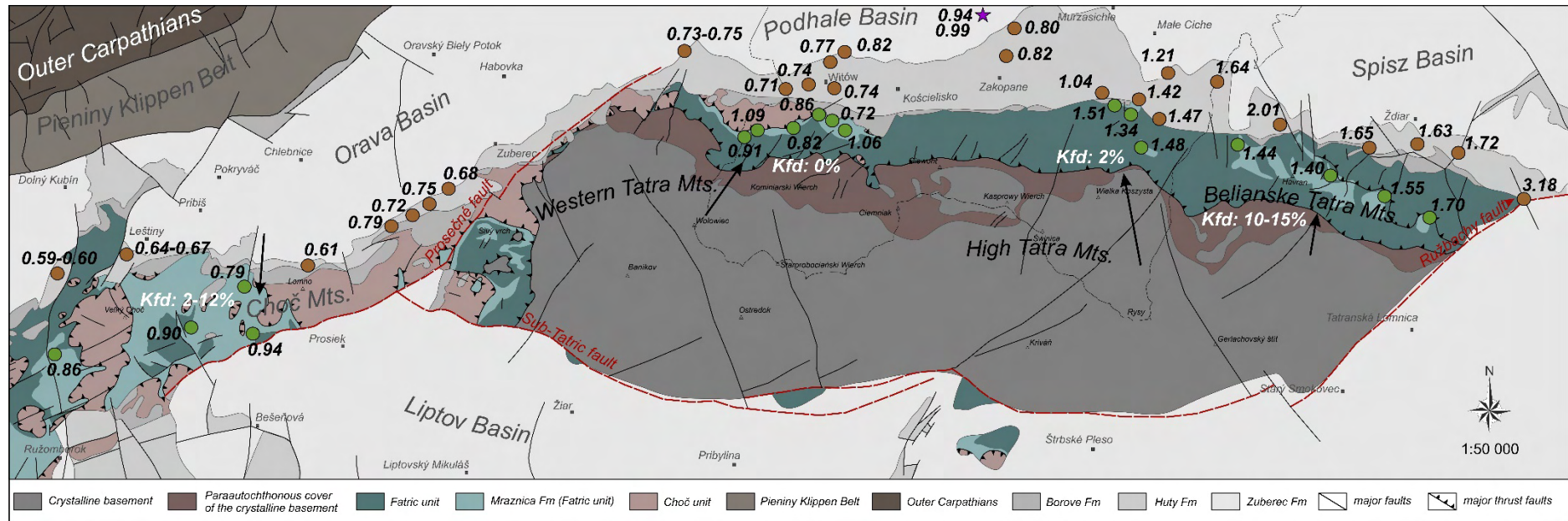
Fig. 4 Paleotemperature distribution in Choč-Tatra Belt. Map compiled after Gross et al. (1993a), Nemčok et al. (1993a), and Piotrowska et al. (2009, 2013). Brown and green dots show the location of Huty and Mraznica Fm. sites, respectively. The star depicts the location of the Furmanowa IG-1 well.

iv. Magnetic proxies of thermal maturity

Magnetic properties of rocks are a rather new tool to assess the thermal maturity of rocks (e.g., Abdelmalak and Polteau, 2020; Caricchi et al., 2024). The presence of some domain sizes and some minerals can be linked with increased thermal impact. Yet, it is rarely the case that the exact paleotemperature range can be estimated using only the magnetic parameters (e.g., Aubourg and Pozzi, 2010). The thermal maturity trend was investigated by applying some parameters in the Mraznica Fm. and the overlying Huty Fm. in a wide belt starting from the Choč Mts. to the Belianske Tatra Mts. (Staneczek et al., 2024b; Staneczek et al., under review).

The magnetic susceptibility reflects the response of a material to the applied external field (e.g., Borradaile, 1988) and can be divided into a component that is in-phase with the applied field and out-of-phase with this field (e.g., Hrouda et al., 2013; 2016; 2022). The first component comprises all minerals (most commonly divided into dia-, para- and ferromagnetic minerals) while the second measures only the response of a part of ferromagnetic minerals (e.g., Hrouda et al., 2013). Different properties of the studied rocks are usually mirrored by the in-phase (Kip[2]) and out-of-phase (Kop) magnetic susceptibility values. Both Kip and Kop are generally quite low but change significantly in the Choč-Tatra Belt and its Paleogene foreland (Fig. 12 in Staneczek et al., under review). The lowest Kip in the Huty and Mraznica Fms. are recorded in the Western Tatra Mts. (Fig. 12 in Staneczek et al., under review), and their values increase slowly towards the most thermally affected Belianske Tatry Mts. This trend is reflected also in the Kop values. However, the Mraznica Fm. samples from the Choč Mts. have higher Kip and Kop values than those for the High Tatra (Fig. 12 in Staneczek et al., under review). The magnetic susceptibility depends strongly on the lithology of the rocks (Rochette, 1987). In the case of Huty and Mraznica Fms. the most common minerals are paramagnetic phyllosilicates. Higher Kip and Kop values could result from a greater contribution of these minerals in the rocks of the Belianske Tatra Mts. However, this would be also reflected in a higher initial slope in the hysteresis experiments, which is not the case (e.g., Fig. S5 in Staneczek et al., under review). Moreover, the Mraznica Fm. in the Belianske Tatra Mts. is characterized by a slightly higher contribution of diamagnetic carbonates, since it was deposited in a shallow marine basin (Vysoka succession; Nemčok et al., 1993a), in contrast to the Mraznica Fm. rocks from the Western Tatra Mts. which were deposited in deeper basin (Zliechov succesion; Nemčok et al., 1993a). The increase in the Kop values towards the

---

[2] In this study we use the volume-normalized magnetic susceptibility denoted as K.

Belianske Tatra Mts. points toward a continuous formation of new ferromagnetic minerals (presumably magnetite and hematite) with elevated temperatures due to illite/smectite transformation, which is commonly reported from many settings (Katz et al., 1998, 2000; Hirt et al., 1993). Anomalously high Kip values in the Mraznica Fm. from the Choč Mts. are most likely linked with the precipitation of magnetite from hydrothermal fluids (Staneczek et al., 2022) documented in this heavily faulted area (Bella and Gaal, 2017), and presumably related also to the south-bounding Choč-Tatra-Ružbachy fault (Bella and Bosak, 2012). The impact of this fault could be especially intense since the Mraznica Fm. form a narrow belt directly adjacent to this fault.

A steady formation of new ferromagnetic minerals can be also traced using the frequency-dependent magnetic susceptibility (Kfd). This parameter compares the high-frequency (15616 Hz) in-phase magnetic susceptibility with the low-frequency (976 Hz) in-phase magnetic susceptibility ($Kfd = 100*(Kip_{976Hz} - Kip_{15616Hz})/Kip_{976Hz}$; Dearing et al., 1996). The obtained result is the approximate percentage value of ferromagnetic grains on the superparamagnetic (SP) domain sizes (Dearing et al., 1996). Similarly to the Kip and Kop pattern, the highest Kfd values are calculated for the Mraznica Fm. samples in the Belianske Tatra Mts. with the absolute maximum of ~15% SP contribution (Fig. 4). The Kfd values decrease towards the less thermally affected Western Tatra Mts. and then increase again in the hydrothermal Choč Mts. The Huty Fm. samples show a lower content of SP particles with a maximum of 3% in the Belianske Tatra foreland (Fig. 5 in Staneczek et al., under review). In the Western and High Tatra foreland, this parameter is zero or close to zero. Only the Choč Mts. shows values above 1% (Fig. S9 in Staneczek et al., under review).

The last parameters are derived from the hysteresis curve and the Isothermal Remanent Magnetization back-field experiments and are presented usually in the Day plot (Day et al., 1977) with added mixing lines and domain state regions after Dunlop (2002; see Fig. 13 in Staneczek et al., under review). The investigated remanent magnetization to saturation magnetization ratio (Mrs/Ms) to the coercivity of remanence to coercivity (Hcr/Hc) ratio sheds light on the domain size and type of the ferromagnetic minerals. In the case of the Huty Fm., a clear trend is not present. Conversely, the diagram for Mraznica Fm. shows a gradual shift towards the PSD-SP mixing area (Fig. 13 in Staneczek et al., under review). The reason for this change could be an increase in the formation of fine-grained iron oxides at high temperatures and, in the case of the Choč Mts., an increased fluid circulation. However, the admixture of hematite in some sites makes it difficult to correctly interpret the Day diagram results.

The parameters discussed above show greater changes for the Mraznica Fm. samples than for the Huty Fm. samples. Still, all magnetic maturity indicators correspond well with the organic maturity parameters. Moreover, the same trend documented for these rocks points toward one major event that affected both units at the same time.

v. Paleotemperature pattern in the CCPB and Tatra Mts.

Different maturity indicators were combined to investigate the paleotemperature pattern. The most important one was the Rc parameter which was further converted into paleotemperatures using two equations described by Barker and Pawlewicz (1994), Burnham and Sweeney (1989) and summaries of various parameters presented by Hunt (1995; see Tab. S1 and S2 in Staneczek and Marynowski, 2025). In the Chochołów PIG-1 well the calculated paleotemperatures increase from ~80°C to ~130°C, and in the Bukowina Tatrzańska PIG-1/GN well, the values continue to increase from ~120°C to >200°C (Tab. S2 in Staneczek and Marynowski, 2025). Unsaturated pentacyclic triterpenoids and ββ-hopanes are present in rocks with vitrinite reflectance values below 0.4-0.5% (Peters et al., 2005) which corresponds roughly to paleotemperatures below 60°C (Fig. 5). The occurrence of thermally unstable dehydroabietane and simonellite in these regions also confirms the low temperatures (Marynowski et al., 2007; Radke, 1987; Simoneit et al., 1986). The next 60-90°C zone covers the majority of the Orava Basin, western Podhale Basin and partly the Šariš Upland (Fig. 5). In this interval, the gymnosperm-based ratios along with the aliphatic indicators can be successfully applied. In the 90-130°C range, the hopanes and steranes are not present, and the most important parameters are the PAH-derived ratios such as Rc calculated from MPI1. The last interval covers the most mature parts of the CCPB, namely the Spiš Basin and a small part of the Levoča Basin. In this zone, Rock-Eval-derived T_{max}, along with Rc and magnetic methods can be successfully applied.
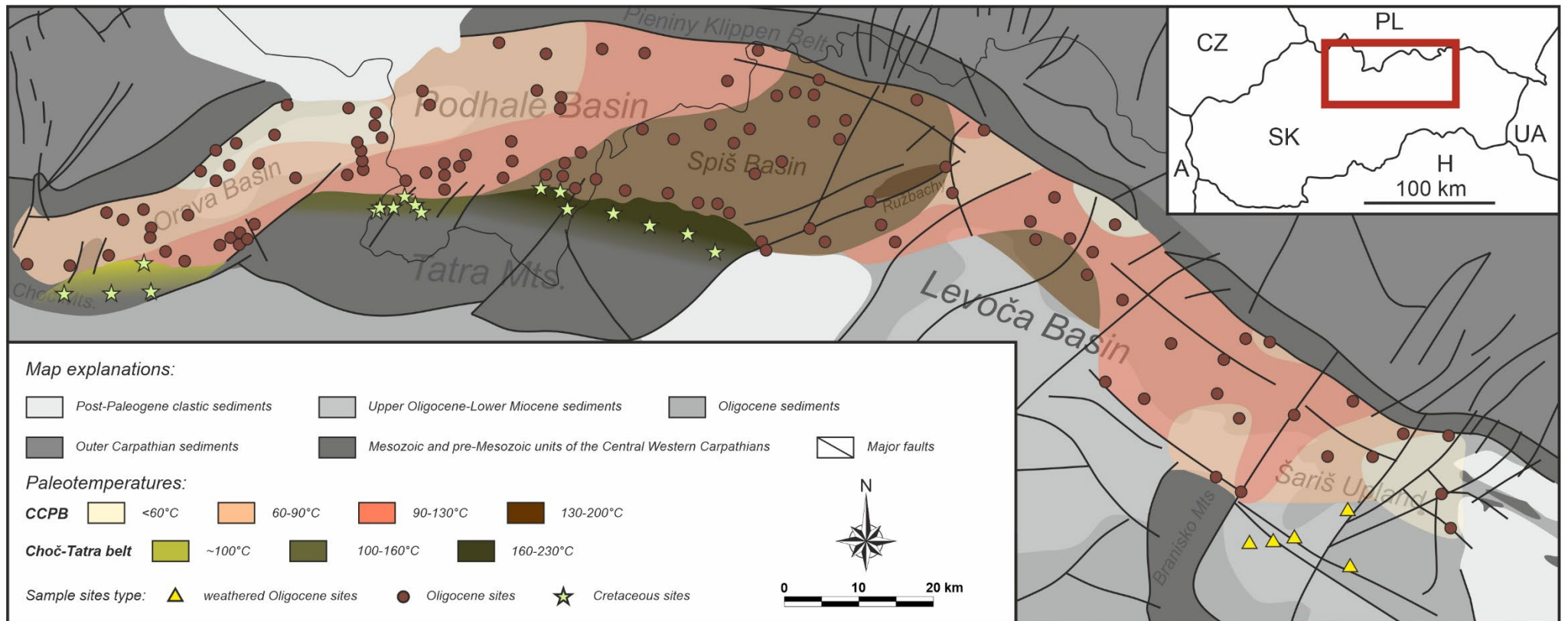
Fig. 5 Paleotemperature distribution in the CCPB and the Choč-Tatra Belt. Map modified after Gross et al. (1993a, 1999), Nemčok et al. (1993a).

The discussed pattern comprises the whole CCPB area but does not cover the Choč-Tatra Belt. Here, the expected paleotemperatures must have been at least the same as those recorded for the Huty Fm. However, they were likely higher due to the additional impact of the now eroded Borove Fm. and possibly also remnants of the Choč thrust nappe. Considering the thermal impact of the additional layers, the paleotemperatures in the Belianske Tatra Mts. could have reached even 230°C (Fig. 5). In the High Tatra Mts., the paleotemperatures dropped to ~160°C, and in the Western Tatra Mts. to over 110-120°C. The paleotemperatures for the Choč Mts. are similar to the Western Tatra Mts. (Fig. 5). However, there, the paleotemperatures originated not only from the sedimentary and tectonic load but also from the localized hydrothermal activity.

vi. Strengths and risks of different maturity parameters in reconstructing thermal maturity based on the CCPB and Tatra Mts. as an example

Organic compounds offer various parameters that can be applied as maturity indicators and can estimate the paleotemperature spectrum in the studied units. However, each investigated basin has its own unique features that must be taken into consideration before choosing the suitable indices. For example, light organic compounds, such as alkylnaphtalenes, and ratios like CPI or Pr/C_{17} and Ph/C_{18}, are susceptible to oxidation, biodegradation, and water washing (Elie et al., 2000; Palmer, 1993); processes that are commonly affecting surface samples. In this study, some sites most likely affected by a paleoweathering pulse in the southern Šariš Upland were sampled. Therefore, all parameters calculated for these sites must be treated cautiously. Another important factor is the different stability of organic compounds. Ratios based on steranes, hopanes, gymnosperm-derived compounds (dehydroabietane, simonellite, retene), and perylene can be applied only to regions where the Rc is lower than 1.2% (George, 1992; Marynowski et al., 2015; Peters et al., 2005; Radke, 1987). Moreover, when examining the maturity maps based on different compounds, it can be noticed, that the assumed maturity zones do not always overlap, which is especially prominent in the least mature areas.

Generally, ratios based on PAHs show higher stability. It is especially valid for the phenylphenanthrene ratio, which was successfully applied even in the highly altered rocks from the Tatra Mts. The most reliable maturity indicator in the case of the CCPB rocks is the MPI1 (and the calculated Rc) based on the distribution of phenanthrene and its methyl derivatives. However, phenanthrene is susceptible to water washing (Palmer, 1993), which must be taken

into consideration when analyzing the surface samples. In overmature rocks (bottom of Bukowina Tatrzańska PIG-1/GN well, Tatra-Ružbachy junction), the Rc ratio starts to decrease due to enhanced phenanthrene (Radke, 1987); and different ratios for calculating paleotemperatures must be used. Conversely, the Rc parameter gives erroneous results below the 0.5 % Rr value (Radke, 1987). Therefore, even the parameters that cover all the maturity ranges must be supplemented by other indicators. In highly altered rocks, aromatic sulfur compounds can be applied, however, they are not typical for terrigenous organic matter reflected in the type III kerogen (Chakhmakhchev et al., 1997; Radke and Willsch, 1994). In the CCPB rocks, thermally stable diamondoids (Chen et al., 1996; Zheng et al., 2023) were very sporadically detected. A careful approach must be adopted when investigating the least mature regions. Applying only the Rc parameter would suggest temperatures over 80°C in the northern Orava Basin. The presence of unstable compounds (oleanenes, lupenes, and $C_{30}\beta\beta$ hopanes) points toward much lower temperatures.

In areas where it is possible, a correlation between surface samples and well samples is a very powerful tool for assessing additional processes that could affect surface samples. Correlations of parameters for surface and well samples, and documenting one common trend of changes need to be considered. Moreover, the gradual changes of parameters with depth in wells are the most important factor for the reliable use of a particular ratio. However, even in the relatively unweathered well samples, there is a possibility of other processes (e.g., the influence of hydrothermal fluids; Bechtel et al., 2001) that may affect the overall maturity trend.

The presumably most common method of thermal maturity estimation is the vitrinite reflectance (Hunt, 1995; Maehlmann and Le Bayon, 2016). However, there are some risks when this method is used without other complementing parameters, and a thorough petrographic investigation. In the CCPB, this risk is related to the presence of dark vitrinites, that surpresses the vitrinite reflectance values. In some samples, especially in the Mraznica Fm., but also in some CCPB samples, the vitrinite grains are small and scattered, which may also lead to underestimated results.

Another common method is the Rock-Eval pyrolysis. While it is generally used to investigate the hydrocarbon potential of rocks, it gives valuable information on the thermal changes in the sedimentary rocks. Some parameters when plotted on a diagram (Hydrogen Index vs. T_{max}; Espitaliè et al., 1985) can potentially indicate the vitrinite reflectance of the analyzed samples. However, for a reliable result, the samples must contain higher levels of TOC. Therefore, this method could not be applied to Mraznica Fm. rocks. An additional strength of this method is recognizing the kerogen type, which helps in choosing suitable

biomarker ratios. Moreover, it can used even if the suspected thermal maturity is high. Still, it may be difficult to estimate the paleotemperatures based only on this method.

Magnetic maturity indicators are developed and applied in many geological settings. The studies most commonly include remagnetized metamorphic rocks (e.g., McClelland Brown, 1981; Schill et al., 2002), but also focus on sedimentary rocks (Aubourg and Pozzi, 2010; Aubourg et al., 2021). The more elaborate methods, the so-called geothermometers, based on the occurrence of different ferromagnetic minerals can estimate the general maximum burial temperature or the metamorphism-related temperature (Aubourg et al., 2021; Schill et al., 2002). However, the majority of studies that dealt with sedimentary rocks were conducted on samples from wells, and not surface samples (see e.g., Aubourg and Pozzi, 2010; Aubourg et al., 2021; Blaise et al., 2014; Tao Yang et al., 2016); therefore the potential weathering of the samples was not taken into consideration. Simple rock magnetic measurements that trace the temperature impact on rocks are applied in more specific settings, such as dykes crossing sedimentary sequences (e.g., Katz et al., 1998). In the case of the Mraznica and Huty Fms. in the Choč-Tatra Belt, a simplified approach (magnetic susceptibility measurements, hysteresis plots, etc.) combined with other non-magnetic methods enabled tracking the maturity changes. However, paleotemperature estimation using magnetic methods needs further research and appears to be a complementary rather than a primary method.

c. Magnetic mineralogy (Staneczek et al., 2024b; Staneczek et al., under review)
i. Mraznica Fm.

The rock magnetic experiments document the general eastward trend of changes in the magnetic mineralogy of the Mraznica Fm. from the Tatra Mts. (with the exception of the Choč Mts.). In the Western and High Tatra Mts., low values of both Kip and Kop along with low ferro/para ratio and hyperbolic decrease of the temperature-dependent in-phase magnetic susceptibility (Figs. 2 and 3 in Staneczek et al., 2024b) suggest that the main magnetic carrier that controls the Kip are paramagnetic minerals (Tab. 2). Considering the lithology of the Mraznica Fm. the minerals in question are phyllosilicates (Grabowski et al., 2013; Lefeld, 1974). The Kop values are slightly higher in the High Tatra specimens and the Kfd parameter equals ~2.5%, which indicates a possible admixture of ferromagnetic (*sensu lato*) minerals (Tab. 2 in Staneczek et al., 2024b). In the Choč Mts., only the magnetic susceptibility was investigated, and similarly to the Mraznica Fm. from the High Tatra Mts. the rather low Kip

and relatively high Kop together with high Kfd values point towards a para-ferromagnetic mixture. More complex is the magnetic mineralogy of the Mraznica Fm. in the Belianske Tatra Mts. Both Kip and Kop show a very broad range of values (Fig. 12 in Staneczek et al., under review). Very low, and even negative Kip along with the diamagnetic shape of the hysteresis curves suggest the presence of diamagnetic minerals, mainly in the BM1 site (Fig. S5 in Staneczek et al., under review). This is also in line with the high carbonate content calculated for this site (97%; Tab. S1 in Staneczek et al., under review). Other specimens show Kip values similar to or much higher than those reported for Western and High Tatra Mts., and Choč Mts.; and the measured Kop is usually significantly higher. Lower carbonate in some Belianske Tatra Mts. sites (e.g., BM2; Tab. S1 in Staneczek et al., under review) content reflects an increase in the clastic supply to the sedimentary basin and the prevalence of paramagnetic phyllosilicates over diamagnetic carbonates. This is additionally confirmed by the hyperbolic decrease of the temperature-dependent in-phase magnetic susceptibility experiment (Fig. S2 in Staneczek et al., under review). However, changes in phyllosilicate content have little effect on Kip and there is no clear correlation with the ferro/para ratio (Tab. S3 in Staneczek et al., under review). In addition, all analyzed sites in the Belianske Tatra Mts. show very high values of the Kfd parameter (~10-15%; Fig. 5 in Staneczek et al., under review) suggesting the presence of ultrafine-grained ferromagnetic mineral (Dearing et al., 1996). Based on these observations the Kip in the Mraznica Fm. in the Belianske Tatra Mts. is mainly governed by ferromagnetic minerals.

Magnetic remanence-based experiments recorded the main ferromagnetic carriers in the Mraznica Fm. (Fig. 6, Tab. 2). The most frequent type, as referred from the acquisition of the Isothermal Remanent Magnetization (IRM) and thermal demagnetization, as well as the hysteresis curves, are low-coercivity minerals (Fig. 2, Tab. 3 and 4 in Staneczek et al., 2024b; Figs. 6, 7, S5, Tab. S2 and S3 in Staneczek et al., under review). In the thermal demagnetization of a three-axis IRM, the maximum unblocking temperature for the low-coercivity curve equaled ~580°C which is the Curie temperature for magnetite (e.g., King and Williams, 2000).

The IRM component analysis revealed that the dominant type of magnetite grains, present in all analyzed Mraznica Fm. specimens has higher coercivities (55-95 mT; Fig. 6; Tab. 4 in Staneczek et al., 2024b; Tab. S2 in Staneczek et al., under review). Since higher coercivities in the magnetite coercivity range correspond with smaller domain sizes (Heider et al., 1996), the grains in question represent most likely stable single-domain (SSD) magnetite (Tab. 2). Its origin is linked with the illite-smectite transformation during the early stages of diagenesis,

where magnetite is formed as a by-product (Hirt et al., 1993). It could also partly form during the thrusting-related burial of the Mraznica Fm.
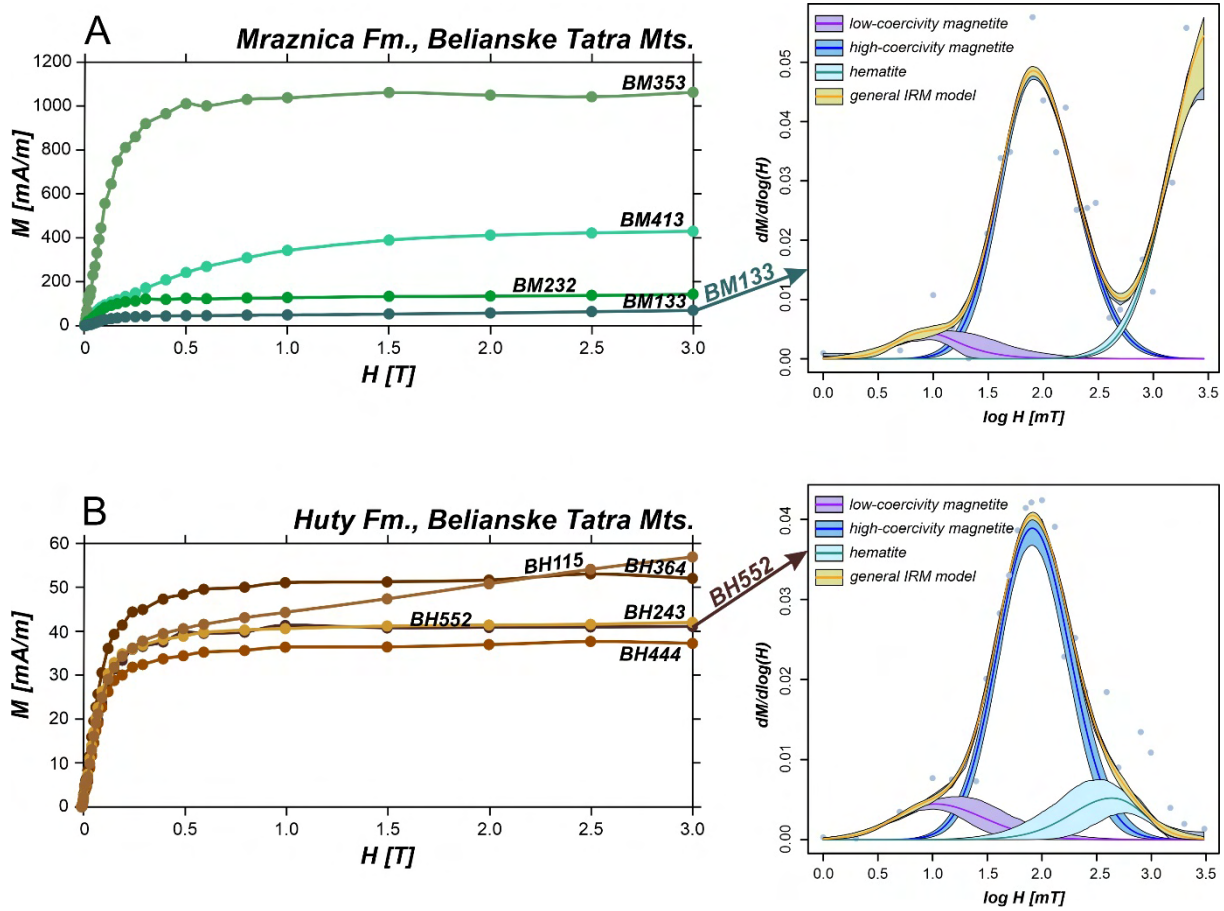
Fig. 6 Acquisition curves of the Isothermal Remanent Magnetization and the IRM component analysis for the Mraznica and Huty Fm. specimens (examples from the Belianske Tatra Mts.). Abbreviations: M – magnetization, H – applied direct field.

A second type of magnetite phase documented in all sites is characterized by very low coercivity (8-16 mT; Fig. 6; Tab. 4 in Staneczek et al., 2024b; Tab. S2 in Staneczek et al., under review) which corresponds with the PSD (pseudo single-domain) or MD (multi-domain) domain size (e.g., Hartstra, 1982). Larger grains could be allochthonous or diagenetic. When the sedimentary environment is oxygen-rich, then detrital iron oxides can be preserved (Canfield et al., 1992; Roberts, 2015), and Kędzierski and Uchmann (1997) reported such depositional conditions for the Mraznica Fm. However, petrographic observations revealed the presence of large quantities of pyrite framboids (Fig. S1 in Staneczek et al., under review), which points towards more oxygen-depleted conditions prohibiting the preservation of iron oxides during sedimentation and early diagenesis (Canfield et al., 1992; Roberts, 2015). Hence, the diagenetic origin of magnetite seems more likely. Presumably, the primary population of SD magnetite could be affected by the continuously elevating paleotemperatures and final

stages of diagenesis during the Oligocene-Miocene burial (Środoń et al., 2006), and thus grow to larger domain sizes. Moreover, PSD-MD magnetite could originate as a result of phyllosilicate transformations which was documented by experimental studies performed by Moreau et al. (2005). The tectonic evolution of the Tatra Mts. suggests the formation of the PSD-MD magnetite population during two stages of diagenesis linked with thrusting and Oligocene-Miocene burial.

Tab. 2 Magnetic mineralogy of the Huty and Mraznica Fms.

No.	Type	Minerals	Origin	Mraznica Fm.	Huty Fm.
1	Diamagnetic	carbonates	sedimentary	Cretaceous	-
2	Paramagnetic	phyllosilicates	sedimentary	Cretaceous	Oligocene
3	Superparamagnetic	magnetite and/or hematite	diagenetic, burial-related, fluid circulation product (Choč Mts.)	Late Cretaceous (Choč Mts.), Oligocene-early Miocene	Oligocene-early Miocene
4	Ferromagnetic, low coercivity	PSD-MD magnetite	burial-related	Oligocene-early Miocene	Oligocene-early Miocene
5	Ferromagnetic, medium coercivity	SSD magnetite	early diagenetic, burial-related	Late Cretaceous, Oligocene-early Miocene	Oligocene, Oligocene-early Miocene
6	Ferromagnetic, high coercivity	hematite	late burial-related (Mraznica Fm.), weathering (Huty Fm.)	Oligocene-early Miocene	undefined
7	Ferromagnetic, high coercivity	goethite	weathering	Late Cretaceous-present	Oligocene-present

Ultrafine-grained iron oxides (superparamagnetic magnetite, possibly alongside superparamagnetic hematite; abbreviation: SP) are detected in the Mraznica Fm. samples from the Belianske and High Tatra Mts. (Tab. 2), and from the Choč Mts. (Fig. 4; Tab. 2 in Staneczek et al., 2024b; Fig. 5 in Staneczek et al., under review). In the Tatra Mts., the Kfd parameter indicates an eastward increase of the SP content in line with the documented thermal maturity increase indicating a burial-related origin typical for this phase (Aubourg and Pozzi, 2010; Kars et al., 2012). It has been documented that during a constant paleotemperature increase to 140°C, the formation of new SP magnetite is faster than the size increase of the older grain population (Aubourg and Pozzi, 2010; Kars et al., 2012). This feature was not investigated in higher temperatures, such as those reported in the Belianske Tatra Mts. However, the high amount of SP iron oxides in the Mraznica Fm. from the Belianske Tatra Mts. in comparison to the High Tatra Mts. (~15% to ~2.5%, respectively) suggests a prolonged and intensified phase of

formation of these iron oxides. In the Choč Mts., the presence of SP particles is most likely linked with the circulation of thermal fluids which was reported by Bella and Gaal (2017) in that area. The Mraznica Fm. in the Belianske Tatra Mts. resembles features typical for remagnetized limestones (wasp-waisted hysteresis curve along with high Kfd values highlighting the presence of SP magnetite; Figs. 5 and S5 in Staneczek at al., under review) as documented by many authors in other geological settings (Channel and McCabe, 1994; Dinarès-Turell and Garcia-Senz, 2000; Jackson and Swanson-Hysell, 2012; Suk et al., 1993). Similar remagnetized Cretaceous rocks belonging to the Krížna nappe were reported by Grabowski et al. (2009) in the nearby Stražov Mts. in central Slovakia.

The last ferromagnetic mineral is hematite (Fig. 6). Its presence is documented by magnetization drops at ~680°C in the thermal demagnetization of a three-axis IRM (Petersen and Bleil, 1982; Figs. 6 and S4 in Staneczek et al., under review), in the IRM acquisition curves and the derived component analysis. In the majority of analyzed samples, the content of the high coercivity fraction is very low, which suggests a weathering-related origin. However, in some samples, the hematite contribution is significant (e.g., Fig. S3 in Staneczek et al., under review). Since the impact of thermal fluids on the Tatra Mts. is rather limited, the origin of hematite in Mraznica Fm. rocks is diagenetic, and most probbaly linked with elevated temperatures during Oligocene-Miocene burial maximum.

ii. Huty Fm.

The magnetic mineralogy of the Huty Fm. records the thermal impact of the Oligocene-Miocene burial maximum. In the Choč-Tatra Belt, except for the Belianske Tatra Mts., the Kip is low and shows similar values. The Kop is very low or reaches 0, as in the Choč Mts (Text S1 in Staneczek et al., under review). In the Belianske Tatra Mts., the Kip and Kop values are significantly higher (Fig. 12 in Staneczek et al., under review). The Kfd values are non-zero only in the Belianske Tatra Mts. and Choč Mts. and average 2-3% (Fig. 5 in Staneczek et al., under review). Moreover, all hysteresis curves have a distinct paramagnetic-related shape and a hyperbolic decrease of in-phase susceptibility during heating (Fig. 2 in Staneczek et al., 2024b). Since the sampled Huty Fm. rocks are mainly shales and siltstones (Appendix 1; for a detailed Huty Fm. description see Gross et al., 1993b), hence the minerals controlling the Kip are paramagnetic phyllosilicates. In the Belianske Tatra Mts. and Choč Mts., an admixture of iron oxides (magnetite) is presumed. The Kop, where measured, is governed by ferromagnetic iron oxides, which will be discussed in the next paragraphs.

Magnetite is the predominant ferromagnetic (*sensu lato*) mineral in the Huty Fm. samples (Tab. 2, Fig. 6). Characteristic unblocking temperatures coinciding with the Curie temperature of magnetite (~580°C; Fig. 2 in Staneczek et al., 2024b; Figs. 6 and S4 in Staneczek et al., under review) in thermomagnetic experiments are the most important evidence of its presence in the samples. Hysteresis shape and hysteresis-derived parameters also suggest the occurrence of this mineral. Moreover, the IRM acquisition and the component analysis distinguish two main magnetite particle sizes: SSD and PSD-MD (Fig. 6). The first component, characterized by relatively high coercivity (70-90 mT; Tab. 4 in Staneczek et al., 2024b; Tab. S2 in Staneczek et al., under review), originated as the product of the illite-smectite transformation during diagenesis (similarly as in the Mraznica Fm.) in the Oligocene, and during the increasing burial up to Miocene. This process could be accelerated via increasing temperatures and/or the impact of organic acids (Brothers at el., 1996). During the continuous burial with elevated temperatures, the first authigenic population of SSD magnetite grew to larger domain sizes (PSD-MD) with lower coercivities (8-21 mT; Fig. 6; Tab. 4 in Staneczek et al., 2024b, Tab. S2 in Staneczek et al., under review). The detrital origin of the larger magnetite phases is highly improbable since they cannot be preserved in dysoxic to euxinic depositional conditions (Canfield et al., 1992; Roberts, 2015) reported for the Huty Fm. In the Belianske Tatra Mts. ultrafine-grained iron oxides of the superparamagnetic fraction are, similarly to the Mraznica Fm., also burial-related. Only in this part of the Tatra Mts., the paleotemperatures were sufficient to generate SP particles. In the Choč Mts., the formation of SP magnetite was most likely facilitated by hydrothermal alterations.

In the majority of analyzed Huty Fm. sites, the content of high coercivity minerals is low (Fig. 6). The coercivity values are generally higher than 250-300 mT (Tab. 4 in Staneczek et al., 2024b, Tab. S2 in Staneczek et al., under review), and the unblocking temperatures on IRM demagnetization diagrams reach 680°C. Both are features typical for hematite (Özdemir and Dunlop, 2014; Petersen and Bleil, 1982). This mineral was documented in all samples. Its origin may be linked to the oxidation of pyrite grains by fluids (Hu et al., 2006). However, since all samples were taken from surface outcrops, it is probable, that the majority of hematite originated as a result of weathering. In contrast to the Mraznica Fm. rocks, it seems that burial did not influence the hematite formation, since hematite does not prevail in any sample.

Lastly, weathering-related goethite was identified in some samples from Huty and/or Mraznica Fms. However, its amount is low and its impact on the magnetic properties is negligible.

d. Anisotropy of in-phase magnetic susceptibility fabrics in the Cretaceous and Paleogene rocks (Staneczek et al., 2024b; Staneczek et al., under review)

Magnetic fabric analysis is a commonly used tool in entangling the tectonic evolution of mountain belts (see e.g., Aubourg et al., 2004; Dudzisz et al., 2016, 2018; Hrouda and Hanák, 1990; Staneczek et al., 2022; Szaniawski et al., 2012, 2017, 2020). Investigating the preferred orientation of minerals sheds light not only on the strain affecting the rocks but also on other processes (diagenesis, burial) during the evolution of the studied mountain belt. In the Carpathians magnetic fabric studies have been performed since the 1980s, and were usually combined with paleomagnetic studies (Grabowski et al., 2009; Gregorová et al., 2009; Hrouda, 1983, 1986; Hrouda and Hanák, 1990; Hrouda and Kahan, 1991; Hrouda and Potfaj, 1993; Hrouda et al., 2009; Madzin et al., 2021; Staneczek et al., 2022, 2024b; Szaniawski et al., 2012, 2017, 2020). However, the development of new techniques in recent decades, especially distinguishing between fabrics controlled by different minerals (so-called subfabrics), offers a new field for in-depth research.

The anisotropy of in-phase magnetic susceptibility (ipAMS) of the Mraznica Fm. in the Western and High Tatra Mts. is, like their ipMS, controlled by the orientation of phyllosilicates. In contrast, the ipAMS of the Belianske Tatra Mts. sites is governed by the orientation of magnetite and hematite. The fabrics in the Western and High Tatra Mts. are mostly planar (T > 0.7) with low corrected anisotropy degrees (Pj < 1.10; Fig. 3 in Staneczek et al., 2024b). In the Belianske Tatra Mts., the T and Pj values are scattered, with Pj values documenting prolate ellipsoids for some sites (Fig. 9 in Staneczek et al., under review). The most commonly occurring fabric is characterized by ENE-WSW to NE-SW oriented magnetic lineation, and with magnetic foliation parallel to the bedding plane (Fig. 7; Fig. 4 in Staneczek et al., 2024b; Fig. 9 in Staneczek et al., under review). Such well-defined magnetic foliation results from compaction and diagenesis (Parés, 2015; Parés et al., 1999), while the magnetic lineation is interpreted to be of tectonic origin. ENE-WSW-oriented magnetic lineations are documented frequently in the Mesozoic of the CWC (Grabowski, 1996; Gregorová et al., 2009; Hrouda and Kahan, 1991; Szaniawski et al., 2020; Staneczek et al., 2022) and correspond well with the assumed NNW orientation of the nappe thrusting during the Turonian reported by many authors (e.g., Jurewicz, 2005; Kováč and Bendík, 2002; Plašienka, 2003; Prokešová, 1994; Prokešová et al., 2012). Therefore, the origin of the ipAMS lineation in the Mraznica Fm. is linked to the stress field during the nappe transport. In Belianske Tatra Mts. ENE-WSW to E-W magnetic lineations are accompanied by a girdle of magnetic foliation poles (Fig. 7; Figs. 9 and S6 in

Staneczek et al., under review). Such a pattern is observed in highly deformed nappes indicating a combination of simple shear and lateral shortening during thrusting (Lamarche and Rochette, 1987; Hrouda and Kahan, 1991). Therefore, the magnetic fabrics support the hypothesis that the Belianske Tatra Mts. have been subjected to intense deformation during the Late Cretaceous (e.g., Hrouda and Kahan, 1991). In two Mraznica Fm. sites, a northerly magnetic lineation is present (Fig. 9 in Staneczek et al., under review). This lineation presumably originated from thrusting-related simple shear deformation resulting from the presence of a thick limestone layer (Muraň Fm) overlying the less competent Mraznica marls and marly limestones (Nemčok et al., 1993ab). Similar magnetic lineations were documented in the Strážov Mts. (Szaniawski et al., 2020). In turn, two Mraznica Fm. sites in the High Tatra Mts. display a different pattern, characterized by scattered magnetic lineation poles perpendicular to the bedding plane, and bedding parallel magnetic foliation (Fig. 9 in Staneczek et al., under review). The most probable cause of such fabric is the prevalence of compaction with no or a minor impact of thrusting-related compression.

The ipAMS in the Huty Fm. rocks in the Tatra Mts. is governed by the orientation of phyllosilicates, with a minor admixture of magnetite in the Belianske Tatra Mts. The Huty Fm. sites recorded one main type of magnetic fabric characterized by oblate ellipsoid shapes and slightly higher corrected anisotropy degrees (Pj reaches 1.15). The magnetic foliation is extremely well-defined and is bedding-parallel. The magnetic lineations are usually well-grouped and undulate from NE-SW orientation in the Western Tatra Mts. to WSW-ENE or E-W orientation in the High and Belianske Tatra Mts. (Fig. 8; Fig. 5 in Staneczek et al., 2024b; Fig. 10 in Staneczek et al., under review). Minor deflections from this trend are likely a result of differential uplift rate in the Tatra Mts. documented by structural studies (Nemčok et al., 1993b; Králiková et al., 2014a). The excellent alignment of the magnetic foliation and bedding results from a combination of compaction during diagenesis and the inherently oblate shape of phyllosilicate grains.

Unit	Age	Process	Fabric type	Fabric example	Sites
Mraznica Fm.	Late Oligocene-Miocene	crystallization of magnetic minerals on a fixed phylosilicate matrix	opAMS, AARM		BM1, BM2, BM3, BM4
		crystallization on a fixed phyllosilicate matrix during burial; minor impact of transpression	opAMS, AARM		Mz8, Mz9, Mz10, Mz11, Mz12
		transpression; burial-related formation of ferromagnetic minerals	opAMS, AARM		MK1, MK2, MK3
	Oligocene	NW-SE to N-S extension during the CCPB formation	opAMS, AARM		Mz7
	Late Cretaceous	simple shear during thrusting	ipAMS		BM1, BM4
		NNW-SSE to NW-SE compression and formation of ferromagnetic minerals linked with nappe thrusting	ipAMS		Mz8, Mz9, Mz10, Mz11, Mz12, MK2, BM2, BM3

Fig. 7 Generalized magnetic fabrics documented in the Mraznica Fm.

The repeatability of the ipAMS lineation and the good grouping suggest a tectonic origin of this fabric element. The ipAMS lineation orientation corresponds with NW-SE to N-S oriented shortening in the Oligocene-Early Miocene documented by structural studies in this area (Králiková et al., 2014a; Pešková et al., 2009; Sůkalová et al., 2012; Vojtko et al., 2010). In the High and Belianske Tatra Mts., the more E-W oriented ipAMS lineation (Fig. 5 in Staneczek et al., 2024b; Fig. 10 in Staneczek et al., under review) could potentially also record the approximately N-S compression during the northward tilting of the Tatra block in the Middle Miocene (Králiková et al., 2014a; Pešková et al., 2009). Since the uplift was larger in

the eastern part of the Tatra block (Śmigielski et al., 2016), the uplift-related compression must have also a stronger impact on the Paleogene rocks. The origin of magnetic lineations in the CCPB rocks is often debated. Madzin et al. (2021) and Márton et al. (2009) interpreted the ipAMS lineation in the Huty Fm. from the Podhale-Spiš regions as a result of paleoflows in the basin. However, such paleocurrents change the depositional environments to aerobic and often lead to the deposition of more sandy facies. Under oxygen-depleted (dysoxic to intermittently euxinic) conditions documented by Staneczek et al. (2024a), paleocurrent cannot occur. Therefore, the ipAMS lineation in the Huty Fm. is of tectonic origin and is linked with the uplift of the Tatra block.

e. Anisotropy of out-phase magnetic susceptibility and anisotropy of anhysteretic remanent magnetization fabrics in the Cretaceous and Paleogene rocks (Staneczek et al., 2024b; Staneczek et al., under review)

The anisotropy of out-of-phase magnetic susceptibility (opAMS) and anisotropy of anhysteretic remanent magnetization (AARM) fabrics are coaxial in the majority of sites, which suggests a common origin. In the Western Tatra Mts. and the Belianske Tatra Mts., the opAMS and AARM foliations of the Mraznica Fm. are parallel or sub-parallel to the bedding plane. The opAMS fabric elements are poorer defined than the AARM. The Pj parameter values are comparable for both investigated fabrics. In contrast, the ellipsoid shapes vary from triaxial to oblate. The opAMS and AARM lineations mirror the ipAMS lineation orientation and, in the case of Western Tatra Mts., are slightly tilted toward a subhorizontal position (Fig. 4 in Staneczek et al., 2024b; Fig. 9 in Staneczek et al., under review). Considering that the carriers of opAMS and AARM in the Mraznica Fm. are predominantly authigenic magnetite populations, the origin of these fabrics must be linked with events of accelerated magnetite formation. The formation of the primary magnetite population in the Late Cretaceous was controlled by the phyllosilicate matrix. The Oligocene-Miocene burial of the nappe rocks and the continuous illite-smectite transformation in elevated temperatures resulted in the formation of a new magnetite population that similarly to the primary one, was formed on the phyllosilicate matrix, strengthening the Late Cretaceous ferromagnetic fabric.

Unit	Age	Process	Fabric type	Fabric example	Sites
Huty Fm.	Early Miocene	crystallization on a fixed phyllosilicate matrix	opAMS, AARM		Ht5, Ht7, Ht14, Ht15, Za3, Za5, BH1, BH3
		compression during uplift	ipAMS		Za1-Za5, Ht5, Ht10, Ht12, Ht14, Ht15, BH1-BH5
	Oligocene	compaction	opAMS		Ht10, Ht12
		NW-SE to N-S extension during the CCPB formation	AARM		Za2, Za3, Za4, Za5, Ht10, Ht11, Ht12, Ht14, Ht15, BH4, BH2

Fig. 8 Generalized magnetic fabrics documented in the Huty Fm.

In the High Tatra Mts., the AARM and opAMS fabrics display vertical or sub-vertical magnetic lineations almost parallel to the pole to bedding, and scattered sub-horizontal magnetic foliation (Fig. 7; Fig. 4 in Staneczek et al., 2024b) with triaxial to oblate ellipsoid shapes and changing Pj values (~1.030-1.110). Interestingly, vertical magnetic lineations are present in sites with both normal-lying and overturned beds and are bedding-independent, suggesting a tectonic origin younger than the nappe emplacement. Similar vertical to sub-vertical ferromagnetic-driven lineations were documented in the nearby Choč Mts. where their origin has been interpreted as transpressional (Staneczek et al., 2022). Sampling sites in the High Tatra Mts. and in the Choč Mts. are located close to large fault zones. In the case of the Choč Mts., it is the continuation of the Sub-Tatric Fault, and in the High Tatra Mts. two parallel NE-SW large faults that cut the Tatra block (Fig. 2 in Staneczek et al., under review; Lexa et al., 2000). Both fault zones were active during the Oligocene-Early Miocene uplift of the Choč-Tatra Belt under a transpressional regime (Anczkiewicz et al., 2015; Fodor, 1995; Froitzheim

et al., 2008; Králiková et al., 2014a; Marko et al., 2005; Peresson and Decker, 1997; Ratschbacher et al., 1993; Sperner et al., 2002). Recent studies also suggest a strike-slip stepover triggered by a transpressional regime as the main process controlling the Miocene exhumation of the Tatra crystalline basement (Campos et al., 2023). Transpression is defined as the simultaneous occurrence of vertical stretching, with horizontal shear and shortening (Sanderson and Marchini, 1984). Such a tectonic regime was active during the maximum of the Oligocene burial and coincided with the episode of a fast magnetite (and hematite) formation. Newly crystallized grains were oriented along the vertical stretching which resulted in vertical or sub-vertical ferromagnetic lineations, a phenomenon reported by many authors (Bilardello, 2016; Housen and van der Pluijm, 1991; Housen et al., 1993ab; Parés, 2015; Weil and Yonkee, 2009). All sites in the Western and some in the Belianske Tatra Mts. are located in the middle of the western and eastern Tatra blocks. Hence, the impact of transpression was minor and resulted only in a small inclination of the AARM and opAMS lineations. In the Belianske Tatra Mts., compaction could prevail over transpression-related deformation due to the highest sedimentary load during the Oligocene-Miocene burial which favored the crystallization along bedding-parallel planar phyllosilicate matrixes.

The majority of the Huty Fm. sites in the Tatra Mts. show a coherent AARM fabric characterized by a well-defined NW-SE-oriented magnetic lineation and bedding-parallel magnetic foliation (Fig. 8; Fig. 5 in Staneczek et al., 2024b; Fig. 10 in Staneczek et al., under review), linked with the crystallization of ferromagnetic grains on a restricted phyllosilicate matrix. In the majority of the Huty Fm. sites the Pj values are relatively high (~1.2), and the AARM ellipsoids are mostly triaxial to oblate. Similarly oriented fabrics were documented in the Huty Fm. from the Choč Mts. (Staneczek et al., 2022) and in the Podhale Basin (Márton et al., 2009). The orientation of this fabric is coaxial with the Oligocene extension documented by structural studies in the Tatra Mts. (Králiková et al., 2014a), and in the Orava and Spiš Basins (Pešková et al., 2009; Vojtko et al., 2010). Such an extensional regime could also affect the basin basement rocks (the nappe units; see Fig. 4 in Staneczek et al., 2024b).

A second fabric in the Huty Fm. displays a NE-SW to ENE-WSW-oriented magnetic lineation present mainly in the opAMS but also in the AARM. It traces the ipAMS lineation orientation (Fig. 5 in Staneczek et al., 2024b; Fig. 10 in Staneczek et al., under review). In the Western Tatra Mts. this lineation orientation is recorded only by opAMS and ipAMS. In the High Tatra Mts. the opAMS and ipAMS lineations are rarely coaxial with the AARM lineation, but in the Belianske Tatra Mts, the overlapping of all three fabrics is frequent. The documented magnetic foliations are bedding-parallel. The AARM and opAMS ellipsoids range from triaxial

to oblate. The opAMS fabric is controlled mainly by ultrafine grains of magnetite fixed in the phyllosilicate matrix. The similar orientation of the ipAMS lineation, opAMS lineations, and some AARM lineations suggests a common origin related to the Early Miocene compression. Perpendicular orientations of AARM and opAMS lineations are likely the result of different magnetite states recording different tectonic events. The older, PSD-MD magnetite populations originated during the Oligocene extension, while the younger SP-SSD is linked with the Oligocene-Miocene maximum burial and uplift-related compression. This is further supported by the frequency of the coinciding opAMS and AARM fabrics. The extensional AARM fabrics could be overwritten by a new generation of magnetite that formed according to the new stress field during the Miocene uplift. This trend is documented in the highly thermally altered Belianske Tatra Mts., where the overlapping of opAMS, AARM, and ipAMS is frequent, in comparison to the less affected Western Tatra Mts.

Interestingly, there is no virtual effect of transpression on the magnetic fabrics of the Huty Fm. even in sites sampled close to fault zones. This phenomenon is presumably linked to the higher phyllosilicate content in the Huty Fm. shales and siltstones than the Mraznica Fm. marls and limestones. The planar phyllosilicate matrix in the Huty Fm. was "stronger" than in the Mraznica Fm. and, therefore, more resistant to vertical stretching, prohibiting the formation of vertical lineations. Similar conclusions were drawn by Staneczek et al. (2022) for the Choč Mts.

f. Summary of the evolution of the CCPB and the Tatra Mts. from the Cretaceous to Neogene (Staneczek et al., 2024ab; Staneczek and Marynowski, 2025; Staneczek et al., under review)

The earliest stage of evolution documented in this work is related to the magnetic mineralogy of the Mraznica Fm., part of the Krížna nappe (the Fatric unit; Fig. 9; Prokešová et al., 2012). The sedimentation occurred during the Lower Cretaceous in two types of basins: a deep marine setting (Zliechov succession in the Western Tatra Mts.; Nemčok et al., 1993ab) and a shallow marine setting (Vysoka succession in the High and Belianske Tatra Mts.; Nemčok et al., 1993ab). The presence of pyrite framboids and laminations suggests an oxygen-depleted sedimentary environment in the part of the Mraznica Fm., which prohibited the preservation of allochthonous magnetite grains. Compaction and diagenesis resulted in the formation of a planar phyllosilicate matrix and, thus, a bedding parallel ipAMS foliation (Fig. 9). In the Turonian, the collision of the North European Platform with Adria- and Europe-derived units

occurred (Castelluccio et al., 2016; Csontos and Vörös, 2004; Kováč et al., 2018; Plašienka, 2018; Plašienka et al., 1997) and the Fatric-Hronic nappe system was thrust in the NNW-NW direction onto the para-autochthonous units of the Central Western Carpathians (Jurewicz, 2005; Kováč and Bendík, 2002; Plašienka, 2003; Prokešová, 1994; Prokešová et al., 2012). The nappe transport affected the magnetic fabric of the Mraznica Fm., resulting in the creation of NNE-SSW to NE-SW ipAMS lineations (Fig. 9). Furthermore, the tectonic overburden has led to increasing pressure and elevated paleotemperatures. During the Late Cretaceous burial of the Mraznica Fm. rocks, the formation of fine-grained magnetite, a by-product of the illite-smectite transformation (Katz et al., 1998, 2000; Hirt et al., 1993), has accelerated (Fig. 9). This primary authigenic ferromagnetic fabric was most likely closely mirroring the phyllosilicate-based ipAMS lineation. However, this pattern was overwritten during further thermal events. The extent of this burial and intensity in different Tatra parts was presumably very similar, with paleotemperatures reaching over 300°C for the crystalline basement (Králiková et al., 2014a).

After the thrusting event, the Tatra Mts. experienced a minor uplift and the exhumation of the crystalline basement, and the nappe sediments were partly eroded (Činčura 1990, 2002; Danišík et al. 2010; Kováč et al. 1994, 2016; Králiková et al. 2014b, 2016; Plašienka 1997; Vojtko et al. 2016). In the Late Eocene, the gravitational collapse of the CWC massifs resulted in a tectonic subsidence of this area (Wagreich, 1995; Castelluccio et al., 2016). The CCPB sedimentation progressed on a basement formed by the eroded nappe sediments with the deposition of basal transgressive lithofacies and shallow marine carbonates (Borove Fm.; Gross et al., 1984, 1993b; Soták et al., 2001). With time, the basin deepened, and the sedimentation of clastic rocks started. The depositional environment of the Oligocene Huty Fm. was characterized by an open marine setting indicated by the sterane distribution and additionally by the dominance of the planktonic kerogen type II, or a mixture of planktonic (with a large contribution of dinoflagellates) and terrestrial organic matter recognized as the kerogen type II/III (Staneczek et al., 2014a). The presence of isorenieratane and aryl isoprenoids points toward the occurrence of intermittent photic zone euxinia (Fig. 9). Bottom waters were generally oxygen-depleted and sporadically disrupted by oxic pulses. The terrestrial organic matter input was low, and the most common biomarkers are conifer-derived compounds. Deep marine basin facilitated the sedimentation of phyllosilicates which, during compaction, formed a very strong and resistant phyllosilicate matrix reflected in the extremely well-defined ipAMS foliation (Fig. 9). Continuous burial and elevated temperatures increased the intensity of the illite-smectite transformation (Fig. 9). The newly formed magnetite population grew along the

NW-SE extension axis, linked with the formation of the CCPB (Králiková et al., 2014a) and in the Orava and Spiš Basins (Pešková et al., 2009; Vojtko et al., 2010).

The transition to the Zuberec Fm. is marked by a transition to an estuarine setting. Gradual shallowing resulted in the formation of restricted subbasins with a common occurrence of photic zone euxinia. The lower Zuberec Fm. shows similar characteristics to the Huty Fm., mainly the moderate productivity, II and II/III kerogen type, and relatively low terrestrial organic matter input. The upper Zuberec Fm. and the Biely Potok Fm. were deposited in a shallow estuarine environment. Sedimentary conditions changed to predominantly oxic, as supported by the presence of large pyrite framboids. The change to the III kerogen type reflects the increased input of the terrestrial organic matter (Fig. 9). In the analyzed samples, high amounts of angiosperm-, gymnosperm- and funghi-derived biomarkers were found, while the algae significance decreased. Petrographic observations revealed the presence of fusinite in many of the samples, indicating the occurrence of wildfires during the Late Oligocene and Early Miocene (Fig. 9). This was further supported by the presence of various PAHs like benzo[*ghi*]fluoranthene, benz[*a*]anthracene, or benzo[*a*]pyrene. Wildfire temperatures were estimated based on the measured fusinite reflectance and ranged from 382°C to 734°C corresponding with surface and crown fires (Scott, 2000, 2010). Based on the distribution of dimethylphenanthrenes, the burned vegetation consisted mainly of hard- and softwood. In the upper Zuberec Fm. the PAHs show a mixed smoke-residue origin, which changes to only residue-related in the Biely Potok Fm. This feature reflects the increasing input of terrestrial organic matter during the Late Oligocene. Moreover, the frequency of wildfires could lead to soil degradation and erosion, resulting in intense terrestrial run-offs.
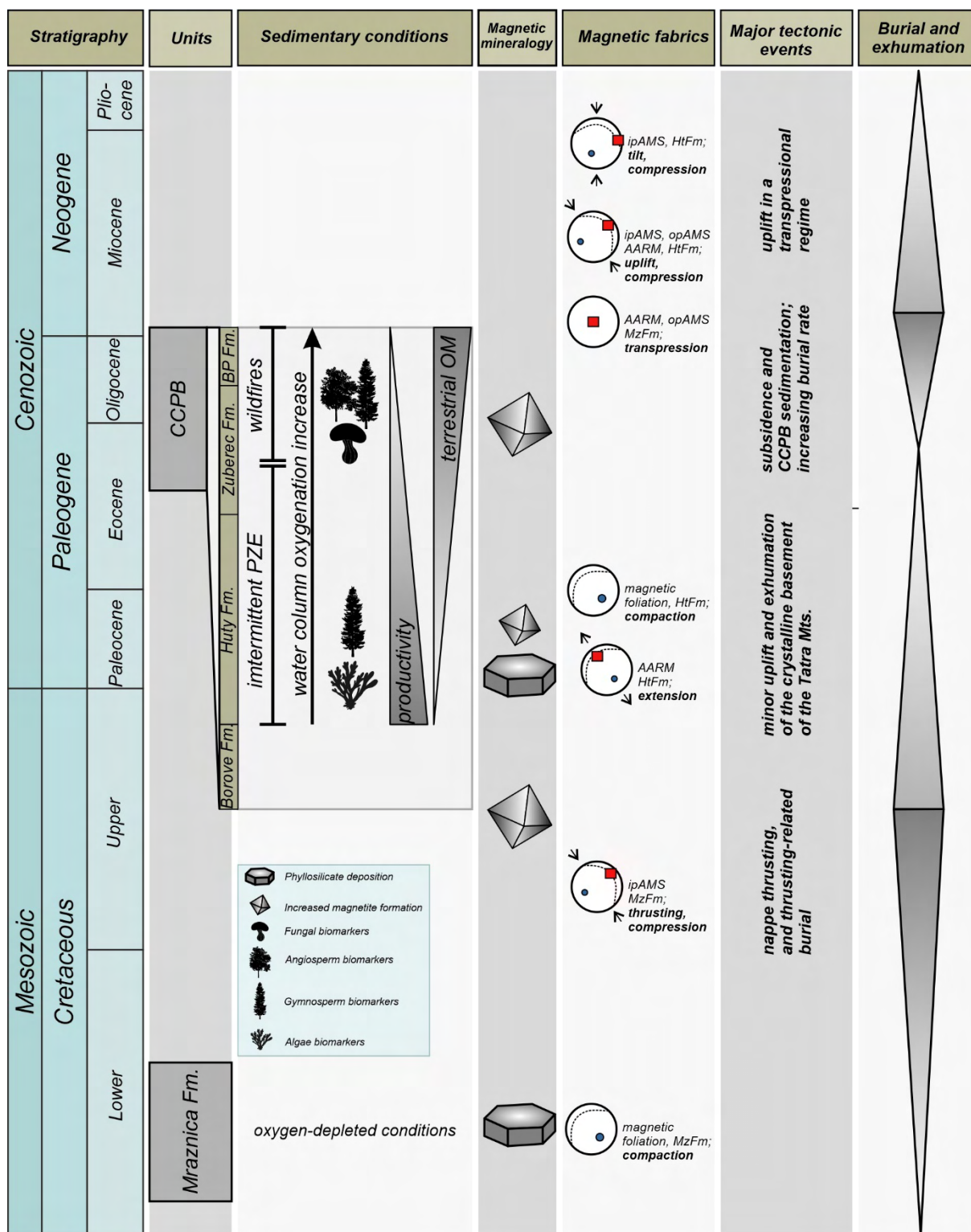
Fig. 9 Main processes documented by organic geochemistry methods, rock magnetism, and magnetic fabric analysis in the CCPB and the Tatra Mts. from the Late Mesozoic to Cenozoic period. Burial (wide part of each triangle) and exhumation were derived from Králiková et al. (2014a).

The burial maximum occurred with the sedimentation of the last CCPB member, the Biely Potok Fm., and coincided presumably with the onset of uplift in the Early Miocene (Králiková et al., 2014a; Vojtko et al., 2010). The thickness of the Paleogene sediments varied throughout the CCPB and the Tatra Mts. area. Biomarker-derived maturity ratios complemented by inorganic parameters suggest that the highest temperatures, and thus the highest sedimentary overload, affected the Belianske Tatra Mts. and the Spiš Basin. Based on the distribution of methyl phenanthrenes converted to the calculated vitrinite reflectance shows values ~3.0% Rc in the Tatra-Ružbachy junction. The measured vitrinite reflectance for the Mraznica Fm. samples is lower and reaches 1.70 % Rr. However, there are several factors that prohibit a reliable measurement of this parameter. The temperatures must have been higher than in the Huty Fm. and the impact of at least the Borove Fm. must be taken into consideration. We therefore assume that temperatures could have been up to 30°C higher. The reported paleotemperatures reach 200°C in the Spiš Basin and 230°C in the Mraznica Fm. in the Belianske Tatra Mts. This area was presumably affected by higher subsidence levels, which in turn caused a prolonged sedimentation. An eastward migration of depocenters toward the Belianske Tatra Mts. and Spiš region was documented by Kováč et al. (2016). Large active fault zones, namely the Ružbachy Fault and a parallel fault cutting the Tatra Mts., could also increase the subsidence rate. Śmigielski et al. (2016) reported their activity related to the fast uplift of the eastern part of the Tatra Mts. in comparison to the western parts. Moreover, these faults seem to bind the region affected by the highest paleotemperatures from the east and west, which further supports their impact on the sedimentation during the Paleogene. When crossing the Ružbachy Fault, the calculated vitrinite reflectance drops significantly from 1.60% to 0.66%. Similar abrupt changes of this parameter (1.42%-1.02%-0.87%) are documented in the High Tatra Mts. The highest recorded paleotemperatures in the CCPB occur along the Mraznica-Huty Fms. contact. The Paleogene outcrops form the lowermost parts of the CCPB and thus were affected by the highest sedimentary overburden. The paleotemperatures documented by biomarker parameters are generally in line with the results from illite crystalline studies (Środoń et al., 2006). However, there are some discrepancies documented mainly in the least mature regions. Środoń et al. (2006) suggest temperatures averaging 95-100°C in the Orava Basin, however, the biomarker proxies indicate much lower temperatures (~50°C). Differences in paleotemperatures estimated using biomarkers and illite/smectite transformation were reported also in other areas, e.g., Ediacaran sedimentary rocks in the East European Craton (Derkowski et al., 2021). The average paleogradient in the northern CCPB, as documented by Środoń et al. (2006) based on data from Poprawa and Marynowski (2005), averaged at 20-

25°C/km. Other authors suggest higher paleogradients, which in turn would result in a lower thickness of the CCPB sediments (Anczkiewicz et al., 2013). However, according to Środoń et al. (2006) the paleogradient was likely close to the current gradient (19-23°C/km; Cebulak et al., 2004). The approximate minimum thickness of CCPB sediments based on these paleogradient values reaches 5-7 km in the Spiš Basin. Moreover, the importance of the Ružbachy Fault is once again highlighted by the difference in the sedimentary overload, which averages 5 km on the northern site and drops to 2-3 km on the southern site. Such high thickness is theoretically possible due to the high estimated thickness of the Biely Potok Fm. which could reach even 3.5 km (Gross et al., 1993b). However, higher values of the paleogradient (Anczkiewicz et al., 2013), resulting in a lower thickness of sedimentary rocks, seem to be more realistic.

The documented paleotemperatures decrease slowly towards the west and southeast. The burial is recorded not only by the biomarker-derived parameters but also by magnetic proxies, especially in the Mraznica Fm. rocks. In the Belianske Tatra Mts., the quantity of iron oxides (magnetite and/or hematite) is significantly higher than in other parts of the Choč-Tatra Belt and is reflected by high ipMS and Kfd values, and characteristic wasp-waisted hysteresis shapes. The content of ferromagnetic minerals decreases slowly towards the Western Tatra Mts. where the Kfd values reach 0. The Choč Mts. were recognized as an area affected by an increased hydrothermal circulation which facilitated the precipitation of magnetite. A similar decreasing trend is documented by the magnetic mineralogy of the Huty Fm., but is less pronounced due to the lower paleotemperatures affecting this unit. The estimated paleotemperatures for the Mraznica Fm. drop from the maximum of 230°C in the Belianske Tatra Mts. to 160-100°C in the Western Tatra Mts. and finally ~100°C in the Choč Mts. In the CCPB, the thermal maturity decreases toward the Orava Basin and Šariš Upland. These least altered regions are characterized by the occurrence of unsaturated compounds, such as oleanenes. The maximum estimated thickness of the sediments in the Orava Basin did not exceed 2 km. The low maturity of these regions is marked additionally by the presence of perylene and simonellite. The hydrocarbon potential of the CCPB rocks is a complex issue. Taking into consideration the organic characteristics of the CCPB units and their thermal maturity, the majority of the studied rocks show rather poor source rock potential. However, some levels in the Huty and Zuberec Fms. display very good or even excellent source rock potential. Moreover, most analyzed samples are early mature or mature, which points to the possibility of hydrocarbon generation. Due to the prevalence of the type III- and II/II kerogen, the rocks are rather gas-prone than oil-prone.

Early Miocene is marked by the beginning of uplift and exhumation of the Tatra crystalline basement along the south-bounding Sub-Tatric Fault (e.g., Králiková et al., 2014a). The main driving force of this process was related to strike-slip stepover during the sinistral transpression (Anczkiewicz et al., 2015; Campos et al., 2023; Fodor, 1995; Froitzheim et al., 2008; Králiková et al., 2014a; Marko et al., 2005; Peresson and Decker, 1997; Ratschbacher et al., 1993; Sperner et al., 2002). The maximum burial and elevated paleotemperatures accelerated the formation of a new population of iron oxides, that were oriented according to the tectonic strain. Transpression-related deformation was documented by opAMS and AARM fabrics in the Mraznica Fm. (Fig. 9). Sites in the High Tatra Mts. located near large faults recorded vertical opAMS and AARM lineation. Similar fabrics were found in the Choč Mts., which form a long fault zone (Staneczek et al., 2022). Similarly, vertical magnetic lineations were commonly documented in other regions affected by transpression (Bilardello, 2016; Housen and van der Pluijm, 1991; Housen et al., 1993ab; Parés, 2015; Weil and Yonkee, 2009). The vertical stretching component of transpression facilitated the crystallization of magnetite and presumably hematite along the extension axis. In the Western Tatra Mts., the impact of transpression was minor due to the relatively large distance from active faults. There, the opAMS and AARM lineations are only slightly inclined. In contrast, in the Belianske Tatra Mts., the lack of transpression-related fabric features could result from the prevalence of compaction due to the large sedimentary load (5-7 km) during the maximum burial. Ferromagnetic minerals crystallized on the preferred planar phyllosilicate matrix, tracing the older ipAMS fabric. The uplift affected also the magnetic fabric of the Huty Fm. creating NE-SW to E-W ipAMS lineations (Fig. 9) perpendicular to the main NW-SE to N-S shortening direction (Králiková et al., 2014a; Pešková et al., 2009; Vojtko et al., 2010; Sůkalová et al., 2012). Some sites in the High and Belianske Tatra Mts. display E-W oriented ipAMS lineations which presumably recorded the Middle Miocene stage of uplift related to the northward tilting of the Tatra block (Králiková et al., 2014a). The exhumation of the Tatra crystalline basement occurred in the Middle to Late Miocene (Anczkiewicz et al. 2015; Burchart 1972; Král, 1977; Králiková et al., 2014a). During this period, the Ružbachy Fault changed from transpressional to normal faulting, with the southeastern side being the hanging wall (Králiková et al., 2014a). This would further explain the large and abrupt differences in paleotemperatures along this structure. The northeastern part would be eroded faster, leading to the exposure of lowermost, highly thermally altered units, whereas the southeastern side would be less affected by erosion. Finally, the latest Miocene to Pliocene uplift acceleration and increased erosion of the CCPB

sediments was followed by the Holocene postglacial denudation, which started to shape their current morphology (Králiková et al., 2014a).

Lastly, it is worth discussing which burial (Turonian or Oligocene-Miocene) affected the Tatra Mts. the most. This problem is the subject of a long-standing discussion. The majority of studies conducted in this area suggest that the Turonian burial was the most prominent (Anczkiewicz et al., 2015; Campos et al., 2023; Grabowski, 2000; Králiková et al., 2014a; Márton et al., 2016; Plašienka et al., 1997; Śmigielski et al., 2016; Środoń et al., 2006). It is important to note, that the majority of these studies focus on the crystalline basement. However, Anczkiewicz et al. (2015), Králiková et al. (2014a), and Śmigielski et al. (2016) suggest a second burial episode in the Oligocene. It is generally agreed upon that the maximum burial and the highest temperatures affected the crystalline basement of the Tatra Mts. in the Late Cretaceous. Still, the age of the most prominent burial of the allochthonous nappe sediments remains in question. Paleomagnetic studies of the Krížna nappe rocks suggest a Late Cretaceous remagnetization linked with thrusting (Grabowski, 1997; Márton et al., 2016). However, some data point toward younger, Paleogene-Neogene remagnetization ages (Grabowski, 1997). However, these studies focused on the Western Tatra Mts., which were less thermally affected than other parts of the massif, which resulted in a lower content of new magnetite formed during the Oligocene-Miocene burial and retaining the Late Cretaceous remagnetization ages. Nemčok et al. (1993b) estimated the thickness of the thrust nappes in the Tatra Mts. to be lower than 4km. If the current nappe sedimentary rocks in the Tatra Mts. represent the lower sections of thrust folds and the Choč nappe once covered the entire Tatra region, the eroded portion was insufficiently thick to generate temperatures reaching 200–230°C. Thermal maturity studies conducted in the Choč-Tatra Belt and the CCPB, document a coherent eastward increase of paleotemperatures detected in both Mraznica and Huty Fms. Moreover, this trend is further supported by maturity studies of Chochołów PIG-1 and Bukowina Tatrzańska PIG-1/GN wells (Poprawa and Marynowski, 2005), vitrinite reflectance studies (Poprawa et al., 2002), T_{max} derived from Rock-Eval analysis (Staneczek and Marynowski, 2025; Staneczek et al., 2024a) and illite/smectite studies (Środoń et al., 2006). Apart from the geochemical proxies, also rock magnetic parameters indicate a clear maturity trend in the Mraznica Fm. which is closely mimicked by Huty Fm. All these trends and patterns documented by various methods clearly suggest that the most prominent burial of the (upper) Krížna nappe sediments occurred during the Oligocene-Miocene.

6. Conclusions

The PhD dissertation provides a study of the geochemical and magnetic evolution of the Central Carpathian Paleogene Basin and the Tatra Mts. from the Late Cretaceous to the Neogene. It focuses on the depositional conditions, organic matter characteristics and maturity, magnetic mineralogy and magnetic fabrics documented in the studied area. The main outcomes of the dissertation are as follows:

- Changes in the depositional conditions during the sedimentation of the CCPB units reflect the changes in the basin morphology and proceeding shallowing. The sedimentary environment shifted from anoxic coupled with intermittent photic zone euxinia to mostly oxic-suboxic.

- Biomarker analysis reveals the input of algae- angiosperm-, gymnosperm- and fungal-derived compounds to the organic matter. The composition of biomarkers changes with time.

- Wildfires (documented by fusinite grains and PAHs) were common during the deposition of the youngest CCPB units. Estimated temperatures correspond to crown and surface fires. Burned vegetation includes both coniferous and deciduous trees.

- Hydrocarbon potential of the CCPB units ranges from poor to excellent, with the most prognostic levels documented in the Zuberec Fm. Organic matter is generally characterized by early mature to mature levels. Some regions show oil-prone characteristics, while others are gas-prone.

- Paleotemperature analysis indicates that the Spiš Basin and the Belianske Tatra Mts. show the highest thermal maturity with temperatures reaching 200°C and 230°C, respectively. The least thermally affected regions are the northern Orava Basin and Šariš Upland, where the temperatures did not exceed 60°C.

- The paleotemperature trend reflected in the CCPB units is mirrored by the paleotemperature pattern present in the Mesozoic thrust nappes of the Choč-Tatra Belt. It suggests a common origin identified as the Oligocene-Miocene burial.

- The paleotemperature pattern was documented by both organic geochemistry, Rock-Eval, and rock magnetic parameters. The study demonstrated the necessity of using multiple proxies for thermal maturity reconstructions.

- Paramagnetic phyllosilicates dominate the magnetic mineralogy of the Huty and Mraznica Fms. Ferromagnetic minerals, mainly magnetite with hematite, are more

prominent in areas with higher paleotemperatures. The formation of iron oxides, reflected by the presence of superparamagnetic phases, accelerated during the Oligocene-Miocene burial.

- The magnetic fabrics recorded in the Mraznica and Huty Fms. show sedimentary-tectonic features with compaction-related magnetic foliation and magnetic lineations of tectonic origin.

- Magnetic fabrics document different stages of the tectonic evolution of the Tatra Mts. The most prevalent fabrics in the Mraznica Fm. shows the impact of the Late Cretaceous thrusting. The Mraznica Fm. fabrics carried by iron oxides recorded the impact of transpression during the Miocene uplift of the Tatra block. The ferromagnetic-driven Huty Fm. fabrics exhibit features linked with the extension during the formation of the CCPB. In turn, the phylosilicate-governed fabrics are characterized by uplift-related magnetic lineations.

7. References

Abdelmalak, M.M., Polteau, S., 2020. The thermal maturity of sedimentary basins as revealed by magnetic mineralogy. Basin Research 32, 1510–1531. https://doi.org/10.1111/bre.12439

Ai, J., Zhong, N., Zhang, T., Zhang, Y., Wang, T., George, S.C., 2021. Oceanic water chemistry evolution and its implications for post-glacial black shale formation: Insights from the Cryogenian Datangpo Formation, South China. Chemical Geology 566, 120083.

Algeo, T.J., Tribovillard, N., 2009. Environmental analysis of paleoceanographic systems based on molybdenum–uranium covariation. Chemical Geology 268, 211–225. https://doi.org/10.1016/j.chemgeo.2009.09.001

Anczkiewicz, A.A., Środoń, J., Zattin, M., 2013. Thermal history of the Podhale Basin in the internal Western Carpathians from the perspective of apatite fission track analyses. Geologica Carpathica 64, 141. https://doi.org/10.2478/geoca-2013-0010

Anczkiewicz, A.A., Danišík, M., Środoń, J., 2015. Multiple low-temperature thermochronology constraints on exhumation of the Tatra Mountains: New implication for the complex evolution of the Western Carpathians in the Cenozoic. Tectonics 34, 2296–2317. https://doi.org/10.1002/2015TC003952

Aubourg, C., Smith, B., Bakhtari, H., Guya, N., Eshragi, A., Lallemant, S., Molinaro, M., Braud, X., Delaunay, S., 2004. Post-Miocene shortening pictured by magnetic fabric across the Zagros-Makran syntaxis (Iran). Geol. Soc. Am. Spec. Pap 383, 17–40. https://doi.org/10.1130/0-8137-2383-3(2004)383[17:PSPBMF]2.0.CO;2

Aubourg, C., Pozzi, J.-P., 2010. Toward a new <250°C pyrrhotite–magnetite geothermometer for claystones. Earth and Planetary Science Letters 294, 47–57. https://doi.org/10.1016/j.epsl.2010.02.045

Aubourg, C., Kars, M., Pozzi, J.-P., Mazurek, M., Grauby, O., 2021. A magnetic geothermometer in moderately buried shales. Minerals 11, 957. https://doi.org/10.3390/min11090957

Barker, C.E., Pawlewicz, M.J., 1994. Calculation of vitrinite reflectance from thermal histories and peak temperatures. A comparison of methods. ACS Symposium Series 570, 216–229.

Bechtel, A., Gratzer, R., Püttmann, W., Oszczepalski, S., 2001. Variable alteration of organic matter in relation to metal zoning at the Rote Fäule front (Lubin-Sieroszowice mining district, SW Poland). Organic Geochemistry 32, 377–395. https://doi.org/10.1016/S0146-6380(01)00002-X

Belcher, C.M., New, S.L., Santín, C., Doerr, S.H., Dewhirst, R.A., Grosvenor, M.J., Hudspith, V.A., 2018. What Can Charcoal Reflectance Tell Us About Energy Release in Wildfires and the Properties of Pyrogenic Carbon? Front. Earth Sci. 6. https://doi.org/10.3389/feart.2018.00169.

Bella, P., Bosak, P., 2012. Speleogenesis along deep regional faults by ascending waters: case studies from Slovakia and Czech Republic. Acta Carsologica 41.

Bella, P., Gaál, Ľ., 2017. Hypogene Caves in Slovakia, in: Klimchouk, A., N. Palmer, A., De Waele, J., S. Auler, A., Audra, P. (Eds.), Hypogene Karst Regions and Caves of the World, Cave and Karst Systems of the World. Springer International Publishing, Cham, pp. 299–311. https://doi.org/10.1007/978-3-319-53348-3_19

Bilardello, D., 2016. Magnetic Anisotropy: Theory, Instrumentation, and Techniques, in: Reference Module in Earth Systems and Environmental Sciences. Elsevier. https://doi.org/10.1016/B978-0-12-409548-9.09516-6

Blaise, T., Barbarand, J., Kars, M., Ploquin, F., Aubourg, C., Brigaud, B., Cathelineau, M., El Albani, A., Gautheron, C., Izart, A., 2014. Reconstruction of low temperature (< 100 C) burial in sedimentary basins: a comparison of geothermometer in the intracontinental Paris Basin. Marine and Petroleum Geology 53, 71–87. https://doi.org/10.1016/j.marpetgeo.2013.08.019

Borradaile, G. J. 1988. Magnetic susceptibility, petrofabrics and strain. Tectonophysics, 156 (1-2), 1-20. https://doi.org/10.1016/0040-1951(88)90279-X

Boretti-Onyszkiewicz, W., 1968. Cios we fliszu zachodniego Podhala. Acta Geologica Polonica 18, 101–152.

Boudinot, F.G., Sepúlveda, J., 2020. Marine organic carbon burial increased forest fire frequency during Oceanic Anoxic Event 2. Nature Geoscience 13, 693–698.

Burchart, J., 1972. Fission-track age determinations of accessory apatite from the Tatra Mountains, Poland. Earth and Planetary Science Letters 15, 418–422. https://doi.org/10.1016/0012-821X(72)90041-6

Burnham, A.K., Sweeney, J.J., 1989. A chemical kinetic model of vitrinite maturation and reflectance. Geochimica et Cosmochimica Acta 53, 2649–2657. https://doi.org/10.1016/0016-7037(89)90136-1

Campos, D., Catlos, E.J., Stockli, D.F., Ketcham, R.A., Miller, N.R., Broska, I., Kohút, M., 2023. Exhumation of the High Tatra Mountains and Implications for the Western Carpathians, Slovakia. Presented at the GSA Connects 2023 Meeting in Pittsburgh, Pennsylvania, GSA.

Canfield, D.E., Raiswell, R., Bottrell, S.H., 1992. The reactivity of sedimentary iron minerals toward sulfide. American Journal of Science 292, 659–683.

Caricchi, C., Aldega, L., Sagnotti, L., Cifelli, F., Corrado, S., Mattei, M., 2024. Magnetic Fabric as a Marker of Thermal Maturity in Sedimentary Basins: A New Approach for Reconstructing the Tectono-Thermal Evolution of Fold-and-Thrust-Belts. Tectonics 43, e2024TC008530. https://doi.org/10.1029/2024TC008530

Castelluccio, A., Mazzoli, S., Andreucci, B., Jankowski, L., Szaniawski, R., Zattin, M., 2016. Building and exhumation of the Western Carpathians: New constraints from sequentially restored, balanced cross sections integrated with low-temperature thermochronometry. Tectonics 35, 2698–2733. https://doi.org/10.1002/2016TC004190

Catlos, E.J., Broska, I., Kohút, M., Etzel, T.M., Kyle, J.R., Stockli, D.F., Miggins, D.P., Campos, D., 2022. Geochronology, geochemistry, and geodynamic evolution of Tatric granites from crystallization to exhumation (Tatra Mountains, Western Carpathians). Geologica Carpathica 73. https://doi.org/10.31577/GeolCarp.73.6

Cebulak, S., Kępińska, B., Marynowski, L., Pająk, L., 2004. Present and past thermal conditions of the Podhale geothermal system. Investigations of Thermal Conditions in the Podhale Geothermal System Using an Oxyreactive Thermal Analysis (OTA) and Mineralogical Methods, IGSMiE PAN, Kraków 80–87.

Çelik, Y., Karayiğit, A.İ., Querol, X., Oskay, R.G., Mastalerz, M., Özer, M.S.K., 2017. Coal characteristics, palynology, and palaeoenvironmental interpretation of the Yeniköy coal of Late Oligocene age in the Thrace Basin (NW Turkey). International Journal of Coal Geology 181, 103–123.

Chakhmakhchev, A., Suzuki, M., Takayama, K., 1997. Distribution of alkylated dibenzothiophenes in petroleum as a tool for maturity assessments. Organic Geochemistry 26, 483–489. https://doi.org/10.1016/S0146-6380(97)00022-3

Channell, J.E.T., McCabe, C., 1994. Comparison of magnetic hysteresis parameters of unremagnetized and remagnetized limestones. J. Geophys. Res. 99, 4613–4623. https://doi.org/10.1029/93JB02578

Chen, J., Fu, J., Sheng, G., Liu, D., Zhang, J., 1996. Diamondoid hydrocarbon ratios: novel maturity indices for highly mature crude oils. Organic Geochemistry 25, 179–190. https://doi.org/10.1016/S0146-6380(96)00125-8

Činčura, J., 1990. Characteristics features of Prealpine and Epipaleoalpine landmass of the West Carpathians. Geologickỳ zborník 41, 29–38.

Činčura, J., 2002. Paleoalpine paleokarst of the Western Carpathians, in: Proceedings of XVII. Congress of Carpathian-Balkan Geological Association. Geol. Carpathica.

Csontos, L., Vörös, A., 2004. Mesozoic plate tectonic reconstruction of the Carpathian region. Palaeogeography, Palaeoclimatology, Palaeoecology 210, 1–56. https://doi.org/10.1016/j.palaeo.2004.02.033

Danišík, M., Kohút, M., Broska, I., Frisch, W., 2010. Thermal evolution of the Malá Fatra Mountains (Central Western Carpathians): insights from zircon and apatite fission track thermochronology. Geologica Carpathica 61, 19–27. https://doi.org/10.2478/v10096-009-0041-0

Day, R., Fuller, M., Schmidt, V., 1977. Hysteresis properties of titanomagnetites: grain-size and compositional dependence. Physics of the Earth and Planetary Interiors 13, 260–267.

Dearing, J.A., Dann, R.J.L., Hay, K., Lees, J.A., Loveland, P.J., Maher, B.A., O'grady, K., 1996. Frequency-dependent susceptibility measurements of environmental materials. Geophysical Journal International 124, 228–240. https://doi.org/10.1111/j.1365-246X.1996.tb06366.x

Derkowski, A., Środoń, J., Goryl, M., Marynowski, L., Szczerba, M., Mazur, S., 2021. Long-distance fluid migration defines the diagenetic history of unique Ediacaran sediments in the East European Craton. Basin Research 33, 570–593. https://doi.org/10.1111/bre.12485

Didyk, B.M., Simoneit, B.R.T., Brassell, S. t, Eglinton, G., 1978. Organic geochemical indicators of palaeoenvironmental conditions of sedimentation. Nature 272, 216–222. https://doi.org/10.1038/272216a0

Dinarès-Turell, J., Garcia-Senz, J., 2000. Remagnetization of Lower Cretaceous limestones from the southern Pyrenees and relation to the Iberian plate geodynamic evolution. J. Geophys. Res. 105, 19405–19418. https://doi.org/10.1029/2000JB900136

Dudzisz, K., Szaniawski, R., Michalski, K., Manby, G., 2016. Applying the anisotropy of magnetic susceptibility technique to the study of the tectonic evolution of the West Spitsbergen Fold-and-Thrust Belt. Polar Research 35, 31683. https://doi.org/10.3402/polar.v35.31683

Dudzisz, K., Szaniawski, R., Michalski, K., Chadima, M., 2018. Rock magnetism and magnetic fabric of the Triassic rocks from the West Spitsbergen Fold-and-Thrust Belt and its foreland. Tectonophysics 728, 104–118. https://doi.org/10.1016/j.tecto.2018.02.007

Dunlop, D.J., 2002. Theory and application of the Day plot (Mrs/Ms versus Hcr/Hc) 2. Application to data for rocks, sediments, and soils. Journal of Geophysical Research: Solid Earth 107, EPM 5-1-EPM 5-15. https://doi.org/10.1029/2001JB000487

Elie, M., Faure, P., Michels, R., Landais, P., Griffault, L., 2000. Natural and Laboratory Oxidation of Low-Organic-Carbon-Content Sediments: Comparison of Chemical Changes in Hydrocarbons. Energy Fuels 14, 854–861. https://doi.org/10.1021/ef9902146

Espitalié, J., Deroo, G., Marquis, F., 1985. La pyrolyse Rock-Eval et ses applications. Deuxième partie. Revue de l'Institut français du Pétrole 40, 755–784.

Fodor, L., 1995. From transpression to transtension: Oligocene-Miocene structural evolution of the Vienna basin and the East Alpine-Western Carpathian junction. Tectonophysics 242, 151–182. https://doi.org/10.1016/0040-1951(94)00158-6

Froitzheim, N., Plašienka, D., Schuster, R., 2008. Alpine tectonics of the Alps and Western Carpathians, in: The Geology of Central Europe Volume 2: Mesozoic and Cenozoic. Geological Society of London. https://doi.org/10.1144/CEV2P.6

Garecka, M., 2005. Calcareous nannoplankton from the Podhale Flysch (Oligocene-Miocene, Inner Carpathians, Poland). Studia Geologica Polonica 124, 353–370.

Gawęda, A., Burda, J., Klötzli, U., Golonka, J., Szopa, K., 2016. Episodic construction of the Tatra granitoid intrusion (Central Western Carpathians, Poland/Slovakia): consequences for the geodynamics of Variscan collision and Rheic Ocean closure. International Journal of Earth Sciences (Geologische Rundschau) 105, 1153–1174. https://doi.org/10.1007/s00531-015-1239-2

George, S.C., 1992. Effect of igneous intrusion on the organic geochemistry of a siltstone and an oil shale horizon in the Midland Valley of Scotland. Organic Geochemistry 18, 705–723. https://doi.org/10.1016/0146-6380(92)90097-H

Goodarzi, F., Snowdon, L., Gentzis, T., Pearson, D., 1994. Petrological and chemical characteristics of liptinite-rich coals from Alberta, Canada. Marine and Petroleum geology 11, 307–319. https://doi.org/10.1016/0264-8172(94)90052-3

Grabowski, J., 1996. Magnetic fabric of the Upper Jurassic sediments, Krížna Unit, Tatra Mts., Poland. Geologica Carpathica 47, 331.

Grabowski, J., 1997. Paleomagnetic results from the cover (High-Tatric) unit and nummulitic Eocene in the Tatra Mts (Central West Carpathians, Poland) and their tectonic implications. Annales Societatis Geologorum Poloniae 67, 13–23.

Grabowski, J., 2000. Palaeo-and rock magnetism of Mesozoic carbonate rocks in the Sub-Tatric series (Central West Carpathians)-palaeotectonic implications. Polish Geological Institute Special Papers 5, 1–88.

Grabowski, J., Michalík, J., Szaniawski, R., Grottek, I., 2009. Synthrusting remagnetization of the Krížna nappe: high resolution palaeo-and rock magnetic study in the Strážovce section, Strážovské vrchy Mts, Central West Carpathians (Slovakia). Acta Geologica Polonica 59, 137–155.

Grabowski, J., Schnyder, J., Sobień, K., Koptíková, L., Krzemiński, L., Pszczółkowski, A., Hejnar, J., Schnabl, P., 2013. Magnetic susceptibility and spectral gamma logs in the Tithonian–Berriasian pelagic carbonates in the Tatra Mts (Western Carpathians, Poland): Palaeoenvironmental changes at the Jurassic/Cretaceous boundary. Cretaceous Research 43, 1–17. https://doi.org/10.1016/j.cretres.2013.02.008

Gregorová, D., Hrouda, F., Kohút, M., 2009. Magnetic fabric of granitic composite pluton of the Velká Fatra Mountains (Western Carpathians, Slovakia): A Variscan remnant within the Alpine edifice? Geodinamica Acta 22, 57–72. https://doi.org/10.3166/ga.22.57-72

Grice, K., Cao, C., Love, G.D., Böttcher, M.E., Twitchett, R.J., Grosjean, E., Summons, R.E., Turgeon, S.C., Dunning, W., Jin, Y., 2005. Photic Zone Euxinia During the Permian-Triassic Superanoxic Event. Science 307, 706–709. https://doi.org/10.1126/science.1104323

Grice, K., Schaeffer, P., Schwark, L., Maxwell, J.R., 1996. Molecular indicators of palaeoenvironmental conditions in an immature Permian shale (Kupferschiefer, Lower Rhine Basin, north-west Germany) from free and S-bound lipids. Organic Geochemistry 25, 131–147. https://doi.org/10.1016/S0146-6380(96)00130-1

Grice, K., Lu, H., Atahan, P., Asif, M., Hallmann, C., Greenwood, P., Maslen, E., Tulipani, S., Williford, K., Dodson, J., 2009. New insights into the origin of perylene in geological samples. Geochimica et Cosmochimica Acta 73, 6531–6543. https://doi.org/10.1016/j.gca.2009.07.029

Gross, P., Buček, S., Ďurkovič, T., Filo, I., Karoli, S., Maglay, J., Nagy, A., Halouzka, R., Spišák, Z., Žec, B., others, 1999. Geological map of Popradská kotlina Basin, Hornádska kotlina Basin, Levočské vrchy Mts, Spišsko-šarišské medzihorie Depression, Bachureň Mts and Šarišská vrchovina highland (scale 1: 50,000). Ministry of Environment of Slovak Republic, Geol. Surv. Slovak Republic.

Gross, P., Filo, I., Halouzka, R., Haško, J., Havrila, M., Kováč, M., Maglay, J., Mello, J., Nagy, A., 1993a. Geological map of southern and eastern part of Orava.

Gross, P., Köhler, E., Haško, J., Halouzka, R., Mello, J., Nagy, A., 1993b. Geology of the southern and eastern Orava. Štátny Geologický Ústav Dionýza Štúra, Bratislava.

Gross, P., Köhler, E., Samuel, O., 1984. New lithostratigraphic classification of the Central Carpathians Paleogene. Geologické Práce, Správy 81, 103–17.

Halicki, B., 1963. Tektonika podhala, in: Annales Societatis Geologorum Poloniae. pp. 349–362.

Hartkopf-Fröder, C., Kloppisch, M., Mann, U., Neumann-Mahlkau, P., Schaefer, R.G., Wilkes, H., 2007. The end-Frasnian mass extinction in the Eifel Mountains, Germany: new insights from organic matter composition and preservation. SP 278, 173–196. https://doi.org/10.1144/SP278.8

Hartstra, R.L., 1982. Grain-size dependence of initial susceptibility and saturation magnetization-related parameters of four natural magnetites in the PSD—MD range. Geophysical Journal International 71, 477–495. https://doi.org/10.1111/j.1365-246X.1982.tb05998.x

Heider, F., Zitzelsberger, A., Fabian, K., 1996. Magnetic susceptibility and remanent coercive force in grown magnetite crystals from 0.1 μm to 6 mm. Physics of the Earth and Planetary interiors 93, 239–256.

Herring, J.R., 2013. Charcoal Fluxes into Sediments of the North Pacific Ocean: The Cenozoic Record of Burning, in: Sundquist, E.T., Broecker, W.S. (Eds.), Geophysical Monograph Series. American Geophysical Union, Washington, D. C., pp. 419–442. https://doi.org/10.1029/GM032p0419

Hirt, A., Banin, A., Gehring, A., 1993. Thermal generation of ferromagnetic minerals from iron-enriched smectites. Geophysical Journal International 115, 1161–1168. https://doi.org/10.1111/j.1365-246X.1993.tb01518.x

Hossain, H.Z., Sampei, Y., Roser, B.P., 2013. Polycyclic aromatic hydrocarbons (PAHs) in late Eocene to early Pleistocene mudstones of the Sylhet succession, NE Bengal Basin, Bangladesh: Implications for source and paleoclimate conditions during Himalayan uplift. Organic Geochemistry 56, 25–39. https://doi.org/10.1016/j.orggeochem.2012.12.001

Housen, B.A., Richter, C., van der Pluijm, B.A., 1993a. Composite magnetic anisotropy fabrics: experiments, numerical models and implications for the quantification of rock fabrics. Tectonophysics 220, 1–12. https://doi.org/10.1016/0040-1951(93)90219-A

Housen, B.A., van der Pluijm, B.A., 1991. Slaty cleavage development and magnetic anisotropy fabrics. Journal of Geophysical Research: Solid Earth 96, 9937–9946. https://doi.org/10.1029/91JB00605

Housen, B.A., Van Der Pluijm, B.A., Van Der Voo, R., 1993b. Magnetite dissolution and neocrystallization during cleavage formation: Paleomagnetic study of the Martinsburg Formation, Lehigh Gap, Pennsylvania. J. Geophys. Res. 98, 13799–13813. https://doi.org/10.1029/93JB01088

Hrouda, F., 1983. Fabric implications of magnetic anisotropy measurements of rocks of the Malé Karpaty (Little Carpathians) Mts. (SW Slovakia). Annuaire Inst. Geol. Geophys. 63, 57–61.

Hrouda, F., 1986. The magnetic fabric of sedimentary rocks of the Malé Karpaty Mts. and its tectonic implications. Sborník geologickỳch věd. Užitá geofyzika 155–167.

Hrouda, F., Hanák, J., 1990. Magnetic fabric of sedimentary formations of the Strazovske vrchy Mts., sedimentological and tectonic implications. Sborník geologickỳch věd. Užitá geofyzika 71–102.

Hrouda, F., Kahan, Š. 1991. The magnetic fabric relationship between sedimentary and basement nappes in the High Tatra Mountains, N. Slovakia. Journal of Structural Geology, 13(4), 431-442. https://doi.org/10.1016/0191-8141(91)90016-C

Hrouda, F., Potfaj, M., 1993. Deformation of sediments in the post-orogenic Intra-Carpathian Paleogene Basin as indicated by magnetic anisotropy. Tectonophysics 224, 425–434. https://doi.org/10.1016/0040-1951(93)90042-I

Hrouda, F., Krejčí, O., Potfaj, M., Stráník, Z., 2009. Magnetic fabric and weak deformation in sandstones of accretionary prisms of the Flysch and Klippen Belts of the Western Carpathians:

Mostly offscraping indicated. Tectonophysics 479, 254–270. https://doi.org/10.1016/j.tecto.2009.08.016

Hrouda, F., Pokornỳ, J., Ježek, J., Chadima, M., 2013. Out-of-phase magnetic susceptibility of rocks and soils: a rapid tool for magnetic granulometry. Geophysical Journal International 194, 170–181. https://doi.org/10.1093/gji/ggt097

Hrouda, F., Chadima, M., Ježek, J., Pokornỳ, J., 2016. Anisotropy of out-of-phase magnetic susceptibility of rocks as a tool for direct determination of magnetic sub-fabrics of some minerals: An introductory study. Geophysical Journal International. https://doi.org/10.1093/gji/ggw399

Hrouda, F., Chadima, M., Ježek, J., 2022. Anisotropy of out-of-phase magnetic susceptibility and its potential for rock fabric studies: a review. Geosciences 12, 234. https://doi.org/10.3390/geosciences12060234

Huang, W.-Y., Meinschein, W.G., 1979. Sterols as ecological indicators. Geochimica et Cosmochimica Acta 43, 739–745. https://doi.org/10.1016/0016-7037(79)90257-6

Hunt, J.M., 1995. Petroleum geochemistry and geology (textbook). Petroleum Geochemistry and Geology (Textbook).(2nd Ed.), WH Freeman Company.

Jackson, M., Swanson-Hysell, N.L., 2012. Rock magnetism of remagnetized carbonate rocks: another look. SP 371, 229–251. https://doi.org/10.1144/SP371.3

Jia, G., Peng, P., Zhao, Q., Jian, Z., 2003. Changes in terrestrial ecosystem since 30 Ma in East Asia: Stable isotope evidence from black carbon in the South China Sea. Geology 31, 1093–1096. https://doi.org/10.1130/G19992.1

Jones, T.P., Scott, Andre.C., Cope, M., 1991. Reflectance measurements and the temperature of formation of modern charcoals and implications for studies of fusain. Bulletin de la Société Géologique de France 162, 193–200.

Jurewicz, E., 2005. Geodynamic evolution of the Tatra Mts. and the Pieniny Klippen Belt (Western Carpathians): problems and comments. Acta Geologica Polonica 55, 295–338.

Jurewicz, E., 2007. Multistage evolution of the granitoid core in Tatra Mountains. Granitoids in Poland. Warsaw University, Warsaw 307–317.

Kaiho, K., Saito, R., Ito, K., Miyaji, T., Biswas, R., Tian, L., Sano, H., Shi, Z., Takahashi, S., Tong, J., 2016. Effects of soil erosion and anoxic–euxinic ocean in the Permian–Triassic marine crisis. Heliyon 2.

Kaiho, K., Miura, M., Tezuka, M., Hayashi, N., Jones, D.S., Oikawa, K., Casier, J.-G., Fujibayashi, M., Chen, Z.-Q., 2021. Coronene, mercury, and biomarker data support a link between extinction magnitude and volcanic intensity in the Late Devonian. Global and Planetary Change 199, 103452. https://doi.org/10.1016/j.gloplacha.2021.103452

Kappenberg, A., Braun, M., Amelung, W., Lehndorff, E., 2019. Fire condensates and charcoals: Chemical composition and fuel source identification. Organic Geochemistry 130, 43–50. https://doi.org/10.1016/j.orggeochem.2019.01.009

Karp, A.T., Behrensmeyer, A.K., Freeman, K.H., 2018. Grassland fire ecology has roots in the late Miocene. Proc. Natl. Acad. Sci. U.S.A. 115, 12130–12135. https://doi.org/10.1073/pnas.1809758115

Karp, A.T., Holman, A.I., Hopper, P., Grice, K., Freeman, K.H., 2020. Fire distinguishers: Refined interpretations of polycyclic aromatic hydrocarbons for paleo-applications. Geochimica et Cosmochimica Acta 289, 93–113. https://doi.org/10.1016/j.gca.2020.08.024

Katz, B., Elmore, R.D., Engel, M.H., 1998. Authigenesis of magnetite in organic-rich sediment next to a dike: implications for thermoviscous and chemical remagnetizations. Earth and Planetary Science Letters 163, 221–234. https://doi.org/10.1016/S0012-821X(98)00189-7

Katz, B., Elmore, R.D., Cogoini, M., Engel, M.H., Ferry, S., 2000. Associations between burial diagenesis of smectite, chemical remagnetization, and magnetite authigenesis in the Vocontian trough, SE France. Journal of Geophysical Research: Solid Earth 105, 851–868. https://doi.org/10.1029/1999JB900309

Kázmér, M., Dunkl, I., Frisch, W., Kuhlemann, J., Ozsvárt, P., 2003. The Palaeogene forearc basin of the Eastern Alps and Western Carpathians: subduction erosion and basin evolution. Journal of the Geological Society 160, 413–428. https://doi.org/10.1144/0016-764902-041

Killops, S.D., Massoud, M.S., 1992. Polycyclic aromatic hydrocarbons of pyrolytic origin in ancient sediments: evidence for Jurassic vegetation fires. Organic Geochemistry 18, 1–7. https://doi.org/10.1016/0146-6380(92)90137-M

King, J.G., Williams, W., 2000. Low-temperature magnetic properties of magnetite. J. Geophys. Res. 105, 16427–16436. https://doi.org/10.1029/2000JB900006

Kohút, M., Kovach, V.P., Kotov, A.B., Salnikova, E.B., Savatenkov, V.M., 1999. Sr and Nd isotope geochemistry of Hercynian granitic rocks from the Western Carpathians–implications for granite genesis and crustal evolution. Geologica Carpathica 50, 477–487.

Kokinos, J.P., Eglinton, T.I., Goñi, M.A., Boon, J.J., Martoglio, P.A., Anderson, D.M., 1998. Characterization of a highly resistant biomacromolecular material in the cell wall of a marine dinoflagellate resting cyst. Organic Geochemistry 28, 265–288. https://doi.org/10.1016/S0146-6380(97)00134-4

Koopmans, M.P., Köster, J., Van Kaam-Peters, H.M., Kenig, F., Schouten, S., Hartgers, W.A., de Leeuw, J.W., Damsté, J.S.S., 1996. Diagenetic and catagenetic products of isorenieratene: Molecular indicators for photic zone anoxia. Geochimica et Cosmochimica Acta 60, 4467–4496. https://doi.org/10.1016/S0016-7037(96)00238-4

Kotański, Z., 1971. Przewodnik geologiczny po Tatrach. Wydawnictwa Geologiczne. Warszawa.

Kotulová, J., Starek, D., Havelcová, M., Pálková, H., 2019. Amber and organic matter from the late Oligocene deep-water deposits of the Central Western Carpathians (Orava–Podhale Basin). International Journal of Coal Geology 207, 96–109. https://doi.org/10.1016/j.coal.2019.02.006

Kováč, M., Král, J., Márton, E., Plašienka, D., Uher, P., 1994. Alpine uplift history of the Central Western Carpathians: geochronological, paleomagnetic, sedimentary and structural data. Geologica Carpathica 45, 83–96.

Kováč, M., Plašienka, D., Soták, J., Vojtko, R., Oszczypko, N., Less, G., Ćosović, V., Fügenschuh, B., Králiková, S., 2016. Paleogene palaeogeography and basin evolution of the Western Carpathians, Northern Pannonian domain and adjoining areas. Global and Planetary Change 140, 9–27.

Kováč, P., Bendík, A., 2002. Structural analysis of Adnet limestones at Zvolen-Donovaly. Miner. Slovaca 34, 3–4.

Král, J., 1977. Fission track ages of apatites from some granitoid rocks in West Carpathians. Geol. Zb. Geol. Carpathica 28, 269–276.

Králiková, S., Vojtko, R., Sliva, L., Minar, J., Fuegenschuh, B., Kováč, M., Hok, J., 2014a. Cretaceous–Quaternary tectonic evolution of the Tatra Mts (Western Carpathians): constraints from structural, sedimentary, geomorphological, and fission track data. Geologica Carpathica 65, 307–326. https://doi.org/10.2478/geoca-2014-0021

Králiková, S., Vojtko, R., Hók, J., Fügenschuh, B., Kováč, M., 2016. Low-temperature constraints on the Alpine thermal evolution of the Western Carpathian basement rock complexes. Journal of Structural Geology 91, 144–160. https://doi.org/10.1016/j.jsg.2016.09.006

Králiková, S., Vojtko, R., Andriessen, P., Kováč, M., Fügenschuh, B., Hók, J., Minár, J., 2014b. Late Cretaceous–Cenozoic thermal evolution of the northern part of the Central Western Carpathians (Slovakia): revealed by zircon and apatite fission track thermochronology. Tectonophysics 615, 142–153. https://doi.org/10.1016/j.tecto.2014.01.002

Lamarche, G., Rochette, P., 1987. Microstructural analysis and origin of lineations in the magnetic fabric of some Alpine slates. Tectonophysics 139, 285–293. https://doi.org/10.1016/0040-1951(87)90102-8

Lefeld, J., 1974. Middle-Upper Jurassic and Lower Cretaceous biostratigraphy and sedimentology of the sub-Tatric succession in the Tatra Mts (Western Carpathians). Acta Geologica Polonica 24, 227–364.

Lefeld, J., Gaździcki, A., Iwanow, A., Krajewski, K., Wójcik, K., 1985. Jurassic and Cretaceous lithostratigraphic units of the Tatra Mountains. Stud. Geol. Pol 84, 1–93.

Lexa, J., Bezák, V., Elečko, M., Mello, J., Polák, M., Potfaj, M., Vozár, J., Schnabel, G., Pálenskỳ, P., Császár, G., others, 2000. Geological map of Western Carpathians and adjacent areas 1: 500 000. Geological Survey of Slovak Republic, Bratislava.

Li, Z., Huang, H., Yan, G., Xu, Y., George, S.C., 2022. Occurrence and origin of perylene in Paleogene sediments from the Tasmanian Gateway, Australia. Organic Geochemistry 168, 104406. https://doi.org/10.1016/j.orggeochem.2022.104406

Ludwiniak, M., 2010. Multi-stage development of the joint network in the flysch rocks of western Podhale (InnerWestern Carpathians, Poland). Acta Geologica Polonica 60, 283–316.

Mackenzie, A., McKenzie, D., 1983. Isomerization and aromatization of hydrocarbons in sedimentary basins formed by extension. Geological Magazine 120, 417–470. https://doi.org/10.1017/S0016756800027461

Madzin, J., Márton, E., Starek, D., Mikuš, T., 2021. Magnetic fabrics in the turbidite deposits of the Central Carpathian Paleogene Basin in relation to sedimentary and tectonic fabric elements. Geologica Carpathica 72, 134–154. https://doi.org/10.31577/GeolCarp.72.2.4

Maehlmann, R.F., Le Bayon, R., 2016. Vitrinite and vitrinite like solid bitumen reflectance in thermal maturity studies: Correlations from diagenesis to incipient metamorphism in different geodynamic settings. International Journal of Coal Geology 157, 52–73. https://doi.org/10.1016/j.coal.2015.12.008

Marko, F., Vojtko, R., Plašienka, D., Sliva, L., Jablonskỳ, J., Reichwalder, P., Starek, D., 2005. A contribution to the tectonics of the Periklippen zone near Zázrivá (Western Carpathians). Slovak Geological Magazine 11, 37–43.

Márton, E., Jelenska, M., Tokarski, A.K., Soták, J., Kovác, M., Spišiak, J., 2009. Current-independent paleomagnetic declinations in flysch basins: a case study from the Inner Carpathians. Geodinamica Acta 22, 73–82. https://doi.org/10.3166/ga.22.73-82

Márton, E., Grabowski, J., Tokarski, A.K., Túnyi, I., 2016. Palaeomagnetic results from the fold and thrust belt of the Western Carpathians: An overview. Geological Society, London, Special Publications 425, 7–36. https://doi.org/10.1144/SP425.1

Marynowski, L., Gawęda A., Poprawa, P., Zywiecki, M.M., Kępińska, B., Merta, H., 2006. Origin of organic matter from tectonic zones in the Western Tatra Mountains Crystalline Basement, Poland: An example of bitumen—source rock correlation. Marine and Petroleum Geology 23, 261–279. https://doi.org/10.1016/j.marpetgeo.2005.08.001

Marynowski, L., Gawęda, A., Cebulak, S., Jędrysek, M., 2001. Hydrocarbons migration in tectonic zones of the Western Tatra Mountains crystalline basement (Central Western Carpathians). Geologica Carpathica 52, 3–14.

Marynowski, L., Smolarek, J., Bechtel, A., Philippe, M., Kurkiewicz, S., Simoneit, B.R., 2013. Perylene as an indicator of conifer fossil wood degradation by wood-degrading fungi. Organic Geochemistry 59, 143–151. https://doi.org/10.1016/j.orggeochem.2013.04.006

Marynowski, L., Smolarek, J., Hautevelle, Y., 2015. Perylene degradation during gradual onset of organic matter maturation. International Journal of Coal Geology 139, 17–25. https://doi.org/10.1016/j.coal.2014.04.013

Marynowski, L., Zatoń, M., Simoneit, B.R., Otto, A., Jędrysek, M.O., Grelowski, C., Kurkiewicz, S., 2007. Compositions, sources and depositional environments of organic matter from the Middle Jurassic clays of Poland. Applied Geochemistry 22, 2456–2485. https://doi.org/10.1016/j.apgeochem.2007.06.015

McClelland Brown, E., 1981. Paleomagnetic estimates of temperatures reached in contact metamorphism. Geology 9, 112–116. https://doi.org/10.1130/0091-7613(1981)9<112:PEOTRI>2.0.CO;2

Moreau, M., Ader, M., Enkin, R., 2005. The magnetization of clay-rich rocks in sedimentary basins: low-temperature experimental formation of magnetic carriers in natural samples. Earth and Planetary Science Letters 230, 193–210. https://doi.org/10.1016/j.epsl.2004.11.013

Nemčok, J., Bezák, V., Biely, A., Gorek, A., Halouzka, R., Janák, M., Kahan, S., Kotański, Z., Lefeld, J., Mello, J., 1993a. Geological Map of the Tatra Mountains 1: 50 000. Bratislava, Geologickỳ ústav D. Štúra.

Nemčok, J, Bezák, V., Janák, M., Kahan, Š., Ryka, W., Kohút, M., Lehotskỳ, I., Wieczorek, J., Zelman, J., Mello, J., others, 1993b. Explanatory notes to the geological map of the Tatra Mts. at 1: 50,000 scale [Vysvetlivky ku geologickej mape Tatier 1: 50 000]. State Geological Institute of Dionỳz Štúr 1–135.

Oskay, R.G., Bechtel, A., Karayiğit, A.İ., 2019. Mineralogy, petrography and organic geochemistry of Miocene coal seams in the Kınık coalfield (Soma Basin-Western Turkey): Insights into depositional environment and palaeovegetation. International Journal of Coal Geology 210, 103205. https://doi.org/10.1016/j.coal.2019.05.012

Otto, A., Simoneit, B.R., 2001. Chemosystematics and diagenesis of terpenoids in fossil conifer species and sediment from the Eocene Zeitz formation, Saxony, Germany. Geochimica et Cosmochimica Acta 65, 3505–3527. https://doi.org/10.1016/S0016-7037(01)00693-7

Özdemir, Ö., Dunlop, D.J., 2014. Hysteresis and coercivity of hematite. Journal of Geophysical Research: Solid Earth 119, 2582–2594. https://doi.org/10.1002/2013JB010739

Palmer, S.E., 1993. Effect of biodegradation and water washing on crude oil composition, in: Organic Geochemistry: Principles and Applications. Springer, pp. 511–533. https://doi.org/10.1306/TrHbk543C4

Parés, J.M., van der Pluijm, B.A., Dinarès-Turell, J., 1999. Evolution of magnetic fabrics during incipient deformation of mudrocks (Pyrenees, northern Spain). Tectonophysics 307, 1–14. https://doi.org/10.1016/S0040-1951(99)00115-8

Parés, J.M., 2015. Sixty years of anisotropy of magnetic susceptibility in deformed sedimentary rocks. Frontiers in Earth Science 3, 4. https://doi.org/10.3389/feart.2015.00004

Passendorfer, E., 1952. Jak powstały Tatry. Państwowe Zakłady Wydawnictw Szkolnych. Warszawa.

Peresson, H., Decker, K., 1997. Far-field effects of Late Miocene subduction in the Eastern Carpathians: E-W compression and inversion of structures in the Alpine-Carpathian-Pannonian region. Tectonics 16, 38–56. https://doi.org/10.1029/96TC02730

Pešková, I., Vojtko, R., Starek, D., Sliva, L., 2009. Late Eocene to Quaternary deformation and stress field evolution of the Orava region (Western Carpathians). Acta Geologica Polonica 59, 73–91.

Peters, K.E., Cassa, M.R., 1994. Applied Source Rock Geochemistry, in: Magoon, L.B., Dow, W.G. (Eds.), The Petroleum System—From Source to Trap. American Association of Petroleum Geologists, p. 0. https://doi.org/10.1306/M60585C5.

Peters, K.E., Moldowan, J.M., 1993. The biomarker guide: interpreting molecular fossils in petroleum and ancient sediments.

Petersen, N., Bleil, U., 1982. 6.2. 5 Curie temperature: 6.2 Magnetic properties of rocks. Subvolume B 415–428.

Petersen, H., Vosgerau, H., 1999. Composition and organic maturity of Middle Jurassic coals, North-East Greenland: evidence for liptinite-induced suppression of huminite reflectance. International Journal of Coal Geology 41, 257–274. https://doi.org/10.1016/S0166-5162(99)00022-1

Petrík, I., Kohút, M., 1997. The evolution of granitoid magmatism during the Hercynian orogen in the Western Carpathians. Geological evolution of the Western Carpathians 235–252.

Piotrowska, K., Kotański, Z., Gawęda, A., Piotrowski, J., Rączkowski, W., 2009. Detailed Geological Map of Poland 1:50000. Tatry Zachodnie sheet. Polish Geological Institute.

Piotrowska, K., Rączkowski, W., Iwanow, A., Zabielski, R., Derkacz, M., Wójcik, A., Michalik, M., Wasiluk, R., 2013. Detailed Geological Map of Poland 1:50000. Tatry Wysokie sheet. Polish Geological Institute.

Plašienka, D., 1997. Cretaceous tectonochronology of the Central Western Carpathians (Slovakia). Geologica Carpathica 48, 99–111.

Plašienka, D., Grecula, P., Putiš, M., Kováč, M., Hovorka, D., 1997. Evolution and structure of the Western Carpathians: an overview. Geological evolution of the Western Carpathians 1–24.

Plašienka, D., 2003. Development of basement-involved fold and thrust structures exemplified by the Tatric–Fatric–Veporic nappe system of the Western Carpathians (Slovakia). Geodinamica Acta 16, 21–38. https://doi.org/10.1016/S0985-3111(02)00003-7

Plašienka, D., 2018. Continuity and episodicity in the early Alpine tectonic evolution of the Western Carpathians: How large-scale processes are expressed by the orogenic architecture and rock record data. Tectonics 37, 2029–2079. https://doi.org/10.1029/2017TC004779

Pokorski, J., 1965. Występowanie łupliwości we fliszu wschodniego Podhala. Geological Quarterly 9, 616–624.

Poprawa, P., Grabowski, J., Grotek, I., 2002. Thermal and burial history of the sub-Tatric nappes and the Podhale basin—Constraints from preliminary maturity analysis and modelling. Geologica Carpathica 53.

Poprawa, P., Marynowski, L., 2005. Thermal history of the Podhale Trough (northern part of the Central Carpathian Paleogene Basin)–preliminary results from 1-D maturity modeling. Mineralogical Society of Poland–Special Papers 25, 352–355.

Prokešová, R., 1994. Structural analysis of the Krížna nappe in its near-root and superficial position. Mineralia Slovaca 26, 347–354.

Prokešová, R., Plašienka, D., Milovskỳ, R., 2012. Structural pattern and emplacement mechanisms of the Krížna cover nappe (Central Western Carpathians). Geologica Carpathica 63, 13–32. https://doi.org/10.2478/v10096-012-0001-y

Radke, M., 1987. Organic geochemistry of aromatic hydrocarbons. Advances in Petroleum Geochemistry 2, 141–207.

Radke, M., Horsfield, B., Littke, R., Rullkötter, J., 1997. Maturation and petroleum generation. Petroleum and Basin Evolution: Insights from Petroleum Geochemistry, Geology and Basin Modeling 169–229.

Radke, M., Welte, D., 1983. The Methylphenanthrene Index (MPI). A maturity parameter based on aromatic hydrocarbons., in: Advances in Organic Geochemistry. J. Wiley and Sons, New York, pp. 504–512.

Radke, M., Welte, D., Willsch, H., 1986. Maturity parameters based on aromatic hydrocarbons: Influence of the organic matter type. Organic Geochemistry 10, 51–63.

Radke, M., Willsch, H., 1994. Extractable alkyldibenzothiophenes in Posidonia Shale (Toarcian) source rocks: Relationship of yields to petroleum formation and expulsion. Geochimica et Cosmochimica Acta 58, 5223–5244. https://doi.org/10.1016/0016-7037(94)90307-7

Ramdahl, T., 1983. Retene—a molecular marker of wood combustion in ambient air. Nature 306, 580–582.

Ratschbacher, L., Linzer, H.-G., Moser, F., Strusievicz, R.-O., Bedelean, H., Har, N., Mogoş, P.-A., 1993. Cretaceous to Miocene thrusting and wrenching along the central South Carpathians due to a corner effect during collision and orocline formation. Tectonics 12, 855–873. https://doi.org/10.1029/93TC00232

Roberts, A.P., 2015. Magnetic mineral diagenesis. Earth-Science Reviews 151, 1–47. https://doi.org/10.1016/j.earscirev.2015.09.010

Rochette, P., 1987. Magnetic susceptibility of the rock matrix related to magnetic fabric studies. Journal of Structural Geology 9, 1015–1020. https://doi.org/10.1016/0191-8141(87)90009-5

Rospondek, M.J., Marynowski, L., Chachaj, A., Góra, M., 2009. Novel aryl polycyclic aromatic hydrocarbons: phenylphenanthrene and phenylanthracene identification, occurrence and

distribution in sedimentary rocks. Organic Geochemistry 40, 986–1004. https://doi.org/10.1016/j.orggeochem.2009.06.001

Rubinkiewicz, J., Ludwiniak, M., 2005. Fracture and fault development in Werfenian quartzitic sandstones–A case study from the autochthonous cover of the Tatra Mts., in: Annales Societatis Geologorum Poloniae. pp. 171–187.

Sage, R.F., 2004. The evolution of C4 photosynthesis. New Phytologist 161, 341–370. https://doi.org/10.1111/j.1469-8137.2004.00974.x

Sanderson, D.J., Marchini, W., 1984. Transpression. Journal of Structural Geology 6, 449–458.

Schill, E., Appel, E., Gautam, P., 2002. Towards pyrrhotite/magnetite geothermometry in low-grade metamorphic carbonates of the Tethyan Himalayas (Shiar Khola, Central Nepal). Journal of Asian Earth Sciences 20, 195–201. https://doi.org/10.1016/S1367-9120(01)00022-0

Scott, A.C., 2000. The Pre-Quaternary history of fire. Palaeogeography, palaeoclimatology, palaeoecology 164, 281–329. https://doi.org/10.1016/S0031-0182(00)00192-9

Scott, A.C., 2010. Charcoal recognition, taphonomy and uses in palaeoenvironmental analysis. Palaeogeography, Palaeoclimatology, Palaeoecology 291, 11–39. https://doi.org/10.1016/j.palaeo.2009.12.012

Seifert, W.K., Moldowan, J.M., 1980. The effect of thermal stress on source-rock quality as measured by hopane stereochemistry. Physics and Chemistry of the Earth 12, 229–237. https://doi.org/10.1016/0079-1946(79)90107-1

Simoneit, B.R., Grimalt, J., Wang, T., Cox, R., Hatcher, P.G., Nissenbaum, A., 1986. Cyclic terpenoids of contemporary resinous plant detritus and of fossil woods, ambers and coals. Organic Geochemistry 10, 877–889. https://doi.org/10.1016/S0146-6380(86)80025-0

Śmigielski, M., Sinclair, H., Stuart, F., Persano, C., Krzywiec, P., 2016. Exhumation history of the Tatry Mountains, Western Carpathians, constrained by low-temperature thermochronology. Tectonics 35, 187–207. https://doi.org/10.1002/2015TC003855

Sokołowski, S., 1959. W sprawie poszukiwań geologicznych w regionie tatrzańskim. Przegląd Geologiczny 7, 341–341.

Soták, J., Pereszlenyi, M., Marschalko, R., Milicka, J., Starek, D., 2001. Sedimentology and hydrocarbon habitat of the submarine-fan deposits of the Central Carpathian Paleogene Basin (NE Slovakia). Marine and Petroleum Geology 18, 87–114. https://doi.org/10.1016/S0264-8172(00)00047-7

Sperner, B., Ratschbacher, L., Nemčok, M., 2002. Interplay between subduction retreat and lateral extrusion: Tectonics of the Western Carpathians. Tectonics 21, 1–1. https://doi.org/10.1029/2001TC901028

Środoń, J., Kotarba, M., Biroň, A., Such, P., Clauer, N., Wójtowicz, A., 2006. Diagenetic history of the Podhale-Orava Basin and the underlying Tatra sedimentary structural units

(Western Carpathians): evidence from XRD and K-Ar of illite-smectite. Clay Minerals 41, 751–774. https://doi.org/10.1180/0009855064130217

Staneczek, D., Szaniawski, R., Szczygieł, J., 2022. Transpression-driven deformations of the Chočské vrchy Mountains (Western Carpathians): Insights from magnetic fabric. Geologica Carpathica 73, 451–471. https://doi.org/10.31577/GeolCarp.73.5.4

Staneczek, D., Więcław, D., Marynowski, L., 2024a. Depositional conditions, wildfires, maturity, and hydrocarbon potential evaluation of Central Carpathian Paleogene Basin based on integrative approach from Orava Basin. International Journal of Coal Geology 285, 104490. https://doi.org/10.1016/j.coal.2024.104490

Staneczek, D., Szaniawski, R., Chadima, M., Marynowski, L., 2024b. Multi-stage tectonic evolution of the Tatra Mts recorded in the para- and ferromagnetic fabrics. Tectonophysics 880, 230338. https://doi.org/10.1016/j.tecto.2024.230338

Staneczek, D., Marynowski, L., 2025. Application of biomarker and non-biomarker parameters to assess maturity using the Central Carpathian Paleogene Basin as a case study. Organic Geochemistry 201, 104933. https://doi.org/10.1016/j.orggeochem.2025.104933

Staneczek, D., Szaniawski, R., Marynowski, L. Under review. Burial impact on the Tatra Mts from a rock magnetic and magnetic fabric perspective. Tectonics.

Starek, D., 2001. Sedimentology and paleodynamics of the Paleogene formations in the Central Western Carpathians (Orava region). Manuscript, PhD. Thesis, Geological Institute of the Slovak Academy of Sciences.

Staszic, S., 1815. O ziemiorództwie Karpatów i innych gór i równin Polski. Warszawa, w Drukarni Rządowej.

Suk, D., Peacor, D.R., der Voo, R.V., 1990. Replacement of pyrite framboids by magnetite in limestone and implications for palaeomagnetism. Nature 345, 611–613.

Sůkalová, L., Vojtko, R., Pešková, I., 2012. Cenozoic deformation and stress field evolution of the Kozie chrbty Mountains and the western part of Hornád Depression (Central Western Carpathians). Acta Geologica Slovaca 4, 53–64.

Summons, R., Powell, T., 1987. Identification of aryl isoprenoids in source rocks and crude oils: biological markers for the green sulphur bacteria. Geochimica et Cosmochimica Acta 51, 557–566. https://doi.org/10.1016/0016-7037(87)90069-X

Synnott, D.P., Schwark, L., Dewing, K., Pedersen, P.K., Sanei, H., 2021. Evidence for widespread wildfires and their environmental impact in the Late Cretaceous Canadian Arctic. Global and Planetary Change 203, 103515. https://doi.org/10.1016/j.gloplacha.2021.103515

Szaniawski, R., Ludwiniak, M., Rubinkiewicz, J., 2012. Minor counterclockwise rotation of the Tatra Mountains (Central Western Carpathians) as derived from paleomagnetic results achieved in hematite-bearing Lower Triassic sandstones. Tectonophysics 560, 51–61. https://doi.org/10.1016/j.tecto.2012.06.027

Szaniawski, R., Mazzoli, S., Jankowski, L., 2017. Controls of structural inheritance on orogenic curvature and foreland basin sedimentation: Insights from the Przemyśl area, Western Carpathians. Journal of Structural Geology 103, 137–150. https://doi.org/10.1016/j.jsg.2017.09.004

Szaniawski, R., Ludwiniak, M., Mazzoli, S., Szczygieł, J., Jankowski, L., 2020. Paleomagnetic and magnetic fabric data from Lower Triassic redbeds of the Central Western Carpathians: new constraints on the paleogeographic and tectonic evolution of the Carpathian region. Journal of the Geological Society 177, 509–522. https://doi.org/10.1144/jgs2018-232

Uhl, D., Spiekermann, R., Wuttke, M., Poschmann, M.J., Jasper, A., 2022. Wildfires during the Paleogene (late Eocene–late Oligocene) of the Neuwied Basin (W-Germany). Review of Palaeobotany and Palynology 297, 104565. https://doi.org/10.1016/j.revpalbo.2021.104565

Uhl, D., Wuttke, M., Jasper, A., 2020. Woody charcoal with traces of pre-charring decay from the Late Oligocene (Chattian) of Norken (Westerwald, Rhineland-Palatinate, W Germany). Acta Palaeobotanica 60, 43–50. https://doi.org/10.35535/acpa-2020-0002

Uhlig, V., 1897. Die Geologie des Tatragebirges. Hof-u. Staatsdruckerei.

Vachula, R.S., Karp, A.T., Denis, E.H., Balascio, N.L., Canuel, E.A., Huang, Y., 2022. Spatially calibrating polycyclic aromatic hydrocarbons (PAHs) as proxies of area burned by vegetation fires: Insights from comparisons of historical data and sedimentary PAH fluxes. Palaeogeography, Palaeoclimatology, Palaeoecology 596, 110995. https://doi.org/10.1016/j.palaeo.2022.110995

Vandenbroucke, M., Largeau, C., 2007. Kerogen origin, evolution and structure. Organic Geochemistry 38, 719–833. https://doi.org/10.1016/j.orggeochem.2007.01.001

Vojtko, R., Králiková, S., Jeřábek, P., Schuster, R., Danišík, M., Fügenschuh, B., Minár, J., Madarás, J., 2016. Geochronological evidence for the Alpine tectono-thermal evolution of the Veporic Unit (Western Carpathians, Slovakia). Tectonophysics 666, 48–65. https://doi.org/10.1016/j.tecto.2015.10.014

Vojtko, R., Tokárová, E., Sliva, L., Pesková, I., 2010. Reconstruction of Cenozoic paleostress fields and revised tectonic history in the northern part of the Central Western Carpathians (the Spisská Magura and Východné Tatry Mountains). Geologica Carpathica 61, 211. https://doi.org/10.2478/v10096-010-0012-5

Wagreich, M., 1995. Subduction tectonic erosion and Late Cretaceous subsidence along the northern Austroalpine margin (Eastern Alps, Austria). Tectonophysics 242, 63–78. https://doi.org/10.1016/0040-1951(94)00151-X

Waliczek, M., Machowski, G., Więcław, D., Konon, A., Wandycz, P., 2019. Properties of solid bitumen and other organic matter from Oligocene shales of the Fore-Magura Unit in Polish Outer Carpathians: Microscopic and geochemical approach. International Journal of Coal Geology 210, 103206. https://doi.org/10.1016/j.coal.2019.05.013

Waliczek, M., Więcław, D., 2012. Maturity of Menilite Shales from Polish Outer Carpathians based on vitrinite reflectance and Rock-Eval pyrolysis data. Geology, Geophysics and Environment 38, 551–552.

Weil, A.B., Yonkee, A., 2009. Anisotropy of magnetic susceptibility in weakly deformed red beds from the Wyoming salient, Sevier thrust belt: Relations to layer-parallel shortening and orogenic curvature. Lithosphere 1, 235–256. https://doi.org/10.1130/L42.1

Wendorff-Belon, M., Rospondek, M., Marynowski, L., 2021. Early Oligocene environment of the Central Paratethys revealed by biomarkers and pyrite framboids from the Tarcău and Vrancea Nappes (Eastern Outer Carpathians, Romania). Marine and Petroleum Geology 128, 105037. https://doi.org/10.1016/j.marpetgeo.2021.105037

Yang, T., Dekkers, M.J., Zhang, B., 2016. Seismic heating signatures in the Japan Trench subduction plate-boundary fault zone: evidence from a preliminary rock magnetic 'geothermometer.' Geophysical Supplements to the Monthly Notices of the Royal Astronomical Society 205, 332–344. https://doi.org/10.1093/gji/ggw013

Zhao, C., Zhang, K., Xiao, L., Uhl, D., Shi, Z., Zhao, W., Zhao, Q., Sun, Y., Liu, B., 2023. Paleoclimate-induced wildfires in a paleomire in the Ordos Basin, Northern China during the Middle Jurassic greenhouse period. Chemical Geology 637, 121677. https://doi.org/10.1016/j.chemgeo.2023.121677

Zheng, X., Schwark, L., Stockhausen, M., Luo, Q., Wu, J., Zhong, N., Schovsbo, N.H., Sanei, H., 2023. Effects of synthetic maturation on phenanthrenes and dibenzothiophenes over a maturity range of 0.6 to 4.7% EASY% Ro. Marine and Petroleum Geology 153, 106285. https://doi.org/10.1016/j.marpetgeo.2023.106285

8. Appendix

Appendix 1. Sampling site location, sampled units, and their lithologies along with conducted analyses. Abbreviations: GC-MS: gas chromatography-mass spectrometry analysis, VR: measured vitrinite reflectance, PyF: measurement of the pyrite framboid diameters, ICP-MS: Inductively Coupled Plasma Mass Spectrometry; FR: fusinite reflectance measurements, TOC&TS&CC: Total Organic Carbon, Total Sulfur and Carbonate Content, AARM: Anisotropy of Anhysteretic Remanent Magnetization, AMS: Anisotropy of in-phase and out-of-phase Magnetic Susceptibility, k/T: temperature-dependent in-phase magnetic susceptibility, IRM+comp.: Isothermal Remanent Magnetization (IRM) acquisition curves and component analysis, hys+IRMbf: hysteresis curves and IRM back-field measurements, MS: in-phase and out-of-phase magnetic susceptibility; LOW: thermal demagnetization of a three-component IRM.

No.	Site/Depth	No. of samples and/or code	Unit	Region	Lithology	Coordinates	Analysis type
1	Pośrednia Kopka hill	Mz7; M: 7; OM: 1	Mraznica Fm.	Western Tatra Mts.	marl	49.2683850 N, 19.8529691 E	AMS, AARM, k/T, IRM+comp., hys+IRMbf, MS, LOW, GC-MS, VR, TOC&TS&CC
2	Lejowa Valley	Mz8; M: 6; OM: 1	Mraznica Fm.	Western Tatra Mts.	marl	49.2723617 N, 19.8489851 E	AMS, AARM, k/T, IRM+comp., hys+IRMbf, MS, LOW, GC-MS, VR, TOC&TS&CC
3	Kryta Valley	Mz9; M: 6; OM: 1	Mraznica Fm.	Western Tatra Mts.	marly limestone	49.2625374 N, 19.8031314 E	AMS, AARM, k/T, IRM+comp., hys+IRMbf, MS, LOW, GC-MS, VR, TOC&TS&CC
4	Wielka Sucha Dolina Valley	Mz10; M: 7; OM: 1	Mraznica Fm.	Western Tatra Mts.	marly limestone	49.2652065 N, 19.8274639 E	AMS, AARM, k/T, IRM+comp., hys+IRMbf, MS, LOW, GC-MS, VR, TOC&TS&CC
5	Długa Valley	Mz11; M: 7; OM: 1	Mraznica Fm.	Western Tatra Mts.	marly limestone	49.2600380 N, 19.7919426 E	AMS, AARM, k/T, IRM+comp., hys+IRMbf, MS, LOW, GC-MS, VR, TOC&TS&CC
6	Wściekły Żleb Gully	Mz 12; M: 7; OM: 1	Mraznica Fm.	Western Tatra Mts.	marl	49.2659777 N, 19.8607750 E	AMS, AARM, k/T, IRM+comp., hys+IRMbf, MS, LOW, GC-MS, VR, TOC&TS&CC
7	Wielka Sucha Dolina Valley	Mz13	Mraznica Fm.	Western Tatra Mts.	limestone	49.2667083 N, 19.8267128 E	GC-MS, VR, TOC&TS&CC
8	Kryta Dolina Valley	KRY_MZ_1A-KRY_MZ_1B	Mraznica Fm.	Western Tatra Mts.	marly limestone	49.2617147 N, 19.8050303 E	GC-MS, TOC&TS&CC
9	Broniarski Żleb Gully	MK1; M: 6; OM: 1	Mraznica Fm.	High Tatra Mts.	marly limestone	49.2831321 N, 20.0582192 E	AMS, AARM, k/T, IRM+comp., hys+IRMbf, MS, LOW, GC-MS, VR, TOC&TS&CC
10	Wojskowy Zrąb Gully	MK2; M: 6; OM: 1	Mraznica Fm.	High Tatra Mts.	limestone	49.2611200 N, 20.0797150 E	AMS, AARM, k/T, IRM+comp., hys+IRMbf, MS, LOW, GC-MS, VR, TOC&TS&CC
11	Jaworzyński Żleb Gully	MK3; M: 7; OM: 1	Mraznica Fm.	High Tatra Mts.	marly limestone	49.2823978 N, 20.0755851 E	AMS, AARM, k/T, IRM+comp., hys+IRMbf, MS, LOW, GC-MS, VR, TOC&TS&CC
12	Medzisteny Valley	BM1; M: 7; OM: 1	Mraznica Fm.	Belianske Tatra Mts.	limestone	49.2619703 N, 20.1552051 E	AMS, AARM, k/T, IRM+comp., hys+IRMbf, MS, LOW, GC-MS, VR, TOC&TS&CC
13	Dolina Bieleho Potoka Valley	BM2; M: 7; OM: 1	Mraznica Fm.	Belianske Tatra Mts.	marly limestone	49.2606628 N, 20.2146249 E	AMS, AARM, k/T, IRM+comp., hys+IRMbf, MS, LOW, GC-MS, VR, TOC&TS&CC
14	Suchá Valley	BM3; M: 7; OM: 1	Mraznica Fm.	Belianske Tatra Mts.	marly limestone	49.2354268 N, 20.2919811 E	AMS, AARM, k/T, IRM+comp., hys+IRMbf, MS, LOW, GC-MS, VR, TOC&TS&CC
15	Tokarenský Potok stream	BM4; M: 5; OM: 1	Mraznica Fm.	Belianske Tatra Mts.	marly limestone	49.2441539 N, 20.2551824 E	AMS, AARM, k/T, IRM+comp., hys+IRMbf, MS, LOW, GC-MS, VR, TOC&TS&CC
16	Lúčky village	CH1; M: 4	Mraznica Fm.	Choč Mts.	limestone	49.1544444 N, 19.3730000 E	MS
17	Magura hill	CH2; M: 7; OM: 1	Mraznica Fm.	Choč Mts.	marly limestone	49.1443333 N, 19.3939444 E	MS, GC-MS, VR, TOC&TS&CC
18	Sestrč Valley	CH3; M: 7; OM: 1	Mraznica Fm.	Choč Mts.	marly limestone	49.1466519 N, 19.4406308 E	MS, GC-MS, VR, TOC&TS&CC
19	Sestrč Valley	CH4; M: 6; OM: 1	Mraznica Fm.	Choč Mts.	marly limestone	49.1637222 N, 19.4319444 E	MS, GC-MS, VR, TOC&TS&CC
20	Hulín hill	CH5; M: 7; OM: 1	Mraznica Fm.	Choč Mts.	marly limestone	49.1280556 N, 19.2947778 E	MS, GC-MS, VR, TOC&TS&CC
21	Bukov hill	CH6; M: 5	Mraznica Fm.	Choč Mts.	limestone	49.1457100 N, 19.3555961 E	MS
22	Oravský Biely Potok village	1_Bi	Biely Potok Fm.	Orava	sandstone	49.2895447 N, 19.5591256 E	GC-MS, TOC&TS&CC, VR, PyF, ICP-MS
23	Chochołów	2_Bi-3_Bi	Biely Potok Fm.	Orava	sandstone	49.3524667 N, 19.8257369 E	GC-MS, TOC&TS&CC, VR, PyF, FR, ICP-MS
24	Čierny Potok stream	4_Bi-5_Bi	Biely Potok Fm.	Orava	sandstone	49.3205297 N, 19.7401319 E	GC-MS, TOC&TS&CC, RE, PyF, FR, ICP-MS
25	Jelešňa stream	6_Bi-7_Bi	Biely Potok Fm.	Orava	mudstone	49.3416038 N, 19.7715595 E	GC-MS, TOC&TS&CC, RE, ICP-MS
26	Krivský Potok stream	8_Bi	Biely Potok Fm.	Orava	mudstone	49.2725067 N, 19.5151614 E	GC-MS, TOC&TS&CC, VR, PyF, FR, ICP-MS
27	Zábiedovo village	9_Bi-10_Bi	Biely Potok Fm.	Orava	mudstone	49.3237981 N, 19.6070806 E	GC-MS, TOC&TS&CC, RE, VR, PyF, ICP-MS
28	Studený Potok stream	11_Bi	Biely Potok Fm.	Orava	sandstone	49.2897486 N, 19.5806603 E	GC-MS, TOC&TS&CC, PyF, ICP-MS
29	Blatná Valley	12_Zu-13_Zu	Zuberec Fm.	Orava	mudstone	49.2739610 N, 19.6569169 E	GC-MS, TOC&TS&CC, VR, PyF, ICP-MS, RE
30	Chlebnice village	15_Zu-16_Zu	Zuberec Fm.	Orava	sandstone	49.2281656 N, 19.4742700 E	GC-MS, TOC&TS&CC, VR, PyF, ICP-MS, RE
31	Jelešňa stream	17_Zu-19_Zu	Zuberec Fm.	Orava	sandstone	49.3482398 N, 19.7735595 E	GC-MS, TOC&TS&CC, VR, PyF, ICP-MS, RE
32	Jelešňa stream	20_Zu	Zuberec Fm.	Orava	mudstone	49.3450281 N, 19.7728728 E	GC-MS, TOC&TS&CC, VR, PyF, ICP-MS, FR
33	Krivský Potok stream	21_Zu-22_Zu	Zuberec Fm.	Orava	black shale	49.2743092 N, 19.5000068 E	GC-MS, TOC&TS&CC, VR, PyF, ICP-MS, FR
34	Malatiná	23_Zu	Zuberec Fm.	Orava	sandstone	49.1882962 N, 19.4231115 E	GC-MS, TOC&TS&CC, PyF, ICP-MS
35	Oravice village	24_Zu-27_Zu	Zuberec Fm.	Orava	black shale	49.3034008 N, 19.7482106 E	GC-MS, TOC&TS&CC, PyF, ICP-MS
36	Oravice village	28_Zu-32_Zu	Zuberec Fm.	Orava	black shale	49.3034008 N, 19.7482106 E	GC-MS, TOC&TS&CC, PyF, ICP-MS, VR
37	Oravica river	33_Zu-34_Zu	Zuberec Fm.	Orava	black shale	49.3178235 N, 19.7462642 E	GC-MS, TOC&TS&CC, PyF, ICP-MS, RE

38	Brezovica village	35_Zu-36_Zu	Zuberec Fm.	Orava	black shale	49.3442772 N, 19.6477197 E	GC-MS, TOC&TS&CC, PyF, ICP-MS, RE, VR, FR
39	Vitanová village	37_Zu	Zuberec Fm.	Orava	black shale	49.3564383 N, 19.7224356 E	GC-MS, TOC&TS&CC, PyF, ICP-MS, RE, FR
40	Medzibrodie nad Oravou	38_Zu	Zuberec Fm.	Orava	black shale	49.2272756 N, 19.3437533 E	GC-MS, TOC&TS&CC, ICP-MS, RE, VR
41	Podbiel	39_Zu-40_Zu	Zuberec Fm.	Orava	black shale	49.2935694 N, 19.5075614 E	GC-MS, TOC&TS&CC, PyF, ICP-MS, RE, FR, VR
42	Pokryváč	41_Zu-45_Zu	Zuberec Fm.	Orava	black shale/coal	49.2079783 N, 19.3906433 E	GC-MS, TOC&TS&CC, PyF, ICP-MS, RE, VR
43	Pribiš	46_Zu	Zuberec Fm.	Orava	mudstone	49.2311251N, 19.4003636 E	GC-MS, TOC&TS&CC, PyF, ICP-MS, RE, VR
44	Pribiš	47_Zu-49_Zu	Zuberec Fm.	Orava	black shale/coal/sandstone	49.2119687 N, 19.4052959 E	GC-MS, TOC&TS&CC, PyF, ICP-MS, RE, VR
45	Pucov	50_Zu-51_Zu	Zuberec Fm.	Orava	mudstone	49.2225997 N, 19.3679462 E	GC-MS, TOC&TS&CC, ICP-MS, VR
46	Oravice	52_Zu-55_Zu	Zuberec Fm.	Orava	black shale	49.3023059 N, 19.7488649 E	GC-MS, TOC&TS&CC, ICP-MS
47	Tvrdošín	56_Zu-57_Zu	Zuberec Fm.	Orava	black shale	49.3051233 N, 19.5205008 E	GC-MS, TOC&TS&CC, PyF, ICP-MS, RE, FR, VR
48	Žaškov	58_Zu	Zuberec Fm.	Orava	sandstone	49.1710747 N, 19.2096264 E	GC-MS, TOC&TS&CC, PyF, ICP-MS, RE, VR
49	Antałowski Potok	59_Ht-61_Ht	Huty Fm.	Podhale	black shale	49.2917233 N, 19.8629594 E	GC-MS, TOC&TS&CC, PyF, ICP-MS, RE, VR
50	Bystrá stream	62_Ht-63_Ht	Huty Fm.	Orava	mudstone	49.2906403 N, 19.7372425 E	GC-MS, TOC&TS&CC, PyF, ICP-MS, RE, VR
51	Kvačianka stream	CH10; M: 5; OM: 1 (64_Ht)	Huty Fm.	Orava	mudstone	49.2135081 N, 19.5556519 E	MS, GC-MS, VR, TOC&TS&CC, RE, VR, ICP-MS
52	Lomné hill	CH11; M: 4; OM: 1 (65_Ht)	Huty Fm.	Orava	sandstone	49.1793089 N, 19.4685319 E	MS, GC-MS, VR, TOC&TS&CC, ICP-MS
53	Huty village	CH8; M: 5; OM: 1 (66_Ht)	Huty Fm.	Orava	mudstone	49.2092600 N, 19.5488889 E	MS, GC-MS, VR, TOC&TS&CC, RE, PyF, ICP-MS
54	Ráztocký stream	CH9; M: 5; OM: 1 (67_Ht)	Huty Fm.	Orava	mudstone	49.2046400 N, 19.5300931 E	MS, GC-MS, VR, TOC&TS&CC, RE, PyF, ICP-MS
55	Jasenová	77_Ht	Huty Fm.	Orava	black shale	49.1706062 N, 19.2958838 E	GC-MS, TOC&TS&CC, RE, ICP-MS
56	Huty village	79_Ht-81_Ht	Huty Fm.	Orava	black shale	49.2127750 N, 19.5556561 E	GC-MS, TOC&TS&CC, RE, VR, PyF, ICP-MS
57	Huty village	82_Ht	Huty Fm.	Orava	black shale	49.2157467 N, 19.5599689 E	GC-MS, TOC&TS&CC, RE, VR, PyF, ICP-MS
58	Huty village	83_Ht	Huty Fm.	Orava	black shale	49.2146533 N, 19.5738736 E	GC-MS, TOC&TS&CC, RE, VR, PyF, ICP-MS
59	Vyšny Kubín	84_Ht-85_Ht	Huty Fm.	Orava	sandstone/coal	49.1820288 N, 19.3424839 E	GC-MS, TOC&TS&CC, RE, VR, PyF, ICP-MS
60	Molkówka meadow	Ht13	Huty Fm.	Western Tatra Mts.	shale	49.2795315 N, 19.8308848 E	GC-MS, TOC&TS&CC, RE, ICP-MS
61	Siwa Woda stream	M: 9 (Ht14); OM: 1 (71_Ht)	Huty Fm.	Western Tatra Mts.	black shale	49.2833529 N, 19.8372670 E	AMS, AARM, k/T, IRM+comp., hys+IRMbf, MS, LOW, GC-MS, VR, TOC&TS&CC, PyF, RE, ICP-MS
62	Molkówka meadow	M: 6 (Ht15); OM: 1 (72_Ht)	Huty Fm.	Western Tatra Mts.	black shale	49.2812580 N, 19.8240323 E	AMS, AARM, k/T, IRM+comp., hys+IRMbf, MS, LOW, GC-MS, VR, TOC&TS&CC, PyF, RE, ICP-MS
63	Kirowa Woda stream	M: 6 (Ht12); OM: 1 (68_Ht)	Huty Fm.	Western Tatra Mts.	mudstone	49.2893128 N 19.8532217 E	AMS, AARM, k/T, IRM+comp., hys+IRMbf, MS, LOW, GC-MS, VR, TOC&TS&CC, PyF, RE, ICP-MS
64	Droga pod Reglami-Jaroniec	76_Ht	Huty Fm.	Western Tatra Mts.	black shale	49.2791775 N, 19.8587803 E	GC-MS, TOC&TS&CC, RE, VR, ICP-MS
65	Głęboki Potok stream	M: 8 (Ht10); OM: 1 (69_Ht)	Huty Fm.	Podhale	black shale	49.3021375 N, 19.8722247 E	AMS, AARM, k/T, IRM+comp., hys+IRMbf, MS, LOW, GC-MS, VR, TOC&TS&CC, PyF, RE, ICP-MS
66	Antałowski Potok stream	M: 6 (Ht5); OM: 3 (73_Ht-75_Ht)	Huty Fm.	Podhale	sandstone	49.2921908 N, 19.8566775 E	AMS, AARM, k/T, IRM+comp., hys+IRMbf, ICP-MS, MS, LOW, GC-MS, VR, TOC&TS&CC, PyF, RE
67	Antałowski Potok stream	ANTPO	Huty Fm.	Podhale	mudstone	49.2895439 N, 19.8681869 E	GC-MS
68	Groń village	GR_ZU_1B-GR_ZU_1C	Huty Fm.	Podhale	mudstone	49.3559795 N, 20.0695022 E	GC-MS, RE
69	Groń village	GR_ZU_2B	Huty Fm.	Podhale	mudstone	49.3723175 N, 20.0652909 E	GC-MS, RE
70	Bachledzki Wierch hill	Ht11; M: 6; OM: 1	Huty Fm.	Podhale	silty sandstone	49.2987386 N, 19.9724381 E	AMS, AARM, k/T, IRM+comp., hys+IRMbf, MS, LOW, GC-MS, VR, TOC&TS&CC
71	Bachledzki Potok stream	Ht7; M: 5; OM:1	Huty Fm.	Podhale	mudstone	49.3036672 N, 19.9678622 E	AMS, AARM, k/T, IRM+comp., hys+IRMbf, MS, LOW, GC-MS, VR, TOC&TS&CC
72	Trybsz stream	Ht9	Huty Fm.	Podhale	mudstone	49.4030078 N, 20.1342183 E	GC-MS, RE
73	Kacwinianka stream	KAC1	Huty Fm.	Podhale	mudstone	49.3842461 N, 20.2875753 E	GC-MS
74	Łapszanka stream	LAP1	Huty Fm.	Podhale	mudstone	49.3620436 N, 20.1835067 E	GC-MS
75	Mały Rogoźnik stream	MARO1	Huty Fm.	Podhale	mudstone	49.3919875 N, 19.9447908 E	TOC&TS&CC, GC-MS
76	Mały Rogoźnik stream	MARO2	Huty Fm.	Podhale	mudstone	49.4115086 N, 19.9798956 E	TOC&TS&CC, GC-MS
77	Sucha Woda Gąsienicowa stream	ZA1; M: 7; OM: 1	Huty Fm.	High Tatra Mts.	black shale	49.2881000 N, 20.0568650 E	AMS, AARM, k/T, IRM+comp., hys+IRMbf, MS, LOW, GC-MS, VR, TOC&TS&CC
78	Zazadnia forester's lodge	ZA2; M: 10; OM: 1	Huty Fm.	High Tatra Mts.	black shale	49.2845138 N, 20.0829667 E	AMS, AARM, k/T, IRM+comp., hys+IRMbf, MS, LOW, GC-MS, VR, TOC&TS&CC

77

No	Location	Sample code	Formation	Region	Lithology	Coordinates	Methods
79	Białka river	ZA3; M: 7; OM: 1	Huty Fm.	High Tatra Mts.	black shale	49.2800444 N, 20.1283947 E	AMS, AARM, k/T, IRM+comp., hys+IRMbf, MS, LOW, GC-MS, VR, TOC&TS&CC
80	Dolina Filipka Valley	ZA4; M: 8; OM: 1	Huty Fm.	High Tatra Mts.	black shale	49.2764134 N, 20.0904376 E	AMS, AARM, k/T, IRM+comp., hys+IRMbf, MS, LOW, GC-MS, VR, TOC&TS&CC
81	Filipczański Potok stream	ZA5; M: 9; OM: 1	Huty Fm.	High Tatra Mts.	black shale	49.2923139 N, 20.0820428 E	AMS, AARM, k/T, IRM+comp., hys+IRMbf, MS, LOW, GC-MS, VR, TOC&TS&CC
82	Dolina Bieleho Potoka Valley	BH1; M: 7; OM: 2	Huty Fm.	Belianske Tatra Mts.	mudstone	49.2683631 N, 20.2284592 E	AMS, AARM, k/T, IRM+comp., hys+IRMbf, MS, LOW, GC-MS, VR, TOC&TS&CC
83	Javorinka stream	BH2; M: 7; OM: 1	Huty Fm.	Belianske Tatra Mts.	mudstone	49.2795911 N, 20.1769178 E	AMS, AARM, k/T, IRM+comp., hys+IRMbf, MS, LOW, GC-MS, VR, TOC&TS&CC
84	Ždiar village	BH3; M: 8; OM: 2	Huty Fm.	Belianske Tatra Mts.	mudstone	49.2697389 N, 20.2655328 E	AMS, AARM, k/T, IRM+comp., hys+IRMbf, MS, LOW, GC-MS, VR, TOC&TS&CC
85	Bachledova Dolina Valley	BH4; M: 8; OM: 2	Huty Fm.	Belianske Tatra Mts.	mudstone	49.2689161 N, 20.3071444 E	AMS, AARM, k/T, IRM+comp., hys+IRMbf, MS, LOW, GC-MS, VR, TOC&TS&CC
86	Lendak stream	M: 5 (BH5); OM:2 (Len_Ht_1A-Len_Ht_1B)	Huty Fm.	Belianske Tatra Mts.	mudstone	49.2479699 N, 20.3419734 E	AMS, AARM, k/T, IRM+comp., hys+IRMbf, MS, LOW, GC-MS, VR, TOC&TS&CC
87	Haligovce village	Hg_Ht_1A	Huty Fm.	Spisz	mudstone	49.3443611 N, 20.4416389 E	GC-MS, TOC&TS&CC, RE
88	Haligovce village	Hg_Ht_2A-Hg_Ht_2B	Huty Fm.	Spisz	mudstone	49.3315278 N, 20.4370833 E	GC-MS, TOC&TS&CC, RE
89	Jezersko village	Jz_Ht_1A	Huty Fm.	Spisz	mudstone	49.2990833 N, 20.3356944 E	GC-MS,TOC&TS&CC, RE, VR
90	Jezersko village	Jz_Ht_2A-Jz_Ht_2C	Huty Fm.	Spisz	mudstone	49.3100833 N, 20.3643333 E	GC-MS, TOC&TS&CC, RE
91	Lechnica village	Lch_Ht_1A-Lch_Ht_1B	Huty Fm.	Spisz	mudstone	49.3805833 N, 20.4078333 E	GC-MS, TOC&TS&CC, RE
92	Lysá nad Dunajcom village	Ly_Ht_1A-Ly_Ht_1B	Huty Fm.	Spisz	mudstone	49.3976944 N, 20.33013889 E	GC-MS, TOC&TS&CC, RE
93	Rieka stream	Rie_Ht_1A	Huty Fm.	Spisz	mudstone	49.3471408 N, 20.6086459 E	GC-MS, TOC&TS&CC, RE, VR
94	Stráňany village	Sn_Ht_1B-Sn_Ht_1C	Huty Fm.	Spisz	mudstone	49.3681944 N, 20.5326389 E	GC-MS, TOC&TS&CC, RE
95	Slovenský Potok stream	Sv_Ht_1A-Sv_Ht_1B	Huty Fm.	Spisz	mudstone	49.2587778 N, 20.4046667 E	GC-MS, TOC&TS&CC, RE
96	Toporec village	Top_Ht_1a	Huty Fm.	Spisz	mudstone	49.2810526 N, 49.2810526 E	GC-MS, TOC&TS&CC, VR
97	Vyšné Ružbachy village	Vr_Ht_1A, Vr_Ht_1C	Huty Fm.	Spisz	mudstone	49.3165975 N, 20.5633272 E	GC-MS, TOC&TS&CC, RE
98	Ždiar village	Zdi_Ht_1A	Huty Fm.	Spisz	mudstone	49.2699819 N, 20.2687192 E	GC-MS, TOC&TS&CC, VR
99	Havka village	Hv_Zu_1C-Hv_Zu_1D	Zuberec Fm.	Spisz	mudstone	49.3640833 N, 20.3802222 E	GC-MS, TOC&TS&CC, RE
100	Havka village	Hv_Zu_2A, Hv_Zu_2D	Zuberec Fm.	Spisz	mudstone	49.3442222 N, 20.4039167 E	GC-MS, TOC&TS&CC, RE
101	Lechnica village	Lch_Zu_2A, Lch_Zu_2D	Zuberec Fm.	Spisz	mudstone	49.376951 N, 20.407869 E	GC-MS, TOC&TS&CC, RE
102	Lendak stream	Len_Zu_2A-Len_Zu_2B	Zuberec Fm.	Spisz	mudstone	49.2441956 N, 20.3448040 E	GC-MS, TOC&TS&CC, RE, VR
103	Modrinok stream	Md_Zu_1D	Zuberec Fm.	Spisz	sandstone	49.2906278 N, 20.5851574 E	GC-MS, TOC&TS&CC, RE
104	Malá Franková village	Mf_Zu_1A, Mf_Zu_1D	Zuberec Fm.	Spisz	mudstone	49.3103056 N, 20.3004722 E	GC-MS, TOC&TS&CC, RE, VR
105	Matiašovce village	Mt_Zu_1A, Mt_Zu_1C-Mt_Zu_1D	Zuberec Fm.	Spisz	mudstone	49.3623056 N, 20.3582222 E	GC-MS, TOC&TS&CC
106	Osturňa village	Os_Zu_1A-Os_Zu_1B	Zuberec Fm.	Spisz	mudstone	49.3220278 N, 20.2309444 E	GC-MS, TOC&TS&CC, RE
107	Osturňa village	Os_Zu_2A	Zuberec Fm.	Spisz	mudstone	49.3284722 N, 20.1962222 E	GC-MS, TOC&TS&CC, RE
108	Osturňa village	Os_Zu_3A-Os_Zu_3B	Zuberec Fm.	Spisz	mudstone	49.33525 N, 20.27325 E	GC-MS, TOC&TS&CC, RE
109	Slovenská Ves village	Slo_Zu_1A-Slo_Zu_1B	Zuberec Fm.	Spisz	mudstone	49.2307249 N, 20.4259603 E	GC-MS, TOC&TS&CC, RE, VR
110	Toporec village	TOP_Zu_2A	Zuberec Fm.	Spisz	mudstone	49.2688461 N, 20.4876889 E	GC-MS, TOC&TS&CC, RE, VR
111	Toporec village	Topr_Zu_1A	Zuberec Fm.	Spisz	sandstone	49.2484406 N, 20.5083819 E	GC-MS, TOC&TS&CC, RE, VR
112	Veľká Franková village	Vf_Zu_1A	Zuberec Fm.	Spisz	mudstone	49.3311944 N, 20.3149167 E	GC-MS, TOC&TS&CC, RE
113	Tichý Potok stream	Ti_Bp_1A-Ti_Bp_1B	Biely Potok Fm.	Levoča Basin & Šariš Upland	sandstone	49.1401994 N, 20.7989481 E	GC-MS, TOC&TS&CC, RE
114	Chminianska Nová Ves village	Cnv_Zu_1A	Zuberec Fm.	Levoča Basin & Šariš Upland	weathered sandstone	49.0050147 N, 21.0900716 E	GC-MS, TOC&TS&CC
115	Fričovce village	Fi_Zu_1A	Zuberec Fm.	Levoča Basin & Šariš Upland	weathered sandstone	49.0183953 N, 20.9738602 E	GC-MS, TOC&TS&CC
116	Hermanovce village	He_Zu_1A	Zuberec Fm.	Levoča Basin & Šariš Upland	weathered sandstone	49.0263330 N, 21.020657 E	GC-MS, TOC&TS&CC
117	Hendrichovce village	Hn_Zu_1A	Zuberec Fm.	Levoča Basin & Šariš Upland	weathered sandstone	49.0250522 N, 20.9912376 E	GC-MS, TOC&TS&CC
118	Malá Svinka stream	Ms_Zu_1A	Zuberec Fm.	Levoča Basin & Šariš Upland	weathered sandstone	49.0518802 N, 21.0837281 E	GC-MS, TOC&TS&CC
119	Lačnov village	Lac_Zu_1A	Zuberec Fm.	Levoča Basin & Šariš Upland	mudstone	49.0718181 N, 20.9234526 E	GC-MS, TOC&TS&CC
120	Lipovce village	Lip_Zu_1A	Zuberec Fm.	Levoča Basin & Šariš Upland	mudstone	49.0624402 N, 20.9520969 E	GC-MS, TOC&TS&CC, RE

121	Plavnica village	Pla_Zu_1C	Zuberec Fm.	Levoča Basin & Šariš Upland	sandstone	49.2714388 N, 20.7775576 E	GC-MS, TOC&TS&CC, RE
122	Stará Ľubovňa town	Sl_Zu_1A-Sl_Zu_1B	Zuberec Fm.	Levoča Basin & Šariš Upland	sandstone	49.300833 N, 20.702222 E	GC-MS, TOC&TS&CC
123	Bajerovce village	Baj_Ht_1A, Baj_Ht_1C-Baj_Ht_1D	Huty Fm.	Levoča Basin & Šariš Upland	mudstone	49.2119208 N, 20.7950319 E	GC-MS, TOC&TS&CC, RE
124	Brezovica village	Bre_Ht_1A	Huty Fm.	Levoča Basin & Šariš Upland	mudstone	49.1377708 N, 20.83008163 E	GC-MS, TOC&TS&CC
125	Červená Voda village	Cv_Ht_1A-Cv_Ht_1B	Huty Fm.	Levoča Basin & Šariš Upland	mudstone	49.1406510 N, 21.0869262 E	GC-MS, TOC&TS&CC, RE
126	Ďačov village	Da_Ht_1B	Huty Fm.	Levoča Basin & Šariš Upland	mudstone	49.1446478 N, 20.9198484 E	GC-MS, TOC&TS&CC, RE
127	Dubovica village	Dub_Ht_1A	Huty Fm.	Levoča Basin & Šariš Upland	mudstone	49.1200249 N, 20.9400288 E	GC-MS, TOC&TS&CC
128	Gregorovce village	Gre_Ht_1A-Gre_Ht_1B	Huty Fm.	Levoča Basin & Šariš Upland	mudstone	49.0681450 N, 21.1980117 E	GC-MS, TOC&TS&CC, RE, VR
129	Jakubianka stream	Ja_Ht_1A	Huty Fm.	Levoča Basin & Šariš Upland	mudstone	49.2602617 N, 20.6847088 E	GC-MS, TOC&TS&CC
130	Jakubovany village	Jbv_Ht_1A-Jbv_Ht_1C	Huty Fm.	Levoča Basin & Šariš Upland	mudstone	49.11315813 N, 21.1461154 E	GC-MS, TOC&TS&CC, RE
131	Jakubova Voľa village	Jv_Ht_1B	Huty Fm.	Levoča Basin & Šariš Upland	mudstone	49.1280243 N, 21.0169421 E	GC-MS, TOC&TS&CC, RE
132	Kamenica village	Kam_Ht_1B	Huty Fm.	Levoča Basin & Šariš Upland	mudstone	49.1840956 N, 20.9508217 E	GC-MS, TOC&TS&CC
133	Krivany village	Krv_Ht_1A	Huty Fm.	Levoča Basin & Šariš Upland	mudstone	49.161111 N, 20.939444 E	GC-MS, TOC&TS&CC
134	Ľubovnianske kúpele	Lk_Ht_1A-Lk_Ht_1B	Huty Fm.	Levoča Basin & Šariš Upland	mudstone	49.276944 N, 20.741111 E	GC-MS, TOC&TS&CC, RE
135	Lúčka village	Lu_Ht_1B, Lu_Ht_1E	Huty Fm.	Levoča Basin & Šariš Upland	mudstone	49.1779882 N, 20.9796123 E	GC-MS, TOC&TS&CC, RE
136	Nová Ľubovňa village	Nl_Ht_1A-Nl_Ht_1B	Huty Fm.	Levoča Basin & Šariš Upland	mudstone	49.2750036 N, 20.6793858 E	GC-MS, TOC&TS&CC, RE
137	Ratvaj village	Ra_Ht_1A	Huty Fm.	Levoča Basin & Šariš Upland	mudstone	49.1167803 N, 21.2062194 E	GC-MS, TOC&TS&CC, RE, VR
138	Sabinov town	Sab_Ht_1B	Huty Fm.	Levoča Basin & Šariš Upland	mudstone	49.0959513 N, 21.1105170 E	GC-MS, TOC&TS&CC, RE
139	Šambron village	Sam_Bp_1A-Sam_Bp_1B	Huty Fm.	Levoča Basin & Šariš Upland	mudstone	49.254444 N, 20.757778 E	GC-MS, TOC&TS&CC, RE
140	Šambron village	Sam_Ht_2A, Sam_Ht_2C	Huty Fm.	Levoča Basin & Šariš Upland	mudstone	49.23196 N, 20.75126 E	GC-MS, TOC&TS&CC, RE
141	Šarišské Dravce village	Sar_Ht_1A-Sar_Ht_1C	Huty Fm.	Levoča Basin & Šariš Upland	mudstone	49.177778 N, 20.859722 E	GC-MS, TOC&TS&CC, RE
142	Šariš Park recreation center	Sp_Ht_1A-Sp_Ht_1B	Huty Fm.	Levoča Basin & Šariš Upland	mudstone	49.0410045 N, 21.2142301 E	GC-MS, TOC&TS&CC, RE, VR
143	Uzovský Šalgov village	Us_Ht_1A	Huty Fm.	Levoča Basin & Šariš Upland	mudstone	49.0944668 N, 21.0506788 E	GC-MS, TOC&TS&CC, RE
144	116 m	CH2	Zuberec Fm.	Chochołów PIG-1 borehole	mudstone	49.3511278 N, 19.8227583 E	TOC&TS&CC; GC-MS; RE
145	193 m	CH193/14_Zu	Zuberec Fm.	Chochołów PIG-1 borehole	mudstone	49.3511278 N, 19.8227583 E	TOC&TS&CC; GC-MS;
146	280 m	CH280	Zuberec Fm.	Chochołów PIG-1 borehole	mudstone	49.3511278 N, 19.8227583 E	TOC&TS&CC; GC-MS;
147	436 m	CH11	Zuberec Fm.	Chochołów PIG-1 borehole	mudstone	49.3511278 N, 19.8227583 E	TOC&TS&CC; GC-MS; RE
148	513 m	CH513	Huty Fm.	Chochołów PIG-1 borehole	mudstone	49.3511278 N, 19.8227583 E	GC-MS
149	593 m	CH593	Huty Fm.	Chochołów PIG-1 borehole	mudstone	49.3511278 N, 19.8227583 E	TOC&TS&CC; GC-MS
150	666 m	CH17	Huty Fm.	Chochołów PIG-1 borehole	mudstone	49.3511278 N, 19.8227583 E	TOC&TS&CC; GC-MS; RE
151	735 m	CH18	Huty Fm.	Chochołów PIG-1 borehole	mudstone	49.3511278 N, 19.8227583 E	TOC&TS&CC; GC-MS; RE
152	820 m	CH820	Huty Fm.	Chochołów PIG-1 borehole	mudstone	49.3511278 N, 19.8227583 E	GC-MS
153	964 m	CH21	Huty Fm.	Chochołów PIG-1 borehole	mudstone	49.3511278 N, 19.8227583 E	TOC&TS&CC; GC-MS; RE
154	1283 m	CH29	Huty Fm.	Chochołów PIG-1 borehole	mudstone	49.3511278 N, 19.8227583 E	TOC&TS&CC; GC-MS; RE
155	1364 m	CH30	Huty Fm.	Chochołów PIG-1 borehole	mudstone	49.3511278 N, 19.8227583 E	TOC&TS&CC; GC-MS; RE
156	1425 m	CH32	Huty Fm.	Chochołów PIG-1 borehole	mudstone	49.3511278 N, 19.8227583 E	TOC&TS&CC; GC-MS; RE
157	1503 m	CH35	Huty Fm.	Chochołów PIG-1 borehole	mudstone	49.3511278 N, 19.8227583 E	TOC&TS&CC; GC-MS; RE
158	1580 m	CH36	Huty Fm.	Chochołów PIG-1 borehole	mudstone	49.3511278 N, 19.8227583 E	TOC&TS&CC; GC-MS; RE
159	1671 m	CH1671	Huty Fm.	Chochołów PIG-1 borehole	mudstone	49.3511278 N, 19.8227583 E	GC-MS
160	1757 m	CH39	Huty Fm.	Chochołów PIG-1 borehole	mudstone	49.3511278 N, 19.8227583 E	TOC&TS&CC; GC-MS; RE
161	1953 m	CH43	Huty Fm.	Chochołów PIG-1 borehole	mudstone	49.3511278 N, 19.8227583 E	TOC&TS&CC; GC-MS; RE
162	2011 m	CH2011	Huty Fm.	Chochołów PIG-1 borehole	mudstone	49.3511278 N, 19.8227583 E	TOC&TS&CC; GC-MS
163	2075 m	CH2075	Huty Fm.	Chochołów PIG-1 borehole	mudstone	49.3511278 N, 19.8227583 E	TOC&TS&CC; GC-MS; RE
164	2127 m	CH48	Huty Fm.	Chochołów PIG-1 borehole	mudstone	49.3511278 N, 19.8227583 E	TOC&TS&CC; GC-MS; RE
165	2214 m	CH49	Huty Fm.	Chochołów PIG-1 borehole	mudstone	49.3511278 N, 19.8227583 E	TOC&TS&CC; GC-MS; RE
166	2264 m	CH52	Huty Fm.	Chochołów PIG-1 borehole	mudstone	49.3511278 N, 19.8227583 E	TOC&TS&CC; GC-MS; RE
167	2410 m	CH2410	Huty Fm.	Chochołów PIG-1 borehole	mudstone	49.3511278 N, 19.8227583 E	TOC&TS&CC; GC-MS

168	2511 m	CH2511	Huty Fm.	Chochołów PIG-1 borehole	mudstone	49.3511278 N, 19.8227583 E	GC-MS
169	2578 m	CH58	Huty Fm.	Chochołów PIG-1 borehole	mudstone	49.3511278 N, 19.8227583 E	TOC&TS&CC; GC-MS; RE
170	2757 m	CH63	Huty Fm.	Chochołów PIG-1 borehole	mudstone	49.3511278 N, 19.8227583 E	TOC&TS&CC; GC-MS
171	2859 m	CH65	Huty Fm.	Chochołów PIG-1 borehole	mudstone	49.3511278 N, 19.8227583 E	TOC&TS&CC; GC-MS; RE
172	2900 m	CH2900	Huty Fm.	Chochołów PIG-1 borehole	mudstone	49.3511278 N, 19.8227583 E	GC-MS
173	102 m	BKT102	Zuberec Fm.	Bukowina Tatrzańska PIG-1/GN borehole	mudstone	49.3295917 N, 20.1009000 E	GC-MS
174	294 m	BKT294	Zuberec Fm.	Bukowina Tatrzańska PIG-1/GN borehole	mudstone	49.3295917 N, 20.1009000 E	TOC&TS&CC; GC-MS; RE
175	504 m	BKT10	Zuberec Fm.	Bukowina Tatrzańska PIG-1/GN borehole	mudstone	49.3295917 N, 20.1009000 E	TOC&TS&CC; GC-MS; RE
176	640 m	BKT640	Huty Fm.	Bukowina Tatrzańska PIG-1/GN borehole	mudstone	49.3295917 N, 20.1009000 E	TOC&TS&CC; GC-MS; RE
177	699 m	BKT14	Huty Fm.	Bukowina Tatrzańska PIG-1/GN borehole	mudstone	49.3295917 N, 20.1009000 E	TOC&TS&CC; GC-MS; RE
178	902 m	BKT902	Huty Fm.	Bukowina Tatrzańska PIG-1/GN borehole	mudstone	49.3295917 N, 20.1009000 E	TOC&TS&CC; GC-MS
179	1005 m	BKT20	Huty Fm.	Bukowina Tatrzańska PIG-1/GN borehole	mudstone	49.3295917 N, 20.1009000 E	TOC&TS&CC; GC-MS; RE
180	1141 m	BKT22	Huty Fm.	Bukowina Tatrzańska PIG-1/GN borehole	mudstone	49.3295917 N, 20.1009000 E	TOC&TS&CC; GC-MS; RE
181	1261 m	BKT1261	Huty Fm.	Bukowina Tatrzańska PIG-1/GN borehole	mudstone	49.3295917 N, 20.1009000 E	GC-MS; RE
182	1382 m	BKT25	Huty Fm.	Bukowina Tatrzańska PIG-1/GN borehole	mudstone	49.3295917 N, 20.1009000 E	TOC&TS&CC; GC-MS; RE
183	1480 m	BKT27	Huty Fm.	Bukowina Tatrzańska PIG-1/GN borehole	mudstone	49.3295917 N, 20.1009000 E	TOC&TS&CC; GC-MS; RE
184	1594 m	BKT1594	Huty Fm.	Bukowina Tatrzańska PIG-1/GN borehole	mudstone	49.3295917 N, 20.1009000 E	GC-MS; RE
185	1649 m	BKT30	Huty Fm.	Bukowina Tatrzańska PIG-1/GN borehole	mudstone	49.3295917 N, 20.1009000 E	TOC&TS&CC; GC-MS; RE
186	1782 m	BKT31	Huty Fm.	Bukowina Tatrzańska PIG-1/GN borehole	mudstone	49.3295917 N, 20.1009000 E	TOC&TS&CC; GC-MS; RE
187	1904 m	BKT35	Huty Fm.	Bukowina Tatrzańska PIG-1/GN borehole	mudstone	49.3295917 N, 20.1009000 E	TOC&TS&CC; GC-MS; RE
188	2043 m	BKT38	Huty Fm.	Bukowina Tatrzańska PIG-1/GN borehole	mudstone	49.3295917 N, 20.1009000 E	TOC&TS&CC; GC-MS; RE
189	2200 m	BKT2200	Huty Fm.	Bukowina Tatrzańska PIG-1/GN borehole	mudstone	49.3295917 N, 20.1009000 E	TOC&TS&CC; GC-MS; RE
190	300 m	PIG_FUR	Huty Fm.	Furmanowa PIG-1 borehole	mudstone	49.3219944 N, 19.9528167 E	TOC&TS&CC; GC-MS
191	505 m	PIG_PR5	Huty Fm.	Furmanowa PIG-1 borehole	mudstone	49.3219944 N, 19.9528167 E	TOC&TS&CC; GC-MS
192	1979 m	FU_PIG1_1979	Huty Fm.	Furmanowa PIG-1 borehole	conglomerate	49.3219944 N, 19.9528167 E	TOC&TS&CC; VR
193	2049 m	FU_PIG1_2049	Cretaceous-Jurassic	Furmanowa PIG-1 borehole	limestone	49.3219944 N, 19.9528167 E	TOC&TS&CC; VR
194	484 m	BAN484	Zuberec Fm.	Bańska IG-1 borehole	mudstone	49.3948417 N, 20.0185028 E	GC-MS
195	0 m	BDUN0	Huty Fm.	Biały Dunajec PAN 1 borehole	mudstone	49.3841389 N, 20.0195278 E	GC-MS
196	111 m	Z111	Huty Fm.	Zakopane IG-1 borehole	mudstone	49.2954833 N, 19.9658444 E	GC-MS

Contribution statements of the co-authors

Załącznik nr 9
do pisma okólnego nr 2
Prorektora ds. nauki i finansów
z dnia 19 lutego 2024 r.

Sosnowiec, 28.02.2025
miejscowość, data

Dorota Staneczek

imię i nazwisko kandydata

ul. Łabędzka 21, Łany Wielkie, 44-153 Sośnicowice
adres do korespondencji

+ 48 507987283
nr telefonu

dorota.staneczek@us.edu.pl
adres e-mail

OŚWIADCZENIE OSOBY UBIEGAJĄCEJ SIĘ O WŁASNYM WKŁADZIE W POWSTAWANIE PRACY

Oświadczam, że w pracy:

Staneczek, D., Więcław, D., Marynowski, L., 2024. Depositional conditions, wildfires, maturity, and hydrocarbon potential evaluation of Central Carpathian Paleogene Basin based on integrative approach from Orava Basin. International Journal of Coal Geology 285, 104490. https://doi.org/10.1016/j.coal.2024.104490

Mój udział polegał na przygotowaniu koncepcji artykułu, pobraniu próbek, prowadzeniu badań laboratoryjnych, przygotowaniu danych do analizy oraz analizie danych, przygotowaniu i edycji tekstu artykułu, przygotowaniu figur i tabel.

....
podpis

Article 1
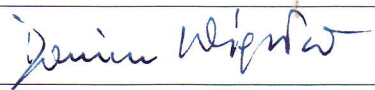
Title: Depositional conditions, wildfires, maturity, and hydrocarbon potential evaluation of Central Carpathian Paleogene Basin based on integrative approach from Orava Basin

Journal: International Journal of Coal Geology

Impact factor: 5.6

Publishing date: 2024

DOI: https://doi.org/10.1016/j.coal.2024.104490

Name and surname	Contribution [%]	Signature
Dorota Staneczek	70%	
Dariusz Więcław	10%	
Leszek Marynowski	20%	

Załącznik nr 9
do pisma okólnego nr 2
Prorektora ds. nauki i finansów
z dnia 19 lutego 2024 r.

Sosnowiec, 28.02.2025

miejscowość, data

Dorota Staneczek

imię i nazwisko kandydata

ul. Łabędzka 21, Łany Wielkie, 44-153 Sośnicowice

adres do korespondencji

+ 48 507987283

nr telefonu

dorota.staneczek@us.edu.pl

adres e-mail

OŚWIADCZENIE OSOBY UBIEGAJĄCEJ SIĘ O WŁASNYM WKŁADZIE W POWSTAWANIE PRACY

Oświadczam, że w pracy:

Staneczek, D., Szaniawski, R., Chadima, M., Marynowski, L., 2024. Multi-stage tectonic evolution of the Tatra Mts recorded in the para- and ferromagnetic fabrics. Tectonophysics 880, 230338. https://doi.org/10.1016/j.tecto.2024.230338

Mój udział polegał na przygotowaniu koncepcji artykułu, uzyskaniu zgód na prowadzenie badań w parku narodowym, pobraniu próbek i wykonaniu pomiarów terenowych, prowadzeniu badań laboratoryjnych, przygotowaniu danych do analizy oraz analizie danych, przygotowaniu i edycji tekstu artykułu, przygotowaniu figur i tabel.

....

podpis

Article 2
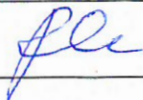
Title: Multi-stage tectonic evolution of the Tatra Mts recorded in the para-and ferromagnetic fabrics

Journal: Tectonophysics

Impact factor: 2.7

Publishing date: 2024

DOI: https://doi.org/10.1016/j.tecto.2024.230338

Name and surname	Contribution [%]	Signature
Dorota Staneczek	85%	
Rafał Szaniawski	5%	
Martin Chadima	5%	co-author not available
Leszek Marynowski	5%	

Załącznik nr 9
do pisma okólnego nr 2
Prorektora ds. nauki i finansów
z dnia 19 lutego 2024 r.

Sosnowiec, 28.02.2025
miejscowość, data

Dorota Staneczek

imię i nazwisko kandydata

ul. Łabędzka 21, Łany Wielkie, 44-153 Sośnicowice
adres do korespondencji

+ 48 507987283
nr telefonu

dorota.staneczek@us.edu.pl
adres e-mail

OŚWIADCZENIE OSOBY UBIEGAJĄCEJ SIĘ O WŁASNYM WKŁADZIE W POWSTAWANIE PRACY

Oświadczam, że w pracy:

Staneczek, D., Marynowski, L., 2025. Application of biomarker and non-biomarker parameters to assess maturity using the Central Carpathian Paleogene Basin as a case study. Organic Geochemistry 201, 104933. https://doi.org/10.1016/j.orggeochem.2025.104933

Mój udział polegał na przygotowaniu koncepcji artykułu, pobraniu próbek, prowadzeniu badań laboratoryjnych, przygotowaniu danych do analizy oraz analizie danych, przygotowaniu i edycji tekstu artykułu, przygotowaniu figur i tabel.

....
podpis

Article 3

Title: Application of biomarker and non-biomarker parameters to assess maturity using the Central Carpathian Paleogene Basin as a case study

Journal: Organic Geochemistry

Impact factor: 2.6

Publishing date: 2025

DOI: https://doi.org/10.1016/j.orggeochem.2025.104933

Name and surname	Contribution [%]	Signature
Dorota Staneczek	80%	
Leszek Marynowski	20%	

Załącznik nr 9
do pisma okólnego nr 2
Prorektora ds. nauki i finansów
z dnia 19 lutego 2024 r.

Sosnowiec, 28.02.2025

miejscowość, data

Dorota Staneczek

imię i nazwisko kandydata

ul. Łabędzka 21, Łany Wielkie, 44-153 Sośnicowice
adres do korespondencji

+ 48 507987283
nr telefonu

dorota.staneczek@us.edu.pl
adres e-mail

OŚWIADCZENIE OSOBY UBIEGAJĄCEJ SIĘ O WŁASNYM WKŁADZIE W POWSTAWANIE PRACY

Oświadczam, że w pracy:

Staneczek, D., Szaniawski, R., Marynowski, L., under review. Burial impact on the Tatra Mts from a rock magnetic and magnetic fabric perspective. Tectonics

Mój udział polegał na przygotowaniu koncepcji artykułu, uzyskaniu zgód na prowadzenie badań w parku narodowym, pobraniu próbek i wykonaniu pomiarów terenowych, prowadzeniu badań laboratoryjnych, przygotowaniu danych do analizy oraz analizie danych, przygotowaniu i edycji tekstu artykułu, przygotowaniu figur i tabel.

....

podpis

Manuscript 1

Title: Burial impact on the Tatra Mts from a rock magnetic and magnetic fabric perspective

Journal: Tectonics, in review

Name and surname	Contribution [%]	Signature
Dorota Staneczek	90%	
Rafał Szaniawski	5%	
Leszek Marynowski	5%	

Article 1

Staneczek Dorota, Więcław Dariusz, Marynowski Leszek, 2024. Depositional conditions, wildfires, maturity, and hydrocarbon potential evaluation of Central Carpathian Paleogene Basin based on integrative approach from Orava Basin. International Journal of Coal Geology 285, 104490.

Depositional conditions, wildfires, maturity, and hydrocarbon potential evaluation of Central Carpathian Paleogene Basin based on integrative approach from Orava Basin

Dorota Staneczek [a], Dariusz Więcław [b], Leszek Marynowski [a,*]

[a] Institute of Earth Sciences, Faculty of Natural Sciences, University of Silesia in Katowice, Będzińska 60, 41-200 Sosnowiec, Poland
[b] Faculty of Geology, Geophysics and Environmental Protection, AGH University of Krakow, Al. Mickiewicza 30, 30-059 Kraków, Poland

A B S T R A C T

Central Carpathian Paleogene Basin (CCPB, Central Western Carpathians) comprises mainly Oligocene clastic autochthonous age-equivalents of the widely known Menilite shale formation from the Outer Carpathians. However, little is known about the paleoenvironment and its subsequent changes during the basin's evolution. Furthermore, the available hydrocarbon potential data are based on anachronous methods and are not investigated on the sub-basin level. Gas chromatography-mass spectrometry (GC–MS) analyses supported by Rock-Eval data along with petrographic measurements enabled us to identify and document the paleoenvironmental evolution of the Orava sub-basin (NW remnant of CCPB). Thermal maturity based on vitrinite reflectance, 22S/(22S + 22R) homohopane ratio and 20S/(20S + 20R) sterane ratio increases from N to S and from Upper to Lower Oligocene. In the least mature samples ββ-hopanes, hopenes, and oleanenes are present, whereas in the most mature deposits less thermally stable compounds dissapeared. This maturation trend is shown also by the Rock-Eval data. Terrestrial organic matter input is documented by the predominance of III- and II/III-type of kerogen and the occurrence of several biomarkers, such as 3,3,7-trimethyl-1,2,3,4-tetrahydrochrysene, cadalene, retene, and perylene. The significant contribution of polycyclic aromatic hydrocarbons (PAHs) may be linked with wildfire-related land degradation and following runoff to the basin. Based on the measured fusinite reflectance values the wildfire types could range from hotter crown fires to colder surface fires. Depositional conditions in Lower Oligocene units are characterized by intermittent euxinia, as derived from small (<5 μm) pyrite framboid diameters and the presence of isorenieratane. Subsequently, a change of conditions to oxic/dysoxic in younger units is observed, and the input of terrestrial organic matter increased.

1. Introduction

The allochthonous Outer Carpathians, composed mainly of Paleogene rocks, belong to one of the largest and oldest oil provinces of Central Europe (ten Haven et al., 1993; Kotarba et al., 2007). The source rocks are considered to be the so-called Menilite shales, mostly dated to the Early Oligocene. Although the importance of these oil fields has now decreased, it is estimated that the Lower Oligocene part of the Menilite Formation could generate from 10 up to 15 t HC/m² (Popescu, 1995; Kosakowski, 2013; Sachsenhofer et al., 2018; Rauball et al., 2019). The organic matter from Menilite shales and Carpathian oils have been the subject of many studies (e.g., ten Haven et al., 1993; Kruge et al., 1996; Rospondek et al., 1997; Köster et al., 1998a; Curtis et al., 2004; Lewan et al., 2006; Kotarba et al., 2007, 2013, 2017; Kosakowski et al., 2018; Jirman et al., 2019; Waliczek et al., 2019; Więcław et al., 2020); including on their depositional conditions (Köster et al., 1998b; Sachsenhofer et al., 2015; Wendorff et al., 2017; Wendorff-Belon et al., 2021; Wójcik-Tabol et al., 2022), much less is known about the autochthonous age-equivalent, the Central Carpathian Paleogene Basin (CCPB).

The CCPB extends over an approximate area of 9000 km² (Fig. 1), having a sediment volume of c.a. 11,500 km³ (Soták et al., 2001), but a large part of the basin has been eroded, mainly during the Miocene Carpathian uplift.

As mentioned above, several studies have been done to identify the thermal maturity of the Paleogene rocks of the CCPB. There is a clear trend of increasing thermal maturity from west to east (from Orava

through Podhale to Spiš; Poprawa and Marynowski, 2005; Środoń et al., 2006; although, in the Levoča Basin, only a single data point is given in the known literature (Francu and Müller, 1983; Soták et al., 2001). Hydrocarbon potential was determined in the extensive study of Soták et al. (2001), and minor signs of hydrocarbon migration were also mentioned by Marynowski et al. (2001, 2006). However, there is no consistent data of sedimentary conditions in the CCPB based on up-to-date petrographic and geochemical methods. In addition, there is also no successive analysis of the evolution of organic matter (OM) with the progression of Oligocene deposition in the CCPB, as well as a discussion about depositional environments and hydrocarbon potential of the particular formations from the CCPB.

In this study, we aim to approach the above issue comprehensively, using a set of independent petrographic, organic, and inorganic geochemical methods. The Orava Basin was chosen as being the least thermally mature part of the CCPB (Środoń et al., 2006); thus, marginally affected by diagenetic transformations and offering the opportunity for use of both organic and inorganic geochemical data of this previously unexplored sedimentary basin.

2. Geological setting

Central Carpathian Paleogene Basin was formed during the Late Eocene as a result of tectonic subsidence linked with the gravitational collapse of Central Western Carpathian (CWC) massifs (Wagreich, 1995; Castelluccio et al., 2016). The sedimentation commenced during the Late Eocene on eroded Mesozoic carbonates, which belong to a widely spread system of thrust nappes in the CWC (Gross et al., 1984; Soták et al., 2001; Králiková et al., 2014). The sedimentary infill of the CCPB is commonly divided into four major lithostratigraphic units (Gross et al., 1984, 1993). The onset of sedimentation in the CCPB realm is marked by the presence of basal transgressive lithofacies that belong to the Borove Fm. (Gross et al., 1984, 1993; Soták et al., 2001; Fig. 1). The oldest coarse-grained facies pass gradually into shallow-water carbonates,

mainly organogenic limestones (so-called 'Eocene Nummulite sediments'). Sporadically in the Orava region, Borove Fm. sediments are overlain by Pucov conglomerates which are interpreted as sediments of submarine alluvial cones (Gross et al., 1984, 1993). The progressive deepening of the basin is indicated by the occurrence of mudstone layers belonging to the Huty Fm., the second Paleogene lithostratigraphic unit. Late Eocene - early Oligocene Huty Fm. is composed mainly of thick layers of calcareous mudstones and black shales, which are intercalated with sandstones (Gross et al., 1993). Locally, lense-like thin coal layers can be found. Gradual increase of sandstone layer volume up to typical rhythmic flysh-like sedimentation marks the transition into Oligocene Zuberec Fm. (Gross et al., 1984; Soták et al., 2001). In the Zuberec Fm., coal seams are more common and tend to be thicker (Gross et al., 1993). The youngest Late Oligocene-Early Miocene Biely Potok Fm. consists predominantly of thick sandstone beds, locally intercalated with conglomerates or thin layers of mudstones, which document the gradual shallowing of the basin (Gross et al., 1993). The CCPB sequence is here eroded due to shortening and basin inversion related to the Miocene uplift of Carpathian massifs.

3. Materials and methods

3.1. Samples description and preparation

A total of eighty-five samples of CCPB rocks were collected from surface outcrops in the Orava Basin area (Fig. 1 and Table 1). Considering the individual formations, 27 samples were collected from Huty Fm., 47 from the Zuberec Fm. and 11 from Biely Potok Fm. The lithology of the rock specimens is described in Table S1. In addition, four analyzed samples (3 in Zuberec Fm. and 1 in Huty Fm.; Table S1) represent coal layers or coal/shale mixture. After removing the weathered layer (usually a few centimeters), a fresh ca. 500–200 g sample was taken.

The collected samples were additionally cleaned with brush, washed with distilled water and dried at room temperature. They were
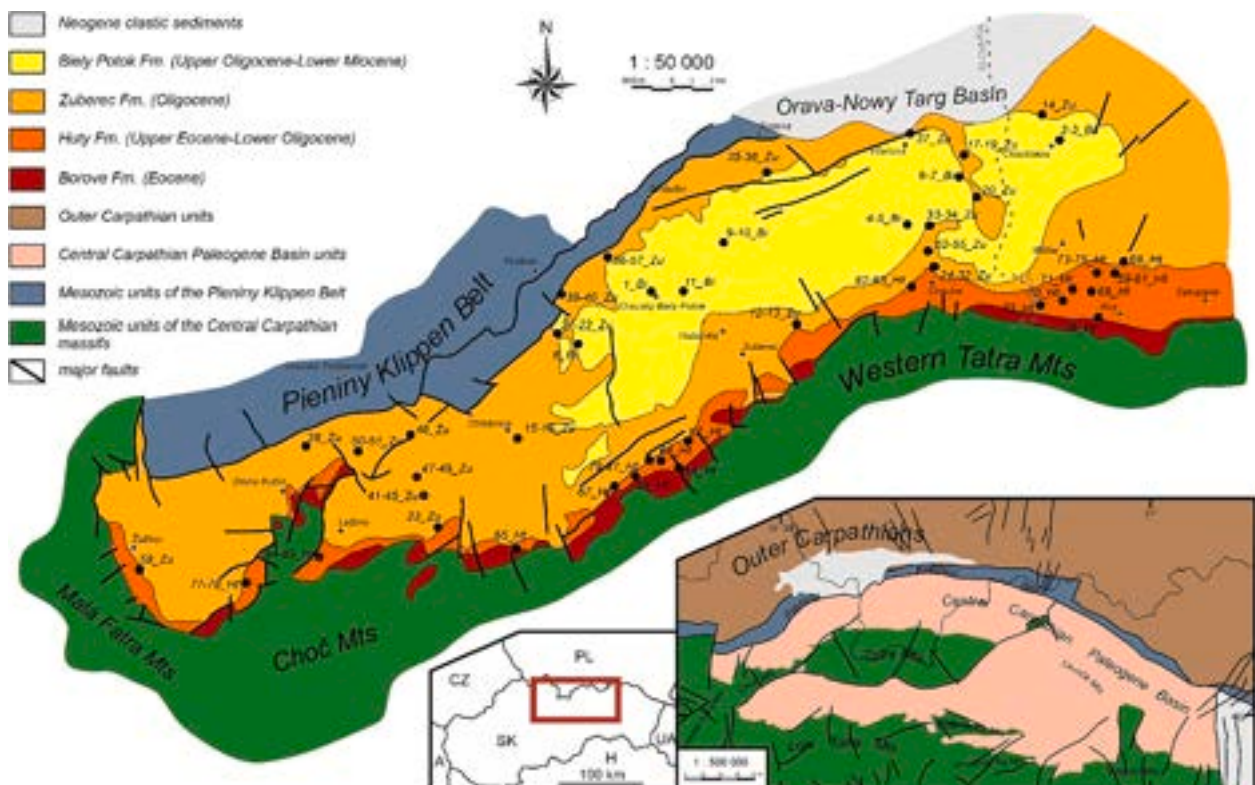
Fig. 1. Simplified geological map of the Orava Basin and adjacent areas showing sampling localities.

Table 1
Maturity parameters derived from hopanes, steranes and aromatic hydrocarbons.

Sample	Hopanes		Steranes		Aromatic hydrocarbons		
	$C_{31}(22S/ 22S + R)$	$C_{30}\alpha\beta/ \beta\alpha$	$C_{29}20S/ (20S + R)$	$C_{29}\beta\beta/ (\alpha\alpha + \beta\beta)$	MPI1	Rc [%]	BeP / (BeP + Pe)
Biely Potok Fm.							
1_Bi	0.54	3.99	0.25	0.37	0.40	0.64	0.81
2_Bi	0.54	3.86	0.18	nd	0.29	0.58	0.27
3_Bi	0.55	2.85	0.18	0.23	0.26	0.56	0.25
4_Bi	0.54	2.33	0.21	0.27	0.43	0.66	0.21
5_Bi	0.51	2.03	0.19	0.26	0.31	0.59	0.20
6_Bi	0.42	1.77	0.07	nd	0.26	0.55	0.08
7_Bi	0.40	2.33	0.10	nd	0.29	0.57	0.06
8_Bi	0.49	4.11	0.12	0.20	0.39	0.63	0.22
9_Bi	0.49	2.37	0.15	nd	0.45	0.67	0.21
10_Bi	0.49	2.46	0.13	0.25	0.46	0.68	0.20
11_Bi	0.42	2.84	0.16	0.12	0.49	0.69	0.65
Zuberec Fm.							
12_Zu	0.59	5.16	0.37	0.35	0.48	0.69	0.94
13_Zu	0.59	3.99	0.38	0.32	0.46	0.68	0.86
14_Zu	0.55	2.82	0.19	0.26	0.26	0.55	0.21
15_Zu	0.59	4.74	0.31	nd	0.57	0.74	0.92
16_Zu	0.59	4.89	0.26	nd	0.36	0.61	0.92
17_Zu	0.45	2.54	0.09	nd	0.38	0.63	0.08
18_Zu	0.48	3.14	0.10	nd	0.43	0.66	0.09
19_Zu	0.48	2.93	0.15	nd	0.41	0.65	0.12
20_Zu	0.49	2.30	0.18	nd	0.37	0.62	0.09
21_Zu	0.54	4.18	0.22	0.22	0.38	0.63	0.14
22_Zu	0.53	4.34	0.20	0.23	0.33	0.60	0.11
23_Zu	0.62	7.67	0.61	0.36	0.75	0.85	1.00
24_Zu	0.59	6.24	0.48	0.43	0.54	0.72	0.90
25_Zu	0.60	6.26	0.43	0.36	0.53	0.72	0.86
26_Zu	0.59	5.17	0.41	0.36	0.52	0.71	0.96
27_Zu	0.59	6.69	0.47	0.43	0.52	0.71	0.95
28_Zu	0.59	4.76	0.43	0.37	0.55	0.73	0.94
29_Zu	0.58	5.81	0.46	0.42	0.56	0.74	0.97
30_Zu	0.59	5.81	0.47	0.40	0.60	0.76	0.96
31_Zu	0.58	5.90	0.48	0.40	0.62	0.77	0.97
32_Zu	0.59	5.99	0.44	0.42	0.53	0.72	0.96
33_Zu	0.56	5.15	0.19	0.25	0.29	0.58	0.73
34_Zu	0.55	3.48	0.22	0.27	0.40	0.64	0.40
35_Zu	0.44	1.78	0.14	nd	0.25	0.55	0.18
36_Zu	0.43	2.05	0.10	0.29	0.28	0.57	0.15
37_Zu	0.50	2.28	0.15	nd	0.31	0.59	0.26
38_Zu	0.58	5.98	0.58	0.51	0.40	0.64	1.00
39_Zu	0.44	2.94	0.07	0.18	0.26	0.56	0.05
40_Zu	0.42	2.09	0.10	nd	0.22	0.53	0.07
41_Zu	0.59	4.43	0.40	nd	0.34	0.60	0.84
42_Zu	0.59	5.98	0.47	nd	0.38	0.63	0.73
43_Zu	0.59	8.24	0.46	nd	0.45	0.67	0.82
44_Zu	0.57	7.49	0.41	nd	0.43	0.66	0.90
45_Zu	0.57	5.82	0.45	nd	0.41	0.64	0.89
46_Zu	0.60	7.25	0.41	nd	0.29	0.58	1.00
47_Zu	0.59	4.40	0.43	nd	0.38	0.63	0.94
48_Zu	0.59	6.14	0.46	nd	0.37	0.62	0.95
49_Zu	0.59	5.82	0.43	nd	0.48	0.69	0.92
50_Zu	0.57	3.00	0.47	nd	0.23	0.54	1.00
51_Zu	0.56	4.59	0.25	0.32	0.25	0.55	0.98
52_Zu	0.59	5.15	0.46	0.40	nd	nd	0.66
53_Zu	0.59	6.16	0.45	0.45	0.55	0.73	1.00
54_Zu	0.59	6.86	0.44	0.43	0.60	0.76	0.97
55_Zu	0.59	5.29	0.42	0.37	0.52	0.71	1.00
56_Zu	0.42	4.44	0.09	0.26	0.24	0.55	0.02
57_Zu	0.42	4.23	0.06	0.23	0.25	0.55	0.05
58_Zu	0.46	2.38	0.20	nd	0.27	0.56	0.07
Huty Fm.							
59_Ht	0.61	6.19	0.49	0.51	0.63	0.78	nd
60_Ht	0.58	6.79	0.53	0.50	0.61	0.77	nd
61_Ht	0.58	6.76	0.54	0.50	0.44	0.67	nd
62_Ht	0.59	6.38	0.46	0.50	0.58	0.75	0.92
63_Ht	0.58	4.79	0.34	0.41	0.55	0.73	0.97
64_Ht	0.58	7.78	0.57	0.58	0.58	0.75	0.97

Table 1 (*continued*)

Sample	Hopanes		Steranes		Aromatic hydrocarbons		
	$C_{31}(22S/ 22S + R)$	$C_{30}\alpha\beta/ \beta\alpha$	$C_{29}20S/ (20S + R)$	$C_{29}\beta\beta/ (\alpha\alpha + \beta\beta)$	MPI1	Rc [%]	BeP / (BeP + Pe)
65_Ht	0.58	5.59	0.47	0.39	0.35	0.61	1
66_Ht	0.56	6.81	0.46	0.56	0.53	0.72	0.97
67_Ht	0.58	7.27	0.53	0.55	0.64	0.79	0.94
68_Ht	0.57	6.57	0.55	0.53	0.57	0.74	0.88
69_Ht	0.59	5.17	0.55	0.51	0.70	0.82	1
70_Ht	0.59	6.21	0.46	0.50	nd	nd	nd
71_Ht	0.57	8.29	0.58	0.56	0.57	0.74	1
72_Ht	0.57	6.98	0.53	0.55	0.52	0.71	1
73_Ht	0.56	4.81	0.44	0.50	0.61	0.77	nd
74_Ht	0.58	6.70	0.59	0.51	0.70	0.82	nd
75_Ht	0.58	6.16	0.54	0.50	0.67	0.80	nd
76_Ht	0.57	5.91	0.54	0.50	0.60	0.76	1
77_Ht	0.58	4.59	0.25	0.33	0.33	0.60	0.88
78_Ht	0.58	4.81	0.29	0.31	0.32	0.59	0.86
79_Ht	0.59	7.02	0.62	0.53	0.51	0.70	0.96
80_Ht	0.58	7.42	0.61	0.54	0.56	0.74	nd
81_Ht	0.58	8.22	0.62	0.55	0.66	0.79	nd
82_Ht	0.57	8.12	0.51	0.49	0.46	0.68	1
83_Ht	0.57	6.28	0.57	0.58	0.57	0.74	1
84_Ht	0.51	3.30	0.28	nd	0.41	0.64	0.84
85_Ht	0.53	4.12	0.25	nd	0.45	0.67	0.85

MPI1 = 1.5 * (3-methylphenanthrene +2-methylphenanthrene)/(phenanthrene +9-methylphenanthrene +1-methylphenanthrene).
Rc = 0.4 + 0.6 * MPI1.
MPI1 = methylphenanthrene index 1, Rc = calculated vitrinite reflectance, BeP/ (BeP + Pe) = benzo[*e*]pyrene to benzo[*e*]pyrene plus perylene ratio, nd = no data.

subsequently crushed and, after quartering, a portion was grounded to a fraction below 0.2 mm for geochemical analyses.

3.2. Total organic carbon (TOC) and total sulphur (TS)

These parameters were measured using an Eltra CS-500 IR-analyzer equipped with a TIC module (Faculty of Natural Sciences, University of Silesia in Katowice, Poland). Lastly, the total organic carbon (TOC) content was calculated from the obtained total carbon (TC) and total inorganic carbon (TIC) values (more details in Marynowski et al., 2017).

3.3. Rock-Eval pyrolysis

The Rock-Eval analysis was conducted using a Vinci Technologies Rock-Eval 6 Turbo apparatus at the Faculty of Geology, Geophysics, and Environmental Protection at AGH University of Krakow applying the Basic cycle of the Bulk Rock method. Briefly, the analysis consisted of two successive steps: firstly, 20–50 mg of rock sample was heated in the pyrolytic oven under nitrogen flow (100 ml/min) at temperatures ranging from 300 (3 min isothermal) to 650 °C at a rate of 25 °C/min; the afterward oxidation was conducted in the oxidation oven in air (100 ml/min) at temperatures ranging from 300 (1 min isothermal) to 850 °C at 20 °C/min (5 min at final temperature). The IFP 160000 standard was used to calibrate the apparatus. Details of the analysis, measured parameters and calculated indices are described elsewhere (Więcław and Sadlik, 2019).

3.4. Vitrinite and fusinite reflectance measurements

Samples for microscopic measurements were prepared according to ISO 7404-2 (2009) procedure. Fifty-five specimens (26, 22, and 7 specimens from Huty, Zuberec, and Biely Potok Fms., respectively) were analyzed in reflected light and immersion oil by Zeiss Axio Imager.A2m (Faculty of Natural Sciences, University of Silesia in Katowice, Poland). It was possible to measure the vitrinite reflectance in 47 specimens (3 specimens from Biely Potok, 21 from Zuberec, and 23 from Huty Fm.;

Table S2). In addition, the vitrinite reflectance values were also calculated based on methylphenanthrene index (MPI1) values for the majority of the analyzed samples (Rc = 0.60 MPI1 + 0.40; Radke and Welte, 1983; Radke, 1988). The inertinite reflectance was analyzed in 10 chosen samples (7 from Zuberec and 3 from Biely Potok Fm.; Table S3). Standards applied for vitrinite reflectance measurements were 0.420%, 0.588%, and 0.898% relative reflectance (Rr), and for inertinite reflectance, 1.42% and 3.09% Rr standards were used.

3.5. Pyrite framboid diameter analysis

Pyrite framboid diameters were measured using an environmental scanning electron microscope Philips XL30 ESEM/TMP (Faculty of Natural Sciences, University of Silesia in Katowice, Poland). Sixty prepared polished rock specimens were analyzed in backscattered electron (BSE) mode. To obtain statistically reliable results, at least 50 framboid diameters were measured. In only one specimen, it was not possible to acquire this number of measurements (see Table S4).

3.6. Biomarker analysis

3.6.1. Extraction, fractionation and derivatization
First, bitumen was extracted with a dichloromethane(DCM)/methanol (1:1, v:v) mixture using a Thermo Scientific Dionex ASE 350 solvent extractor. Extracts were further separated into aliphatic, aromatic and polar fractions by applying the column chromatography method. Prepared Pasteur pipettes were filled with silica gel (heated for 24 h at 120 °C), and the fractions were separated and collected using *n*-pentane, *n*-pentane/DCM (7:3) and DCM/methanol (1:1), respectively. Obtained aliphatic and aromatic fractions were dried and prepared for gas chromatography–mass spectrometry (GC–MS) analysis by dissolving in ethyl acetate. The polar fractions of selected (less mature) samples were additionally derivatised by reaction with *N,O*-bis-(trimethylsilyl)trifluoroacetamide (BSTFA, Sigma-Aldrich, St. Louis, MO, USA), dissolved in dehydrated *n*-hexane and then heated for 3 h in 70 °C (details are reported in Simoneit et al., 2021).

3.6.2. Gas chromatography-mass spectrometry (GC–MS)
GC–MS analyses were conducted with an Agilent Technologies 7890 A gas chromatograph (GC) and an Agilent 5975C Network mass spectrometer with Triple-Axis Detector (MSD) at the Faculty of Natural Sciences, Sosnowiec, Poland. Separation was obtained on an Agilent J&W HP5-MS (50 m × 0.32 mm i.d., 0.25 μm film thickness) fused silica capillary column coated with a chemically bonded phase (5% phenyl, 95% methylsiloxane), for which the GC oven temperature was programmed from 45 °C (1 min) to 100 °C at 20 °C /min, then to 300 °C (hold 60 min) at 3 °C /min, with a solvent delay of 10 min. Helium (6.0 Grade) was used as a carrier gas at a constant flow of 2.6 ml/min. The GC column outlet was connected directly to the ion source of the MSD. The GC–MS interface was set at 280 °C, while the ion source and the quadrupole analyzer were set at 230 and 150 °C, respectively. Mass spectra were recorded starting from *m/z* 45 to 550 (0–40 min) and *m/z* 50–700 (>40 min). The MSD was operated in the electron impact mode, with an ionization energy of 70 eV.

3.7. Inorganic geochemistry

The eighty-one samples (26, 46 and 9 from Huty, Zuberec and Biely Potok Fms., respectively) were analyzed at AcmeLabs, Vancouver, Canada in order to measure the content of 37 elements (Mo, Cu, Pb, Zn, Ag, Ni, Co, Mn, Fe, As, U, Au, Th, Sr, Cd, Sb, Bi, V, Ca, P, La, Cr, Mg, Ba, Ti, B, Al, Na, K, W, Sc, Tl, S, Hg, Se, Te, and Ga). Four samples suspected of being partially weathered were omitted (Marynowski et al., 2017). Approximately 5 g of each powdered sample was digested using modified aqua regia digestion (1:1:1; HNO_3:HCl:H_2O). Subsequently, the content of the previously mentioned elements was measured by using Optical Emission Spectroscopy (OES) and Inductively Coupled Plasma Mass Spectrometry (ICP-MS) techniques.

4. Results

4.1. General organic geochemical and petrological data

Measured total organic carbon (TOC) values are generally low to moderate for most of the samples (Table S1). The exceptions are the coal samples, where the TOC reaches 82.5 wt%. In Huty Fm., the content of TOC rarely exceeds 1 wt%, apart from a few samples displaying slightly higher values. Samples taken from Zuberec Fm. are characterized by on average higher TOC content than from Huty Fm., sometimes reaching c. a. 10 wt% in black shales. Sandstones and mudstones of the Biely Potok Fm. show the lowest values of TOC, in the range of 0.02 to 2.4 wt% (Table S1).

Total sulphur (TS) content in analyzed units changes coherently with the TOC values and reaches the highest levels in Zuberec Fm. samples. In Huty Fm., the TS content is not higher than 2.5 wt% and equals 0.6–0.7 wt% on average. The TS content in Biely Potok Fm. samples is the lowest in all measured units and in some samples drops almost to zero (Table S1). Calculated carbonate content (CC) values are strongly site-dependent. There is no clear trend in the CC values in the analyzed units; however, it seems that the average CC is the highest in Huty Fm. (~20%) and decreases in younger units (Table S1).

Vitrinite reflectance values obtained using two different methods differ significantly. The calculated values (based on the methylphenanthrene index 1; MPI1) are c.a. 0.2–0.3% higher than the measured ones. The measured vitrinite reflectance values could be used with caution since, as already pointed out by Marynowski et al. (2006). This is due to the occurrence of both dark hydrogen-rich vitrinites and reworked vitrinites observed in the studied samples from Oligocene sequences. Especially dark vitrinites occur in large numbers (Fig. S1) and prevent proper measurement of reflectance. However, the MPI1 parameter converted to calculated vitrinite reflectance (Rc) works very well for CCPB rocks (Poprawa and Marynowski, 2005). The results of both methods follow more or less the same distribution pattern. The highest vitrinite reflectance values are reported in the south and southeast of the Orava region in the Huty Fm. Generally, in this unit, the obtained values range from 0.59 to 0.82% Rc. Slightly lower values are documented in the Zuberec Fm. Similarly to Huty Fm., the vitrinite reflectance increases towards the southeast (Fig. 3; Table S2). The values in the northern part of the Orava Basin tend to be the lowest, averaging at 0.50–0.55% Rc. However, the vitrinite reflectance of the southernmost Zuberec Fm. samples do not differ from those measured in Huty Fm. samples. In the Biely Potok Fm., the vitrinite reflectance values are similar to the values obtained for the northern Zuberec Fm. samples (0.5–0.7%), and follow the same maturity trend (the lowest values in the north, the highest in the southern parts).

Fusinite reflectance was possible to be measured only in Zuberec and Biely Potok Fm. samples. Fusinite grains were small and relatively rare (Fig. S1), generally more common in Biely Potok Fm. than in Zuberec Fm. Higher reflectance values were recorded in the Zuberec Fm. and ranged from 1.89% to 4.66%, corresponding with theoretical combustion temperatures (calculated based on Jones and Lim, 2000, and Petersen and Lindström, 2012 formulas) between 407 °C and 734 °C (Table S3). In turn, fusinite reflectance, which was measured in Biely Potok Fm. samples vary from 1.68% to 2.98%. Calculated combustion temperatures for these samples range from 382 °C to 536 °C (Table S3).

4.2. Rock-Eval analysis

The TOC concentrations determined by the Rock-Eval analysis (Table S5) are comparable to values presented in Chapter 4.1 (Table S1). Statistically, the best source rock levels are recorded within Zuberec Fm. with medians of TOC and hydrocarbon potential ($S_1 + S_2$) reaching 1.97

wt% and 4.4 mg HC/g rock, respectively (Fig. 4). Within this formation some coal seams or lenses were recorded with TOC content up to 92.6 wt % and S1 + S2 values up to 321 mg HC/g rock (Fig. 4). Huty and Biely Potok formations show poor source rock properties with median TOC values of 0.50 and 0.45 wt%, respectively and median hydrocarbon contents (S1 + S2) of 0.85 and 0.42 mg HC/g rock, respectively (Fig. 4). However within Huty Fm. levels rich organic matter (even coals – sample 85_Ht) are recorded.

The hydrogen index (HI) values of all studied samples ranges between 50 and 380 mg HC/g TOC (Table S5). The lowest values, below 100 mg HC/g TOC are recorded for Biely Potok Fm. For Zuberec and Huty formations values of this index below 200 mg HC/g TOC dominate, but for some samples (42_Zu from Zuberec and 77_Ht, 78_Ht and 82_Ht from Huty Fm.) values above 300 mg HC/g TOC are recorded (Fig. 5a). Similar results were also obtained from the Levoca Basin, part of the CCPB (Soták et al., 2001).

The production index (PI) values range from 0.02 to 0.48 (Table S5, Fig. 5b). For Biely Potok and Zuberec Fms. values of this index usually do not exceed 0.1 (both medians equal 0.09), whereas for the Huty Fm. are mainly from 0.2 to 0.4 (median 0.29) with a maximal value of 0.48 for 79_Ht sample (Fig. 5b). All studied samples reach a range of T_{max} values from 421 to 458 °C (Table S5). The lowest T_{max} temperature was recorded for the coal sample (42_Zu) collected from Zuberec Fm. (Fig. 5a), but remaining coals (85_Ht, 45_Zu and 48_Zu) evidence much higher values of this parameter (445–457 °C, Table S5). Statistically, organic matter present within Biely Potok and Zuberec formations is characterized by lower T_{max} values, mainly 430–440 °C whereas values of this parameter for organic material present in Huty Fm. are from 440 to 450 °C (Fig. 5).

4.3. Pyrite framboid size analysis

Out of the total number of 60 inspected specimens (chosen based on TS values), pyrite framboids were present in 20 specimens from Huty Fm., 24 from the Zuberec Fm. and 6 from the Biely Potok Fm. (Table S4). In the majority of examined specimens, it was possible to measure 100 framboid diameters, otherwise at least 50 measurements were taken. Only in one specimen, the number of measurements was significantly lower (14; Table S4).

In all analyzed samples, pyrite framboids with small (<2 μm) and large (>20 μm) diameters were present. The mean value of framboid diameters was generally coherent in Zuberec and Huty Fms. and equaled c.a. 6 μm. In Biely Potok Fm. average framboid diameter values were only slightly larger (c.a. 6.5 μm). The calculated percentage of pyrite framboids with diameters smaller than 5 μm was similar in Huty and Zuberec Fms. and varied around 45%. Moreover, in Huty Fm., the calculated percentage for each sample was rather homogenous, while in Zuberec Fm., the values are more dispersed, changing from 78% to 12%. In the specimens from the youngest analyzed unit, the Biely Potok Fm., the percentage of the framboids with diameters below 5 μm was much lower (c.a. 30%).

4.4. Biomarker analysis

4.4.1. Aliphatic fraction

The most prominent compound groups present in the analyzed samples are *n*-alkanes, hopanes, and steranes. Among other identified compounds are acyclic isoprenoids (pristane, phytane), diterpanes and angiosperm derivatives. Based on aliphatic compounds distribution, several ratios were calculated (Table S1).

The distribution of *n*-alkanes depends both on the maturity and lithology of the samples and is rather uniform in each unit. This homologue series generally ranges from *n*-C_{12} to *n*-C_{37} (sporadically to *n*-C_{38} for some Zuberec and Huty Fm. samples). The calculated values of two Carbon Preference Indexes (CPI_{Total} and $CPI_{25–31}$; Bray and Evans, 1961; Marynowski and Zatoń, 2010) are generally close to unity in both Huty

and Zuberec Fms. However, in the Huty Fm., the CPI values are rather coherent, while in the Zuberec Fm., they show a distinct dispersion ranging from 0.79 to 2.22. In the Biely Potok Fm., the values of both indexes are usually above 1.15 with few exceptions. The terrigenous versus aquatic *n*-alkane ratio (TAR, Bourbonniere and Meyers, 1996) shows a bimodal distribution with values grouping at 0.7–0.8 or over 1.2 in Huty Fm. samples. In Zuberec Fm., the TAR values are even more dispersed, ranging from 0.17 to 37.81. A similar situation occurs in the Biely Potok samples. The highest reported values (>20) result most likely from a very low OM content and therefore a poor quality of the obtained data and will be not taken into account in further analyses. There is no clear trend in the spatial distribution of samples with high or low TAR values.

Two acyclic isoprenoids identified in all samples are pristane (Pr) and phytane (Ph). The calculated Pr/Ph ratio is strongly site-dependent and differs significantly according to the unit level. However, the changes between all three units are minor. Mean values vary generally between 1 and 5, only a few samples show Pr/Ph ratio below 1. The second calculated indicator is the Pr/*n*-C_{17} ratio, which seems to increase in the profile from Huty to Biely Potok Fm. In Huty Fm., the Pr/*n*-C_{17} ratio rarely reaches 3 or higher values, which on the contrary are noted frequently in Zuberec and Biely Potok Fms. The highest values are documented in Zuberec Fm., up to 11.74 (Table S1). Such an increasing trend is not related with the Ph/*n*-C_{18} ratio. In Huty Fm. the Ph/*n*-C_{18} values are predominantly below 1, while in Zuberec and Biely Potok Fms., the documented values are higher, and even reach 5.75 (Table S1).

Hopanes are abundant in all sampled formations. The dominant compounds are C_{30} αβ hopane and C_{31} αβS homohopane (Fig. 6), but in some samples C_{29} αβ hopane is also one of the major compound. The homohopane C_{31} 22S/(S + R) ratio values are the highest in the Huty Fm. samples and those Zuberec Fm. samples which are located in the southern part of the Orava basin (Fig. 3). In this two groups, the values are quite uniform and vary between 0.55 and 0.60, reaching equilibrium (Peters et al., 2005). The values are somewhat lower in the northern Zuberec Fm. and Biely Potok Fm., and equal 0.4–0.5 (Table 1). The $C_{30}αβ/βα$ (hopane to moretane ratio), shows a clear decreasing trend from the oldest units to the youngest. In Huty Fm., the content of the C_{30} αβ hopanes is over six times higher than the C_{30} βα moretanes. This ratio decreases slightly over 4 in Zuberec Fm., and over 2 in Biely Potok Fm. A few samples of Zuberec and Biely Potok Fms. contain small amounts of C_{30} and C_{31} ββ-hopanes and hop-(13)18-enes, which were not previously identified in the Podhale Basin (Marynowski et al., 2006). Gammacerane was found in a few samples of Huty and Zuberec Fms. (Fig. 6).

Steranes were identified in all analyzed samples (Table 1). In order to assess the maturity of the studied rocks, the $C_{29}ααα$ 20S/(S + R) ratio was determined. Similarly to the hopane-derived ratios, it shows a consistent decrease in the profile. Huty Fm. samples display the highest values (up to 0.62), while the Zuberec samples, located in the north of Orava and all Biely Potok Fm. samples are characterized by much lower values (up to 0.25). Zuberec Fm. sites in the central Orava have intermediate values of this ratio. In all samples containing regular steranes, C_{27}-C_{29} sterane homologues were identified and in most of them, C_{30} steranes were also found. In Huty Fm., the most dominant are, with a few exceptions, cholestanes (C_{27} steranes). In Zuberec Fm., the percentage contribution of ergostanes (C_{28}) and stigmastanes (C_{29}) is approximately equal, while in the youngest studied unit, Biely Potok Fm., the stigmastanes are prevalent. This relationship is clearly visualised in Fig. 7. In some samples of Biely Potok and Zuberec Fms. diaster-13(17)-enes were found with the domination of C_{29} (20R and 20S epimer) compounds.

In most of the samples, angiosperm (flowering land plant) markers, including 18α + 18β-oleanane, norlupanes, and bisnorlupanes were found (Moldowan et al., 1994; Nytoft et al., 2002; Curiale, 2006). Moreover, in less mature samples, olean-13(18)-ene, olean-12-ene, and taraxer-14-ene compounds, all derived from angiosperms, were identified (ten Haven and Rullkötter, 1988; Nytoft et al., 2016). The content of

angiosperm biomarkers is diverse and generally increases towards the younger formations (Fig. 6).

Gymnosperm markers are represented by tricyclic and tetracyclic diterpanes, between which 16α(H)- and 16β(H)-phyllocladanes, 16α(H)- and 16β(H)-kauranes, abietane, 8α(H)- 8β(H)-labdanes as well as 4α(H)- and 4β(H)-fichtelite. The 8β(H)-labdane is usually the dominating compound; nevertheless, 8α(H)-labdane is minor or absent. Additionally, phyllocladanes and abietane usually dominate over kauranes (Fig. 8). These compounds are present in less mature samples only, mainly in Zuberec and Biely Potok Fm.

4.4.2. Aromatic fraction

The molecular composition of the aromatic fraction is diverse and depends strongly on the OM maturity level. Mature samples, namely from Huty Fm. and a few Zuberec Fm. samples, are characterized by similar molecular composition dominated by gymnosperm biomarkers, mainly retene and cadalene which relatively high quantities are documented in each sample (Fig. 9). In slightly less mature Zuberec Fm. and few Huty Fm. samples low quantities of simonellite and 6-isopropyl-2-methyl-1-(4-methylpentyl) naphthalene (ip-iHMN) were also identified. Angiosperm-related biomarkers are also documented in the mature samples, but their quantity and diversity are rather limited in comparison to the least mature samples (Fig. 9). Chrysene and picene derivatives, such as 1,2,9-trimethyl-1,2,3,4-tetrahydropicene, 2,2,9-trimethyl-1,2,3,4-tetrahydropicene, 3,3,7-trimethyl-1,2,3,4-tetrahydrochrysene, 2,2,9,9-tetramethyl-1,2,3,4,9,10,11,12-octahydropicene, 2,2-dimethyl-1,2,3,4-tetrahydropicene (Laflamme and Hites, 1979; Wakeham et al., 1980) are common in many samples of all formations. Other compounds documented in low quantities are triterpene-related des-*E*-D;C-friedo-25-norhopa-5,7,9-triene and oleanane derivatives (e.g., des-A-dinoroleana-5,7,9,11,15-pentaene) and they are more typical for Zuberec and Biely Potok Fms. (Fig. 9). Polycyclic aromatic hydrocarbons (PAHs) were detected in all samples, but their abundances are diverse. Their quantities vary significantly with the maturity level of the sample and stratigraphic position. PAHs characteristic for pyrolytic processes, including phenanthrene, anthracene, 4H-cycopenta[*def*]phenanthrene, fluoranthene, pyrene, benzo[*ghi*]fluoranthene, benz[*a*]anthracene, chrysene, triphenylene, as well as typical five-ring PAHs including benzofluoranthenes, benzo[*a*]pyrene, benzo[*e*]pyrene were found in almost all samples. On the other hand, two-ring aromatic hydrocarbons (like naphthalene or acenaphthene) and their alkyl derivatives were found in some samples only, mainly in Huty Fm.

However, PAHs are highly abundant in Biely Potok and upper Zuberec Fms. (Fig. S2). Perylene was virtually not present or at very low quantities in the most mature samples (most Huty Fm. samples) and gradually reoccurring in the less mature Zuberec and Biely Potok Fms. Generally, the abundance of perylene in less mature samples is usually higher or at similar abundance to benzo[*a*]pyrene and benzo[*e*]pyrene (Fig. S3).

Other PAHs documented in these samples are naphthalene and its methyl derivatives, phenanthrene and its methyl derivatives and less abundant methyl derivatives of other PAHs. Aromatic sulphur compounds such as methyldibenzothiophenes or benzonaphthothiophenes are of low content and present only in some samples.

In less mature rocks (all Biely Potok Fm. and some Zuberec Fm. samples), gymnosperm-related biomarkers contain not only retene, ip-iHMN and cadalene as for the most Huty Fm., but also less thermally stable compounds like simonellite and dehydroabietane. Similarly, for the angiosperm biomarkers, their abundance and variety are greater in the northern Zuberec and Biely Potok Fms. All compounds mentioned in the paragraph above are present in these samples and, additional others are documented, like des-A-dinoroleana-5,7,8,11,13-pentaene and 23,25-bisnor-des-E-oleana-1,3,5(10)-triene (Fig. 9).

Almost all analyzed samples contain some amount of triaromatic dinosteroids (Table S6). They are most abundant in Huty Fm. and some Zuberec Fm. samples but generally their content decreases with the age

of sediments. Based on the *m/z* 245 chromatogram and known elution times (Ma et al., 2008; Brocks et al., 2016; Wendorff-Belon et al., 2021) it was possible to identify D1–7 isomers of these compounds (Fig. S4). In most samples, D3 and D7 are the most prominent isomers.

In addition, we calculated three indices based on the quantity of aromatic compounds (Table 1; Fig. 3) used when assessing the maturity of organic matter: the methylphenanthrene index (MPI) (Radke and Welte, 1983), and the ratio of benzo[*e*]pyrene/(benzo[*e*]pyrene + perylene) (Marynowski et al., 2015), and Rc. The MPI parameter values change from c.a. 0.2 to c.a. 0.7 in Biely Potok to Huty Fms. respectively, and from the northern parts of Orava to the southern. Based on the MPI values the theoretical calculated vitrinite reflectance values were obtained (Table 1; Fig. 3; Fig. S5). The Rc values do not exceed 0.9%. The second maturity-related parameter, the benzo[*e*]pyrene/(benzo[*e*]pyrene + perylene) ratio, documents values close to one in all Huty Fm. samples and southern, and south-central Zuberec Fm. samples. Only a few analyzed sites were characterized by intermediate values (c.a. 0.4). The ratio significantly drops to 0.02 in the northern Zuberec Fm. samples. A detailed spatial distribution of this parameter is documented in Fig. S5.

Some mudstones from the Huty and lower Zuberec Fms. contained low amounts of isorenieratane, the green sulphur bacteria biomarker, and its diaryl and monoaryl (aryl isoprenoid) degradation products (Fig. 10; Grice et al., 1996; Koopmans et al., 1996).

4.4.3. Polar compounds

Three samples, containing immature organic matter were selected to identify and interpret polar compounds. The most abundant compounds were *n*-carboxylic acids, but benzoic or hydroxybenzoic acids as well as hydroxyacetophenons and hydroxybenzaldehydes were also present in significant amounts (Table 2). The other lignin-degradation products were isopropylphenol, catechol, vanillin, 3-phenylphenol and protocatechoic acid (Table 2). The additional identified polar compounds characteristic of terrestrial organic matter were dehydroabietic acid, four tocopherol isomers, and β-sitosterol (Table 2). High-molecular-weight *n*-carboxylic acids with a noticeable predominance of even-carbon homologues typical for terrestrial OM were also found. Characteristic fragmentation for all identified compounds (as trimethylsilyl derivatives) is listed in Table 2, together with their molecular masses, abundances and likely sources.

4.5. Inorganic bulk rock geochemistry

The ICP-MS analysis documented the presence and content of trace elements in the Oligocene rocks samples. Molybdenum content is strongly formation-dependent and reaches the highest values in Zuberec Fm. and one Huty Fm. sample (up to 30.27 ppm; Table S7). The lowest content of this element is reported in Biely Potok Fm. samples, while in Huty Fm. the values are intermediate. The authigenic uranium (U_{aut}), uranium- and molybdenum enrichment factors (U_{EF} and Mo_{EF}, respectively) values were calculated following the procedure by Wignall (1994), Algeo and Tribovillard (2009) and Tribovillard et al. (2012). U_{aut}, U_{EF} and Mo_{EF} highest values are documented in the Zuberec Fm. samples. Although the values are generally dispersed, the mean value of U_{aut} for this unit is close to 1. The values of these two parameters for Biely Potok and Huty Fms. display a greater coherence but are lower. Calculated Mo_{EF} values depend strongly on the unit. In the Biely Potok Fm. Mo_{EF} values are rather low (c.a. 10–15) in comparison with other formations. In Huty Fm., this parameter shows a greater dispersion, but the values are higher than in Biely Potok Fm. The highest Mo_{EF} values are documented in Zuberec Fm. samples, where this parameter often exceeds 100.

In addition, U/Th, V/Cr, TOC/P, U/Mo ratios were calculated (Table S7). The U/Th ratio shows consistently low values (0.1–0.7) in Huty Fm. (except coal sample) while being slightly higher and/or more dispersed in Zuberec (up to 1.4) and Biely Potok Fms. (up to 0.4). This

Table 2

Main polar compounds (by elution order on DB-5MS column) and proportions (%) in selected low mature samples. Identification based on literature data (Kuroda, 2000; Otto and Simoneit, 2001; Fabbri et al., 2002, 2009; Dickens et al., 2007; Rybicki et al., 2017, 2020) and mass spectra interpretation; *molecular mass (as trimethylsilyl derivative in parentheses).

Compound	Mol. mass*	Characteristic fragments *m/z* (%)	Source	35_Zu	37_Zu	56_Zu
Hexanoic acid-TMS	116(188)	75(100), 73(80), 173(80), 117(40)	Bacteria?	30	30	
2-Ethylhexanol	130(202)	75(100), 103(80), 73(7), 187(70)	Bacteria?		8	
Levulinic acid-TMS	116(188)	75(100), 145(40), 173(40)	Saccharide degradation	10	8	3
Heptanoic acid-TMS	130(202)	75(100), 73(80), 187(80), 117(40)	Bacteria?	6	10	3
Cyclohexanecarboxylic acid-TMS	128(200)	73(100), 75(70), 185(40), 200(5)	Higher plants?	6	8	
Isopropylphenol-TMS	134(208)	193(100), 73(50), 208(30)	Lignin	2	4	
Benzoic acid-TMS	122(194)	105(100), 179(90), 77(80), 135(50), 194(8)	Lignin	10	2	10
3Me-cyclohexanecarboxylic acid-TMS	142(214)	73(100), 75(70), 199(40), 214(5)	Higher plants	5	2	
Octanoic acid-TMS	144(216)	75(100), 73(98), 201(85), 117(60)	Bacteria?	15	10	4
2'-Hydroxyacetophenon-TMS	136(208)	198(100), 208(50), 151(30), 73(20)	Lignin	5	8	
Glycerol-TMS	92(308)	73(100), 147(55), 205(45), 117(30)	Saccharide degradation	6	6	15
3'-Hydroxyacetophenon-TMS	136(208)	198(100), 208(50), 151(30), 73(20)	Lignin	7	9	
4'-Hydroxyacetophenon-TMS	136(208)	198(100), 208(50), 151(30), 73(20)	Lignin	5	9	
Succinic acid-TMS	118(262)	147(100), 73(50), 247(10)	Resin/Higher plants	20		
Catechol	110(254)	73(100), 254(30), 239(10)	Lignin	15	5	
3-Hydroxybenzaldehyde-TMS	122(194)	179(100), 194(80), 151(65)	Lignin	25	6	
Carvacrol-TMS	150(222)	207(100), 222(80), 73(50), 165(20)	Higher plants/Lignin	8	8	4
Nonanoic acid-TMS	158(230)	75(100), 73(98), 201(85), 117(60)	Bacteria?	25	35	13
4-Hydroxybenzaldehyde-TMS	122(194)	179(100), 194(80), 151(65)	Lignin	25	7	
Pentanedioic acid	132(276)	147(100), 73(70), 261(50), 158(25)	Higher plants?	20		
Decanoic acid-TMS	172(244)	75(100), 229(98), 73(95), 117(80), 129(45), 132(30)	Bacteria?	27	10	12
4-(Methylcarboxyl)phenol-TMS	152(224)	209(100), 224(75), 193(30), 135(30)	Lignin			4
Vanillin-TMS	152(224)	194(100), 209(50), 224(30), 73(30)	Lignin	1		2
1-Dodecanol-TMS	186(258)	243(100), 75(50), 103(20), 73(20)	Bacteria?		3	1
Adipic acid-TMS	146(290)	73(100), 111(80), 147(60), 275(20)	Higher plants?	3		
Dodecanoic acid-TMS	186(258)	117(100), 243(98), 73(80), 75(75), 129(45), 145(20)	Bacteria?	50	5	10
m-Hydroxybenzoic acid-TMS	138(282)	267(100), 73(60), 193(50), 223(40), 282(40)	Lignin	50	4	
p-Hydroxybenzoic acid-TMS	138(282)	73(100), 267(85), 193(50), 223(50), 282(20)	Lignin	50	5	
Dodecanoic acid-TMS	200(272)	257(100), 73(98), 75(95), 117(90), 237(50), 129(48)	Bacteria?	**100**	25	10
3-Phenylphenol-TMS	170(242)	227(100), 242(80), 211(60), 152(20)	Lignin	10	5	
Tridecenoic acid-TMS	214(286)	73(100), 117(95), 271(90), 75(90), 129(50), 132(45)	Bacteria?	85	15	12
2-Naphthoic acid-TMS	172(244)	127(100), 155(100), 229(90), 185(90), 244(50)	Diverse	3	1	
4-Phenylphenol-TMS	170(242)	227(100), 242(80), 211(60), 152(20)	Lignin	10	7	
1-Naphthoic acid-TMS	172(244)	127(100), 155(100), 229(90), 185(75), 244(50)	Diverse	5	0.5	
Protocatechoic acid-TMS	154(370)	198(100), 73(60), 370(45), 355(20)	Lignin	10		
Anthrone	194	194(100), 165(90), 82(10)	Diverse	8		
Tetradecanoic acid-TMS	228(300)	73(100), 285(95), 117(90), 75(80), 129(50), 132(45)	Bacteria?	80	20	20
Pentadecanoic acid-TMS	242(314)	73(100), 299(95), 117(90), 75(80), 129(60), 132(45)	Bacteria?	50	15	20
1-Hexadecanol-TMS	242(314)	299(100), 75(50), 103(20), 73(20)	Bacteria or higher plants		7	15
6-Phenanthridinol-TMS	195(267)	252(100), 266(80), 267(40), 178(30)	?			5
Hexadecanoic acid-TMS	256(328)	73(100), 117(100), 313(95), 75(80), 129(60), 132(50)	Bacteria or higher plants	90	**100**	**100**
Octadec-1-ol-TMS	268(340)	75(100), 82(40), 96(40), 129(25), 325(25), 340(5)	Bacteria or higher plants	15		12
Phytanic acid	312(384)	73(100), 159(85), 117(80), 369(50), 143(40)	Marine photosynthesizers	20	5	10
Octadecanoic acid-TMS	284(356)	73(100), 117(95), 341(85), 75(80), 129(50), 132(50)	Bacteria or higher plants	60	95	70
Nonadecanoic acid-TMS	298(370)	117(100), 355(100), 73(95), 75(80), 129(60), 132(60)	Bacteria or higher plants	10	5	10
Dehydroabietic acid-TMS	300(372)	239(100), 73(40), 255(10), 357(10), 372(8)	Pine resin	5		3
Eicosanoic acid-TMS	312(384)	73(100), 117(95), 369(85), 75(75), 129(50), 132(50)	Higher plants	5	7	15
Heneicosanoic acid-TMS	326(398)	117(100), 383(95), 73(90), 132(60), 75(55), 129(50)	Higher plants	5	5	8
Docosanoic acid-TMS	340(412)	117(100), 73(90), 397(90), 132(60), 75(55), 129(50)	Higher plants	20	10	15
Tricosanoic acid-TMS	354(426)	117(100), 73(95), 411(85), 75(70), 132(60), 129(50)	Higher plants	20	6	10
Tetracosanoic acid-TMS	368(440)	117(100), 73(95), 425(90), 75(60), 132(60), 145(60)	Higher plants	30	7	17
δ-Tocopherol-TMS	402(474)	474(100), 209(50), 73(50), 208(45), 249(20)	Higher plants			8
Pentacosanoic acid-TMS	382(454)	117(100), 73(98), 439(80), 75(75), 132(60), 145(60)	Higher plants	20	5	8
β-Tocopherol-TMS	416(488)	488(100), 223(60), 73(50)	Higher plants			4
Υ-Tocopherol-TMS	416(488)	488(100), 223(80), 73(50)	Higher plants			4
Hexacosanoic acid-TMS	396(468)	73(100), 117(95), 453(90), 75(75), 129(50), 132(50)	Higher plants	40	6	13
α-Tocopherol-TMS	430(502)	502(100), 237(75), 73(50)	Higher plants			0.3
Heptacosanoic acid-TMS	410(482)	73(100), 117(90), 467(75), 75(70), 129(50), 132(50)	Higher plants	20	2	5
Octacosanoic acid-TMS	424(496)	117(100), 73(98), 481(80), 75(65), 145(60), 132(50)	Higher plants	30	6	15
Nonacosanoic acid-TMS	438(510)	117(100), 73(90), 495(80), 75(70), 145(65), 132(55)	Higher plants	8	1	3
β-Sitosterol-TMS	414(486)	129(100), 357(85), 396(65), 486(40), 381(30), 471(10)	Higher plants	5	2	10
Triacontanoic acid-TMS	452(524)	73(100), 117(92), 509(60), 75(65), 145(60), 132(55)	Higher plants	15	3	5

applies as well to the U/Mo ratio, in which calculated values have an average between 0.5 and 0.6 in Huty Fm. and are more or less consistent, whereas in Zuberec and Biely Potok samples, the dispersion is much greater. The V/Cr ratio seems to be rather coherent in all units, with values usually not exceeding 4. The TOC/P ratio reaches the highest values in coal samples (e.g., 85_Ht). In Huty Fm., the TOC/P ratio averages 20–25, with only two values being significantly higher. In Zuberec Fm. samples with values close to or higher than 100 are more frequent. In Biely Potok Fm. reported TOC/P values are generally lower than in the two previously mentioned units.

5. Discussion

5.1. Maturity assessment

Organic compound parameters, supported by measured vitrinite

reflectance, were used to determine the maturity of the Orava Basin. Moreover, the maturity of organic matter present in analyzed formations was evaluated based on T_{max} and PI values received from Rock-Eval analysis (Table S5, Fig. 5). T_{max} values of all analyzed samples vary from 421 to 458 °C (Table S5), indicating their changeable maturity. A few samples from Biely Potok and Zuberec formations T_{max} have values below 430 °C, suggesting low maturity of organic matter (Fig. 5); for most of the samples (from all formations), values of this parameter range from 430 to 460 °C, which fulfills the whole range of the oil window (after Peters and Cassa, 1994). The largest differences in T_{max} temperature were recorded for samples collected from Zuberec Fm. whereas organic material from Huty Fm. show the narrowest range of this parameter, from 440 to 450 °C (Fig. 5). The PI values generally very well correlate with T_{max} values (Fig. 5b). Only for some samples from all formations, characterized by T_{max} values from 430 to 460 °C (oil window range) PI values are untypically below 0.1 (Fig. 5b). This feature may be related to the evaporation of the volatile (free) hydrocarbons (S1) from outcropping rocks. However, rocks rich in terrestrial OM also, regardless of maturity, are usually characterized by low (<0.1) values of this index (Espitalié et al., 1986).

The main organic indices used to determine thermal maturity were: methylphenanthrene index 1 (MPI1) converted to Rc (Radke and Welte, 1983), 20S/(S + R) for C_{29} steranes, 22S/(S + R) for C_{31} homohopanes (Peters et al., 2005) and the ratio of benzo[e]pyrene and perylene: BeP/(BeP + Pe) (Marynowski et al., 2015). Some organic indices have previously been used in thermal maturity changes in the Podhale Basin, showing high precision and a gradual increase with depth (Poprawa and Marynowski, 2005; Marynowski et al., 2015). Most organic maturity indices correlate well with each other (Fig. 11), indicating their potential usefulness. However, other parameters like the Pr/n-C_{17}, Ph/n-C_{18}, $C_{30}\alpha\beta/\beta\alpha$ or $\beta\beta/(\alpha\alpha + \beta\beta)$ ratios (Tables 1 and S1) indicate a general trend of changes in thermal maturity, although their correlation with each other is less convincing.

Certain limitations to the application of organic parameters must not be ignored. Vitrinite reflectance shows underestimated values due to the presence of reworked (Marynowski et al., 2006), and dark vitrinites noticed also in the Oligocene of Outer Carpathians (Waliczek and Więcław, 2012; Waliczek et al., 2019). The main reason for the occurrence of dark vitrinite and reflectance suppression is the presence of resinite (Fig. S1), which generated hydrocarbons that were adsorbed on vitrinites (Petersen and Vosgerau, 1999; see also Mansour et al., 2020). Sanders et al. (2022) show that free radicals and volatile organic matter from liptinite-rich kerogen during maturation slows vitrinite aromatization (but see also Lewan, 2023). In extreme cases, vitrinite reflectance values can be underestimated by up to 0.4% Rr (Goodarzi et al., 1994). Moreover, TOC values and S2 peak are, in some cases too low to reliably determine T_{max} values. According to organic compounds, MPI1 is dedicated to type III kerogen and fails for immature samples (Ro < c.a. 0.55–0.6%; see Radke, 1988), while the BeP/(BeP + Pe) ratio is not useful above 0.7% of Ro, because of the complete degradation of perylene (Marynowski et al., 2015). Moreover, C_{31} 22S/(S + R) homohopane ratio reaches equilibrium (c.a. 0.58 to 0.6) at Ro = 0.6% (Peters et al., 2005).

Using all of the aforementioned indicators allows the determination of thermal maturity for the studied Oligocene rocks of the Orava Basin. The schematic maps (Figs. 3 and S5) present the data of organic indicators and show the presumed temperature ranges (based on calculations presented in Hunt, 1995; Peters et al., 2005), corresponding to changes in overburden thickness. By far, the lowest temperatures occurred in the N-E part of the basin and in the western part, but only one point was measured there, due to the lack of exposures (Figs. 3 and S5). The lowermost values were recorded near Tvrdosin, as thermally unstable $\beta\beta$-hopanes, hopenes and oleanenes are present in the extracts (samples: 35–36, 39–40, 56–57), all within Zuberec Fm. (Fig. 6). The same samples and a few samples of Biely Potok Fm. (samples: 2–3, 6–7, 9–10) contain unsaturated and relatively unstable diaster-13(17)-enes.

As the thermal maturity of these samples is low, the MPI1 and Rc values are overestimated (Radke, 1988); nevertheless, but other parameters (e.g., C_{31} 22S/(22S + R) and C_{29}20S/(20S + R)) show the lowest values (Figs. 3 and S5; Table 1). Temperatures estimated by Środoń et al. (2006), at 95–100 °C may be considered suitable in the SE part of the Orava Basin; on the other hand, but are far too high for the whole Orava Basin area, especially its NE part. According to the formula proposed by Waliczek et al. (2021), worked out for Polish Outer Carpathian rocks, such concentrations of smectite in illite/smectite diagenetic conversion temperatures in this area do not exceed 80 °C. Nevertheless, temperatures above 70 °C are not possible for samples containing the unstable organic compounds listed above (Peters et al., 2005). The problem with the discrepancy between % smectite and biomarker indicators has also been raised previously (Derkowski et al., 2021). Although there are some objections are still existing, it should be noted that the Orava Basin was estimated to be the least mature among CCPB sediments (Środoń et al., 2006), which is also confirmed here.

5.2. Evaluation of hydrocarbon potential

The best source rock potential was recorded for Zuberec Fm.; this level may be considered as a good source rock, since median values of TOC and hydrocarbon potential (S1 + S2) are ca. 2.0 wt% and 4.4 mg HC/g rock, respectively (Fig. 4). Due to specific, concentrated form of OM of coals, despite high TOC and S1 + S2 values (Fig. 4), their source-rock potential should be considered with caution (Sykes and Snowdon, 2002; Petersen, 2006; Dembicki, 2009; Karayigit et al., 2021). The remaining analyzed formations (Huty and Biely Potok) are poor source rocks, but within Huty Fm. good or even excellent hydrocarbon potential levels were recorded (Fig. 4).

Values of the hydrogen index of all studied formations are usually below 200 mg HC/g TOC indicating domination of the gas-prone type-III kerogen (Fig. 5a; see also Soták et al., 2001); presence of the reworked type-IV kerogen is not excluded. In some samples from Zuberec and Huty formations values of the HI are above 300 mg HC/g TOC indicating their elevated share of the oil-prone type-II kerogen (Fig. 5a). However, in one of these samples (42_Zu), OM content is above 50 wt%, evidencing the presence of coal there (Schopf, 1956). The maturation path of coaly OM is another than dispersed organic matter (Espitalié et al., 1985). Therefore, the type-III kerogen most probably dominates in this sample (Fig. 5a).

5.3. Reconstruction of depositional environments in CCPB

A combination of organic and inorganic geochemical methods, and analysis of pyrite framboid diameters of the Orava Basin deposits were used to reconstruct the sedimentary conditions of the CCPB Oligocene rocks (Fig. 2). As differences in the oxygenation of the sedimentary basin during the deposition of the particular formations are apparent, these will be discussed separately.

5.3.1. Huty Fm.

The content of TOC in the Huty Fm. is within 1 wt% for most of the samples (Table S1). TOC values of four samples are below 0.5 wt% and five samples are above or near 2.0 wt% (excluding the coal sample). Although TOC strongly depends on redox conditions and productivity (Calvert and Pedersen, 1993; Tribovillard et al., 1994), the measured values are not typical of anoxic conditions but of a dysoxic or oxic environment. The TS content is also relatively similar (0.5–1 wt%), although individual samples contain a minimal amount of TS, or on the contrary, >2 wt% (Table S1). As it is mainly sulphidic sulphur (no or little organic sulphur compounds in extracts), pyrites could be formed both in the sediment and in the water column.

The basic organic parameter indicating organic matter depositional conditions is the ratio of two isoprenoids, pristane and phytane (Pr/Ph). The values of this ratio for all samples from the Huty Fm. are higher than
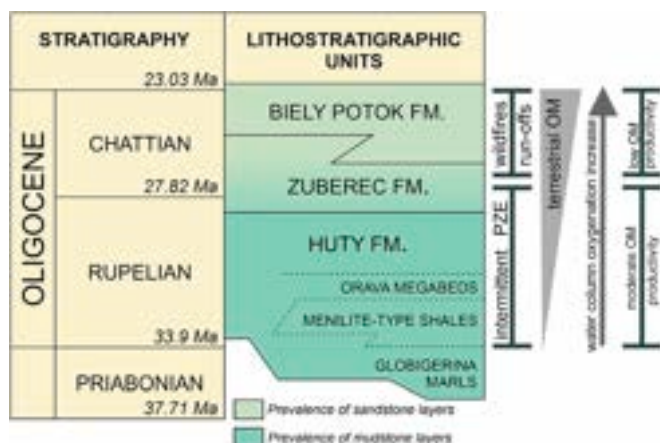
Fig. 2. Oligocene lithostratigraphy of the CCPB and the main processes described in the paper. PZE = photic zone euxinia.

1 (Table S1), and for more than half of the samples, the values are between 2.0 and 5.5. Such data suggest aerobic conditions for sedimentation of organic matter (Didyk et al., 1978), although there are many exceptions, such as multiple pristane origins (for example, from tocopherols identified in some immature samples; Rontani et al., 2010).

In Fig. 7, samples from Huty Fm. cluster mostly in the field characteristic of open marine organic matter (Huang and Meinschein, 1979). Even though the ternary diagram was developed for sterols, not steranes, and does not always reflect the real depositional conditions (e.g., Peters et al., 2005), especially for Paleozoic and older samples (Schwark and Empt, 2006), in the case of the CCPB it appears to reflect the nature of a shallowing sedimentary basin. The Huty Fm. was deposited in the deepest fully marine basin, only rarely shallowing, while the basin slowly became more shallow during the sedimentation of the younger formations. Marine conditions are further supported by the occurrence of algal biomarkers. Dinosteroids, which are the derivatives of

compounds linked to modern dinoflagellates (Kokinos et al., 1998) are most abundant in Huty Fm. samples.

Hopane distribution in samples of the Huty Fm. is classical, with C_{30} $\alpha\beta$ hopane predominance (Fig. 6). Among the homohopanes, C_{31} 22S and 22R epimers dominate, and abundance decreases towards the higher mass homohopanes up to C_{35} (Fig. 6c). Such a distribution of homohopanes is characteristic of the organic matter deposition under oxic to dysoxic conditions (Peters et al., 2005).

Isorenieratane and its derivatives are commonly used biomarkers of green sulphur bacteria and the occurrence of photic zone euxinia (PZE) in the water column (Summons and Powell, 1987; Koopmans et al., 1996; Grice et al., 1996, 2005). Aryl isoprenoids were found in a few samples of the Huty Fm., and only one has other isorenieratane decomposition derivatives, but isorenieratane was not found. This may be related to the fact that these compounds undergo decay with increasing temperature (Requejo et al., 1992), whereas rocks from the Huty Fm. are exposed in the southern part of the study area and have the highest (with a few exceptions) thermal maturity (Fig. 3). Small abundances of gammacerane (Fig. 6) were also identified in several samples that contained aryl isoprenoids. This compound is interpreted as an indicator of water column stratification (Sinninghe Damsté et al., 1995). However, it is probable that, unlike in the Oligocene sediments of the Outer Carpathians (Köster et al., 1998b; Kotarba et al., 2007), the PZE occurred sporadically in the Huty Fm., at least when considering this part of the CCPB and comparing data to inorganic proxies and framboids (Fig. 2).

The ternary diagram of the Fe-TS-TOC relation (Fig. S6), which is based on pyrite formation in water column and sediments (Dean and Arthur, 1989; Arthur and Sageman, 1994), defines the general depositional conditions, and should be applied to samples where the vitrinite reflectance (Ro) is lower than 0.8% (Dean and Arthur, 1989). Based on these criteria during deposition of the Huty Fm., the dysoxic to oxic conditions prevail while the anoxic conditions occured only localy (Fig. S6). Values of the Th/U, Ni/Co and V/Cr ratios suggest domination of the aerobic conditions during the Huty Fm. sedimentation (Fig. 12). The same evaluation is received applying the U_{aut}, where its values are
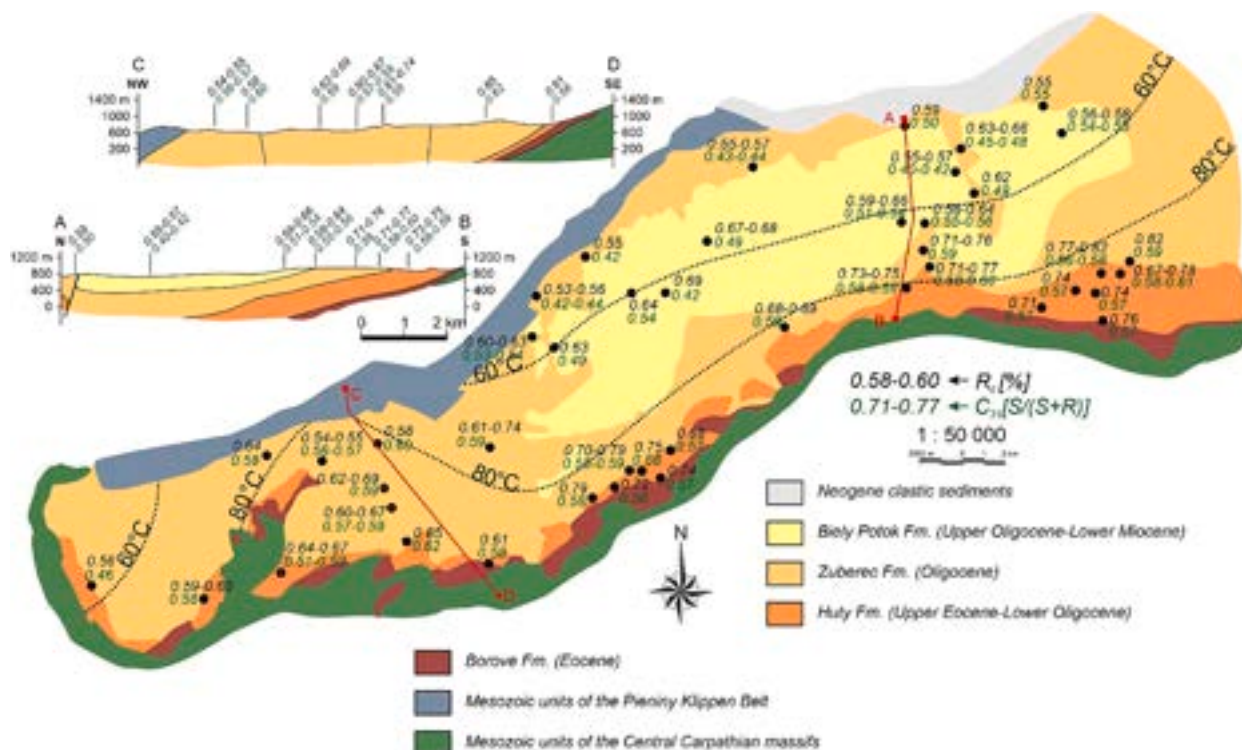
Fig. 3. Schematic map showing the distribution of calculated vitrinite reflectance (Rc) and C_{31} 22S/(22S + R) homohopane ratio for the Orava Basin area.

9
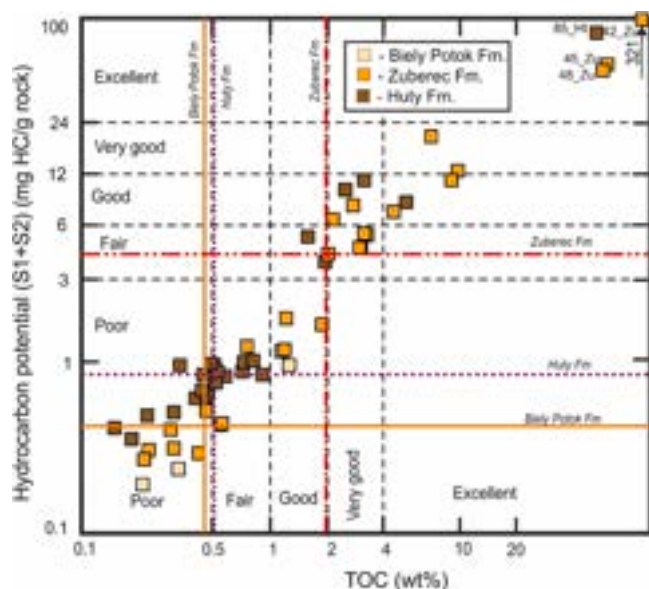
Fig. 4. Petroleum source quality diagram according to criteria of Peters and Cassa (1994). Solid lines represent median values of TOC and S1 + S2 for Biely Potok Fm., dotted lines represent median values of TOC and S1 + S2 for Huty Fm. and dashed–double dotted lines represent median values of TOC and S1 + S2 for Zuberec Fm.

below 2 for most samples (Table S7), and suggest aerobic conditions (Wignall, 1994). However, short euxinic pulses, are not necessarily recorded in inorganic proxies because, for example, uranium can be oxidized to the soluble U^{6+} form during the recurrence of oxic conditions on the seafloor (Tribovillard et al., 2006; Pollack et al., 2009). In the Mo_{EF} vs. U_{EF} diagram (Fig. 13), they are located in an uncharacteristic field (probably aerobic to suboxic conditions), or in a field typical of a particulate shuttle, when conditions were dysoxic on the seafloor and oxic in the water column (Chen et al., 2022). Generally, Mo enrichment in relation to U suggests unstable depositional conditions with intermittent events of suboxic-anoxic conditions in the generally oxic water column (Algeo and Tribovillard, 2009; Ai et al., 2021). This is additionally supported by TOC/P ratio values, which differ significantly in the analyzed Huty Fm. samples varying from as low as 7 to over 4000 in coaly beds (Table S7).

The biomarkers and inorganic geochemical data are well supported by the pyrite framboid diameter study. For the Huty Fm., in seven of the twenty samples measured, the population of tiny pyrites (<5 μm in diameter) is not <50% (Table S4; Fig. 14). Moreover, there are at least 45% tiny pyrites in a further four samples.

Such data may suggest the intermittent occurrence of euxinia in the water column and the formation of tiny pyrites (Wilkin et al., 1996; Bond and Wignall, 2010). However, larger pyrites formed in the sediment, under variable, generally dysoxic conditions.

5.3.2. Zuberec Fm.

In the Zuberec Fm., TOC values are more varied than in the Huty Fm. There are more black shales whose TOC values are higher than 2.0 wt%, reaching up to 9–10 wt%, although rocks containing <0.5 wt% (mainly sandstones) are also present (Table S1). The TS values are similar to those recorded for Huty Fm. (Table S1), and as with this formation, it is mainly inorganic sulphur.

In Zuberec Fm., the Pr/Ph ratio values are in fact very similar to values noted for Huty Fm. (Table S1). Only two samples were characterized by values slightly below 1, while for about half of the samples, the Pr/pH values were higher than 2, suggesting, that oxic conditions can also be indicated as occurring during the organic matter sedimentation.
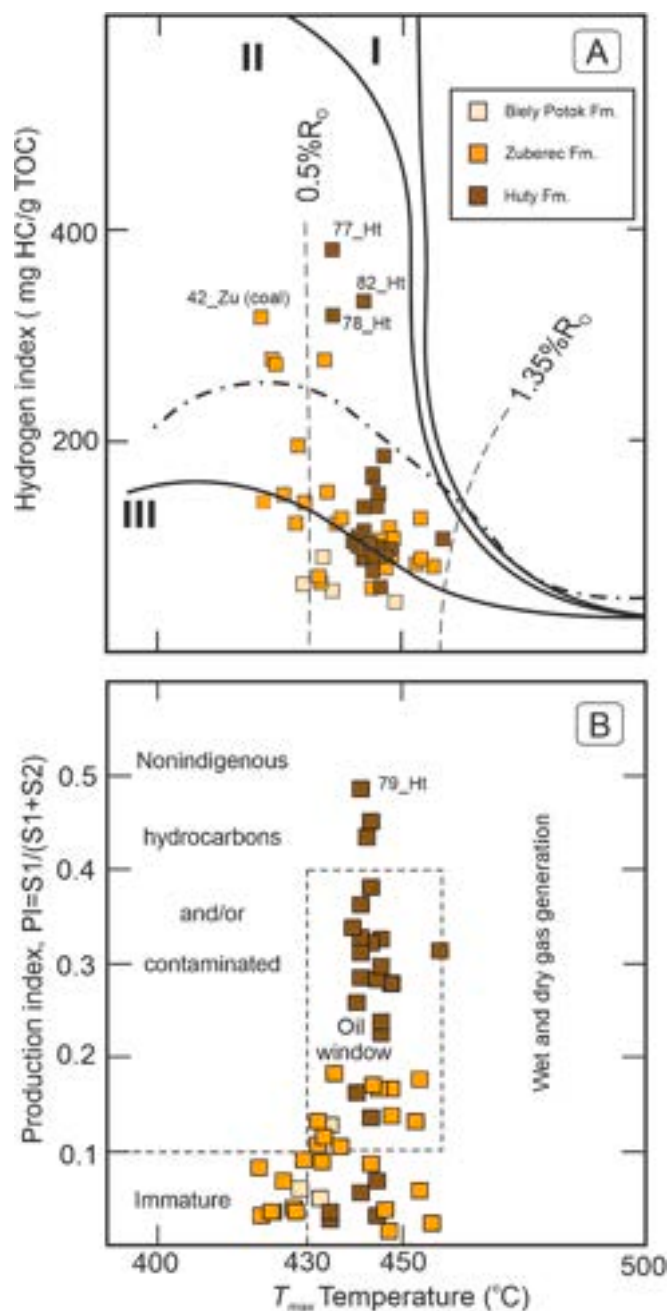
Fig. 5. T_{max} temperature versus (A) hydrogen index and (B) production index. Maturation paths for kerogens and maturity ranges after Espitalié et al. (1985). Dashed-dotted line represents the maturity path of organic matter concentrated in lenses or seams (coals).

In the sterane ternary diagram (Fig. 7), samples from Zuberec Fm. are located in estuarine and terrestrial fields. We believe that the basin was surrounded by land (at least partially) and the water was brackish due to the numerous river outputs. However, at least in the lower part of Zuberec Fm., the estuarine type was rather intermittent (Day, 1981), and marine conditions could prevail over relatively wide intervals which is additionally documented by relatively high content of dinosteroids in most samples (Table S6, Fig. S4). In the upper part of the Zuberec Fm., the basin became shallow to the extent that clastic material dominated over clay deposition, and organic matter was represented with mainly the terrestrial type.

Homohopanes in samples of Zuberec Fm. are also characterized by the predominance of C_{31} 22S and 22R epimers, with a gradual decrease
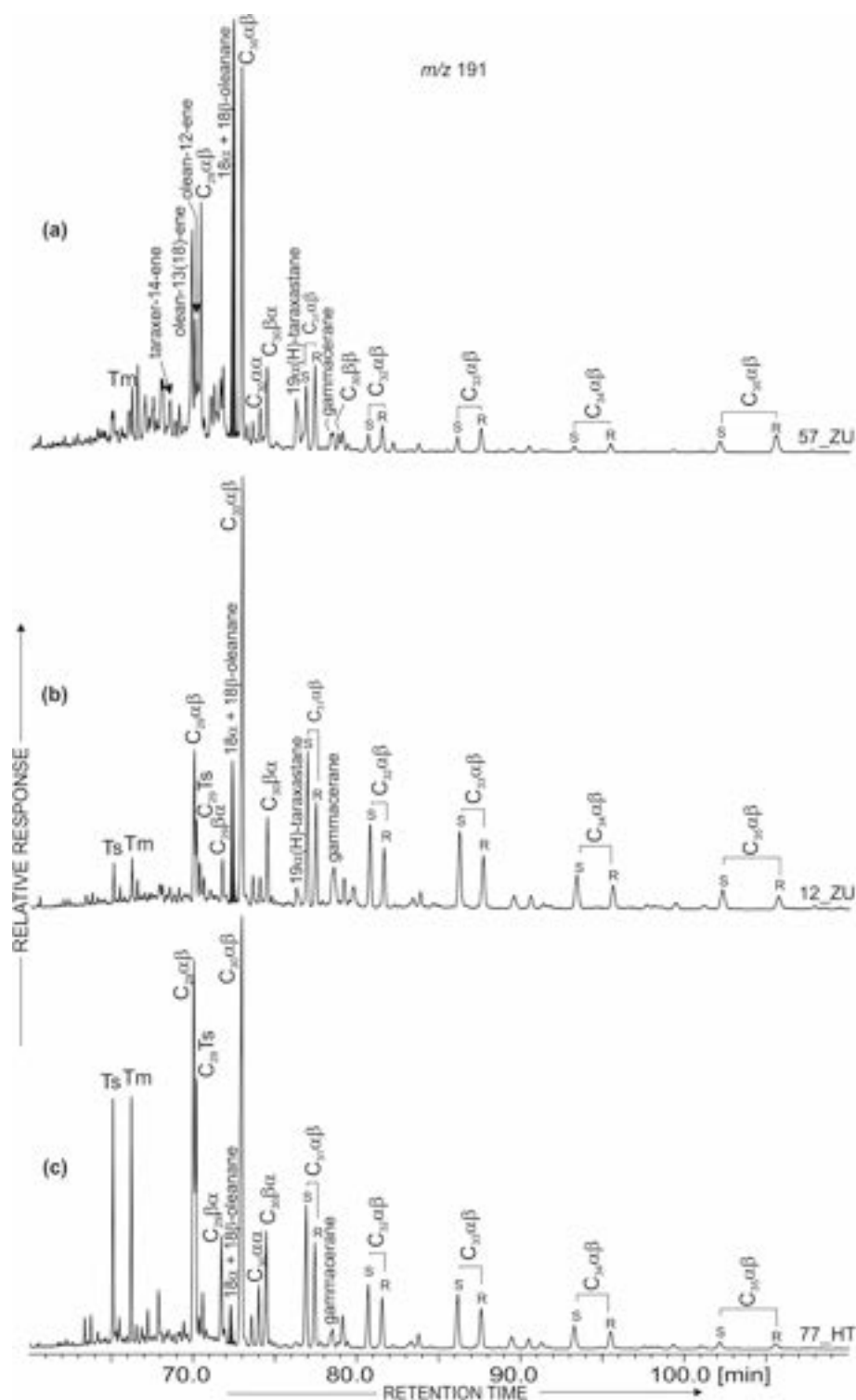
Fig. 6. Partial *m/z* 191 mass chromatograms for sample extracts from Zuberec (a) and (b) and Huty (c) Formations, showing the diverse distributions of pentacyclic triterpenoids.

towards higher masses, but in some cases, there is a slight increase in the higher mass homohopanes, for example at C_{35} (Fig. 6a). However, this situation is rare, mostly in samples that contain isorenieratane and its derivatives.

Isorenieratane and its derivatives, including aryl isoprenoids, are more common in Zuberec Fm., than in Huty Fm. Although isorenieratane was identified in very low abundance only in one sample (12_Zu; Fig. 10), the other diaromatic isorenieratane derivatives and

aryl isoprenoids were found in two profiles from the Oravice village (samples: 23_Zu – 32_Zu and 52_Zu – 55_Zu; eight samples in total) and four samples from Tvrdosin area (Fig. 1). Gammacerane was also found in several samples (Fig. 6). The basin appears to have been fragmented into smaller, more restrictive sub-basins or bays during the deposition of the Zuberec Fm. due to progressive shallowing. This caused PZE in the water column. Continuous pulses of shallowing and delivery of terrigenous material into the reservoir interrupted the anoxia, oxygenating
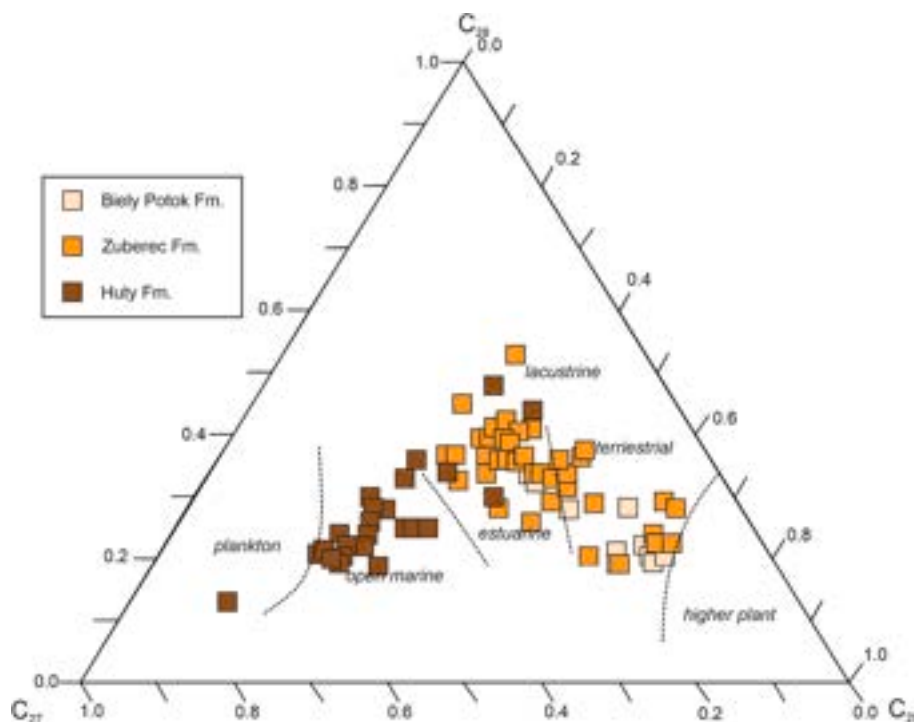
Fig. 7. Ternary diagram showing the distribution of C_{27}, C_{28} and C_{29} regular steranes for the rock extracts from the Huty, Zuberec and Biely Potok Fms.

the bottom waters.

Inorganic indicators for the Zuberec Fm. show similar values to those of the Huty Fm. For the Fe-TS-TOC ternary diagram, a bit more samples fall within the anoxic conditions (Fig. S6) In the case of the Mo_{EF} vs. U_{EF} diagram, more samples are enriched in Mo and are in the range of the particulate shuttle field (Fig. 13). In this respect, the samples differ from the Oligocene from the Outer Carpathians, as these rocks fall within suboxic to anoxic conditions (Wójcik-Tabol et al., 2022). Also, U_{aut} values and TOC/P ratio are quite higher than in the case of Huty Fm. (Table S7). Based on inorganic proxies, depositional conditions appear to have been similar for both formations, with the Zuberec Fm. tending to be a little more restrictive.

In ten of the twenty-four samples, the amount of tiny framboidal pyrite is greater than or equal to 50% (Table S4; Fig. 14). In addition, 3 samples contain >70% of tiny framboids. This fact, together with the presence of isorenieratane and its derivatives in part of the samples, suggests periodic euxinia in the water column, primarily in the lower part of the Zuberec Fm. The framboid diameter values obtained are generally larger than those measured for the Outer Carpathians (Wendorff-Belon et al., 2021; fine framboids accounted for 80% or more in most of the samples), indicating more reducing conditions during sedimentation of the early Oligocene Menilite shales.

5.3.3. Biely Potok Fm.

TOC values in Biely Potok Fm. are more or less similar to other studied Oligocene formations, with the measured values falling rather within the lower limits of TOC (mostly below 2 wt%; Table S1). TS values are also in the lower ranges, not exceeding 1 wt%.

The Pr/Ph ratio values are higher than 1 (with two exceptions) and generally similar to other formations, tentatively suggesting aerobic conditions (but see ten Haven et al., 1987).

The distribution of steranes in Biely Potok Fm. is characteristic of terrestrial organic matter (Fig. 7), with rare estuarine intercalations, suggesting a successive shallowing of the basin, up to terrestrial conditions in the latest Oligocene and early Miocene. Algal-derived biomarkers like steranes and dinosteranes are still present but their content is the lowest in comparison to other units (Fig. 7; Table S6).

In the case of Biely Potok Fm. homohopanes in all samples show a distribution typical of oxic conditions, with a clear dominance of C_{31} 22 (S + R) epimers and very low abundances of the higher mass homohopanes. In contrast, very high amounts of 18α + 18β-oleananes, norlupanes, and bisnorlupanes were detected. Frequently these hydrocarbons were the main compounds present in the aliphatic fraction, confirming the terrestrial character of organic matter.

During the sedimentation of Biely Potok Fm., there is no indication of restricted depositional conditions or PZE. Isorenieratane, its derivatives and aryl isoprenoids were not found in any sample.

In the Biely Potok Fm., all samples show an aerobic or occasionally dysoxic character (Figs. 12 and 13). TOC/P values seem to be the lowest in regard to other analyzed units. Individual samples are slightly enriched in Mo, which may suggest an occasional dysoxic bottom-water environment (Ai et al., 2021), but the majority were deposited in oxic conditions, with relatively rapid sedimentation.

In the Biely Potok Fm. deposits, the percentage of tiny framboids is low. Only in one sample it exceeds 40%, and in the others, the values range from 20 to 38%. Such data again confirm the generally oxic character of the sedimentation of this formation (Fig. 2).

5.4. Terrestrial organic matter and evidence of wildfires

5.4.1. Terrestrial biomarkers

The terrestrial OM was detected in Orava part of the CCPB sedimentary rocks based on different groups of compounds, including *n*-alkanes (CPI and TAR values), bicyclic, tricyclic, and tetracyclic diterpenoids, pentacyclic triterpenoids, aromatic biomarkers and polar compounds (Tables 2, S1 and S8).

According to the GC–MS results, three different types of terrestrial organic matter were detected in all three formations. The first type is organic matter from angiosperm higher plants. Compounds associated with flowering plants were found in both aliphatic and aromatic fractions. Saturated biomarkers common in Oligocene samples are oleananes and lupanes, including 18α- + 18β-oleananes, 24-norlupane, 24,28-bisnorlupanes, and 24,28-bisnor-18a-oleanane. In some less mature Biely Potok samples 17α(H)- and 17β(H)-24,28-bisnorlupanes
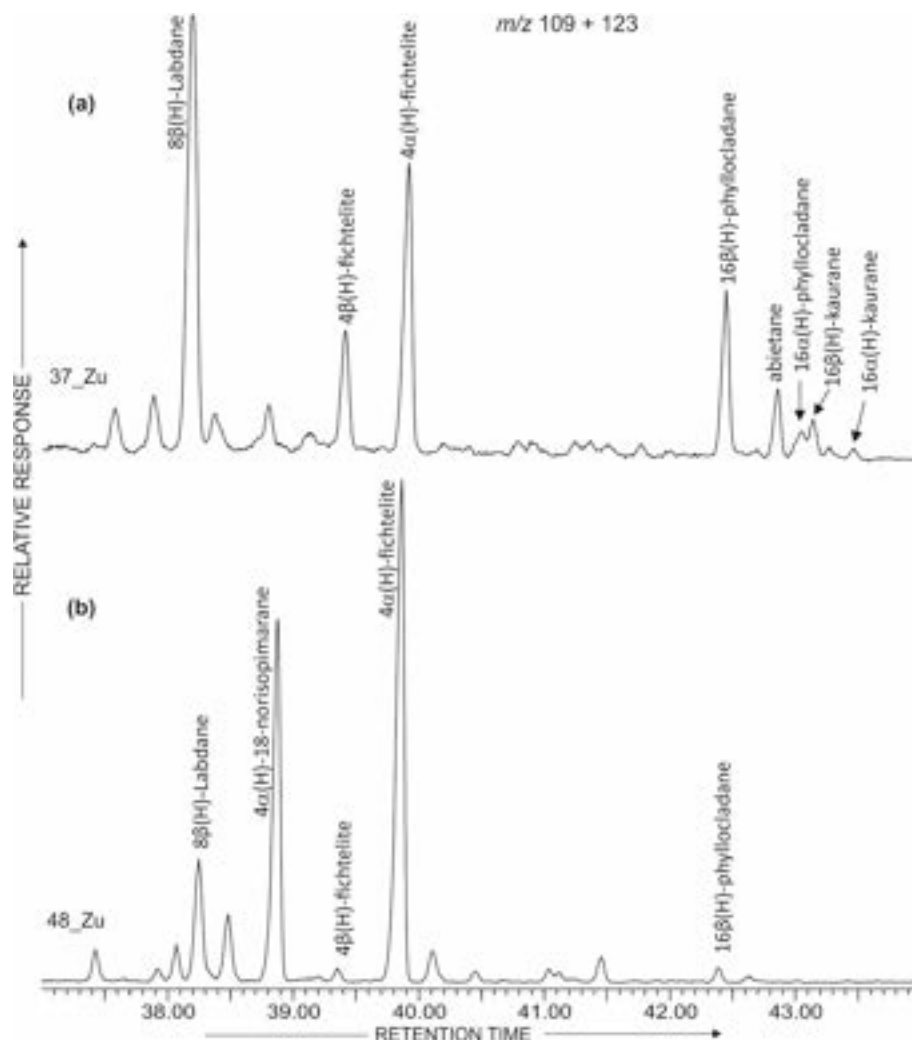
Fig. 8. Summed mass fragmentograms (*m/z* 109 + 123) showing the distribution of diterpanes in rock (a) and coal (b) sample of Zuberec Fm.

and 24-norlupane are dominant peaks in the fraction. Aromatic angiosperm-related compounds are more diverse. Many of the identified compounds are presented in Fig. 9. A more varied representation of aromatic α- and β-amyrin derivatives is found in the rocks of the Biely Potok and upper Zuberec Fms., which may be due to differences in thermal maturity associated with gradual degradation of less stable compounds. For this reason, these compounds are more poorly represented in Huty Fm. (Fig. 9).

The second type is organic matter originating from gymnosperms. In aliphatic fractions, the organic compounds representing the conifers are bicyclic, tricyclic, and tetracyclic diterpenoids, among which labdane, norisopimarane, fichtelite, phyllocladane, abietane, and kaurane have been identified (Fig. 8). Their distribution varies between rock and coal samples (Fig. 8). In coals, bi- and tricyclic diterpenoids dominate with traces of tetracyclic diterpenoids while in rocks all groups of diterpenoids are present with different proportions (but labdane is usually the major). The more thermally altered rock samples from the southern part of the Orava Basin usually do not contain diterpenoids.

Representatives of aromatic biomarkers from gymnosperms include cadalene, retene, 6-isopropyl-1-isohexyl-2-methylnaphthalene (iP-iHMN), dehydroabietane, and simonellite, with the latter two compounds identified only in non-thermally transformed rocks (Table S8). Methyl derivatives of retene and simonellite were also identified. Dehydroabietic acid is a typical compound of conifers found in the polar fraction (Otto and Simoneit, 2001). Moreover, Kotulová et al. (2019)

found amber near the Kojsówka village (Podhale Basin) in the fine-grained sandstones of the Zuberec Fm., thus confirming the significant contribution of resinous plants.

Due to the split of biomarkers from angiosperm and gymnosperm plants between aliphatic and aromatic fractions and their differential degradation pathways under diagenesis, it is not possible to quantify the relationships between these two groups. In general, it can be concluded that the proportion of higher plants in the kerogen in all three formations was significant (as also indicated by the type of kerogen), and gymnosperm and angiosperm higher plants were abundantly represented.

A biomarker of terrestrial origin, most likely from fungi, found in all less thermally transformed samples is perylene (Grice et al., 2009; Marynowski et al., 2013; Oskay et al., 2019; Li et al., 2022). As shown by Marynowski et al. (2015) this compound disappears in samples where vitrinite reflectance exceeds values of c.a. 0.7%, which corresponds well to the presence of perylene in the studied rocks (Table 1). In less mature Biely Potok and upper Zuberec Fms. perylene is one of the major fraction constituents (Fig. 9), significantly superior in quantity to other five-ring PAHs (Fig. S2). High perylene abundances are sometimes linked to humid climates, as fungi thrive more intensively in such conditions (e.g., Hossain et al., 2013), leading to organic matter decay (Oskay et al., 2019). In the case of the samples studied, the origin of perylene in the mainly marine CCPB may be related to runoffs from surrounding land, possibly in association with intense wildfires (Fig. 2). Such post-wildfire
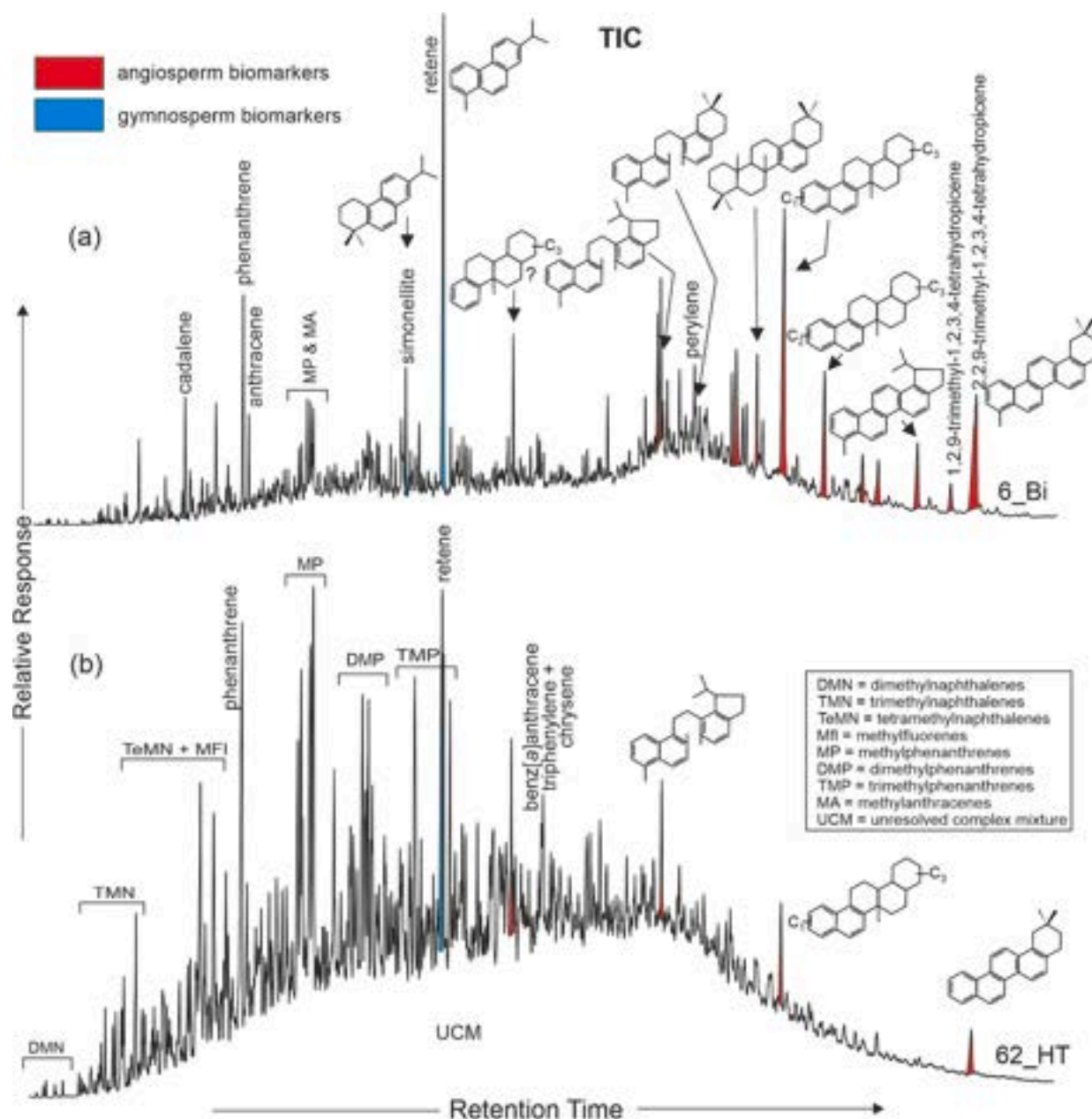
Fig. 9. Total ion chromatograms (TIC) of the aromatic fraction showing differences in aromatic compounds distribution between Biely Potok (a) and Huty (b) Fms.

soil erosion events were previously reported in numerous studies (e.g., DeBano et al., 1998; Santín et al., 2008; Uglik and Nowak, 2015).

5.4.2. Evidences of wildfires

In the rocks of the Biely Potok and upper Zuberec Formations, microscopic observations revealed numerous macerals of the inertinite group (mainly fusinite; Fig. S1). Experimentally, it was shown that as the fusinite reflectance increased, the temperature affecting the wood during the fire was higher (Jones et al., 1991; Belcher et al., 2018). Fusinite reflectance measurements were made on ten samples (3 from Biely Potok Fm. and 7 from Zuberec Fm.) to determine the type of fires (Scott, 2000, 2010) occurring in the middle and upper Oligocene in the area around the CCPB (Table S3). The results indicate diverse fire types, ranging from surface and crown fires in the middle Oligocene (Zuberec Fm.), where average temperatures exceeded 700 °C, to mainly surface fires in the upper Oligocene (Biely Potok Fm.), with temperatures not exceeding 550 °C.

A second, independent indication for the occurrence of wildfires in the middle and upper Oligocene is the significant contribution of unsubstituted polycyclic aromatic hydrocarbons (PAHs) in the samples (Fig. S2). A high content of PAHs in marine sedimentary rocks and coal seams may indicate wildfires on land (Killops and Massoud, 1992) or hydrothermal processes (Simoneit and Fetzer, 1996). As there is no evidence of early-diagenetic hydrothermal activity within the CCPB, the source of the PAHs must be fire-related. In Zuberec and Biely Potok Fm. samples, among other PAHs, as anthracene and methylanthracenes, 4H-cyclopenta[*def*]phenanthrene, benzo[*ghi*]fluoranthene, benz[*a*]anthracene and benzo[*a*]pyrene were identified (Fig. S2), all characteristic for pyrolytic processes (Nabbefeld et al., 2010; Denis et al., 2012; Marynowski et al., 2014; Synnott et al., 2021). Coronene, 6-ring PAH was found only in some of the samples. This organic compound requires higher temperatures to be formed (Kaiho et al., 2021), hence it was not found in samples 2_Bi, 22_Zu, and 37_Zu. In all of these samples, the measured temperatures were relatively low (Table 3). Moreover, some
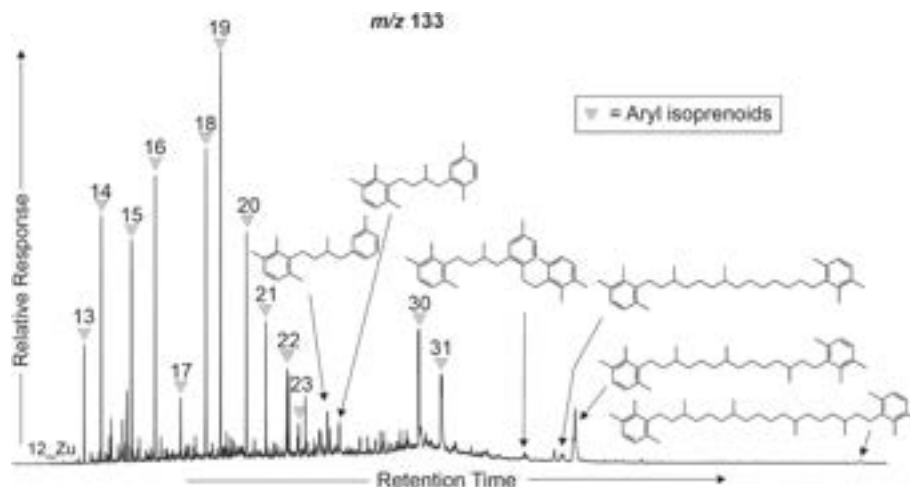
Fig. 10. Partial mass chromatogram *m/z* 133 of the mudstone from Zuberec Fm. showing aryl isoprenoids distribution and isorenieratane and its derivatives. Numbers denote individual carbon number pseudohomologues.
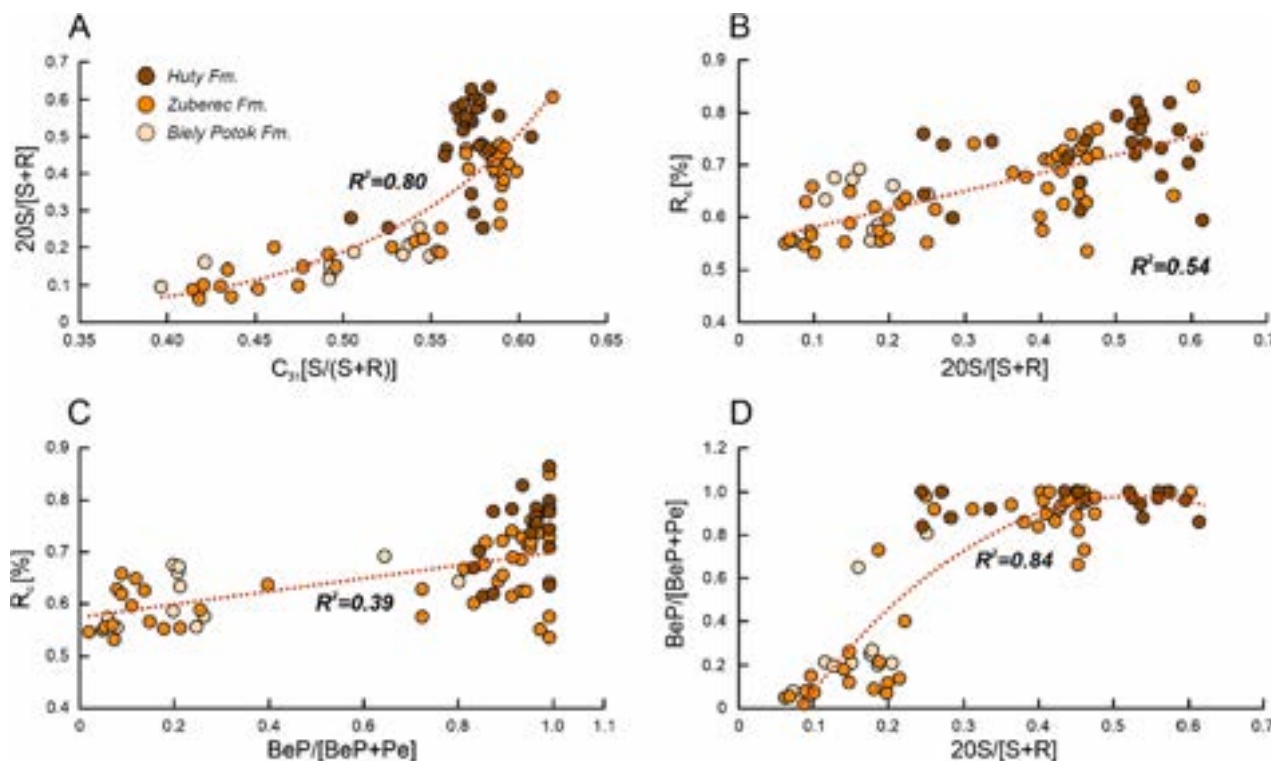
Fig. 11. Cross plots of main maturity parameters showing their mutual correlation.

other common compounds in Oligocene samples, like, e.g., retene could also be (at least partially) generated by wildfires (Ramdahl, 1983). However, high concentrations of retene do not necessarily indicate the dominance of coniferous forest fires on the land (e.g., Karp et al., 2020), as other biomarkers of gymnosperm plants such as simonellite, dehydroabietane, cadalene, or bi-, tri- and tetracyclic diterpanes (Figs. 8 and 9) are also present in samples containing elevated unsubstituted PAHs. This means that the retene is largely derived from unburned organic matter of terrestrial origin.

The ratios of dimethylphenanthrenes were applied to determine the source of burned vegetation (Kappenberg et al., 2019; Karp et al., 2020; Zhao et al., 2023). Thermal experiments have shown that 1,7-DMP is characteristic of softwood burning, 1,2-DMP for hardwood, whereas grass combustion generates both isomers in similar proportions

(Kappenberg et al., 2019). Our data point to grasses as the main source of biomass burned (Fig. 15). However, grasses and other C4 plants did not develop until the Miocene (Karp et al., 2018), and before that, their importance was minor (Sage, 2004). For this reason, and given the presence of biomarkers derived from angiosperms and gymnosperms in the organic matter (Figs. 8 and 9), it appears that we are observing a dimethylphenanthrenes mix derived from both hardwoods and softwoods combustion. During the Late Oligocene in the Thrace Basin (NW Turkey, located further south than the CCPB), the woody vegetation was mixed, abundant in both conifers as well as angiosperms such as *Ulmus*, *Carya*, *Zelkova*, *Alnus*, *Pterocarya* and *Quercus* (Çelik et al., 2017). Furthermore, the effect of diagenesis (thermal maturity) should be taken into account, which may affect the dimethylphenanthrenes distribution (e.g., 1,7-DMP is less stable and its distribution changes with maturity,
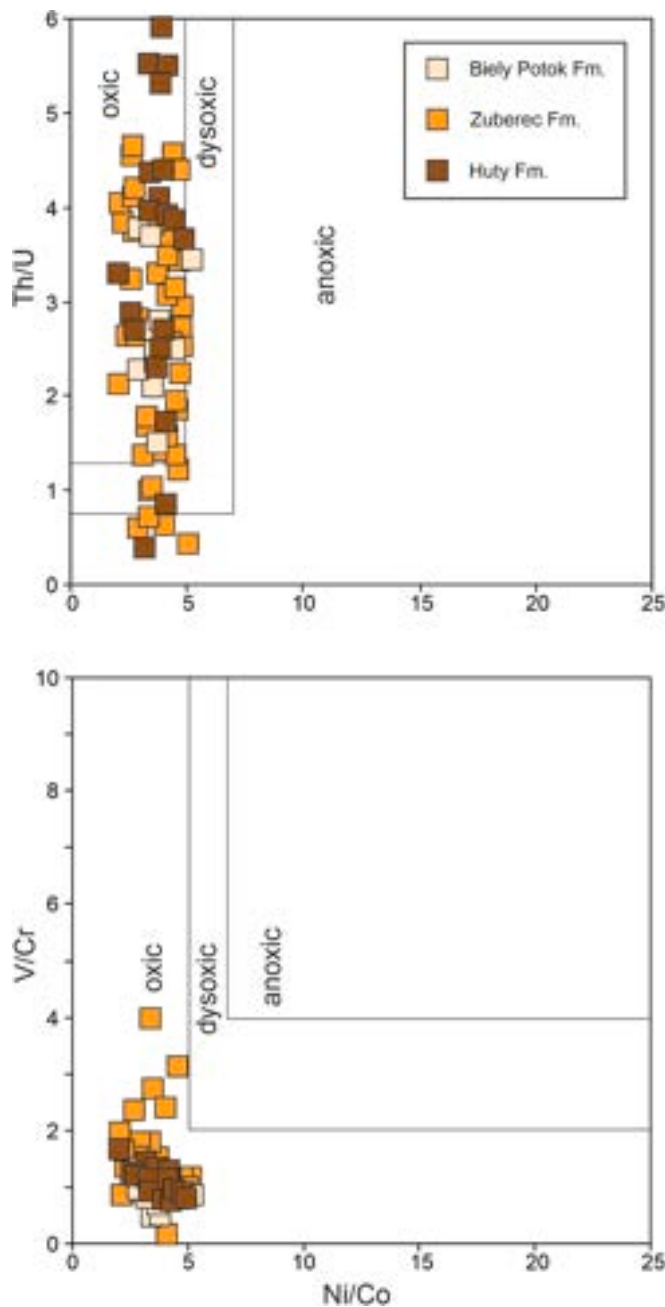
Fig. 12. Cross-plot of trace metal ratios showing paleoredox environments adopted from Hartkopf-Fröder et al. (2007).

Fig. 13. Mo_EF versus U_EF diagram for the Oligocene deposits of the Orava Basin.

Zheng et al., 2023). For this reason, for geological samples, dimethyl-phenanthrenes should be used with caution in determining the source of wildfires (Zhao et al., 2023).

We also tested whether PAHs were derived from smoke or residues, using a low-molecular-weight PAHS to total PAHs ratio (LMW/Total; Table 3; Karp et al., 2020; Vachula et al., 2022). Low-molecular-weight PAHs including phenanthrene, anthracene, fluoranthene, and pyrene are more common in smoke migration, while high-molecular-weight PAHs are rather adsorbed on charcoal fragments (Karp et al., 2020). Most of the examined samples reach LMW/Total values of 0.7–0.8 (Table 3), which suggests PAHs' mixed (smoke and residue) character. However, this proxy generally had higher values for samples from Zuberec Fm. (Table 3) suggesting an origin of PAHs to a greater extent from smoke. This is consistent with the bathymetry of the CCPB, as the basin became shallower during Biely Potok Fm. sedimentation,

deposition was more dynamic, and more organic matter (including charcoal) was transported from the land. In oxic conditions during Biely Potok Fm. deposition, charcoals were preserved as more resistant to weathering than unburned terrestrial organic matter (Kubik et al., 2020). As a consequence, LMW/Total values are lower in Biely Potok Fm. (Table 3), indicating a residue source of PAHs transported from the land.

Oligocene wildfires have been relatively frequently reported from numerous sedimentary basins, starting from the Eocene – Oligocene boundary (Selkin et al., 2015) and continuing throughout the Oligocene (Miao et al., 2022). Late Oligocene wildfires have been reported from the Neuwied Basin in western Germany (Uhl et al., 2022), from the Norken area (Westerwald, Rhineland-Palatinate) (Uhl et al., 2020) and from Northern Hesse, central Germany (Uhl and Jasper, 2018) in all cases as limnic-brackish or brackish-marine deposits. Conifers were the main fuel in these regions (Uhl and Jasper, 2018; Uhl et al., 2022), and surface fires predominated (Uhl et al., 2020). Oligocene wildfires were
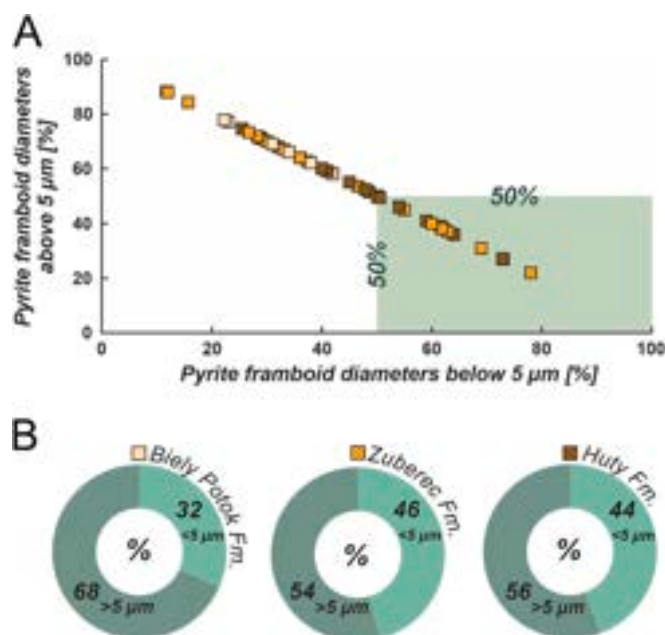
Fig. 14. Cross-plot showing percentage of pyrite with diameters above and below 5 μm (a) and graphs showing the percentage of pyrite diameters in each formation (b).

also documented with black carbon detection in marine formations of the northern South China Sea (Jia et al., 2003), charcoals in the North Pacific Ocean (Herring, 1985), as well as in marginal lacustrine and fluvial deposits of the northern Tibetan Plateau based on microcharcoal detection (Miao et al., 2022). Low content of inertodetrinite was also reported from the late Oligocene coal seams in the Malkara coalfield from the Thrace Basin (NW Turkey), documenting wildfire episodes in paleomires (Karayigit et al., 2021). Moreover, low-temperature wildfires in the late Eocene to early Miocene of NE Bengal Basin were determined using PAH detection, during the early to middle phase of the Himalayan uplift (Hossain et al., 2013).

Here, based on organic geochemical data, we suggest that Oligocene wildfires have contributed to land degradation, which resulted in the

intensification of continental run-off, and in consequence, increased terrigenous OM deposition in the CCPB (Fig. 2). Intensive soil erosion and runoff processes are commonly associated with wildfires in various geological periods (Boudinot and Sepúlveda, 2020; Synnott et al., 2021). Furthermore, enhanced soil erosion (also confirmed by perylene) and its migration into the CCPB could potentially be responsible for nutrient inputs into the basin and periodically enhanced productivity (e.g., Kaiho et al., 2016). However, because the rocks from the upper Zuberec and Biely Potok Fms. are generally organic-poor (Table S1), this process had limited impact in this case.

6. Conclusions

Biomarker and Rock-Eval studies revealed increased thermal maturity from the northern to southern part of the Orava sub-basin, and from Biely Potok Fm. (Upper Oligocene) to Huty Fm. (Lower Oligocene). The gas-prone type-III kerogen occurs in most Paleogene samples but in some rocks taken from Zuberec and Huty Fms. oil-prone type-II kerogen dominates. The best source rock potential was documented for Zuberec Fm., and it may be considered as fair to good source rock interval. The Huty and Biely Potok Fms. are poor source rocks. The maturity of the Oligocene sedimentary rocks from the Orava sub-basin is well defined by the lipid biomarkers. The occurrence of ββ-hopanes, hopenes, oleanenes, and low values of 22S/(22S + 22R) homohopane ratio (reaching c.a. 0.4), as well as 20S/(20S + 20R) sterane ratio (reaching c.a. 0.1–0.2), suggest immature organic matter in northern and northeastern parts of the Orava sub-basin. On the contrary, the S part is characterized by relatively high values of 22S/(22S + 22R) ratio (>0.5) and 20S/(20S + 20R) ratio (>0.4), and lack of unsaturated compounds, indicating that these units have reached the oil window stage.

The dominance of type-III and type-II/III kerogen in both the Lower and Upper Oligocene suggests terrestrial organic matter input to the marine sedimentary rocks. Biomarkers of terrestrial origin, including both angiosperm and gymnosperm affinity, were detected in all samples. Moreover, the high content of perylene in less mature samples indicates fungal input to organic matter, most possibly associated with soil erosion. In the upper part of Zuberec and Biely Potok Fms. the evidence of wildfires was found in several sites. Both, fusinites and elevated pyrolytic PAHs were found. The results indicate diverse fire types, ranging from crown fires in the middle Oligocene (Zuberec Fm.), when average
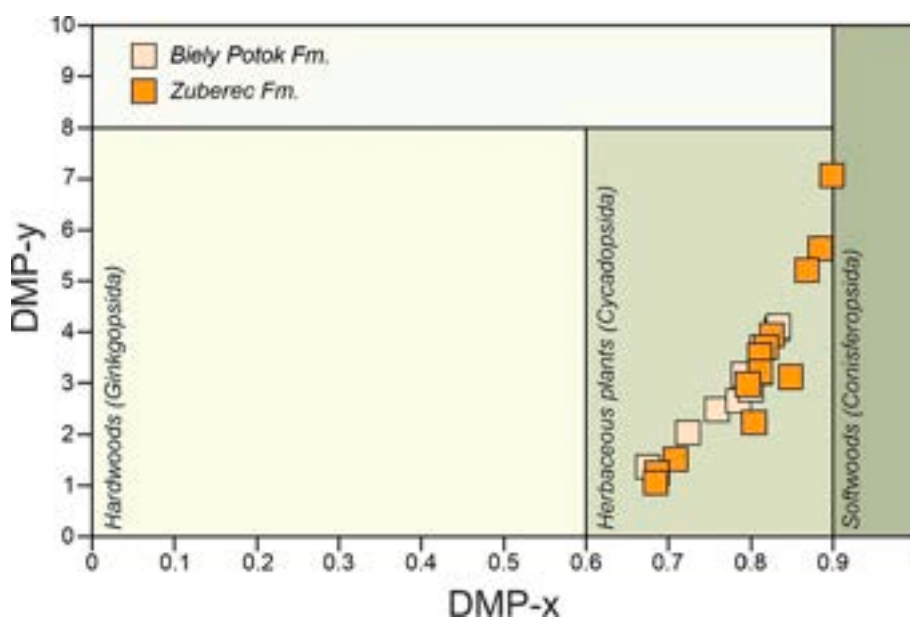
Fig. 15. Cross-plot of the DMPx = (1,7-DMP + 2,6-DMP + 3,5-DMP)/(1,7-DMP + 2,6-DMP + 3,5-DMP + 1,2-DMP) vs. DMPy = 1,7-DMP/1,2-DMP denoting the source of dimethylphenanthrenes in the Oligocene Orava Basin samples.

Table 3

Distribution of dimethylphenanthrenes with calculated ratios and low molecular weight to total PAHs ratio for Biely Potok and Zuberec Fms.

Sample code	DMPx	DMPy	LMW/Total
Biely Potok Fm.			
2_Bi	0.68	1.36	0.75
8_Bi	0.80	2.88	0.77
1_Bi	0.79	3.16	0.50
3_Bi	0.81	3.69	0.67
4_Bi	0.72	2.03	0.45
5_Bi	0.76	2.48	0.73
6_Bi	0.83	4.10	0.74
7_Bi	0.83	4.03	0.65
11_Bi	0.78	2.66	0.16
Zuberec Fm.			
20_Zu	0.81	3.51	0.79
22_Zu	0.71	1.51	0.83
36_Zu	0.85	3.12	0.66
37_Zu	0.80	2.95	0.84
40_Zu	0.80	2.23	0.88
56_Zu	0.82	3.68	0.84
57_Zu	0.83	3.93	0.78
39_Zu	0.81	3.21	0.86
17_Zu	0.87	5.20	0.79
18_Zu	0.90	7.06	0.55
19_Zu	0.88	5.63	0.47
21_Zu	0.69	1.24	0.81
58_Zu	0.68	1.05	0.75

DMPx = (1,7- + 2,6- + 3,5-DMP)/(1,2- + 1,7- + 2,6- + 3,5-DMP).

DMPy = 1,7−/1,2-DMP.

LMW/Total = (Phen + Ant + Flu + Pyr)/(Phen + Ant + Flu +Pyr + BaA + Chry + BkfF + BeP + BaP + IP + BghiPe).

temperatures exceeded 700 °C, to mainly surface fires in the Late Oligocene (Biely Potok Fm.), when temperatures did not exceed 550 °C.

Sedimentary conditions in the Oligocene of Central Carpathian Paleogene Basin changed from predominantly anaerobic to aerobic. In the Lower Oligocene (Huty and lower part of Zuberec Fms.), dysoxic to intermittently euxinic depositional environments were present, which is manifested by the occurrence of isorenieratane and its derivatives, as well as high content of small (<5 μm) pyrite framboids. During the Upper Oligocene, the conditions in the basin were oxic, with increased input of terrestrial organic matter caused by soil erosion, and intensive runoff associated with wildfires.

CRediT authorship contribution statement

Dorota Staneczek: Writing – review & editing, Writing – original draft, Visualization, Validation, Methodology, Investigation, Formal analysis, Data curation, Conceptualization. **Dariusz Więcław:** Writing – review & editing, Writing – original draft, Visualization, Investigation. **Leszek Marynowski:** Writing – review & editing, Writing – original draft, Visualization, Supervision, Methodology, Funding acquisition, Conceptualization.

Declaration of competing interest

None.

Data availability

Data will be made available on request.

Acknowledgments

Appendix A. Supplementary data

Supplementary data to this article can be found online at https://doi.org/10.1016/j.coal.2024.104490.

References

Ai, J., Zhong, N., Zhang, T., Zhang, Y., Wang, T., George, S.C., 2021. Oceanic water chemistry evolution and its implications for post-glacial black shale formation: Insights from the Cryogenian Datangpo Formation, South China. Chem. Geol. 566, 120083.

Algeo, T., Tribovillard, N., 2009. Environmental analysis of paleoceanographic systems based on molybdenum–uranium covariation. Chem. Geol. 268, 211–225.

Arthur, M.A., Sageman, B.B., 1994. Marine black shales: depositional mechanisms and environments of ancient deposits. Annu. Rev. Earth Planet. Sci. 22, 499–551.

Belcher, C.M., New, S.L., Santín, C., Doerr, S.H., Dewhirst, R.A., Grosvenor, M.J., Hudspith, V.A., 2018. What can charcoal reflectance tell us about energy release in wildfires and the properties of pyrogenic carbon? Front. Earth Sci. 6, 169. https://doi.org/10.3389/feart.2018.00169.

Bond, D.P.G., Wignall, P.B., 2010. Pyrite framboid study of marine Permian-Triassic boundary sections: a complex anoxic event and its relationship to contemporaneous mass extinction. GSA Bull. 122, 1265–1279.

Boudinot, F.G., Sepúlveda, J., 2020. Marine organic carbon burial increased forest fire frequency during Oceanic Anoxic Event 2. Nat. Geosci. 13, 693–698.

Bourbonniere, R.A., Meyers, P.A., 1996. Sedimentary geolipid records of historical changes in the watersheds and productivities of Lakes Ontario and Erie. Limnol. Oceanogr. 41, 352–359.

Bray, E.E., Evans, E.D., 1961. Distribution of n-paraffins as a clue to recognition of source beds. Geochim. Cosmochim. Acta 22, 2–15.

Brocks, J.J., Jarrett, A.J.M., Sirantoine, E., Kenig, F., Moczydłowska, M., Porter, S., Hope, J., 2016. Early sponges and toxic protists: possible sources of cryostane, an age diagnostic biomarker antedating Sturtian Snowball Earth. Geobiology 14, 129–149.

Calvert, S.E., Pedersen, T.F., 1993. Geochemistry of recent oxic and anoxic marine sediments: Implications for the geological record. Mar. Geol. 13, 67–88.

Castelluccio, A., Mazzoli, S., Andreucci, B., Jankowski, L., Szaniawski, R., Zattin, M., 2016. Building and exhumation of the Western Carpathians: New constraints from sequentially restored, balanced cross sections integrated with low-temperature thermochronometry. Tectonics 35, 2698–2733.

Çelik, Y., Karayiğit, A.I., Querol, X., Oskay, R.G., Mastalerz, M., Özer, M.S.K., 2017. Coal characteristics, palynology, and palaeoenvironmental interpretation of the Yeniköy coal of late Oligocene age in the Thrace Basin (NW Turkey). Int. J. Coal Geol. 181, 103–123.

Chen, X., Li, S., Newby, S.M., Lyons, T.W., Wu, F., Owens, J.D., 2022. Iron and manganese shuttle has no effect on sedimentary thallium and vanadium isotope signatures in Black Sea sediments. Geochim. Cosmochim. Acta 317, 218–233.

Curiale, J.A., 2006. The occurrence of norlupanes and bisnorlupanes in oils of Tertiary deltaic basins. Org. Geochem. 37, 1846–1856.

Curtis, J.B., Kotarba, M.J., Lewan, M.D., Więcław, D., 2004. Oil/source rock correlations in the Polish Flysch Carpathians and Mesozoic basement and organic facies of the Oligocene Menilite Shales: insights from hydrous pyrolysis experiments. Org. Geochem. 35, 1573–1596.

Day, J.H., 1981. Estuarine Ecology. Rotterdam, A. A. Balkema, p. 411.

Dean, W.E., Arthur, M.A., 1989. Iron–sulfur–carbon relationships in organic-carbon-rich sequences: I. Cretaceous Western Interior Seaway. Am. J. Sci. 289, 708–743.

DeBano, L.F., Neary, D.G., Ffolliott, P.F., 1998. Fire's Effects on Ecosystems. J. Wiley, New York, p. 333.

Dembicki, H., 2009. Three common source rock evaluation errors made by geologists during prospect or play appraisals. AAPG Bull. 93, 341–356.

Denis, E.H., Toney, J.L., Tarozo, R., Scott Anderson, R., Roach, L.D., Huang, Y., 2012. Polycyclic aromatic hydrocarbons (PAHs) in lake sediments record historic fire events: Validation using HPLC-fluorescence detection. Org. Geochem. 45, 7–17.

Derkowski, A., Środoń, J., Goryl, M., Marynowski, L., Szczerba, M., Mazur, S., 2021. Long-distance fluids migration defines diagenetic history of unique Ediacaran sediments in the east European Craton. Basin Res. 33, 570–593.

Dickens, A.F., Gudeman, J.A., Gélinas, Y., Baldock, J.A., Tinner, W., Hu, F.S., Hedges, J.I., 2007. Sources and distribution of CuO-derived benzene carboxylic acids in soils and sediments. Org. Geochem. 38, 1256–1276.

Didyk, B.M., Simoneit, B.R.T., Brassell, S.C., Eglinton, G., 1978. Organic geochemical indicators of palaeoenvironmental conditions of sedimentation. Nature 272, 216–222.

Espitalié, J., Deroo, G., Marquis, F., 1985. La pyrolyse Rock Eval et ses applications (part two). Rev. Inst. Fr. Pétrol. 40, 755–784. https://doi.org/10.2516/ogst:1985045.

Espitalié, J., Deroo, G., Marquis, F., 1986. La pyrolyse Rock Eval et ses applications (part three). Rev. Inst. Fr. Pétrol. 41, 73–89. https://doi.org/10.2516/ogst:1986003.

Fabbri, D., Vassura, I., Snape, C.E., 2002. Simple off-line flash pyrolysis procedure with in situ silylation for the analysis of hydroxybenzenes in humic acids and coals. J. Chromatogr. A 967, 235–242.

Fabbri, D., Torri, C., Simoneit, B.R.T., Marynowski, L., Rushdi, A.I., Fabiańska, M.J., 2009. Levoglucosan and other cellulose and lignin markers in emissions from burning of Miocene lignites. Atmos. Environ. 43, 2286–2295.

Francu, J., Müller, P., 1983. Organic matter maturity in Peri-Klippen Flysch of the Inner Carpathian Mts (East Slovakia). Geol. Carpath. 34, 483–494.

Goodarzi, F., Snowdon, L., Gentzis, T., Pearson, D., 1994. Petrological and chemical characteristics of liptinite-rich coals from Alberta, Canada. Mar. Pet. Geol. 11, 307–319.

Grice, K., Schaeffer, P., Schwark, L., Maxwell, J.R., 1996. Molecular indicators of palaeoenvironmental conditions in an immature Permian shale (Kupferschiefer, lower Rhine Basin, N.W. Germany) from free and sulfide-bound lipids. Org. Geochem. 25, 131–147.

Grice, K., Cao, C., Love, G.D., Bottcher, M.E., Twitchett, R., 2005. Photic zone euxinia during the Permian-Triassic superanoxic event. Science 307, 706–709.

Grice, K., Lu, H., Atahan, P., Asif, M., Hallmann, C., Greenwood, P., Maslen, E., Tulipani, S., Williford, K., Dodson, J., 2009. New insights into the origin of perylene in geological samples. Geochim. Cosmochim. Acta 73, 6531–6543.

Gross, P., Köhler, E., Samuel, O., 1984. New lithostratigraphic classification of the Central Carpathians Paleogene. Geol. Práce, Správy 81, 103–117.

Gross, P., Köhler, E., Haško, J., Halouzka, R., Mello, J., Nagy, A., 1993. Geology of the Southern and Eastern Orava. Štátny Geologický Ústav Dionýza Štúra, Bratislava.

Hartkopf-Fröder, C., Kloppisch, M., Mann, U., Neumann-Mahlkau, P., Schaefer, R.G., Wilkes, H., 2007. The end-Frasnian mass extinction in the Eifel Mountains, Germany: New insights from organic matter composition and preservation. In: Becker, R.T., Kirchgasser, W.T. (Eds.), Devonian Events and Correlations: Geological Society, 278. Special Publications, London, pp. 173–196.

Herring, J.R., 1985. Charcoal fluxes into sediments of the North Pacific Ocean: the Cenozoic record of burning. Geophysical Monograph Series. The Carbon Cycle Atmos. CO2: Nat. Variat. Arch. Present 32, 419–442. https://doi.org/10.1029/gm032p0419.

Hossain, H.M.Z., Sampei, Y., Roser, B.P., 2013. Polycyclic aromatic hydrocarbons (PAHs) in late Eocene to early Pleistocene mudstones of the Sylhet succession, NE Bengal Basin, Bangladesh: Implications for source and paleoclimate conditions during Himalayan uplift. Org. Geochem. 56, 25–39.

Huang, W.-Y., Meinschein, W.G., 1979. Sterols as ecological indicators. Geochim. Cosmochim. Acta 43, 739–745.

Hunt, J.M., 1995. Petroleum Geochemistry and Geology. W.H. Freeman, New York, p. 743.

ISO 7404-2, 2009. Methods for the Petrographic Analysis of Coals – Part 2: Methods of Preparing Coal Samples. International Organization for Standardization, Switzerland.

Jia, G., Peng, P., Zhao, Q., Jian, Z., 2003. Changes in terrestrial ecosystem since 30 Ma in East Asia: stable isotope evidence from black carbon in the South China Sea. Geology 31, 1093–1096.

Jirman, P., Geršlová, E., Bubík, M., Sachsenhofer, R.F., Bechtel, A., Więcław, D., 2019. Depositional environment and hydrocarbon potential of the Oligocene Menilite Formation in the Western Carpathians: a case study from the Loučka section (Czech Republic). Mar. Pet. Geol. 107, 334–350.

Jones, T.P., Lim, B., 2000. Extraterrestrial impacts and wildfires. Palaeogeogr. Palaeoclimatol. Palaeoecol. 164, 57–66.

Jones, T.P., Scott, A.C., Cope, M., 1991. Reflectance measurements and the temperature of formation of modern charcoals and implications for studies of fusain. Bull. Soc. Géol. France 162, 193–200.

Kaiho, K., Saito, R., Ito, K., Miyaji, T., Biswas, R., Tian, L., Sano, H., Shi, Z., Takahashi, S., Tong, J., Liang, L., Oba, M., Nara, F.W., Tsuchiya, N., Chen, Z.-Q., 2016. Effects of soil erosion and anoxic-euxinic ocean in the Permian-Triassic marine crisis. Heliyon 2, e00137. https://doi.org/10.1016/j.heliyon.2016.e00137.

Kaiho, K., Miura, M., Tezuka, M., Hayashi, N., Jones, D.S., Oikawa, K., Casier, J.-G., Fujibayashi, M., Chen, Z.-Q., 2021. Coronene, mercury, and biomarker data support a link between extinction magnitude and volcanic intensity in the late Devonian. Glob. Planet. Chang. 199, 103452.

Kappenberg, A., Braun, M., Amelung, W., Lehndorff, E., 2019. Fire condensates and charcoals: chemical composition and fuel source identification. Org. Geochem. 130, 43–50.

Karayigit, A.I., Oskay, R.G., Çelik, Y., 2021. Mineralogy, petrography, and Rock-Eval pyrolysis of late Oligocene coal seams in the Malkara coal field from the Thrace Basin (NW Turkey). Int. J. Coal Geol. 244, 103814.

Karp, A.T., Behrensmeyer, A.K., Freeman, K.H., 2018. Grassland fire ecology has roots in the late Miocene. Proc. Natl. Acad. Sci. 115, 12130–12135.

Karp, A.T., Holman, A.I., Hopper, P., Grice, K., Freeman, K.H., 2020. Fire distinguishers: Refined interpretations of polycyclic aromatic hydrocarbons for paleo-applications. Geochim. Cosmochim. Acta 289, 93–113.

Killops, S.D., Massoud, M.S., 1992. Polycyclic aromatic hydrocarbons of pyrolitic origin in ancient sediments: evidence for vegetation fires. Org. Geochem. 18, 1–7.

Kokinos, J.P., Eglinton, T.I., Gõni, M.A., Boon, J.J., Martoglio, P.A., Anderson, D.M., 1998. Characterization of a highly resistant biomacromolecular material in the cell wall of a marine dinoflagellate resting cyst. Org. Geochem. 28, 265–288.

Koopmans, M.P., Köster, J., van Kaam-Peters, H.M.E., Kenig, F., Schouten, S., Hartgers, W.A., de Leeuw, J.W., Sinninghe Damsté, J.S., 1996. Diagenetic and catagenetic products of isorenieratene: molecular indicators for photic zone anoxia. Geochim. Cosmochim. Acta 60, 4467–4496.

Kosakowski, P., 2013. 1D modelling of hydrocarbon generation and expulsion from Oligocene Menilite source rocks in the San and Stryi rivers region (polish and Ukrainian Carpathians). Geol. Quarter. 57, 307–324.

Kosakowski, P., Koltun, Y., Machowski, G., Poprawa, P., Papiernik, B., 2018. The geochemical characteristics of the Oligocene – lower Miocene Menilite Formation in the polish and Ukrainian Outer Carpathians: a review. J. Pet. Geol. 41, 319–335.

Köster, J., Kotarba, M., Lafargue, E., Kosakowski, P., 1998a. Source rock habitat and hydrocarbon potential of Oligocene Menilite Formation (Flysch Carpathians, Southeast Poland): an organic geochemical and isotope approach. Org. Geochem. 29, 543–558.

Köster, J., Rospondek, M., Schouten, S., Kotarba, M., Zubrzycki, A., Sinninghe Damsté, J. S., 1998b. Biomarker geochemistry of a Foreland Basin: the Oligocene Menilite Formation in the flysch Carpathians of Southeast Poland. Org. Geochem. 29, 649–669.

Kotarba, M.J., Więcław, D., Koltun, Y.V., Marynowski, L., Kuśmierek, J., Dudok, I.V., 2007. Organic geochemical study and genetic correlation of natural gas, oil and Menilite source rocks in the area between San and Stryi rivers (polish and Ukrainian Carpathians). Org. Geochem. 38, 1431–1456.

Kotarba, M.J., Więcław, D., Dziadzio, P., Kowalski, A., Bilkiewicz, E., Kosakowski, P., 2013. Organic geochemical study of source rocks and natural gas and their genetic correlation in the central part of the Polish Outer Carpathians. Mar. Pet. Geol. 45, 106–120.

Kotarba, M.J., Więcław, D., Bilkiewicz, E., Dziadzio, P., Kowalski, A., 2017. Organic geochemical study of source rock and natural gas and their genetic correlation in the eastern part of the Polish Outer Carpathians and Paleozoic-Mesozoic basement east of Kraków (southern Poland). Geol. Quarter. 61, 795–824.

Kotulová, J., Starek, D., Havelcová, M., Pálková, H., 2019. Amber and organic matter from the late Oligocene deep-water deposits of the Central Western Carpathians (Orava–Podhale Basin). Int. J. Coal Geol. 207, 96–109.

Králiková, S., Vojtko, R., Sliva, L., Minar, J., Fuegenschuh, B., Kováč, M., Hok, J., 2014. Cretaceous–Quaternary tectonic evolution of the Tatra Mts (Western Carpathians): constraints from structural, sedimentary, geomorphological, and fission track data. Geol. Carpath. 65, 307–326.

Kruge, M.A., Mastalerz, M., Solecki, A., Stankiewicz, B.A., 1996. Organic geochemistry and petrology of oil source rocks, Carpathian Overthrust region, southeastern Poland: implications for petroleum generation. Org. Geochem. 24, 897–912.

Kubik, R., Marynowski, L., Uhl, D., Jasper, A., 2020. Co-occurrence of charcoal, polycyclic aromatic hydrocarbons and terrestrial biomarkers in an early Permian swamp to lagoonal depositional system, Paraná Basin, Rio Grande do Sul, Brazil. Int. J. Coal Geol. 230, 103590.

Kuroda, K.-I., 2000. Pyrolysis-trimethylsilylation analysis of lignin: Preferential formation of cinnamyl alcohol derivatives. J. Anal. Appl. Pyrolysis 56, 79–87.

Laflamme, R.E., Hites, R.A., 1979. Tetra- and pentacyclic, naturally-occurring, aromatic hydrocarbons in recent sediments. Geochim. Cosmochim. Acta 43, 1687–1691.

Lewan, M.D., 2023. Comment: Suppression of vitrinite reflectance by bitumen generated from liptinite during hydrous pyrolysis of artificial source rock by Peters et al. (2018). Org. Geochem. 181, 104628.

Lewan, M.D., Kotarba, M.J., Curtis, J.B., Więcław, D., Kosakowski, P., 2006. Oil-generation kinetics for organic facies with Type-II and-IIS kerogen in the Menilite Shales of the Polish Carpathians. Geochim. Cosmochim. Acta 70, 3351–3368.

Li, Z., Huang, H., Yang, G., Xu, Y., George, S.C., 2022. Occurrence and origin of perylene in Paleogene sediments from the Tasmanian Gateway, Australia. Org. Geochem. 168, 104406.

Ma, A., Zhang, S., Zhang, D., 2008. Ruthenium ion-catalyzed oxidation of asphaltenes of heavy oils in Lunnan and Tahe oilfields in Tarim Basin, NW China. Org. Geochem. 39, 1502–1511.

Mansour, A., Gentzis, T., Carvajal-Ortiz, H., Tahoun, S.S., Elewa, A.M., Mohamed, O., 2020. Source rock evaluation of the Cenomanian Raha Formation, Bakr Oil Field, Gulf of Suez, Egypt: observations from palynofacies, RGB-based sporomorph microscopy, and organic geochemistry. Mar. Pet. Geol. 122, 104661.

Marynowski, L., Zatoń, M., 2010. Organic matter from the Callovian (Middle Jurassic) deposits of Lithuania: compositions, sources and depositional environments. Appl. Geochem. 25, 933–946.

Marynowski, L., Gawęda, A., Cebulak, S., Jędrysek, M.O., 2001. Hydrocarbons migration in tectonic zones of the Western Tatra Mountains crystalline basement (Central Western Carpathians). Geol. Carpath. 52, 3–14.

Marynowski, L., Gawęda, A., Poprawa, P., Żywiecki, M.M., Kępińska, B., Merta, H., 2006. Origin of organic matter from tectonic zones in the Western Tatra Mountains Crystalline Basement, Poland: an example of bitumen – source rock correlation. Mar. Pet. Geol. 23, 261–279.

Marynowski, L., Smolarek, J., Bechtel, A., Philippe, M., Kurkiewicz, S., Simoneit, B.R.T., 2013. Perylene as an indicator of conifer fossil wood degradation by wood-degrading fungi. Org. Geochem. 59, 143–151.

Marynowski, L., Kubik, R., Uhl, D., Simoneit, B.R.T., 2014. Molecular composition of fossil charcoal and relationship with incomplete combustion of wood. Org. Geochem. 77, 22–31.

Marynowski, L., Smolarek, J., Hautevelle, Y., 2015. Perylene degradation during gradual onset of organic matter maturation. Int. J. Coal Geol. 139, 17–25.

Marynowski, L., Pisarzowska, A., Derkowski, A., Rakociński, M., Szaniawski, R., Środoń, J., Cohen, A.S., 2017. Strong influence of palaeoweathering on trace metal concentrations and environmental proxies in black shales. Palaeogeogr. Palaeoclimatol. Palaeoecol. 472, 177–191.

Miao, Y., Chang, H., Li, L., Cheng, F., Garzione, C., Yang, Y., 2022. Early Oligocene—late Miocene wildfire history in the Northern Tibetan Plateau and links to temperature-driven precipitation changes. Front. Earth Sci. 10, 850809 https://doi.org/10.3389/feart.2022.850809.

Moldowan, J.M., Dahl, J., Huizinga, B.J., Fago, F.J., Hickey, L.J., Peakman, T.M., Taylor, D.W., 1994. The molecular fossil record of oleanane and its relationship to angiosperms. Science 265, 768–771.

Nabbefeld, B., Grice, K., Summons, R.E., Hays, L.E., Cao, Ch., 2010. Significance of polycyclic aromatic hydrocarbons (PAHs) in Permian/Triassic boundary sections. Appl. Geochem. 25, 1374–1382.

Nytoft, H.P., Bojesen-Koefoed, J.A., Christiansen, F.G., Fowler, M.G., 2002. Oleanane or Lupane? Reappraisal of the presence of oleanane in Cretaceous-Tertiary oils and sediments. Org. Geochem. 33, 1225–1240.

Nytoft, H.P., Kildahl-Andersen, G., Rise, F., 2016. Unusual hexacyclic oleananes in late cretaceous/Tertiary terrigenous oils: NMR characterisation of the major hexacyclic oleanane in Niger Delta oil. Org. Geochem. 101, 196–206.

Oskay, R.G., Bechtel, A., Karayiğit, A.I., 2019. Mineralogy, petrography and organic geochemistry of Miocene coal seams in the Kınık coalfield (Soma Basin-Western Turkey): Insights into depositional environment and palaeovegetation. Int. J. Coal Geol. 210, 103205.

Otto, A., Simoneit, B.R.T., 2001. Chemosystematics and diagenesis of terpenoids in fossil conifer species and sediment from the Eocene Zeitz Formation, Saxony, Germany. Geochim. Cosmochim. Acta 65, 3505–3527.

Peters, K.E., Cassa, M.R., 1994. Applied source rock geochemistry. In: Magoon, L.B., Dow, W.G. (Eds.), The Petroleum System - from Source to Trap, vol. 60. AAPG Memoir, pp. 93–120.

Peters, K.E., Walters, C.C., Moldowan, J.M., 2005. The Biomarker Guide: Interpreting Molecular Fossils in Petroleum and Ancient Sediments. Prentice-Hall, New Jersey.

Petersen, H.I., 2006. The petroleum generation potential and effective oil window of humic coals related to coal composition and age. Int. J. Coal Geol. 67, 221–248.

Petersen, H., Lindström, S., 2012. Synchronous wildfire activity rise and mire deforestation at the Triassic–Jurassic boundary. PLoS One 7, e47236.

Petersen, H.I., Vosgerau, H., 1999. Composition and organic maturity of Middle Jurassic coals North-East Greenland: evidence for liptinite-induced suppression of huminite reflectance. Int. J. Coal Geol. 41, 257–274.

Pollack, G.D., Krogstad, E.J., Bekker, A., 2009. U–Th–Pb–REE systematics of organic-rich shales from the ca. 2.15 Ga Sengoma Argillite Formation, Botswana: evidence for oxidative continental weathering during the Great Oxidation Event. Chem. Geol. 260, 172–185.

Popescu, B.M., 1995. Romania's petroleum systems and their remaining potential. Pet. Geosci. 1, 337–350.

Poprawa, P., Marynowski, L., 2005. Thermal history of the Podhale Trough (northern part of the Central Carpathian Paleogene Basin)–preliminary results from 1-D maturity modeling. Mineral. Soc. Poland–Spe. Paper. 25, 352–355.

Radke, M., 1988. Application of aromatic compounds as maturity indicators in source rocks and crude oils. Mar. Pet. Geol. 5, 224–236.

Radke, M., Welte, D.H., 1983. The Methylphenanthrene Index (MPI). A maturity parameter based on aromatic hydrocarbons. In: Bjorøy, M., et al. (Eds.), Advances in Organic Geochemistry 1981. J. Wiley and Sons, New York, pp. 504–512.

Ramdahl, T., 1983. Retene - a molecular marker of wood combustion in ambient air. Nature 306, 580–582.

Rauball, J.F., Sachsenhofer, R.F., Bechtel, A., Ćorić, S., Gratzer, R., 2019. The oligocene–miocene Menilite Formation in the Ukrainian Carpathians: a world-class source rock. J. Pet. Geol. 42, 393–416.

Requejo, A.G., Allan, J., Creany, S., Gray, N.R., Cole, K.S., 1992. Aryl isoprenoids and diaromatic carotenoids in Paleozoic source rocks and oils from the Western Canada and Williston basins. Org. Geochem. 23, 205–222.

Rontani, J.-F., Nassiry, M., Michotey, V., Guasco, S., Bonin, P., 2010. Formation of pristane from α-tocopherol under simulated anoxic sedimentary conditions: a combination of biotic and abiotic degradative processes. Geochim. Cosmochim. Acta 74, 252–263.

Rospondek, M.J., Köster, J., Sinninghe Damsté, J.S., 1997. Novel C26 highly branched isoprenoid thiophenes and alkane from the Menilite Formation, Outer Carpathians, Southeast Poland. Org. Geochem. 26, 295–304.

Rybicki, M., Marynowski, L., Stukins, S., Nejbert, K., 2017. Age and origin of the well-preserved organic matter in internal sediments from the Silesian-Cracow Lead-Zinc deposits, Southern Poland. Econ. Geol. 112, 775–798.

Rybicki, M., Marynowski, L., Simoneit, B.R.T., 2020. Composition of organic compounds from low-temperature burning of lignite and their application as tracers in ambient air. Chemosphere 249, 126087.

Sachsenhofer, R.F., Hentschke, J., Bechtel, A., Ćorić, S., Gratzer, R., Gross, D., Horsfield, B., Rachetti, A., Soliman, A., 2015. Hydrocarbon potential and depositional environments of oligo-miocene rocks in the eastern Carpathians (Vrancea nappe, Romania). Mar. Pet. Geol. 68, 269–290.

Sachsenhofer, R.F., Popov, S.V., Ćorić, S., Mayer, J., Misch, D., Morton, M.T., Pupp, M., Rauball, J., Tari, G., 2018. Paratethyan petroleum source rocks: an overview. J. Pet. Geol. 41, 219–246.

Sage, R.F., 2004. The evolution of C4 photosynthesis. New Phytol. 161, 341–370.

Sanders, M.M., Jubb, A.M., Hackley, P.C., Peters, K.E., 2022. Molecular mechanisms of solid bitumen and vitrinite reflectance suppression explored using hydrous pyrolysis of artificial source rock. Org. Geochem. 165, 104371.

Santín, C., Knicker, H., Fernández, S., Menéndez-Duarte, R., Álvarez, M.A., 2008. Wildfires influence on soil organic matter in an Atlantic mountainous region (NW of Spain). Catena 74, 286–295.

Schopf, J.M., 1956. A definition of coal. Econ. Geol. 51, 521–527. https://doi.org/10.2113/gsecongeo.51.6.521.

Schwark, L., Empt, P., 2006. Sterane biomarkers as indicators of palaeozoic algal evolution and extinction events. Palaeogeogr. Palaeoclimatol. Palaeoecol. 240, 225–236.

Scott, A.C., 2000. The Pre-Quaternary history of fire. Palaeogeogr. Palaeoclimatol. Palaeoecol. 164, 281–329.

Scott, A.C., 2010. Charcoal recognition, taphonomy and uses in palaeoenvironmental analysis. Palaeogeogr. Palaeoclimatol. Palaeoecol. 291, 11–39.

Selkin, P.A., Strömberg, C.A.E., Dunn, R., Kohn, M.J., Carlini, A.A., Davies-Vollum, K.S., Madden, R.H., 2015. Climate, dust, and fire across the Eocene-Oligocene transition, Patagonia. Geology 43, 567–570.

Simoneit, B.R.T., Fetzer, J.C., 1996. High molecular weight polycyclic aromatic hydrocarbons in hydrothermal petroleums from the Gulf of California and Northeast Pacific Ocean. Org. Geochem. 24, 1065–1077.

Simoneit, B.R.T., Rybicki, M., Goryl, M., Bucha, M., Otto, A., Marynowski, L., 2021. Monoterpenylabietenoids, novel biomarkers from extant and fossil Taxodioideae and sedimentary rocks. Org. Geochem. 154, 104172.

Sinninghe Damsté, J.S., Kenig, F., Koopmans, M.P., Köster, J., Schouten, S., Hayes, J.M., de Leeuw, J.W., 1995. Evidence for gammacerane as an indicator of water column stratification. Geochim. Cosmochim. Acta 59, 1895–1900.

Soták, J., Pereszlenyi, M., Marschalko, R., Milicka, J., Starek, D., 2001. Sedimentology and hydrocarbon habitat of the submarine-fan deposits of the Central Carpathian Paleogene Basin (NE Slovakia). Mar. Pet. Geol. 18, 87–114.

Środoń, J., Kotarba, M., Biroň, A., Such, P., Clauer, N., Wójtowicz, A., 2006. Diagenetic history of the Podhale-Orava Basin and the underlying Tatra sedimentary structural units (Western Carpathians): evidence from XRD and K-Ar of illite-smectite. Clay Miner. 41, 751–774.

Summons, R.E., Powell, T.G., 1987. Identification of aryl isoprenoids in source rocks and crude oils: Biological markers for the green sulfur bacteria. Geochim. Cosmochim. Acta 51, 557–566.

Sykes, R., Snowdon, L., 2002. Guidelines for assessing the petroleum potential of coaly source rocks using Rock-Eval. Org. Geochem. 33, 1441–1455.

Synnott, D.P., Schwark, L., Dewing, K., Pedersen, P.K., Sanei, H., 2021. Evidence for widespread wildfires and their environmental impact in the late cretaceous Canadian Arctic. Glob. Planet. Chang. 203, 103515.

ten Haven, H.L., Rullkötter, J., 1988. The diagenetic fate of taraxer-14-ene and oleanene isomers. Geochim. Cosmochim. Acta 52, 2543–2548.

ten Haven, H.L., de Leeuw, J.W., Rullkötter, J., Sinninghe Damsté, J.S., 1987. Restricted utility of the pristane/phytane ratio as a palaeoenvironmental indicator. Nature 330, 641–643.

ten Haven, H.L., Lafargue, E., Kotarba, M., 1993. Oil/oil and oil/source rock correlations in the Carpathian Foredeep and overthrust, south-East Poland. Org. Geochem. 20, 935–959.

Tribovillard, N.P., Desprairies, A., Lallier-Vergès, E., Bertrand, P., Pradier, B., Moureau, N., Ramdani, A., Ramanampisoa, L., 1994. Geochemical study of organic-matter rich cycles from the Kimmeridge Clay Formation of Yorkshire (UK): productivity versus anoxia. Palaeogeogr. Palaeoclimatol. Palaeoecol. 108, 165–181.

Tribovillard, N., Algeo, T.J., Lyons, T., Riboulleau, A., 2006. Trace metals as paleoredox and paleoproductivity proxies: an update. Chem. Geol. 232 (1–2), 12–32.

Tribovillard, N., Algeo, T.J., Baudin, F., Riboulleau, A., 2012. Analysis of marine environmental conditions based on molybdenum-uranium covariation – applications to Mesozoic paleoceanography. Chem. Geol. 324–325, 46–58.

Uglik, M., Nowak, G.J., 2015. Petrological recognition of bituminous inertinite enriched coals of the lower Silesian Coal Basin (Central Sudetes, SW Poland). Int. J. Coal Geol. 139, 49–62.

Uhl, D., Jasper, A., 2018. Charred conifer remains from the late Oligocene – early Miocene of Northern Hesse (Germany). Acta Palaeobot. 58, 175–184.

Uhl, D., Wuttke, M., Jasper, A., 2020. Woody charcoal with traces of pre-charring decay from the late Oligocene (Chattian) of Norken (Westerwald, Rhineland-Palatinate, W-Germany). Acta Palaeobot. 60, 43–50.

Uhl, D., Spiekermann, R., Wuttke, M., Poschmann, M.J., Jasper, A., 2022. Wildfires during the Paleogene (late Eocene–late Oligocene) of the Neuwied Basin (W-Germany). Rev. Palaeobot. Palynol. 297, 104565.

Vachula, R.S., Karp, A.T., Denis, E.H., Balascio, N.L., Canuel, E.A., Huang, Y., 2022. Spatially calibrating polycyclic aromatic hydrocarbons (PAHs) as proxies of area burned by vegetation fires: Insights from comparisons of historical data and sedimentary PAH fluxes. Palaeogeogr. Palaeoclimatol. Palaeoecol. 596, 110995.

Wagreich, M., 1995. Subduction tectonic erosion and late cretaceous subsidence along the northern Austroalpine margin (Eastern Alps, Austria). Tectonophysics 242, 63–78.

Wakeham, S.G., Schaffner, C., Giger, W., 1980. Polycyclic aromatic hydrocarbons in recent lake sediments - II. Compounds derived from biogenic precursors during early diagenesis. Geochim. Cosmochim. Acta 44, 415–429.

Waliczek, M., Więcław, D., 2012. Maturity of Menilite Shales from Polish Outer Carpathians based on vitrinite reflectance and Rock-Eval pyrolysis data. Geol. Geophys. Environ. 38, 551–552.

Waliczek, M., Machowski, G., Więcław, D., Konon, A., Wandycz, P., 2019. Properties of solid bitumen and other organic matter from Oligocene shales of the Fore-Magura Unit in Polish Outer Carpathians: Microscopic and geochemical approach. Int. J. Coal Geol. 210, 103206.

Waliczek, M., Machowski, G., Poprawa, P., Świerczewska, A., Więcław, D., 2021. A novel VRo, Tmax, and S indices conversion formulae on data from the fold-and-thrust belt of the Western Outer Carpathians (Poland). Int. J. Coal Geol. 234, 103672.

Wendorff, M., Rospondek, M., Kluska, B., Marynowski, L., 2017. Organic matter maturity and hydrocarbon potential of the lower Oligocene Menilite facies in the Eastern Flysch Carpathians (Tarcău and Vrancea Nappes), Romania. Appl. Geochem. 78, 295–310.

Wendorff-Belon, M., Rospondek, M., Marynowski, L., 2021. Paleoenvironment of the early Oligocene environment of the Central Paratethys revealed by biomarkers and

pyrite framboids from the Tarcău and Vrancea Nappes (Eastern Outer Carpathians, Romania). Mar. Pet. Geol. 128, 105037.

Więcław, D., Sadlik, M., 2019. Evaluation of ground pollution by hydrocarbons using Rock-Eval pyrolysis. Pol. J. Chem. Technol. 21, 8–12.

Więcław, D., Bilkiewicz, E., Kotarba, M.J., Lillis, P.G., Dziadzio, P.S., Kowalski, A., Kmiecik, N., Romanowski, T., Jurek, K., 2020. Origin and secondary processes in petroleum in the eastern part of the Polish Outer Carpathians. Int. J. Earth Sci. 109, 63–99.

Wignall, P.B., 1994. Black Shales. Clarendon Press, Oxford, p. 144.

Wilkin, R.T., Barnes, H.L., Brantley, S.L., 1996. The size distribution of framboidal pyrite in modern sediments: an indicator of redox conditions. Geochim. Cosmochim. Acta 60, 3897–3912.

Wójcik-Tabol, P., Wendorff-Belon, M., Kosakowski, P., Zakrzewski, A., Marynowski, L., 2022. Paleoenvironment, organic matter maturity and hydrocarbon potential of the menilite shales (Silesian unit, Polish Outer Carpathians) – organic and inorganic geochemical proxies. Mar. Pet. Geol. 142, 105767.

Zhao, C., Zhang, K., Xiao, L., Uhl, D., Shi, Z., Zhao, W., Zhao, Q., Sun, Y., Liu, B., 2023. Paleoclimate-induced wildfires in a paleomire in the Ordos Basin, Northern China during the Middle Jurassic greenhouse period. Chem. Geol. 637, 121677.

Zheng, X., Schwark, L., Stockhausen, M., Luo, Q., Wu, J., Zhong, N., Schovsbo, N.H., Sanei, H., 2023. Effects of synthetic maturation on phenanthrenes and dibenzothiophenes over a maturity range of 0.6 to 4.7% EASY%Ro. Mar. Pet. Geol. 153, 106285.

Supplementary materials to the article 1

Supplementary Materials

Depositional conditions, wildfires, maturity, and hydrocarbon potential evaluation of Central Carpathian Paleogene Basin based on integrative approach from Orava Basin

Dorota STANECZEK[1], Dariusz WIĘCŁAW[2], Leszek MARYNOWSKI[1]

[1]*Institute of Earth Sciences, Faculty of Natural Sciences, University of Silesia in Katowice, Będzińska 60, 41-200 Sosnowiec, Poland;*
[2]*Faculty of Geology, Geophysics and Environmental Protection, AGH University of Krakow, Al. Mickiewicza 30, 30-059 Kraków, Poland.*
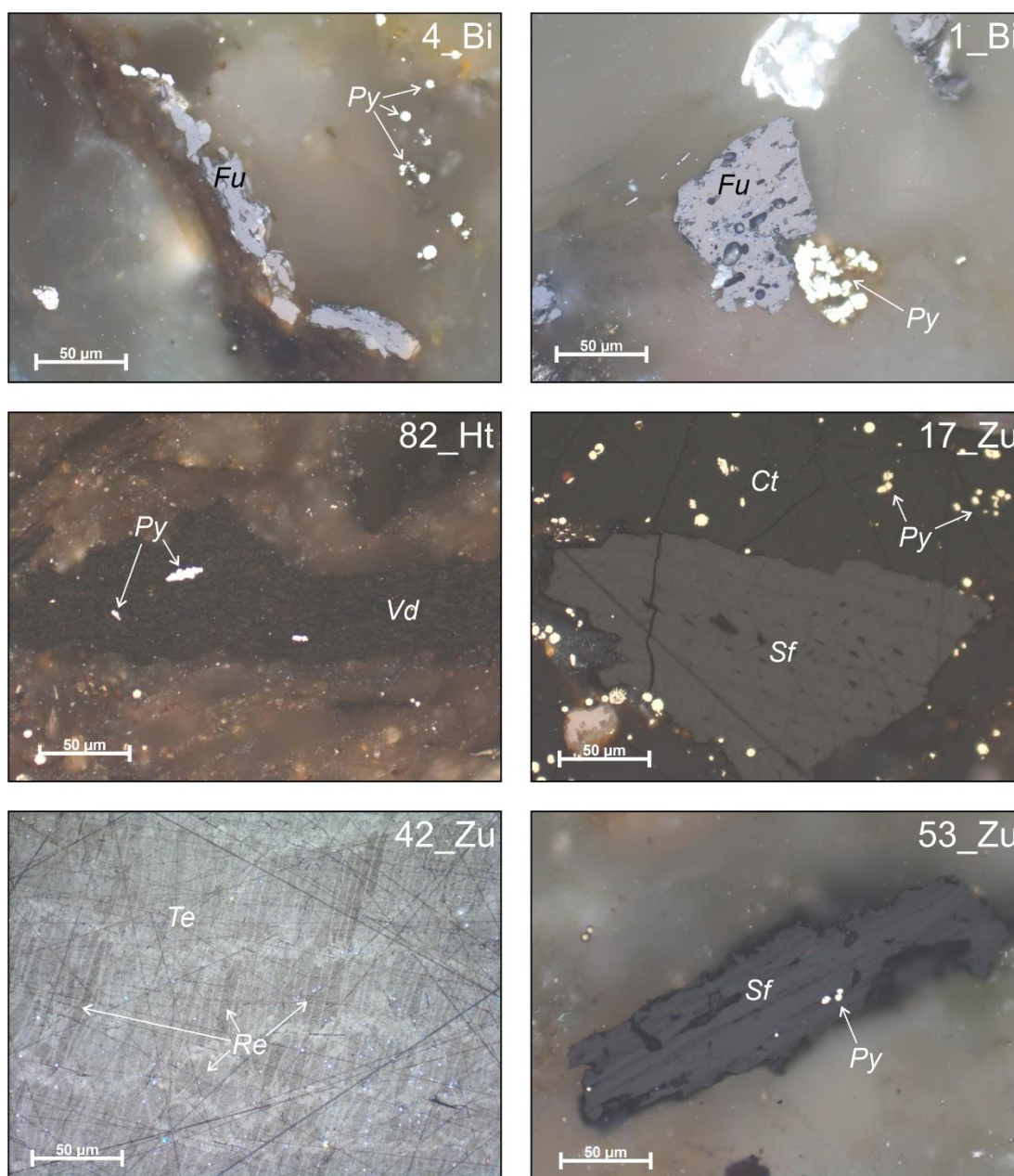
Fig. S1. Examples of macerals observed in reflected light. Abbreviations: Te – tellinite; Ct – collotellinite; Py – pyrite; Re – resinite; Vd- vitrodetrinite; Sf – semifusinite; Fu – fusinite.
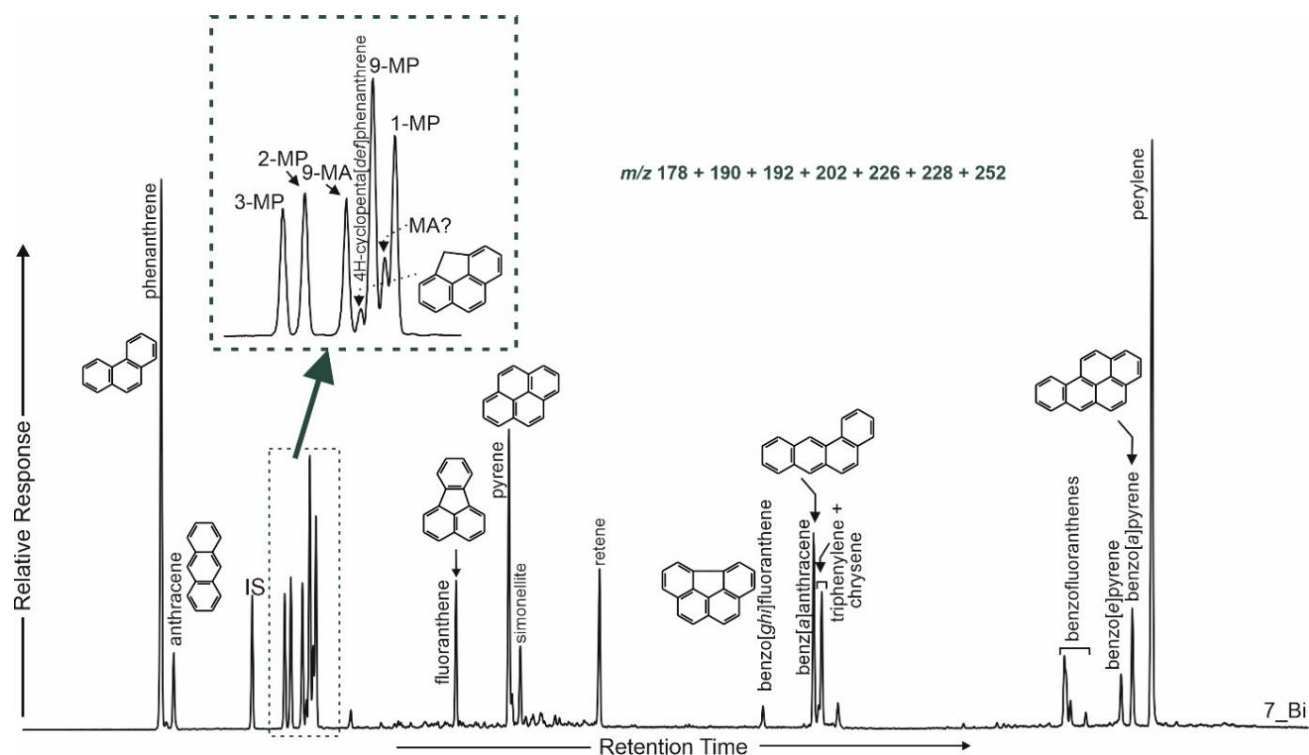
Fig. S2. Summed mass fragmentogram (*m/z* 178 + 190 + 192 + 202 + 226 + 228 + 252) showing distribution of pyrolytic PAHs in extract of Biely Potok sample (for the abbreviations see the legend to the Fig. 9 in the manuscript).

2
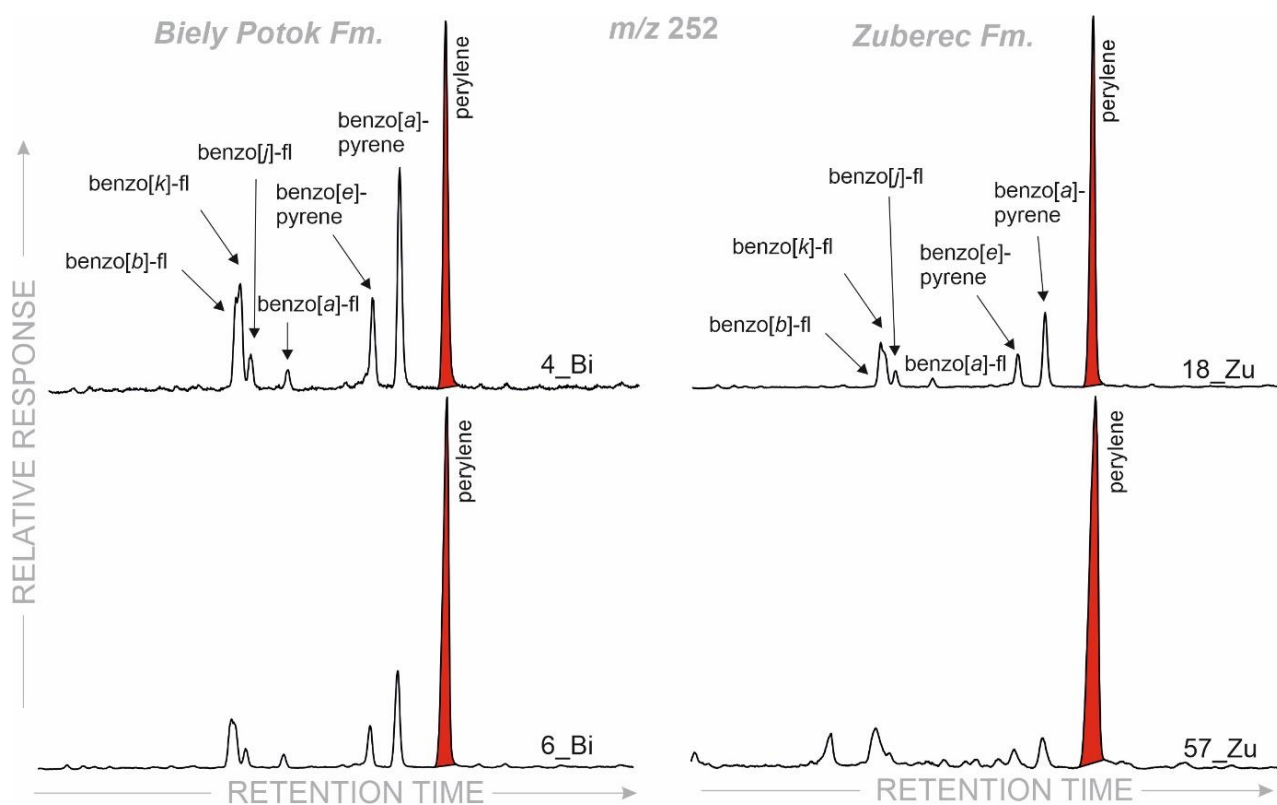
Fig. S3. Partial *m/z* 252 mass chromatograms showing high content of perylene in relation to other pericondensed pentacyclic PAHs in Zuberec and Biely Potok samples.
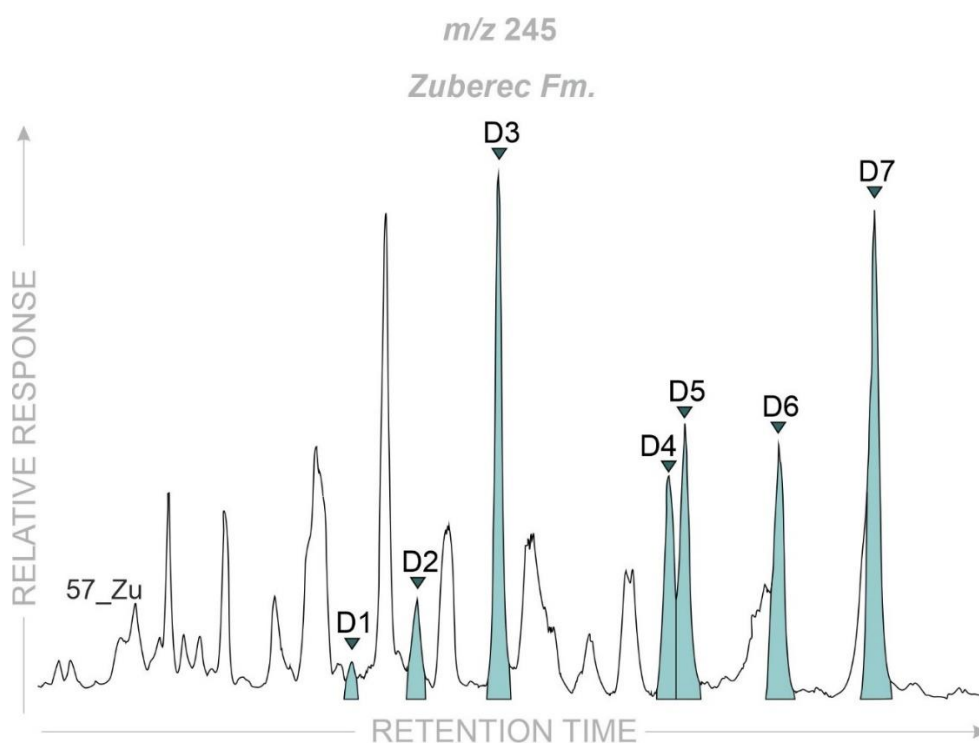
Fig. S4. Distribution of D1-D7 isomers of triaromatic dinosteroids in a Zuberec Fm sample extract.

3
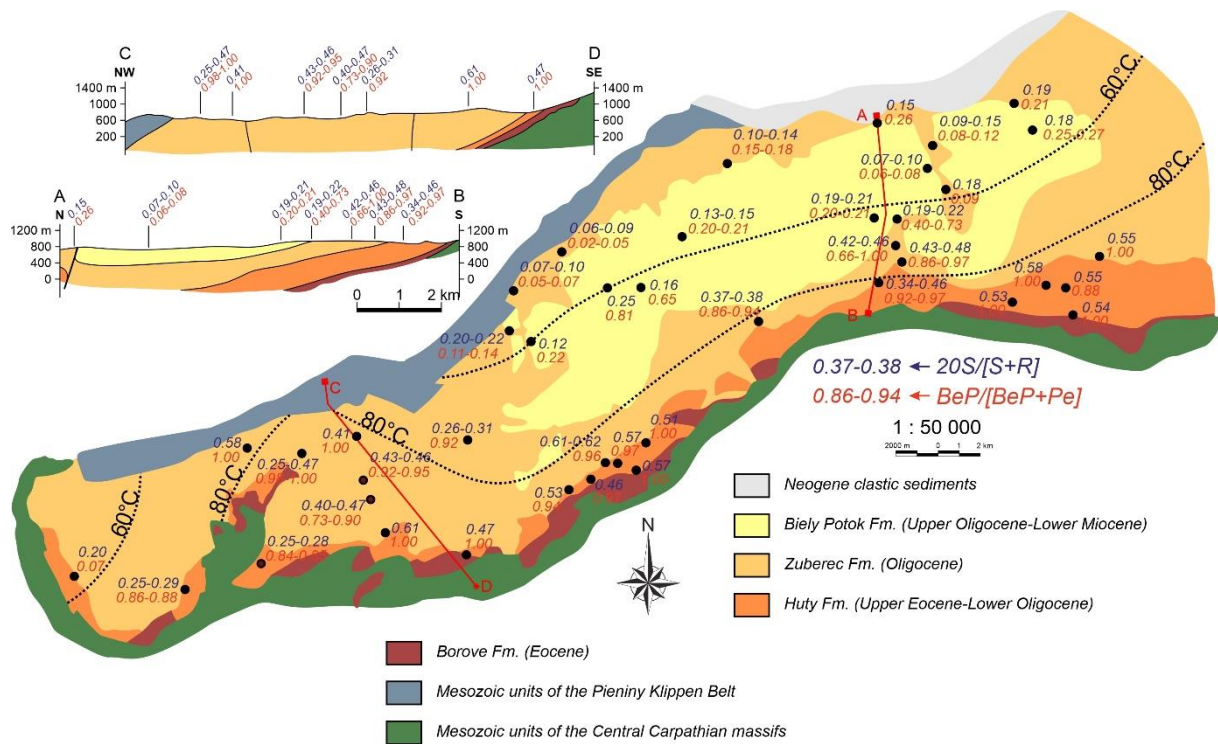
Fig. S5. Schematic map showing the C29 20S/[S+R] sterane parameter distribution and BeP/[BeP+Pe] ratio values for the Orava Basin area.
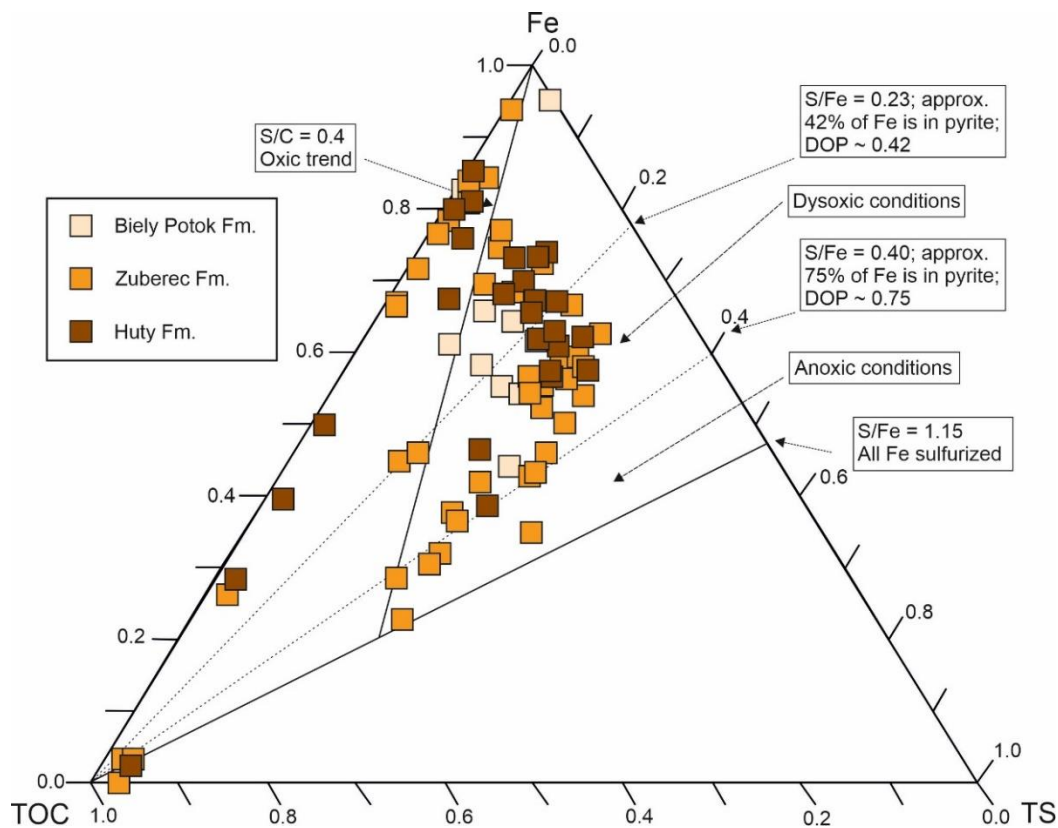
Fig. S6. TOC–TS–Fe ternary diagram for the Palaeogene samples from Orava Basin. DOP = degree of pyritisation.

Tables

Table S1. Sample lithology, bulk geochemical data and *n*-alkanes derived parameters.

Sample code	Lithology	TOC [wt%]	TS [wt%]	CC [wt%]	CPI_{Total}	CPI_{25-31}	Pr/Ph	Pr/n-C_{17}	Ph/n-C_{18}	TAR
Biely Potok Fm.										
1_Bi	sandstone	0.02	0.04	33.29	1.02	1.07	0.60	1.53	0.25	35.20
2_Bi	mudstone	0.89	0.46	8.07	1.15	1.18	3.12	3.77	1.37	4.87
3_Bi	mudstone	0.60	0.28	11.47	1.32	1.47	3.14	4.08	1.81	3.69
4_Bi	sandstone	0.59	0.57	18.68	1.25	1.34	0.56	3.11	0.53	16.33
5_Bi	sandstone	2.43	0.71	9.01	1.50	1.35	3.49	4.27	2.38	2.65
6_Bi	mudstone	1.24	0.97	19.41	1.17	1.34	2.66	4.46	1.44	5.81
7_Bi	mudstone	0.54	0.36	16.68	1.17	1.44	1.63	4.35	0.96	11.09
8_Bi	sandstone	1.08	0.89	11.34	1.28	1.41	1.71	1.63	2.06	0.98
9_Bi	mudstone	0.89	0.27	11.94	1.35	1.30	1.96	2.38	0.84	0.73
10_Bi	mudstone	0.50	0.36	13.27	1.43	1.35	2.65	2.36	1.19	0.69
11_Bi	sandstone	0.36	0.00	10.64	0.94	0.98	1.10	3.23	0.27	24.45
Zuberec Fm.										
12_Zu	mudstone	1.37	1.27	9.80	1.25	1.28	1.66	1.34	1.78	0.43
13_Zu	mudstone	2.20	2.37	11.38	1.26	1.37	2.39	1.94	0.90	1.32
14_Zu	shale	-	-	-	1.28	1.71	3.75	3.50	1.15	0.58
15_Zu	sandstone	0.37	0.17	21.29	1.07	1.19	1.12	4.12	0.94	5.11
16_Zu	sandstone	0.55	0.23	15.47	1.06	1.15	1.87	3.19	0.87	3.02
17_Zu	sandstone	3.15	1.71	17.53	1.44	1.38	3.57	4.47	2.60	0.78
18_Zu	sandstone	0.76	0.69	19.25	1.27	1.28	1.13	4.65	1.68	4.55
19_Zu	sandstone	0.19	0.02	26.71	0.99	1.11	0.85	2.80	0.23	34.55
20_Zu	mudstone	3.55	3.40	18.70	1.34	1.33	4.36	3.79	2.96	1.88
21_Zu	shale	0.76	1.28	19.29	1.30	1.48	3.48	5.41	1.79	2.77
22_Zu	shale	1.09	1.15	16.61	1.39	1.57	4.62	3.47	1.70	1.72
23_Zu	sandstone	0.62	0.00	14.19	1.06	1.06	1.18	0.99	0.74	3.00
24_Zu	shale	1.47	1.53	14.34	1.12	1.14	1.63	1.72	1.44	0.67
25_Zu	shale	0.90	1.38	17.98	1.19	1.25	2.25	1.55	1.21	0.90
26_Zu	shale	0.83	1.10	19.04	1.18	1.18	1.73	1.00	1.16	0.74
27_Zu	shale	0.85	1.36	16.55	1.13	1.09	1.48	1.44	1.84	0.73
28_Zu	shale	0.78	1.26	17.06	1.13	1.19	2.35	2.08	1.17	1.27
29_Zu	shale	0.98	1.34	16.25	1.11	1.15	1.92	1.95	1.15	1.13
30_Zu	shale	0.89	1.46	13.80	1.10	1.14	1.40	1.18	1.13	0.99
31_Zu	shale	0.87	0.60	13.79	1.09	1.14	1.54	1.57	1.10	1.22
32_Zu	shale	1.56	2.02	14.07	1.14	1.14	1.91	1.56	1.45	0.87
33_Zu	shale	0.68	0.02	0.01	1.21	1.38	1.13	4.69	0.73	9.60
34_Zu	shale	0.67	0.73	8.76	1.10	1.23	1.44	4.95	0.89	5.22
35_Zu	shale	9.91	4.16	5.16	2.22	1.87	4.37	1.13	4.38	1.12
36_Zu	shale	2.32	1.45	9.25	1.83	1.53	4.21	6.09	1.81	0.68
37_Zu	shale	5.01	2.46	7.51	1.38	1.17	3.99	2.91	2.53	1.04
38_Zu	shale	1.06	0.01	16.37	0.98	1.17	3.99	2.27	0.58	0.26

5

39_Zu	shale	6.99	3.27	6.10	1.96	2.16	3.15	11.74	4.13	5.25
40_Zu	shale	3.50	1.87	7.30	1.38	1.42	5.17	9.25	2.52	2.04
41_Zu	shale	3.00	0.79	9.68	1.19	1.24	5.48	2.38	0.63	0.45
42_Zu	coal	82.51	0.92	0.23	1.09	1.16	2.19	0.62	0.35	0.40
43_Zu	shale	3.05	0.97	10.43	1.20	1.22	2.20	1.41	0.55	1.24
44_Zu	shale	1.61	0.00	7.35	0.79	1.32	1.68	1.30	0.70	0.30
45_Zu	shale + coal	56.44	0.71	0.28	1.04	0.88	2.35	0.83	0.45	0.17
46_Zu	mudstone	0.75	0.00	27.04	1.07	1.08	1.16	0.61	0.46	1.34
47_Zu	shale	10.11	0.09	13.81	1.27	1.32	4.20	1.78	1.76	1.84
48_Zu	coal	56.00	0.53	0.38	1.02	1.33	5.09	5.26	1.43	1.21
49_Zu	sandstone	0.45	0.21	23.76	1.08	1.14	1.36	3.52	0.70	6.49
50_Zu	mudstone	0.41	0.00	41.99	0.79	1.06	1.74	2.23	0.06	28.65
51_Zu	mudstone	0.22	0.00	0.35	0.88	1.11	1.25	1.27	0.06	37.81
52_Zu	shale	0.67	1.54	11.99	1.14	1.20	2.49	1.67	0.87	1.65
53_Zu	shale	0.50	0.81	14.56	1.09	1.12	1.42	1.19	1.20	0.78
54_Zu	shale	1.89	2.04	12.54	1.14	1.14	1.48	1.47	1.62	0.59
55_Zu	shale	2.46	2.31	13.56	1.10	1.11	2.19	2.12	1.38	1.07
56_Zu	shale	2.08	2.04	16.88	1.14	0.83	1.20	6.96	5.75	1.79
57_Zu	shale	5.65	2.08	0.00	1.46	1.92	0.93	3.95	5.62	1.89
58_Zu	sandstone	0.48	0.07	16.77	0.97	1.04	1.61	5.69	1.74	2.35

Huty Fm.

59_Ht	shale	0.78	0.94	18.05	1.13	1.24	1.20	3.52	0.70	3.36
60_Ht	shale	0.87	1.12	18.02	1.10	1.17	3.21	2.86	0.73	1.00
61_Ht	shale	0.76	0.61	16.62	1.09	1.19	2.63	2.77	0.71	1.43
62_Ht	mudstone	0.85	1.49	15.27	1.07	1.15	1.96	1.83	0.95	1.31
63_Ht	sandstone	0.94	1.08	8.90	1.07	1.15	2.26	1.65	0.65	1.74
64_Ht	mudstone	0.44	0.07	35.67	1.08	1.10	1.31	1.23	0.90	0.82
65_Ht	sandstone	0.37	0.01	36.27	1.04	1.10	1.08	2.74	0.99	2.48
66_Ht	mudstone	0.31	0.04	36.81	1.07	1.11	1.93	5.16	0.97	2.72
67_Ht	mudstone	0.58	0.39	25.13	1.11	1.18	2.20	2.15	0.81	1.29
68_Ht	mudstone	0.59	0.59	16.85	1.08	1.11	2.86	2.57	0.57	1.51
69_Ht	shale	0.65	0.86	18.45	1.09	1.18	2.39	3.23	0.79	1.81
70_Ht	shale	0.57	0.00	13.79	1.09	1.15	2.24	1.89	0.45	2.42
71_Ht	shale	0.66	1.16	17.77	1.09	1.18	3.04	2.40	0.71	0.73
72_Ht	shale	1.10	0.25	14.81	1.23	1.27	5.27	2.17	0.53	1.46
73_Ht	sandstone	0.64	0.59	16.39	1.21	1.51	1.99	2.67	1.27	0.85
74_Ht	sandstone	0.40	0.44	22.76	1.07	1.21	1.59	2.66	0.69	1.63
75_Ht	sandstone	0.62	0.58	19.02	1.09	1.17	3.04	2.67	0.64	1.15
76_Ht	shale	1.03	1.20	18.14	1.09	1.14	2.01	1.65	0.87	1.09
77_Ht	shale	2.72	0.03	7.24	1.21	1.41	2.66	3.12	1.35	0.68
78_Ht	shale	1.98	0.01	14.93	1.07	1.27	2.39	3.46	1.64	0.69
79_Ht	shale	0.76	0.94	24.87	1.08	1.16	3.35	1.60	0.46	0.68
80_Ht	shale	0.87	0.88	22.32	1.14	1.18	2.24	1.77	0.70	0.90
81_Ht	shale	1.02	0.62	68.42	1.07	1.11	1.60	0.93	0.58	0.46
82_Ht	shale	3.19	2.17	5.04	1.10	1.06	2.28	2.00	1.00	0.16

6

Sample code	Rock type	TOC	TS	CC	CPI_Total	CPI_25-31	Pr/Ph	Pr/n-C17	Ph/n-C18	TAR
83_Ht	shale	2.20	1.31	13.30	1.13	1.07	2.11	0.80	0.39	0.29
84_Ht	sandstone	5.39	0.04	11.48	0.99	1.36	1.64	1.94	0.57	0.56
85_Ht	coal	50.64	0.66	1.62	1.12	1.23	3.33	1.55	0.56	0.30

TOC = total organic carbon; TS = total sulphur, CC = carbonate content, CPI_{Total} = Carbon Preference Index, $CPI_{25\text{-}31}$ = Carbon Preference Index for long chain *n*-alkanes, Pr/Ph = pristane/phytane ratio, Pr/*n*-C_{17} = pristane/ C_{17} *n*-alkane ratio, Ph/*n*-C_{18} = phytane/ C_{18} *n*-alkane ratio, TAR = terrigenous vs. aquatic *n*-alkane ratio

CPI_{Total} = $(C_{17}+C_{19}...+C_{27}+C_{29})+(C_{19}+C_{21}...+C_{29}+C_{31})/[2(C_{18}+C_{20}...+C_{28}+C_{30})]$

$CPI_{25\text{-}31}$ = $(C_{25}+C_{27}+C_{29})+(C_{27}+C_{29}+C_{31})/[2(C_{26}+C_{28}+C_{30})]$

TAR = $(C_{27} + C_{29} + C_{31})/(C_{15}+C_{17}+C_{19})$

Table S2. Measured and calculated vitrinite reflectance values.

Sample code	Vitrinite reflectance [%]					Calculated vitrinite reflectance [%]
	Min	Max	Avg	SD	N	
Biely Potok Fm.						
1_Bi	0.14	0.59	0.26	0.09	55	0.64
2_Bi	0.17	0.72	0.51	0.12	100	0.58
9_Bi	0.11	0.66	0.37	0.11	53	0.67
Zuberec Fm.						
13_Zu	0.21	0.61	0.38	0.09	55	0.68
15_Zu	0.18	0.69	0.44	0.11	64	0.74
17_Zu	0.28	0.65	0.45	0.07	100	0.63
20_Zu	0.14	0.77	0.55	0.10	101	0.62
22_Zu	0.17	0.68	0.39	0.12	100	0.60
23_Zu	0.21	0.55	0.37	0.07	100	0.85
32_Zu	0.11	0.86	0.49	0.16	100	0.72
35_Zu	0.20	0.58	0.47	0.07	102	0.55
36_Zu	0.21	0.68	0.50	0.09	103	0.57
38_Zu	0.33	0.68	0.53	0.08	102	0.64
39_Zu	0.28	0.59	0.42	0.06	100	0.56
40_Zu	0.27	0.58	0.43	0.06	102	0.53
42_Zu	0.37	0.58	0.50	0.04	100	0.63
43_Zu	0.31	0.64	0.49	0.06	103	0.67
46_Zu	0.20	0.63	0.39	0.08	51	0.58
47_Zu	0.26	0.65	0.44	0.07	101	0.63
48_Zu	0.12	0.60	0.46	0.08	66	0.62
50_Zu	0.44	1.12	0.84	0.20	25	0.54
55_Zu	0.12	0.90	0.46	0.19	101	0.71
57_Zu	0.21	0.47	0.33	0.06	100	0.55
58_Zu	0.20	0.72	0.43	0.11	100	0.56
Huty Fm.						
59_Ht	0.23	0.78	0.45	0.14	50	0.78
60_Ht	0.23	0.77	0.50	0.14	55	0.77
61_Ht	0.25	0.68	0.47	0.10	54	0.67

7

62_Ht	0.21	0.85	0.48	0.12	100	0.75
63_Ht	0.27	0.60	0.45	0.06	50	0.73
64_Ht	0.16	0.52	0.35	0.10	50	0.75
65_Ht	0.25	0.80	0.44	0.17	30	0.61
66_Ht	0.20	0.65	0.41	0.09	100	0.72
67_Ht	0.26	0.81	0.55	0.10	100	0.79
68_Ht	0.25	0.79	0.55	0.13	57	0.74
69_Ht	0.25	0.68	0.41	0.12	31	0.82
71_Ht	0.22	0.74	0.53	0.11	61	0.74
72_Ht	0.31	0.86	0.62	0.15	30	0.71
73_Ht	0.21	0.75	0.53	0.13	58	0.77
76_Ht	0.27	0.80	0.57	0.13	61	0.76
78_Ht	0.09	0.46	0.27	0.08	50	0.59
79_Ht	0.38	0.79	0.58	0.10	59	0.70
80_Ht	0.33	0.88	0.54	0.12	53	0.74
81_Ht	0.28	0.87	0.57	0.15	54	0.79
82_Ht	0.28	0.73	0.47	0.13	55	0.68
83_Ht	0.21	0.81	0.49	0.12	101	0.74
84_Ht	0.33	0.58	0.44	0.04	100	0.64
85_Ht	0.38	0.54	0.45	0.03	100	0.67

Rc = 0.60 * MPI1 + 0.40

Min = minimum vitrinite reflectance value [%], Max = maximum vitrinite reflectance value [%], Avg = average vitrinite reflectance value [%], SD = standard deviation, N = number of measurements.

Table S3. Measured fusinite reflectance values and calculated combustion temperatures (abbreviations as in Table S2).

Sample code	Fusinite reflectance [%]					Combustion temp [°C]		
	Min	Max	Avg	SD	N	Avg	Min	Max
Biely Potok Fm.								
2_Bi	0.71	6.20	1.68	0.72	100	382	268	914
5_Bi	1.55	2.76	2.35	0.26	50	461	367	510
8_Bi	0.93	4.92	2.98	1.14	104	536	294	765
Zuberec Fm.								
20_Zu	3.15	5.85	4.66	0.65	50	734	556	874
22_Zu	1.00	4.54	2.43	1.01	53	471	302	720
36_Zu	0.60	6.08	2.25	1.45	41	449	255	902
37_Zu	0.88	3.80	1.89	0.66	20	407	287	632
40_Zu	2.12	6.08	4.50	0.91	51	715	434	902
56_Zu	1.54	5.57	3.27	1.27	36	570	366	841
57_Zu	0.89	6.08	3.35	1.58	33	580	289	902

Table S4. Pyrite framboid diameter measurements with statistical data and calculated framboid parameter.

Sample	Min FD [μm]	Max FD [μm]	Mean [μm]	SD	N	% F <5 μm
Biely Potok Fm.						
1_Bi	1.87	19.96	6.46	3.51	50	42
2_Bi	2.48	13.06	6.08	2.29	100	38
5_Bi	1.83	11.86	5.76	1.96	100	31
8_Bi	2.23	14.69	6.56	2.89	100	34
10_Bi	2.73	29.32	7.87	4.78	101	22
11_Bi	1.63	18.03	6.50	2.63	100	23
Zuberec Fm.						
13_Zu	1.55	14.85	4.38	1.82	100	73
15_Zu	1.74	22.87	6.71	4.06	50	36
17_Zu	2.08	13.12	6.09	2.21	100.0	33
20_Zu	1.19	38.48	7.25	4.58	100	31
22_Zu	1.87	34.93	7.15	5.53	100	40
23_Zu	2.56	23.57	7.61	4.86	50	40
29_Zu	1.56	14.85	4.14	1.81	100	78
30_Zu	1.59	9.23	4.19	1.37	100	78
32_Zu	1.69	13.00	4.97	1.88	100	55
33_Zu	2.32	24.66	7.16	3.70	100	30
35_Zu	1.96	26.55	6.51	3.13	100	36
36_Zu	2.87	15.84	6.09	2.08	101	28
37_Zu	1.75	14.15	5.83	2.05	101	37
39_Zu	1.84	13.24	5.43	1.99	100	50
40_Zu	2.47	12.21	5.52	1.71	100	41
43_Zu	1.94	13.37	4.87	1.94	100	60
46_Zu	3.21	27.32	9.12	5.00	50	12
47_Zu	1.91	15.21	6.82	2.60	101	27
53_Zu	2.14	26.38	6.76	4.74	101	47
54_Zu	1.31	13.88	4.68	1.82	100	60
55_Zu	2.12	11.37	4.63	1.70	97	62
56_Zu	1.86	10.86	4.43	1.85	100	69
57_Zu	1.48	19.59	4.94	2.35	100	63
58_Zu	2.58	24.45	10.17	4.95	51	16
Huty Fm.						
59_Ht	2.29	14.28	5.45	1.95	50	48
60_Ht	1.84	12.27	5.52	1.91	103	49
61_Ht	2.43	19.60	5.64	2.58	101	50
62_Ht	1.43	15.07	4.60	1.99	100	64
63_Ht	1.67	17.37	6.78	3.16	100	33
66_Ht	2.87	33.20	9.39	5.55	51	12

9

67_Ht	1.71	22.76	5.90	3.27	100	45
68_Ht	2.28	25.10	6.02	2.96	100	41
69_Ht	2.96	25.92	7.21	4.59	50	36
71_Ht	1.54	9.99	5.57	2.26	100	45
72_Ht	1.60	7.88	5.03	2.50	100	59
73_Ht	2.30	53.44	8.70	8.36	51	25
74_Ht	3.60	20.38	7.63	4.02	14	29
75_Ht	2.72	19.26	6.78	2.75	100	29
79_Ht	2.23	25.53	5.50	3.46	50	54
80_Ht	2.01	15.58	5.06	2.26	101	61
81_Ht	1.91	10.69	4.51	1.46	100	62
82_Ht	1.99	13.44	5.78	2.12	100	32
83_Ht	1.69	17.03	4.39	2.32	103	73
84_Ht	2.17	12.05	5.91	2.15	50	40

Min, Max FD = the smallest/largest pyrite framboid diameter; SD = standard deviation; N = number of measurements; %F < 5 μm = percentage of pyrite framboids with diameter equal or lower than 5 μm.

Table S5. Rock-Eval analysis for CCPB rocks.

Sample code	TOC (wt%)	T_{max} (°C)	S1	S2	S3	PI	HI	OI	MINC (wt%)
Biely Potok Fm.									
5_Bi	1.16	434	0.06	1.08	0.05	0.05	93	4	2.5
6_Bi	1.28	430	0.06	0.89	0.09	0.06	69	7	2.4
7_Bi	0.33	436	0.03	0.21	0.03	0.13	61	7	2.2
9_Bi	0.56	448	0.14	0.28	0.46	0.33	50	83	1.62
10_Bi	0.21	n.a.	0.07	0.12	0.30	n.a.	56	138	1.79
11_Bi	0.07	n.a.	n.a.	n.a.	n.a.	n.a.	n.a.	n.a.	1.58
Zuberec Fm.									
12_Zu	1.23	438	0.19	1.58	0.03	0.10	128	2	1.18
13_Zu	2.2	434	0.58	6.0	0.02	0.09	276	1	1.29
16_Zu	0.23	448	0.05	0.25	0.01	0.17	109	5	2.3
17_Zu	3.1	422	0.15	4.4	0.05	0.03	144	2	2.3
18_Zu	0.56	433	0.05	0.38	0.05	0.11	68	9	2.5
23_Zu	0.30	446	0.07	0.33	0.31	0.17	108	103	1.92
33_Zu	0.43	444	0.03	0.27	0.47	0.09	62	110	0.15
34_Zu	0.92	446	0.22	0.60	0.02	0.27	65	2	1.10
35_Zu	9.8	428	0.50	12.2	1.78	0.04	124	18	1.26
36_Zu	1.88	433	0.21	1.40	0.26	0.13	74	14	1.37
37_Zu	4.6	430	0.67	6.6	0.59	0.09	145	13	1.44
38_Zu	0.76	454	0.21	0.98	0.49	0.18	128	64	2.2
39_Zu	7.2	424	0.71	19.6	0.84	0.03	272	12	1.19
40_Zu	3.3	426	0.37	5.0	0.48	0.07	151	14	1.20
41_Zu	3.0	437	0.83	3.7	0.03	0.18	124	1	1.22
42_Zu	92.6	421	26.2	294.7	0.05	0.08	318	0	1.72
43_Zu	3.2	435	0.63	4.9	0.00	0.11	153	0	1.33
44_Zu	1.19	454	0.07	1.08	0.53	0.06	90	44	1.11
45_Zu	61.4	457	1.23	51.5	16.7	0.02	84	27	2.19
46_Zu	0.47	448	0.07	0.44	0.57	0.14	94	120	3.6
47_Zu	9.2	448	0.17	10.9	3.4	0.02	118	37	2.17

48_Zu	58.0	447	1.79	46.9	18.2	0.04	81	31	2.74
49_Zu	0.22	445	0.05	0.22	0.00	0.17	101	0	3.2
50_Zu	0.03	n.a.	n.a.	n.a.	n.a.	n.a.	n.a.	n.a.	5.0
51_Zu	0.07	n.a.	n.a.	n.a.	n.a.	n.a.	n.a.	n.a.	0.20
56_Zu	2.1	429	0.15	4.0	0.07	0.04	196	3	2.1
57_Zu	2.8	424	0.28	7.6	0.14	0.04	276	5	3.0
58_Zu	0.31	453	0.04	0.27	0.11	0.13	85	35	2.2
Huty Fm.									
59_Ht	0.59	448	0.23	0.59	0.16	0.28	100	27	2.4
60_Ht	0.72	446	0.20	0.67	0.12	0.23	94	17	2.4
61_Ht	0.47	446	0.15	0.47	0.07	0.24	100	16	2.3
62_Ht	0.82	441	0.16	0.84	0.02	0.16	101	2	1.69
64_Ht	0.23	445	0.14	0.35	0.15	0.28	152	64	4.5
65_Ht	0.06	n.a.	n.a.	n.a.	n.a.	n.a.	n.a.	n.a.	4.6
66_Ht	0.15	446	0.12	0.29	0.12	0.30	187	76	4.7
67_Ht	0.34	444	0.36	0.58	0.15	0.38	171	44	2.2
68_Ht	0.48	446	0.21	0.44	0.11	0.33	91	22	2.2
69_Ht	0.41	444	0.27	0.33	0.11	0.45	81	27	2.4
70_Ht	0.31	458	0.16	0.34	0.75	0.31	109	239	1.97
71_Ht	0.46	444	0.21	0.44	0.10	0.32	94	22	2.4
72_Ht	0.52	442	0.24	0.50	0.07	0.33	96	14	2.3
73_Ht	0.44	441	0.17	0.49	0.09	0.26	110	21	2.2
74_Ht	0.19	442	0.13	0.22	0.11	0.36	116	57	3.0
75_Ht	0.45	443	0.36	0.47	0.13	0.43	104	28	2.5
76_Ht	0.73	442	0.31	0.68	0.11	0.31	93	14	2.4
77_Ht	2.5	436	0.26	9.6	0.65	0.03	380	26	1.15
78_Ht	1.59	436	0.18	5.1	0.62	0.03	319	39	2.0
79_Ht	0.52	442	0.45	0.48	0.09	0.48	93	17	3.1
80_Ht	0.53	440	0.29	0.57	0.10	0.34	107	19	2.9
81_Ht	0.49	442	0.27	0.68	0.64	0.28	139	130	7.9
82_Ht	3.2	442	0.63	10.5	0.10	0.06	332	3	0.86
83_Ht	1.96	444	0.51	3.3	0.19	0.14	165	9	1.84
84_Ht	5.3	445	0.26	8.0	1.68	0.03	151	32	1.61
85_Ht	53.3	445	5.3	74.5	13.4	0.07	140	25	1.91

TOC = total organic carbon; T_{max} = temperature of the S2 peak maximum; S1 = oil and gas yield (mg HC/g rock);

S2 = residual petroleum potential (mg HC/g rock); S3 = CO_2 from decomposition of the organic matter (mg CO_2 /g rock);

PI = production index; HI = hydrogen index (mg HC/g TOC); OI = oxygen index (mg CO_2/g TOC); MINC = mineral carbon; n.a. = not applicable

Table S6. Distribution (relative peak areas in %) of D1-D7 isomers of triaromatic dinosteroids. The abbreviations for peak areas correspond to the peak areas in Fig. S4.

Sample code	D1	D2	D3	D4	D5	D6	D7
Biely Potok Fm.							
1_Bi	-	-	-	-	-	-	-
2_Bi	12	15	13	15	14	15	16

3_Bi	3	11	21	12	17	17	20
4_Bi	8	10	11	13	17	15	26
5_Bi	8	11	14	13	21	11	23
6_Bi	9	18	9	16	20	12	17
7_Bi	3	20	14	17	16	13	17
8_Bi	4	11	20	14	15	14	21
9_Bi	18	7	16	6	18	17	17
10_Bi	13	9	20	15	15	12	16
11_Bi	27	9	16	12	8	9	19

Zuberec Fm.

12_Zu	1	11	15	13	17	16	27
13_Zu	5	11	16	13	17	14	24
14_Zu	3	8	16	12	13	26	21
15_Zu	2	17	14	8	15	20	24
16_Zu	2	13	13	12	16	17	26
17_Zu	12	6	18	14	23	12	16
18_Zu	23	9	16	9	12	9	23
19_Zu	29	8	15	10	12	7	19
20_Zu	32	13	18	10	10	8	10
21_Zu	6	12	20	11	13	10	28
22_Zu	33	10	12	8	10	9	17
23_Zu	3	10	14	11	21	10	30
24_Zu	4	17	18	9	17	16	19
25_Zu	4	15	17	11	17	14	22
26_Zu	3	18	17	12	18	13	19
27_Zu	4	18	19	11	16	13	20
28_Zu	5	18	17	10	14	14	22
29_Zu	4	15	19	11	15	16	21
30_Zu	4	17	19	9	17	16	18
31_Zu	3	14	19	10	15	15	23
32_Zu	3	14	17	9	16	16	25
33_Zu	6	10	16	12	16	15	23
34_Zu	30	7	13	7	11	12	21
35_Zu	8	9	9	5	34	20	15
36_Zu	4	9	15	8	28	16	20
37_Zu	11	10	19	12	12	19	17
38_Zu	8	17	9	12	24	13	16
39_Zu	4	9	23	9	16	12	27
40_Zu	11	14	20	7	20	10	18
41_Zu	44	7	11	4	6	13	15
42_Zu	6	13	8	8	6	22	36
43_Zu	6	12	15	12	14	19	23
44_Zu	19	13	10	11	11	14	22
45_Zu	22	13	8	9	12	19	17
46_Zu	6	16	17	11	15	14	20

47_Zu	37	8	13	6	5	23	8
48_Zu	19	15	12	16	11	13	14
49_Zu	4	16	15	10	16	19	21
50_Zu	-	-	-	-	-	-	-
51_Zu	3	10	21	14	14	14	25
52_Zu	-	-	-	-	-	-	-
53_Zu	2	14	19	12	15	16	21
54_Zu	2	14	19	12	16	14	24
55_Zu	2	15	17	11	18	15	22
56_Zu	2	6	25	14	14	13	26
57_Zu	2	15	16	11	16	15	24
58_Zu	8	14	15	15	14	14	19
Huty Fm.							
59_Ht	9	12	19	11	16	12	20
60_Ht	8	10	15	11	18	18	20
61_Ht	-	-	-	-	-	-	-
62_Ht	5	12	16	11	16	14	26
63_Ht	11	13	17	10	14	12	23
64_Ht	2	10	16	12	16	19	24
65_Ht	3	8	17	12	17	20	23
66_Ht	7	20	12	6	25	12	19
67_Ht	2	10	16	11	13	25	24
68_Ht	4	13	18	10	14	19	21
69_Ht	6	14	14	11	14	20	21
71_Ht	6	10	16	10	18	15	25
72_Ht	9	15	19	10	18	13	16
73_Ht	6	15	12	9	18	15	25
74_Ht	8	14	19	12	18	12	17
75_Ht	5	12	19	13	19	14	19
76_Ht	5	9	17	11	13	24	21
77_Ht	1	10	21	13	16	14	24
78_Ht	2	15	29	10	14	10	19
79_Ht	4	14	15	12	21	18	15
80_Ht	5	11	15	12	18	16	23
81_Ht	4	10	13	12	17	22	22
82_Ht	3	9	17	13	16	20	23
83_Ht	5	12	17	11	14	21	19
84_Ht	5	12	28	10	10	14	21
85_Ht	10	10	24	8	10	15	22

Table S7. Ratios of U/Th, V/Cr, TOC/P, U/Mo, concentrations of authigenic uranium and contents of Mo and the average enrichment factors of U and Mo.

Sample code	U/Th	V/Cr	TOC/P	U/Mo	Mo [ppm]	U_{aut} [ppm]	U_{EF}	Mo_{EF}

Biely Potok Fm.

1_Bi	0.22	0.82	0.72	3.64	0.11	0.67	2.22	1.90
2_Bi	0.26	1.34	15.06	0.88	1.14	0.79	3.54	12.53
3_Bi	0.16	0.93	12.21	2.44	0.41	0.48	2.81	3.57
4_Bi	0.21	0.51	14.35	0.69	0.87	0.64	2.55	11.45
5_Bi	0.25	0.69	63.89	0.58	1.2	0.75	2.89	15.38
6_Bi	0.40	1.37	33.49	1.01	0.99	1.20	4.96	15.23
7_Bi	0.29	1.20	17.27	1.30	0.46	0.86	3.28	7.80
8_Bi	0.24	1.10	20.74	0.23	4.44	0.73	3.01	41.50
9_Bi	0.17	0.86	23.98	0.48	0.83	0.52	1.84	11.86
10_Bi	0.24	0.81	13.29	1.25	0.48	0.72	2.65	6.58
11_Bi	0.16	0.49	9.88	1.71	0.35	0.49	3.07	5.56

Zuberec Fm.

12_Zu	0.18	1.01	30.55	0.28	3.59	0.55	2.52	28.05
13_Zu	0.23	0.99	48.89	0.06	27.73	0.70	4.06	205.4
15_Zu	0.14	1.09	8.85	0.35	1.13	0.43	1.50	13.14
16_Zu	0.16	1.35	14.18	0.56	0.72	0.48	1.54	8.57
17_Zu	0.44	1.34	49.20	0.42	3.32	1.31	5.87	43.12
18_Zu	0.23	1.11	14.55	0.66	1.21	0.69	2.87	13.44
19_Zu	0.38	0.17	8.35	1.11	0.45	1.15	6.20	17.31
20_Zu	0.31	3.14	91.15	0.20	3.95	0.92	3.74	57.25
21_Zu	0.22	1.15	16.15	0.53	2.07	0.66	2.88	16.83
22_Zu	0.19	1.00	23.65	0.53	1.52	0.57	2.21	12.99
23_Zu	0.15	0.83	13.84	0.80	0.5	0.44	1.74	6.76
24_Zu	0.27	1.13	37.61	0.16	11.79	0.80	4.20	80.75
25_Zu	0.16	0.92	24.20	0.36	3.02	0.49	2.29	19.48
26_Zu	0.17	0.94	21.24	0.41	2.71	0.52	2.46	18.82
27_Zu	0.17	0.87	24.23	0.19	5.73	0.52	2.52	40.64
28_Zu	0.13	0.92	20.09	0.24	3.32	0.39	1.47	18.86
29_Zu	0.20	0.94	23.80	0.16	8.15	0.61	2.83	55.07
30_Zu	0.23	0.86	21.23	0.10	15.55	0.70	3.25	104.4
31_Zu	0.14	0.93	21.80	0.13	6.8	0.41	1.89	44.16
32_Zu	0.24	0.94	32.48	0.29	5.25	0.71	3.38	36.71
33_Zu	0.08	0.84	14.49	2.05	0.39	0.24	1.58	2.39
34_Zu	0.13	1.51	14.78	0.52	0.96	0.39	0.93	5.52
35_Zu	0.83	3.99	300.4	0.56	5.36	2.50	10.41	57.63
36_Zu	0.35	1.33	52.66	0.69	1.75	1.06	3.52	15.91
37_Zu	0.60	1.80	143.3	0.30	5.94	1.80	6.60	67.50
38_Zu	0.16	1.65	19.66	1.09	0.46	0.47	1.25	3.57
39_Zu	0.42	1.52	142.7	0.14	23.64	1.26	7.17	164.17
40_Zu	0.36	1.56	67.31	0.34	4.39	1.07	3.90	35.40
41_Zu	0.23	1.40	65.31	0.83	1.21	0.68	1.91	7.16
42_Zu	1.00	178	82510	0.11	0.91	3.00	4.03	113.75
43_Zu	0.21	1.72	64.98	0.71	1.4	0.64	1.89	8.19
44_Zu	0.15	2.35	38.37	0.74	0.94	0.44	1.46	6.06

45_Zu	0.58	2.75	2015	2.00	1.1	1.74	7.39	11.46
46_Zu	0.16	0.99	12.50	0.42	1.89	0.47	2.63	19.29
47_Zu	0.28	1.97	259	1.04	1.06	0.85	2.46	7.36
48_Zu	0.95	2.41	2800	1.32	1.44	2.85	9.43	22.15
49_Zu	0.13	1.39	9.32	1.29	0.31	0.39	1.29	3.10
50_Zu	0.08	0.94	6.09	5.00	0.08	0.24	1.01	0.63
51_Zu	0.03	0.92	6.01	2.22	0.09	0.09	0.29	0.41
52_Zu	0.09	0.85	12.61	0.67	0.9	0.26	1.22	5.66
53_Zu	0.20	1.13	10.12	0.39	2.03	0.59	2.12	16.64
54_Zu	0.44	0.97	26.29	0.16	16.37	1.31	7.57	142.4
55_Zu	0.49	1.03	35.66	0.17	20.14	1.48	8.12	149.2
56_Zu	0.32	1.09	48.29	0.18	12.82	0.97	6.18	106.8
57_Zu	1.39	1.17	94.20	0.69	13.99	4.16	25.86	115.6
58_Zu	0.19	1.06	11.59	1.00	0.5	0.56	1.17	3.62
Huty Fm.								
60_Ht	0.16	0.84	21.83	0.71	1.27	0.49	2.18	9.55
61_Ht	0.09	0.83	16.87	0.48	1.04	0.28	1.07	6.89
62_Ht	0.15	0.81	21.69	0.12	6.93	0.46	2.17	58.24
63_Ht	0.22	0.80	15.94	0.99	0.81	0.67	2.19	6.86
64_Ht	0.22	1.21	9.14	0.68	0.88	0.67	2.48	11.28
65_Ht	0.35	1.25	9.12	1.40	0.57	1.04	4.37	9.66
66_Ht	0.21	1.26	7.07	0.66	0.76	0.63	2.18	10.27
67_Ht	0.14	1.10	10.93	0.54	1.3	0.41	1.69	9.70
68_Ht	0.09	0.90	13.40	0.69	0.72	0.26	0.93	4.14
69_Ht	0.09	0.80	12.53	0.83	0.6	0.26	1.18	4.38
70_Ht	0.10	0.80	13.47	0.34	1.78	0.30	1.40	12.90
71_Ht	0.11	0.87	16.84	0.35	1.71	0.33	1.32	11.63
72_Ht	0.09	0.78	24.93	0.76	0.66	0.26	1.10	4.49
73_Ht	0.14	0.88	10.95	0.58	1.04	0.41	1.74	9.37
74_Ht	0.15	0.93	8.28	0.65	0.77	0.45	1.77	8.46
75_Ht	0.15	0.91	11.08	0.56	1.07	0.44	1.74	9.64
76_Ht	0.16	0.89	25.77	0.47	1.93	0.47	2.13	14.19
77_Ht	0.09	0.83	75.55	1.40	0.43	0.26	1.51	3.36
78_Ht	0.11	0.94	53.51	1.49	0.47	0.34	2.03	4.23
79_Ht	0.09	0.96	17.61	0.59	0.85	0.28	1.20	6.34
80_Ht	0.11	1.03	20.19	0.25	2.04	0.33	1.21	15.34
81_Ht	0.26	1.30	16.14	0.56	1.07	0.78	2.58	14.27
82_Ht	0.70	1.10	62.64	0.13	30.27	2.11	11.52	270.3
83_Ht	0.24	1.03	42.26	0.24	4.96	0.72	2.81	35.94
84_Ht	0.18	1.67	125.5	1.25	0.48	0.55	2.25	5.58
85_Ht	1.53	1.45	4219	1.28	1.79	4.60	23.93	57.74

$U_{aut} = U_{TOTAL} - (Th/3)$

$U_{EF} = (U_{TOTAL}/Al_{TOTAL})$ / Post-Archean Australian Shale U/Al ratio

$Mo_{EF} = (Mo_{TOTAL}/Al_{TOTAL})$/ Post-Archean Australian Shale Mo/Al ratio

Table S8. Peak areas of selected angiosperm and gymnosperm biomarkers (in percentage values for angiosperms and gymnosperms respectively).

| | Angiosperms | | | | | | | | | | | Gymnosperms | | | | |
| | m/z292 | m/z213 | m/z254 | m/z324 | | | m/z218 | m/z327 | m/z292 | | m/z145 | m/z219 | m/z237 | m/z255 | m/z183 | m/z197 |
Sample code	Des-A-26,27-dinor-5,7,9,11,13-pentaene	27-28-Bisnoroleana-13,15,17-triene	Des-E-D;C-friedo-25-norhopa-5,7,9-triene	2,2-Dimethyl-1,2,3,4-tetrahydropicene	1,2,9-Trimethyl-1,2,3,4-tetrahydropicene	2,2,9-Trimethyl-1,2,3,4-tetrahydropicene	3,3,7-trimethyl-1,2,3,4-tetrahydrochrysene	2,2,9,9-Tetramethyl-1,2,3,4,9,10,11,12-octahydropicene	des-A-dinoroleana-5,7,8,11,13-pentaene	des-A-dinoroleana-5,7,9,11,15-pentaene	23,25-Bisnor-des-E-oleana-1,3,5(10)-triene	Retene	Simonellite	Dehydroabietane	Cadalene	ip-iHMN
Biely Potok Fm.																
1_Bi	-	16	10	-	-	16	10	-	-	-	47	47	16	3	6	28
2_Bi	4	11	5	1	2	34	4	1	1	4	33	69	9	1	11	10
3_Bi	5	10	7	1	2	31	6	2	1	5	30	16	16	1	52	15
4_Bi	4	11	10	1	2	18	6	2	1	4	42	62	21	1	1	15
5_Bi	4	9	10	1	1	20	5	2	1	4	44	35	12	1	41	10
6_Bi	4	5	4	1	6	54	5	1	1	4	18	69	11	1	14	6
7_Bi	5	4	3	1	8	52	6	-	1	5	15	78	11	-	6	5
8_Bi	5	19	7	1	1	18	6	1	4	5	34	48	19	1	21	10
9_Bi	2	14	12	-	4	5	5	-	1	2	54	30	29	1	27	12
10_Bi	2	9	11	-	3	27	4	2	1	2	39	28	25	2	30	15
11_Bi	4	16	4	2	9	33	5	2	1	3	22	31	55	4	1	9
Zuberec Fm.																
12_Zu	4	16	5	2	-	36	7	2	1	4	22	89	3	-	5	3
13_Zu	6	11	4	2	-	34	8	3	1	6	25	89	2	-	3	6
14_Zu	5	4	5	1	2	43	6	3	1	5	24	48	3	-	46	3
15_Zu	3	5	2	2	-	44	21	-	1	3	18	99	-	-	1	1
16_Zu	5	6	3	2	-	48	25	-	1	5	6	98	-	-	1	1
17_Zu	11	17	7	-	2	20	3	1	1	11	27	62	18	1	14	4
18_Zu	8	9	5	1	4	42	4	1	1	8	16	70	20	1	5	4
19_Zu	4	5	4	1	7	48	6	1	1	4	20	76	16	1	-	6
20_Zu	4	10	9	1	2	23	6	1	1	4	38	46	12	-	35	7
21_Zu	1	78	2	-	-	7	3	-	-	1	7	49	19	1	20	11
22_Zu	5	21	5	1	-	23	14	1	1	5	24	46	16	-	25	12
23_Zu	5	4	6	4	1	31	26	2	-	5	15	94	4	-	1	-
24_Zu	4	13	10	1	1	6	8	-	1	3	52	83	4	-	10	3
25_Zu	3	13	6	2	-	31	8	1	-	3	33	85	2	-	9	4
26_Zu	5	13	8	1	-	20	11	1	1	5	35	83	2	-	11	4
27_Zu	4	17	8	2	-	16	9	1	1	5	38	83	4	-	8	5
28_Zu	4	14	8	1	-	21	10	1	1	4	36	87	2	-	6	4
29_Zu	3	14	7	3	-	29	8	1	-	3	31	89	2	-	5	3
30_Zu	3	14	8	3	-	22	9	1	-	4	35	90	3	-	4	3
31_Zu	2	11	6	4	-	41	7	1	-	2	26	91	2	-	3	4
32_Zu	2	10	5	3	-	42	7	1	-	2	28	88	2	-	7	3
33_Zu	5	16	3	2	1	44	4	2	1	5	16	18	78	2	1	2
34_Zu	3	8	5	2	1	47	5	2	1	3	24	61	14	-	13	11

35_Zu	2	22	10	-	1	10	2	2	1	2	48	14	13	5	62	5
36_Zu	2	13	14	-	-	-	4	1	1	2	63	15	23	2	51	9
37_Zu	-	-	-	-	-	-	-	-	2	6	93	99	-	-	1	-
38_Zu	-	-	3	-	-	29	17	-	-	6	44	-	-	-	-	-
39_Zu	11	60	1	2	1	8	4	-	1	1	10	22	28	-	34	16
40_Zu	6	37	2	1	1	16	11	-	2	2	21	40	24	-	22	13
41_Zu	10	5	4	1	-	19	22	-	1	10	27	95	1	-	3	1
42_Zu	7	2	13	1	-	38	16	-	1	7	15	42	-	-	57	1
43_Zu	9	4	3	2	-	29	24	-	1	9	19	95	1	-	4	1
44_Zu	6	3	1	2	4	51	11	1	1	6	14	95	-	-	3	2
45_Zu	18	7	1	1	1	6	7	-	2	18	39	94	-	-	5	1
46_Zu	4	12	7	3	1	17	15	-	3	4	33	86	14	-	-	-
47_Zu	4	9	1	1	-	12	9	-	2	11	50	97	-	-	1	2
48_Zu	6	9	1	4	-	36	14	1	1	6	23	97	-	-	1	2
49_Zu	5	8	2	2	-	31	28	-	-	5	17	98	-	-	-	1
50_Zu	4	4	1	1	3	63	10	-	-	4	10	90	10	-	-	-
51_Zu	3	14	1	2	5	51	9	-	-	3	11	53	45	-	-	2
52_Zu	-	2	-	3	8	85	-	-	-	-	3	100	-	-	-	-
53_Zu	4	5	3	4	-	40	11	1	1	4	29	92	2	-	5	1
54_Zu	2	10	5	3	-	54	4	1	-	2	19	85	4	-	7	4
55_Zu	3	9	5	3	-	42	7	1	1	3	26	88	3	-	7	2
56_Zu	8	30	5	1	1	9	9	1	3	8	24	31	45	1	20	3
57_Zu	10	24	6	1	1	10	8	1	7	11	22	68	14	1	14	3
58_Zu	10	23	3	1	1	15	16	1	3	11	16	80	9	-	6	5

Huty Fm.

59_Ht	-	12	-	3	2	47	8	2	-	-	25	100	-	-	-	-
60_Ht	-	9	-	4	2	50	8	3	-	-	24	100	-	-	-	-
61_Ht	-	7	-	-	-	54	10	-	-	-	29	100	-	-	-	-
62_Ht	3	6	6	3	1	36	11	-	-	3	31	94	3	-	3	1
63_Ht	2	3	5	3	0	44	10	-	-	2	32	96	0	-	4	-
64_Ht	5	3	3	3	1	28	20	-	-	5	32	99	1	-	-	-
65_Ht	2	8	18	-	-	26	16	1	-	2	27	91	6	-	-	3
66_Ht	2	2	2	3	1	29	14	-	-	2	45	99	1	-	-	-
67_Ht	3	5	8	2	-	19	17	-	-	3	42	98	-	-	1	-
68_Ht	3	2	6	2	-	18	10	3	1	3	52	13	57	5	25	-
69_Ht	1	3	7	2	-	38	9	2	-	1	38	96	2	-	2	-
71_Ht	1	53	2	1	1	8	3	1	-	1	30	78	4	-	18	-
72_Ht	3	19	6	2	3	25	7	2	-	2	33	28	21	7	44	-
73_Ht	-	-	-	4	2	63	10	1	-	-	20	93	-	-	7	-
74_Ht	-	-	-	3	2	62	8	-	-	-	24	99	-	-	1	-
75_Ht	-	-	-	4	2	67	9	1	-	-	18	97	-	-	3	-
76_Ht	2	24	3	2	1	21	8	-	-	2	39	92	-	-	8	-
77_Ht	3	30	13	2	-	16	20	2	1	3	10	75	5	-	15	5
78_Ht	2	29	11	3	-	18	22	2	1	2	9	80	5	-	9	6
79_Ht	2	2	3	4	2	53	11	1	-	2	21	64	-	-	36	-

17

80_Ht	5	2	3	4	1	45	16	1	1	5	17	86	-	-	14	-
81_Ht	4	-	2	5	1	48	20	3	1	4	12	84	-	-	16	-
82_Ht	4	5	3	5	1	46	17	1	-	4	14	94	-	-	6	-
83_Ht	3	19	-	5	2	33	17	-	-	3	18	94	-	-	6	-
84_Ht	6	23	2	1	-	22	10	1	1	6	27	90	1	-	2	7
85_Ht	7	20	2	1	-	18	12	1	1	7	31	96	-	-	2	2

18

Article 2

Staneczek Dorota, Szaniawski Rafał., Chadima Martin, Marynowski Leszek, 2024. Multi-stage tectonic evolution of the Tatra Mts recorded in the para- and ferromagnetic fabrics. Tectonophysics 880, 230338.

Contents lists available at ScienceDirect

Tectonophysics

Multi-stage tectonic evolution of the Tatra Mts recorded in the para- and ferromagnetic fabrics

Dorota Staneczek [a],[*], Rafał Szaniawski [b], Martin Chadima [c],[d], Leszek Marynowski [a]

[a] Institute of Earth Sciences, University of Silesia in Katowice, Będzińska 60, 41-200 Sosnowiec, Poland
[b] Institute of Geophysics, Polish Academy of Sciences, Księcia Janusza 64, 01-452 Warszawa, Poland
[c] AGICO Ltd., Purkynova 3050/99a, 612 00 Brno, Czech Republic
[d] Institute of Geology, Academy of Sciences of Czech Republic, Rozvojová 135, 165 00 Prague, Czech Republic

A B S T R A C T

The Tatra Mts form the highest part of the Carpathian mountain chain; however, their tectonic and thermal evolution is still debatable. Previous magnetic fabric studies have primarily focused on the crystalline basement and its autochthonous cover. We investigate the magnetic fabrics of Cretaceous marly limestones from a Mesozoic nappe unit and post-thrusting Oligocene shales and mudstones to unravel the most recent tectonic evolution of the Tatra massif. In addition to standard petromagnetic measurements such as the acquisition of the Isothermal Remanent Magnetization or temperature-dependent susceptibility analyses, we investigated the paleotemperature of the Tatra region because high temperatures are known to significantly affect the magnetic mineralogy. The most common minerals in the studied units are paramagnetic phyllosilicates which govern the in-phase Anisotropy of Magnetic Susceptibility. The ferromagnetic fraction is represented by fine-grained magnetite with a minor contribution of hematite. Measured and counted vitrinite reflectances document an eastward increase in maturity, which is also reflected in the magnetite–hematite grain size ratios. Because the paleotemperatures recorded in the Cretaceous rocks follow the same increasing trend as the post-thrusting shales, it appears that both units were affected by a single major thermal event linked presumably to the Late Oligocene/ Early Miocene burial. We propose that magnetic fabrics carried by phyllosilicates document the impact of crucial tectonic phases such as Miocene uplift and Cretaceous thrusting, whereas the out-of-phase Anisotropy of Magnetic Susceptibility and Anisotropy of Anhysteretic Remanent Magnetization fabrics most likely record the stress orientation during major burial episodes. Finally, the conspicuous vertical ferromagnetic lineation present in some Cretaceous sites documents the transpression-controlled tectonic regime in the Oligocene–Early Miocene.

1. Introduction

Magnetic fabric methods such as Anisotropy of in-phase Magnetic Susceptibility (ipAMS), Anisotropy of out-of-phase Magnetic Susceptibility (opAMS), or Anisotropy of Anhysteretic Remanent Magnetization (AARM) are frequently used to decipher the tectonic evolution of mountain belts (e.g., Aubourg et al., 2004; Dudzisz et al., 2016, 2018; Hrouda and Hanák, 1990; Szaniawski et al., 2012, 2017, 2020). These methods focus on investigating the mineral-preferred orientation: diamagnetic, paramagnetic, and ferromagnetic (for AMS) or only ferromagnetic minerals (for AARM) in rocks. Studies have shown that magnetic fabrics are good indicators of the strain orientation in rock formations (e.g., Aubourg et al., 1991; Averbuch et al., 1992; Parés,

2015). Applying magnetic fabric methods enables studying the tectonic deformation in areas where natural outcrops are not sufficiently exposed to use traditional structural geology methods or where macroscopic indicators of deformation are absent and/or in an incipient stage. Modern magnetic anisotropy methods can identify fabrics originating from different mineral generations formed during separate stages of tectonic evolution (see Biedermann et al., 2020 and references therein). Thorough analysis and comparison of all detected magnetic subfabrics enable us to trace the geotectonic evolution of orogenic belts.

The AMS and AARM methodologies have been extensively applied to study the tectonic evolution of the Carpathians (i.e., Grabowski et al., 2009; Gregorová et al., 2009; Hrouda and Potfaj, 1993; Hrouda, 1983, 1986; Hrouda and Hanák, 1990; Hrouda and Kahan, 1991; Hrouda et al.,

---

* Corresponding author.
  E-mail address: dorota.staneczek@us.edu.pl (D. Staneczek).

2009; Madzin et al., 2021; Szaniawski et al., 2012, 2017, 2020). In the Tatra Mts, which are the highest part of the Carpathians, ipAMS studies are relatively scarce and existing studies largely focused on the crystalline basement and its autochthonous cover (Hrouda and Kahan, 1991; Szaniawski et al., 2012, 2020). To the best of our knowledge, opAMS and AARM data throughout the Tatra Mts are substantially lacking.

Studies have shown that the paleotemperature determines the magnetic mineralogy (e.g., Aubourg and Pozzi, 2010; Aubourg et al., 2019); however, research that combines temperature estimations, magnetic fabrics, and regional tectonic studies is limited (e.g., Antolín Tomas, 2010). Most commonly, vitrinite reflectance analyses are applied to study mineralogical changes related to changing depth in well samples (e.g., Kitamura et al., 2005). Paleotemperature estimations based on vitrinite reflectance data can detect a relatively broad temperature spectrum (even up to 300 °C; Hunt, 1996). Insights into the temperature range, especially below 200 °C can also be derived from extracted organic compounds (biomarker) analyses. To most effectively track the paleotemperature changes in the Tatra area, we apply both biomarker analyses and vitrinite reflectance measurements.

This study aims to analyze new rock magnetic, magnetic fabric, and paleotemperature estimate data from the Mesozoic thrust nappe and the Paleogene post-thrusting cover in the Tatra Mts (divided here into the Western and High Tatra Mts; Figs. 1 and S.1), to evaluate the main stages of the Cretaceous–Neogene tectonic evolution. A joint interpretation of the magnetic fabrics and paleotemperatures allows for a more in-depth understanding of the tectonic evolution of the Tatra Mountains and adjacent areas, as well as mountain belts in general.

2. Geological setting

The tectonic evolution of the Tatra Mts started in the Late Paleozoic with the granitic intrusions and Variscan metamorphic events that formed the present crystalline basement (e.g., Burchart, 1972; Kohút et al., 1999; Král, 1977; Petrík and Kohút, 1997; Plašienka et al., 1997).

The Triassic period was dominated by the formation of oceanic regions under an extensional regime and the onset of carbonate sedimentation that followed the deposition of conglomerates and sandstones (Plašienka et al., 1997). This extensional regime continued during the Jurassic. In the Cretaceous, the collision of the North European Platform with Adria- and Europe-derived units resulted in the emplacement of nappe systems, here represented by the Fatric-Hronic nappe system (Castelluccio et al., 2016; Csontos and Vörös, 2004; Kováč et al., 2018; Plašienka, 2018; Plašienka et al., 1997). In the Tatra Mts, the thrusting lasted until the Late Cretaceous (Anczkiewicz et al., 2015; Castelluccio et al., 2016; Csontos and Vörös, 2004; Kováč et al., 2018; Plašienka, 2018). Afterward, at the beginning of the Paleogene, the Tatra region was subjected to a minor uplift and terrestrial erosion, followed by the opening of the Central Carpathian Paleogene Basin (CCPB) and subsequent burial of the Mesozoic nappe units under a stack of clastic Paleogene sediments (Soták et al., 2001). The sedimentation in the CCPB was terminated presumably in the earliest Miocene (Garecka, 2005; Soták et al., 2001). During the Neogene, the Tatra horst was elevated and asymmetrically tilted to the north along the Sub-Tatric fault (Jurewicz, 2005; Rubinkiewicz and Ludwiniak, 2005; Sperner et al., 2002; Szaniawski et al., 2012).

In this study, we investigate two formations (the Huty and Mraznica Fms) that have previously been proven to be suitable for magnetic analyses in the neighboring Choč Mts (Staneczek et al., 2022). These formations belong to different geological units (Podhale Basin, part of the CCPB; and the Krížna nappe, part of the Fatric unit, respectively). The sedimentation of the younger Huty Fm predates the uplift of the Tatra Mt.; thus, it likely recorded the tectonic strain related to this major event. Therefore, studying these two formations may provide new insights into the geological evolution of the Tatras starting from the Cretaceous. The first formation, the Mraznica Fm (the Kościeliska Marl Fm in Polish terminology; see Lefeld, 1974), is part of a Mesozoic nappe system (Krížna nappe, Fatric unit) that was thrust over the crystalline basement of the Tatra Mts and its sedimentary cover in the Late
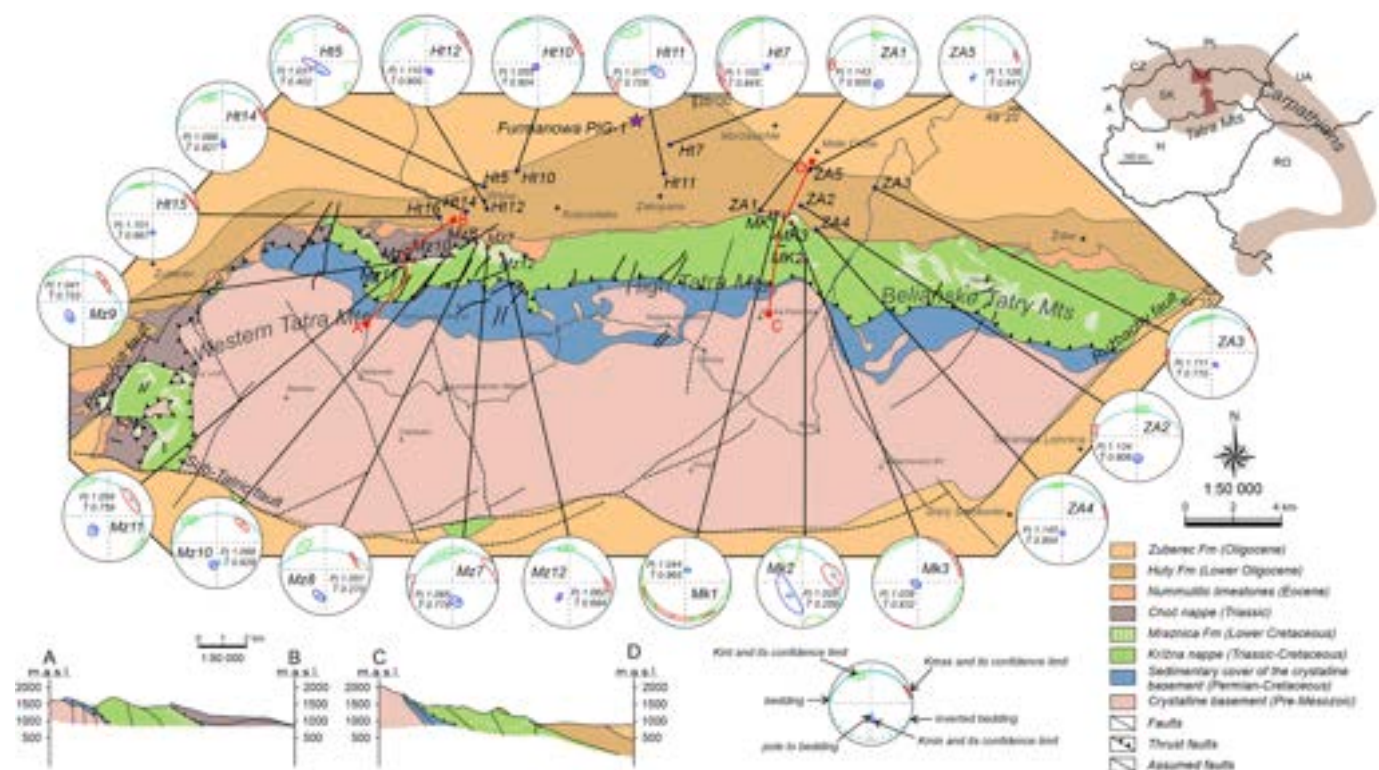
Fig. 1. Simplified geological map of the study area after Piotrowska et al. (2009, 2013) and Nemčok et al., 1993 with the cross-sections, sampling site locations, and ipAMS diagrams (the *Pj* and *T* parameters of the mean tensor are plotted for each diagram).

Cretaceous (Turonian). The Mraznica Fm comprises Lower Cretaceous light to dark gray marly limestones and marls, sometimes intercalated by turbiditic calcareous sandstones (Kędzierski and Uchman, 1997; Lefeld, 1974; Lefeld et al., 1985). In the Tatra Mts, the Mraznica Fm occurs in two slightly different types of successions: the Zliechov and Vysoka types. The Zliechov succession in the Western Tatra Mts comprises deeper marine deposits, while the Vysoka type (High Tatra Mts) consists of shallower water marine sedimentation (Nemčok et al., 1993). Both types of successions were sampled for this study. In the Western Tatra Mts, the Mraznica Fm strata are normal-lying; conversely, in some parts of the High Tatra Mts the bedding is overturned (Bac-Moszaszwili et al., 1979).

The second unit selected, the Huty Fm (Zakopane beds in Polish terminology; Westwalewicz-Mogilska, 1986), is a member of the CCPB cover. In the Podhale Basin, the Lower Oligocene unit consists of dark gray to nearly black siltstones and shales), representing deposition in marine conditions depleted in oxygen, locally intercalated with silty sandstones and conglomerates (Gross et al., 1993).

3. Materials and methods

3.1. Sampling sites

Nine sites were sampled in the Cretaceous Mraznica Fm (Fig. 1). Six of these sites are located in the Western Tatra Mts, and the remaining three are in the High Tatra Mts. All sites in the Western Tatras and one site in the High Tatras (Mk2) were sampled in beds with a normal position, whereas two sites in the High Tatras represent overturned Mraznica Fm strata. The Krížna nappe outcrops in the High Tatra area expose predominantly overturned layers; therefore, sampling normal-laying strata is not possible. The samples represent dark gray marly limestones. Twelve Huty Fm (Lower Oligocene) sites were sampled in a

2-km-wide belt along the Mesozoic outcrops of the Tatra Mts. Given that we were interested in resolving a record of the tectonic deformation, we sampled fine-grained rocks, mostly dark gray siltstones and shales, because these lithologies are less likely to have a magnetic fabric influenced by turbiditic paleocurrents (Table 1). The collected rock samples were used for the magnetic and geochemical analyses. Samples from the Furmanowa PIG-1 well were used for an additional comparison of the thermal maturity results for the Cretaceous and Paleogene rocks. Areas where local intensive tectonic deformations were present were strictly avoided during sampling.

3.2. Rock magnetic methods

First, the magnetic mineralogies of the Mraznica and Huty Fms were investigated by applying standard rock magnetic techniques. Volume-normalized in-phase (Kip) and out-of-phase (Kop) magnetic susceptibilities for each specimen were measured using an MFK1-FA Kappabridge (AGICO, Inc.) in 200 A/m field at two different frequencies (976 Hz and 15,616 Hz). The average percentage loss of susceptibility for the in-phase values was calculated using the equation of Dearing et al. (1996).

Temperature-dependent susceptibility measurements were performed to obtain information concerning the paramagnetic- and ferromagnetic contents. Powdered rock samples were examined using a KLY − 5 A Kappabridge with a CS4 high-temperature unit (AGICO, Czech Republic). The changes in the magnetic susceptibility were measured at temperatures between room temperature and 700 °C in a 400 A/m field intensity and 1220 Hz operating frequency.

The properties of the ferromagnetic components were subsequently characterized to identify the type and domain state of the ferromagnetic minerals present in the studied units. Specimens chosen for the acquisition of Isothermal Remanent Magnetization (IRM) measurements were

Table 1
Lithology and geochemical parameters of the sampled sites.

Sample	Lithology	Location	TOC	TS	CC	MPI1	Rc [%]	Rr [%]
Huty Fm								
Ht5	silty sandstone		0.55	0.54	19.39	0.61	0.77	0.53
Ht7	mudstone		0.85	1.09	16.38	0.67	0.80	0.57
Ht10	mudstone		0.70	0.86	18.45	0.70	0.82	0.41
Ht11	silty sandstone	*Western Tatra Mts*	0.77	1.25	17.52	0.69	0.82	0.40
Ht12	mudstone		0.59	0.59	16.85	0.57	0.74	0.55
Ht14	black shale		0.66	1.16	17.77	0.57	0.74	0.53
Ht15	mudstone		1.10	0.25	14.81	0.52	0.71	0.62
ZA1	black shale		1.59	1.39	34.85	1.07	1.04	0.92
ZA2	black shale		1.41	0.74	18.41	1.70	1.42	1.30
ZA3	black shale	*High Tatra Mts*	0.59	1.04	18.28	2.07	1.64	1.07
ZA4	black shale		0.65	1.10	21.99	1.78	1.47	1.18
ZA5	black shale		0.59	1.33	17.90	1.35	1.21	1.10
PIG_FUR	mudstone	*PIG1_FUR*	1.92	4.13	5.50	0.74	0.84	–
PIG_PR5	mudstone		2.24	0.70	14.76	0.90	0.94	–
Mraznica Fm								
MZ7	marl		0.12	0.00	68.17	0.44	0.66	0.72
MZ8	marl		0.13	0.00	65.43	0.45	0.67	0.86
MZ9	marly limestone		0.10	0.00	74.48	0.41	0.65	1.09
MZ10	marly limestone		0.10	0.08	73.38	0.35	0.61	0.82
MZ11	marly limestone	*Western Tatra Mts*	0.10	0.17	49.37	0.44	0.66	0.91
MZ12	marl		0.10	0.00	67.20	0.55	0.73	1.06
MZ13	limestone		0.14	0.00	81.53	0.46	0.67	0.72
KRY_MZ_1A	marly limestone		0.41	0.00	61.32	0.47	0.68	–
KRY_MZ_2A	marly limestone		0.56	0.00	57.21	0.41	0.65	–
MK1	marly limestone		0.10	0.06	69.58	0.64	0.79	1.51
MK2	limestone	*High Tatra Mts*	0.10	0.00	55.76	1.71	1.43	1.48
MK3	marly limestone		0.10	0.00	84.15	1.24	1.14	1.34
Eocene-Jurassic								
FU_PIG1_1979	conglomerate	*PIG1_FUR*	0.01	0.04	61.13	–	–	0.94
FU_PIG1_2049	limestone		0.52	0.00	56.21	–	–	0.99

Rr = random vitrinite reflectance.
MPI1 = methylphenanthrene index MPI1 = 1.5 (2-MP + 3-MP)/(P + 1-MP + 9-MP) (Radke and Welte, 1983).
Rc [%] = 0.4 + 0.6 x MPI1; Ph = phenantrene; MP = methylophenanthrene.

magnetized along the $+z$ axis using the MMPM10 pulse magnetizer (Magnetic Measurements, UK) in 28 steps up to 3 T. After each step, the acquired IRM was measured using a 2G SQUID cryogenic magnetometer (2G Enterprises, USA). A component analysis of the IRM acquisition data was performed using the Maxunmix software (https://maxunmix.shinyapps.io/).

Thermal demagnetization of the three-component IRM experiments (Lowrie, 1990) was performed for specimens for which IRM acquisition was previously performed. Each specimen was magnetized along three perpendicular axes (z: 3 T, y: 0.5 T, x: 0.15 T) using an MMPM10 pulse magnetizer followed by thermal demagnetization in 25–50 °C steps up to 700 °C (MMTDSC thermal demagnetizer, Magnetic Measurements, UK). After the initial IRM application and each demagnetization step, the remanence was measured using the 2G SQUID cryogenic magnetometer.

Hysteresis curves were acquired and IRM back-field experiments were conducted using a Micro-Mag vibrating sample magnetometer. Samples were demagnetized prior to hysteresis experiments in a 1 T field. Hysteresis curves were acquired in fields up to 1 T (500 mT for the Mraznica Fm and 1 T for the Huty Fm). Paramagnetic slope correction was applied at 70% of the highest field.

3.3. AMS and AARM

To analyze the magnetic fabrics of all the magnetic minerals in the studied units, ipAMS and opAMS measurements were repeated three times for each specimen to enhance the data quality. We used a KLY-5 A induction bridge with a 1220 Hz operating frequency and a 700 Am^{-1} field intensity. Standard-size cylindrical and cubic specimens were measured using the automated three-dimensional rotator, and the obtained susceptibilities were volume-normalized (κ, SI units). In total, 209 and 155 specimens were measured from the Huty and Mraznica Fms, respectively. The AMS ellipsoids and quantitative parameters of the AMS ellipsoid were calculated using the Anisoft5 software (AGICO).

To study the ferromagnetic fabrics, we applied the Anisotropy of the Anhysteretic Remanent Magnetization method. Measurements were performed on 118 Huty Fm specimens and 89 Mraznica Fm specimens in the 0–130 mT coercivity window. Directional Anhysteretic Remanent Magnetization was applied in six different directions: either along six phase diagonals of specimens coordinate system axes or along three principal specimen coordinate axes and their antipodals (B- and C-modes, respectively, see: https://www.agico.com/downloads/documents/agicoprints/arm_guide.pdf). After each magnetization-measurement step, the sample was demagnetized in a 140 mT alternating field (LDA-5 demagnetizer, AGICO). Directional ARM measurements and AARM calculations were conducted using a JR-6 A spinner magnetometer (AGICO) and the Rema6 software using full-vector method, respectively. Quantitative ellipsoid parameters were calculated via the Anisoft5 software. All magnetic fabric analyses were conducted in the Paleomagnetic Laboratory of the Institute of Geophysics, Polish Academy of Sciences in Warsaw (Poland), and in the magnetic laboratory of AGICO in Brno (Czech Republic).

3.4. Total organic carbon and total sulfur

The total carbon (TC), total sulfur (TS), and total inorganic carbon (TIC) contents were measured using an Eltra CS-500 IR-analyzer with a TIC module (Faculty of Natural Sciences, University of Silesia in Katowice, Poland).

3.5. Vitrinite reflectance

The sample preparation process followed the procedure described in ISO 7404-2 (2009). Freshly polished rock chips were examined in reflected light and immersion oil using an Axio Imager.A2m (Faculty of Natural Sciences, University of Silesia in Katowice, Poland). The

standards used were 0.898% and 1.71% relative reflectance (Rr).

3.6. Gas chromatography–mass spectrometry

Gas chromatography–mass spectrometry (GC–MS) was performed on an Agilent Technologies 7890 A gas chromatograph and an Agilent 5975C Network mass spectrometer with a Triple-Axis Detector (MSD). Separation was conducted on a fused silica capillary column (J&W HP5-MS, 60 m × 0.25 mm i.d., 0.25 μm film thickness) coated with a chemically bonded phase (5% phenyl and 95% methylsiloxane), for which the GC oven temperature was programmed to increase from 45 °C (1 min) to 100 °C at a rate of 20 °C/min, and then to 300 °C at a rate of 3 °C/min (holding time: 40 min), with a solvent delay of 10 min. Helium (6.0 grade) was used as the carrier gas at a constant flow rate of 2.6 ml/min.

The GC column outlet was directly connected to the ion source of the MSD. The GC–MS interface was set to 280 °C, while the ion source and quadrupole analyzer were set to 230 °C and 150 °C, respectively. Mass spectra were recorded from m/z 45–550 (0–40 min) and m/z 50–700 (> 40 min). MS was conducted in the electron impact mode, with an ionization energy of 70 eV. Spectra from the Wiley Registry of Mass Spectral Data (9th edition) and from the literature were used for the MS data comparison. Quantification of the compounds to calculate the molecular parameters was performed using Agilent Technologies MSD ChemStation E.02.01.1177 via integration of the peak areas on the appropriate mass chromatograms or total ion currents. The concentration of the selected aromatic compounds was calculated via comparisons of the peak area for an internal standard (9-phenylindene) with those of the individual compounds. The analysis was performed at the Faculty of Natural Sciences, University of Silesia in Katowice, Poland.

4. Results

4.1. Petromagnetic investigations

The in-phase magnetic susceptibility in the lower frequency is fairly consistent in the Huty Fm samples. The highest measured values are recorded in ZA3 and in Ht14 (Table 2). The lowest values are recorded for the samples from sites Ht7 and Ht11. The average Kip values in the Mraznica Fm sites are lower than the Kip measured for the Huty Fm samples. In general, the average obtained values range from 4.858 × 10^{-5} [SI] to 1.164 × 10^{-4} [SI]. There are no significant differences between the samples from the Western and High Tatra Mts (or their forelands). The Kip values were also measured at a higher frequency, and the obtained results were nearly identical. Moreover, the differences between the susceptibilities measured at different frequencies at most sites fluctuate at the sensitivity limit of the MFK1A. Therefore, the calculated average percentage loss of susceptibility for the majority of sites is close to zero. The Xfd parameter is higher, at ~2% (Table 2), only for three Mraznica Fm sites from the High Tatra Mts.

The temperature-dependent susceptibility measurements show consistent results for the sampled shales and limestones, respectively. The thermomagnetic curves show a hyperbolic decrease in the susceptibility up to 400 °C; this is followed by a sharp increase in the susceptibility values and a subsequent drop at ~575 °C. The estimated ferro/para ratio (according to the method proposed by Hrouda et al. (1997) shows a general prevalence of paramagnetic minerals and varies at the specimen level (Fig. 2). Ferro/para ratio obtained from the hysteresis experiments also suggests a high paramagnetic contribution in Huty and Mraznica Fms (Table 3). This is mirrored by the characteristics of the hysteresis loops in these units. The uncorrected loops show a nearly linear trend indicating the prevalence of paramagnetic minerals (Fig. 2).

The hysteresis loop experiments show consistent values of the hysteresis-related parameters at the lithology-level (Table 3; Fig. 2). In the Mraznica Fm, the magnetization (M) uncorrected for the paramagnetic slope reaches a maximum value of ~30 mAm^2·kg^{-1} in the 500

Table 2
Site-average volume-normalized magnetic susceptibility for each sampling site measured at low and high frequencies.

Site	Unit	Location	Average Kip 976 Hz [SI]	Average Kip 15,616 Hz [SI]	Kip 976 Hz - Kip 15,616 Hz	Average Xfd [%]
Za1			1.822E-04	1.828E-04	-5.802E-07	−0.318
Za2			1.827E-04	1.825E-04	2.245E-07	0.123
Za3		High Tatra Mts	2.267E-04	2.272E-04	−4.798E-07	−0.212
Za4			1.709E-04	1.715E-04	−6.174E-07	−0.361
Za5			1.853E-04	1.856E-04	−3.411E-07	−0.184
Ht5	Huty Fm		1.725E-04	1.737E-04	−1.214E-06	−0.704
Ht7			1.587E-04	1.593E-04	−5.173E-07	−0.326
Ht10			1.977E-04	1.983E-04	−5.550E-07	−0.281
Ht11		Western Tatra Mts	1.636E-04	1.623E-04	1.302E-06	0.795
Ht12			1.978E-04	1.989E-04	−1.074E-06	−0.543
Ht14			2.050E-04	2.047E-04	3.696E-07	0.180
Ht15			1.799E-04	1.796E-04	2.464E-07	0.137
Mk1			7.497E-05	7.289E-05	2.076E-06	2.770
Mk2		High Tatra Mts	1.164E-04	1.130E-04	3.324E-06	2.856
Mk3			5.188E-05	5.070E-05	1.172E-06	2.260
Mz7			8.205E-05	8.201E-05	4.200E-08	0.051
Mz8	Mraznica Fm		8.874E-05	8.883E-05	−9.518E-08	−0.107
Mz9		Western Tatra Mts	4.858E-05	4.849E-05	8.953E-08	0.184
Mz10			8.738E-05	8.768E-05	−3.077E-07	−0.352
Mz11			8.724E-05	8.725E-05	−1.200E-08	−0.014
Mz12			8.166E-05	8.178E-05	−1.264E-07	−0.155

mT applied field, while the saturation magnetization (Ms) reaches 3.031 mAm^2·kg^{-1} and the remanence magnetization (Mr) is up to 180.3 μAm^2·kg^{-1} after the paramagnetic slope correction. All three parameters have slightly lower values for the High Tatra samples. The mean coercivity (Hc) and remanence coercivity (Hcr; obtained from backfield experiments) differ somewhat in the Western and High Tatra samples, having values of ~10 mT and ~ 24 mT, respectively. The hysteresis parameters (apart from the mean coercivity) for the Huty Fm show some distinct differences from those determined for sites sampled in the Western and High Tatra Mts. The M (~60.15 μAm^2·kg^{-1}) and Hcr (~49 mT) values are higher for samples from the Western Tatra Mts, while the saturation magnetization and remanent magnetization values are significantly higher in the High Tatra Mts (1151.66 μAm^2·kg^{-1} and 126.87 μAm^2·kg^{-1}, respectively).

The IRM acquisition curves are fairly homogeneous in each sampled unit (Fig. 2; Table 4). In the Huty Fm specimens, the saturation IRM (SIRM) reaches a maximum of 140 mA/m. The values of the magnetization grow quickly until an applied field of approximately 130 mT. Then, the curves flatten slowly until 500 mT and there is only a very subtle increase in the magnetization in higher fields. The Mraznica Fm specimens show similar behavior with respect to the magnetization curve as the Huty Fm specimens in fields of up to 500 mT. The SIRM values are quite high and reach 108 mA/m. Afterward, the magnetization values continue to increase gradually until the maximum applied field.

The IRM component analysis revealed four main components in the Huty and Mraznica Fms (Table 4). Components 1 and 2 are similar in both sampled units. The first component is characterized by low B1/2 values (11–21 mT) and the dispersion parameter (DP) averaging 0.35. The second component has higher coercivity values (~75 mT) and, for the majority of the analyzed specimens, is the dominant component of the IRM. The B1/2 values for the third component range from 150 mT to 300 mT and the DP averages from 0.30 to 0.35. The contribution of this component is rather low in the Huty Fm and in most Mraznica Fm specimens; however some Mraznica Fm specimens from the Western Tatra Mts, it is the main IRM constituent. The fourth distinguished component is not present in all the analyzed specimens and is characterized by high coercivity, reaching even >6 T.

The thermal demagnetization of a three-component IRM follows different patterns for the Mraznica and Huty Fm specimens. The pattern typical for the Huty Fm shows a dominance of the low coercivity magnetic phase characterized by a maximum unblocking temperature of 575 °C, while the magnetization values for the intermediate and high

coercivity curves are close to zero. The second pattern, the Mraznica pattern, is characterized by higher magnetization values of the high and intermediate coercivity curves than those measured for the Huty Fm. While the drops in the magnetization values on the intermediate coercivity curves are not consistent for the analyzed specimens, the high coercivity curves experience drops at 675 °C for a considerable number of specimens. Regardless, the low coercivity magnetic phase displays the highest magnetization values, which drop to zero at the 575 °C demagnetization step.

4.2. Magnetic fabrics

The in-phase magnetic susceptibility (Kip) measured for the nine Mraznica Fm sites ranges from 0.25×10^{-5} to 1.51×10^{-4} [SI] (Fig. 3). The corrected anisotropy degree (Pj; Jelínek, 1981) is low (~1.05) and is relatively consistent in each site. The ellipsoid shape for the majority of the analyzed specimens is predominantly oblate. There are virtually no differences in the ellipsoid parameters between the sites sampled in the Western and High Tatra Mts. The IpAMS foliation in all of the Mraznica Fm sites is well defined and bedding-parallel (Fig. 4). In the Western Tatras, the k_{max} axes are moderately (Mz7 and Mz11) or well-grouped (Mz8–10 and Mz12). The ipAMS lineation is approximately NE-SW to ENE-WSW oriented and parallel to the bedding. In sites Mk1 and Mk3 in the High Tatra Mts, the maximum ellipsoid axes form a girdle that is sub-parallel to the bedding plane. Site Mk2, which represents the beds of the Mraznica Fm. at a normal stratigraphic position in the High Tatra Mts, is characterized by an ipAMS fabric similar to those documented in the Mraznica Fm sites in the Western Tatras. The IpAMS foliation traces the bedding plane and the quite well-defined ipAMS lineation has an approximate ENE-WSW orientation.

The out-of-phase magnetic susceptibility (Kop) in Mraznica Fm sites is lower than the in-phase magnetic susceptibility (Fig. 3B). The Pj values are generally higher than those documented by ipAMS measurements, which is typical for opAMS fabrics (Hrouda et al., 2022). The T values are much lower, corresponding primarily to prolate ellipsoid shapes. In the Western Tatra Mts, the magnetic fabric typically shows a moderate dispersion of ellipsoid axes (Fig. 4). The OpAMS foliation tends to be rather sub-parallel to the bedding and is more poorly defined than the magnetic lineation. The opAMS lineation is inclined with respect to the bedding plane (except at sites Mz7 and Mz12). In the High Tatra Mts, the opAMS lineation is vertical in all sites while the opAMS foliation is sub-perpendicular to the bedding.

The in-phase magnetic susceptibility measured for the 12 Huty Fm
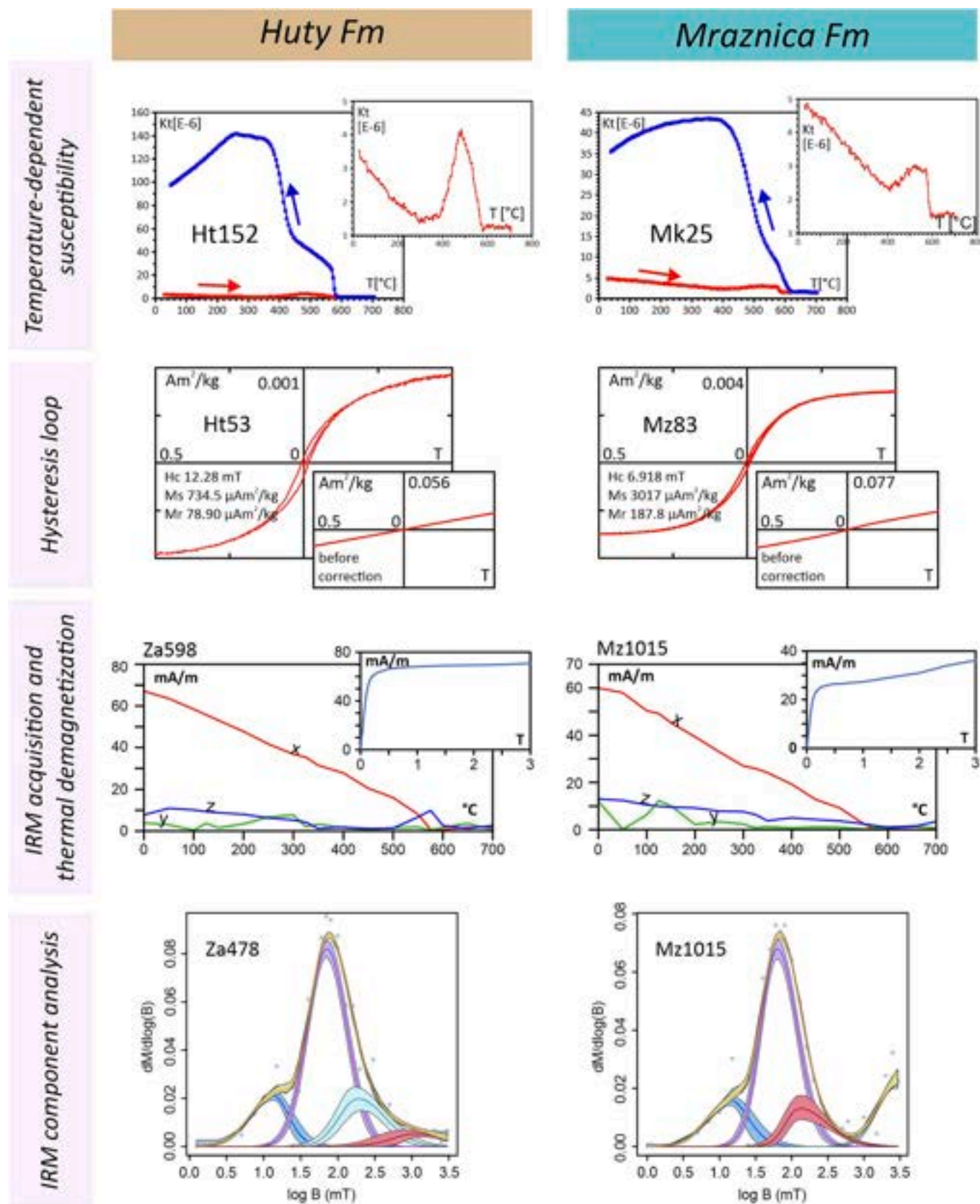
Fig. 2. Results of petromagnetic investigations for selected Mraznica and Huty Fm samples.

Table 3

Hysteresis and isothermal remanent magnetization (IRM) back-field parameters.

Formation	Site	Sample values								
		Sample	Hysteresis loop (after holder correction)		Hysteresis loop (after slope correction)					IRM back-curve	Ferro/para content (%)
			Ms (mAm²/kg)	Initial slope (mAm²/T*kg)	Ms (µAm²/kg)	Mr (µAm²/kg)	Hc (mT)	Initial slope (mAm²/T*kg)	Slope correction (mAm²/T*kg)	Hcr (mT)	
Huty Fm, Western Tatra Mts	Ht5	Ht53	50.4	53.8	734.5	78.9	12.28	4.072	−49.73	25.75	7.57
		Ht55	70.72	87.49	3268	168.2	5.735	19.94	−67.55	22.68	22.79
	Ht7	Ht72	28.34	64.36	1081	65.92	5.15	9.819	−54.54	21.67	15.26
		Ht74	24.55	58.81	1274	80.14	5.094	12.24	−46.57	15.48	20.81
	Ht10	Ht102	71.93	75.19	807.6	50.45	7.042	3.959	−71.23	16.84	5.27
		Ht103	79.45	83.41	790.9	72.37	9.632	4.638	−78.77	16.01	5.56
	Ht11	Ht111	24.16	55.75	1006	60.95	5.51	9.427	−46.32	15.68	16.91
		Ht115	29.62	73.65	2241	181.5	7.369	18.87	−54.78	20.35	25.62
	Ht12	Ht121	60.5	62.92	492.6	47.01	9.416	2.833	−60.09	10.86	4.50
		Ht122	54.83	57.91	569	86.87	14.08	3.569	−54.34	18.98	6.16
	Ht14	Ht147	62.92	65.85	679.2	64.21	9.391	3.521	−62.33	21.9	5.35
		Ht145	55.86	60.7	1400	60.33	7.442	6.165	−54.54	21.78	10.16
	Ht15	Ht154	73.92	77.12	733.7	50.59	6.438	3.832	−73.29	17.47	4.97
		Ht156	68.85	72.26	765.3	64.46	7.935	4.073	−68.19	19.17	5.64
Average values			**54.00**	**67.80**	**1131.63**	**80.85**	**8.04**	**7.64**	**−60.16**	**18.90**	**11.18**
Standard deviation			**18.93**	**10.13**	**732.24**	**40.04**	**2.59**	**5.53**	**9.91**	**3.68**	**7.27**
Huty Fm, High Tatra Mts	ZA1	ZA14	28.09	59.37	674.40	64.07	8.72	4.50	−54.87	18.64	7.58
		ZA18	29.86	62.95	508.00	51.19	10.41	4.21	−58.74	18.74	6.69
	ZA2	ZA24	13.19	34.13	947.80	119.00	7.89	9.62	−24.51	24.20	28.18
		ZA28	33.31	83.26	1926.00	212.80	6.82	20.45	−62.81	18.81	24.56
	ZA3	ZA33	32.95	73.90	1252.00	121.80	8.26	10.46	−63.44	22.40	14.15
		ZA35	7.33	18.03	423.70	57.31	8.76	4.20	−13.83	19.54	23.29
	ZA4	ZA46	27.91	63.07	1003.00	100.60	7.89	9.20	−53.87	19.43	14.59
		ZA47	28.03	63.70	946.70	109.90	9.00	9.48	−54.22	20.51	14.88
	ZA5	ZA54	31.49	82.99	2205.00	260.00	6.78	24.37	−58.62	20.06	29.36
		ZA59	31.06	75.47	1630.00	172.00	7.02	16.58	−58.89	21.22	21.97
Average values			**26.32**	**61.69**	**1151.66**	**126.87**	**8.15**	**11.31**	**−50.38**	**20.36**	**18.53**
Standard deviation			**8.34**	**19.84**	**567.95**	**65.36**	**1.08**	**6.64**	**16.09**	**1.71**	**7.68**
Mraznica Fm, Western Tatra Mts	Mz7	Mz73	31.19	46.65	3031	180.3	6.648	18.45	−28.2	25.29	39.55
		Mz74	28.72	31.27	485.9	58.97	11.63	2.995	−28.28	23.48	9.58
	Mz8	Mz82	17.51	19.26	385.1	39.11	14.71	2.109	−17.15	30.67	10.95
		Mz83	45.1	60.45	3017	187.8	6.918	18.31	−42.14	25.17	30.29
	Mz9	Mz91	6.216	8.117	358.1	39.24	10.25	2.251	−5.866	25.47	27.73
		Mz96	11.15	18.4	1061	57.51	4.32	8.298	−10.1	13.99	45.10
	Mz10	Mz101	19	21.04	410.3	48.59	11.52	2.422	−18.61	23.42	11.51
		Mz106	31.42	33.54	472.2	51.19	11.97	2.551	−30.99	21.83	7.61
	Mz11	Mz112	21.83	23.78	376.5	49.52	14.08	2.295	−21.49	18.48	9.65
		Mz113	27.97	30.05	349.3	45.11	11.59	2.394	−27.66	19.38	7.97
	Mz12	Mz122	26.46	28.12	295.7	52.53	13.82	1.919	−26.2	28.2	6.82
		Mz127	29.76	31.78	441.1	46.94	10.2	2.424	−29.36	22.98	7.63
Average values			**24.69**	**29.37**	**890.27**	**71.40**	**10.64**	**5.53**	**−23.84**	**23.20**	**15.02**
Standard deviation			**9.90**	**13.13**	**972.70**	**50.73**	**3.07**	**5.97**	**9.42**	**4.26**	**13.28**
Mraznica Fm, High Tatra Mts	MK1	MK11	9.62	22.47	421.20	52.63	8.11	4.06	−18.41	22.20	18.07
		MK13	6.46	17.16	506.80	77.17	8.53	5.25	−11.92	24.78	30.57
	MK2	MK25	18.87	43.03	726.40	113.70	11.03	6.71	−36.32	25.77	15.59
		MK27	12.54	28.94	514.50	74.94	9.46	4.87	−24.07	24.76	16.83
	MK3	MK34	7.44	17.88	365.30	52.75	8.80	3.72	−14.16	24.21	20.81
		MK35	7.33	18.03	423.70	57.31	8.76	4.20	−13.83	26.44	23.29
Average values			**10.38**	**24.59**	**492.98**	**71.42**	**9.11**	**4.80**	**−19.79**	**24.69**	**20.86**
Standard deviation			**4.29**	**9.19**	**116.47**	**21.35**	**0.95**	**0.99**	**8.39**	**1.33**	**5.03**

sites varies significantly from 3.42×10^{-5} to 2.62×10^{-4} [SI] (Fig. 3). The shape of the AMS ellipsoid is oblate. The corrected anisotropy degree varies with the lithology of the sampling site. In shales and siltstones (sites Ht7, Ht10, Ht12, 14, 15, and Za1–5), it is significantly higher (1.022–1.149) than in more sandy sites (Ht5 and Ht11; 1.022–1.055). The IpAMS fabric is consistent in all Huty Fm sites. It is characterized by well-defined and bedding-parallel magnetic foliation (Fig. 5) and similarly oriented magnetic lineations (ENE-WSW in the Western Tatras and E-W in the High Tatras). Only in site Ht5 are the k_{max} axes more NE-SW oriented.

The out-of-phase magnetic susceptibility values for the Huty Fm are low and range from 4.11×10^{-8} to 7.33×10^{-7} [SI] (Fig. 3). The corrected anisotropy degree reaches higher values than those reported for ipAMS (a typical feature of opAMS fabrics; Hrouda et al., 2022). The T parameter varies from 0.9 to nearly 0, corresponding primarily to triaxial to oblate ellipsoid shapes. The out-of-phase magnetic fabric orientation is highly consistent in the High and Western Tatra Mts. The OpAMS foliation follows the bedding, and the magnetic lineation is generally well defined (and NE-SW oriented Fig. 5). In sites Ht10, Ht11 and Ht12, maximum ellipsoid axes are dispersed, and, therefore, the opAMS lineation is poorly defined.

The AARM was measured in the 0–130 mT coercivity range for the nine Mraznica Fm sites. The anhysteretic remanence values range from 3.25×10^{-3} [SI] to 148.0×10^{-3} [A/m] (Table S.1; Supplementary materials). The shape of the AARM ellipsoid varies at the specimen level from oblate to prolate, and the corrected anisotropy degree ranges from 1.077 to 1.114 (Fig. 3). In the majority of sites in the Western Tatra Mts, the magnetic r_{min} axes (the minimum axes of the AARM ellipsoid) are

Table 4
Analysis of IRM components.

Sample	Unit	Location	Component 1			Component 2			Component 3			Component 4		
			logB1/2	B1/2 [mT]	DP	logB1/2	B1/2 [mT]	DP	logB1/2	B1/2 [mT]	DP	logB1/2	B1/2 [mT]	DP
Ht524			1.20	15.93	0.34	1.88	75.52	0.24	2.38	241.61	0.35	3.63	4293.35	0.37
Ht725			1.08	12.01	0.29	1.86	72.62	0.26	2.27	188.16	0.28	3.14	1386.06	0.40
Ht1082		*Western Tatra*	1.25	17.77	0.36	1.88	76.42	0.25	2.31	205.17	0.34	2.93	852.94	0.27
Ht1132			1.32	21.11	0.40	1.91	81.95	0.25	2.36	231.23	0.31	2.94	862.81	0.27
Ht1213			1.23	17.00	0.35	1.87	73.59	0.24	2.26	183.65	0.28	2.87	736.15	0.78
Ht1474	*Huty Fm*		1.17	14.74	0.35	1.88	75.79	0.28	2.36	230.95	0.31	3.23	1714.41	0.42
Ht1564			1.25	17.95	0.39	1.90	80.10	0.28	2.55	358.32	0.45	–	–	–
Za133			1.20	15.90	0.36	1.85	71.21	0.23	2.16	143.77	0.22	3.02	1043.22	0.47
Za284			1.24	17.56	0.39	1.89	77.13	0.27	2.40	251.51	0.35	3.12	1324.93	0.20
Za352		*High Tatra*	1.24	17.54	0.39	1.91	80.51	0.26	2.49	307.43	0.32	3.22	1678.27	0.44
Za478			1.05	11.32	0.26	1.86	72.80	0.26	2.36	230.40	0.32	3.15	1403.87	0.37
Za598			1.06	11.52	0.27	1.87	74.55	0.27	2.49	307.32	0.43	3.79	6164.70	0.29
Mz742			1.10	12.49	0.28	1.88	75.06	0.24	2.49	307.92	0.31	3.50	3188.97	0.31
Mz825			1.18	15.12	0.32	1.81	65.02	0.23	2.19	153.76	0.28	3.48	3019.71	0.24
Mz953		*Western Tatra*	1.22	16.69	0.36	1.85	71.07	0.24	2.31	204.50	0.32	3.52	3313.99	0.25
Mz1015			1.10	12.70	0.29	1.84	68.93	0.25	2.27	184.85	0.33	3.58	3772.58	0.30
Mz1136	*Mraznica Fm*		1.21	16.15	0.36	1.84	68.80	0.26	2.23	170.10	0.19	3.39	2461.00	0.47
Mz1223			1.21	16.32	0.40	1.87	73.52	0.25	2.34	217.42	0.28	3.48	2998.01	0.27
Mk142			1.12	12.63	0.32	1.87	75.63	0.24	2.16	228.51	0.37	3.58	3123.83	0.34
Mk263		*High Tatra*	1.22	16.66	0.36	1.87	73.52	0.26	2.22	164.91	0.30	3.56	3631.28	0.51
Mk334			1.10	12.63	0.33	1.88	75.63	0.25	2.36	228.51	0.32	3.49	3123.83	0.38
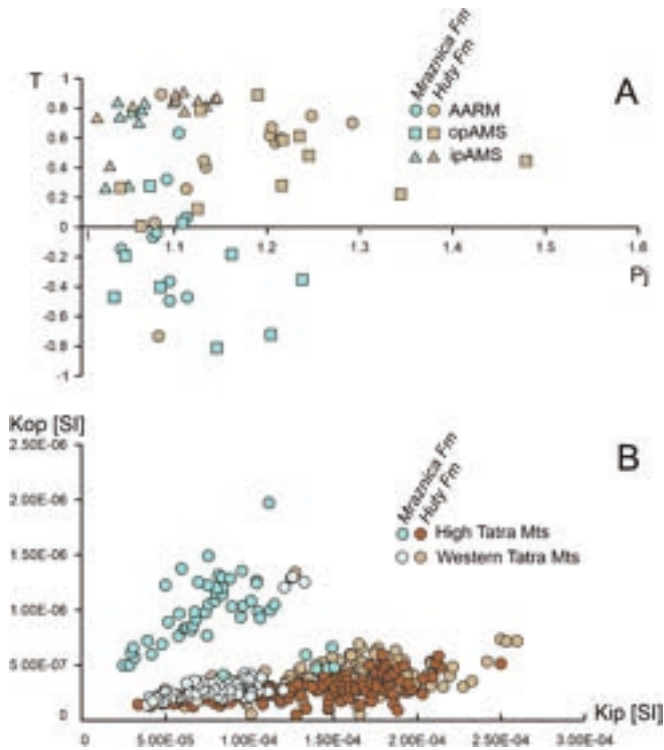
Fig. 3. Magnetic susceptibility and ipAMS, opAMS and AARM ellipsoid parameters (*Pj*: corrected anisotropy degree, *T*: ellipsoid shape parameter, Kip: in-phase magnetic susceptibility, Kop: out-of-phase magnetic susceptibility).

grouped rather well (Mz9, Mz10, and Mz12) or are somewhat dispersed (Mz7, and Mz11), and the mean AARM foliation plane is parallel to the bedding (Fig. 4). Only in site Mz8 site do the r_{min} axes form a girdle. The AARM lineation is rather well defined in each site. The mean AARM lineation orientations lie on the bedding plane (Mz7, Mz11, and 12) or are or are gently dipping with respect to the bedding planes. After applying the bedding correction, they are generally NNE-SSW to NE-SW oriented. In the High Tatra Mts, the AARM ellipsoid characteristics differ

from those reported in the Western Tatra Mts and are similar to the features of the opAMS ellipsoid. The minimum ellipsoid axes are dispersed, and only for site Mk1 are they well-grouped and horizontally oriented. The magnetic AARM lineation is well defined and sub-vertical in all High Tatra Mts sites.

The ARM in the 0–130 mT coercivity range for the 12 Huty Fm sites ranges from 4.13×10^{-3} to 37.7×10^{-3} [A/m]. The ellipsoid shapes are oblate to triaxial and the Pj parameter values are nearly 20% greater than those for the Mraznica Fm, varying from 1.079 to 1.292 (Fig. 5). In all sites, the AARM foliation is parallel to the bedding. The r_{max} axes (the maximum axes of the AARM ellipsoid) are generally well-grouped and lie within the bedding plane. The AARM lineation varies slightly by site, however, it is generally NW-SE oriented.

4.3. Bulk geochemical data and vitrinite reflectance

The bulk geochemical data for the Mraznica Fm (Lower Cretaceous) and Huty Fm (Lower Oligocene) samples vary widely. Samples of the Mraznica Fm are characterized by low TOC and TC contents. In most samples, the TOC contents oscillate in the range of 0.1 wt%, and the TOC values reach 0.4 wt% and 0.5 wt% in only two Mraznica samples. In addition, the TS contents are very low, not exceeding 0.2 wt%, and are below the detection range in most samples. All the samples from the Mraznica Fm are marly limestones with carbonate contents in the range of 55–85 wt%. In the Lower Oligocene samples from the Huty Fm, TOC content is higher, ranging from 0.5 wt% to 1.6 wt%. Moreover, the total sulfur values are >1.0 wt% in half of the samples and are not below 0.5 wt% for all samples. Carbonates are present in all samples but are below 20 wt% in most samples (only two samples contain higher carbonate content, reaching 22 wt% and 35 wt%; Table 1).

The vitrinite reflectance was measured for all of the outcrop samples from the Huty and Mraznica Fms (Table 1). Only two Mraznica samples did not contain vitrinite, or the grains were too small. The vitrinite reflectance was not measured for the Huty samples from the Furmanowa well. The obtained results differ significantly between the Western and High Tatra Mts. For the Mraznica Fm in the Western Tatra Mts, the measured vitrinite reflectance ranges from 0.7% to 1.1% Rr (Table 1). For the Mraznica Fm samples from the High Tatra Mts, the vitrinite reflectance values are higher, in the range of 1.3%–1.5% Rr (Table 1). The same situation applies to the Huty Fm. The measured vitrinite
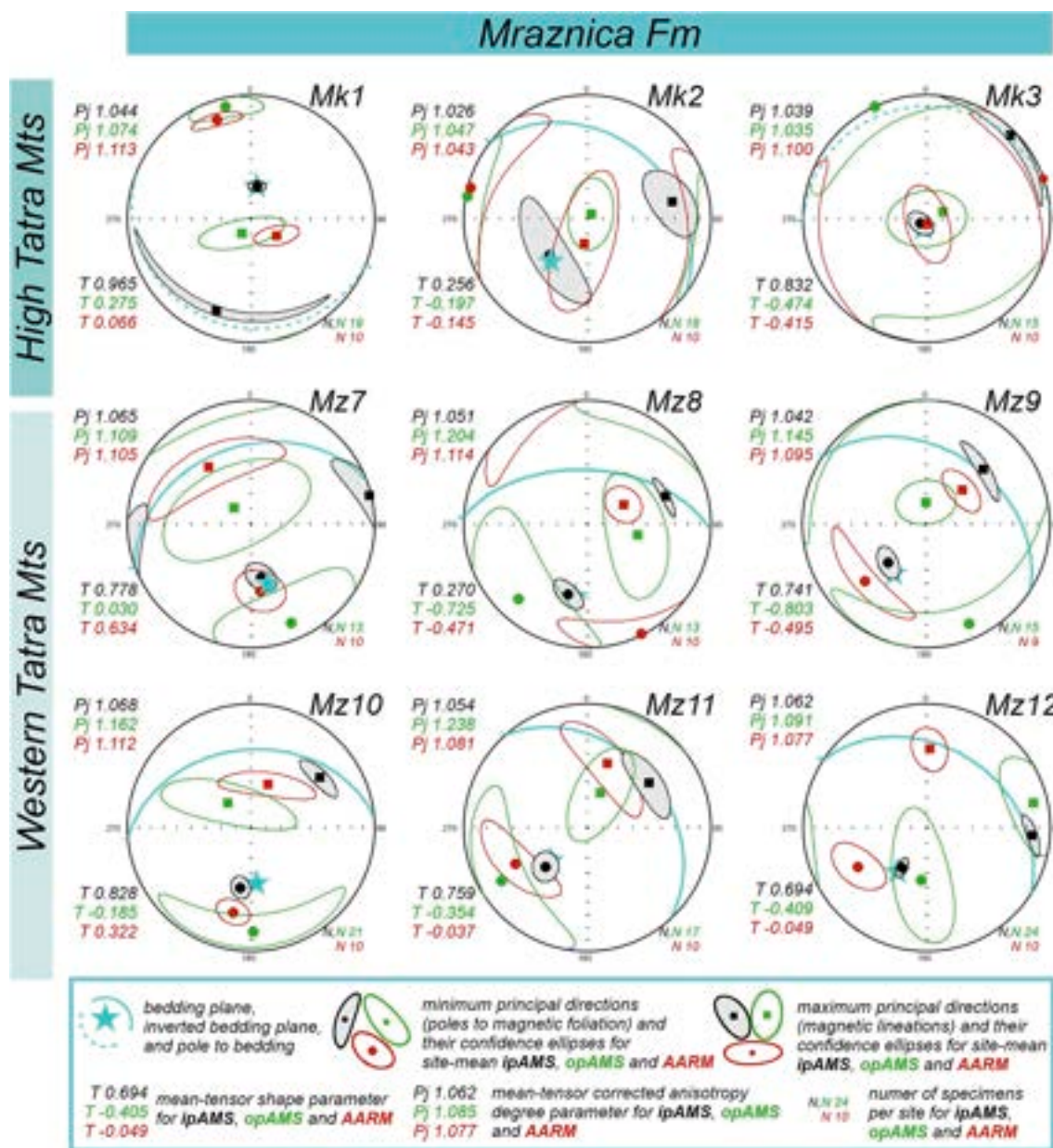
Fig. 4. Magnetic fabrics recorded in the Mraznica Fm rocks. All fabrics are plotted in lower hemisphere projections in geographic coordinates. Squares and circles represent the maximum and minimum ellipsoid axes derived from the site-mean tensor, respectively. Black colour indicates the ipAMS fabric, green indicates the opAMS, and red indicates the AARM fabric. The blue great circle indicates the bedding orientation, and the blue stars indicate the pole to bedding. *(For interpretation of the references to colour in this figure legend, the reader is referred to the web version of this article.)*

reflectance values for the High Tatra Mts range from 0.9% to 1.3%, while the values for the Western Tatra Mts do not exceed 0.65%. The measured vitrinite reflectance values from the Western Tatra Mts are consistent but much lower than previously published data (Poprawa et al., 2002). However, for the Huty Fm samples, the measured vitrinite reflectance values do not correspond to those previously mentioned by Marynowski et al. (2006) and Środoń et al. (2006). The measured values are too low compared to the biomarker or clay mineral maturity parameters. This may be related to the suppression of the measured values as a result of the saturation of vitrinites with bitumens, given that the rocks are in the oil window maturity range (Staneczek et al., 2024).

4.4. Maturity parameters based on GC–MS analyses

The organic compounds used to determine the thermal maturity of the Mraznica and Huty Fms in the Western and High Tatra Mts were methylphenanthrenes (MP). The methylphenanthrene index (MPI1) was calculated and then converted to a theoretical value of the vitrinite reflectance (Table 1; Radke and Welte, 1983; Radke et al., 1986). This group of compounds has previously been used in thermal maturity studies of Oligocene rocks and shows a consistent increase in value with depth in the Chochołów PIG1 and Bukowina Tatrzańska IG1 boreholes (Marynowski et al., 2015; Poprawa and Marynowski, 2005).

The MPI1 and Rc values differ for samples from the Western and High Tatra Mts (Table 1). The MPI1 values for the Huty Fm from the High Tatra Mts range from ~1 to 2, corresponding to Rc values in the range from 1% to 1.65% Rc. In the Huty Fm sites in the Western Tatra Mts, MPI1 varies insignificantly (from 0.5 to 0.7), resulting in Rc values from 0.7% to 0.82%. The MPI1 and Rc values for Mraznica Fm are similar but relatively lower than those for the Huty Fm samples (Table 1). However, MPI1 is not recommended for the marine organic matter type (Radke et al., 1986), which is typical for the marly
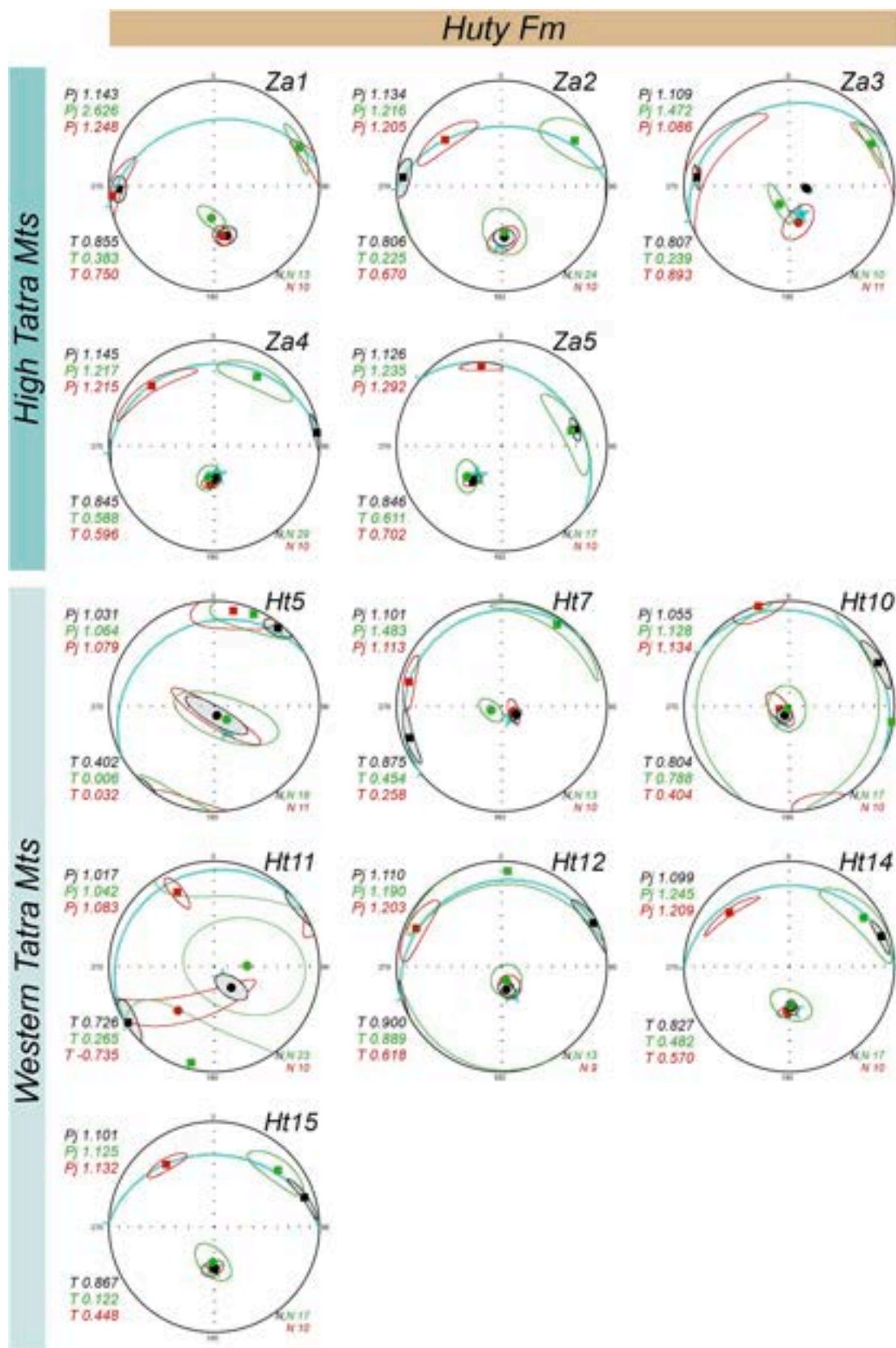
Fig. 5. Magnetic fabrics recorded in the Huty Fm rocks (symbol explanation as in Fig. 4).

limestones of the Mraznica Fm. Therefore, we used the values of the measured vitrinite reflectance (Ro) for these rocks. The MP distribution is similar in Huty and Mraznica Fms in the Western Tatra Mts, and Huty and Mraznica Fms from the High Tatra Mts, and clearly differs between the mentioned Tatra parts (Fig. 6). In addition, phenylphenanthrenes (PhP), compounds whose distributions vary with thermal maturity (Grafka et al., 2015; Huang et al., 2016; Rospondek et al., 2009), show clear differences for the Western and High Tatra mountain samples (Fig. 7).

5. Discussion

5.1. Paleotemperature changes across the southern part of the Podhale Basin and the Tatra Mts

This study aims to measure the maturity range of the youngest deposits of the Krížna nappe and the oldest deposits of the Paleogene in both the Western and High Tatra Mts. Note that the presented data were derived from two independent methods and converged in both cases. Our results show no distinct differences between the maturities of the Mesozoic (Mraznica Fm) and Cenozoic (Huty Fm) deposits in both the Western and High Tatra Mts (Fig. 8), as well as in the central part of the southern Podhale (Furmanowa PIG-1 well; Fig. 8). The vitrinite reflectance measurements gave optimal results for the Mraznica Fm, and MPI1 was converted to reflectance values (Rc) for the Huty Fm (Table 1). If the two data groups are compared, there are no significant differences between the maturities of the Mraznica and Huty Fms in the Western Tatra Mts, and the Mraznica and Huty Fms in the High Tatra Mts. The only differences arise from the locations of individual points (Fig. 8) because the thermal maturity increases toward the SE direction, as also reported by Środoń et al. (2006). This means that the maximum burial (and maximum temperatures) of the Lower Cretaceous (Mraznica Fm) rocks

occurred after the Oligocene, which is consistent with a previous reconstruction of the burial and thermal history of the Podhale Trough (Poprawa et al., 2002; Marynowski et al., 2006). If this is the case, at least part of the Mesozoic Krížna nappe reached maximum temperatures long after the Late Cretaceous thrusting event. Fission track data presented by Králiková et al. (2014) and Śmigielski et al. (2016) also show significant differences in the temperature influence for the Western and High Tatra Mts; this may, however, be associated with differences in the thicknesses of Mesozoic nappes. The lack of important differences between the thermal maturity of the Mraznica Fm and the directly overlying Huty Fm rocks presented here raises a question where the thermal influence of the Paleogene overburden ends and that of the Cretaceous begins (see Králiková et al., 2014). In other words, the new data suggest that the probable tectonic cover of the Krížna nappe with other nappes (e.g. Choč) had a lower temperature effect than the Paleogene to earliest Miocene burial.

5.2. Main magnetic carriers and their origins

The rock magnetic investigations (temperature-dependent susceptibility and hysteresis loop experiments) document the dominance of the paramagnetic minerals over the ferromagnetic minerals in the Mraznica and Huty Fms (Fig. 2). These results agree with previous magnetic investigations of the Mraznica Fm in the Tatra Mts (Grabowski et al., 2013), Choč Mts (Staneczek et al., 2022) and Strážov Mts (Grabowski et al., 2009) and of the Huty Fm (Hrouda and Potfaj, 1993; Hrouda et al., 2018; Madzin et al., 2021; Márton et al., 2009). Considering the lithology of the marly limestones in the Mraznica Fm, the most likely paramagnetic mineral group is phyllosilicates (Grabowski et al., 2013; Lefeld, 1974). Similarly, for the siltstones and shales in the Huty Fm, the paramagnetic minerals are primarily phyllosilicates identified in previous mineralogical studies as biotite, muscovite, illite, and montmorillonite (Gross et al., 1999).

The IRM component analyses as well as the mean coercivity and coercivity of the remanence derived from hysteresis and IRM back-field experiments, indicate that low-coercivity minerals are prevalent in both the Huty and Mraznica Fms. Thermal demagnetization results document a $\sim 580\ °C$ maximum unblocking temperature of the low coercivity component, which is the Curie temperature for magnetite (Dunlop, 1986). Considering the coercivity values derived from the IRM analysis, the magnetite in the Huty and Mraznica Fms occurs in two grain sizes: single domain (SD, higher coercivity values; second component of the IRM; Table 4) and pseudo-single domain (PSD, lower coercivity values; first component of the IRM). The origin of SD-magnetite can likely be attributed to diagenetic processes and/or later mineral recrystallizations (which are also coherent with the remagnetizations of the analyzed rocks; Grabowski, 1995, 2000; Grabowski et al., 2009; Jackson et al., 1988; Katz et al., 1998, 2000; Márton et al., 2016). In the case of the Mraznica Fm, the latter explanation is more likely because such an event is documented by paleomagnetic studies of the Mraznica Fm in the Strážov Mts (Grabowski et al., 2009). The crystallization of new magnetite grains is interpreted as being an effect of the Cretaceous nappe thrusting. However, we suggest that the high burial-related temperatures during the Late Oligocene documented by biomarker analysis and vitrinite reflectance results indicate the possibility of a second episode of magnetite formation. This has already been discussed in the Choč Mts area by Staneczek et al. (2022) and the Tatra Mts by Grabowski (1997) and Márton et al. (2016). Nevertheless, in the latter study, the whole-rock remagnetization was interpreted as being a result of a Mid-Miocene thermal event, as also suggested by fission-track studies (Anczkiewicz et al., 2013; Danišík et al., 2012). Our data suggest a clear link between the organic matter maturity of the Cretaceous and Oligocene rocks and the Paleogene burial. If a Mid-Miocene thermal event did occur, its significance was mostly local because of the pronounced differences in the maturities of the Cretaceous and Oligocene rocks between the Western and High Tatras.
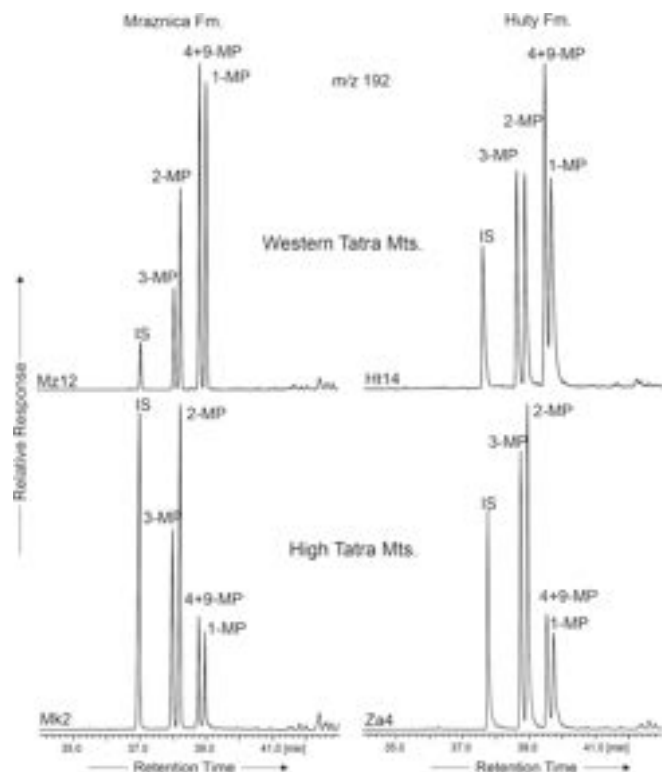
Fig. 6. Mass chromatograms (*m/z* 192) showing changes in the distribution of the methylphenanthrenes (MP) between the Western and High Tatra Mts. The more thermodynamically stable 2-MP and 3-MP clearly dominate in the High Tatra Mts. IS indicates the internal standard (9-phenylindene).
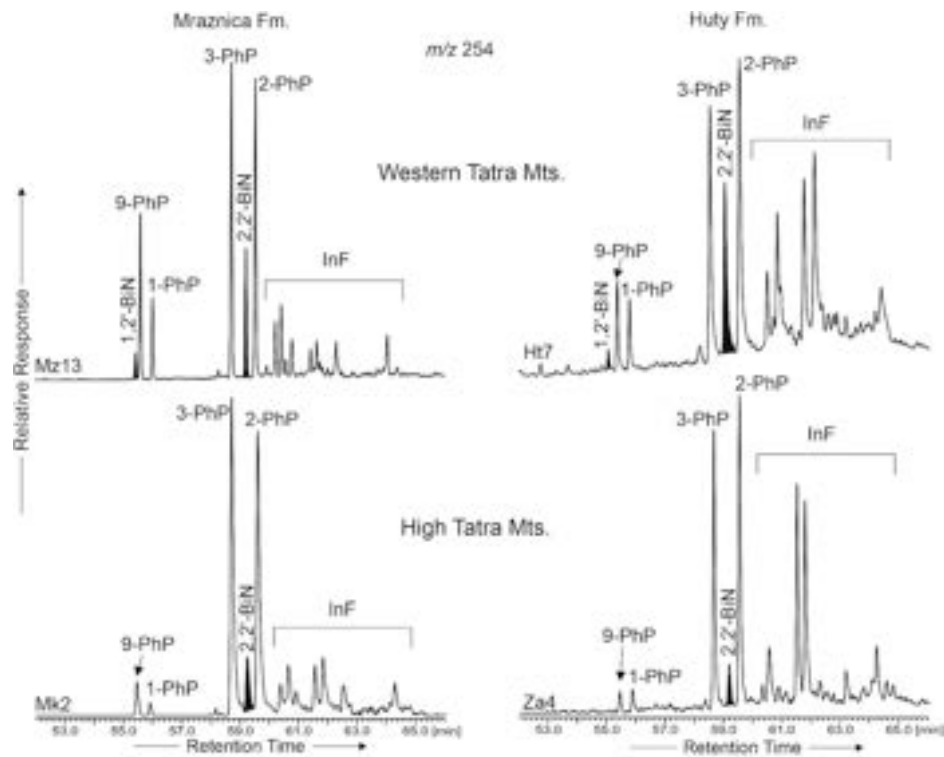
Fig. 7. Mass chromatograms (*m/z* 254) showing changes in the distribution of the phenylphenanthrenes (PhP) and binaphthyls (BiN) between the Western and High Tatra Mts. The more thermodynamically stable 2-PhP and 3- PhP dominate in the High Tatra Mts.

Fig. 8. Comparison of the vitrinite reflectance changes in the Podhale–Tatra area. Note the significant differences in the maturity values for the Western and High Tatra Mts for the Mraznica Fm (red points) and Huty Fm (blue points). The purple asterisk denotes the location of the Furmanowa PIG-1 well, and the two adjacent numbers show the measured vitrinite reflectances of two samples from different depths. *(For interpretation of the references to colour in this figure legend, the reader is referred to the web version of this article.)*

The younger remagnetization (crystallization of new magnetite) could have been driven by a few mechanisms, such as precipitation from migrating mineralized fluids (Lewchuk and Symons, 1995; Symons and Sangster, 1992), oxidization of pyrite grains by fluids (Suk et al., 1990), illite/smectite transformations (Katz et al., 1998, 2000) or hydrocarbon migration and maturation of organic matter (Abdulkarim et al., 2022; Badejo et al., 2021a, 2021b; Banerjee et al., 1997; Blumstein et al., 2004; Brothers et al., 1996; Elmore et al., 1987; McCabe and Elmore,

1989). The TOC values measured for the Mraznica Fm are low (Table 1), such that the by-products of the organic matter maturity (organic acids, Brothers et al., 1996) could not result in a faster magnetite formation. Hydrocarbon migration paths from the Western Tatra Mts have been reported (Marynowski et al., 2001) but are limited to tectonic zones and are therefore negligible at the orogenic scale. Therefore, bitumen-related remagnetization can also be excluded. Taking into consideration the lithology of the Mraznica Fm, which includes phyllosilicates

(Lefeld, 1974), a possible remagnetization mechanism would be the illite/smectite transformation under an elevated temperature regime which is a commonly reported process in clay-rich rocks (Elmore et al., 1993; Gill et al., 2002; Hirt et al., 1993; Katz et al., 2000). In addition, experimental studies performed by Moreau et al. (2005) show that even larger PSD grains of magnetite can form as a result of phyllosilicate transformations as demonstrated on our k(T) curves (Fig. 2). This could explain the presence of a population of larger grains in the Mraznica Fm. Because there are no indications of large-scale mineralized (ore-type) fluid migrations in the Tatra Mts, the precipitation of magnetite from these fluids is rather unlikely. However, migrations of hydrothermal or meteoric fluids could have affected the thrust nappe rocks. Therefore, we suggest that magnetite formation from pyrite oxidation was a second, presumably less important remagnetization mechanism during the Oligocene in the Mraznica Fm rocks.

The origin of authigenic SD-magnetite in the Huty Fm is seemingly related to illite/smectite transformations during diagenesis because the Huty Fm is composed predominantly of clay minerals (Gross et al., 1993). This process could be accelerated via increasing temperatures and/or the impact of organic acids. Studies from other parts of the CCPB also suggest a mainly diagenetic origin of the SD-magnetite in the Huty Fm (Madzin et al., 2021; Márton et al., 1999, 2009; Staneczek et al., 2022).

PSD-size grains were documented in both the Mraznica and Huty Fm. Similar to the SD-magnetite, their origin is likely related to different stages of diagenesis. In addition, the magnetite in Mraznica Fm could be detrital and/or related to illite/smectite transformations under elevated temperatures. In organic-rich rocks (such as the dark shales of Huty Fm), larger detrital magnetite (also MD-magnetite) is likely to dissolve (Canfield and Berner, 1987). Therefore we interpret these grains as PSD-magnetite with a purely diagenetic origin.

The rock magnetic investigations revealed the presence of a third ferromagnetic mineral in the analyzed units. High coercivities (>600 mT) and the highest unblocking temperatures (~680 °C) imply that the mineral in question is hematite. Apart from a detrital origin, hematite could be authigenic (Jackson and Swanson-Hysell, 2012), especially in the Mraznica Fm, where it contributes significantly to the IRM.Similarly to magnetite, hematite may have formed as a result of the oxidation of pyrite grains by fluids (Hu et al., 2006). In addition, weathering of surface rocks could also affect the increase in the hematite content in both the Huty and Mraznica Fms.

We identified the last, fourth component as goethite because of its very high coercivities, which are attributable to this mineral (e.g., Kruiver et al., 2001). Its presence in nearly all of the analyzed specimens is likely linked to the surface weathering of rocks.

5.3. Correlation of magnetic and geochemical data

To better understand the magnetic susceptibility and its carriers, we compared the obtained geochemical data with the magnetic properties of the analyzed units. The relationship between the carbonate content (CC; Table 1) and the magnetic susceptibility was determined (Fig. 9). Both the in-phase and out-of-phase susceptibilities decrease with increasing carbonate contribution. These changes likely result from changes in the clastic input rates. The increased input of terrigenous material correlates with higher susceptibilities as well as low CC values (Grabowski et al., 2013; Grabowski and Sobień, 2015). However, this trend is also present in the out-of-phase magnetic susceptibility measurements. Here, the negative correlation with CC is related to the most common formation mechanism, namely, the illite/smectite transformations. If the clastic input rates were lower, the amount of terrigenous hematite would also be lower. In addition, with the decreasing clastic input, the content of phyllosilicates which are mainly responsible for "producing" new magnetite via illite/smectite transformations, would decrease. Therefore, the lower content of phyllosilicates compared with carbonates results in a lower amount of newly formed
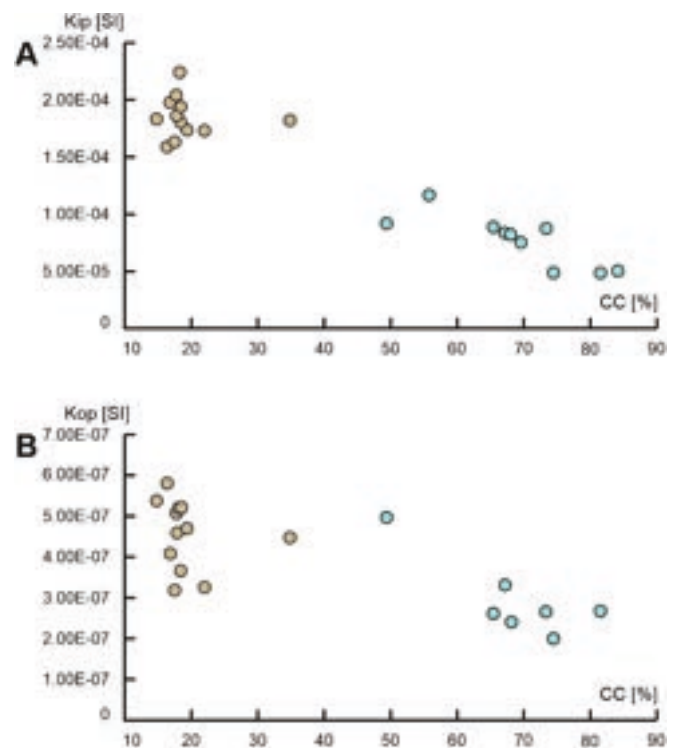
Fig. 9. Correlation of the magnetic and geochemical data highlighting a link between the carbonate content and the in-phase and out-of-phase magnetic susceptibilities (blue dots indicate the Mraznica Fm, and brown dots indicate the Huty Fm). *(For interpretation of the references to colour in this figure legend, the reader is referred to the web version of this article.)*

diagenetic magnetite.

Next, we plotted the remanent magnetization/saturation magnetization and remanence coercivity/mean coercivity ratios (Mrs/Ms. and Hcr/Hc) of our samples on a Day diagram (Day et al., 1977) with added mixing lines and domain state regions after Dunlop (2002). However, the results must be interpreted carefully due to the presence of not only magnetite but also hematite and goethite in our samples. The Day diagram is valid for magnetite purely compositions, and the addition of other ferromagnetic minerals may lead to erroneous interpretations (Roberts et al., 2018, 2019). Interestingly, the samples affected by higher paleotemperatures in both the Huty and Mraznica Fms appear to group very well in the PSD-magnetite window, whereas samples with lower measured vitrinite reflectances are more scattered and display less coherent Mrs./Ms. and Hcr/Hc values (Fig. 10A). The samples from the Western and High Tatra Mts can also be distinguished. Mraznica Fm specimens in the High Tatra Mts appear to contain a larger amount of high coercivity ferromagnetic minerals, which could also have formed as a result of increased burial temperatures. In the Huty Fm the content of SD-magnetite grains appears to increase with increasing vitrinite reflectance. Similarly, coherent Mrs./Ms. and Hcr/Hc ratios for samples from the High Tatra Mts point to a single major remagnetization event that affected both the Mraznica and Huty Fm samples. The temperature impact can also be observed in the Rr to Mrs./Ms. ratio diagram (Fig. 10B). The differences in the hysteresis parameters in the Western and High Tatra samples suggest that increased temperatures were a major trigger for faster magnetite formation mainly for the Huty Fm sites.

5.4. Origin and comparison of magnetic fabrics

The ipAMS, opAMS, and AARM measurements revealed variable fabrics in the analyzed Huty and Mraznica Fm rocks (Figs. 4 and 5).

Changes in the magnetic fabrics are controlled by the unit (Huty or Mraznica Fm), lithology (siltstone/shale or sandstone), and/or location (High or Western Tatra Mts). The ipAMS fabrics show the most consistent patterns, while the detected opAMS and AARM fabrics may vary within the same lithology and/or location.

The ipAMS investigations of the Mraznica Fm rocks revealed primarily planar fabrics ($T > 0.7$) with low mean anisotropy degrees ($Pj < 1.068$). The calculated Pj values are slightly higher in the Western Tatra Mts than in the High Tatra Mts. The differences are likely a result of the changing sedimentation in the shallower (High Tatra Mts) or deeper (Western Tatra Mts) basins (Nemčok et al., 1993), which favored the sedimentation of phyllosilicates. In all sites, the ipAMS foliation is well developed and parallel to the bedding plane. However, in addition to these features, which are typical for sedimentary rocks affected by compaction (e.g. Parés, 2015; Parés et al., 1999), a clear ipAMS lineation is usually present. Sites in the Western Tatra Mts and site Mk2 in the High Tatras, have a coherent, approximately ENE-WSW lineation orientation and lie on the bedding plane. Similarly oriented ipAMS lineations are present in other Central Western Carpathian massifs (Grabowski, 1996; Gregorová et al., 2009; Hrouda and Kahan, 1991;

Staneczek et al., 2022; Szaniawski et al., 2020). The documented ENE-WSW orientation corresponds well with the approximate NW orientation of nappe thrusting in the Central Western Carpathians reported by many structural studies (Jurewicz, 2005; Kováč and Bendík, 2002; Plašienka, 2003; Prokešová, 1994; Prokešová et al., 2012). The repeatability of this pattern/orientation indicates that the ipAMS lineation is of tectonic origin. However, the presence of bedding-parallel magnetic foliation and low Pj values suggests that the deformation was in its initial stage. We suggest that the ipAMS lineation in most of the Mraznica Fm sites originated during layer-parallel shortening, which predated the folding and thrusting processes (Fig. 11).

Fabrics carried by ferromagnetic minerals (opAMS and AARM) are generally coaxial. Minor discrepancies in the orientations of the magnetic foliation and lineation are likely a result of different minerals

Fig. 11. Tectonic interpretation of magnetic fabrics in the Huty and Mraznica Fm. Explanations of symbols as in Figs. 3 and 4.

Fig. 10. (A) Mrs./Ms. versus Hcr/Hc plot for the Mraznica and Huty Fm samples showing the changes in the sizes of the magnetite grains and the relationship between the magnetic data and the thermal maturity; (B) Mrs./Ms. to vitrinite reflectance (for Mraznica Fm) and calculated vitrinite reflectance (taken from MPI1; for Huty Fm); blue dots indicate the Mraznica Fm, brown dots indicate the Huty Fm. *For interpretation of the references to colour in this figure legend, the reader is referred to the web version of this article.)*

145:4317188683

contributing to the opAMS and AARM. The coercivity window applied in the AARM measurements (0–130 mT) records the orientation of the whole magnetite spectrum (SD-PSD-MD magnetite grains). The opAMS fabric could be influenced by the orientation of ultra-fine magnetite (superparamagnetic to stable single domain size), hematite, and even some ferromagnetic iron sulfides (Hrouda et al., 2016, 2022), which are relatively common in the Mraznica Fm rocks. In the Western Tatra Mts sites, the opAMS and AARM foliations tend to follow the bedding plane, with the confidence ellipses for the minimum ellipsoid axes being significantly larger/broader for opAMS than AARM. Magnetic lineation usually traces the orientation of the ipAMS lineation (sites 8, 9, 10, 11, and 12 for opAMS), being typically slightly deflected toward sub-horizontal orientations. Because we assume that the minerals that control the opAMS and AARM fabrics in the analyzed unit are mostly authigenic fine magnetite grains, the possible genesis of these fabrics is related to episodes of diagenetic magnetite formation. The majority of the newly formed magnetite grains were likely formed as a by-product of the illite/smectite transformation during the Paleogene burial, when the conditions were suitable for a faster magnetite formation (see paragraph 5.2). Magnetite grains could be controlled primarily by the phyllosilicate matrix, resulting in a similar orientation of the tectonic ipAMS lineation and both the opAMS and AARM lineations. Such magnetite crystallization, restricted by the preexisting mineral fabric, is a commonly reported phenomenon (Borradaile and Lagroix, 2000; Calvín et al., 2018; Hirt and Gehring, 1991; Li and Kodama, 2005). The magnetic lineation in both the opAMS and AARM fabrics in the Western Tatras more or less traces the ipAMS lineation orientation. An older population of magnetite grains related to the first stages of diagenesis was most likely also present in these rocks, and, in the case of the Western Tatra Mts, this older fabric has been strengthened by the crystallization of new magnetite. Sub-vertical to vertical ferromagnetic lineations (opAMS and AARM) are present in the High Tatra Mts (see next paragraph) and in the Choč Mts, where it has been attributed to transpression (Staneczek et al., 2022). In the Western Tatra Mts, the transpression (inducing uplift) was weaker than that in the High Tatra Mts and the ferromagnetic lineation retained the phyllosilicate-matrix-related orientation (Fig. 11).

In the High Tatra Mts, the mean/general opAMS and AARM fabrics for the Mraznica Fm differ from the fabric most commonly documented in the Western Tatras but are similar to AARM fabrics reported in the Choč Mts (Staneczek et al., 2022). The orientation of the fabric elements points to a significant tectonic imprint. The most striking feature of these fabrics is the sub-vertical magnetic lineation that is almost parallel to the pole to bedding (Fig. 4), whereas the minimum ellipsoid axes are sub-horizontal. This conspicuous fabric is consistent in both normal-laying strata and in overturned strata and tends to be bedding-independent, which suggests an event younger than the emplacement of the thrust nappes. Note, that the magnetic lineations of the AARM fabrics in the nearby Choč Mts also display a similar sub-vertical orientation (Staneczek et al., 2022). However, such lineation is not present in the Western Tatra Mts sites, where the documented lineations are slightly inclined. A potential clue toward disentangling the origin of this specific opAMS and AARM lineation may be the presence of large fault zones in the vicinity of the sampled sites. Cretaceous sedimentary rocks of the Krížna nappe in the High Tatra Mts are close to two parallel, *NE*-SW-oriented major faults that cut the Tatra block in two (Fig. S.1; Lexa et al., 2000). The Western Tatra Mts are located in the middle of the western block, and therefore the Mraznica Fm sampling sites are far from major tectonic zones. Similarly, the Choč Mts are limited from the south by the continuation of the Sub-Tatric fault (Gross et al., 1994; Lexa et al., 2000; Sperner et al., 2002; Fig. S.1).

The activity of these faults is linked to the Oligocene-Early Miocene uplift of the Central Western Carpathians in a sinistral transpressional regime that was especially pronounced in the highly elevated Tatra Mts (Anczkiewicz et al., 2015; Fodor, 1995; Froitzheim et al., 2008; Králiková et al., 2014; Marko et al., 2005; Peresson and Decker, 1997;

Ratschbacher et al., 1993; Sperner et al., 2002). Transpression is characterized by the co-occurrence of vertical stretching along horizontal shear and shortening (Sanderson and Marchini, 1984). Crystallization of fine-grained magnetite in the presence of such a vertical extension is likely to result in vertical or sub-vertical magnetic lineation (Bilardello, 2016; Housen and van der Pluijm, 1991; Housen et al., 1993a, 1993b; Parés, 2015; Weil and Yonkee, 2009). Therefore, the onset of transpression could likely coincide with the maximum burial and burial-related crystallization of ferromagnets, as proposed for the Choč Mts (Staneczek et al., 2022). In addition, the impact of higher burial temperatures in the eastern part of the Tatra massif would increase the rate of magnetite formation. However, we cannot exclude a possible reorientation of the older population of ferromagnetic minerals, which originated during the first, Cretaceous remagnetization. Such mimetic growth of secondary minerals over preexisting fabrics has been previously documented by many authors, e.g., Li and Kodama (2005). The resulting fabric can subsequently rotate with the original paramagnetic fabric. In cleaved rocks, the strain related to the cleavage formation can induce the dissolution and recrystallization of ferromagnetic minerals, which affects the previously established ferromagnetic fabric (e.g., Housen et al., 1993a, 1993b). Nevertheless, the petromagnetic investigations in our study point to a close link between the magnetic mineralogy and the paleotemperatures. Moreover, the occurrence of this fabric in both normal and overturned bedding links its origin to post-folding processes. It is worth mentioning, that recent studies on the tectonic evolution of the High Tatra Mts identify strike-slip stepover controlled by a transpressional regime as the driving force for the Miocene exhumation and uplift (Campos et al., 2023). Therefore, we suggest that the opAMS and AARM magnetic fabrics of the Mraznica Fm in the High Tatra Mts, which originated during the sinistral transpression in the Oligocene-Early Miocene, are more representative because of the vicinity of a minor fault zone (Fig. S.1) and the faster formation of ferromagnetic minerals at higher temperatures (Fig. 11). This agrees with the observation of vertical AARM axes present in the Choč Mts by Staneczek et al. (2022). Vertical magnetic lineations have been reported by studies performed in other transpression-controlled settings (e.g., Archanjo et al., 1999; De Wall et al., 2012; Di Chiara et al., 2020). In the Western Tatra Mts, the impact of transpression on the fabrics was lower, which resulted in only a slight inclination of the AARM lineations in comparison to the ipAMS fabric.

The ipAMS investigations in the Huty Fm documented one main pattern that was present in all sites. Relatively high Pj and T values point to a highly oblate fabric which is expected for rocks predominantly composed of phyllosilicates (Parés, 2015; Parés et al., 1999). The ipAMS foliation follows the bedding plane and likely results from both the clayey, flat mineralogy and the compaction processes during diagenesis. Apart from a well-developed ipAMS foliation, a distinct magnetic lineation lying within the bedding plane is also present. The orientation of this ipAMS lineation varies with the bedding, undulating from the primarily NE-SW in the Western Tatra Mts to E-W in the High Tatra Mts. The formation of ipAMS lineations in CCPB clastic rocks is usually attributed to paleocurrents in sedimentary basins (Madzin et al., 2021; Márton et al., 2009). A NE-oriented paleo-transport has been reported, e. g., in the Podhale subbasin (Marszałko and Radomski, 1960). However, such magnetic lineations are characterized by rather wide/broad confidence ellipses as a result of the larger scattering of the ipAMS axes (Hrouda and Chadima, 2020; Hrouda et al., 2009; Parés et al., 1999; Stachowska et al., 2020). In addition, note that paleocurrents are more likely to affect coarse-grained rocks (Schwab, 2003). Therefore, to avoid purely sedimentary fabrics, we sampled mainly silty strata. In light of these data, we propose a tectonic origin of the ipAMS lineation in the Huty Fm sites (Fig. 11). The detected NE-SW to E-W orientation of the ipAMS lineation points to an approximately NW-SE to N-S compression, which coincides roughly with the Oligocene-Early Miocene transpression-related shortening orientation derived from structural studies of CCPB rocks (Králiková et al., 2014; Pešková et al., 2009;

Vojtko et al., 2010). The ipAMS lineation in the High Tatra Mts' sites is slightly more E-W oriented, such that it could also be an effect of the Middle to Late Miocene northward tilting in the N-S oriented compression. Because the uplift is known to be larger in the eastern part of the Tatra Mts (Śmigielski et al., 2016), the compression related to the uplift could also have had a greater impact on the CCPB rocks in the High Tatra foreland. Additionally, small differences in the orientation of the ipAMS lineation could be explained by differential uplift in the Tatra area (Nemčok et al., 1993; Králiková et al., 2014).

Ferromagnetic fabrics recorded by opAMS and AARM methods display some major differences in the analyzed Huty Fm rocks. In general, fabrics detected by both methods document a well-developed magnetic foliation. The origin of this foliation is related to the growth of magnetite restricted by the phyllosilicate matrix of the Huty Fm, which was shaped by compaction processes. In addition, a better-defined (AARM) or slightly more scattered (opAMS) magnetic lineation is present, which we attribute to tectonic processes. The detected magnetic lineation in the AARM fabric of the Huty Fm was coherent in all of the Western and High Tatra sites. The mean NNW-SSE to NW-SE orientation is approximately perpendicular to the ipAMS phyllosilicate fabric. A similar AARM lineation has been reported in the Choč Mts (Staneczek et al., 2022). Several authors have proposed that the magnetite population that controlled the AARM lineation there crystallized during the early stages of compaction and diagenesis in an NW-SE to N-S extensional regime linked to the formation of the CCPB, which is reported in multiple structural studies (Pešková et al., 2009; Vojtko et al., 2010; Králiková et al., 2014); we agree with this interpretation. In addition, this extensional regime could also affect the Cretaceous rocks. Site Mz7 in the Western Tatras records a similar NW-SE orientation of the magnetic lineation in the ferromagnetic-controlled fabrics that is approximately perpendicular to the phyllosilicate-governed ipAMS lineation. Similar to the Huty Fm sites, the carrier of the AARM magnetic fabric in site Mz7 is magnetite that has crystallized in this NW-SE to N-S extensional regime (Fig. 11).

Our observations lead to a few, sometimes contrasting interpretations. The NW-SE orientation of the AARM lineation in the Oligocene rocks has also been reported by Márton et al. (2009) in the Podhale Basin. Another possible alternative is that this conspicuous orientation of the magnetic lineation could develop independently from the phyllosilicate matrix in fractures or joints as a result of crystallization from migrating fluids. NNW-SSE-oriented calcite-filled joints have been reported from the western part of Podhale by Ludwiniak (2010) and other authors (Boretti-Onyszkiewicz, 1968; Halicki, 1963; Pokorski, 1965).

It is rarely the case that neither the opAMS nor the AARM magnetic lineations coincide with the phyllosilicate-controlled ipAMS lineation. In most sites, the confidence ellipses of the opAMS and ipAMS lineations overlap, while the confidence ellipse of the AARM lineation has a different orientation. The ipAMS fabric carried by phyllosilicates and the opAMS fabric governed by ultrafine-grained magnetite fixed in the phyllosilicate matrix both document the same Early Miocene compression event. These ultrafine grains of magnetite could have originated from this shortening event. Because superparamagnetic magnetite has no magnetic remanence, the AARM fabric is carried by larger magnetite grains that originated during the Oligocene extension. Therefore, the differences in those fabrics are easily explained by the different grain sizes that govern the two fabrics. A second possibility is that the magnetite grains are of the same age, yet some of them were later recrystallized into larger SD/PSD sizes. The ultrafine magnetite grains embedded in the phyllosilicates (similarly as documented by Borradaile and Lagroix, 2000) would be more likely to rotate with the paramagnetic matrix; however, the larger grains could preserve their original orientation. The convergence of the opAMS and ipAMS lineations could also result from the contribution of hematite to both fabrics. Nevertheless, the reported hematite content in the ferromagnetic fraction is below 16% and thus appears to be too low to actively influence the fabric.

Consequently, we suggest that the fine-grained magnetite formed either in two populations as a response to different tectonic phases (Oligocene extension and Late Oligocene/Early Miocene compression) or that different grain sizes of magnetite aligned along two different favorable directions with the exact ages of their crystallization being debatable.

Finally, it is worth mentioning that even though the Huty Fm rocks in the High Tatras were sampled in the vicinity of a fault zone where transpression would be a major trigger of the fabric evolution, the ferromagnetic fabrics do not display such transpression-related vertical magnetic lineations (Fig. S.1). This phenomenon was also observed in the Choč Mts (Staneczek et al., 2022). We believe that, because the phyllosilicate content in the Huty Fm shales is much larger than that in the Mraznica Fm marls, the phyllosilicate matrix was therefore "stronger" and prohibited the formation of such vertical AARM or opAMS lineations. This hypothesis is further supported by the values of the initial slopes prior to the slope correction in the hysteresis experiments (Table 3). The Huty Fm samples display over two times higher values of the initial slope (on average 60 mA·m^2·T^{-1}·kg^{-1}) than the Mraznica Fm samples (~25–30 mA·m^2·T^{-1}·kg^{-1}). This is in agreement with the interpretation of the vertical AARM lineations in Staneczek et al. (2022).

6. Conclusions

Petromagnetic investigations of the Mraznica and Huty Fm rocks indicate that paramagnetic minerals control the magnetic susceptibility in both studied units. These minerals are mostly phyllosilicates such as biotite and muscovite. The ferromagnetic fraction is dominated by SD-magnetite with some PSD-magnetite and a minor addition of hematite. The origin of fine-grained magnetite is related to two major remagnetization events: Cretaceous nappe thrusting and Oligocene burial. Because the percentage of ferromagnetic minerals is relatively low, the ipAMS fabric is dominantly controlled by paramagnetics.

The maturity data show a gradual increase in the paleotemperatures in both studied formations toward the southeast. Furthermore, the paleotemperature changes in the Mraznica Fm are related to those reported in the Huty Fm, pointing toward a single major recrystallization event during the Oligocene. The occurrence of small-sized magnetite grains with the highest vitrinite reflectance confirms the impact of a single recrystallization event that affected both the Oligocene and Cretaceous rocks.

Analyses of the magnetic fabrics of the 9 Mraznica Fm and 12 Huty Fm sites enabled us to distinguish some major deformation events in the Tatra Mts ranging from the Late Cretaceous to the Miocene. All of the analyzed sites display sedimentary-tectonic features, indicating an early deformation stage. Fabrics governed by paramagnetic minerals (ipAMS) document major tectonic events, such as Late Cretaceous nappe thrusting (most Mraznica Fm sites) or compression related to the onset of the Miocene uplift of the Tatra horst (Huty Fm). The origins of fabrics carried by ferromagnetic minerals differ in the Huty and Mraznica Fm. In the latter, the opAMS and AARM fabrics are relatively homogeneous and result from the transpression-controlled tectonic regime in the Oligocene-Early Miocene. Conversely, in a few Huty Fm sites, the opAMS lineation is nearly perpendicular to the AARM lineation. We attribute this peculiar orientation of the magnetic lineations either to a reorienting of two sizes of magnetite grains along two perpendicular directions/axes or to the result of two major tectonic phases: NW-SE extension during the late stages of CCPB formation and the incipient uplift stage of the Tatra Mts in the Late Oligocene/Early Miocene.

CRediT authorship contribution statement

Dorota Staneczek: Writing – original draft, Visualization, Validation, Methodology, Investigation, Formal analysis, Data curation, Conceptualization. **Rafał Szaniawski:** Writing – review & editing,

Supervision, Methodology, Conceptualization. **Martin Chadima:** Writing – review & editing, Formal analysis. **Leszek Marynowski:** Writing – review & editing, Supervision, Methodology, Conceptualization.

Declaration of competing interest

None.

Data availability

Data will be made available on request.

Appendix A. Supplementary data

Supplementary data to this article can be found online at https://doi. org/10.1016/j.tecto.2024.230338.

References

Abdulkarim, M.A., Muxworthy, A.R., Fraser, A., Sims, M., Cowan, A., 2022. Effect of Hydrocarbon Presence and Properties on the magnetic Signature of the Reservoir Sediments of the Catcher Area Development Region, UK North Sea. Front. Earth Sci. 10.

Anczkiewicz, A.A., Środoń, J., Zattin, M., 2013. Thermal history of the Podhale Basin in the internal Western Carpathians from the perspective of apatite fission track analyses. Geol. Carpath. 64, 141.

Anczkiewicz, A.A., Danišík, M., Środoń, J., 2015. Multiple low-temperature thermochronology constraints on exhumation of the Tatra Mountains: New implication for the complex evolution of the Western Carpathians in the Cenozoic. Tectonics 34, 2296–2317.

Antolín Tomas, B., 2010. Tectonic Evolution of the Tethyan Himalaya in SE Tibet Deduced from Magnetic Fabric, Structural, Metamorphic and Paleomagnetic Data (PhD Thesis).. Universität Tübingen.

Archanjo, C.J., da Silva, E.R., Caby, R., 1999. Magnetic fabric and pluton emplacement in a transpressive shear zone system: the Itaporanga porphyritic granitic pluton (Northeast Brazil). Tectonophysics 312, 331–345.

Aubourg, C., Pozzi, J.-P., 2010. Toward a new <250°C pyrrhotite–magnetite geothermometer for claystones. Earth Planet. Sci. Lett. 294, 47–57. https://doi.org/10.1016/j.epsl.2010.02.045.

Aubourg, C., Rochette, P., Vialon, P., 1991. Subtle stretching lineation revealed by magnetic fabric of Callovian-Oxfordian black shales (French Alps). Tectonophysics 185, 211–223.

Aubourg, C., Smith, B., Bakhtari, H., Guya, N., Eshragi, A., Lallemant, S., Molinaro, M., Braud, X., Delaunay, S., 2004. Post-Miocene shortening pictured by magnetic fabric across the Zagros-Makran syntaxis (Iran). Geol. Soc. Am. Spec. Pap. 383, 17–40.

Aubourg, C., Jackson, M., Ducoux, M., Mansour, M., 2019. Magnetite-out and pyrrhotite-in temperatures in shales and slates. Terra Nova 31, 534–539. https://doi.org/10.1111/ter.12424.

Averbuch, O., de Lamotte, D.F., Kissel, C., 1992. Magnetic fabric as a structural indicator of the deformation path within a fold-thrust structure: a test case from the Corbières (NE Pyrenees, France). J. Struct. Geol. 14, 461–474.

Bac-Moszaszwili, M., Burchart, J., G\lazek, J., Iwanow, A., Jaroszewski, W., Kotański, Z., Lefeld, J., Mastella, L., Ozimkowski, W., Roniewicz, P., 1979. Geological Map of the Polish Tatra Mountains 1: 30 000. Wyd. Geol, Warszawa.

Badejo, S.A., Muxworthy, A.R., Fraser, A., Neumaier, M., Perkins, J.R., Stevenson, G.R., Davey, R., 2021a. Using magnetic techniques to calibrate hydrocarbon migration in petroleum systems modelling: a case study from the lower Tertiary, UK Central North Sea. Geophys. J. Int. 227, 617–631. https://doi.org/10.1093/gji/ggab236.

Badejo, S.A., Muxworthy, A.R., Fraser, A., Stevenson, G.R., Zhao, X., Jackson, M., 2021b. Identification of magnetic enhancement at hydrocarbon-fluid contacts. AAPG Bull. 105, 1973–1991. https://doi.org/10.1306/07062019207.

Banerjee, S., Elmore, R.D., Engel, M., 1997. Chemical remagnetization and burial diagenesis: Testing the hypothesis in the Pennsylvanian Belden Formation, Colorado. J. Geophys. Res. Solid Earth 102, 24825–24842.

Biedermann, A.R., Jackson, M., Bilardello, D., Feinberg, J.M., 2020. Anisotropy of full and partial anhysteretic remanence across different rock types: 2—Coercivity dependence of remanence anisotropy. Tectonics 39 e2018TC005285.

Bilardello, D., 2016. Magnetic anisotropy: theory, instrumentation, and techniques. In: Reference Module in Earth Systems and Environmental Sciences. Elsevier. https://doi.org/10.1016/B978-0-12-409548-9.09516-6.

Blumstein, A.M., Elmore, R.D., Engel, M.H., Elliot, C., Basu, A., 2004. Paleomagnetic dating of burial diagenesis in Mississippian carbonates, Utah. J. Geophys. Res. Solid Earth 109.

Boretti-Onyszkiewicz, W., 1968. Joints in the flysh of Western Podhale. Acta Geol. Pol. 18, 101–152 (in Polish).

Borradaile, G.J., Lagroix, F., 2000. Thermal Enhancement of magnetic Fabrics in High Grade Gneisses. Geophys. Res. Lett. 27, 2413–2416. https://doi.org/10.1029/2000GL008522.

Brothers, L., Engel, M., Elmore, R., 1996. The late diagenetic conversion of pyrite to magnetite by organically complexed ferric iron. Chem. Geol. 130, 1–14.

Burchart, J., 1972. Fission-track age determinations of accessory apatite from the Tatra Mountains, Poland. Earth Planet. Sci. Lett. 15, 418–422.

Calvín, P., Villalaín, J.J., Casas-Sainz, A.M., 2018. Anisotropic magnetite growth in remagnetized limestones: Tectonic constraints and implications for basin history. Geology 46, 751–754.

Campos, D., Catlos, E., Stockli, D., Ketcham, R., Miller, N., Broska, I., Kohut, M., 2023. Exhumation of the High Tatra Mountains and Implications for the Western Carpathians, Slovakia. https://doi.org/10.1130/abs/2023AM-393919.

Canfield, D.E., Berner, R.A., 1987. Dissolution and pyritization of magnetite in anoxic marine sediments. Geochim. Cosmochim. Acta 51, 645–659.

Castelluccio, A., Mazzoli, S., Andreucci, B., Jankowski, L., Szaniawski, R., Zattin, M., 2016. Building and exhumation of the Western Carpathians: New constraints from sequentially restored, balanced cross sections integrated with low-temperature thermochronometry. Tectonics 35, 2698–2733.

Csontos, L., Vörös, A., 2004. Mesozoic plate tectonic reconstruction of the Carpathian region. Palaeogeogr. Palaeoclimatol. Palaeoecol. 210, 1–56.

Danišík, M., Kohut, M., Evans, N.J., McDonald, B.J., 2012. Eo-Alpine metamorphism and the 'mid-Miocene thermal event' in the Western Carpathians (Slovakia): new evidence from multiple thermochronology. Geol. Mag. 149, 158–171.

Day, R., Fuller, M., Schmidt, V., 1977. Hysteresis properties of titanomagnetites: grain-size and compositional dependence. Phys. Earth Planet. Inter. 13, 260–267.

De Wall, H., Pandit, M.K., Dotzler, R., Just, J., 2012. Cryogenian transpression and granite intrusion along the western margin of Rodinia (Mt. Abu region): magnetic fabric and geochemical inferences on Neoproterozoic geodynamics of the NW Indian block. Tectonophysics 554, 143–158.

Dearing, J.A., Dann, R.J.L., Hay, K., Lees, J.A., Loveland, P.J., Maher, B.A., O'grady, K., 1996. Frequency-dependent susceptibility measurements of environmental materials. Geophysical Journal International 124, 228–240.

Di Chiara, A., Morris, A., Anderson, M.W., Menegon, L., Tremblay, A., 2020. Magnetic anisotropy reveals Acadian transpressional fabrics in an Appalachian ophiolite (Thetford Mines, Canada). Geophys. J. Int. 222, 1034–1045.

Dudzisz, K., Szaniawski, R., Michalski, K., Manby, G., 2016. Applying the anisotropy of magnetic susceptibility technique to the study of the tectonic evolution of the West Spitsbergen Fold-and-Thrust Belt. Polar Res. 35, 31683.

Dudzisz, K., Szaniawski, R., Michalski, K., Chadima, M., 2018. Rock magnetism and magnetic fabric of the Triassic rocks from the West Spitsbergen Fold-and-Thrust Belt and its foreland. Tectonophysics 728, 104–118.

Dunlop, D.J., 1986. Hysteresis properties of magnetite and their dependence on particle size: a test of pseudo-single-domain remanence models. J. Geophys. Res. Solid Earth 91, 9569–9584.

Dunlop, D.J., 2002. Theory and application of the Day plot (Mrs/Ms versus Hcr/Hc) 2. Application to data for rocks, sediments, and soils. J. Geophys. Res. 107 https://doi.org/10.1029/2001JB000487.

Elmore, R.D., Engel, M., Crawford, L., Nick, K., Imbus, S., Sofer, Z., 1987. Evidence for a relationship between hydrocarbons and authigenic magnetite. Nature 325, 428–430.

Elmore, R.D., London, D., Bagley, D., Fruit, D., Gao, G., 1993. Remagnetization by basinal fluids: testing the hypothesis in the Viola Limestone, southern Oklahoma. J. Geophys. Res. Solid Earth 98, 6237–6254.

Fodor, L., 1995. From transpression to transtension: Oligocene-Miocene structural evolution of the Vienna basin and the East Alpine-Western Carpathian junction. Tectonophysics 242, 151–182.

Froitzheim, N., Plašienka, D., Schuster, R., 2008. Alpine Tectonics of the Alps and Western Carpathians.

Garecka, M., 2005. Calcareous nannoplankton from the Podhale Flysch (Oligocene-Miocene, Inner Carpathians, Poland). Stud. Geol. Polon. 124, 353–370.

Gill, J.D., Elmore, R., Engel, M., 2002. Chemical remagnetization and clay diagenesis: testing the hypothesis in the cretaceous sedimentary rocks of northwestern Montana. Phys. Chem. Earth, Parts A/B/C 27, 1131–1139.

Grabowski, J., 1995. New palaeomagnetic data from the lower Sub-Tatric radiolarites, Upper Jurassic (Western Tatra Mts.). Geol. Quart. 39, 61–74.

Grabowski, J., 1996. Magnetic fabric of the Upper Jurassic sediments, Krížna Unit, Tatra Mts., Poland. Geol. Carpath. 47, 331–337.

Grabowski, J., 1997. Paleomagnetic results from the cover (High-Tatric) unit and nummulitic Eocene in the Tatra Mts (Central West Carpathians, Poland) and their tectonic implications. Ann. Soc. Geol. Pol. 67, 13–23.

Grabowski, J., 2000. Palaeo-and rock magnetism of Mesozoic carbonate rocks in the Sub-Tatric series (Central West Carpathians)-palaeotectonic implications. In: Polish Geological Institute Special Papers, 5, pp. 1–88.

Grabowski, J., Sobień, K., 2015. Variation in clastic input in the Berriasian of the lower Sub-Tatric (Krížna) succession in the Tatra Mountains (Central Western Carpathians,

Poland): data from magnetic susceptibility and inorganic geochemistry. Ann. Soc. Geol. Pol. 85, 139–150. https://doi.org/10.14241/asgp.2015.004.

Grabowski, J., Michalík, J., Szaniawski, R., Grotek, I., 2009. Synthrusting remagnetization of the Krížna nappe: high resolution palaeo-and rock magnetic study in the Strážovce section, Strážovské vrchy Mts, Central West Carpathians (Slovakia). Acta Geol. Pol. 59, 137–155.

Grabowski, J., Schnyder, J., Sobień, K., Koptíková, L., Krzemiński, L., Pszczółkowski, A., Hejnar, J., Schnabl, P., 2013. Magnetic susceptibility and spectral gamma logs in the Tithonian–Berriasian pelagic carbonates in the Tatra Mts (Western Carpathians, Poland): Palaeoenvironmental changes at the Jurassic/Cretaceous boundary. Cretac. Res. 43, 1–17.

Grafka, O., Marynowski, L., Simoneit, B.R., 2015. Phenyl derivatives of polycyclic aromatic compounds as indicators of hydrothermal activity in the Silurian black siliceous shales of the Bardzkie Mountains, Poland. Int. J. Coal Geol. 139, 142–151.

Gregorová, D., Hrouda, F., Kohút, M., 2009. Magnetic fabric of granitic composite pluton of the Velká Fatra Mountains (Western Carpathians, Slovakia): a Variscan remnant within the Alpine edifice? Geodin. Acta 22, 57–72.

Gross, P., Köhler, E., Haško, J., Halouzka, R., Mello, J., Nagy, A., 1993. Geology of the Southern and Eastern Orava. Štátny Geologický Ústav Dionýza Štúra, Bratislava.

Gross, P., Filo, I., Halouzka, R., Haško, J., Havrila, M., Kováč, M., Maglay, J., Mello, J., Nagy, A., 1994. Geological Map of Southern and Eastern Part of Orava. Štátny Geologický Ústav Dionýza Štúra, Bratislava.

Gross, P., Buček, S., Ďurkovič, T., Filo, I., Karoli, S., Maglay, J., Nagy, A., Halouzka, R., Spišák, Z., Žec, B., Others, 1999. Geological map of Popradská kotlina Basin, Hornádska kotlina Basin, Levočské vrchy Mts, Spišsko-šarišské medzihorie Depression, Bachureň Mts and Šarišská vrchovina highland (scale 1: 50,000). Ministry of Environment of Slovak Republic, Geol. Surv, Slovak Republic.

Halicki, B., 1963. Tectonics of Podhale. Ann. Soc. Geol. Pol. 349–362 (in Polish).

Hirt, A., Gehring, A., 1991. Thermal alteration of the magnetic mineralogy in ferruginous rocks. J. Geophys. Res. Solid Earth 96, 9947–9953.

Hirt, A., Banin, A., Gehring, A., 1993. Thermal generation of ferromagnetic minerals from iron-enriched smectites. Geophys. J. Int. 115, 1161–1168.

Housen, B.A., van der Pluijm, B.A., 1991. Slaty cleavage development and magnetic anisotropy fabrics. J. Geophys. Res. Solid Earth 96, 9937–9946. https://doi.org/10.1029/91JB00605.

Housen, B.A., Richter, C., van der Pluijm, B.A., 1993a. Composite magnetic anisotropy fabrics: experiments, numerical models and implications for the quantification of rock fabrics. Tectonophysics 220, 1–12. https://doi.org/10.1016/0040-1951(93)90219-A.

Housen, B.A., van der Pluijm, B.A., van der Voo, R., 1993b. Magnetite dissolution and neocrystallization during cleavage formation: paleomagnetic study of the Martinsburg Formation, Lehigh Gap, Pennsylvania. J. Geophys. 98 (B8), 13,799–13,813.

Hrouda, F., 1983. Fabric implications of magnetic anisotropy measurements of rocks of the Malé Karpaty (Little Carpathians) Mts. (SW Slovakia). Annuaire Inst. Geol. Geophys. 63, 57–61.

Hrouda, F., 1986. The magnetic fabric of sedimentary rocks of the Malé Karpaty Mts. and its tectonic implications. Sborník Geol. věd. Užitá Geofyzika 155–167.

Hrouda, F., Chadima, M., 2020. Examples of tectonic overprints of magnetic fabrics in rocks of the Bohemian Massif and Western Carpathians. Int. J. Earth Sci. 109, 1321–1336.

Hrouda, F., Hanák, J., 1990. Magnetic fabric of sedimentary formations of the Strazovske vrchy Mts., sedimentological and tectonic implications. Sborník Geol. věd. Užitá Geofyzika 71–102.

Hrouda, F., Jelínek, V., Zapletal, K., 1997. Refined technique for susceptibility resolution into ferromagnetic and paramagnetic components based on susceptibility temperature-variation measurement. Geophysical Journal International 129, 715–719.

Hrouda, F., Kahan, S., 1991. The magnetic fabric relationship between sedimentary and basement nappes in the High Tatra Mountains, N. Slovakia. J. Struct. Geol. 13, 431–442.

Hrouda, F., Potfaj, M., 1993. Deformation of sediments in the post-orogenic Intra-Carpathian Paleogene Basin as indicated by magnetic anisotropy. Tectonophysics 224, 425–434.

Hrouda, F., Krejčí, O., Potfaj, M., Stráník, Z., 2009. Magnetic fabric and weak deformation in sandstones of accretionary prisms of the Flysch and Klippen Belts of the Western Carpathians: mostly offscraping indicated. Tectonophysics 479, 254–270.

Hrouda, F., Chadima, M., Ježek, J., Pokorný, J., 2016. Anisotropy of out-of-phase magnetic susceptibility of rocks as a tool for direct determination of magnetic sub-fabrics of some minerals: an introductory study. Geophys. J. Int. 208, 385–402.

Hrouda, F., Gilder, S., Wack, M., Ježek, J., 2018. Diverse response of paramagnetic and ferromagnetic minerals to deformation from Intra-Carpathian Paleogene sedimentary rocks: Comparison of magnetic susceptibility and magnetic remanence anisotropies. J. Struct. Geol. 113, 217–224.

Hrouda, F., Chadima, M., Ježek, J., 2022. Anisotropy of out-of-phase magnetic susceptibility and its potential for rock fabric studies: a review. Geosciences 12, 234.

Hu, G., Dam-Johansen, K., Wedel, S., Hansen, J.P., 2006. Decomposition and oxidation of pyrite. Prog. Energy Combust. Sci. 32, 295–314.

Huang, S.-Y., Li, M.-J., Zhang, K., Wang, T.-G., Xiao, Z.-Y., Fang, R.-H., Zhang, B.-S., Wang, D.-W., Zhao, Q., Yang, F.-L., 2016. Distribution and geochemical significance of phenylphenanthrenes and their isomers in selected oils and rock extracts from the Tarim Basin, NW China. Pet. Sci. 13, 183–191.

Hunt, J.M., 1996. Petroleum Geochemistry and Geology. W.H. Freeman and Company, New York, p. 743. ISBN 0–7167–2441-3.

ISO 7404-2, 2009. Methods for the Petrographic Analysis of Coals – Part 2: Methods of Preparing Coal Samples. International Organization for Standardization, Switzerland.

Jackson, M., Swanson-Hysell, N.L., 2012. Rock magnetism of remagnetized carbonate rocks: another look. Geol. Soc. Lond. Spec. Publ. 371 (1), 229–251.

Jackson, M., McCabe, C., Ballard, M.M., Van der Voo, R., 1988. Magnetite authigenesis and diagenetic paleotemperatures across the northern Appalachian basin. Geology 16, 592–595.

Jelínek, V., 1981. Characterization of the magnetic fabric of rocks. Tectonophysics 79, T63–T67.

Jurewicz, E., 2005. Geodynamic evolution of the Tatra Mts. and the Pieniny Klippen Belt (Western Carpathians): problems and comments. Acta Geol. Pol. 55, 295–338.

Katz, B., Elmore, R., Engel, M., 1998. Authigenesis of magnetite in organic-rich sediment next to a dike: implications for thermoviscous and chemical remagnetizations. Earth Planet. Sci. Lett. 163, 221–234.

Katz, B., Elmore, R.D., Cogoini, M., Engel, M.H., Ferry, S., 2000. Associations between burial diagenesis of smectite, chemical remagnetization, and magnetite authigenesis in the Vocontian trough, SE France. J. Geophys. Res. Solid Earth 105, 851–868.

Kędzierski, M., Uchman, A., 1997. Age and palaeoenvironment of the Koscieliska Marl Formation (lower cretaceous) in the Tatra Mountains, Poland: preliminary results. Ann. Soc. Geol. Pol. 67, 237–247.

Kitamura, Y., Sato, K., Ikesawa, E., Ikehara-Ohmori, K., Kimura, G., Kondo, H., Ujiie, K., Onishi, C.T., Kawabata, K., Hashimoto, Y., Mukoyoshi, H., Masago, H., 2005. Mélange and its seismogenic roof décollement: a plate boundary fault rock in the subduction zone—an example from the Shimanto Belt, Japan. Tectonics 24. https://doi.org/10.1029/2004TC001635.

Kohút, M., Kovach, V.P., Kotov, A.B., Salnikova, E.B., Savatenkov, V.M., 1999. Sr and Nd isotope geochemistry of Hercynian granitic rocks from the Western Carpathians–implications for granite genesis and crustal evolution. Geol. Carpath. 50, 477–487.

Kováč, P., Bendík, A., 2002. Structural analysis of Adnet limestones at Zvolen-Donovaly. Miner. Slovaca 34, 3–4.

Kováč, M., Halásová, E., Hudáčková, N., Holcova, K., Hyžný, M., Jamrich, M., Ruman, A., 2018. Towards better correlation of the Central Paratethys regional time scale with the standard geological time scale of the Miocene Epoch. Geol. Carpath. 69, 283–300.

Král, J., 1977. Fission track ages of apatites from some granitoid rocks in West Carpathians. Geol. Zb. Geol. Carpath. 28, 269–276.

Králiková, S., Vojtko, R., Sliva, L., Minár, J., Fuegenschuh, B., Kováč, M., Hok, J., 2014. Cretaceous–Quaternary tectonic evolution of the Tatra Mts (Western Carpathians): constraints from structural, sedimentary, geomorphological, and fission track data. Geol. Carpath. 65, 307–326.

Kruiver, P.P., Dekkers, M.J., Heslop, D., 2001. Quantification of magnetic coercivity components by the analysis of acquisition curves of isothermal remanent magnetisation. Earth Planet. Sci. Lett. 189, 269–276.

Lefeld, J., 1974. Middle-Upper Jurassic and lower cretaceous biostratigraphy and sedimentology of the sub-Tatric succession in the Tatra Mts (Western Carpathians). Acta Geol. Pol. 24, 227–364.

Lefeld, J., Gaździcki, A., Iwanow, A., Krajewski, K., Wójcik, K., 1985. Jurassic and cretaceous lithostratigraphic units of the Tatra Mountains. Stud. Geol. Pol 84, 1–93.

Lewchuk, M., Symons, D., 1995. Age and duration of Mississippi Valley–type ore-mineralizing events. Geology 23, 233–236.

Lexa, J., Bezák, V., Elečko, M., Mello, J., Polák, M., Potfaj, M., Vozár, J., Schnabel, G., Pálenský, P., Császár, G., Others, 2000. Geological Map of Western Carpathians and Adjacent Areas 1: 500 000. Geological Survey of Slovak Republic, Bratislava.

Li, Y.-X., Kodama, K.P., 2005. Assessing thermal effects on magnetic fabrics of sedimentary rocks: Results from synthetic and natural samples. Geophysical Research Letters 32. https://doi.org/10.1029/2004GL022049.

Lowrie, W., 1990. Identification of ferromagnetic minerals in a rock by coercivity and unblocking temperature properties. Geophysical Research Letters 17, 159–162. https://doi.org/10.1029/GL017i002p00159.

Ludwiniak, M., 2010. Multi-stage development of the joint network in the flysch rocks of Western Podhale (Inner Western Carpathians, Poland). Acta Geol. Pol. 60, 283–316.

Madzin, J., Márton, E., Starek, D., Mikuš, T., 2021. Magnetic fabrics in the turbidite deposits of the Central Carpathian Paleogene Basin in relation to sedimentary and tectonic fabric elements. Geol. Carpath. 72, 134–154.

Marko, F., Vojtko, R., Plašienka, D., Sliva, L., Jablonský, J., Reichwalder, P., Starek, D., 2005. A contribution to the tectonics of the Periklippen zone near Zázrivá (Western Carpathians). Slovak Geol. Magaz. 11, 37–43.

Marszałko, R., Radomski, A., 1960. Preliminary results of investigations of current directions in the flysch basin of the Central Carpathians. Ann. Soc. Geol. Pol. 30, 259–272.

Márton, E., Mastella, L., Tokarski, A., 1999. Large counterclockwise rotation of the Inner West Carpathian Paleogene flysch—evidence from paleomagnetic investigations of the Podhale Flysch (Poland). Phys. Chem. Earth Solid Earth Geod. 24, 645–649.

Márton, E., Jelenska, M., Tokarski, A.K., Soták, J., Kováč, M., Spišiak, J., 2009. Current-independent paleomagnetic declinations in flysch basins: a case study from the Inner Carpathians. Geodin. Acta 22, 73–82.

Márton, E., Grabowski, J., Tokarski, A.K., Túnyi, I., 2016. Palaeomagnetic results from the fold and thrust belt of the Western Carpathians: an overview. Geol. Soc. Lond. Spec. Publ. 425, 7–36.

Marynowski, L., Gawęda, A., Cebulak, S., Jędrysek, M., 2001. Hydrocarbons migration in tectonic zones of the Western Tatra Mountains crystalline basement (Central Western Carpathians). Geol. Carpath. 52, 3–14.

Marynowski, L., Gaweda, A., Poprawa, P., Zywiecki, M.M., Kępińska, B., Merta, H., 2006. Origin of organic matter from tectonic zones in the Western Tatra Mountains

Crystalline Basement, Poland: an example of bitumen—source rock correlation. Mar. Pet. Geol. 23, 261–279.

Marynowski, L., Smolarek, J., Hautevelle, Y., 2015. Perylene degradation during gradual onset of organic matter maturation. Int. J. Coal Geol. 139, 17–25.

McCabe, C., Elmore, R.D., 1989. The occurrence and origin of late Paleozoic remagnetization in the sedimentary rocks of North America. Rev. Geophys. 27, 471–494.

Moreau, M., Ader, M., Enkin, R., 2005. The magnetization of clay-rich rocks in sedimentary basins: low-temperature experimental formation of magnetic carriers in natural samples. Earth Planet. Sci. Lett. 230, 193–210.

Nemčok, J., Bezák, V., Janák, M., Kahan, Š., Ryka, W., Kohút, M., Lehotský, I., Wieczorek, J., Zelman, J., Mello, J., Others, 1993. Explanatory notes to the geological map of the Tatra Mts. at 1: 50,000 scale [Vysvetlivky ku geologickej mape Tatier 1: 50 000]. State Geological Institute of Dionýz Štúr, pp. 1–135.

Parés, J.M., 2015. Sixty years of anisotropy of magnetic susceptibility results in deformed sedimentary rocks. Front. Earth Sci. 3, 4. https://doi.org/10.3389/feart.2015.00004.

Parés, J.M., van der Pluijm, B.A., Dinarès-Turell, J., 1999. Evolution of magnetic fabrics during incipient deformation of mudrocks (Pyrenees, northern Spain). Tectonophysics 307, 1–14.

Peresson, H., Decker, K., 1997. Far-field effects of late Miocene subduction in the Eastern Carpathians: E-W compression and inversion of structures in the Alpine-Carpathian-Pannonian region. Tectonics 16, 38–56.

Pešková, I., Vojtko, R., Starek, D., Sliva, L., 2009. Late Eocene to Quaternary deformation and stress field evolution of the Orava region (Western Carpathians). Acta Geol. Pol. 59, 73–91.

Petrík, I., Kohút, M., 1997. The Evolution of Granitoid Magmatism during the Hercynian Orogen in the Western Carpathians. Geological evolution of the Western Carpathians. Mineralia Slovaca Monograph, Bratislava, pp. 235–252.

Piotrowska, K., Kotański, Z., Gawęda, A., Piotrowski, J., Rączkowski, W., 2009. Detailed Geological Map of Poland. Western Tatra MTS Sheet. Polish Geological Institute-National Research Institute, Warsaw.

Piotrowska, K., Rączkowski, W., Iwanow, A., Zabielski, R., Derkacz, M., Wójcik, A., Michalik, M., Wasiluk, R., 2013. Detailed Geological Map of Poland. High Tatra Mts sheet. Polish Geological Institute-National Research Institute, Warsaw.

Plašienka, D., 2003. Development of basement-involved fold and thrust structures exemplified by the Tatric–Fatric–Veporic nappe system of the Western Carpathians (Slovakia). Geodin. Acta 16, 21–38.

Plašienka, D., 2018. Continuity and episodicity in the early Alpine tectonic evolution of the Western Carpathians: how large-scale processes are expressed by the orogenic architecture and rock record data. Tectonics 37, 2029–2079.

Plašienka, D., Grecula, P., Putiš, M., Kováč, M., Hovorka, D., 1997. Evolution and Structure of the Western Carpathians: An Overview. Geological evolution of the Western Carpathians, Mineralia Slovaca Monograph, Bratislava, pp. 1–24.

Pokorski, J., 1965. Occurence of cleavage in the flysch deposits of the east Podhale region. Geol. Quart. 9, 616–624.

Poprawa, P., Marynowski, L., 2005. Thermal history of the Podhale Trough (northern part of the Central Carpathian Paleogene Basin)–preliminary results from 1-D maturity modeling. In: Mineralogical Society of Poland–Special Papers, 25, pp. 352–355.

Poprawa, P., Grabowski, J., Grotek, I., 2002. Thermal and burial history of the sub-Tatric nappes and the Podhale basin—Constraints from preliminary maturity analysis and modelling. In: Proceedings of XVII. Congress of Carpathian-Balkan Geological Association Bratislava, September 1st - 4th 2002, Geologica Carpathica Vol. 53 Special Issue.

Prokešová, R., 1994. Structural analysis of the Krížna nappe in its near-root and superficial position. Mineral. Slov. 26, 347–354.

Prokešová, R., Plašienka, D., Milovský, R., 2012. Structural pattern and emplacement mechanisms of the Krížna cover nappe (Central Western Carpathians). Geol. Carpath. 63, 13–32.

Radke, M., Welte, D., 1983. The Methylphenanthrene Index (MPI). A maturity parameter based on aromatic hydrocarbons. In: Advances in Organic Geochemistry. J. Wiley and Sons, New York, pp. 504–512.

Radke, M., Welte, D., Willsch, H., 1986. Maturity parameters based on aromatic hydrocarbons: Influence of the organic matter type. Org. Geochem. 10, 51–63.

Ratschbacher, L., Linzer, H.-G., Moser, F., Strusievicz, R.-O., Bedelean, H., Har, N., Mogoş, P.-A., 1993. Cretaceous to Miocene thrusting and wrenching along the

central South Carpathians due to a corner effect during collision and orocline formation. Tectonics 12, 855–873.

Roberts, A.P., Tauxe, L., Heslop, D., Zhao, X., Jiang, Z., 2018. A critical Appraisal of the "Day" Diagram. J. Geophys. Res. Solid Earth 123, 2618–2644. https://doi.org/10.1002/2017JB015247.

Roberts, A.P., Hu, P., Harrison, R.J., Heslop, D., Muxworthy, A.R., Oda, H., Sato, T., Tauxe, L., Zhao, X., 2019. Domain State Diagnosis in Rock Magnetism: Evaluation of potential Alternatives to the Day Diagram. J. Geophys. Res. Solid Earth 124, 5286–5314. https://doi.org/10.1029/2018JB017049.

Rospondek, M.J., Marynowski, L., Chachaj, A., Góra, M., 2009. Novel aryl polycyclic aromatic hydrocarbons: phenylphenanthrene and phenylanthracene identification, occurrence and distribution in sedimentary rocks. Org. Geochem. 40, 986–1004.

Rubinkiewicz, J., Ludwiniak, M., 2005. Fracture and fault development in Werfenian quartzitic sandstones–A case study from the autochthonous cover of the Tatra Mts. In: Annales Societatis Geologorum Poloniae, pp. 171–187.

Sanderson, D.J., Marchini, W., 1984. Transpression. J. Struct. Geol. 6, 449–458.

Schwab, F.L., 2003. Sedimentary Petrology. In: Meyers, R.A. (Ed.), Encyclopedia of Physical Science and Technology, Third edition. Academic Press, New York, pp. 495–529. https://doi.org/10.1016/B0-12-227410-5/00678-5.

Śmigielski, M., Sinclair, H., Stuart, F., Persano, C., Krzywiec, P., 2016. Exhumation history of the Tatry Mountains, Western Carpathians, constrained by low-temperature thermochronology. Tectonics 35, 187–207.

Soták, J., Pereszlenyi, M., Marschalko, R., Milicka, J., Starek, D., 2001. Sedimentology and hydrocarbon habitat of the submarine-fan deposits of the Central Carpathian Paleogene Basin (NE Slovakia). Mar. Pet. Geol. 18, 87–114.

Sperner, B., Ratschbacher, L., Nemčok, M., 2002. Interplay between subduction retreat and lateral extrusion: Tectonics of the Western Carpathians. Tectonics 21, 1–24.

Środoń, J., Kotarba, M., Biron, A., Such, P., Clauer, N., Wójtowicz, A., 2006. Diagenetic history of the Podhale-Orava Basin and the underlying Tatra sedimentary structural units (Western Carpathians): evidence from XRD and K-Ar of illite-smectite. Clay Miner. 41, 751–774.

Stachowska, A., Łoziński, M., Śmigielski, M., Wysocka, A., Jankowski, L., Ziółkowski, P., 2020. Anisotropy of magnetic susceptibility as an indicator for palaeocurrent analysis in folded turbidites (Outer Western Carpathians, Poland). Sedimentology 67, 3783–3808.

Staneczek, D., Szaniawski, R., Szczygieł, J., 2022. Transpression-driven deformations of the Chočské vrchy Mountains (Western Carpathians): Insights from magnetic fabric. Geol. Carpath. 73, 451–471.

Staneczek, D., Więcław, D., Marynowski, L., 2024. Depositional conditions, wildfires, maturity, and hydrocarbon potential evaluation of Central Carpathian Paleogene Basin based on integrative approach from Orava Basin. International Journal of Coal Geology 285, 104490. https://doi.org/10.1016/j.coal.2024.104490.

Suk, D., Peacor, D.R., der Voo, R.V., 1990. Replacement of pyrite framboids by magnetite in limestone and implications for palaeomagnetism. Nature 345, 611–613.

Symons, D., Sangster, D., 1992. Late Devonian paleomagnetic age for the Polaris Mississippi Valley-type Zn–Pb deposit, Canadian Arctic Archipelago. Can. J. Earth Sci. 29, 15–25.

Szaniawski, R., Ludwiniak, M., Rubinkiewicz, J., 2012. Minor counterclockwise rotation of the Tatra Mountains (Central Western Carpathians) as derived from paleomagnetic results achieved in hematite-bearing lower Triassic sandstones. Tectonophysics 560, 51–61.

Szaniawski, R., Mazzoli, S., Jankowski, L., 2017. Controls of structural inheritance on orogenic curvature and foreland basin sedimentation: Insights from the Przemyśl area, Western Carpathians. J. Struct. Geol. 103, 137–150.

Szaniawski, R., Ludwiniak, M., Mazzoli, S., Szczygieł, J., Jankowski, L., 2020. Paleomagnetic and magnetic fabric data from lower Triassic redbeds of the Central Western Carpathians: new constraints on the paleogeographic and tectonic evolution of the Carpathian region. J. Geol. Soc. Lond. 177, 509–522.

Vojtko, R., Tokárová, E., Sliva, L.A., Pešková, I., 2010. Reconstruction of Cenozoic paleostress fields and revised tectonic history in the northern part of the Central Western Carpathians (the Spišská Magura and Východné Tatry Mountains). Geol. Carpath. 61, 211.

Weil, A.B., Yonkee, A., 2009. Anisotropy of magnetic susceptibility in weakly deformed red beds from the Wyoming salient, Sevier thrust belt: Relations to layer-parallel shortening and orogenic curvature. Lithosphere 1, 235–256.

Westwalewicz-Mogilska, E., 1986. New insights into the genesis of the sediments of the Podhale flysch. Prz. Geol. 34, 690–698 (in Polish).

Supplementary materials to the article 2

Supplementary Materials

Multi-stage tectonic evolution of the Tatra Mts recorded in the para- and ferromagnetic fabrics

Dorota STANECZEK[1*], Rafał SZANIAWSKI[2], Martin CHADIMA[3,4], Leszek MARYNOWSKI[1]

[1]*Institute of Earth Sciences, University of Silesia in Katowice, Będzińska 60, 41-200 Sosnowiec, Poland;*

[2]*Institute of Geophysics, Polish Academy of Sciences, Księcia Janusza 64, 01-452 Warszawa, Poland;*

[3]*AGICO Ltd., Purkynova 3050/99a, 621 00 Brno, Czech Republic;*

[4]*Institute of Geology, Academy of Sciences of Czech Republic, Rozvojová 135, 165 00 Prague, Czech Republic*

[*]*corresponding author: dorota.staneczek@us.edu.pl*
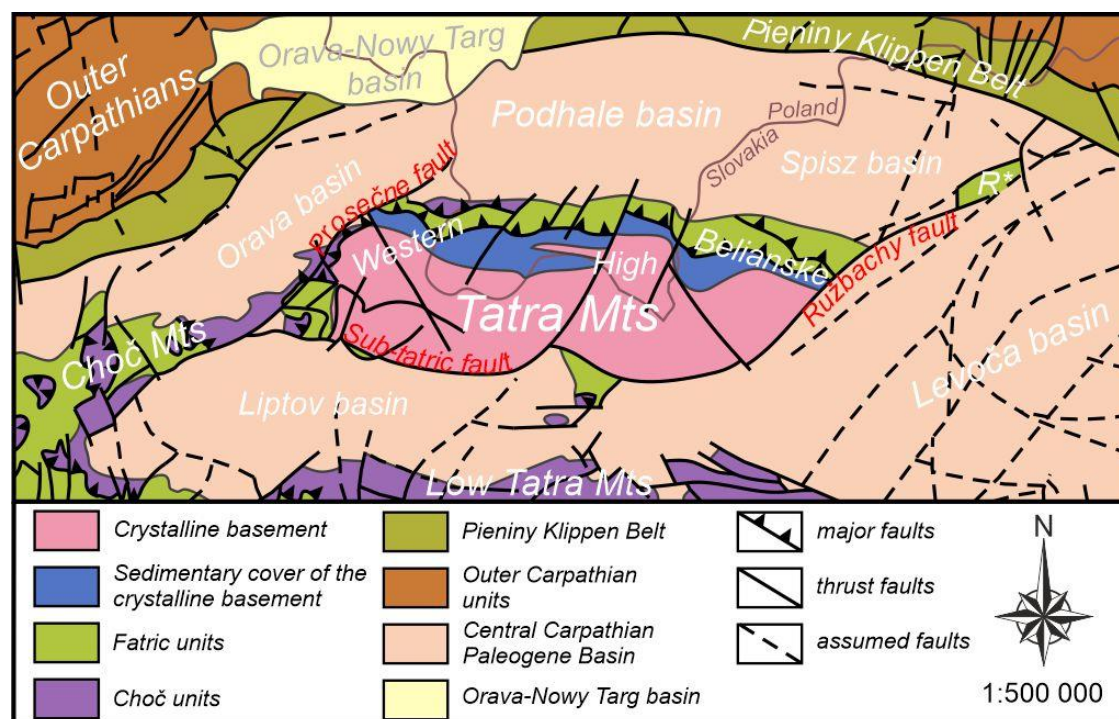
Figure S.1. Simplified tectonic setting of the Tatra Mts area (after Lexa et al., 2000). R* - Ružbachy horst.

Supplementary materials to the article 2

Table S.1 Anisotropy of anhysteretic remanent magnetization measurements for the Huty and Mraznica Fms. specimens

Site	Specimen	Mean ARM	K1	K2	K3	K1_Dec	K1_Inc	K2_Dec	K2_Inc	K3_Dec	K3_Inc	L	F	P	Pj	T	U	Q	E	FTest_F	FTest_F12	FTest_F23	E12	E23	E13
	HT511	3.53E-05	1.078141	1.001368	0.9204899	171.468746	39.7614853	25.0594576	45.0337406	276.668868	17.4907892	1.076668	1.087865	1.171269	1.171401	6.54E-02	2.60E-02	0.6437194	1.010399	1.9	1.1	1.2	18.5	17.6	9.2
	HT512	7.58E-05	1.056105	1.013909	0.9299858	167.902533	35.400942	59.7768988	23.6412649	303.614385	45.206822	1.041616	1.090242	1.135614	1.138684	0.3587698	0.3308663	0.4017778	1.046683	6.7	1.8	7.2	14.7	7.5	5
	HT521	3.63E-05	1.036115	1.009455	0.9544306	13.5180477	14.9394633	277.319074	22.0333487	134.979487	62.9230744	1.02641	1.057651	1.085584	1.087545	0.3651203	0.3472409	0.3900281	1.030437	0.8	0.2	0.9	38.2	20.9	14.4
	HT522	7.71E-05	1.049852	1.01207	0.9380786	10.0196751	8.75320913	277.635565	15.1187144	129.103618	72.4240889	1.037331	1.078875	1.119151	1.121683	0.3488277	0.3239535	0.4067728	1.040049	3.5	1	3.7	19.7	10.4	6.9
	HT531	3.85E-05	1.045305	1.008637	0.9460576	0.14383714	30.7872973	259.885089	16.6417214	145.506742	54.0893039	1.036353	1.066148	1.104906	1.10638	0.2841239	0.2610933	0.4531651	1.02875	4.5	1.5	4.4	16.1	9.6	6.1
Ht5	HT533	8.15E-05	1.051664	1.012601	0.9357351	350.873555	33.8274453	251.459441	13.7167388	142.726588	52.7646419	1.038577	1.082145	1.123891	1.126575	0.3518386	0.3260852	0.4052303	1.04195	1.3	0.4	1.4	30.5	16.7	11.2
	HT542	4.03E-05	1.029777	1.003816	0.9664072	314.494526	18.1576708	46.6710687	6.60553724	155.867592	70.5984706	1.025863	1.038709	1.065573	1.066005	0.1959366	0.1806376	0.5152184	1.012522	0.4	0.2	0.3	41.8	31.9	20.1
	HT543	8.60E-05	1.048061	1.02024	0.9316995	344.884246	23.8609297	254.469831	0.93680008	162.353318	66.1183783	1.027269	1.095031	1.124892	1.131258	0.5427827	0.5218123	0.2715577	1.065963	6.7	0.9	8.8	20.7	6.8	5.2
	HT555	8.86E-05	1.072036	1.002138	0.9258261	345.342198	20.0099702	246.466977	22.9604119	112.206257	58.7410826	1.069749	1.082426	1.157924	1.158106	8.03E-02	4.39E-02	0.6282352	1.01185	17.8	10.1	12.1	6.3	5.8	3
	HT561	8.24E-05	1.049857	1.015945	0.9341981	175.639805	10.4518518	80.7584265	24.7631034	286.7136	62.8408432	1.03338	1.087505	1.123806	1.127931	0.4373747	0.4135813	0.3435796	1.052376	8.6	1.8	10.2	14.9	6.3	4.5
	HT563	3.74E-05	1.097303	1.017368	0.8853284	51.1908244	7.91123907	142.521537	9.48754846	281.99228	77.5995646	1.07857	1.149143	1.239431	1.243275	0.2952664	0.2458079	0.4647178	1.065431	1.1	0.4	1	29.8	19.1	12.2
	HT713	4.30846E-05	1.051312	0.9996969	0.9489913	312.094291	1.62472739	222.062844	1.1083309	97.7762421	88.0330758	1.051631	1.053431	1.10782	1.107826	0.01670611	-0.00888706	0.67459	1.001712	5.7	3.6	3.5	20.9	21.2	10.7
	HT721	5.89015E-05	1.045937	1.012216	0.9418461	271.103965	15.5146267	3.9847777	10.2621012	126.224116	71.2535335	1.033314	1.074715	1.110518	1.113215	0.3747558	0.3520866	0.3865735	1.040066	9.6	2.4	10.5	25.2	12.4	8.4
	HT722	2.92839E-05	1.034515	1.01249	0.9529954	309.898713	14.5705551	218.470421	5.47752981	108.395997	74.3908971	1.021753	1.062429	1.08554	1.088843	0.4756175	0.4596383	0.3123802	1.03981	0.5	0.1	0.6	51.7	25.1	18.9
	HT723	2.71546E-05	1.080068	0.9652621	0.9546704	283.633665	17.5957388	164.061508	57.2750863	22.7824859	26.6273388	1.118937	1.011095	1.131351	1.146348	-0.8211946	-0.831071	1.688456	0.9036203	1.7	2.9	0	11.7	65.9	10.7
Ht7	HT732	3.38298E-05	1.058785	1.013572	0.9276431	269.211978	5.93618649	179.126059	0.82624805	81.2311609	84.0061787	1.044608	1.092631	1.141371	1.144254	0.3399154	0.3104678	0.4165767	1.045973	10.9	3.1	11.4	22.3	11.9	7.9
	HT733	1.55352E-05	1.05087	0.9944345	0.9546953	295.163764	1.95475451	204.78933	10.839339	35.2589282	78.9816032	1.056751	1.041625	1.100739	1.101135	-0.150212	-0.1736052	0.8304605	0.9856859	2.3	1.9	1	14.2	19.8	8.5
	HT741	0.000032539	1.058154	1.019423	0.9224235	276.935572	4.80904438	186.305226	7.44990859	39.5070675	81.1179033	1.037993	1.105157	1.147145	1.152541	0.456729	0.4292936	0.3328419	1.064705	0.7	0.1	0.8	44	21.1	15.4
	HT742	7.07411E-05	1.049261	1.015909	0.93483	249.464144	7.4373904	342.678689	23.2462969	142.852491	65.4574566	1.03283	1.086731	1.122409	1.126543	0.4405384	0.41708	0.3411802	1.052188	0.8	0.2	1	72.4	38.3	28.2
	HT751	3.65084E-05	1.057805	1.017656	0.9245389	285.419203	12.2232775	17.0790297	7.61574355	138.299744	75.5355099	1.039453	1.100717	1.144143	1.148729	0.42529	0.3974603	0.3547003	1.05894	7.7	1.7	9	29.9	13.4	9.4
	HT752	1.95156E-05	1.048376	1.01569	0.9359339	301.845144	9.20824538	32.370922	3.23987153	141.561502	80.2290348	1.032181	1.085215	1.120139	1.124212	0.4416343	0.4186175	0.3401271	1.051381	5.9	1.2	7	18.1	7.6	5.4
	HT1013	2.71386E-05	1.067973	1.031011	0.9010164	174.215492	0.48847044	84.0701974	16.5639229	265.857276	73.4284598	1.03585	1.144275	1.185298	1.196556	0.5856044	0.5572281	0.2489421	1.104673	8.1	0.9	11.1	39.4	12.1	9.4
	HT1022	5.67187E-05	1.094915	1.011336	0.8937485	327.835457	7.68191585	58.1775818	2.53486654	166.31458	81.9058608	1.082642	1.131567	1.225082	1.227041	0.2177216	0.1690592	0.5244085	1.04519	2.9	1.2	2.4	34.3	25.1	15
	HT1032	5.96825E-05	1.082759	1.016762	0.9004788	324.869102	6.10349243	55.3947371	4.90370151	183.930237	82.1589281	1.064908	1.129135	1.202425	1.206129	0.3176912	0.2758796	0.442092	1.060312	3.2	1	3.1	37.4	22.3	14.4
	HT1041	3.11396E-05	1.082998	1.020032	0.8969706	353.750501	2.01117158	84.1054891	10.0063274	252.508054	79.7894731	1.06173	1.137196	1.207395	1.212385	0.3643438	0.323041	0.4074333	1.071079	71.2	19.7	75.3	9.1	4.7	3.1
Ht10	HT1051	2.30297E-05	1.08383	1.040377	0.8757936	355.228413	7.22934731	265.125424	0.81178933	168.753084	82.7247339	1.041766	1.187925	1.23754	1.253831	0.6160228	0.5822576	0.2332285	1.140299	57.9	5.7	81.4	16.8	4.5	3.5
	HT1062	6.07202E-05	1.059883	1.017312	0.922805	343.006143	12.877907	74.667476	7.22709679	193.28684	75.1714166	1.041846	1.102413	1.148545	1.152907	0.4080079	0.3788857	0.3676442	1.058134	18.1	4.2	20.5	19.5	8.9	6.2
	HT1071	7.50042E-05	1.033082	1.002389	0.9645286	347.744973	4.74114608	79.2795557	17.8951874	243.438958	71.4459509	1.030619	1.039253	1.071074	1.071255	0.1214983	0.1045642	0.5768512	1.008377	1.1	0.6	0.9	47.7	40.2	23.5
	HT1072	3.55728E-05	1.032847	1.012144	0.9550087	338.386404	11.3869846	72.1215633	17.9244122	217.545209	68.5525791	1.020455	1.059827	1.081506	1.084746	0.4831563	0.4680473	0.3067739	1.038583	0.9	0.2	1.2	41.8	18	13.4
	HT1081	7.57533E-05	1.064869	0.9982802	0.9368514	166.675892	35.5859726	69.5607942	9.8205469	326.441554	52.6699837	1.066703	1.06557	1.136646	1.136648	-0.00830148	-0.04030316	0.7029797	0.9989374	4.3	2.9	2.5	23.2	25	12.3
	HT1083	3.41339E-05	1.051521	0.9981684	0.9503108	165.054669	40.6009061	67.4672502	8.75741369	327.595451	48.0594972	1.05345	1.05036	1.106502	1.106518	-0.02903002	-0.0542919	0.7158159	0.9970663	0.7	0.5	0.4	26.6	29.2	14.8
	HT1114	5.83E-05	1.088032	0.9675017	0.9444659	332.862776	32.0708474	95.7075018	40.8788362	219.271151	32.5671459	1.124579	1.02439	1.152007	1.163478	-0.6594126	-0.679091	1.446925	0.9109103	8.1	12.4	0.5	11.4	51.8	9.6
	HT1121	2.77E-05	1.086895	0.9742315	0.9388738	336.268518	14.8459196	184.434752	73.2653188	68.2816728	7.54932783	1.115643	1.03766	1.157658	1.164462	-0.4949713	-0.5222614	1.228751	0.9300999	2.7	3.6	0.4	10.5	30.6	8
	HT1124	5.68E-05	1.046979	1.001595	0.9514259	324.034576	18.509973	73.1058682	44.303317	217.781706	39.8949708	1.045312	1.052731	1.100432	1.100527	7.39E-02	5.01E-02	0.6228821	1.007097	4.3	2.5	3	25.1	22.8	12.2
	HT1131	6.28E-05	1.036067	1.022458	0.9414754	129.153147	18.3385564	18.1442015	47.2449604	233.607349	36.9811641	1.01331	1.086017	1.100472	1.109336	0.7237856	0.7122589	0.1550221	1.071752	30.2	1.3	47.3	33.1	5.9	5
Ht11	HT1141	5.64E-05	1.028796	1.011371	0.9598328	324.29191	38.2950707	223.502403	13.3374302	117.900282	48.6043468	1.017229	1.053696	1.071849	1.074982	0.5076244	0.4946733	0.2891985	1.035849	1	0.11	1.3	74.6	33.9	26
	HT1142	2.61E-05	1.049461	0.9915602	0.9589792	352.530431	48.8309476	92.2503408	8.39849209	189.34943	39.931794	1.058393	1.033975	1.094352	1.095448	-0.2588862	-0.279831	0.9409932	0.9769285	1.2	1.2	0.4	18.2	30.3	11.9
	HT1152	2.99E-05	1.049303	0.9836053	0.9670915	148.724513	7.81426911	350.970182	81.5660464	239.157724	3.1534456	1.066793	1.017076	1.085009	1.089932	-0.5849503	-0.5982602	1.330918	0.9533958	0.9	1.3	0.1	17.4	51.3	14.1
	HT1153	6.71E-05	1.048601	0.9845662	0.9668329	157.106818	16.1920291	263.535493	44.2449116	52.3329412	41.2892269	1.065039	1.018342	1.084573	1.08895	-0.5522556	-0.5662553	1.287115	0.9561545	8.3	11.5	0.9	11.9	39.7	9.3
	HT1161	5.94E-05	1.04759	1.015707	0.936703	332.415325	29.3021645	238.801033	6.40887671	137.642351	59.8687083	1.031389	1.084343	1.11838	1.122496	0.4475093	0.4249586	0.3357949	1.051342	6.9	1.4	8.3	32.9	13.9	10
	HT1212	1.97E-05	1.089472	1.047759	0.86277	320.670265	11.7403013	54.4602519	17.6436203	198.665123	68.5886785	1.039811	1.214413	1.26276	1.283923	0.6653289	0.6320029	0.2026414	1.167916	2.1	0.2	3	42.1	11.5	9.4
	HT1214	4.47E-05	1.092635	1.023405	0.8839598	288.622207	25.1870854	25.0975203	13.4849054	140.69645	60.9695287	1.067646	1.157751	1.236068	1.24239	0.3822991	0.3364848	0.3977332	1.084396	3.9	1	4.2	37.1	19.5	13.1
Ht12	HT1221	4.29E-05	1.080225	1.028825	0.8909501	302.840359	18.4733898	34.2487487	4.20777056	136.599919	71.0193705	1.04996	1.15475	1.212442	1.221786	0.4938421	0.4568725	0.3142307	1.099804	4.8	0.8	6	40.6	16.3	12
	HT1231	4.22E-05	1.073865	1.038121	0.8880143	295.090338	12.1864825	29.0885268	17.8932202	172.57136	68.1132695	1.034432	1.169036	1.209288	1.224744	0.6437213	0.6153451	0.2127902	1.130124	1.5	0.1	2.1	78.2	26.9	22
	HT1241	4.29E-05	1.093678	1.021422	0.8848996	287.202592	9.16712099	18.9656297	10.7938659	157.694294	75.7665701	1.070741	1.15428	1.235935	1.241379	0.3546593	0.3078223	0.4185097	1.078021	3	0.9	3.1	40	22.5	14.9

	HT1242	2.08E-05	1.071753	1.041611	0.8866367	307.851585	13.5295359	40.4606983	10.7128127	167.632542	72.6141269	1.028937	1.174789	1.208784	1.226885	0.6991121	0.6743515	0.177255	1.14175	4.3	0.2	6.5	35.5	7.9	6.6
	HT1243	2.05E-05	1.082214	1.033169	0.8846174	306.821543	14.4712146	40.6357842	14.4537261	173.694836	69.3172046	1.04747	1.167927	1.223369	1.235131	0.53992	0.5035849	0.2833755	1.114998	1.3	0.2	1.7	39.2	15.1	11.5
	HT1252	6.12E-05	1.05213	1.043377	0.9044926	241.108981	3.97879888	150.236305	12.3511284	348.649682	77.004476	1.008389	1.15355	1.163227	1.18527	0.889501	0.8814329	6.11E-02	1.143954	3.9	0	6.8	101.6	15.4	14.5
	HT1262	6.13E-05	1.054173	1.019068	0.9267598	250.566932	10.0466381	344.401344	20.6794645	136.145881	66.8039556	1.034448	1.099603	1.137482	1.142886	0.4741657	0.4489547	0.3195432	1.062985	1.9	0.3	2.3	58.1	25.9	19.1
	HT1411	2.57E-05	1.072931	1.025404	0.9016648	318.057593	28.0639415	62.2317919	24.6692314	186.828082	51.0298414	1.04635	1.137234	1.189945	1.197736	0.4789436	0.4449914	0.3222121	1.086859	9	1.6	11	30.3	12.1	8.8
	HT1421	4.58E-05	1.099323	1.01862	0.8820575	308.433484	26.2809831	59.5041753	36.0561617	191.464393	42.5635699	1.079227	1.154823	1.246316	1.250614	0.3074652	0.257105	0.4561689	1.070046	13.1	4.4	12.7	18.9	11.3	7.1
	HT1432	4.04E-05	1.081741	1.009901	0.9083583	269.62594	8.80595474	5.59208116	33.8598714	166.986244	54.7031597	1.071136	1.111787	1.190874	1.192446	0.2132319	0.1713123	0.5226152	1.037951	165.3	70.3	140.4	4.8	3.4	2
Ht14	HT1442	3.76E-05	1.065599	1.010031	0.9243699	310.321791	21.6692922	52.4480633	27.8654093	187.923785	53.4407255	1.055017	1.092669	1.152785	1.154439	0.2466385	0.2130738	0.4898274	1.035689	15.7	6	14.2	16.3	10.7	6.5
	HT1452	2.49E-05	1.082619	1.037898	0.8794842	340.563486	29.742853	77.0119401	11.1201725	185.228984	57.8404168	1.043088	1.180121	1.23097	1.245681	0.5939848	0.5596919	0.2473855	1.131373	3.9	0.4	5.3	28.5	8.7	6.8
	HT1454	4.88E-05	1.065582	1.047068	0.8873501	326.153636	25.7612904	64.6078249	16.9432591	184.351138	58.4472689	1.017681	1.179995	1.200858	1.223842	0.8084906	0.7922555	0.1095626	1.159493	2.9	0.1	4.7	89.4	18.3	16.4
	HT1461	5.15E-05	1.074847	1.031471	0.8936814	310.148533	19.5230747	50.0334936	25.8345729	187.492993	56.6904029	1.042053	1.154182	1.202719	1.213837	0.5536717	0.5211429	0.2719897	1.107604	1.6	0.2	2.2	66.7	26.5	20.5
	HT1471	4.81E-05	1.07559	1.027725	0.8966851	0.52355296	33.9394263	91.5425413	1.51372182	183.789299	56.0174286	1.046574	1.146138	1.199518	1.208445	0.4995364	0.4649065	0.3088646	1.095133	1	0.2	1.2	72.4	34.5	26
	HT1481	5.57E-05	1.096489	1.012265	0.8912459	321.028918	23.6560201	64.995452	28.8535111	198.11251	51.1272371	1.083203	1.135787	1.230288	1.232503	0.2287277	0.1792805	0.5162924	1.048545	2.5	1	2.1	37.1	26.8	16.2
	HT1491	4.95E-05	1.097015	1.039219	0.8637667	285.5038	19.57542	26.1836796	27.5263344	164.740697	55.1919824	1.055615	1.203124	1.270036	1.284911	0.5471716	0.5044261	0.2828274	1.139738	3.8	0.5	5	48.2	17.8	13.5
	HT1511	2.56E-05	1.04957	1.03396	0.9164706	14.5313388	23.950306	276.759678	16.9319453	154.899848	60.0258869	1.015097	1.128198	1.14523	1.160313	0.7790027	0.7654417	0.1245848	1.111418	0.6	0	1	69.9	19.9	17.7
	HT1512	5.23E-05	1.086169	0.9863465	0.9274848	315.392954	24.4357829	59.0088194	27.3887366	190.152086	51.7811548	1.101204	1.063464	1.171091	1.172588	-0.2208041	-0.2581262	0.917713	0.9657283	1.6	1.5	0.5	31.1	48.6	20.1
	HT1521	4.78E-05	1.049592	1.023512	0.9268961	324.149445	30.2184148	66.2027989	19.7241884	184.279156	52.7007176	1.02548	1.104236	1.132372	1.140481	0.5952078	0.5748962	0.2378272	1.0768	0.8	0.1	1.1	84.9	35.5	28.6
	HT1541	4.79E-05	1.074946	0.9939917	0.9310624	308.688185	26.3082369	59.6451481	35.8828025	191.536763	42.7072263	1.081444	1.067589	1.154537	1.15476	-8.97E-02	-0.1252747	0.7828746	0.9871885	1.6	1.3	0.8	33.6	41.7	19.7
Ht15	HT1542	2.62E-05	1.057142	1.000476	0.9423816	328.188541	30.9341922	73.5441024	23.8389167	194.290072	49.162768	1.056639	1.061647	1.121777	1.121813	4.11E-02	1.25E-02	0.6556429	1.00474	4.5	2.7	2.9	12.1	11.8	6
	HT1551	5.17E-05	1.047782	1.022969	0.9292486	318.492063	28.3258375	56.898615	15.174868	171.773806	57.1868028	1.024255	1.100857	1.127558	1.135497	0.6007492	0.5813406	0.2338002	1.074787	2.5	0.2	3.6	63.7	21	16.7
	HT1552	2.41E-05	1.038007	1.027125	0.934868	314.088553	15.7653244	50.4520325	21.4345609	190.586977	62.911041	1.010595	1.098684	1.110325	1.122143	0.798586	0.7889769	0.1113879	1.087166	1.3	0	2.1	64.3	13.7	12.3
	HT1553	2.34E-05	1.061833	1.004324	0.9338427	335.343077	22.5538262	72.0650958	15.7400067	194.044092	61.9794951	1.057261	1.075475	1.137058	1.137487	0.1329835	0.1013613	0.5795124	1.017228	1.3	0.6	1	23.9	19.9	11.3
	HT1561	4.44E-05	1.054633	1.026957	0.9184093	49.2893567	18.2486643	310.028908	26.0147808	170.312261	57.3901346	1.02695	1.118191	1.148326	1.158096	0.6154453	0.5936662	0.2261387	1.088847	0.6	0.1	0.8	91.8	40.4	33.2
	HT1562	2.38E-05	1.043993	1.022363	0.9336448	323.705275	14.2789922	60.3662136	24.5016003	206.189755	61.1499424	1.021157	1.095023	1.118191	1.126106	0.6251721	0.6079642	0.217317	1.072336	0.4	0	0.6	62.5	25.1	20.7
	ZA113	5.44E-05	1.081307	1.055022	0.8636709	345.901708	45.0030777	245.573589	10.1632158	145.878127	43.2118238	1.024915	1.221555	1.25199	1.27957	0.7809914	0.7584456	0.1285396	1.191861	15.3	0.5	24.8	51.1	8.1	7.1
	ZA131	5.29E-05	1.091756	1.02375	0.8844945	277.091597	20.0911197	31.4632264	48.4465241	172.491806	34.5720062	1.066428	1.157441	1.234327	1.240817	0.3890077	0.3437668	0.3925113	1.085343	35.8	9.3	38.9	13.2	6.5	4.4
	ZA132	2.12E-05	1.066302	1.035074	0.8986239	279.290141	19.9263789	24.7865133	36.3905683	166.55951	46.8265762	1.03017	1.151843	1.186594	1.200606	0.6525314	0.6275237	0.2053612	1.11811	1.5	0.1	2.2	45.9	13.3	10.9
	ZA141	4.92E-05	1.086646	1.037875	0.8754784	273.970984	5.63572608	10.7371864	50.0516898	179.323968	39.3860328	1.046991	1.185495	1.241203	1.255678	0.5749693	0.5380832	0.2611114	1.132288	15.5	1.9	20.8	28.3	8.8	6.8
ZA1	ZA142	1.45E-05	1.079308	1.036761	0.8839314	81.6664198	6.964599	344.927298	43.8498782	178.75914	45.3073981	1.041039	1.172897	1.221031	1.2352	0.5971965	0.564457	0.2443811	1.12666	29	3.1	40.1	11.3	3.2	2.5
	ZA161	4.79E-05	1.076516	1.034004	0.8894799	72.0340078	10.2705059	335.904277	30.5107612	178.523091	57.445785	1.041115	1.162481	1.210276	1.222853	0.5777607	0.5454077	0.2564401	1.116574	21.8	2.6	29.6	24.5	7.4	5.7
	ZA163	1.11E-05	1.091297	1.023603	0.885099	57.6933182	12.7315126	323.307149	18.7006532	180.035348	67.1039409	1.066133	1.156485	1.232966	1.239397	0.3884323	0.3434084	0.392768	1.084747	39.4	10.2	42.7	6.3	3.1	2.1
	ZA171	4.88E-05	1.098	1.072181	0.82982	289.046222	19.4416403	30.6962176	29.7735264	170.79575	53.2871055	1.024081	1.292064	1.323178	1.364152	0.8300549	0.8074504	0.1011436	1.261682	862.6	16.4	1446.8	9.9	1.1	1
	ZA174	1.00E-05	1.095703	1.059756	0.844541	63.1964772	10.7988785	326.15818	32.7170412	169.068619	55.1071003	1.033921	1.25483	1.297395	1.327566	0.743754	0.7137511	0.1541562	1.213662	8.7	0.4	13.7	29.8	5.5	4.7
	ZA181	3.55E-05	1.087486	1.056811	0.8557026	284.465878	11.7818424	22.8430647	34.9335805	178.658195	52.55919	1.029026	1.235021	1.270869	1.299308	0.7612621	0.735312	0.141722	1.200185	15.8	0.6	25.2	46.9	8	7
	ZA211	4.03E-05	1.043836	1.025316	0.9308476	320.146738	39.8380104	66.7645972	18.9212015	176.172736	44.1093436	1.018063	1.101486	1.121383	1.131175	0.687474	0.6721735	0.1785463	1.081943	6.5	0.4	9.9	55.3	12.8	10.7
	ZA231	4.36E-05	1.08249	1.017538	0.899972	291.570448	28.1249242	31.2960668	17.5390073	149.213463	55.9794927	1.063832	1.130633	1.202804	1.206801	0.3298053	0.2882716	0.4328889	1.062793	3	0.9	3.1	38.7	22.6	14.8
	ZA241	3.96E-05	1.060436	1.040265	0.8992985	277.70453	30.7713182	38.7658342	40.909214	164.216341	33.7964567	1.019391	1.156751	1.179182	1.197524	0.7669542	0.7496334	0.1335419	1.134747	8.3	0.3	13.4	61.8	11	9.6
	ZA251	4.47E-05	1.059246	1.013581	0.9271727	287.355911	24.0535288	43.3247466	44.4514302	178.522082	35.8765755	1.045053	1.093196	1.142447	1.145324	0.3381893	0.3084923	0.41802	1.046067	1.5	0.4	1.5	52.9	31.1	21
ZA2	ZA252	2.01E-05	1.057666	1.015201	0.9271337	7.24232054	45.2489504	271.54227	5.62330254	176.04764	44.2008201	1.041829	1.094988	1.140791	1.14433	0.377809	0.3493537	0.3885203	1.051025	1.2	0.3	1.3	33.2	17.5	12
	ZA262	3.89E-05	1.083155	1.032542	0.8843037	293.701144	29.9116848	51.9864944	39.4777619	178.899186	36.0980037	1.049017	1.167633	1.224867	1.236213	0.528144	0.4909507	0.2916394	1.113073	4.5	0.7	5.7	44.5	16.7	12.5
	ZA271	3.34E-05	1.097634	1.076084	0.8262815	324.100302	29.7194691	65.8890936	19.6923794	184.437877	53.1706585	1.020026	1.302322	1.328402	1.373114	0.8603537	0.8411683	0.0826997	1.276753	83.8	1.1	143.6	36.5	3.4	3.1
	ZA281	4.51E-05	1.112065	1.018787	0.8691475	306.141868	22.1560235	50.698054	31.6836294	187.430828	49.7142272	1.091558	1.172168	1.27949	1.283859	0.2890897	0.2320198	0.4752322	1.073849	41.7	15.1	38.9	10.4	6.5	4
	ZA282	1.98E-05	1.090681	1.038198	0.8711209	21.349529	21.5026913	285.057514	15.5458961	161.975109	62.9945287	1.050552	1.191796	1.252043	1.266531	0.5612032	0.5219267	0.2714839	1.134447	5.5	0.7	7.3	22.6	7.4	5.7
	ZA291	3.52E-05	1.099896	1.061839	0.838265	329.03332	38.0801345	85.2214485	29.3898877	201.312366	37.9839869	1.035841	1.26671	1.312111	1.34371	0.7407271	0.7090731	0.1568731	1.22288	7.4	0.3	11.6	57.7	11.8	10.1
ZA3	ZA311	6.33E-05	1.043501	0.9964606	0.9600382	291.451997	28.7481403	74.6631525	55.5890735	191.638012	17.260704	1.047207	1.037938	1.086937	1.087108	-0.1066484	-0.1272188	0.7847582	0.9911488	13.1	10.3	6.2	12.5	16.1	7.1
	ZA312	2.76E-05	1.023965	0.9931042	0.982931	221.49052	82.9003197	9.75871819	6.04696099	100.1519	3.70634513	1.031075	1.01035	1.041746	1.043463	-0.4964741	-0.5041522	1.205325	0.9798998	0.1	0.2	0	39.1	67.9	31.4

	ID																							
	ZA321	5.31E-05	1.053549	1.024043	0.922408	262.685637	1.301714	353.455018	30.5800674	170.484848	59.3861892	1.028813	1.110184	1.142173	1.150284	0.5726224	0.5500085	0.2535157	1.079092	12.1	1.4	16.5	32.5	9.9	7.7
	ZA332	6.28E-05	1.040828	1.025255	0.9339162	102.329312	2.66991002	10.6680223	31.8686821	196.607946	57.9928485	1.015189	1.097802	1.114477	1.124592	0.7218319	0.7086862	0.157098	1.081378	8.4	0.4	13.1	55.1	11.1	9.5
	ZA333	1.29E-05	1.023106	1.014679	0.9622148	26.166526	18.9555527	118.832127	7.71130426	229.974828	69.4235256	1.008305	1.054525	1.063282	1.068861	0.7304345	0.7232256	0.1486747	1.04584	2.2	0.1	3.6	49.4	10.6	9.2
	ZA334	1.46E-05	1.024734	1.012053	0.9632137	43.1291657	12.4850658	307.815111	22.6983603	159.806762	63.7485695	1.01253	1.050704	1.06387	1.067689	0.5977452	0.5877365	0.2298182	1.037701	0.7	0.1	1	53.3	19.2	15.5
	ZA351	4.98E-05	1.039891	1.034073	0.9260355	330.475486	38.1452583	68.8980988	10.5643664	171.688064	49.8872781	1.005627	1.116667	1.12295	1.139716	0.9032245	0.8977921	5.24E-02	1.110419	2.7	0	4.7	108.7	18.3	17.4
	ZA362	4.63E-05	1.039288	1.036924	0.9237884	327.779042	34.0251456	66.7080787	12.9469122	174.426513	52.9332691	1.00228	1.122469	1.125028	1.144236	0.9613413	0.9590661	2.07E-02	1.119916	7.7	0	14.2	114.6	10.7	10.5
	ZA364	9.90E-06	1.054001	1.010811	0.9351872	29.1424281	19.7401945	293.168541	16.1737501	166.612509	64.0363492	1.042728	1.080865	1.127048	1.129062	0.3003452	0.2729865	0.4442506	1.036575	3	1	2.9	19.9	11.7	7.5
	ZA371	4.62E-05	1.037863	1.030572	0.9315652	241.020662	13.1026412	335.571762	18.8245942	118.173346	66.7748382	1.007075	1.10628	1.114107	1.128517	0.8695002	0.862807	7.10E-02	1.098507	8.9	0.1	15.4	84.8	10.3	9.6
ZA4	ZA412	3.54E-05	1.087149	1.07874	0.834111	51.4842846	22.8706067	314.748607	15.539159	193.46275	61.8334192	1.007796	1.293281	1.303363	1.351956	0.9413822	0.9335328	3.38E-02	1.283277	51.1	0.1	92.5	79.9	4.2	4.1
	ZA421	2.63E-05	1.073144	1.009757	0.9170991	12.7935325	25.9974776	103.717446	1.89372959	197.591355	63.9232033	1.062775	1.101033	1.170151	1.171698	0.2250658	0.187571	0.509748	1.035998	7	2.9	6.1	11.8	8.1	4.8
	ZA422	5.51E-05	1.062943	1.048864	0.8881928	289.039193	16.9170253	26.3775554	22.7802973	165.714948	61.0300425	1.013423	1.180897	1.196748	1.221574	0.85152	0.8388636	8.40E-02	1.165255	83.7	1.1	143.4	36	3.4	3.1
	ZA441	4.24E-05	1.162007	0.9393551	0.8986378	300.511289	12.5202143	34.7691559	18.4869569	178.250189	67.411493	1.237026	1.04531	1.293076	1.316264	-0.6551798	-0.6907968	1.464399	0.8450184	6.1	9.4	0.3	13.1	59	11.1
	ZA451	5.06E-05	1.057231	1.039837	0.9029319	291.025843	16.6768542	29.3658403	25.8352388	171.699934	58.5477727	1.016728	1.151623	1.170887	1.189324	0.7896895	0.7745394	0.1194639	1.132675	11.6	0.3	19.1	59.4	9.2	8.2
	ZA462	5.17E-05	1.081388	1.038691	0.8799208	306.554064	25.2420263	49.0128259	24.5885101	177.096592	53.4294921	1.041107	1.180437	1.228961	1.244271	0.6092096	0.5761368	0.237051	1.133829	4.9	0.5	6.9	49.9	15.2	12.1
	ZA463	2.22E-05	1.076774	1.030334	0.8928931	0.43041711	31.8034685	92.0342701	2.58429907	186.187187	58.0666392	1.045073	1.153927	1.205938	1.216285	0.5291347	0.4948891	0.2890567	1.10416	4.1	0.6	5.3	24.4	8.7	6.5
	ZA473	4.92E-05	1.10155	1.003868	0.8945819	306.59707	13.1526445	43.1199613	25.9264621	192.234457	60.4695878	1.097306	1.122164	1.231358	1.231852	0.1076356	5.61E-02	0.6177469	1.022654	6.4	3.6	4.5	21	18.8	10.1
	ZA482	5.42E-05	1.106611	1.017054	0.8763348	311.001013	13.0369202	49.9739192	33.963791	203.138629	52.9514093	1.088055	1.160577	1.262772	1.26651	0.2765668	0.2221788	0.482792	1.066653	7.4	2.8	6.8	23.7	15.3	9.4
ZA5	ZA511	7.20E-05	1.084749	1.078266	0.8369852	98.9288769	22.2208301	358.396711	24.1057656	226.498007	56.1775657	1.006012	1.288274	1.296019	1.344484	0.9537694	0.9476739	2.65E-02	1.280576	27	0	49.2	98.1	5.8	5.6
	ZA521	7.83E-05	1.081268	1.070525	0.8482059	23.9931544	27.6507781	119.214625	9.8541062	226.985304	60.3545482	1.010035	1.262106	1.274771	1.316188	0.9177378	0.90781	4.72E-02	1.249566	77.5	0.3	138.3	58.5	3.4	3.3
	ZA531	6.46E-05	1.108173	1.036622	0.8552059	352.725855	28.2619278	91.5479399	15.9227709	207.418257	56.8223356	1.069023	1.212131	1.295796	1.308768	0.4848411	0.4343051	0.3294378	1.133868	47.6	9	57.5	13.4	5.3	3.8
	ZA542	3.18E-05	1.113815	1.070478	0.8157074	12.8235898	25.7038023	107.487216	9.58745118	216.267813	62.3157511	1.040484	1.312331	1.365459	1.403678	0.7451879	0.7092526	0.1567687	1.26127	6.3	0.3	9.9	33.4	6.4	5.5
	ZA544	7.37E-05	1.100592	1.039732	0.8596749	335.219734	20.1404532	79.7165817	34.315761	220.586675	48.6553067	1.058534	1.209448	1.280242	1.295317	0.5394855	0.494767	0.2891369	1.142569	9.3	1.4	12.1	32.6	11.6	8.7
	ZA551	8.75E-05	1.094335	1.061059	0.8446061	331.848684	19.6122978	72.2707979	26.9159296	210.360274	55.6985611	1.031362	1.256276	1.295675	1.32706	0.7615744	0.7334988	0.1427622	1.218075	127.2	4.8	202.6	18.2	2.8	2.5
	ZA561	6.45E-05	1.101532	1.070751	0.827717	329.328738	12.1231516	69.5097917	39.2363652	225.335668	48.1671196	1.028747	1.29362	1.330808	1.370139	0.8016587	0.7751701	0.1191098	1.257471	2.8	0.1	4.5	87.2	18.7	16.6
	ZA571	7.24E-05	1.084974	1.05732	0.857706	349.97642	24.7784896	88.3768163	17.5615341	210.030549	58.9072249	1.026155	1.23273	1.264972	1.294082	0.7803123	0.7566382	0.1295636	1.20131	44.7	1.4	72.3	32.5	4.8	4.2
	ZA581	7.27E-05	1.080344	1.004345	0.9153113	338.689472	24.0720297	112.391867	57.1137759	238.814283	21.0018509	1.07567	1.097271	1.180302	1.180771	0.1199384	7.90E-02	0.598263	1.020081	1.1	0.6	0.8	47.6	41.9	24.1
	ZA591	6.76E-05	1.082983	1.045621	0.8713967	0.91278135	32.9420875	105.653424	21.4388249	222.573494	49.0641722	1.035732	1.199936	1.242813	1.262875	0.6769813	0.6468377	0.1936814	1.15854	8.9	0.6	13.2	46.2	11.1	9.1
MK1	MK111	7.21E-05	1.067844	1.025423	0.9067328	239.481298	20.3876281	101.629101	63.3766925	335.749688	16.3720474	1.041369	1.130899	1.177683	1.185708	0.5042968	0.4734017	0.3032176	1.085974	19.4	3.1	24.5	22.3	8.2	6
	MK112	3.16E-05	1.035982	1.013174	0.9508441	143.619275	66.9160595	266.181478	12.9195564	0.65744323	18.7888903	1.022511	1.065552	1.089539	1.093078	0.4808039	0.46421	0.3093286	1.042093	0.9	0.1	1.1	43.1	18.9	14.1
	MK122	9.95E-05	1.058794	0.9977823	0.9434234	133.701048	60.6649225	248.597921	13.3106091	345.113311	25.6230797	1.061147	1.057619	1.122289	1.122307	-2.89E-02	-5.77E-02	0.7189294	0.9966747	0.3	0.2	0.2	65.2	69.8	40.7
	MK131	7.40E-05	1.06659	0.9882944	0.9451152	105.351402	65.4573393	253.42109	21.1830758	348.073036	11.8201549	1.079223	1.045687	1.128529	1.130072	-0.2610717	-0.289084	0.9510323	0.9689256	3.4	3.4	1	21.4	36.9	14
	MK132	3.71E-05	1.064236	0.9823498	0.9534143	175.990318	75.7188948	72.6430163	3.36298298	341.812089	13.8631095	1.083357	1.030349	1.116236	1.120431	-0.4562171	-0.4777997	1.171833	0.9510707	2.8	3.6	0.4	10.6	27.8	7.8
	MK141	8.31E-05	1.089273	0.9714886	0.9392384	111.411549	56.3658369	270.58664	31.8732536	6.64054147	9.62642909	1.121241	1.034336	1.159741	1.16806	-0.5443872	-0.5700978	1.292314	0.9224921	13.3	18.5	1.4	9.4	32.6	7.4
	MK151	7.27E-05	1.051947	1.011003	0.93705	94.3669625	50.5021212	241.993874	34.8442899	343.686148	16.2303891	1.040498	1.078921	1.122615	1.124727	0.3135209	0.2872969	0.4336104	1.036928	1.3	0.4	1.3	54.3	33.5	22.3
	MK153	3.47E-05	1.046847	1.010452	0.9427013	81.7064082	70.3093727	219.392061	14.8223867	312.801773	12.6667507	1.036019	1.071868	1.110476	1.112504	0.324637	0.3010727	0.4234546	1.034603	0.6	0.2	0.7	39.1	23.6	15.9
	MK161	9.29E-05	1.053951	0.99896	0.947089	153.328149	70.7105261	251.972232	3.01109359	343.012085	19.034522	1.055048	1.054769	1.112832	1.112832	-2.47E-03	-2.92E-02	0.6928717	0.9997355	2	1.3	1.2	33.4	35.1	17.9
	MK162	4.14E-05	1.0688	0.9802392	0.9509607	106.60208	81.3165246	233.668285	5.25947675	324.305623	6.88992775	1.090347	1.030788	1.123917	1.128893	-0.4808427	-0.5030801	1.203947	0.9453767	1.4	1.8	0.2	14.9	38.8	11.3
MK2	MK221	7.40E-05	1.039284	1.003377	0.9573384	342.205617	59.2308153	102.395527	16.6678555	200.444185	25.0628631	1.035786	1.048091	1.085597	1.085904	0.1437926	0.1236477	0.5611082	1.01188	1.2	0.6	0.9	47.8	39	23.1
	MK241	7.03E-05	1.035022	1.013585	0.9513927	319.393012	10.7201226	61.9014845	48.8433685	220.52841	39.1450206	1.02115	1.06537	1.087902	1.091698	0.5031743	0.4873349	0.2940154	1.043304	2.7	0.4	3.4	54	21.5	16.1
	MK242	3.18E-05	1.048149	1.00776	0.944092	73.4185365	51.3719228	339.97067	2.75139435	247.780465	38.492648	1.040078	1.067438	1.110219	1.111406	0.2483378	0.2237097	0.481613	1.026305	1	0.4	0.9	30.1	20.2	12.7
	MK243	3.01E-05	1.025155	1.015115	0.9597302	18.4266548	43.3395206	132.340815	23.2469768	241.697867	37.6535033	1.009891	1.057708	1.06817	1.073743	0.7015017	0.693064	0.1662228	1.047349	1.8	0.1	2.8	49.3	11.9	10.1
	MK262	6.55E-05	1.091125	0.9596906	0.9491847	191.522053	41.4093427	339.99349	44.024547	86.4980822	16.3798646	1.136955	1.011068	1.149539	1.167607	-0.8420281	-0.8519669	1.724338	0.8892776	35.4	61.1	0.4	5.2	54.7	4.8
	MK264	3.14E-05	1.039347	1.002705	0.9579481	139.167046	77.4442306	359.034838	9.70040092	267.67652	7.89501848	1.036543	1.046722	1.084972	1.085183	0.119826	9.97E-02	0.5808947	1.00982	0.8	0.4	0.6	28.8	24.3	13.9
	MK271	8.57E-05	1.060388	1.014425	0.9251872	344.975569	62.0906027	184.867471	26.4769721	90.7536937	8.19581421	1.04531	1.096454	1.146134	1.149302	0.350217	0.3200729	0.4095859	1.048927	4.5	1.3	4.7	34	18.3	12.2
	MK273	6.43E-05	1.045376	0.9963769	0.9582479	45.6554172	41.7432758	233.59356	47.9825252	139.192443	3.95502126	1.049177	1.03979	1.090924	1.091093	-0.1032664	-0.1247551	0.7823713	0.9910535	1.2	0.9	0.6	20.1	25.2	11.6
	MK281	7.89E-05	1.04704	1.002833	0.9501268	341.044235	70.8705001	159.359842	19.1218364	249.540641	0.52145672	1.044083	1.055473	1.102001	1.102223	0.1117083	8.77E-02	0.590933	1.010909	4.1	2.1	3	26.9	22.8	12.6

Group	Sample																							
	MK282	3.56E-05	1.03987	1.015737	0.9443924	173.910973	61.4767836	14.2945779	26.9965062	279.916269	8.52245881	1.023759	1.075546	1.1011	1.105652	0.5123799	0.4944801	0.2893248	1.050585	3.4	0.5	4.4	26.4	9.5	7.2
MK3	MK321	7.82E-05	1.047269	1.00569	0.9470405	151.881259	33.2073872	272.203686	37.6429414	34.7310876	34.8819049	1.041344	1.061929	1.105834	1.106534	0.1945844	0.1703128	0.5234103	1.019768	5.7	2.4	4.8	25.2	18.2	10.8
	MK322	3.18E-05	1.079547	0.9705595	0.949894	163.554499	35.8279031	311.770572	49.6578169	61.5679361	16.0485734	1.112293	1.021756	1.136492	1.146845	-0.6635725	-0.6812177	1.450087	0.9186028	4.3	6.6	0.2	7.8	35.9	6.6
	MK323	3.43E-05	1.076452	0.990989	0.9325589	124.292977	2.18039501	18.8952919	81.8397775	214.594117	7.85970171	1.086241	1.062656	1.1543	1.154945	-0.1529793	-0.1878704	0.8448187	0.9782876	4.5	3.9	1.8	10.1	14.6	6
	MK331	2.84E-05	1.034082	1.006559	0.9593588	272.904802	69.0041522	100.022947	20.8479851	9.11678225	2.37801042	1.027344	1.0492	1.077889	1.078944	0.2806697	0.2633371	0.4514779	1.021275	0.4	0.1	0.4	42.6	28.2	18.7
	MK332	3.63E-05	1.035709	0.9832888	0.981002	180.900885	41.6425009	84.1401192	7.54196391	345.871914	47.3654624	1.053311	1.002331	1.055766	1.063284	-0.9141886	-0.9163985	1.839504	0.9516002	1	1.8	0	29.1	117.9	28
	MK351	4.20E-05	1.086604	0.967896	0.9455004	31.4926666	48.8935315	147.166749	20.7083658	251.747258	33.6603131	1.122645	1.023687	1.149237	1.160617	-0.663397	-0.6825637	1.45209	0.9118524	2.9	4.4	0.2	18.9	72.9	16
	MK352	1.87E-05	1.126406	0.9852859	0.8883086	34.5645939	73.422641	185.438597	14.5764261	277.45981	7.72389771	1.143228	1.109171	1.268034	1.268848	-0.1273555	-0.1853983	0.8423202	0.9702098	0.7	0.6	0.3	47.2	60.7	29.8
	MK361	3.95E-05	1.0739	0.9920351	0.9340645	186.531431	62.3851902	31.5588216	25.3608976	296.663164	10.2065305	1.082523	1.062063	1.149707	1.150206	-0.1367747	-0.1708766	0.8277313	0.9810999	4.3	3.7	1.8	10.4	14.9	6.2
	MK362	1.46E-05	1.091882	0.9841149	0.924004	245.634825	66.9980016	37.2024611	20.4711464	130.991335	10.0379922	1.109506	1.065055	1.181685	1.183649	-0.2449287	-0.2838718	0.9453691	0.959936	2	2	0.6	14.1	24.2	9.1
	MK363	1.53E-05	1.099688	1.005482	0.8948302	200.716158	74.51212	23.9789031	15.4639782	293.746708	0.83930234	1.093692	1.123657	1.228934	1.229659	0.1311178	8.03E-02	0.5971639	1.027398	5.8	3.1	4.2	11.4	9.8	5.3
Mz7	MZ711	3.25E-05	1.075061	1.00698	0.9179592	303.023686	14.4504018	54.1375459	54.4210236	203.862852	31.708218	1.067609	1.096977	1.171142	1.17205	0.1717701	0.1332866	0.5532299	1.027508	4.5	2.1	3.6	26.9	20.9	12
	MZ712	1.61E-05	1.041909	1.017545	0.9405459	350.598262	37.1360894	259.711972	1.17013498	168.167788	52.8390913	1.023944	1.081866	1.107771	1.11312	0.5376216	0.5192658	0.2732014	1.056568	0.6	0.1	0.9	50.4	20.9	16.2
	MZ713	1.30E-05	1.099652	0.9955777	0.9047711	356.663131	37.40911	89.0719836	3.14553623	183.165957	52.412286	1.104536	1.100364	1.215392	1.215407	-1.94E-02	-6.81E-02	0.7285869	0.9962229	2.2	1.6	1.2	15.6	17.8	8.5
	MZ731	3.53E-05	1.075207	0.9916284	0.9331648	281.73729	43.4987377	54.8780054	35.77648	164.915962	25.430937	1.084284	1.062651	1.152215	1.152765	-0.1422376	-0.1768119	0.8336759	0.9800487	3.2	2.7	1.3	23.7	33	14.2
	MZ733	1.67E-05	1.056136	1.016977	0.9268874	349.297556	61.0265259	79.4671447	9.39E-02	169.519148	28.9732935	1.038506	1.097196	1.139444	1.143785	0.4211321	0.3940469	0.3570682	1.056514	3.5	0.8	4.1	22	9.9	7
	MZ741	2.83E-05	1.041366	1.020227	0.9384073	12.1779026	30.0582275	272.238424	16.6080273	157.243891	54.7816974	1.02072	1.08719	1.109716	1.116605	0.6060009	0.5893618	0.2288085	1.06512	0.5	0	0.6	95.5	45.2	37.3
	MZ751	3.64E-05	1.072147	1.010639	0.9172143	80.4085129	10.7424212	339.958593	43.7121442	181.076521	44.2967394	1.060861	1.101856	1.168916	1.170703	0.2429309	0.206	0.4953213	1.038644	1.2	0.5	1.1	51.7	36.8	23.2
	MZ752	1.27E-05	1.031119	1.02846	0.9404213	269.036341	19.1575704	14.3395571	37.2241949	157.552987	46.5109854	1.002585	1.093616	1.096444	1.110551	0.9439174	0.9413717	2.98E-02	1.090797	0.5	0	0.9	85.5	20.8	20.2
	MZ761	2.32E-05	1.051217	1.018564	0.9302189	291.323782	51.8873429	57.8438828	25.0247762	161.428587	26.7087555	1.032058	1.094972	1.130075	1.135379	0.4839021	0.4602644	0.3119621	1.060959	3.7	0.6	4.6	45.5	18.5	13.6
	MZ771	2.47E-05	1.035605	0.990052	0.9743423	169.858065	3.64579531	78.110053	25.5821386	267.405486	64.1216716	1.046011	1.016123	1.062876	1.065276	-0.4754002	-0.4871418	1.183626	0.9714268	1	1.3	0.1	34	73.9	25.9
Mz8	MZ822	1.54E-05	1.076381	0.995503	0.9281164	27.2797359	63.0043307	237.304724	23.8007624	141.927817	11.9944105	1.081243	1.072606	1.159747	1.159831	-5.41E-02	-9.10E-02	0.7500793	0.9920117	6	4.5	3.1	9.5	11.3	5.2
	MZ823	2.98E-05	1.074195	1.008493	0.9173115	45.6988372	50.5215497	187.392964	32.8774875	290.496567	19.3281256	1.065149	1.099401	1.171026	1.17226	0.2004761	0.1624116	0.5297149	1.032157	9.6	4.2	8	19.5	14.1	8.3
	MZ824	1.48E-05	1.075482	0.9917271	0.9327917	51.1003761	69.6041165	228.373391	20.3746874	318.704193	0.89061014	1.084453	1.063182	1.152971	1.1535	-0.1391705	-0.1739372	0.8307937	0.9803851	5.3	4.5	2.2	9.5	13.3	5.6
	MZ831	4.62E-05	1.043407	1.034242	0.9223507	90.4294749	19.9960696	307.138292	65.5862116	185.41236	13.4248369	1.008862	1.121311	1.131248	1.147503	0.8569191	0.8485842	7.87E-02	1.111462	1.3	0	2.2	107.9	26.2	24.3
	MZ842	1.63E-05	1.077572	0.9746319	0.9477963	64.0366045	58.0361353	283.398219	25.7547762	184.594374	17.6012221	1.105619	1.028314	1.136924	1.144511	-0.5648549	-0.5864314	1.314594	0.9300792	1.2	1.7	0.1	15.3	46.4	12.2
	MZ843	3.34E-05	1.048682	0.9890347	0.962283	63.3205274	66.6710924	267.710697	21.4437961	174.242763	8.75507372	1.060309	1.0278	1.089786	1.091814	-0.3621655	-0.380742	1.054301	0.9693405	0.4	0.4	0.1	53	84.4	39.5
	MZ851	1.53E-05	1.05653	0.9947142	0.948756	34.4589087	78.9564302	182.51336	9.40348515	273.467002	5.73873993	1.062144	1.04844	1.113595	1.113885	-0.1206925	-0.1471354	0.8041987	0.9870982	0.7	0.5	0.3	25.6	32.8	15.4
	MZ852	3.04E-05	1.071553	1.020125	0.9083224	101.853353	58.005445	232.32154	22.0711049	331.718935	21.9344028	1.050413	1.123087	1.179705	1.18497	0.4047889	0.3698741	0.373976	1.069186	81.6	19.4	91.6	9.2	4.2	2.9
	MZ853	1.41E-05	1.079212	0.9796417	0.9411467	80.9384478	64.7656462	262.393612	25.2272288	172.129221	0.56114639	1.101639	1.040902	1.146699	1.151135	-0.4142934	-0.4423645	1.127889	0.9448667	0.7	0.8	0.1	21.4	45.3	15.7
	MZ861	4.23E-05	1.07162	0.9880733	0.9403068	56.55963	47.2900446	305.191081	18.5900783	200.630299	36.7769504	1.084555	1.050799	1.139649	1.141096	-0.241884	-0.2724797	0.9330674	0.9688755	24	23.7	7.8	8.3	14.4	5.3
Mz9	MZ911	1.54E-05	1.063278	0.9820051	0.9547171	65.6533979	55.5511402	317.755416	11.9044321	220.249501	31.7839577	1.082762	1.028582	1.11371	1.118178	-0.4766507	-0.4972759	1.196517	0.9499617	4.6	5.9	0.7	16.4	44.5	12.4
	MZ912	9.17E-06	1.073254	0.9768494	0.9498968	77.930109	63.9346355	333.354848	7.01748411	240.069467	24.9653389	1.098689	1.028374	1.129864	1.136472	-0.5416889	-0.5630141	1.282744	0.9360011	1.2	1.6	0.1	15.6	44.9	12.3
	MZ922	2.01E-05	1.07489	0.9860368	0.9390732	78.3269653	44.1160661	336.708864	11.73347	235.335971	43.5136612	1.090111	1.050011	1.144629	1.146602	-0.277463	-0.3084277	0.9722398	0.963214	6	6.2	1.7	16.1	29.4	10.6
	MZ931	1.89E-05	1.080667	0.9701624	0.9491709	23.0680407	44.593139	117.666938	4.64943442	212.33672	45.0303834	1.113903	1.022116	1.138538	1.149032	-0.6628054	-0.6807279	1.449357	0.9175983	1.8	2.8	0.1	23.5	81.3	19.9
	MZ942	2.00E-05	1.057739	1.003649	0.9386122	47.6851449	55.4301032	158.368808	13.6791444	256.79469	31.0497072	1.053893	1.06929	1.126918	1.127248	0.1213872	9.19E-02	0.5874114	1.01461	0.6	0.3	0.5	59	51.7	31.2
	MZ951	7.96E-06	1.040823	0.9892018	0.969975	28.2056385	56.3157402	154.80752	21.67354	255.213609	24.4417025	1.052184	1.019822	1.073041	1.07548	-0.4431474	-0.4572356	1.146181	0.9692425	1.2	1.4	0.2	16.5	38.4	12.2
	MZ952	1.60E-05	1.04542	1.000413	0.9541672	14.6045856	56.414733	135.827005	18.9937969	235.739552	26.5705814	1.044988	1.048467	1.095636	1.095658	3.64E-02	1.36E-02	0.6546549	1.003329	0.6	0.3	0.4	56.9	55.8	32
	MZ961	9.04E-06	1.055977	1.012024	0.9319994	40.8623501	63.3327308	252.648771	23.117932	157.191911	12.5579906	1.043431	1.085863	1.133023	1.135408	0.3191684	0.2909486	0.43091	1.040666	1	0.3	1	32.4	19.2	12.7
	MZ964	1.52E-05	1.030917	0.9949301	0.9741523	328.372832	62.4691911	94.1873523	16.9625863	190.914523	21.0092833	1.036171	1.021329	1.058271	1.058916	-0.2547293	-0.2679371	0.9281895	0.9856766	1	0.9	0.3	38.5	59	25.5
Mz10	MZ1011	1.95E-05	1.071169	0.9693685	0.9594619	346.681006	56.1858069	103.273074	16.6901187	202.629518	28.4680321	1.105018	1.010325	1.116427	1.129387	-0.8134578	-0.8226321	1.67416	0.9143069	1.3	2.1	0	13.6	68.2	12.5
	MZ1013	3.98E-05	1.027557	1.001087	0.9713564	336.524719	47.0210571	78.3164273	10.78138	177.831853	40.9623594	1.026441	1.030607	1.057858	1.057909	7.20E-02	5.80E-02	0.6160673	1.004059	0.1	0.1	0.1	93.2	89.5	65.7
	MZ1021	4.00E-05	1.035947	1.031634	0.9324198	294.728595	20.693341	62.878475	58.5542579	195.696181	22.5685644	1.004181	1.106405	1.11103	1.12664	0.92075	0.9166787	4.25E-02	1.101798	4.3	0	7.7	108.1	14.5	13.9
	MZ1031	1.93E-05	1.038087	1.001419	0.9604947	66.9482824	29.134121	326.264558	18.3976256	208.430957	54.5350342	1.036616	1.042607	1.080783	1.08086	7.42E-02	5.48E-02	0.6187875	1.005779	1	0.6	0.7	25.5	23.1	12.7
	MZ1035	3.43E-05	1.051028	0.9810531	0.9679188	59.6512107	34.774858	259.953671	53.4851135	156.5137	9.76383382	1.071327	1.01357	1.085864	1.092395	-0.6727606	-0.6839287	1.454124	0.9460882	0.7	1.1	0	35.5	96.4	30.4
	MZ1042	5.13E-05	1.051442	1.020204	0.9283534	338.999105	61.3332761	102.561745	16.8178882	199.753064	22.4973003	1.030619	1.09894	1.132588	1.138718	0.515525	0.492432	0.2906675	1.06629	6.1	0.9	7.8	39.3	14.4	10.8

	MZ1061	2.54E-05	1.038422	1.034369	0.9272103	322.893291	35.1970912	81.282458	33.9830232	201.313524	36.5920712	1.003918	1.115571	1.119942	1.137238	0.9309517	0.9271097	3.71E-02	1.111216	11.1	0	19.9	64.5	4.5	4.4
	MZ1062	4.45E-05	1.048445	1.018943	0.9326122	50.19553	47.5415326	299.911071	17.5997051	196.01734	37.1247446	1.028954	1.092569	1.124202	1.129855	0.5124044	0.4906095	0.2918635	1.061825	5.3	0.8	6.8	41.4	15.3	11.5
	MZ1072	2.44E-05	1.058492	0.9793781	0.9621299	354.632812	70.3826271	97.8639302	4.66378276	189.474535	19.0105865	1.08078	1.017927	1.100155	1.106858	-0.6276972	-0.6420119	1.392723	0.9418453	0.5	0.7	0	22.3	62	18.6
	MZ1073	4.07E-05	1.057216	0.998988	0.9437956	32.1276238	62.9843489	266.940476	16.3734167	170.510191	20.8656687	1.058287	1.058479	1.120175	1.120175	1.60E-03	-2.68E-02	0.6906747	1.000181	61	40.2	36.1	6.4	6.7	3.3
	MZ1111	3.25E-04	1.045211	1.0081	0.9466886	72.4508499	51.3679472	164.944198	1.99126226	256.532434	38.5611125	1.036813	1.06487	1.10407	1.105388	0.269702	0.2466537	0.4640759	1.027061	5.9	2.1	5.6	27.2	16.8	10.6
	MZ1122	3.06E-05	1.102931	0.9737526	0.9233164	352.082442	27.0408361	128.568698	54.8609969	250.980337	20.6690469	1.132661	1.054625	1.194532	1.200178	-0.4015869	-0.4383952	1.123042	0.9311042	1.8	2.2	0.3	26.4	57.7	19.3
	MZ1131	3.62E-04	1.114165	1.003406	0.8824296	79.5770327	43.4007746	325.063272	23.689235	215.569989	37.2555132	1.110384	1.137094	1.262611	1.26312	0.1019395	4.41E-02	0.6280462	1.024055	3.3	1.9	2.2	28.5	26.2	14.1
	MZ1134	2.23E-05	1.050539	0.9997423	0.9497182	29.6340571	58.0625707	128.912083	5.73895948	222.414737	31.2957441	1.05081	1.052673	1.106159	1.106165	1.76E-02	-7.67E-03	0.6735002	1.001772	4.8	3	3	11.5	11.6	5.8
Mz11	MZ1141	2.89E-05	1.103215	0.9549102	0.9418751	10.8199617	15.2220047	232.826066	69.8877557	104.372617	12.8289566	1.155307	1.013839	1.171296	1.191455	-0.82614	-0.8384147	1.700986	0.8775496	3.3	5.7	0	16.8	95.2	15.5
	MZ1153	1.63E-05	1.024114	1.00122	0.9746665	358.512631	51.8305122	206.391726	34.7926296	106.618943	13.7280733	1.022866	1.027243	1.050732	1.050797	8.63E-02	7.40E-02	0.6024623	1.00428	0.1	0	0	65	61.6	44.8
	MZ1154	3.26E-05	1.040954	1.001491	0.9575553	47.6741927	160.747865	40.5219286	259.576198	10.1793507	1.039404	1.045883	1.087095	1.087179	7.44E-02	5.36E-02	0.6198297	1.006234	5.3	3	3.7	22.9	20.7	11.1
	MZ1162	3.80E-05	1.025088	1.000684	0.9742278	278.415539	18.9819652	37.771009	54.9439544	177.762231	28.2552931	1.024387	1.027156	1.052205	1.05223	5.31E-02	4.04E-02	0.6312589	1.002704	2	1.2	1.4	35.1	32.6	17.7
	MZ1163	1.44E-05	1.043278	0.9851543	0.971568	56.9470622	47.483341	187.339487	30.7165309	294.387516	26.263364	1.058999	1.013984	1.073808	1.078421	-0.6099785	-0.6210757	1.362866	0.9574925	0.5	0.7	0	22.4	60.4	18.4
	MZ1171	3.32E-05	1.033944	1.012972	0.9530839	6.04973673	49.187274	152.102659	35.6167921	254.962909	17.259777	1.020704	1.062836	1.084841	1.088408	0.4967126	0.4812754	0.2980081	1.041278	4.4	0.7	5.6	44.1	16.9	12.6
	MZ1211	3.48E-05	1.04816	1.000926	0.9509137	343.987549	30.7830522	111.899265	45.8866085	235.398773	28.1515657	1.04719	1.052594	1.102266	1.102316	5.29E-02	2.86E-02	0.6415132	1.00516	43.6	25.7	28.8	8	7.5	3.9
	MZ1212	1.74E-05	1.051507	0.9914245	0.9570683	18.0722168	32.2378425	124.153456	23.7122737	243.445041	48.0843054	1.060603	1.035897	1.098675	1.099751	-0.2504556	-0.2724157	0.9329987	0.9767064	1.5	1.4	0.5	16.4	27.3	10.6
	MZ1221	2.68E-05	1.084664	0.9885307	0.9268051	3.20406054	30.1495186	189.13619	59.7166928	94.7055502	2.58299624	1.097249	1.0666	1.170326	1.171319	-0.1801206	-0.2179671	0.8755948	0.9720677	4.4	4	1.6	19.9	30.2	12.3
	MZ1231	4.05E-05	1.048236	0.9982582	0.9535051	346.54526	50.8663784	113.20317	25.9095598	217.591601	27.0914076	1.050066	1.046935	1.099351	1.099368	-3.15E-02	-5.52E-02	0.7166137	0.9970192	0.8	0.5	0.4	48.1	52.4	27.7
Mz12	MZ1241	3.80E-05	1.040212	1.017846	0.9419419	351.117397	20.8606206	95.0963627	32.3708269	234.123994	49.9838219	1.021974	1.080583	1.104327	1.109965	0.5619378	0.5448074	0.256822	1.057349	0.9	0.1	1.2	80.5	34.5	27.3
	MZ1251	3.37E-05	1.058474	0.9852285	0.9562976	355.56769	36.4261037	119.119477	36.8308865	237.570457	32.4608813	1.074343	1.030253	1.106845	1.109997	-0.4128023	-0.4337054	1.117334	0.9589608	6.2	7.4	1.2	14.7	35.2	10.6
	MZ1261	3.44E-05	1.037877	0.9987013	0.9634222	63.545736	60.9292506	319.775122	7.53814075	225.758333	27.8944753	1.039226	1.036619	1.077281	1.077297	-3.38E-02	-5.23E-02	0.7140098	0.9974905	2.6	1.8	1.5	28.7	31.6	15.6
	MZ1262	1.77E-05	1.028691	0.9955476	0.9757612	7.87251027	60.7108745	108.460445	5.88450431	201.678851	28.5779269	1.033292	1.020278	1.054245	1.054777	-0.239938	-0.2523569	0.9115871	0.9874054	0.2	0.2	0.1	38.3	52.9	26.3
	MZ1271	3.59E-05	1.031617	1.005975	0.9624082	2.75637069	18.9166112	104.264425	30.2061378	245.453004	53.2362495	1.02549	1.045268	1.071912	1.072845	0.2750891	0.2589923	0.454747	1.019287	0.4	0.1	0.4	76	54.8	37.9
	MZ1273	1.41E-05	1.026163	1.00936	0.9644783	165.810357	7.96556798	68.9041753	40.6733308	264.819544	48.2166957	1.016647	1.046535	1.063956	1.066318	0.467372	0.4552011	0.31535	1.029398	0.3	0	0.4	57.7	30.6	23.3

C

Article 3

Staneczek Dorota, Marynowski Leszek, 2025. Application of biomarker and non-biomarker parameters to assess maturity using the Central Carpathian Paleogene Basin as a case study. Organic Geochemistry 201, 104933.

Application of biomarker and non-biomarker parameters to assess maturity using the Central Carpathian Paleogene Basin as a case study☆

Dorota Staneczek , Leszek Marynowski [*]

Institute of Earth Sciences, Faculty of Natural Sciences, University of Silesia in Katowice, Będzińska 60, 41-200 Sosnowiec, Poland

ARTICLE INFO

ABSTRACT

This study employs an integrated approach to investigate the thermal maturity of sedimentary rocks within the Central Carpathian Paleogene Basin (CCPB) by combining biomarker and non-biomarker parameters. The research primarily applies biomarker ratios based on the distribution of aliphatic and aromatic hydrocarbons and compares them with other paleotemperature indicators such as Rock-Eval pyrolysis. The results reveal a notable thermal gradient across the CCPB. The highest maturity levels are recorded in the Spiš Basin with calculated vitrinite reflectance values exceeding 2.0 %, and the least mature in the Orava Basin and Šariš Upland. The latter two contain unsaturated compounds, indicating immature organic matter. The variations in the paleotemperature pattern emerge from the changing thickness of overlying rocks in these areas. The findings suggest that the calculated vitrinite reflectance derived from the methylphenanthrene index (MPI1) is the most appropriate method for characterizing the broadest maturity range. When comparing the results of the illite/smectite-derived paleotemperatures with biomarker-derived ones, there is a good agreement in the results of the rocks with a higher degree of maturity. In contrast, at lower maturities, the illite/smectite-derived paleotemperatures appear to be overestimated. This study highlights the limitations of using a single maturity indicator and argues for a comprehensive approach combining different parameters to accurately reconstruct paleotemperatures. These results advance our understanding of the geological evolution of the CCPB and provide valuable information for future hydrocarbon exploration in the region. The CCPB is an excellent testing ground for comparing different maturity parameters.

1. Introduction

The thermal maturity of sedimentary rocks is one of the most important parameters considered in fossil fuel exploration (Hunt, 1995). However, the correct estimation of thermal maturity is not always straightforward as it requires the use of more than one investigation indicator and the results obtained may not always agree.

There are numerous methods for determining thermal maturity. These can be broadly divided into methods based on the properties of organic matter and other, i.e., mineralogical methods. Methods using organic matter to estimate thermal maturity are broad and include both petrographic and chemical techniques. Vitrinite reflectance is a widely used technique, covering a wide temperature range (Taylor et al., 1998), often supplemented by the fluorescence of organic matter (Pradier et al., 1991). Vitrinite reflectance values can be converted to temperature, but these are usually approximate and dependent on the age of the rocks

(Hunt, 1995). Graptolites, zooclasts and solid bitumens are also used to measure reflectance for maturity determination (Radke et al., 1997; Hartkopf-Fröder et al., 2015). Rock Eval pyrolysis T_{max} values increase with increasing thermal maturity. It has been correlated with vitrinite reflectance, and works well for type III kerogen (Poelchau et al., 1997; Radke et al., 1997). There are many more thermal maturity parameters known, such as those based on the color of spores or conodonts (TAI, CAI), API gravity (Radke et al., 1997; Hartkopf-Fröder et al., 2015), or the application of biomarkers (Radke et al., 1997; Peters et al., 2005). The latter are based on aromatization of cyclic organic compounds or the isomerization of less stable biomarkers into more thermally stable ones. Many types of organic compounds have been applied as maturity parameters, covering a variety of thermal maturity intervals, but usually within the range of the oil window (Peters et al., 2005). The most frequently applied parameters are ratios based on the distribution of hopanes, steranes, and methylphenanthrenes (Radke and Welte, 1983;

☆ This article is part of a special issue entitled: 'Xplorer, hybrid and early-career' published in Organic Geochemistry.
* Corresponding author.
  E-mail address: leszek.marynowski@us.edu.pl (L. Marynowski).

Peters et al., 2005) or other polycyclic aromatic compounds (PACs; e.g., Kruge, 2000; Asif et al., 2011; Noah et al., 2020). The calculated vitrinite reflectance derived from the methylphenanthrenes can be treated like measured vitrinite reflectance and converted into paleotemperatures (Barker and Pawlewicz, 1994). Conversely, ratios based on PACs can provide insight not only into the maturity of the studied rocks but also into other characteristics, such as the paleoenvironment or the occurrence of paleofires (e.g., Argiriadis et al., 2024; Jiao et al., 2024). Furthermore, the thermal maturity of the rock can be evaluated by observing the presence or absence of unsaturated and biologically configured compounds, such as hopenes, oleanenes, lupenes, and ββ-hopanes (e.g., Staneczek et al., 2024a), to detect the immature organic matter. The most frequently employed aliphatic hydrocarbon parameters are derived from the distribution of hopanes and steranes and are typically applied in lower to moderate maturity ranges (e.g., Zumberge, 1987; Yuan et al., 2024).

An example of a 'non-organic' technique is the illitization of smectite, commonly known as the illite/smectite method (Eslinger et al., 1979; Środoń, 1999). It relies on the fact that, as the temperature increases, smectite gradually transforms into illite. Another method is the measurement of rock porosity, which gradually decreases during diagenesis (Mondol et al., 2007) or fission track analysis (Gleadow et al., 1986; Petmecky et al., 1999; Anczkiewicz et al., 2013). An additional technique is the homogenization temperature of fluid inclusions, although in this case, the temperature of migrated hydrothermal fluids rather than the maturity of rock complexes is more frequently assessed (Wilkinson, 2001).

Here, we use a variety of different organic compounds and T_{max} to characterize the maturity of the Central Carpathian Paleogene Basin (CCPB) in eastern Central Europe (Fig. 1). The basin provides an excellent case study area featuring a wide maturity range, homogeneous kerogen types, and well characterized and understood lithologies (Marynowski et al., 2006; Środoń et al., 2006; Staneczek et al., 2024a). Moreover, for a large part of the study area, the results can be compared to illite/smectite data (Środoń et al., 2006), which expands the possibilities of interpretation. The use of a broad spectrum of biomarkers, supported by other methods for determining thermal maturity, provides an example of research that can be used in future oil and gas exploration, potentially including the study area.

2. Geological setting

The evolution of the CCPB began during the Late Eocene in the Central Western Carpathian area (Soták et al., 2001) and is documented throughout the Paleogene. The age of the onset of sedimentation varies slightly in the different subbasins, and the rock facies also show subtle variations (Soták et al., 2001). Here, we focus on the most common units in the whole CCPB area. Generally, sedimentation started with basal transgressive lithofacies (conglomerates) followed by carbonates, commonly represented by limestones known as the Borove Fm. (Gross et al., 1984, 1993; Soták et al., 2001). The Early Oligocene basin deepening is reflected by the deposition of siltstones and dark to black shales sometimes intercalated with sandstones and conglomerates of the Huty Fm. (Fig. 2). Initially, more coarse-grained layers were rare, but with time their occurrence increased. The Zuberec Fm. was then deposited and is characterized by a rhythmic sequence of sandstones, siltstones, and shales (Gross et al., 1984, 1993). The youngest documented unit, the Biely Potok Fm. (Fig. 2), is composed predominantly of thick sandstone layers with the sporadic occurrence of siltstones. The increasing deposition of sandstones in this unit provides evidence for the upward coarsening nature and shallowing of the basin and the subsequent termination of sedimentation (Gross et al., 1984, 1993). The generalized stratigraphic thickness of the CCPB units estimated by Gross et al. (1984) is 1.2 km for the Huty Fm., 1 km for the Zuberec Fm., and 3 km for the Biely Potok Fm. However, the thickness of each unit varies in different areas and depends on various factors, e.g., differential subsidence (Soták, 1998). In the Orava region, the Huty, Zuberec and Biely Potok Fms. only reach thicknesses of 450 m, 1000 m, and 500 m, respectively (Gross et al., 1993). In the Levoča Basin, the estimated thickness of these units is higher and reaches 800 m for the Huty Fm., 1450 m for the Zuberec Fm., and 900 m for the Biely Potok Fm. (Gross et al., 1999).
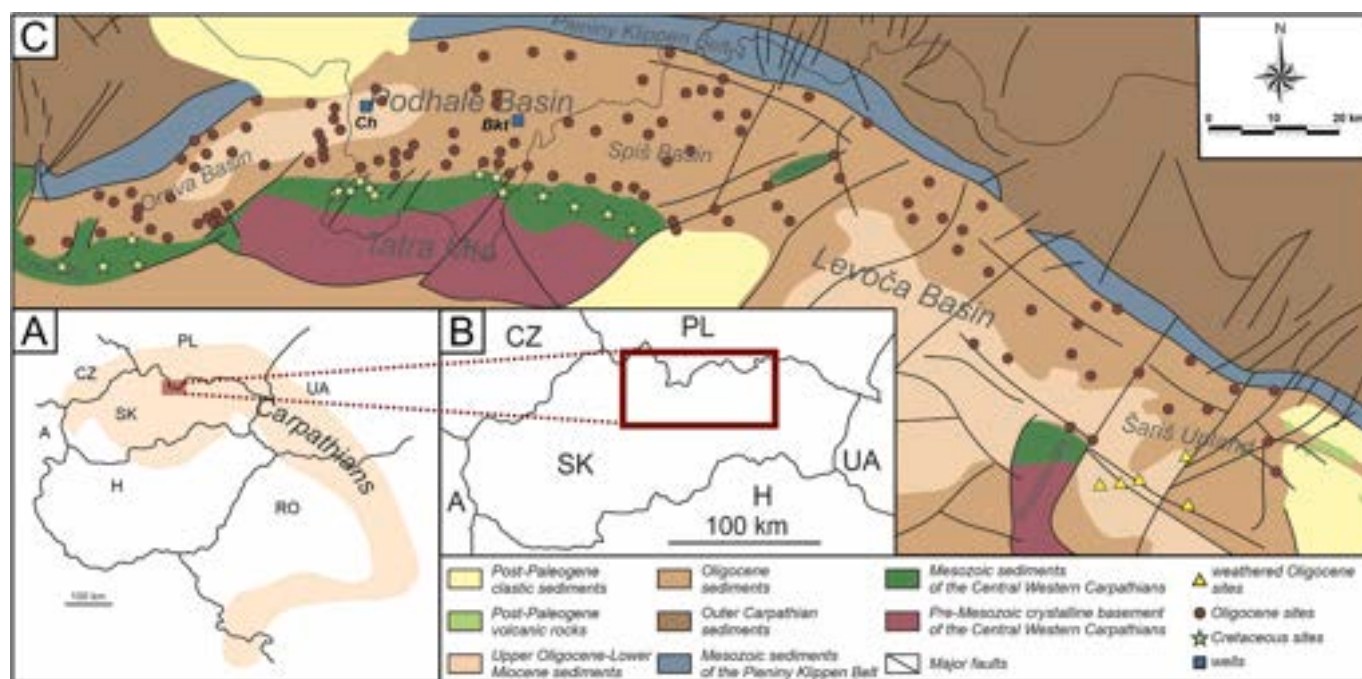

Fig. 1. Simplified geological map of the Central Carpathian Paleogene Basin (modified after Gross et al., 1994, 1999; Nemčok et al., 1993) and adjacent areas with marked sampling localities. Ch = Chochołów PIG1 borehole, Bkt = Bukowina Tatrzańska PIG1 borehole.
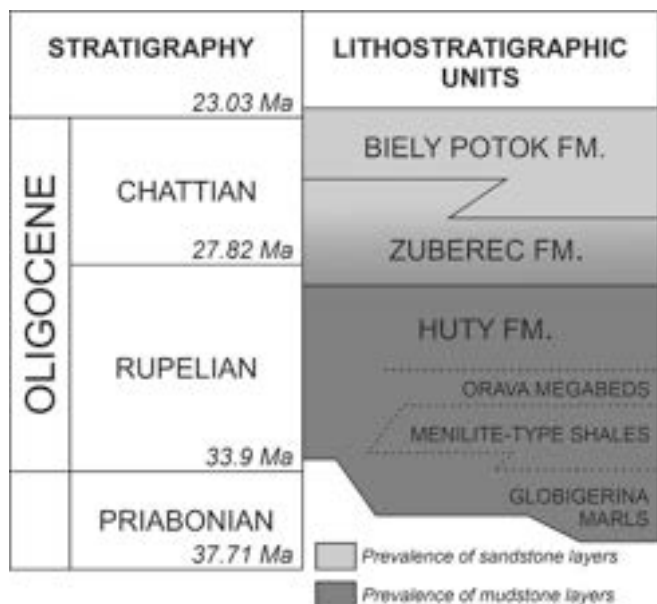
Fig. 2. Lithostratigraphy of the Central Carpathian Paleogene Basin (CCPB) units (simplified after Gross et al., 1984; Starek, 2001).

3. Samples and methods

Altogether, 241 rock samples were analyzed in this study. A total of 202 single samples from 126 sampling sites were collected from rock outcrops in streams, rivers and outcrops from the northern part of the CCPG (Fig. 1). In some sites, more than one rock sample was analyzed to improve the data precision and allow for further data comparison. Mostly mudstones and shales were sampled except from sites in the upper Zuberec Fm. and in Biely Potok Fm., where sandstone layers are dominant and mudstone layers are relatively rare. The samples were collected mostly from fresh outcrops where possible. However, five samples from the Šariš Upland were taken from sites interpreted as paleoweathered (Fig. 1). The sampling sites from the Orava Basin were derived from Staneczek et al. (2024a). In addition, 39 mudstone samples from the Chochołów PIG-1 (22) and Bukowina Tatrzańska PIG-1/GN (17) boreholes were analyzed. All samples were prepared for analyses by washing with distilled water, drying, and crushing to a <0.2 mm fraction size.

Total carbon (TC), total sulfur (TS), and total inorganic carbon (TIC) were measured using an Eltra CS-500 IR-analyzer with a TIC module (Faculty of Natural Sciences, University of Silesia in Katowice, Poland). Total organic carbon (TOC) was calculated from the previously obtained TC and TIC parameters (for details see Marynowski et al., 2017).

Rock-Eval analysis was conducted using the Rock-Eval 6 Turbo apparatus in three research centers: the Faculty of Geology, Geophysics, and Environmental Protection at AGH University of Krakow, the Oil and Gas Institute – National Research Institute, Krakow and the Polish Geological Institute – National Research Institute, Warszawa. In this study, only T_{max} values were applied. Further details can be found in Staneczek et al. (2024a).

For vitrinite reflectance measurements, samples for microscopic observations were prepared according to the ISO 7404-2 (2009) procedure. Samples were analyzed in reflected light and immersion oil using a Zeiss Axio Imager.A2m.

The crushed and powdered rocks were extracted using a Thermo Scientific Dionex ASE 350 solvent extractor with a dichloromethane (DCM)/methanol (1:1, v:v) mixture. Column chromatography method was used to separate the extractable organic matter into aliphatic, aromatic, and polar fractions. Pasteur pipettes filled with silica gel (heated for 24 h at 120 °C) were sequentially eluted with *n*-pentane, *n*-pentane/

DCM (7:3) and DCM/methanol (1:1) and the fractions were then collected. Dried aliphatic and aromatic fractions were dissolved in ethyl acetate and prepared for gas chromatography-mass spectrometry (GC–MS) analysis. Detailed method descriptions can be found in Staneczek et al. (2024a). The polar fraction was not analyzed in this study.

4. Results

4.1. General geochemical data

The TOC content in surface samples of the CCPB lithologies is generally moderate (Table S.1). In mudstones and shales from the Biely Potok, Zuberec, and Huty Fms., the obtained TOC content ranges usually from 0.5 wt% to 2.5 wt%, and only in the sandstones with plant detritus present, and in the coal beds the content was higher. Similarly, in the borehole samples, the TOC values are also moderate, with a maximum of 3.4 wt% in the Chochołów PIG-1 borehole (Table S.2). The measured TS content is very low in both surficial and borehole samples, sometimes even showing values close to 0 wt%. Few samples show TS content higher than 2.0 wt%.

4.2. Vitrinite reflectance measurements

The vitrinite reflectance was measured in 60 surface samples (Table S.1, Fig. S1). Maximum reflectance values were recorded in the Spiš Basin and the eastern part of the Podhale Basin reaching 1.61 %. The measured reflectance was significantly lower in the Orava and Šariš part of the CCPB and usually varied in the 0.3–0.5 % range. The measured reflectance was slightly higher in the Huty Fm. samples. The vitrinite reflectance was not measured in borehole samples. Due to the prevalence of dark vitrinites with suppressed reflectance by the presence of resinite (Staneczek et al., 2024a), this method was not used to estimate the thermal maturity of the CPPB.

4.3. Rock-Eval

Rock-Eval analysis was performed for 114 samples from rock outcrops and 35 samples from boreholes (Tables S.1, S.2). Most of the samples represent kerogen type III, and sometimes II/III and incidentally II (Soták et al., 2001; Staneczek et al., 2024a). Generally, the recorded temperatures are almost always higher than 420 °C. The obtained T_{max} values are quite consistent in each of the CCPB subbasins (Fig. S2). In Huty Fm. samples, especially in the Spiš Basin, the T_{max} values were noticeably higher than those documented in other units (up to 606 °C). The lowest values for the Huty Fm. are documented in the Šariš Upland (up to 426 °C). In the Zuberec and Biely Potok Fms., the temperatures are similar and usually coherent, ranging from 420 °C to 450 °C, except for the Spiš Basin, where T_{max} reaches a maximum of 594 °C. In the samples from boreholes, the measured T_{max} values increase with depth (Fig. 3). In the Chochołów PIG-1 well, the T_{max} values start from 430 °C in the upper samples and reach 456 °C in the lower samples. In the Bukowina Tatrzańska PIG-1 borehole, T_{max} values are higher than in Chochołów PIG-1 borehole and span from 448 °C in the upper samples to over 500 °C in the lower borehole.

4.4. Aliphatic ratios

We investigated the spatial distribution of three parameters based on aliphatic compounds (Table S.3, Fig. 4), but the data were also supplemented by additional sterane and hopane indicators (Tables S.3, S.4). The $C_{31}S/(S+R)$ homohopane (Seifert and Moldowan, 1980) parameter ranged from 0.28 to 0.62. The vast majority of the studied area is characterized by values varying from 0.50 to 0.62. Only a few areas, mainly in the Zuberec and Biely Potok Fms. in the northern Orava Basin and the Huty Fm. in the southeastern Šariš Upland and northern parts of the Levoča, show values below 0.50, reaching a minimum in the south-
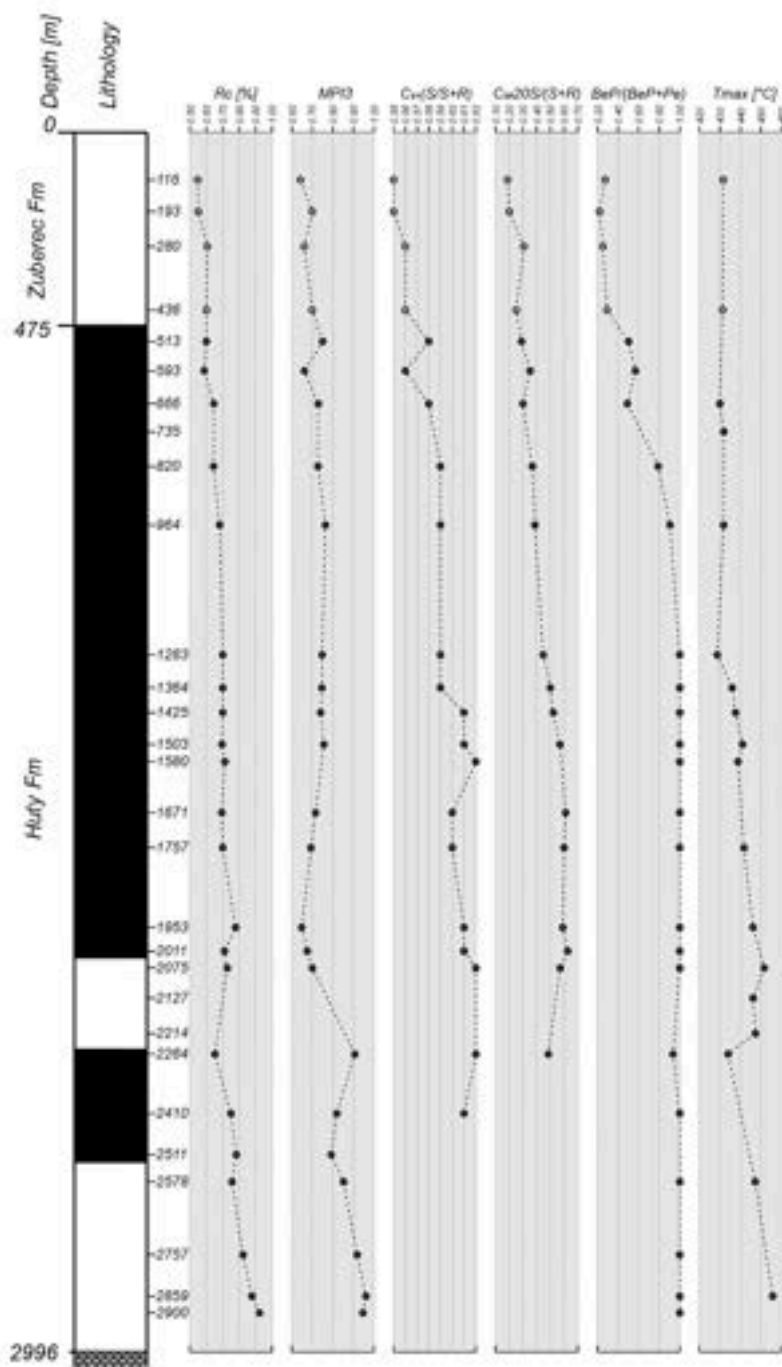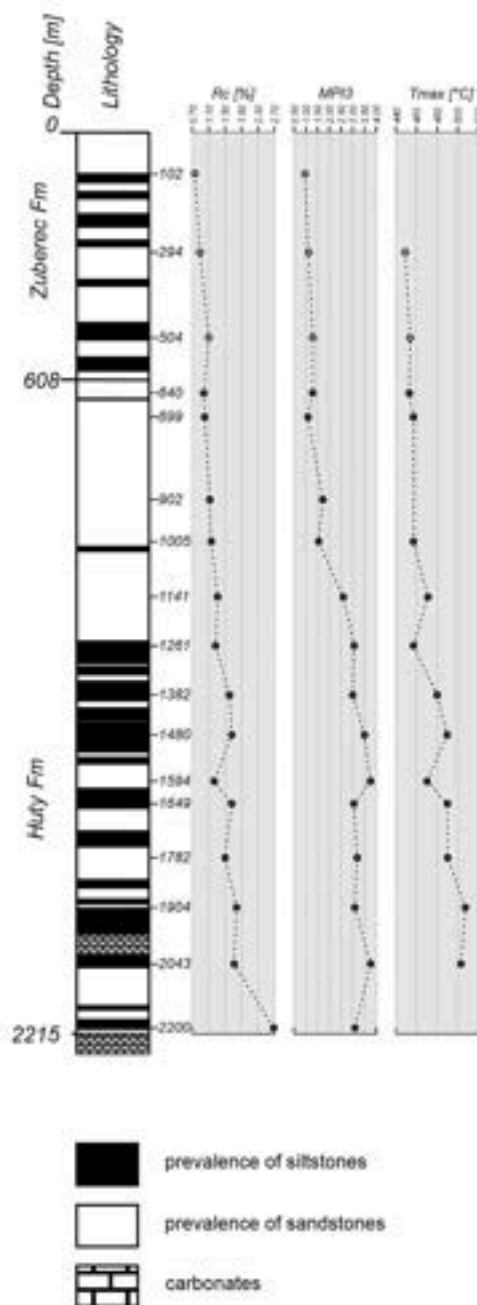
Fig. 3. Geochemical and biomarker-derived parameter changes in the Bukowina Tatrzańska PIG-1 and Chochołów PIG-1 boreholes. Abbreviations are given below Table S.3.

east Šariš Uplan (0.28). In the Chochołów PIG-1 borehole, the values of the applied parameter slowly increased from 0.55 to 0.62 down to 2500 m, below which hopanes are not preserved (Fig. 3). This parameter was not applicable in the Spiš Basin, eastern Podhale, and the Bukowina Tatrzańska PIG-1 borehole that lacked hopanes due to higher maturity.

The second parameter is the C_{29}-$\alpha\alpha\alpha$ 20S/(S+R) ratio (Tables S.3, S.4; Mackenzie and McKenzie, 1983). Similarly to the hopane ratio, this parameter cannot be applied in the Spiš, eastern Podhale and Bukowina Tatrzańska PIG-1 borehole due to the lack of steranes (Tables S.3, S.4, Fig. 4). The range of calculated values reaches from 0.03 to 0.68. The highest values (0.41–0.68) characterize the central Podhale, southern Orava, and central Levoča areas. These values were documented mostly

in Huty Fm. samples. Intermediate values (0.20–0.40) were recorded in Huty Fm. from the Levoča and Podhale Basins, and the Zuberec Fm. from the Orava Basin. The lowest values of the sterane parameter, which suggest the lowest maturity, occur in the northern Orava (Biely Potok and Zuberec Fms.; ratio values 0.07–0.20), northern Levoča (Zuberec Fm., <0.20), and southeastern Šariš Upland (Huty Fm., values as low as 0.03). In the Chochołów PIG-1 borehole, the parameter values increase with depth from 0.19 to 0.63 (Fig. 3). Steranes were not detected in samples below 2300 m.

The last applied parameter is based on the presence of immature compounds, i.e., oleanenes, lupenes and $C_{30}\beta\beta$ hopanes (Table S.3). We calculated a ratio based on the sum of oleanenes, lupenes and $C_{30}\beta\beta$
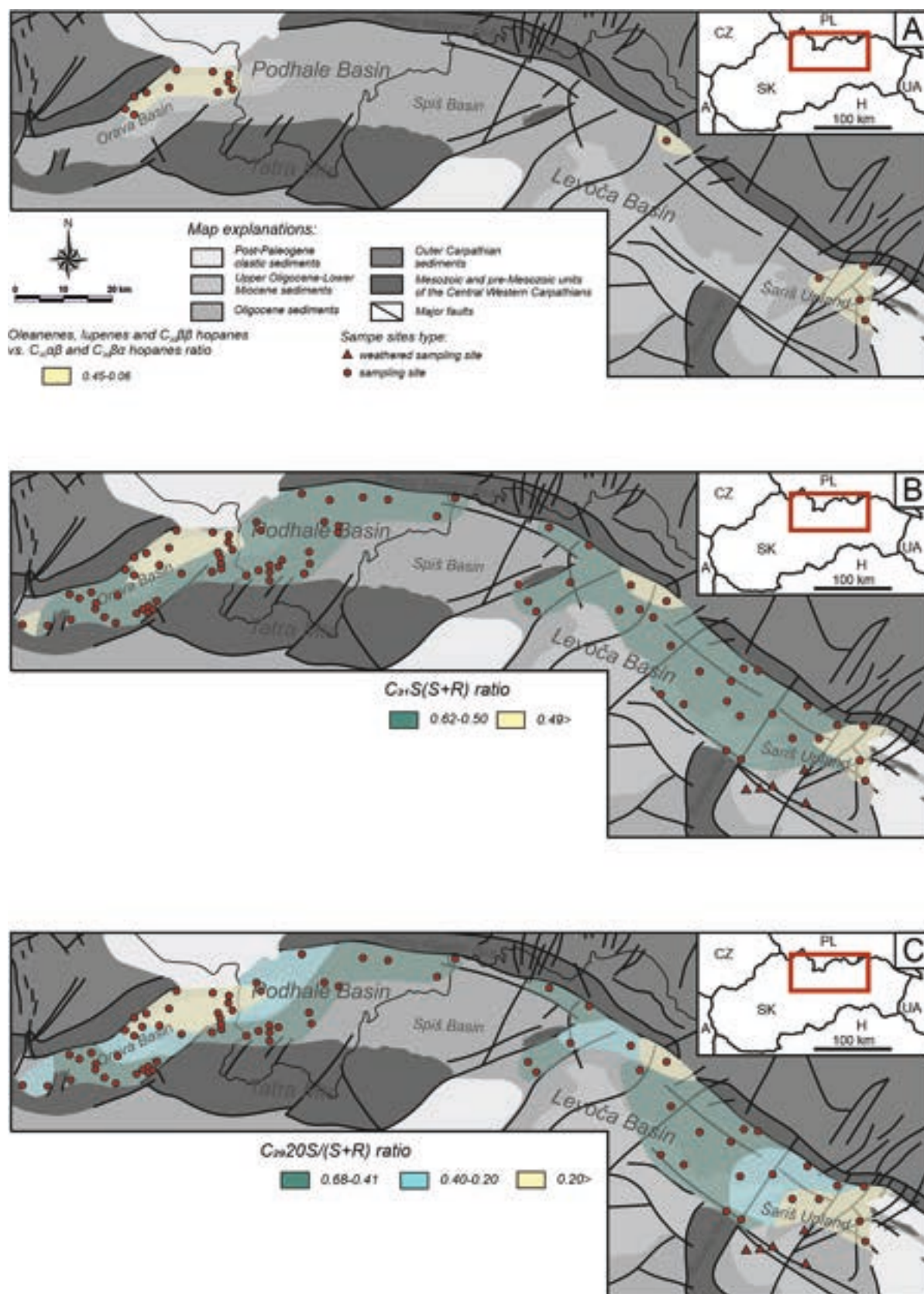
Fig. 4. Spatial distribution of the values of aliphatic ratios in the CCPB surface samples.

hopanes vs. $C_{30}\alpha\beta$ and $C_{30}\beta\alpha$ hopanes. The ratio values ranged from 0.06 to 0.45. These compounds are only present in Biely Potok and Zuberec Fms. for samples from the northern Orava Basin, as well as Zuberec and Huty Fms. of the northern Levoča Basin and the Huty Fm. in the southeastern Šariš Upland (Fig. 4). These compounds were not found in the borehole samples. An example of hopane distribution for samples with different thermal maturity is presented in Staneczek et al. (2024a).

4.5. Aromatic ratios

Seven different maturity ratios based on aromatic compounds were also calculated for surface and borehole samples (Tables S.3, S.4; Figs. 5, 6, S3, S4, S5, S6).

The first two parameters are based on phenanthrene and methylphenanthrenes compound distribution (Tables S.3, S.4). Firstly, the methylphenanthrene index was calculated (MPI1; Radke and Welte, 1983), whose values vary between 0.11 and 3.70 in the samples. The highest ratios are documented in the Huty and Zuberec Fms. of the Spiš Basin, especially in areas close to the Tatra Mountains. Usually, the MPI1 parameter values recorded in the Tatra Mountains are higher than 2.0. In the Podhale Basin, the recorded values slowly decrease from east to west (above 1.5 to 0.5), and from the north to the south (0.5 to above 1.5). The slight decrease in values also occurs in the Orava Basin, where the recorded values are, with few exceptions, below 0.6, with the lowest values in the northern part of the basin (below 0.25). A more complicated spatial distribution of the MPI1 parameter occurs in the Levoča Basin and Šariš Upland. The lowest values occur in the southeastern part of the Šariš Upland, where the MPI1 parameter shows values below 0.5. Usually, the documented values increase towards the Spiš region with the MPI1 equaling 0.65; however, in some areas, the values can be as low as 0.11, and in others as high as 1.30. In the Chochołów PIG-1 borehole, the MPI1 values increase gradually with depth starting from 0.23 and reaching 0.88. In the Bukowina Tatrzańska PIG-1 borehole, the surface values reach 0.65 and increase significantly to 2.16 with depth. The next parameter, MPI3 (Radke, 1987), does not include phenanthrene in the equation. Its values follow a comparable spatial distribution as the MPI1 parameter (Figs. 6, S3). However, its values are slightly higher and vary from 0.45 to 4.33 (Tables S.3, S.4). Similar to MPI1, the lowest values are recorded in the Orava region and the southeastern Šariš Upland, with the highest being in the Spiš area. In the samples from boreholes, the MPI3 values increase with depth, from 0.64 to 0.94 in Chochołów PIG-1, to 0.95–3.73 in Bukowina Tatrzańska PIG-1 boreholes (Fig. 3). The MPI1 values were converted to a calculated vitrinite reflectance (Rc; Tables S.3, S.4). Two formulas were used. The first: Rc = 0.55 MPI1+0.44 for most samples, and Rc = 0.50 MPI1+2.27 for the highly mature samples with vitrinite reflectance above 1.5–1.7 % (Radke, 1987). The lowest Rc values are documented in the Zuberec and Biely Potok Fms. of the northern Orava Basin, where they reach 0.55 % (Fig. 6). The values slowly increase towards the east, and in the Podhale region show 0.60–0.87 % Rc. In the eastern Tatra foreland, the Rc reaches its highest values, which in general are higher than 2.0 %.

Towards the southeast from the Spiš region, after crossing the Ružbachy Fault, the Rc values start to decrease with an average of 0.65–0.85 % (Fig. 6). In the Chochołów PIG-1 borehole, the calculated reflectance increases steadily, similar to MPI1, from 0.54 to 0.93 %. In the Bukowina Tatrzańska PIG-1 borehole, the Rc values of the shallow samples are around 0.79 % and increase with depth to 2.68 % (Fig. 3, Table S.4).

The third ratio is based on the five-ring polycyclic aromatic hydrocarbon (PAH) compounds, i.e., benzo[*e*]pyrene (B*e*P), benzo[*a*]pyrene (B*a*P), and perylene (Pe). B*e*P is the most thermally stable compound (Marynowski et al., 2015), and, therefore, is present in all surface and borehole samples. B*a*P is documented in most of the samples, and its amount decreased with maturity, which was documented in the Chochołów PIG-1 borehole (Marynowski et al., 2015). The least stable compound, perylene (Holman et al., 2024), is recorded mainly in

samples from the Orava Basin and Šariš Upland, the northern part of Podhale, and up to 1000 m in the Chochołów PIG-1 borehole (Marynowski et al., 2015). The Biely Potok and Zuberec Fms. samples generally contain perylene, except for samples from the Spiš Basin. Conversely, in samples from the Huty Fm., perylene does not usually occur. However, in the Šariš Upland, all Huty Fm. samples contain perylene. Based on these organic compounds, the B*e*P/(B*e*P+Pe) ratio was calculated (Tables S.3, S.4). The ratio values vary from as low as 0.02 (northern Orava and eastern Šariš) to 1.00 (Spiš and Podhale). Generally, the Biely Potok and Zuberec Fms. record the lowest values of B*e*P/(B*e*P+Pe) ratios, especially in the Orava region. The Huty Fm. samples are characterized by the highest values of this parameter; but, interestingly they also display the lowest documented values in the eastern Šariš Upland.

A next parameter was derived from the ratio of three gymnosperm biomarkers: retene (R), simonellite (S), and dehydroabietane (D), which have different thermal stability. Retene is the most thermally stable compound and occurs in areas where the vitrinite reflectance values are lower than 1.0 % (Radke, 1987). Simonellite is much less stable and disappears near the first jump of carbonization (ca. 0.55 % Ro; Radke, 1987), while dehydroabietane is present in immature organic matter only (Simoneit et al., 1986; Marynowski et al., 2007). R/(R+S+D) expresses thermal maturity over most of the study area, except the southeastern part of Podhale and the Spiš basin (Fig. 5). In the rest of the Podhale area and the majority of sites in the Levoča Basin, retene is the only compound present (R/(R+S+D) = 1). Simonellite is documented in less mature rocks. It occurs in the northern and central parts of the Orava Basin and in a few sampling sites in the Šariš Upland and the Podhale Basin. R/(R+S+D) in these areas generally ranges from 0.81 up to 0.94. The least mature regions are characterized by the occurrence of dehydroabietane (Table S.3). This includes some samples of the Biely Potok and Zuberec Fms. in the Orava region and Huty Fm. in southeastern Šariš (Fig. 5). There, in the Šariš Upland, the R/(R+S+D) parameter shows the lowest values, generally below 0.81, but in some sites even below 0.5. In the Chochołów PIG-1 borehole, simonellite is present in samples up to 700 m and retene up to 2300 m (Table S.4). These ratio values are quite high, ranging from 0.9 to 1.0. However, none of the described compounds is present in the Bukowina Tatrzańska PIG-1 borehole samples.

The ratio of retene to the sum of retene and 3-methylphenanthrene (R/(R+3-MP); Fig. 5, Tables S.3, S.4) provides another thermal maturity parameter showing a broad range from 0.01 to 0.96. Due to the lack of retene, this parameter cannot differential maturity in the Spiš and eastern Podhale regions, including the Bukowina Tatrzańska PIG-1 boreholes. In samples where retene is detected, the lowest R/(R+3-MP) values (implying the highest maturity) occur in the Podhale Basin, as well as areas neighboring the Pieniny Klippen Belt (PKB), and the central Levoča basin (Fig. 5). These values usually range from 0.01 to 0.50. Intermediate values of this parameter occur in samples from the eastern Orava (Zuberec and Huty Fms.) and eastern Šariš (Huty Fm., 0.70 to 0.51). The highest values are documented in Zuberec and Biely Potok Fms. samples from the Orava basin and the easternmost Huty Fm. samples from the Šariš Upland. There, the parameter reaches a maximum value of 0.96. In the Chochołów PIG-1 borehole, a decreasing trend of R/(R+3-MP) values is observed (Table S.4). The parameter changes from 0.66 to 0.10.

The final aromatic parameter is calculated from the ratio of phenylphenanthrenes (2-PhP + 3-PhP)/[(2-PhP+3-PhP)+(4-PhP+1-PhP+9-PhP)] (Rospondek et al., 2009; Tables S.3, S.4, Figs. 6, S4). Although other ratios have also been proposed based on the distribution of phenylphenanthrenes and binaphthyls (Li et al., 2012), in the case of the CCPB only the values of the ratio (2-PhP+3-PhP)/[(2-PhP+3-PhP)+(4-PhP+1-PhP+9-PhP)] increased with depth in the boreholes (Fig. S4). The highest values of this parameter are documented in the Spiš area, as well as in the eastern Tatra foreland, and some parts of the Levoča Basin, where they range from 0.9 to 1.0 (Fig. 6B). The central Podhale and Šariš
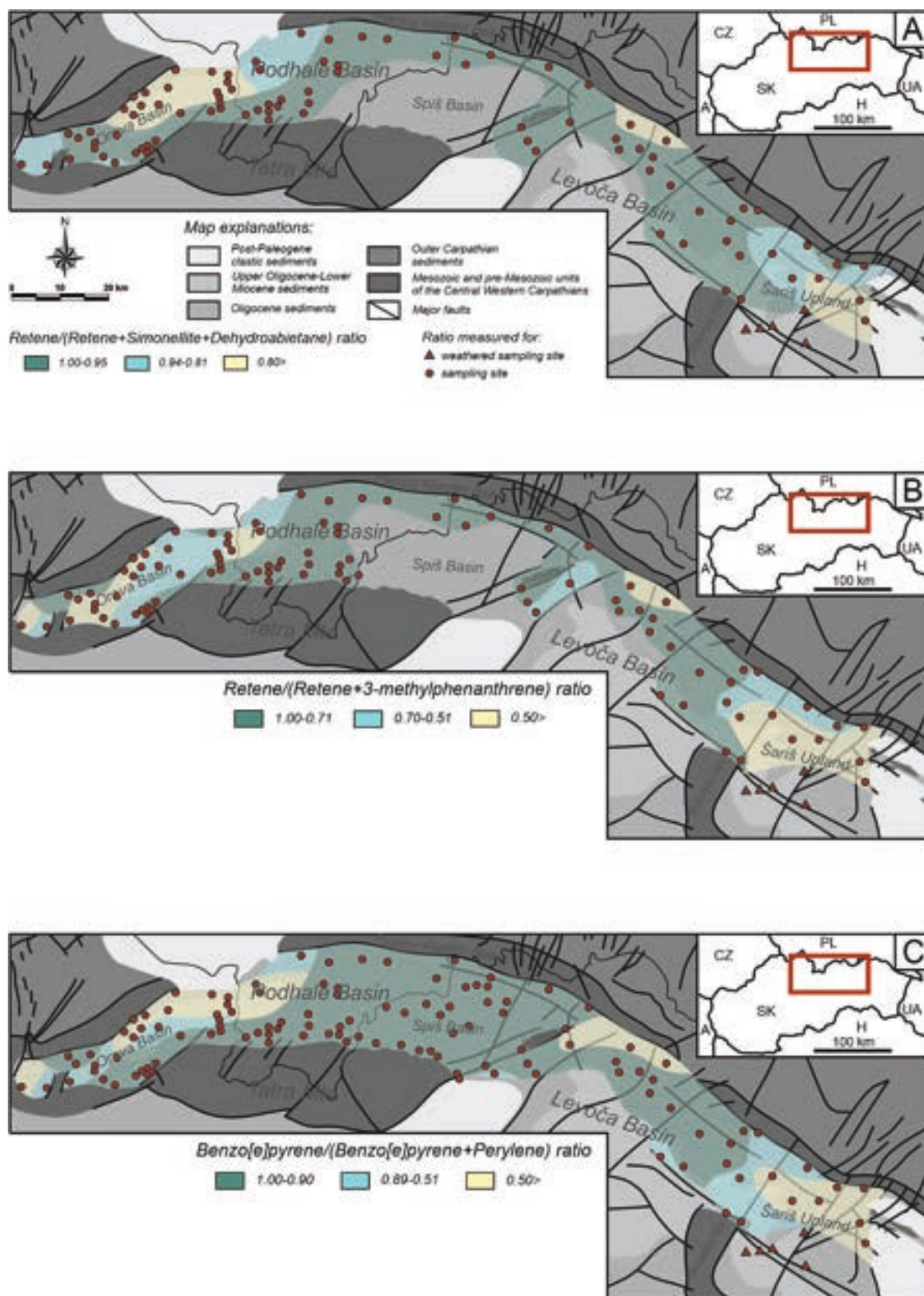
Fig. 5. Spatial distribution of the values of aromatic ratios in the CCPB surface samples.
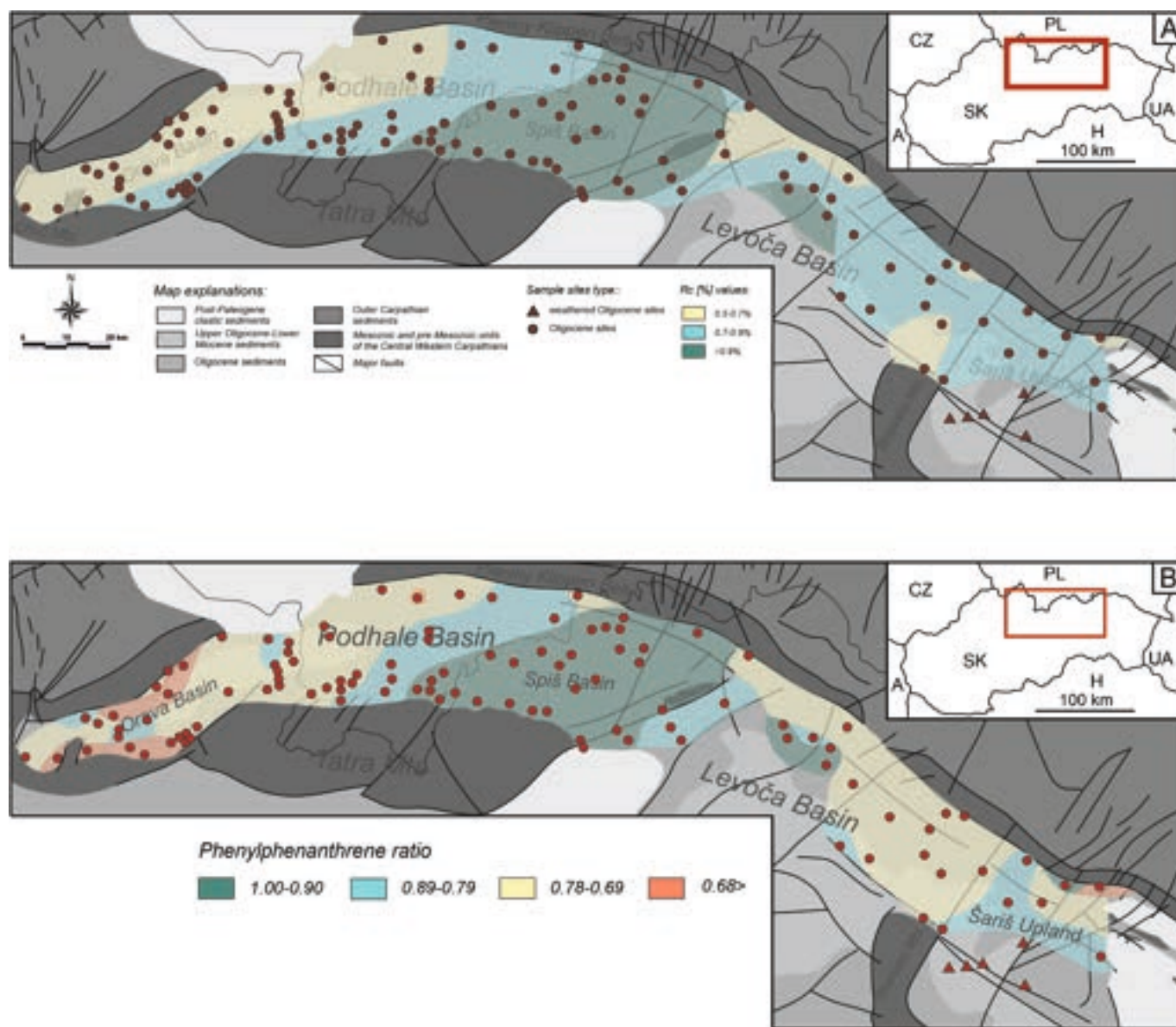
Fig. 6. Spatial distribution of the calculated vitrinite reflectance values and the phenylphenanthrene ratio in the CCPB surface samples.

regions are characterized by intermediate (0.89–0.80) values of the phenylphenanthrene ratio. Low values of the analyzed parameter (0.79–0.70) are recorded in the eastern Orava, western Podhale area, and in the majority of the Levoča Basin and Šariš Upland. Only in a few regions did the phenylphenanthrene parameter reach values below 0.70, mainly in northern Orava and the easternmost Šariš Upland. In the well samples, the parameter values increase slowly with depth. In the Chochołów PIG-1 borehole, they increase from approximately 0.70 to 0.90, and in the Bukowina Tatrzańska PIG-1 borehole from 0.88 to 0.98.

5. Discussion

5.1. Changes in thermal maturity of key parameters in Chochołów PIG-1 and Bukowina Tatrzańska PIG-1 boreholes

Out of the several maturity parameters investigated in this study, the MPI1 and the calculated Rc values appear to be the most suitable to characterize the maturity changes with increasing depth in the boreholes (Fig. 3). The Rc values increase steadily with depth to approximately 2200 m in the Bukowina Tatrzańska PIG-1 borehole. In addition,

this parameter covers the widest maturity range in comparison to other ratios. However, its applicability seems to be limited above 1.7–1.8 % Rc where the MPI values start to be inverted. In this case, an alternative formula for the recalculated vitrinite reflectance should be used (Radke, 1987). Moreover, the calculated Rc values in the bottom of Chochołów PIG-1 borehole correspond to the uppermost Bukowina Tatrzańska PIG-1 borehole samples (Fig. 3). Other parameters showing this phenomenon are MPI3, T_{max} and PhP ratio (Figs. 3, S4). All three are characterized by more or less consistent increases that cover a large range in maturity. An exception is the PhP ratio, which can be applied only to approximately 1.60 % Rc (~1300 m in the Bukowina Tatrzańska PIG-1 borehole), and above there is no value change due to the very low content of less stable PhP.

Some parameters listed above are suitable for characterizing maturity changes in the lower maturity range. The sterane, hopane and perylene ratios show an increasing trend (Fig. 3). A gradual rise with only minor variations is characteristic of perylene and sterane ratios. In turn, the homohopane parameter displays more deviations in trend. The range of the perylene parameter is the smallest in comparison to the other ratios used and spans to ~0.7 % Rc and to ~1300 m in the

Chochołów PIG-1 well. In our samples, both sterane and hopane parameters can be applied to investigate maturity to approximately 0.8–0.9 % Rc and are present up to 2264 m and 2400 m depth in the Chochołów PIG-1 borehole, respectively. This may be related to the generally low concentrations of hopanes and especially steranes in immature samples, as these compounds are normally present at higher maturities (Peters et al., 2005). Retene can also be applied in the lower maturity range. In contrast to the previously discussed parameters, the values of R/(R+3MP) decrease with depth (Fig. 3, Table S.4). Retene is detected in a sample 2264 m deep in the Chochołów PIG-1 borehole; however, below depths of 2000 m depth, the values of this parameter start to deviate from the trend. This may be related to differences in the initial concentrations of this compound in the rocks because they were deposited in a marine basin into which terrestrial organic matter was supplied (Staneczek et al., 2024a).

Several parameters presented above show no gradual changes with depth in both boreholes. However, these parameters can complement the temperature distribution in the CCPB area. Consequently, all ratios can be applied for maturity assessment in surface samples, providing a cohesive picture of thermal maturity in the study area.

5.2. Distribution of thermal maturity in surface samples within the CCPB

The most fundamental parameter applied for characterizing the thermal maturity of surface samples was calculated vitrinite reflectance based on MPI1 (Fig. 6). Overall, this parameter is suitable for documenting the general trend of maturity changes and enables a simplified reconstruction of the maturity zones. However, there are some drawbacks to this parameter and, therefore, it must be supported by additional biomarker ratios that are shown effectively in the boreholes or were found only in certain areas. The calculated vitrinite reflectance gives erroneous results below the 0.5 % Rc value (Radke, 1987). However, in areas where this value was suspected, unsaturated pentacyclic triterpenoids and ββ-hopanes were also found (Fig. 4). Generally, these thermally unstable compounds are representative of immature organic matter, with vitrinite reflectance below 0.4–0.5 % (Peters et al., 2005), and thus they were not present in core samples and limited to small areas of the CCPB (Fig. 4). The analyzed ratio derived from these compounds allowed detection in the areas that experienced only minor thermal alterations. The lowest maturity is documented in the Šariš Upland, northern Orava Basin, and central Levoča Basin (Fig. 4).

The calculated vitrinite reflectance values suggest that the Spiš and eastern Podhale Basins are the most mature areas in the CCPB. Two biomarker parameters from aliphatic fractions [$C_{31}S(S+R)$, $C_{29}20S/(S+R)$] and three from aromatic fractions [R/(R+S+D), R/(R+3-MP) and BeP/(BeP+Pe)] cannot be applied to estimate the maturity of these regions (Figs. 4 and 5). The limitation of these ratios is due to the thermal stability of steranes, hopanes, simonellite, retene, and perylene, which are not present in rocks showing Rc values higher than 1.2 % (Radke, 1987; George, 1992; Peters et al., 2005; Marynowski et al., 2015). Where retene is detected, the R/(R+S+D) parameter shows the lowest values in Šariš Upland, northern Orava Basin, and a small part of Levoča Basin (Fig. 5), similar to the R/(R+3-MP) parameter. However, the R/(R+3-MP) ratio in the Orava Basin has more scattered values, and does not show such the trend seen in R/(R+S+D) ratio. As with the boreholes, these divergences may be due to the differences in the input of terrestrial organic matter derived from gymnosperms (Simoneit, 1977; Simoneit et al., 1986; Otto and Simoneit, 2001) to the basin. Yet, both parameters are similar to the maturity trend documented by the Rc values. We were able to apply the five-ring PAH compounds ratio to the whole CCPB area due to the high stability of benzo[e]pyrene (Table S.3, Fig. 5), but in eastern Podhale and the Spiš Basin ratio values are equal to 1 (Table S.3). Highly altered regions include Spiš, the eastern Podhale Basin, central Levoča, and the Choč-Tatra foreland. However, this parameter is not particularly effective in identifying the most thermally mature areas since the highest values occur both in the Spiš Basin and

also in the Western Tatra foreland, which shows distinctive changes in Rc values (Fig. 6, Table S.3). This parameter is suitable for characterizing the maturity of less thermally altered regions of the CCPB. A clear decreasing trend consistent with the previous observations is nicely shown in the Šariš Upland and the northern Orava Basin (Fig. 5).

Ratios based on aliphatic compounds are useful in characterizing moderately mature areas. Both steranes and hopanes are not present in the Spiš Basin and eastern Podhale Basin. Parameters based on the S/(S+R) homohopane ratio show relatively limited effectiveness in the characterization of the thermal maturity of CCPB rocks (Fig. 4). However, it can be helpful in the identification of areas with the lowest maturity levels, which in the case of the CCPB, are the Šariš Upland and northern Orava Basin. The parameter based on the sterane distribution more accurately depicts gradual changes in maturity (Fig. 7), which is reflected clearly in the changes observed in the Orava Basin and from the
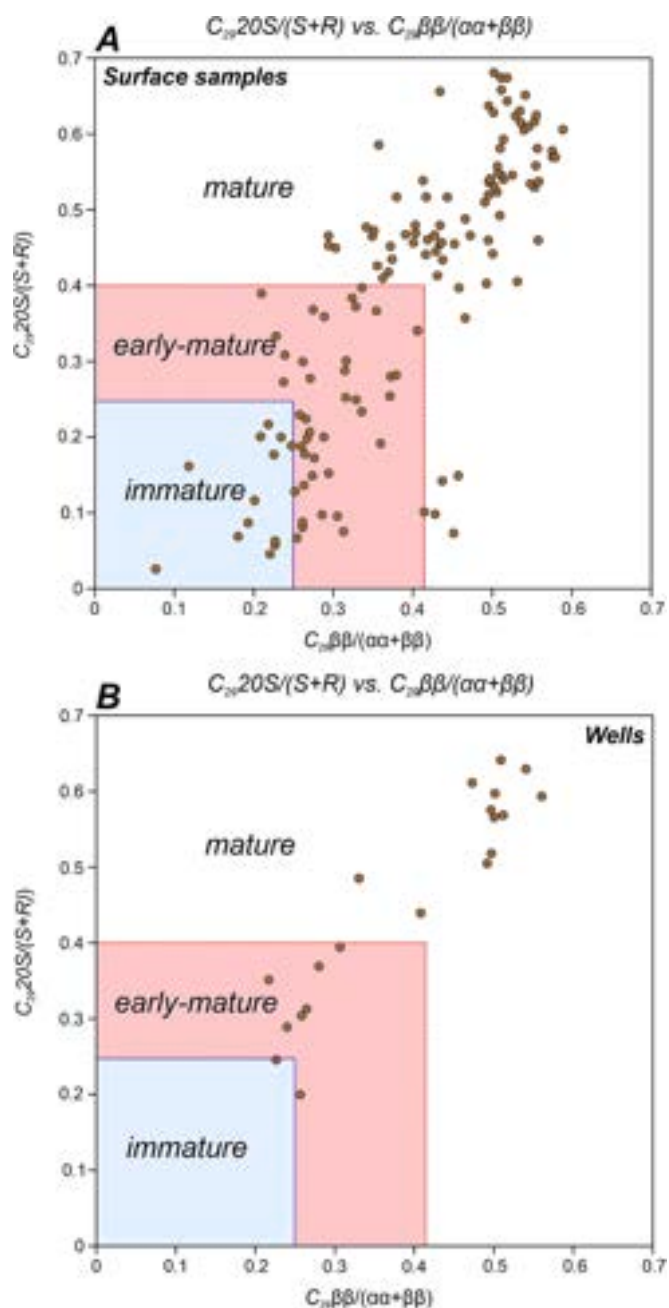

Fig. 7. Correlation of sterane indicators for CCPB surface samples (A) and wells (B).

Levoča Basin to the Šariš Upland (Fig. 4). The trend documented by this parameter is very similar to that presented by Rc, excluding areas with high maturity.

The parameter based on phenylphenanthrenes can be applied even in the areas characterized by the highest maturity (Fig. 6B). However, similar to the (R/(R+3-MP) ratio, the PhP ratio shows some inconsistency in the Orava Basin. In this region, the CCPB units and their lithologies change frequently in a relatively small area (Gross et al., 1993). Therefore, the lithology, and preserved organic matter may vary more than in other regions. Moreover, in all areas except the Orava Basin, the samples were derived mainly from Huty Fm., and were mostly mudstones. There, the general trend of maturity change is gradual and does not vary significantly when applying other parameters.

Rock-Eval T_{max} (Fig. S2) can be successfully applied even in the most mature samples. Therefore, this parameter, similar to Rc, shows an increase in thermal maturity from the PKB to the Mesozoic Carpathian massifs (i.e., Staneczek et al., 2024b) and from the Orava and Levoča basins to the Spiš Basin. In addition, this parameter supports the previous findings, and documents that the Šariš Upland and Orava Basin show the lowest maturity.

The maturity maps created by applying different biomarker methods and T_{max} parameters generally are similar and complement the picture outlined by the Rc values. The thermal maturity trend is directed from the Orava Basin towards the Spiš Basin, and from the Šariš Upland to the Spiš Basin. The Rc and T_{max} parameters also documented an N-S trend of increasing paleotemperatures present mainly in the Orava, Podhale, and Spiš basins.

In summary, there is no single parameter that accurately describes thermal maturity in the CCPB area. Measured vitrinite reflectance does not show relevant data, due to the presence of dark vitrinites (Staneczek et al., 2024a), which are also present in the Outer Carpathians (Waliczek and Więcław, 2012; Wendorff et al., 2017; Waliczek et al., 2019). Fig. S1 shows the measured vitrinite reflectance values. The large discrepancies in relation to other parameters make this method unsuitable for the CCPB. The most universal parameter for CCPB is MPI1, which is converted to a vitrinite reflectance equivalent. However, it needs to be complemented by other indicators, especially those based on thermally unstable biomarkers such as simonellite, dehydroabietane, oleanenes, lupenes and $\beta\beta$ hopanes. Ratios of regular steranes and homohopanes can also be useful up to peak oil generation.

5.3. The evolution of the Paleogene deposits of the CCPB

Based on the Rc values, supplemented by other biomarker data, we have attempted to estimate the paleotemperature distribution influenced by the Paleogene rocks in the CCPB. The highest paleotemperatures were recorded in the southernmost part of the Spiš Basin, where the Rc values can reach even 2.62 %, which corresponds roughly to approximately 200 °C (after the calculations of Burnham and Sweeney, 1989; Barker and Pawlewicz, 1994) Elevated maturity in the Spiš Basin was confirmed by the high T_{max} values (Table S.1; Fig. S2). Moreover, in the deepest sample of the Bukowina Tatrzańska PIG-1 borehole and in the areas closest to the Ružbachy Fault where the vitrinite reflectance is ~2.0 %, the MPI1 (and Rc) values start to decrease due to enhanced phenanthrene (Radke, 1987; Fig. 6A and Fig. 3).

In comparison to the Spiš Basin, the paleotemperatures decrease continuously towards the west, east, and north. In the Tatra foreland of the eastern Podhale Basin, the recorded temperatures are high (~130–150 °C), but noticeably lower than in the Spiš Basin. The temperatures tend to decrease along the Tatra-Choč Mountains and reach a minimum of 60–80 °C in the westernmost Orava Basin. This N-S increasing trend present in the Orava-Podhale-Spiš area documents a large change: from below 50 °C to 70–80 °C in the Orava Basin, 60 °C to 150 °C in Podhale Basin, and finally from 100 °C up to 200 °C in the Spiš Basin. In contrast, paleotemperatures in the Spiš Basin change abruptly when crossing the Ružbachy Fault Zone, which was also observed by

Środoń et al. (2006). The change is significant, ranging from almost 200 °C in the samples before the fault to even 70 °C after crossing the fault. This characteristic feature occurs along the whole fault zone, which may indicate that the fault was active in the Paleogene and caused subsidence on its western side (i.e., Środoń et al., 2006; Kováč et al., 2016). Continuing eastward, the paleotemperatures decrease slowly (with few exceptions) towards the Šariš Upland, where, similar to the Orava Basin, they drop below 50 °C (Fig. 4). It is notable that in the Levoča Basin near Lipany and Šambron, methane and paraffinic oils have been found in boreholes (Soták et al., 2001) and vitrinite reflectance in the boreholes range from 1.3 % close to the surface to 1.6–1.7 % at a depth of 2000 m (Francû and Müller, 1983).

Another study of paleotemperatures in the northern part of the CCPB (Orava to Spiš Basins) based on the illite–smectite transformation (Środoń et al., 2006) generally shows a very similar temperature trend, i. e., paleotemperatures are increasing towards the Spiš Basin, and decrease towards the PKB. Also, Gedl (2000) showed that black palynomorphs occurred only in the southeastern part of the Podhale Basin. However, the paleotemperatures estimated by Środoń et al. (2006) are quite different from those reported in this paper. It is especially noticeable in the case of the Orava Basin, where the difference in recorded temperatures reaches 50 °C. Yet, temperatures ~95–100 °C (Środoń et al., 2006) in the Orava Basin are unlikely, due to the presence of compounds characteristic of immature rocks (unsaturated compounds and $\beta\beta$-hopanes; see Staneczek et al., 2024a). Similarly, the biomarker-based parameters document a lower maturity of the units on the Western Tatra foreland, where the estimated temperatures could reach a maximum of 90 °C. This temperature shift occurs in all studied regions up to the Spiš Basin. Similar discrepancies between illite/smectite transformation and biomarker data have also been found for the Ediacaran sedimentary rocks in the East European Craton (Derkowski et al., 2021). Despite attempts to explain these differences by migration of hydrothermal fluids, the problem remains unaddressed.

Środoń et al. (2006) did not continue the paleotemperature research beyond the Ružbachy Fault Zone (apart from a few points in the Levoča Basin). However, some data points located eastward of the fault suggest an increase in the content of smectite in comparison to samples located westward from the fault, which would suggest a lower maturity of these rocks. The results of our study are consistent with these findings. Moreover, the obtained results seem to highlight the importance of the Ružbachy Fault Zone as a potential factor influencing the abrupt paleotemperature change.

Additionally, Środoń et al. (2006), based on Suggate (1998) and data from Poprawa and Marynowski (2005), calculated the average paleogradient in the northern CCPB at 20 °C–25 °C/km. However, there are reports that suggest a higher paleogradient, implying a lower thickness of overlying rocks up to about 2 km (Anczkiewicz et al., 2013 and references therein). As stated by Środoń et al. (2006), it is close to the current gradient, which averages 19–23 °C/km (Cebulak et al., 2004). Applying this gradient to our results, we can calculate the minimum thickness of the eroded Paleogene cover. The lowest thickness would be recorded in the Orava Basin and Šariš Upland, and would not exceed 2 km. Meanwhile, in the Spiš Basin, the thickness of the eroded units could likely be even 5–7 km (i.e., Środoń et al., 2006). This peculiar difference is once again highlighted near the Ružbachy Fault Zone, with over 5 km to the western side of the fault, and around 2–3 km to the eastern side. This is theoretically possible, as the maximum thickness of the Biely Potok Fm. is estimated at 3–3.5 km (Gross et al., 1993). However, the higher paleogradient and the lower thickness of the eroded Paleogene cover postulated by Anczkiewicz et al. (2013) seem to be more realistic.

Such observed paleotemperature patterns in the CCPB can result from a variety of processes. This is likely caused by changes in the sedimentation rates and subsidence levels in different parts of the CCPB. Kováč et al. (2016) report an eastward migration of depocentres during the sedimentation of Paleogene units. Such a phenomenon would cause a prolonged deposition, mainly in the eastern Podhale and Spiš area.

Another possible factor contributing to this hypothesis is the presence of large fault zones, mainly the Ružbachy Fault Zone and a parallel fault cutting the High Tatra Mountains (Nemčok et al., 1993), which could be active during the CCPB sedimentation and causing faster subsidence of the Spiš and eastern Podhale areas. Moreover, the mentioned faults are known to be active during the uplift of the Tatra Mountains and presumably are linked to the faster uplift of the eastern Tatra Mountains in comparison to the western part of this massif (Śmigielski et al., 2016). The movement along the Ružbachy Fault Zone could also affect the Spiš area, which is supported by the abrupt change in paleotemperatures on both sides of the fault (Fig. 8). An increased overburden of the eastern Tatra Mountains resulted in noticeable thermal alteration of Tatra nappe units, which was reported by Staneczek et al. (2024b). The measured vitrinite reflectance in the Tatra Mountains increases from the western part to the eastern part. This trend also is recorded by biomarker and rock magnetic parameters (Staneczek et al., 2024b). Noteworthy, the paleotemperature trend recorded in the Tatra nappe units follows closely the trend present in the CCPB units.

The second trend present mostly in the northern part of the CCPB is the increase of paleotemperatures from the PKB to the Mesozoic Carpathian massifs (Figs. 4, 5, 8, S2 and S3).

The highest values are documented near the massifs, which is probably linked with the presence of the older Paleogene strata directly overlying the Mesozoic units. These rocks were slightly tilted during the uplift of the Carpathian massifs and now form outcrops, e.g., along the Tatra Mountains. Castelluccio et al. (2016) suggested that the PKB formed an elevated ridge during the Paleogene and the sedimentary infill could likely be lower than in other parts of the basin. Our data support this hypothesis.

Lower paleotemperatures also were reported in the Šariš Upland and in the Orava Basin (Fig. 8). The immaturity of these rocks suggests a relatively small thickness of overlying sedimentary rocks. Even though the exact extent of the CCPB is not currently known due to erosion of these rocks, it can be inferred that these regions were close to the margins of the CCPB. The deepening of the basin is reflected by the higher paleotemperatures in the hinterland of the Šariš Upland and Levoča Basins, reaching a maximum paleotemperature in the Spiš Basin.

Generally, the maturity patterns result prevailingly from basin architecture and its depth changes. These factors heavily influence sedimentation rates. The tectonic processes, which affected mostly the core along the Mesozoic massifs and the PKB are also important.

5.4. Implications for hydrocarbon exploration and paleotemperature reconstruction

Thermal maturity data are one of the key parameters for estimating and assessing the hydrocarbon potential of sedimentary rocks. Partial data for the Orava Basin area are presented in Staneczek et al. (2024a). The lithology of the Paleogene rocks is relatively homogeneous (Marynowski et al., 2006; Środoń et al., 2006; Day-Stirrat et al., 2008), especially for the Huty and Zuberec Fms. TOC and S1+S2 values for these rocks are similar to those in the Orava Basin, and range in generative potentials from poor to excellent (according to criteria of Peters and Cassa, 1994). Gas-prone type-III kerogen is dominant, but parts of the black shales of the Zuberec and Huty Fms. are characterized by oil-prone type-II kerogen (Soták et al., 2001; Staneczek et al., 2024a). All data suggest that the Paleogene rocks of the Huty and Zuberec Fms. could be a potential source of gaseous and even liquid hydrocarbons (e. g., Tissot and Welte, 1984). This is confirmed by the presence of liquid hydrocarbons found in the LHV and Tichy Potok boreholes in the Levoča Basin (Soták et al., 2001). In Fig. 6A, the regions marked in blue (Rc = 0.7–0.9 %) could potentially be oil-prone areas. In contrast, green regions where Rc > 0.9 % measured for the surface samples are areas of potential gas occurrence. Fig. 7 shows the correlation between the sterane indicators of C_{29} 20S/(S+R) vs. C_{29} αα/(αα+ββ) for surface samples (Fig. 7A), and boreholes (Fig. 7B). Only 12 samples were classified as immature among the surface samples and none are from the boreholes. Most of the samples were placed in the early mature or mature fields, which confirms their ability to generate hydrocarbons.

Although the presence of other concentrations of liquid and/or gaseous hydrocarbons in the CCPB area cannot be completely ruled out, their presence should be regarded as unlikely. There were recorded manifestations of hydrocarbon migration in the area of the Tatra Mountains and Podhale Basin, but their source was linked to Mesozoic source rocks (Marynowski et al., 2001; 2006). Other autochthonous Paleogene-source oils were found in Moravia (Western Carpathians; Picha and Peters, 1998), far from the area of research in this study. Many boreholes in the CCPB have no detectable hydrocarbons. Nevertheless, the problem requires further research in the context of Paleogene rocks as a source of shale gas.

There are many methods for reconstructing palaeotemperatures based on indicators derived from organic matter. Temperatures are usually correlated with vitrinite reflectance (Hunt, 1995; Selley and Sonnenberg, 2022 and references therein. Since sedimentary basins vary
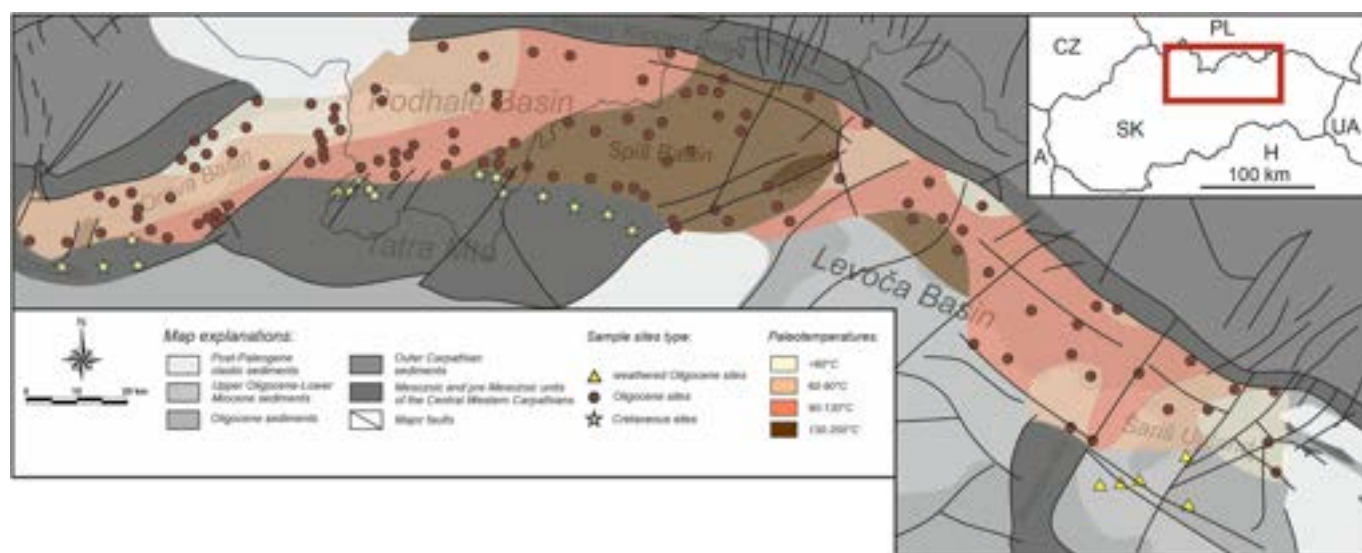
Fig. 8. Estimated paleotemperatures considering data from organic indicators in the CCPB (based on Barker and Pawlewicz, 1994; Hunt, 1995; Selley and Sonnenberg, 2022).

in age, rock lithology, facies and organic matter content, the estimated temperatures should be considered as approximate. Here we present temperature map (Fig. 8) estimates based on typical diagrams (e.g., Hunt, 1995), but the temperatures are within the range that corresponds to the respective values of the Rc.

5.5. Usefulness of biomarker indicators in reconstructing thermal maturity of the CCPB. Strengths and risks

It is widely accepted that vitrinite reflectance is treated as the optimal method for determining thermal maturity, especially when supported by an alternative approach (e.g., Hunt, 1995; Mählmann and Le Bayon, 2016). However, each sedimentary basin has its own characteristics, and there is no universal method to study the thermal maturity of sedimentary rocks of different ages and facies (e.g., Tissot and Welte, 1984). This is the case for the CCPB, where vitrinite reflectance does not give reliable results due to the presence of resinite and reworked vitrinite macerals (Staneczek et al., 2024a).

Indicators based on organic compounds also must be carefully selected. For example, in the case of the CCPB, the analysis of alkyl-naphthalenes, which, as light compounds, are susceptible to oxidation, biodegradation, and water washing in surface samples, was not considered (Palmer, 1993; Elie et al., 2000). For the same reason, indicators such as CPI or Pr/C_{17} and Ph/C_{18} also were not considered. The reliable use of biomarker indicators can be questioned for oxidized samples (Elie et al., 2000; Marynowski et al., 2011). Such samples are present in the southern part of the Šariš Upland and are most likely related to a pulse of paleoweathering in the area (yellow triangles in Fig. 1). Data from these samples should be treated with caution.

Some organic compounds that could be potentially used, especially in samples of highly thermally transformed rocks, were only present in some samples. This is especially true for aromatic sulfur compounds, which are not typical of terrigenous type-III kerogen (Radke and Willsch, 1994; Chakhmakhchev et al., 1997) and diamondoids (Chen et al., 1996; Zheng et al., 2023), which were sporadically detected.

The methods used to verify the individual indicators were based on

Fig. 9. Cross plots of the main maturity parameters from the CCPB of the surface and well samples. An explanation of abbreviations is below Table S.3.

the observation of changes in their values with depth in the boreholes (Figs. 3 and S4) and of their correlation with each other (Figs. 9, S5, and S6). 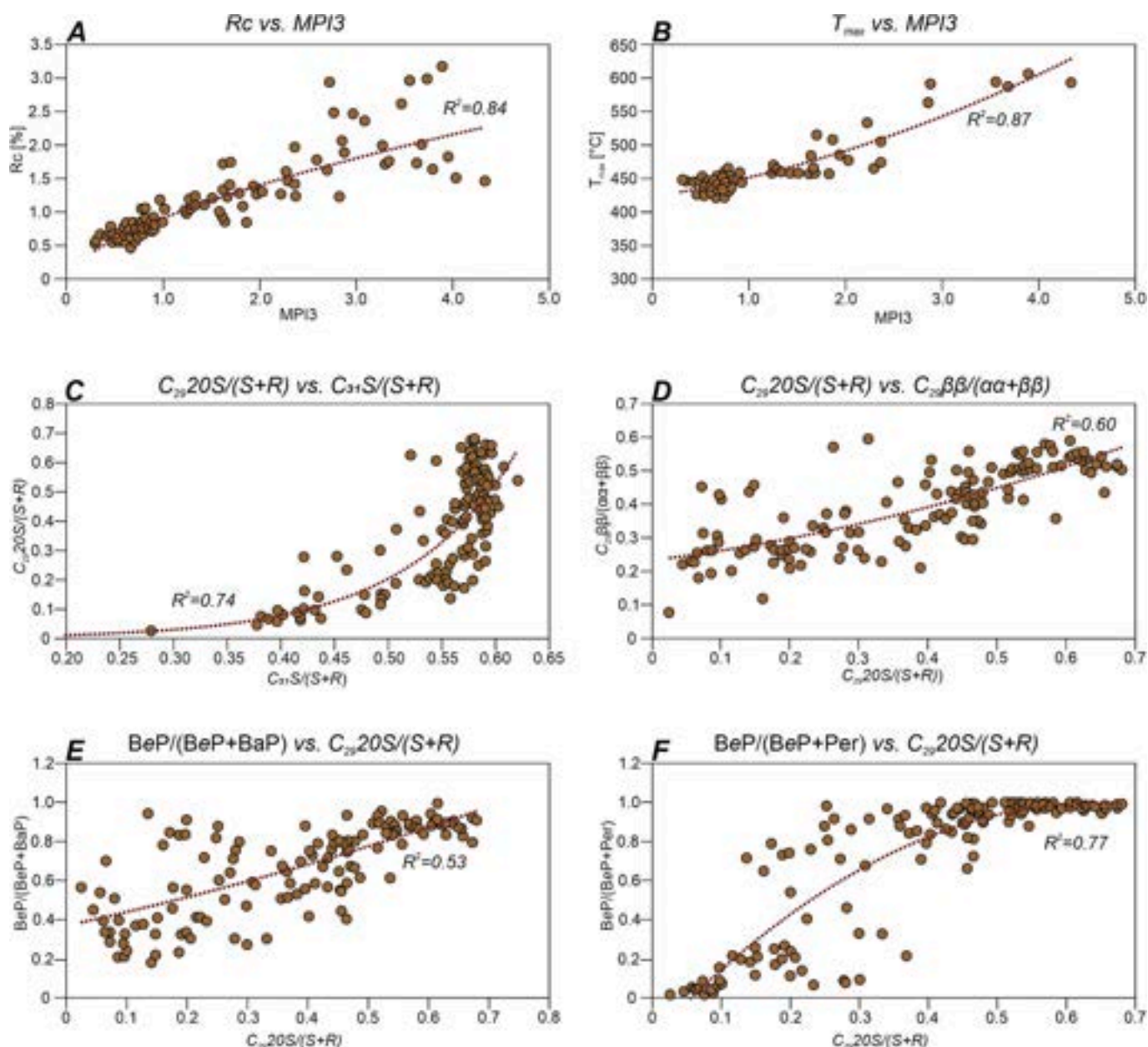It should be noted that with all the indicators used, there were deviations from a gradual trend with depth for individual samples. Such deviations can be attributed to a number of possible factors, for example, variable organic input, a change in clay mineral content (van Kaam-Peters et al., 1998), diagenetic methylation of some aromatic compounds (Alexander et al., 1995), or the influence of hydrothermal fluids (Bechtel et al., 2001). However, despite fluctuating values, consistent changes together with depth were the main indication for the reliable use of a particular ratio. The second factor verifying the suitability of individual ratios is their correlation to each other (Figs. 9, S5, and S6). In optimal cases, the correlation coefficient is at $R^2 > 0.8$, but even correlations of $R^2 = \sim 0.5$ for such a large number of samples seem sufficient.

In summary, organic compounds (including biomarkers), if properly selected, can be a powerful tool to assess the thermal maturity of sedimentary rocks. In this context, the CCPB is an experimental model due to its wide range of maturity, numerous natural exposures and boreholes and significant TOC content. It is highly likely that a single biomarker parameter is not sufficient to adequately determine paleotemperatures. It is also useful to use alternative methods not based on organic matter studies.

6. Conclusions

Using parameters based on organic compounds and T_{max}, the thermal maturity of a large part of the Central Carpathian Paleogene Basin (CCPB) was determined. The data obtained confirm earlier reports of maximum paleotemperatures recorded in the Spiš Basin, and a gradual decrease westwards, reaching a minimum in the Orava Basin. In contrast, towards the east, thermal maturity drops sharply after crossing the Ružbachy Fault Zone, especially in the northern part of the Levoča Basin. The thermal maturity of the CCPB then reaches a minimum in the easternmost area (Šariš Upland). The parameter that spans the widest range of maturity and increases gradually with depth is the methylphenanthrene index (MPI1), that yields a calculated vitrinite reflectance (Rc). This index does not perform well below the reflectance of 0.5 %, where several biomarkers, such as oleanenes, lupenes, and ββ-hopanes, 22R-homohopanes, and 20R-steranes are particularly diagnostic.

When comparing the illite/smectite method with biomarker techniques, the results for more mature rocks show strong agreement, while at lower maturity levels, the illite/smectite ratio seems to be overestimated, especially in areas where unsaturated and thermodynamically unstable biomarkers are present. This discrepancy highlights the limitations of relying on a single maturity indicator and underscores the importance of an integrated approach that combines multiple methodologies. Most of the organic matter from the Paleogene rocks of the CCPB area is at the marginally mature or mature level, while part of the Spiš area and deeper samples from the Bukowina Tatrzańska PIG-1 borehole are overmature. Regions within the CCPB with Rc values between 0.7 % and 0.9 % (as indicated on the thermal maturity maps) are identified as potentially oil-prone areas. In contrast, areas with Rc > 0.9 % are more likely to be associated with gas hydrocarbon occurrences. The CCPB's unique characteristics, including its wide maturity range and significant TOC content, make it an ideal model and case study for testing and developing new approaches to thermal maturity assessment and paleotemperature reconstruction.

CRediT authorship contribution statement

Dorota Staneczek: Writing – review & editing, Writing – original draft, Visualization, Methodology, Investigation, Formal analysis, Data curation, Conceptualization. **Leszek Marynowski:** Writing – review & editing, Writing – original draft, Supervision, Project administration, Methodology, Funding acquisition, Conceptualization.

Declaration of competing interest

The authors declare that they have no known competing financial interests or personal relationships that could have appeared to influence the work reported in this paper.

Acknowledgments

Appendix A. Supplementary data

Supplementary data to this article can be found online at https://doi.org/10.1016/j.orggeochem.2025.104933.

Data availability

Data will be made available on request.

References

Alexander, R., Bastow, T.P., Fisher, S.J., Kagi, R.I., 1995. Geosynthesis of organic compounds: II. Methylation of phenanthrene and alkylphenanthrenes. Geochimica et Cosmochimica Acta 59, 4259–4266.

Anczkiewicz, A.A., Środoń, J., Zattin, M., 2013. Thermal history of the Podhale Basin in the internal Western Carpathians from the perspective of apatite fission track analyses. Geologica Carpathica 64, 141–151.

Argiriadis, E., Denniston, R.F., Ondei, S., Bowman, D.M., Genuzio, G., Nguyen, H.Q.A., Thompson, J., Baltieri, M., Azenon, J., Cugley, J., 2024. Polycyclic aromatic hydrocarbons in tropical Australian stalagmites: a framework for reconstructing paleofire activity. Geochimica et Cosmochimica Acta 366, 250–266.

Asif, M., Nazir, A., Fazeelat, T., Grice, K., Nasir, S., Saleem, A., 2011. Applications of polycyclic aromatic hydrocarbons to assess the source and thermal maturity of the crude oils from the Lower Indus Basin, Pakistan. Petroleum Science and Technology 29, 2234–2246.

Barker, C.E., Pawlewicz, M.J., 1994. Calculation of vitrinite reflectance from thermal histories and peak temperatures. A comparison of methods. ACS Symposium Series 570, 216–229.

Bechtel, A., Gratzer, R., Püttmann, W., Oszczepalski, S., 2001. Variable alteration of organic matter in relation to metal zoning at Rote Fäule front (Lubin-Sieroszowice mining district, SW Poland). Organic Geochemistry 32, 377–395.

Burnham, A.K., Sweeney, J.J., 1989. A chemical kinetic model of vitrinite maturation and reflectance. Geochimica et Cosmochimica Acta 53, 2649–2657.

Castelluccio, A., Mazzoli, S., Andreucci, B., Jankowski, L., Szaniawski, R., Zattin, M., 2016. Building and exhumation of the Western Carpathians: new constraints from sequentially restored, balanced cross sections integrated with low-temperature thermochronometry. Tectonics 35, 2698–2733.

Cebulak, S., Kępińska, B., Marynowski, L., Pająk, L., 2004. Present and past thermal conditions of the Podhale geothermal system. In: Kępińska, B. (Ed.) Investigations of Thermal Conditions in the Podhale Geothermal System Using an Oxyreactive Thermal Analysis (OTA) and Mineralogical Methods, IGSMiE PAN, Kraków, 80-87 pp. (in Polish).

Chakhmakhchev, A., Suzuki, N., Takayama, K., 1997. Distribution of alkylated dibenzothiophenes in petroleum as a tool for maturity assessments. Organic Geochemistry 26, 483–490.

Chen, J., Fu, J., Sheng, G., Liu, D., Zhang, J., 1996. Diamondoid hydrocarbon ratios: novel maturity indices for highly mature crude oils. Organic Geochemistry 25, 179–190.

Day-Stirrat, R.J., Aplin, A.C., Środoń, J., van der Pluijm, B.A., 2008. Diagenetic reorientation of phyllosilicate minerals in Paleogene mudstones of the Podhale Basin, southern Poland. Clays and Clay Minerals 56, 100–111.

Derkowski, A., Środoń, J., Goryl, M., Marynowski, L., Szczerba, M., Mazur, S., 2021. Long-distance fluids migration defines diagenetic history of unique Ediacaran sediments in the East European Craton. Basin Research 33, 570–593.

Elie, M., Faure, P., Michels, R., Landais, P., Griffault, L., 2000. Natural and laboratory oxidation of low-organic-carbon-content sediments: comparison of chemical changes in hydrocarbons. Energy & Fuels 14, 854–861.

Eslinger, E., Highsmith, P., Albers, D., de Mayo, B., 1979. Role of iron reduction in the conversion of smectite to illite in bentonites in the disturbed belt, Montana. Clays & Clay Minerals 27, 327–338.

Francû, J., Müller, P., 1983. Organic matter maturity in peri-klippen flysch of the Inner Carpathian Mts. (East Slovakia). Geologica Carpathica 34, 483–494.

Gedl, P., 2000. Biostratigraphy and paleoenvironment of the Podhale Paleogene (Inner Carpathians, Poland) in the light of palynological studies. Part I. Studia Geologica Polonica 117, 69–154 (in Polish).

George, S.C., 1992. Effect of igneous intrusion on the organic geochemistry of a siltstone and an oil shale horizon in the Midland Valley of Scotland. Organic Geochemistry 18, 705–723.

Gleadow, A.J.W., Duddy, I.R., Lovering, J.F., 1986. Fission track analysis: a new tool for the evaluation of thermal histories and hydrocarbon potential. APEA Journal 23, 93–102.

Gross, P., Filo, I., Halouzka, R., Haŝko, J., Havrila, M., Kováč, M., Maglay, J., Mello, J., Nagy, A., 1994. Geological Map of Southern and Eastern Part of Orava. State Geological Institute of Dionỳz Štúr. Bratislava.

Gross, P., Buček, S., Ďurkovič, T., Filo, I., Karoli, S., Maglay, J., Nagy, A., Halouzka, R., Spišák, Z., Žec, B., Vozár, J. Borza, V., Lukáčik, E., Mello, J., Polák, M., Janočko, J., 1999. Geological map of the Popradská Kotlina Basin, Hornádska Kotlina Basin, Levočské Vrchy Mt., Spišsko-Šarišske Medzihorie Depression, Bachureň Mts. and Šarišska Vrchovina Highland. State Geological Institute of Dionỳz Štúr. Bratislava.

Gross, P., Köhler, E., Samuel, O., 1984. New lithostratigraphic classification of the Central Carpathians Paleogene. Geologické Práce, Správy 81, 103–117.

Gross, P., Köhler, E., Haŝko, J., Halouzka, R., Mello, J., Nagy, A., 1993. Geológia južnej a východnej Oravy (Geology of the southern and eastern Orava). Štátny Geologickỳ Ústav Dionýza Štúra, Bratislava, p. 319 (in Slovak).

Hartkopf-Fröder, Ch., Königshof, P., Littke, R., Schwarzbauer, J., 2015. Optical thermal maturity parameters and organic geochemical alteration at low grade diagenesis to anchimetamorphism: a review. International Journal of Coal Geology 150–151, 74–119.

Holman, A.I., Poropat, S.F., Greenwood, P.F., Bhandari, R., Tripp, M., Hopper, P., Schimmelmann, A., Brosnan, L., Rickard, W.D.A., Wolkenstein, K., Grice, K., 2024. Significance of lignin and fungal markers in the Devonian (407 Ma) Rhynie Chert. Geobiology 22.

Hunt, J.M., 1995. Petroleum Geochemistry and Geology. W.H. Freeman, New York.

ISO 7404-2, 2009. Methods for the Petrographic Analysis of Coals – Part 2: Methods of Preparing Coal Samples. International Organization for Standardization, Switzerland.

Jiao, S., Zhang, H., Cai, Y., Jin, C., Shen, S., 2024. Polycyclic aromatic hydrocarbons (PAHs) evidence for frequent combustion events on land during the Permian–Triassic transition in Northwest China. Palaeogeography, Palaeoclimatology, Palaeoecology 642, 112152.

Kováč, M., Plašienka, D., Soták, J., Vojtko, R., Oszczypko, N., Less, G., Ćosović, V., Fügenschuh, B., Králiková, S., 2016. Paleogene palaeogeography and basin evolution of the Western Carpathians, Northern Pannonian domain and adjoining areas. Global and Planetary Change 140, 9–27.

Kruge, M.A., 2000. Determination of thermal maturity and organic matter type by principal components analysis of the distributions of polycyclic aromatic compounds. International Journal of Coal Geology 43, 27–51.

Li, M., Shi, S., Wang, T.-G., Zhong, N., Wang, G., Cui, J., 2012. The occurrence and distribution of phenylphenanthrenes, phenylanthracenes and binaphthyls in Palaeozoic to Cenozoic shales from China. Applied Geochemistry 27, 2560–2569.

Mackenzie, A.S., McKenzie, D., 1983. Isomerization and aromatization of hydrocarbons in sedimentary basins formed by extension. Geological Magazine 120, 417–470.

Mählmann, R.F., Le Bayon, R., 2016. Vitrinite and vitrinite like solid bitumen reflectance in thermal maturity studies: correlations from diagenesis to incipient metamorphism in different geodynamic settings. International Journal of Coal Geology 157, 52–73.

Marynowski, L., Gawęda, A., Cebulak, S., Jędrysek, M., 2001. Hydrocarbons migration in tectonic zones of the Western Tatra Mountains crystalline basement (Central Western Carpathians). Geologica Carpathica 52, 3–14.

Marynowski, L., Gawęda, A., Poprawa, P., Żywiecki, M.M., Kępińska, B., Merta, H., 2006. Origin of organic matter from tectonic zones in the Western Tatra Mountains Crystalline Basement, Poland: an example of bitumen – source rock correlation. Marine and Petroleum Geology 23, 261–279.

Marynowski, L., Zatoń, M., Simoneit, B.R.T., Otto, A., Jędrysek, M.O., Grelowski, C., Kurkiewicz, S., 2007. Compositions, sources and depositional environments of organic matter from the Middle Jurassic clays of Poland. Applied Geochemistry 22, 2456–2485.

Marynowski, L., Kurkiewicz, S., Rakociński, M., Simoneit, B.R.T., 2011. Effects of weathering on organic matter: I. Changes in molecular composition of extractable organic compounds caused by paleoweathering of a Lower Carboniferous (Tournaisian) marine black shale. Chemical Geology 285, 144–156.

Marynowski, L., Smolarek, J., Hautevelle, Y., 2015. Perylene degradation during gradual onset of organic matter maturation. International Journal of Coal Geology 139, 17–25.

Marynowski, L., Pisarzowska, A., Derkowski, A., Rakociński, M., Szaniawski, R., Środoń, J., Cohen, A.S., 2017. Strong influence of palaeoweathering on trace metal concentrations and environmental proxies in black shales. Palaeogeography, Palaeoclimatology, Palaeoecology 472, 177–191.

Mondol, N.H., Bjørlykke, K., Jahren, J., Høeg, K., 2007. Experimental mechanical compaction of clay mineral aggregates—changes in physical properties of mudstones during burial. Marine and Petroleum Geology 24, 289–311.

Nemčok, J., Bezák, V., Biely, A., Gorek, A., Halouzka, R., Janák, M., Kahan, S., Kotański, Z., Lefeld, J., Mello, J., 1993. Geological Map of the Tatra Mountains 1: 50 000. Geologickỳ Ústav Dionýza ŠtúraBratislava, Bratislava.

Noah, M., Horsfield, B., Han, S., Wang, C., 2020. Precise maturity assessment over a broad dynamic range using polycyclic and heterocyclic aromatic compounds. Organic Geochemistry 148, 104099.

Otto, A., Simoneit, B.R.T., 2001. Chemosystematics and diagenesis of terpenoids in fossil conifer species and sediment from the Eocene Zeitz Formation, Saxony, Germany. Geochimica et Cosmochimica Acta 65, 3505–3527.

Palmer, S., 1993. Effect of biodegradation and water washing on crude oil composition. In: Engel, M.H., Macko, S.A. (Eds.), Organic Geochemistry. Plenum Press, New York, pp. 511–533.

Peters, K.E., Cassa, M.R., 1994. Applied source rock geochemistry. In: Magoon, L.B., Dow, W.G. (Eds.), The Petroleum System - from Source to Trap. AAPG Memoir, pp. 93–120.

Peters, K.E., Walters, C.C., Moldowan, J.M., 2005. The BIomarker Guide, vol. 2. Cambridge University Press, Cambridge, UK.

Petmecky, A., Meier, L., Reiser, H., Littke, R., 1999. High thermal maturity in the Lower Saxony Basin: intrusion or deep burial? Tectonophysics 304, 317–344.

Picha, F.J., Peters, K.E., 1998. Biomarker oil-to-source rock correlation in the Western Carpathians and their foreland, Czech Republic. Petroleum Geoscience 4, 289–302.

Poelchau, H.S., Baker, D.R., Hantschel, Th, Horsfield, B., Wygrala, B., 1997. Basin simulation and the design of the conceptual basin model. In: Welte, D.H., Horsfield, B., Baker, D.R. (Eds.), Petroleum and Basin Evolution. Springer-Verlag, pp. 3–62.

Poprawa, P., Marynowski, L., 2005. Thermal history of the Podhale Trough (northern part of the Central Carpathian Paleogene Basin) – preliminary results from 1-D maturity modeling. Mineralogical Society of Poland – Special Papers 25, 352–355.

Pradier, B., Bertrand, P., Martinez, L., Laggoun-Defarge, F., 1991. Fluorescence of organic matter and thermal maturity assessment. Organic Geochemistry 17, 511–524.

Radke, M., 1987. Organic geochemistry of aromatic hydrocarbons. In: Brooks, J., Welte, D. (Eds.), Advances in Petroleum Geochemistry, vol. 2. Academic Press, London, pp. 141–207.

Radke, M., Welte, D.H., 1983. The Methylphenanthrene Index (MPI). A maturity parameter based on aromatic hydrocarbons. In: Bjorøy, M. (Ed.), Advances in Organic Geochemistry. Wiley and Sons, New York, pp. 504–512.

Radke, M., Willsch, H., 1994. Extractable alkyldibenzothiophenes in Posidonia Shale (Toarcian) source rocks: relationship of yields to petroleum formation and expulsion. Geochimica et Cosmochimica Acta 58, 5223–5244.

Radke, M., Horsfield, B., Littke, R., Rullkötter, J., 1997. Maturation and petroleum generation. In: Welte, D.H., Horsfield, B., Baker, D.R. (Eds.), Petroleum and Basin Evolution. Springer-Verlag, pp. 169–229.

Rospondek, M.J., Marynowski, L., Chachaj, A., Góra, M., 2009. Novel aryl polycyclic aromatic hydrocarbons: phenylphenanthrene and phenylanthracene identification, occurrence and distribution in sedimentary rocks. Organic Geochemistry 40, 986–1004.

Seifert, W.K., Moldowan, J.M., 1980. The effect of thermal stress on source-rock quality as measured by hopane stereochemistry. Physics and Chemistry of the Earth 12, 229–237.

Selley, R., Sonnenberg, S., 2022. Elements of Petroleum Geology, fourth ed. Elsevier Science Publishing Co Inc., p. 608

Simoneit, B.R.T., 1977. Diterpenoid compounds and other lipids in deep-sea sediments and their geochemical significance. Geochimica et Cosmochimica Acta 41, 463–476.

Simoneit, B.R.T., Grimalt, J.O., Wang, T.G., Cox, R.E., Hatcher, P.G., Nissenbaum, A., 1986. Cyclic terpenoids of contemporary resinous plant detritus and of fossil woods, ambers and coal. Organic Geochemistry 10, 877–889.

Śmigielski, M., Sinclair, H., Stuart, F., Persano, C., Krzywiec, P., 2016. Exhumation history of the Tatry Mountains, Western Carpathians, constrained by low temperature thermochronology. Tectonics 35, 187–207.

Soták, J., 1998. Sequence stratigraphy approach to the Central Carpathian Paleocene (Eastern Slovakia): eustasy and tectonics as controls of deep-sea fan deposition. Slovak Geolocal Magazine 4, 185–190.

Soták, J., Pereszlenyi, M., Marschalko, R., Milicka, J., Starek, D., 2001. Sedimentology and hydrocarbon habitat of the submarine-fan deposits of the Central Carpathian Paleogene Basin (NE Slovakia). Marine and Petroleum Geology 18, 87–114.

Środoń, J., 1999. Use of clay minerals in reconstructing geological processes: recent advances and some perspectives. Clay Minerals 34, 27–37.

Środoń, J., Kotarba, M., Biroń, A., Such, P., Clauer, N., Wójtowicz, A., 2006. Diagenetic history of the Podhale-Orava Basin and the underlying Tatra sedimentary structural units (Western Carpathians): evidence from XRD and K-Ar of illite-smectite. Clay Minerals 41, 751–774.

Staneczek, D., Więcław, D., Marynowski, L., 2024a. Depositional conditions, wildfires, maturity, and hydrocarbon potential evaluation of Central Carpathian Paleogene Basin based on integrative approach from Orava Basin. International Journal of Coal Geology 285, 104490.

Staneczek, D., Szaniawski, R., Chadima, M., Marynowski, L., 2024b. Multi-stage tectonic evolution of the Tatra Mts recorded in the para- and ferromagnetic fabrics. Tectonophysics 880, 230338.

Starek, D., 2001. Sedimentology and paleodynamics of the Paleogene formations of the Central Western Carpathians. Slovak Academy of Sciences, Bratislava, pp. 1–152.

Suggate, R.P., 1998. Relations between depth of burial, vitrinite reflectance and geothermal gradient. Journal of Petroleum Geology 21, 5–32.

Taylor, G.H., Teichmüller, M., Davis, A., Diessel, C.F.K., Littke, R., Robert, R., 1998. Organic Petrology. A New Handbook Incorporating Some Revised Parts of Stach's Textbook of Coal Petrology. Gebrüder Borntraeger, Berlin.

Tissot, B.P., Welte, D.H., 1984. Petroleum Formation and Occurrence, second ed. Springer Verlag, Dordrecht, p. 728.

van Kaam-Peters, H.M.E., Köster, J., van der Gaast, S.J., Dekker, M., de Leeuw, J.W., Sinninghe Damsté, J.S., 1998. The effect of clay minerals on diasterane/sterane ratios. Geochimica et Cosmochimica Acta 62, 2923–2929.

Waliczek, M., Więcław, D., 2012. Maturity of Menilite Shales from Polish Outer Carpathians based on vitrinite reflectance and Rock-Eval pyrolysis data. Geology, Geophysics and Environment 38, 551–552.

Waliczek, M., Machowski, G., Więcław, D., Konon, A., Wandycz, P., 2019. Properties of solid bitumen and other organic matter from Oligocene shales of the Fore-Magura Unit in Polish Outer Carpathians: microscopic and geochemical approach. International Journal of Coal Geology 210, 103206.

Wendorff, M., Rospondek, M., Kluska, B., Marynowski, L., 2017. Organic matter maturity and hydrocarbon potential of the Lower Oligocene Menilite facies in the Eastern Flysch Carpathians (Tarcău and Vrancea Nappes), Romania. Applied Geochemistry 78, 295–310.

Wilkinson, J.J., 2001. Fluid inclusions in hydrothermal ore deposits. Lithos 55, 229–272.

Yuan, Z., Shi, S., Wu, X., Wang, S., Tian, W., 2024. Aliphatic and polycyclic aromatic compounds in coal and coal-based solid wastes: Relationship with coal-forming paleoenvironment and implications for environmental pollution. Science of the Total Environment 951, 175394.

Zheng, T., Zhang, Q., Deng, E., 2023. Applications of low molecular weight polycyclic aromatic hydrocarbons (PAHs) and diamondoids ratios/indices on the maturity assessment of coal-bearing source rock: insight from mature to overmature Longtan Shale. International Journal of Coal Geology 269, 104209.

Zumberge, J.E., 1987. Terpenoid biomarker distributions in low maturity crude oils. Organic Geochemistry 11, 479–496.

Supplementary materials to the article 3

Supplementary Materials

Application of biomarkers and non-biomarker parameters to assess maturity using the Central Carpathian Paleogene Basin as a case study

Dorota Staneczek[1], Leszek Marynowski[1*]

[1]Institute of Earth Sciences, Faculty of Natural Sciences, University of Silesia in Katowice, Będzińska 60, 41-200 Sosnowiec, Poland

Figures
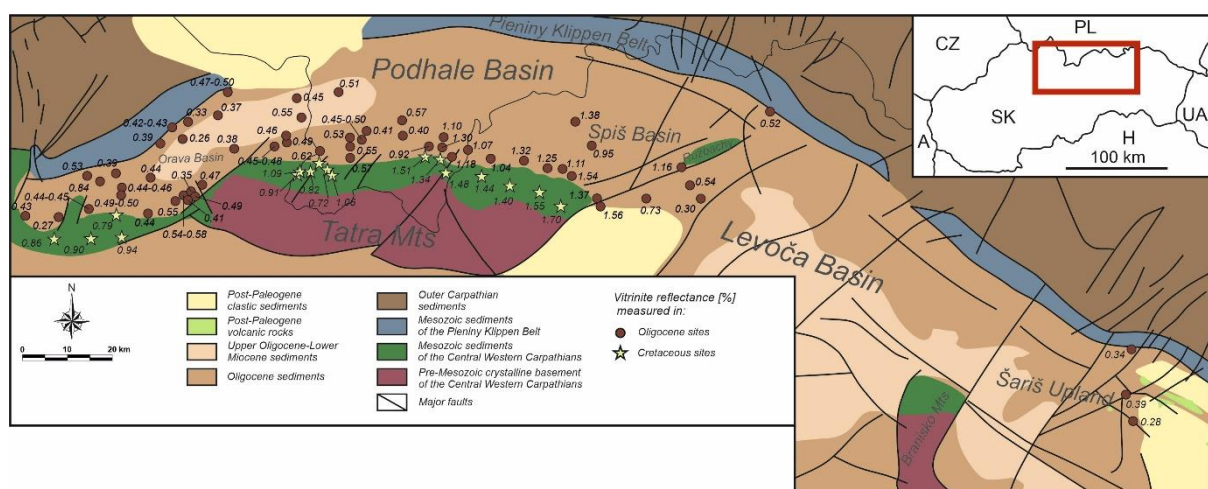
Fig. S1. The distribution of the vitrinite reflectance (*Rr*) values in the CCPB surface samples.
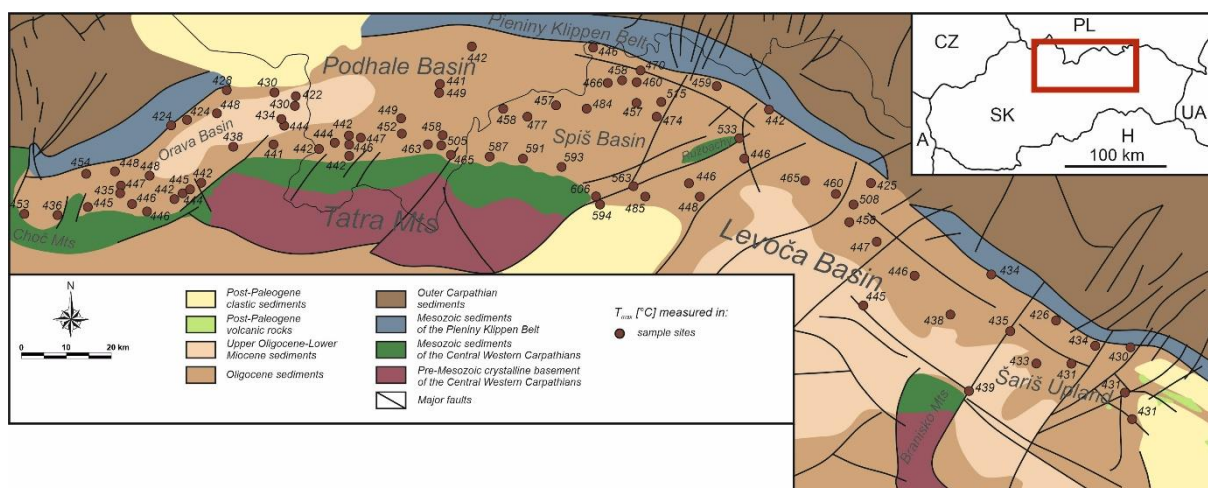
Fig. S2. The distribution of the T_{max} values in the CCPB surface samples.
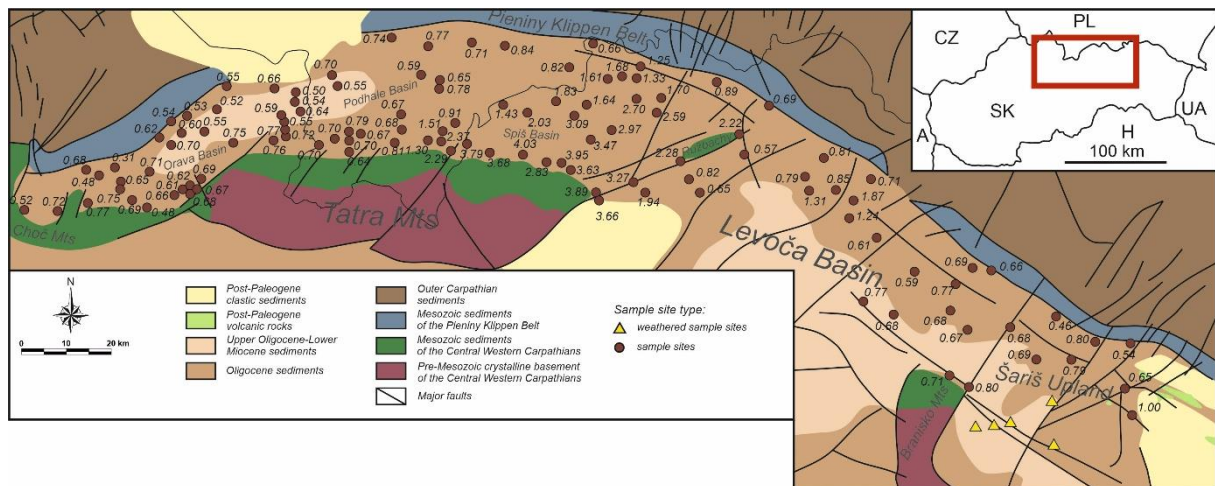
Fig. S3. The distribution of the MPI3 ratio values in the CCPB surface samples.
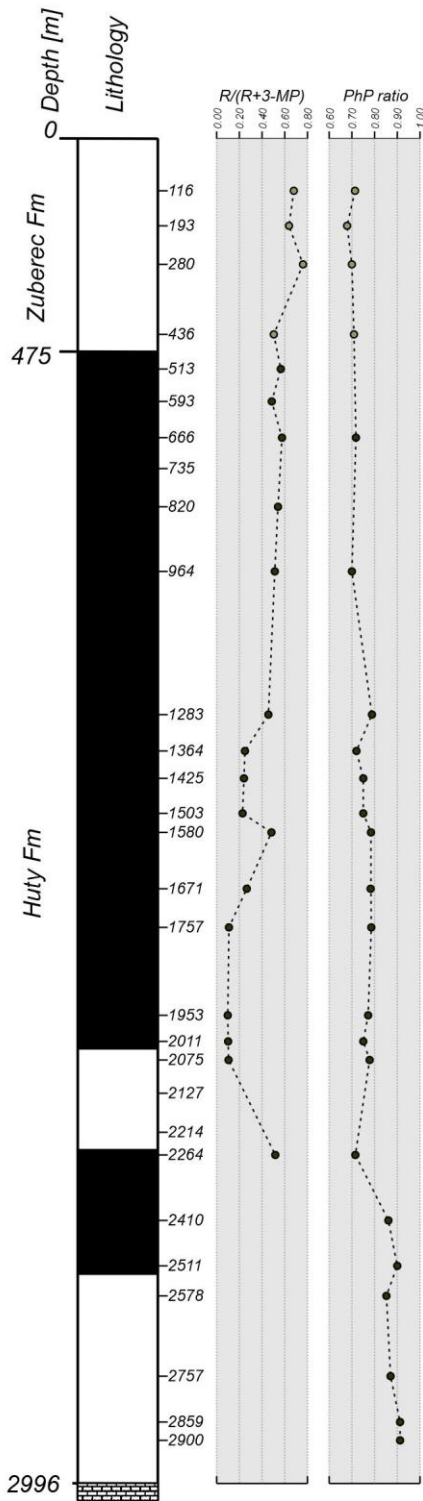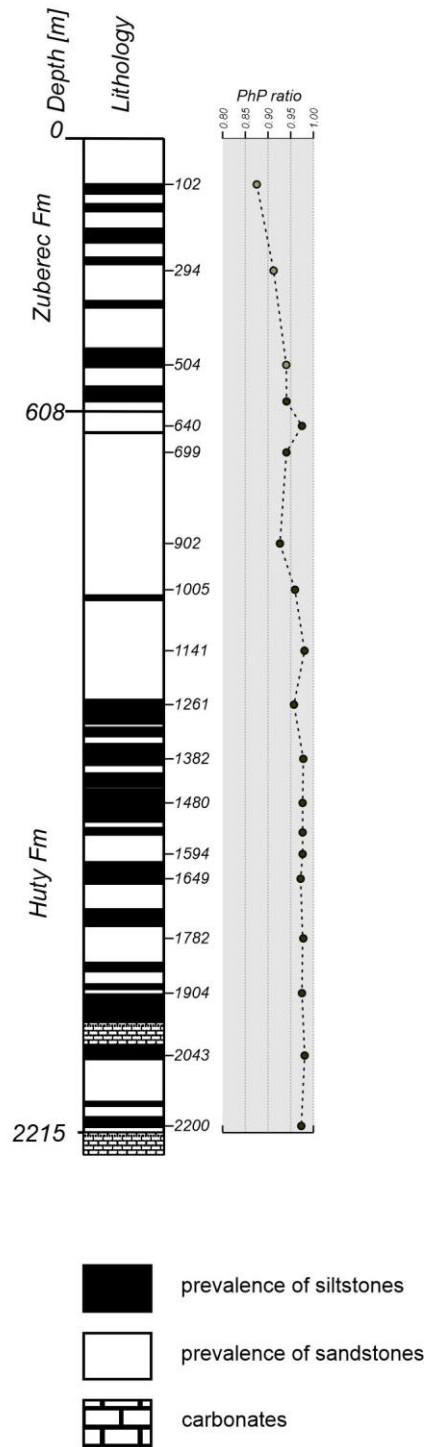
Fig. S4. Organic parameter changes in the Chochołów PIG-1 and Bukowina Tatrzańska PIG-1 wells. An explanation of abbreviations is below Table S.3.
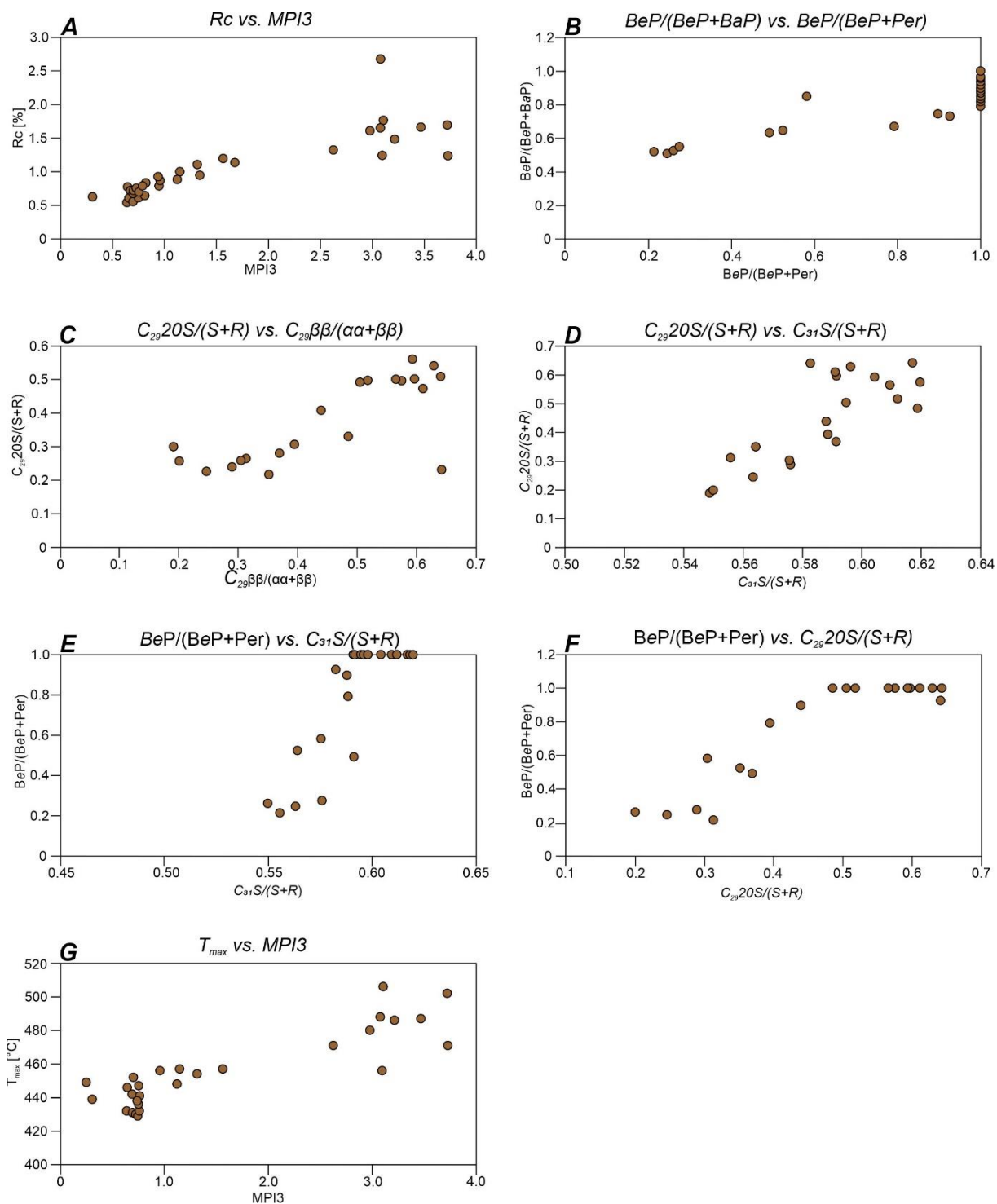
Fig. S5. Correlation of biomarker-derived parameters for Chochołów PIG-1 and Bukowina Tatrzańska PIG-1 well samples. An explanation of abbreviations is below Table S.3.
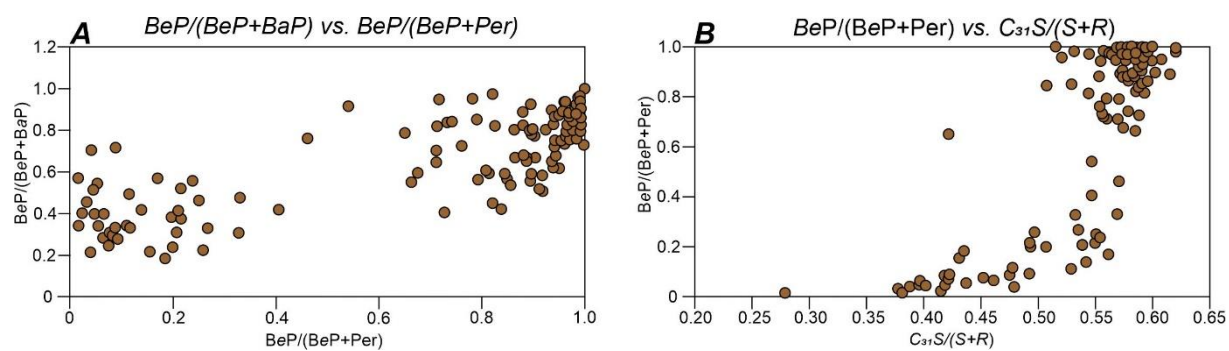
Fig. S6. Correlation of aromatic ratios for surface samples. An explanation of abbreviations is below Table S.3.

Tables

Tab. S1 Sample lithology and bulk geochemical data of the CCPB samples.

Sample code	Lithology	Unit	Geochemical parameters			Rock-Eval		Vitrinite reflectance	Temperature [°C]	
			TOC [%]	TS [%]	CC [%]	S2	Tmax [°C]	Rr [%]	(lnRc + 1.68)/0.0124*	(lnRc+1.19)/0.00782*
*Orava Basin**										
1_Bi	sandstone	Biely Potok	0.02	0.04	33.29	-	-	0.26	100	96
2_Bi	mudstone	Biely Potok	0.89	0.46	8.07	-	-	0.51	91	82
3_Bi	mudstone	Biely Potok	0.60	0.28	11.47	-	-	-	88	77
4_Bi	sandstone	Biely Potok	0.59	0.57	18.68	-	-	-	102	99
5_Bi	sandstone	Biely Potok	2.43	0.71	9.01	1.08	434	-	92	84
6_Bi	mudstone	Biely Potok	1.24	0.97	19.41	0.89	430	-	88	77
7_Bi	mudstone	Biely Potok	0.54	0.36	16.68	0.21	436	-	91	81
8_Bi	sandstone	Biely Potok	1.08	0.89	11.34	-	-	-	99	94
9_Bi	mudstone	Biely Potok	0.89	0.27	11.94	0.28	448	0.37	104	101
10_Bi	mudstone	Biely Potok	0.50	0.36	13.27	-	-	-	104	102
11_Bi	sandstone	Biely Potok	0.36	0.00	10.64	-	-	-	106	105
12_Zu	mudstone	Zuberec	1.37	1.27	9.80	1.58	438	-	105	104
13_Zu	mudstone	Zuberec	2.20	2.37	11.38	6.03	434	0.38	104	102
14_Zu	black shale	Zuberec	-	-	-	-	-	-	88	77
15_Zu	sandstone	Zuberec	0.37	0.17	21.29	-	-	0.44	111	114
16_Zu	sandstone	Zuberec	0.55	0.23	15.47	0.25	448	-	96	90
17_Zu	sandstone	Zuberec	3.15	1.71	17.53	4.41	422	0.45	98	93
18_Zu	sandstone	Zuberec	0.76	0.69	19.25	0.38	433	-	102	99
19_Zu	sandstone	Zuberec	0.19	0.02	26.71	-	-	-	101	97
20_Zu	mudstone	Zuberec	3.55	3.40	18.70	-	-	0.55	97	91
21_Zu	black shale	Zuberec	0.76	1.28	19.29	-	-	-	98	92
22_Zu	black shale	Zuberec	1.09	1.15	16.61	-	-	0.39	94	86
23_Zu	sandstone	Zuberec	0.62	0.00	14.19	0.33	446	-	123	132

24_Zu	black shale	Zuberec	1.47	1.53	14.34	-	-	-	109	111
25_Zu	black shale	Zuberec	0.90	1.38	17.98	-	-	-	109	110
26_Zu	black shale	Zuberec	0.83	1.10	19.04	-	-	-	108	109
27_Zu	black shale	Zuberec	0.85	1.36	16.55	-	-	-	108	109
28_Zu	black shale	Zuberec	0.78	1.26	17.06	-	-	-	110	112
29_Zu	black shale	Zuberec	0.98	1.34	16.25	-	-	-	111	113
30_Zu	black shale	Zuberec	0.89	1.46	13.80	-	-	-	114	117
31_Zu	black shale	Zuberec	0.87	0.60	13.79	-	-	-	114	119
32_Zu	black shale	Zuberec	1.56	2.02	14.07	-	-	0.49	109	110
33_Zu	black shale	Zuberec	0.68	0.02	0.01	0.27	444	-	91	81
34_Zu	black shale	Zuberec	0.67	0.73	8.76	0.60	446	-	99	95
35_Zu	black shale	Zuberec	9.91	4.16	5.16	12.22	428	0.47	88	76
36_Zu	black shale	Zuberec	2.32	1.45	9.25	1.40	433	0.50	90	79
37_Zu	black shale	Zuberec	5.01	2.46	7.51	6.63	430	-	93	84
38_Zu	black shale	Zuberec	1.06	0.01	16.37	0.98	454	0.53	100	95
39_Zu	black shale	Zuberec	6.99	3.27	6.10	19.55	424	0.42	88	77
40_Zu	black shale	Zuberec	3.50	1.87	7.30	5.00	426	0.43	84	71
41_Zu	black shale	Zuberec	3.00	0.79	9.68	3.72	437	-	94	87
42_Zu	coal	Zuberec	82.51	0.92	0.23	294.65	421	0.50	98	93
43_Zu	black shale	Zuberec	3.05	0.97	10.43	4.85	435	0.49	103	101
44_Zu	weathered coal	Zuberec	1.61?	0?	7.35?	1.08?	454?	-	101?	98?
45_Zu	black shale + coal	Zuberec	56.44	0.71	0.28	51.54	457	-	100	96
46_Zu	mudstone	Zuberec	0.75	0.00	27.04	0.44	448	0.39	91	81
47_Zu	black shale	Zuberec	10.11	0.09	13.81	10.88	448	0.44	98	92
48_Zu	coal	Zuberec	56.00	0.53	0.38	46.93	447	0.46	98	92
49_Zu	sandstone	Zuberec	0.45	0.21	23.76	0.22	445	-	105	105
50_Zu	mudstone	Zuberec	0.41	0.00	41.99	-	-	0.84	85	72
51_Zu	mudstone	Zuberec	0.22	0.00	0.35	-	-	-	87	76
52_Zu	black shale	Zuberec	0.67	1.54	11.99	-	-	-	-	-
53_Zu	black shale	Zuberec	0.50	0.81	14.56	-	-	-	110	112

54_Zu	black shale	Zuberec	1.89	2.04	12.54	-	-	-	113	117
55_Zu	black shale	Zuberec	2.46	2.31	13.56	-		0.46	108	108
56_Zu	black shale	Zuberec	2.08	2.04	16.88	4.01	429	-	87	75
57_Zu	black shale	Zuberec	5.65	2.08	0.00	7.63	424	0.33	87	76
58_Zu	sandstone	Zuberec	0.48	0.07	16.77	0.27	453	0.43	89	78
59_Ht	black shale	Huty	0.78	0.94	18.05	0.59	448	0.45	115	120
60_Ht	black shale	Huty	0.87	1.12	18.02	0.67	446	0.50	114	118
61_Ht	black shale	Huty	0.76	0.61	16.62	0.47	446	0.47	103	100
62_Ht	mudstone	Huty	0.85	1.49	15.27	0.84	441	0.48	112	115
63_Ht	sandstone	Huty	0.94	1.08	8.90	-	-	0.45	110	112
64_Ht	mudstone	Huty	0.44	0.07	35.67	0.35	445	0.35	112	115
65_Ht	sandstone	Huty	0.37	0.01	36.27	-	-	0.44	96	89
66_Ht	mudstone	Huty	0.31	0.04	36.81	0.29	446	0.41	109	110
67_Ht	mudstone	Huty	0.58	0.39	25.13	0.58	444	0.55	116	121
68_Ht	mudstone	Huty	0.59	0.59	16.85	0.44	446	0.55	111	114
69_Ht	black shale	Huty	0.65	0.86	18.45	0.33	444	0.41	119	127
70_Ht	black shale	Huty	0.57	0.00	13.79	0.34	458	-	-	-
71_Ht	black shale	Huty	0.66	1.16	17.77	0.44	444	0.53	112	114
72_Ht	black shale	Huty	1.10	0.25	14.81	0.50	442	0.62	108	108
73_Ht	sandstone	Huty	0.64	0.59	16.39	0.49	441	0.53	114	118
74_Ht	sandstone	Huty	0.40	0.44	22.76	0.22	442	-	120	127
75_Ht	sandstone	Huty	0.62	0.58	19.02	0.47	443	-	118	124
76_Ht	black shale	Huty	1.03	1.20	18.14	0.68	442	0.57	113	117
77_Ht	black shale	Huty	2.72	0.03	7.24	9.58	436	-	94	86
78_Ht	black shale	Huty	1.98	0.01	14.93	5.08	436	0.27	93	86
79_Ht	black shale	Huty	0.76	0.94	24.87	0.48	442	0.58	107	107
80_Ht	black shale	Huty	0.87	0.88	22.32	0.57	440	0.54	111	113
81_Ht	black shale	Huty	1.02	0.62	68.42	0.68	442	0.57	117	123
82_Ht	black shale	Huty	3.19	2.17	5.04	10.49	442	0.47	104	103
83_Ht	black shale	Huty	2.20	1.31	13.30	3.25	444	0.49	111	114

84_Ht	sandstone	Huty	5.39	0.04	11.48	7.98	445	0.44	100	96
85_Ht	coal	Huty	50.64	0.66	1.62	74.48	445	0.45	103	101

Podhale Basin

ANTPO	mudstone	Huty	-	-	-	-	-	-	108	109
GR_ZU_1B	mudstone	Huty	0.65	0.42	13.67	0.47	449	-	119	126
GR_ZU_1C	mudstone	Huty	0.67	0.79	10.01	-	-	-	120	128
GR_ZU_2B	mudstone	Huty	0.71	1.03	12.66	0.53	449	-	124	134
Ht11	silty sandstone	Huty	0.77	1.25	17.52	0.43	452	0.40	119	126
Ht7	mudstone	Huty	0.85	1.09	16.38	0.57	449	0.57	118	124
Ht8	mudstone	Huty	3.21	1.20	18.14	0.68	442	-	113	117
Ht9	mudstone	Huty	3.21	1.27	17.71	0.79	442	-	114	119
KAC1	mudstone	Huty	-	-	-	-	-	-	113	116
LAP1	mudstone	Huty	-	-	-	-	-	-	116	121
MARO1	mudstone	Huty	2.49	-	-	-	-	-	108	108
MARO2	mudstone	Huty	5.11	-	-	-	-	-	99	94
ZA1	black shale	Huty	1.59	1.39	34.85	1.09	463	0.92	139	158
ZA2	black shale	Huty	1.41	0.74	18.41	0.58	505	1.30	164	197
ZA3	black shale	Huty	0.59	1.04	18.28	0.15	468	1.07	175	216
ZA4	black shale	Huty	0.65	1.10	21.99	0.19	465	1.18	166	201
ZA5	black shale	Huty	0.59	1.33	17.90	0.27	458	1.10	151	177
BDUN0	mudstone	Huty	-	-	-	-	-	-	102	100
BAN484	mudstone	Zuberec	-	-	-	-	-	-	105	104
BKT102	mudstone	Zuberec	-	-	-	-	-	-	116	122
CHL193	mudstone	Zuberec	-	-	-	-	-	-	88	77
Z111	mudstone	Huty	-	-	-	-	-	-	117	123

Spisz Basin

BH1_1	mudstone	Huty	0.55	0.94	8.71	0.06	591	1.32	187	234
BH1_2	mudstone	Huty	0.89	0.96	17.17	-	-	-	169	205

BH2_1	mudstone	Huty	0.95	0.83	16.53	0.12	587	1.04	192	242
BH3_1	mudstone	Huty	1.15	1.04	8.40	0.16	593	1.11	166	201
BH3_2	mudstone	Huty	0.95	0.91	14.72	-	-	-	184	229
BH4_1	mudstone	Huty	0.73	0.92	22.88	0.11	344	1.54	179	221
BH4_2	mudstone	Huty	0.99	0.80	14.46	-	-	-	180	222
Hg_Ht_1A	mudstone	Huty	0.76	0.01	0.00	0.08	515	-	180	223
Hg_Ht_2A	mudstone	Huty	1.32	2.27	6.27	0.14	474	-	190	239
Hg_Ht_2B	mudstone	Huty	1.33	2.06	4.28	-	-	-	182	226
Jz_Ht_1A	mudstone	Huty	0.74	0.94	18.09	0.21	481	0.95	213	275
Jz_Ht_2B	mudstone	Huty	0.79	1.26	20.32	0.15	477	-	209	269
Jz_Ht_2C	mudstone	Huty	0.72	0.85	17.18	-	-	-	208	268
Lch_Ht_1A	mudstone	Huty	1.26	2.13	10.14	-	-	-	143	164
Lch_Ht_1B	mudstone	Huty	1.65	2.53	9.66	1.06	470	-	137	155
Len_Ht_1A	mudstone	Huty	0.70	0.57	17.14	-	-	-	224	292
Len_Ht_1B	mudstone	Huty	0.71	0.61	17.11	0.05	606	1.37	229	300
Ly_Ht_1A	mudstone	Huty	0.75	0.67	20.96	-	-	-	109	111
Ly_Ht_1B	mudstone	Huty	1.17	1.02	20.38	0.95	446	-	120	128
Rie_Ht_1A	mudstone	Huty	2.32	1.74	41.65	3.95	442	0.52	121	129
Sn_Ht_1B	mudstone	Huty	0.86	0.75	17.60	0.59	459	-	129	142
Sn_Ht_1C	mudstone	Huty	0.75	0.66	12.05	-	-	-	128	140
Sv_Ht_1A	mudstone	Huty	0.87	0.04	9.92	-	-	-	191	240
Sv_Ht_1B	mudstone	Huty	0.83	0.55	12.92	0.09	563	-	194	245
Top_Ht_1A	mudstone	Huty	0.49	0.01	2.67	-	-	1.16	174	213
Vr_Ht_1A	mudstone	Huty	0.40	0.01	1.27	-	-	-	-	-
Vr_Ht_1C	mudstone	Huty	0.55	0.01	0.05	0.05	533	-	155	183
Zdi_Ht_1A	mudstone	Huty	0.89	0.64	18.15	-	-	1.25	152	179
Hv_Zu_1C	mudstone	Zuberec	0.39	0.86	14.96	-	-	-	156	184
Hv_Zu_1D	mudstone	Zuberec	1.38	0.86	11.96	0.22	458	-	162	194
Hv_Zu_2A	mudstone	Zuberec	1.18	0.26	8.64	-	-	-	175	214
Hv_Zu_2D	mudstone	Zuberec	0.87	1.38	15.15	0.15	457	-	179	222

Sample	Lithology	Formation								
Lch_Zu_2A	mudstone	Zuberec	0.87	0.74	21.43	-	-	-	150	175
Lch_Zu_2D	mudstone	Zuberec	1.13	0.75	18.13	0.47	460	-	153	179
Len_Zu_2A	mudstone	Zuberec	0.92	1.51	14.94	0.05	594	1.61	223	291
Len_Zu_2B	mudstone	Zuberec	0.78	1.15	20.09	-	-	1.56	222	290
Md_Zu_1A	sandstone	Zuberec	0.89	0.01	1.07	0.38	446	-	96	90
Mf_Zu_1A	mudstone	Zuberec	0.96	0.58	16.08	0.29	475	-	205	262
Mf_Zu_1D	mudstone	Zuberec	0.88	0.58	17.40	0.51	466	1.38	181	224
Mt_Zu_1A	mudstone	Zuberec	1.43	0.03	11.48	-	-	-	136	153
Mt_Zu_1C	mudstone	Zuberec	1.18	1.00	13.21	-	-	-	130	143
Mt_Zu_1D	mudstone	Zuberec	1.78	0.05	0.09	-	-	-	152	179
Os_Zu_1A	mudstone	Zuberec	0.95	1.15	14.52	-	-	-	157	186
Os_Zu_1B	mudstone	Zuberec	2.88	1.18	4.27	1.36	477	-	153	180
Os_Zu_2A	mudstone	Zuberec	0.89	0.40	10.94	0.29	458	-	144	165
Os_Zu_3A	mudstone	Zuberec	0.94	0.59	16.94	0.24	457	-	142	163
Os_Zu_3B	mudstone	Zuberec	0.79	0.62	16.93	-	-	-	154	182
Slo_Zu_1A	mudstone	Zuberec	0.85	0.42	19.07	0.31	485	0.73	162	194
Slo_Zu_1B	mudstone	Zuberec	0.50	0.27	19.61	-	-	-	163	196
TOP_Zu_2A	mudstone	Zuberec	4.60	2.47	5.12	5.81	446	0.54	128	141
Topr_Zu-1A	sandstone	Zuberec	1.17	0.02	4.51	0.55	448	0.30	102	99
Vf_Zu_1A	mudstone	Zuberec	0.66	0.01	0.02	0.14	484	-	123	132

Lewocza Basin & Šariš Upland

Sample	Lithology	Formation								
Cnv_Zu_1A	weathered sandstone	Zuberec	0.33?	0?	12.09?	-	-	-	149?	174?
Fi_Zu_1A	weathered sandstone	Zuberec	0.46?	0.01?	15.95?	-	-	-	139?	158?
He_Zu_1A	weathered sandstone	Zuberec	0.26?	0?	18.21?	-	-	-	110?	112?
Hn_Zu_1A	weathered sandstone	Zuberec	0.34?	0?	6.81?	-	-	-	123?	133?
Ms_Zu_1A	weathered sandstone	Zuberec	0.45?	0?	15.07?	-	-	-	140?	160?
Lac_Zu_1A	mudstone	Zuberec	0.48	0.71	20.14	-	-	-	100	96
Lip_Zu_1A	mudstone	Zuberec	0.87	1.09	13.00	0.75	439	-	112	116
Pla_Zu_1C	sandstone	Zuberec	5.09	4.45	6.35	5.72	425	-	89	78

Sl_Zu_1A	sandstone	Zuberec	0.17	0.10	5.81	-	-	-	120	128
Sl_Zu_1B	sandstone	Zuberec	0.38	0.16	7.90	-	-	-	123	132
Baj_Ht_1A	mudstone	Huty	0.70	0.68	14.83	-	-	-	113	117
Baj_Ht_1C	mudstone	Huty	0.52	0.93	14.45	-	-	-	114	119
Baj_Ht_1D	mudstone	Huty	0.99	1.08	11.21	0.85	447	-	117	122
Bre_Ht_1A	mudstone	Huty	0.40	0.48	13.20	-	-	-	118	125
Cv_Ht_1A	mudstone	Huty	0.84	1.09	5.60	-	-	-	110	112
Cv_Ht_1B	mudstone	Huty	0.66	2.89	18.41	0.83	426	-	116	121
Da_Ht_1B	mudstone	Huty	0.73	0.40	19.51	0.65	438	-	113	116
Dub_Ht_1A	mudstone	Huty	0.49	0.31	15.28	-	-	-	73	54
Gre_Ht_1A	mudstone	Huty	1.14	0.34	18.24	1.25	431	0.39	110	112
Gre_Ht_1B	mudstone	Huty	1.02	0.60	15.68	-	-	-	103	101
Ja_Ht_1A	mudstone	Huty	0.48	0.48	16.62	-	-	-	145	167
Jbv_Ht_1A	mudstone	Huty	0.55	0.27	8.99	0.29	434	-	110	111
Jbv_Ht_1C	mudstone	Huty	0.51	0.02	11.61	-	-	-	118	124
Jv_Ht_1B	mudstone	Huty	0.85	0.49	17.89	0.90	435	-	110	112
Kam_Ht_1B	mudstone	Huty	0.46	0.01	17.05	-	-	-	114	118
Krv_Ht_1A	mudstone	Huty	0.40	0.02	1.00	-	-	-	102	99
Lk_Ht_1A	mudstone	Huty	0.87	0.01	3.71	0.46	469	-	114	118
Lk_Ht_1B	mudstone	Huty	0.83	0.05	7.77	-	-	-	117	123
Lu_Ht_1B	mudstone	Huty	0.85	0.69	13.81	-	-	-	101	97
Lu_Ht_1E	mudstone	Huty	0.75	0.88	17.41	0.67	434	-	108	109
Nl_Ht_1A	mudstone	Huty	0.95	0.19	13.46	0.51	465	-	118	124
Nl_Ht_1B	mudstone	Huty	0.41	0.08	0.51	-	-	-	112	115
Ra_Ht_1A	mudstone	Huty	1.13	1.53	10.33	1.61	430	0.34	87	75
Sab_Ht_1B	mudstone	Huty	0.67	0.56	9.08	0.39	431	-	119	127
Sam_Bp_1A	mudstone	Huty	0.59	0.00	15.03	-	-	-	159	189
Sam_Bp_1B	mudstone	Huty	0.57	0.00	14.86	0.09	508	-	122	131
Sam_Ht_2A	mudstone	Huty	0.71	0.02	10.59	0.30	458	-	137	154
Sam_Ht_2C	mudstone	Huty	0.70	0.60	7.97	-	-	-	144	165

Sample	Rock type	Formation	TOC	TS	CC	S2				
Sar_Ht_1A	mudstone	Huty	0.39	0.10	16.73	-	-	-	116	121
Sar_Ht_1B	mudstone	Huty	0.53	1.20	18.95	-	-	-	113	116
Sar_Ht_1C	mudstone	Huty	1.54	1.73	13.37	3.85	446	-	120	128
Sp_Ht_1A	mudstone	Huty	2.10	2.09	11.70	-	-	-	123	132
Sp_Ht_1B	mudstone	Huty	0.70	0.36	11.46	0.43	431	0.28	118	125
Us_Ht_1A	mudstone	Huty	0.64	0.31	13.83	0.34	433	-	101	98
Ti_Bp_1A	sandstone	Biely Potok	7.79	0.12	0.68	4.47	445	-	108	108
Ti_Bp_1B	sandstone	Biely Potok	0.19	0.07	10.54	-	-	-	89	78

TOC = total organic carbon; TS = total sulphur, CC = carbonate content

S2 = mg HC/g

*Staneczek et al. (2024)

**Barker and Pawlewicz, 1994

Tab. S2 Sample lithology, depth and bulk geochemical data of the well samples.

Sample code	Lithology	Depth [m]	Unit	Geochemical parameters			Rock-Eval		Temperature [°C]	
				TOC [%]	TS [%]	CC [%]	S2	*Tmax [°C]*	*(lnRc + 1.68)/0.0124**	*(lnRc+1.19)/0.00782**
Chochołów										
CH2	mudstone	116	Zuberec	1.76 -	-	-	0.64	432	85.83	73.44
CH193	mudstone	193	Zuberec	-	-	-	- -		87.82	76.60
CH280	mudstone	280	Zuberec	-	-	-	- -		95.44	88.67
CH11	mudstone	436	Zuberec	2.29 -	-	-	0.81	431	94.48	87.16
CH513	mudstone	513	Huty	-	-	-	- -		94.24	86.77
CH593	mudstone	593	Huty	0.10 -	-	-	- -		91.00	81.64
CH17	mudstone	666	Huty	1.82 -	-	-	1.18	430	99.29	94.78
CH18	mudstone	735	Huty	0.44	0.90	15.45	0.83	432 -	-	
CH820	mudstone	820	Huty	-	-	-	- -		99.25	94.71
CH21	mudstone	964	Huty	2.62 -	-	-	0.95	432	103.88	102.07
CH29	mudstone	1283	Huty	3.4 -	-	-	0.22	429	106.47	106.16
CH30	mudstone	1364	Huty	0.95	1.27	16.68	2.26	436	106.48	106.18
CH32	mudstone	1425	Huty	0.86	1.79	9.52	1.67	438	106.82	106.72
CH35	mudstone	1503	Huty	0.84	0.84	11.46	1.47	441	105.15	104.07
CH36	mudstone	1580	Huty	0.42	0.46	18.68	1.09	439	97.58	92.07
CH1671	mudstone	1671	Huty	-	-	-	-	-	106.08	105.54
CH39	mudstone	1757	Huty	0.67	1.05	17.10	1.01	442	107.06	107.11
CH43	mudstone	1953	Huty	0.64	1.58	14.80	1.50	446	114.79	119.35
CH2011	mudstone	2011	Huty	2.50 -	-	-	-	-	109.03	110.22
CH2075	mudstone	2075	Huty	0.52 -	-	-	0.82	452	109.74	111.36
CH48	mudstone	2127	Huty	0.76	1.98	6.13	1.31	447 -	-	
CH49	mudstone	2214	Huty	1.31	1.64	9.12	2.29	448 -	-	
CH52	mudstone	2264	Huty	0.28	0.51	21.77	0.67	434	100.00	95.91
CH2410	mudstone	2410	Huty	0.48	1.24	15.57	- -		112.28	115.38

Sample	Lithology	Depth	Formation	TOC	TS	CC	S2	Tmax		
CH2511	mudstone	2511	Huty	-	-	-	-	-	116.33	121.81
CH58	mudstone	2578	Huty	2.6	-	-	0.89	447	113.43	117.20
CH63	mudstone	2757	Huty	2.65	-	-	-	-	120.92	129.09
CH65	mudstone	2859	Huty	0.15	0.67	22.86	0.40	456	124.05	134.05
CH2900	mudstone	2900	Huty	-	-	-	-	-	129.31	142.38

Bukowina

Sample	Lithology	Depth	Formation	TOC	TS	CC	S2	Tmax		
BKT102	mudstone	102	Zuberec	-	-	-	-	-	116.27	121.70
BKT294	mudstone	294	Zuberec	0.66	-	-	0.75	448	125.63	136.54
BKT10	mudstone	504	Zuberec	0.56	0.56	14.89	0.48	454	143.61	165.06
BKT640	mudstone	640	Huty	0.75	-	-	0.69	452	131.12	145.25
BKT14	mudstone	699	Huty	0.91	1.70	14.20	0.70	457	135.48	152.17
BKT902	mudstone	902	Huty	1.00	-	-	-	-	145.79	168.51
BKT20	mudstone	1005	Huty	0.94	1.46	12.26	0.49	471	150.02	175.23
BKT22	mudstone	1141	Huty	1.07	1.10	11.44	0.42	456	158.12	188.07
BKT1261	mudstone	1261	Huty	-	-	-	0.52	456	153.02	179.98
BKT25	mudstone	1382	Huty	0.99	1.14	14.99	0.33	480	173.89	213.08
BKT27	mudstone	1480	Huty	0.69	0.51	17.78	0.28	487	176.54	217.27
BKT1594	mudstone	1594	Huty	-	-	-	0.57	471	152.71	179.49
BKT30	mudstone	1649	Huty	1.17	2.06	5.73	0.37	488	176.02	216.45
BKT31	mudstone	1782	Huty	1.23	2.34	6.61	0.30	486	167.28	202.60
BKT35	mudstone	1904	Huty	0.94	1.83	7.73	0.23	506	181.31	224.84
BKT38	mudstone	2043	Huty	0.53	1.38	16.91	0.17	502	178.12	219.78
BKT2200	mudstone	2200	Huty	0.94	-	-	0.29	330	214.99	278.24

TOC = total organic carbon; TS = total sulphur, CC = carbonate content

S2 = mg HC/g

*Barker and Pawlewicz, 1994

Tab. S3 Biomarker-derived parameter values calculated for the CCPB samples.

Sample code	Aromatic maturity parameters							Aliphatic maturity parameters						
	m/z 252	m/z 178+192			m/z 219+237+255	m/z 192+219	m/z 254	m/z 191		m/z 217		m/z 218+191	m/z 217	m/z 191
	BeP / (BeP + Pe)	MPI1	MPI3	Rc [%]	R/(R+D+S)	R/(R+3-MP)	PhP ratio	C31(S/S+R)	C30αβ/βα	20S/(S+R)	C29ββ/(αα+ββ)		DIA/(DIA+REG)	Ts/(Ts+Tm)
*Orava Basin**														
1_Bi	0.81	0.40	0.69	0.64	0.71	0.43	0.00	0.54	3.99	0.25	0.37	0.00	0.17	0.29
2_Bi	0.27	0.29	0.55	0.58	0.88	0.76	0.79	0.54	3.86	0.18	0.36	0.07	0.06	0.50
3_Bi	0.25	0.26	0.55	0.56	0.49	0.32	0.74	0.55	2.85	0.18	0.23	0.27	0.15	0.13
4_Bi	0.21	0.43	0.47	0.66	0.74	0.63	0.80	0.54	2.33	0.21	0.27	0.14	0.08	0.22
5_Bi	0.20	0.31	0.59	0.59	0.72	0.50	0.80	0.51	2.03	0.19	0.26	0.40	0.07	0.21
6_Bi	0.08	0.26	0.54	0.55	0.86	0.93	0.76	0.42	1.77	0.07	0.45	0.19	0.02	0.43
7_Bi	0.06	0.29	0.55	0.57	0.87	0.96	0.78	0.40	2.33	0.10	0.31	0.51	0.06	0.30
8_Bi	0.22	0.39	0.70	0.63	0.71	0.71	0.67	0.49	4.11	0.12	0.20	0.53	0.06	0.32
9_Bi	0.21	0.45	0.52	0.67	0.50	0.65	0.00	0.49	2.37	0.15	0.29	0.00	0.10	0.00
10_Bi	0.20	0.46	0.45	0.68	0.51	0.62	0.00	0.49	2.46	0.13	0.25	0.00	0.06	0.00
11_Bi	0.65	0.49	0.55	0.69	0.34	0.67	0.87	0.42	2.84	0.16	0.12	0.00	0.08	0.28
12_Zu	0.94	0.48	0.75	0.69	0.97	0.68	0.75	0.59	5.16	0.37	0.35	0.00	0.16	0.42
13_Zu	0.86	0.46	0.73	0.68	0.98	0.72	0.76	0.59	3.99	0.38	0.32	0.00	-	-
14_Zu	0.21	0.26	0.70	0.55	0.93	0.63	0.55	0.55	2.82	0.19	0.27	0.00	0.15	0.39
15_Zu	0.92	0.57	0.71	0.74	1.00	0.87	0.80	0.59	4.74	0.31	0.37	0.00	0.15	0.25
16_Zu	0.92	0.36	0.74	0.61	1.00	0.84	0.86	0.59	4.89	0.26	0.38	0.46	0.21	0.36
17_Zu	0.08	0.38	0.66	0.63	0.76	0.80	0.68	0.45	2.54	0.09	0.37	0.25	0.00	0.45
18_Zu	0.09	0.43	0.61	0.66	0.77	0.86	0.71	0.48	3.14	0.10	0.43	0.31	0.08	0.25
19_Zu	0.12	0.41	0.50	0.65	0.81	0.96	0.75	0.48	2.93	0.15	0.46	0.40	0.08	0.27
20_Zu	0.09	0.37	0.64	0.62	0.78	0.80	0.73	0.49	2.30	0.18	0.32	0.06	0.02	0.41
21_Zu	0.14	0.38	0.64	0.63	0.71	0.74	0.76	0.54	4.18	0.22	0.22	0.09	0.10	0.25
22_Zu	0.11	0.33	0.63	0.60	0.74	0.73	0.66	0.53	4.34	0.20	0.23	0.00	0.13	0.29
23_Zu	1.00	0.75	0.69	0.85	0.96	0.75	0.65	0.62	7.67	0.61	0.41	0.00	0.26	0.04
24_Zu	0.90	0.54	0.77	0.72	0.96	0.34	0.60	0.59	6.24	0.48	0.43	0.00	0.21	0.54

25_Zu	0.86	0.53	0.79	0.72	0.98	0.49	0.71	0.60	6.26	0.43	0.36	0.00	0.24	0.40
26_Zu	0.96	0.52	0.88	0.71	0.98	0.46	0.68	0.59	5.17	0.41	0.36	0.00	0.25	0.46
27_Zu	0.95	0.52	0.78	0.71	0.96	0.43	0.72	0.59	6.69	0.47	0.43	0.00	0.22	0.57
28_Zu	0.94	0.55	0.77	0.73	0.97	0.48	0.71	0.59	4.76	0.43	0.37	0.00	0.20	0.41
29_Zu	0.97	0.56	0.72	0.74	0.97	0.51	0.69	0.58	5.81	0.46	0.42	0.00	0.20	0.54
30_Zu	0.96	0.60	0.72	0.76	0.97	0.54	0.68	0.59	5.81	0.47	0.40	0.00	0.21	0.54
31_Zu	0.97	0.62	0.72	0.77	0.98	0.55	0.70	0.58	5.90	0.48	0.40	0.00	0.19	0.54
32_Zu	0.96	0.53	0.73	0.72	0.97	0.45	0.74	0.59	5.99	0.44	0.42	0.00	0.19	0.54
33_Zu	0.73	0.29	0.54	0.58	0.19	0.63	0.75	0.56	5.15	0.19	0.25	0.52	0.14	0.33
34_Zu	0.40	0.40	0.55	0.64	0.81	0.55	0.80	0.55	3.48	0.22	0.27	0.44	0.11	0.25
35_Zu	0.18	0.25	0.54	0.55	0.44	0.60	0.00	0.44	1.78	0.14	0.44	0.18	0.01	0.00
36_Zu	0.15	0.28	0.55	0.57	0.38	0.58	0.79	0.43	2.05	0.10	0.29	0.22	0.06	0.61
37_Zu	0.26	0.31	0.66	0.59	1.00	0.44	0.84	0.50	2.28	0.15	0.27	0.44	0.00	0.51
38_Zu	1.00	0.40	0.68	0.64 -		0.24	0.80	0.58	5.98	0.58	0.51	0.57	0.09	0.23
39_Zu	0.05	0.26	0.53	0.56	0.43	0.92	0.00	0.44	2.94	0.07	0.18	0.00	0.03	0.13
40_Zu	0.07	0.22	0.47	0.53	0.62	0.89	0.67	0.42	2.09	0.10	0.41	0.00	0.02	0.26
41_Zu	0.84	0.34	0.71	0.60	0.99	0.87	0.83	0.59	4.43	0.40	0.49	0.00	0.04	0.33
42_Zu	0.73	0.38	0.75	0.63	0.99	0.79	0.83	0.59	5.98	0.47	0.35	0.00	0.04	0.42
43_Zu	0.82	0.45	0.77	0.67	0.99	0.80	0.84	0.59	8.24	0.46	0.44	0.00	0.43	0.43
44_Zu	0.9?	0.43?	0.79?	0.66?	1.00?	0.80?	0.84?	0.57?	7.49?	0.41?	0.43?	0.00?	0.05?	0.42?
45_Zu	0.89	0.41	0.75	0.64	1.00	0.70	0.82	0.57	5.82	0.45	0.43	0.00	0.08	0.43
46_Zu	1.00	0.29	0.31	0.58	0.86	0.24	0.60	0.60	7.25	0.41	0.51	0.00	0.27	0.73
47_Zu	0.94	0.38	0.66	0.63	1.00	0.88	0.88	0.59	4.40	0.43	0.47	0.00	0.02	0.12
48_Zu	0.95	0.37	0.69	0.62	1.00	0.83	0.89	0.59	6.14	0.46	0.56	0.00	0.02	0.14
49_Zu	0.92	0.48	0.65	0.69	1.00	0.94	0.86	0.59	5.82	0.43	0.47	0.00	0.19	0.53
50_Zu	1.00	0.23	0.30	0.54	0.90	0.79	0.74	0.57	3.00	0.47	0.47	0.00	0.15	0.00
51_Zu	0.98	0.25	0.48	0.55	0.54	0.86	0.74	0.56	4.59	0.25	0.32	0.00	0.07	0.44
52_Zu	0.66 -		-	-	1.00	1.00	0.00	0.59	5.15	0.46	0.40	0.00	0.20	0.48
53_Zu	1.00	0.55	0.71	0.73	0.98	0.48	0.69	0.59	6.16	0.45	0.45	0.00	0.15	0.53
54_Zu	0.97	0.60	0.72	0.76	0.96	0.60	0.67	0.59	6.86	0.44	0.43	0.00	0.20	0.57

	C1	C2	C3	C4	C5	C6	C7	C8	C9	C10	C11	C12	C13	C14
55_Zu	1.00	0.52	0.73	0.71	0.97	0.44	0.64	0.59	5.29	0.42	0.37	0.00	0.22	0.47
56_Zu	0.02	0.24	0.60	0.55	0.40	0.90	0.52	0.42	4.44	0.09	0.26	0.45	0.13	0.29
57_Zu	0.05	0.25	0.54	0.55	0.82	0.96	0.50	0.42	4.23	0.06	0.23	0.48	0.05	0.37
58_Zu	0.07	0.27	0.52	0.56	0.89	0.94	0.75	0.46	2.38	0.20	0.51	0.00	0.03	0.43
59_Ht	-	0.63	0.67	0.78	1.00	0.30	0.73	0.61	6.19	0.49	0.50	0.00	0.24	0.00
60_Ht	-	0.61	0.71	0.77	1.00	0.24	0.76	0.58	6.79	0.53	0.50	0.00	0.35	0.65
61_Ht	-	0.44	0.35	0.67	1.00	0.66	0.00	0.58	6.76	0.54	0.50	0.00	0.28	0.61
62_Ht	0.92	0.58	0.73	0.75	0.97	0.49	0.79	0.59	6.38	0.46	0.41	0.00	0.23	0.59
63_Ht	0.97	0.55	0.76	0.73	1.00	0.38	0.79	0.58	4.79	0.34	0.58	0.00	0.14	0.32
64_Ht	0.97	0.58	0.62	0.75	0.99	0.34	0.66	0.58	7.78	0.57	0.39	0.00	0.15	0.08
65_Ht	1.00	0.35	0.48	0.61	0.94	0.68	0.58	0.58	5.59	0.47	0.56	0.00	0.14	0.39
66_Ht	0.97	0.53	0.61	0.72	0.99	0.33	0.69	0.56	6.81	0.46	0.55	0.00	0.23	0.30
67_Ht	0.94	0.64	0.66	0.79	1.00	0.53	0.64	0.58	7.27	0.53	0.53	0.00	0.31	0.54
68_Ht	0.88	0.57	0.70	0.74	0.17	0.19	0.80	0.57	6.57	0.55	0.51	0.00	0.37	0.62
69_Ht	1.00	0.70	0.93	0.82	0.98	0.35	0.70	0.59	5.17	0.55	-	0.00	0.32	0.56
70_Ht	-	-	-	-	-	-		0.59	6.21	0.46	0.56	0.00	-	-
71_Ht	1.00	0.57	0.72	0.74	0.95	0.06	0.58	0.57	8.29	0.58	0.55	0.00	0.33	0.66
72_Ht	1.00	0.52	0.70	0.71	0.50	0.15	0.67	0.57	6.98	0.53	-	0.00	0.42	0.65
73_Ht	-	0.61	0.67	0.77	1.00	0.30	0.75	0.56	4.81	0.44	0.50	0.00	0.31	0.57
74_Ht	-	0.70	0.66	0.82	1.00	0.24	0.71	0.58	6.70	0.59	0.51	0.00	0.33	0.55
75_Ht	-	0.67	0.73	0.80	1.00	0.66	0.75	0.58	6.16	0.54	0.50	0.00	0.31	0.56
76_Ht	1.00	0.60	0.64	0.76	1.00	0.26	0.77	0.57	5.91	0.54	0.51	0.00	0.35	0.65
77_Ht	0.88	0.33	0.72	0.60	0.94	0.59	0.67	0.58	4.59	0.25	0.33	0.00	0.04	0.47
78_Ht	0.86	0.32	0.71	0.59	0.94	0.61	0.68	0.58	4.81	0.29	0.31	0.00	0.06	0.43
79_Ht	0.96	0.51	0.70	0.70	1.00	0.21	0.73	0.59	7.02	0.62	0.53	0.00	0.39	0.68
80_Ht	-	0.56	0.69	0.74	1.00	0.18	0.72	0.58	7.42	0.61	0.54	0.00	0.24	0.63
81_Ht	-	0.66	0.67	0.79	1.00	0.20	0.73	0.58	8.22	0.62	0.55	0.00	0.17	0.62
82_Ht	1.00	0.46	0.68	0.68	1.00	0.22	0.67	0.57	8.12	0.51	0.49	0.00	0.27	0.50
83_Ht	1.00	0.57	0.68	0.74	1.00	0.34	0.79	0.57	6.28	0.57	0.58	0.00	0.42	0.67
84_Ht	0.84	0.41	0.43	0.64	0.99	0.86	0.65	0.51	3.30	0.28	0.33	0.00	0.10	0.29

85_Ht	0.85	0.45	0.77	0.67	1.00	0.90	0.64	0.53	4.12	0.25	0.44	0.00	0.01	0.28

Podhale Basin

ANTPO	0.96	0.52	0.68	0.71	1.00	0.17	0.73	0.59	8.91	0.52	0.44	0.00	0.27	0.13
GR_ZU_1B	1.00	0.69	0.81	0.81	1.00	0.06	0.88	0.60	3.45	0.00	0.00	0.00	0.00	0.67
GR_ZU_1C	1.00	0.71	0.65	0.83	1.00	0.12	0.00	0.00	0.00	0.00	0.00	0.00	0.00	0.70
GR_ZU_2B	0.96	0.78	0.78	0.87	1.00	0.12	0.84	0.59	6.15	0.66	0.51	0.00	0.34	0.62
Ht11	0.96	0.69	0.68	0.82	1.00	0.11	0.84	0.52	2.91	0.62	0.56	0.00	0.55	0.49
Ht7	0.97	0.67	0.67	0.80	1.00	0.08	0.82	0.54	5.00	0.61	0.59	0.00	0.47	0.07
Ht8	1.00	0.60	0.64	0.76	1.00	0.26	0.77	0.58	5.52	0.54	0.51	0.00	0.35	0.65
Ht9	0.96	0.62	0.71	0.77	1.00	0.28	0.77	0.58	6.65	0.56	0.51	0.00	0.36	0.61
KAC1	0.98	0.59	0.82	0.76	1.00	0.03	0.85	0.58	7.14	0.55	0.51	0.00	0.19	0.22
LAP1	0.98	0.63	0.84	0.78	1.00	0.08	0.86	0.59	9.34	0.58	0.58	0.00	0.30	0.31
MARO1	0.68	0.52	0.74	0.71	0.93	0.49	0.55	0.57	4.02	0.31	0.24	0.00	0.13	0.23
MARO2	0.33	0.39	0.72	0.63	0.91	0.56	0.70	0.53	2.76	0.33	0.23	0.00	0.05	0.13
ZA1	1.00	1.07	1.30	1.04	1.00	0.00	0.91	-	-	-	0.00	0.00	0.00	0.00
ZA2	1.00	1.70	2.37	1.42	1.00	0.03	0.95	-	-	-	0.00	0.00	0.00	0.00
ZA3	1.00	2.07	3.79	1.64	1.00	0.01	0.96	-	-	-	0.00	0.00	0.03	0.00
ZA4	1.00	1.78	2.29	1.47	1.00	0.02	0.95	-	-	-	0.00	0.00	0.00	0.00
ZA5	1.00	1.35	1.51	1.21	1.00	0.04	0.92	-	-	-	0.00	0.00	0.05	0.00
BDUN0	0.95	0.44	0.59	0.66	1.00	0.18	0.61	0.61	7.50	0.36	0.36	0.00	0.32	0.35
BAN484	1.00	0.47	0.77	0.68	1.00	0.08	0.00	-	-	-	0.00	0.00	0.00	0.00
BKT102	1.00	0.65	0.91	0.79	1.00	0.05	0.90	-	-	-	0.00	0.00	0.00	0.00
CHL193	0.21	0.26	0.70	0.55	0.93	0.63	0.72	0.55	2.39	0.27	0.27	0.00	0.18	0.07
Z111	1.00	0.66	0.81	0.80	1.00	0.04	0.84	0.52	6.45	-	0.00	0.00	1.00	0.00

Spisz Basin

BH1_1	1.00	2.48	2.88	1.89	-	0.00	0.99	-	-	-	0.00	0.00	0.00	0.00
BH1_2	1.00	1.85	4.03	1.51	-	0.00	1.00	-	-	-	0.00	0.00	0.00	0.00
BH2_1	1.00	2.69	3.68	2.01	-	0.00	1.00	-	-	-	0.00	0.00	0.00	0.00

BH3_1	1.00	1.78	4.33	1.47	-		0.00	0.99	-	-	-	0.00	0.00	0.00	0.00
BH3_2	1.00	2.38	3.95	1.83	-		0.00	1.00	-	-	-	0.00	0.00	0.00	0.00
BH4_1	1.00	2.19	3.30	1.72	-		0.00	0.00	-	-	-	0.00	0.00	0.00	0.00
BH4_2	1.00	2.22	3.63	1.73	-		0.00	0.00	-	-	-	0.00	0.00	0.00	0.00
Hg_Ht_1A	1.00	2.24	1.70	1.75	-		0.00	0.98	-	-	-	0.00	0.00	0.00	0.00
Hg_Ht_2A	1.00	2.62	2.36	1.97	-		0.00	1.00	-	-	-	0.00	0.00	0.00	0.00
Hg_Ht_2B	1.00	2.30	2.59	1.78	-		0.00	0.98	-	-	-	0.00	0.00	0.00	0.00
Jz_Ht_1A	1.00	3.70	3.47	2.62	-		0.00	1.00	-	-	-	0.00	0.00	0.00	0.00
Jz_Ht_2B	1.00	3.47	2.77	2.48	-		0.00	1.00	-	-	-	0.00	0.00	0.00	0.00
Jz_Ht_2C	1.00	3.44	2.97	2.47	-		0.00	1.00	-	-	-	0.00	0.00	0.00	0.00
Lch_Ht_1A	1.00	1.17	1.34	1.10	1.00		0.01	0.92	-	-	-	0.00	0.00	0.00	0.66
Lch_Ht_1B	1.00	1.03	1.25	1.02	1.00		0.03	0.93	-	-	-	0.00	0.00	0.00	0.00
Len_Ht_1A	1.00	1.44	3.73	2.99**	-		0.00	0.97	-	-	-	0.00	0.00	0.00	0.32
Len_Ht_1B	1.00	1.81	3.89	3.18**	-		0.00	0.95	-	-	-	0.00	0.00	0.00	0.79
Ly_Ht_1A	0.97	0.54	0.66	0.72	1.00		0.26	0.77	0.58	8.90	0.67	0.52	0.00	0.23	0.61
Ly_Ht_1B	0.98	0.72	0.75	0.83	1.00		0.19	0.79	0.60	7.73	0.63	0.53	0.00	0.27	0.61
Rie_Ht_1A	0.95	0.72	0.69	0.83	1.00		0.06	0.70	0.57	8.34	0.65	0.54	0.00	0.61	0.05
Sn_Ht_1B	0.99	0.87	0.90	0.92	1.00		0.06	0.89	0.60	2.53	0.66	0.43	0.00	0.43	0.78
Sn_Ht_1C	0.97	0.85	0.89	0.91	1.00		0.05	0.90	0.58	2.25	-	0.00	0.00	1.00	0.92
Sv_Ht_1A	1.00	2.66	3.27	1.99	-		0.00	1.00	-	-	-	0.00	0.00	0.00	0.00
Sv_Ht_1B	1.00	2.77	2.85	2.06	-		0.00	1.00	-	-	-	0.00	0.00	0.00	0.00
Top_Ht_1A	0.96	2.01	2.28	1.60	1.00		0.16	0.98	0.57	4.35	-	0.00	0.00	1.00	0.34
Vr_Ht_1A	-		-	-	-	-		0.00	0.00	-	-	-	0.00	0.00	0.00	0.00
Vr_Ht_1C	0.98	1.45	2.22	1.27	-		0.00	0.00	-	-	-	0.00	0.00	0.00	0.00
Zdi_Ht_1A	1.00	1.38	2.83	1.23	-		0.00	0.98	-	-	-	0.00	0.00	0.00	0.50
Hv_Zu_1C	1.00	1.47	1.79	1.28	-		0.00	0.96	-	-	-	0.00	0.00	0.00	0.00
Hv_Zu_1D	1.00	1.64	1.68	1.39	-		0.00	0.96	-	-	-	0.00	0.00	0.00	0.00
Hv_Zu_2A	1.00	2.04	2.70	1.63	-		0.00	1.00	-	-	-	0.00	0.00	0.00	0.00
Hv_Zu_2D	1.00	2.20	1.62	1.72	-		0.00	1.00	-	-	-	0.00	0.00	0.00	0.47
Lch_Zu_2A	0.98	1.32	1.27	1.19	-		0.00	0.94	-	-	-	0.00	0.00	0.00	0.00

Lch_Zu_2D	0.99	1.40	1.33	1.24	-		0.00	0.94	-	-	-		0.00	0.00
Len_Zu_2A	1.00	1.39	3.56	2.96**	-		0.00	0.98	-	-	-		0.00	0.00
Len_Zu_2B	1.00	1.34	2.73	2.94**	-		0.00	0.93	-	-	-		0.00	0.00
Md_Zu_1A	0.33	0.36	0.57	0.61	0.98		0.62	0.81	0.57	2.95	0.30		0.26	0.00
Mf_Zu_1A	0.99	3.27	3.09	2.36	-		0.00	1.00	-	-	-		0.00	0.00
Mf_Zu_1D	1.00	2.26	3.34	1.76	-		0.00	0.00	-	-	-		0.00	0.00
Mt_Zu_1A	0.78	1.01	1.59	1.01	1.00		0.03	0.95	-	-	-		0.00	0.00
Mt_Zu_1C	0.99	0.88	1.61	0.93	1.00		0.01	0.95	-	-	-		0.00	0.00
Mt_Zu_1D	1.00	1.38	1.67	1.23	1.00		0.05	0.96	-	-	-		0.00	0.00
Os_Zu_1A	0.98	1.51	2.03	1.31	-		0.00	0.96	-	-	-		0.00	0.00
Os_Zu_1B	0.99	1.40	2.37	1.24	-		0.00	0.96	-	-	-		0.00	0.00
Os_Zu_2A	0.98	1.18	1.43	1.11	-		0.00	0.94	-	-	-		0.00	0.00
Os_Zu_3A	0.98	1.15	1.83	1.09	-		0.00	0.96	-	-	-		0.00	0.00
Os_Zu_3B	0.98	1.44	1.97	1.27	-		0.00	0.97	-	-	-		0.00	0.00
Slo_Zu_1A	0.71	1.65	1.94	1.39	-		0.00	0.96	-	-	-		0.00	0.00
Slo_Zu_1B	0.83	1.68	1.69	1.41	-		0.00	0.96	-	-	-		0.00	0.00
TOP_Zu_2A	0.94	0.86	0.82	0.92	1.00		0.04	0.88	0.55	8.07	0.41		0.53	0.00
Topr_Zu-1A	0.90	0.43	0.65	0.66	1.00		0.66	0.85	0.60	3.53	0.45		0.30	0.00
Vf_Zu_1A	0.99	0.76	1.64	0.86	-		0.00	0.95	-	-	-		0.00	0.00

Lewocza Basin & Šariš Upland

Cnv_Zu_1A	0.72?	1.30?	0.97?	1.18?	-		0.00?	0.00?	0.56?	4.10?	0.14?	0.26?	0.00?	0.07?
Fi_Zu_1A	0.74?	1.08?	0.79?	1.05?	1.00?		0.74?	0.00?	0.58?	7.77?	0.20?	0.27?	0.00?	0.07?
He_Zu_1A	0.79?	0.55?	0.92?	0.73?	-		0.00?	0.00?	0.57?	4.03?	0.17?	0.28?	0.00?	0.17?
Hn_Zu_1A	0.54?	0.77?	0.63?	0.86?	-		0.00?	0.78?	0.55?	3.78?	0.20?	0.29?	0.00?	0.13?
Ms_Zu_1A	0.82?	1.10?	0.82?	1.06?	-		0.00?	0.00?	0.00?	0.00?	0.00?	0.00?	0.00?	1.00?
Lac_Zu_1A	0.79	0.41	0.71	0.64	1.00		0.48	0.81	0.56	4.14	0.40	0.34	0.00	0.21
Lip_Zu_1A	0.94	0.59	0.80	0.75	1.00		0.32	0.73	0.60	5.31	0.47	0.35	0.00	0.24
Pla_Zu_1C	0.04	0.27	0.71	0.56	0.80		0.78	0.76	0.48	2.64	0.09	0.19	0.84	0.02
Sl_Zu_1A	0.11	0.71	0.89	0.82	0.74		0.84	0.00	0.00	0.00	0.00	0.00	0.00	0.00

Sl_Zu_1B	0.09	0.75	0.81	0.85	0.73	0.38	0.00	0.42	3.03	0.28	0.27	0.00	0.08	0.39
Baj_Ht_1A	0.99	0.60	0.67	0.76	1.00	0.03	0.78	0.59	6.84	0.64	0.50	0.00	0.32	0.74
Baj_Ht_1C	0.99	0.62	0.61	0.77	1.00	0.08	0.79	0.58	9.01	0.68	0.50	0.00	0.00	0.00
Baj_Ht_1D	0.99	0.65	0.69	0.79	1.00	0.05	0.79	0.58	7.36	0.52	0.50	0.00	0.46	0.75
Bre_Ht_1A	0.90	0.68	0.68	0.81	1.00	0.34	0.74	0.59	5.61	0.27	0.42	0.00	0.24	0.36
Cv_Ht_1A	0.71	0.55	0.61	0.73	0.85	0.57	0.80	0.56	2.83	0.23	0.24	0.00	0.14	0.25
Cv_Ht_1B	0.76	0.64	0.46	0.78	0.48	0.63	0.74	0.55	5.17	0.00	0.26	0.00	0.10	0.26
Da_Ht_1B	0.90	0.59	0.68	0.76	1.00	0.61	0.74	0.58	3.55	0.36	0.00	0.00	1.00	0.19
Dub_Ht_1A	0.88	0.11	0.67	0.46	0.95	0.91	0.75	0.55	3.19	0.07	0.29	0.00	0.15	0.15
Gre_Ht_1A	0.04	0.55	0.65	0.73	0.77	0.98	0.00	0.39	2.24	0.03	0.25	0.30	0.06	0.20
Gre_Ht_1B	0.02	0.45	0.56	0.67	0.75	0.97	0.00	0.28	2.26	0.00	0.08	0.39	0.06	0.38
Ja_Ht_1A	0.97	1.20	1.31	1.12	1.00	0.02	0.93	0.56	2.30	0.39	0.00	0.00	1.00	0.00
Jbv_Ht_1A	0.71	0.55	0.80	0.73	1.00	0.24	0.87	0.57	1.63	0.28	0.21	0.00	0.04	0.04
Jbv_Ht_1C	0.46	0.67	0.76	0.80	1.00	0.51	0.92	0.57	1.54	0.20	0.38	0.00	0.05	0.03
Jv_Ht_1B	0.24	0.55	0.68	0.73	0.82	0.81	0.72	0.55	2.30	0.40	0.21	0.00	0.13	0.06
Kam_Ht_1B	0.97	0.61	0.69	0.76	1.00	0.37	0.74	0.57	6.06	0.52	0.46	0.00	0.14	0.31
Krv_Ht_1A	0.94	0.44	0.77	0.66	1.00	0.27	0.75	0.59	4.59	0.61	0.50	0.00	0.24	0.38
Lk_Ht_1A	0.99	0.61	0.75	0.76	1.00	0.03	0.85	0.57	7.01	0.64	0.55	0.00	0.22	0.77
Lk_Ht_1B	0.98	0.66	0.85	0.80	1.00	0.03	0.85	0.58	7.34	0.47	0.52	0.00	0.25	0.81
Lu_Ht_1B	0.81	0.42	0.66	0.65	1.00	0.54	0.78	0.59	3.00	0.45	0.29	0.00	0.19	0.14
Lu_Ht_1E	0.89	0.52	0.67	0.71	1.00	0.62	0.79	0.58	2.92	0.00	0.29	0.00	0.15	0.17
Nl_Ht_1A	0.90	0.67	0.79	0.80	1.00	0.06	0.90	0.00	0.00	0.00	0.00	0.00	1.00	0.92
Nl_Ht_1B	0.94	0.58	0.79	0.75	1.00	0.11	0.89	0.00	0.00	0.08	0.00	0.00	1.00	0.90
Ra_Ht_1A	0.02	0.24	0.54	0.55	0.82	0.96	0.53	0.38	4.04	0.05	0.31	0.18	0.16	0.21
Sab_Ht_1B	0.03	0.70	0.79	0.82	0.59	0.78	0.74	0.38	2.03	0.00	0.22	0.27	0.06	0.07
Sam_Bp_1A	0.98	1.55	1.62	1.33	1.00	0.07	0.00	0.53	2.65	0.00	0.00	0.00	0.00	0.48
Sam_Bp_1B	0.98	0.74	1.87	0.85	1.00	0.02	0.97	0.62	3.21	0.00	0.00	0.00	0.00	0.00
Sam_Ht_2A	0.99	1.02	1.24	1.01	1.00	0.02	0.94	0.00	0.00	0.00	0.00	0.00	0.00	0.87
Sam_Ht_2C	0.97	1.18	1.30	1.11	1.00	0.03	0.93	0.00	0.00	0.62	0.00	0.00	0.00	0.00
Sar_Ht_1A	0.99	0.64	0.59	0.78	1.00	0.10	0.77	0.58	7.34	0.67	0.54	0.00	0.41	0.79

Sar_Ht_1B	0.99	0.59	0.64	0.76	1.00	0.05	0.78	0.58	6.48	0.56	0.51	0.00	0.39	0.80
Sar_Ht_1C	1.00	0.72	0.65	0.83	1.00	0.06	0.78	0.59	7.01	0.06	0.56	0.00	0.43	0.85
Sp_Ht_1A	0.05	0.75	1.00	0.85	0.76	0.84	0.80	0.40	1.92	0.08	0.23	0.28	0.04	0.04
Sp_Ht_1B	0.04	0.68	0.80	0.81	0.72	0.86	0.00	0.40	1.75	0.18	0.26	0.00	0.00	0.00
Us_Ht_1A	0.17	0.42	0.69	0.65	0.89	0.83	0.81	0.56	2.21	0.48	0.26	0.00	0.10	0.08
Ti_Bp_1A	0.90	0.52	0.77	0.71	1.00	0.21	0.83	0.57	4.00	0.00	0.34	0.00	0.01	0.11
Ti_Bp_1B	0.89	0.27	0.64	0.56	1.00	0.20	0.00	0.62	4.23	0.00	0.00	0.00	0.00	0.00

MPI1: methylphenanthrene index 1; MPI3: methylphenanthrene index 3; Rc: calculated vitrinite reflectance; PhP ratio: phenylphenathrene ratio.

BeP/(BeP + Pe) = benzo[e]pyrene/(benzo[e]pyrene + perylene)

MPI1 = 1.5*(3-methylphenanthrene + 2-methylphenanthrene)/(phenanthrene + 9-methylphenanthrene + 1-methylphenanthrene)

MPI3 = (3-methylphenanthrene + 2-methylphenanthrene)/(9-methylphenanthrene + 1-methylphenanthrene)

Rc = 0.4 + 0.6 * MPI1
R/(R + D + S) = retene/(renete+dehydroabietane+simonellite)

R/(R + 3-MP) = retene/(retene + 3-methylphenanthrene)

PhP ratio: (2- + 3-PhP)/[(2- + 3-PhP) + (4- + 1- + 9-PhP)] = (2- + 3-phenylphenanthrene)/ [(2- + 3-phenylphenanthrene)+(4- + 1-+ 9-phenylphenanthrene)]

m/z 218 + 191 = (oleanenes + lupenes +C30ββ hopanes)/(C30αβ and C30βα hopanes)

Ts/(Ts+Tm) = 18a(H)-22,29,30-trisnorneohopane/ (18a(H)-22,29,30-trisnorneohopane + 17a(H)-22,29,30-trisnorhopane)

DIA/(DIA+REG) = C_{27} diasteranes/ (C_{27} diasteranes + C_{29} steranes)

*Staneczek et al. (2024)

**the value calculated using Rc = 0.5*MPI1 + 2.27 equation (Radke , 1987)

Tab. S4 Biomarker-derived parameter values calculated for the well samples.

Sample code	Aromatic maturity parameters								Aliphatic maturity parameters						
	m/z 252		m/z 178+192			m/z 219+237+255	m/z 192+219	m/z 254	m/z 191		m/z 217		m/z 218+191	m/z 217	m/z 191
	BeP / (BeP + Pe)	BeP / (BeP + BaP)	MPI1	MPI3	Rc [%]	R/(R+D+S)	R/(R+3-MP)	PhP ratio	C31(S/S+R)	C30αβ/βα	20S/(S+R)	C29ββ/(αα+ββ)		DIA/(DIA+REG)	Ts/(Ts+Tm)
Chochołów															
CH2	0.26	0.53	0.23	0.64	0.54	0.96	0.66	0.72	0.55	2.41	0.19	0.30	0.00	0.14	0.10
CH193	0.21	0.52	0.26	0.70	0.55	0.93	0.63	0.68	0.55	2.39	0.20	0.26	0.00	0.24	0.08
CH280	0.25	0.51	0.35	0.66	0.61	0.94	0.77	0.70	0.56	2.52	0.31	0.26	0.00	0.16	0.07
CH11	0.28	0.55	0.34	0.70	0.60	0.94	0.53	0.71	0.56	3.09	0.25	0.23	0.00	0.12	0.10
CH513	0.52	0.65	0.33	0.75	0.60	0.94	0.56	0	0.58	2.92	0.29	0.24	0.00	0.11	0.10
CH593	0.58	0.85	0.29	0.66	0.58	0.84	0.51	0.55	0.56	0.11	0.35	0.22	0.00	0.00	0.00
CH17	0.49	0.63	0.40	0.73	0.64	0.63	0.51	0.72	0.58	2.99	0.30	0.26	0.00	0.20	0.10
CH18	-	-	-	-	-	-	-	-	-	-	-	-	-		
CH820	0.79	0.67	0.40	0.73	0.64	1.00	0.58	0.00	0.59	2.95	0.37	0.28	0.00	0.17	0.00
CH21	0.90	0.75	0.46	0.76	0.68	1.00	0.54	0.70	0.59	4.55	0.39	0.31	0.00	0.24	0.35
CH29	1.00	0.79	0.50	0.75	0.70	1.00	0.52	0.79	0.59	5.44	0.44	0.41	0.00	0.18	0.49
CH30	1.00	0.90	0.50	0.75	0.70	1.00	0.47	0.73	0.59	1.48	0.50	0.49	0.00	0.34	0.64
CH32	1.00	0.91	0.50	0.74	0.70	1.00	0.25	0.75	0.61	2.78	0.52	0.50	0.00	0.24	0.59
CH35	1.00	0.85	0.48	0.76	0.69	1.00	0.22	0.75	0.61	3.05	0.57	0.50	0.00	0.29	0.61
CH36	1.00	0.84	0.38	0.31	0.63	1.00	0.55	0.79	0.62	0.21	0.58	0.50	0.00	0.32	0.64
CH1671	1.00	0.87	0.49	0.72	0.69	1.00	0.55	0.79	0.59	6.33	0.61	0.47	0.00	0.34	0.56
CH39	1.00	0.89	0.50	0.69	0.70	1.00	0.27	0.79	0.59	7.86	0.60	0.50	0.00	0.31	0.68
CH43	1.00	0.96	0.62	0.64	0.77	1.00	0.13	0.77	0.60	9.74	0.59	0.56	0.00	0.20	0.79
CH2011	1.00	0.96	0.53	0.67	0.72	1.00	0.10	0.75	0.60	9.05	0.63	0.54	0.00	0.31	0.81
CH2075	1.00	0.94	0.54	0.70	0.73	1.00	0.11	0.78	0.62	0.11	0.57	0.51	0.00	0.33	0.70
CH48	-	-	-	-	-	-	-	-	-	-	-	-	-	-	-
CH49	-	-	-	-	-	-	-	-	-	-	-	-	-	-	-

CH52	0.93	0.73	0.41	0.81	0.64	1.00	0.20	0.72	0.62	5.13	0.49	0.33	0.00	0.21	0.29
CH2410	1.00	0.95	0.58	0.73	0.75	0.00	0.00	0.86	0.60	7.65	0.00	0.00	0.00	0.39	0.31
CH2511	1.00	0.96	0.65	0.79	0.79	0.00	0.00	0.90	0.00	0.00	0.00	0.00	0.00	0.00	0.47
CH58	1.00	1.00	0.60	0.75	0.76	0.00	0.00	0.85	0.00	0.00	0.00	0.00	0.00	0.00	0.87
CH63	1.00	1.00	0.72	0.82	0.83	0.00	0.00	0.87	0.00	0.00	0.00	0.00	0.00	0.00	0.84
CH65	1.00	0.93	0.78	0.96	0.87	0.00	0.00	0.91	0.00	0.00	0.00	0.00	0.00	0.00	0.80
CH2900	1.00	0.94	0.88	0.94	0.93	0.00	0.00	0.91	0.00	0.00	0.00	0.00	0.00	0.00	0.00
Bukowina															
BKT102	1.00	0.92	0.65	0.95	0.79	0.00	0.00	0.88	0.00	0.00	0.00	0.00	0.00	0.00	0.00
BKT294	1.00	0.94	0.81	1.12	0.88	0.00	0.00	0.91	0.00	0.00	0.00	0.00	0.00	0.00	0.00
BKT10	1.00	0.92	1.18	1.32	1.11	0.00	0.00	0.94	0.00	0.00	0.00	0.00	0.00	0.00	0.00
BKT640	1.00	0.93	0.91	1.34	0.95	0.00	0.00	0.94	0.00	0.00	0.00	0.00	0.00	0.00	0.00
BKT14	1.00	0.94	1.00	1.15	1.00	0.00	0.00	0.93	0.00	0.00	0.00	0.00	0.00	0.00	0.00
BKT902	1.00	0.89	1.23	1.68	1.14	0.00	0.00	0.97	0.00	0.00	0.00	0.00	0.00	0.00	0.00
BKT20	1.00	0.94	1.33	1.56	1.20	0.00	0.00	0.96	0.00	0.00	0.00	0.00	0.00	0.00	0.00
BKT22	1.00	0.86	1.54	2.63	1.32	0.00	0.00	0.98	0.00	0.00	0.00	0.00	0.00	0.00	0.00
BKT1261	1.00	0.89	1.40	3.09	1.24	0.00	0.00	0.96	0.00	0.00	0.00	0.00	0.00	0.00	0.00
BKT25	1.00	0.89	2.02	2.98	1.61	0.00	0.00	0.98	0.00	0.00	0.00	0.00	0.00	0.00	0.00
BKT27	1.00	0.82	2.11	3.47	1.66	0.00	0.00	0.98	0.00	0.00	0.00	0.00	0.00	0.00	0.00
BKT1594	1.00	0.91	1.40	3.73	1.24	0.00	0.00	0.98	0.00	0.00	0.00	0.00	0.00	0.00	0.00
BKT30	1.00	0.87	2.09	3.08	1.65	0.00	0.00	0.97	0.00	0.00	0.00	0.00	0.00	0.00	0.00
BKT31	1.00	0.88	1.81	3.21	1.48	0.00	0.00	0.98	0.00	0.00	0.00	0.00	0.00	0.00	0.00
BKT35	1.00	0.87	2.28	3.11	1.77	0.00	0.00	0.97	0.00	0.00	0.00	0.00	0.00	0.00	0.00
BKT38	1.00	0.86	2.16	3.72	1.70	0.00	0.00	0.98	0.00	0.00	0.00	0.00	0.00	0.00	0.00
BKT2200	1.00	0.94	0.83	3.08	2.68*	0.00	0.00	0.97	0.00	0.00	0.00	0.00	0.00	0.00	0.00

MPI1: methylphenanthrene index 1; MPI3: methylphenanthrene index 3; Rc: calculated vitrinite reflectance; PhP ratio: phenylphenathrene ratio.
BeP/(BeP + Pe) = benzo[e]pyrene/(benzo[e]pyrene + perylene)

MPI1 = 1.5*(3-methylphenanthrene + 2-methylphenanthrene)/(phenanthrene + 9-methylphenanthrene + 1-methylphenanthrene)

MPI3 = (3-methylphenanthrene + 2-methylphenanthrene)/(9-methylphenanthrene + 1-methylphenanthrene)

Rc = 0.4 + 0.6 * MPI1
R/(R + D + S) =
retene/(renete+dehydroabietane+simonellite)

R/(R + 3-MP) = retene/(retene + 3-methylphenanthrene)
PhP ratio: (2- + 3-PhP)/[(2- + 3-PhP) + (4- + 1- + 9-PhP)] = (2- + 3-phenylphenanthrene)/ [(2- + 3-phenylphenanthrene)+(4- + 1-+ 9-phenylphenanthrene)]
m/z 218 + 191 = (oleanenes + lupenes +C30ββ hopanes)/(C30αβ and C30βα
hopanes)

Ts/(Ts+Tm) = 18a(H)-22,29,30-trisnorneohopane/ (18a(H)-22,29,30-trisnorneohopane + 17a(H)-22,29,30-trisnorhopane)

DIA/(DIA+REG) = C_{27} diasteranes/ (C_{27} diasteranes + C_{29} steranes)

* the value calculated using Rc = 0.5*MPI1 + 2.27 equation (Radke , 1987)

Manuscript 1

Staneczek Dorota, Szaniawski Rafał, Marynowski Leszek. Under review. Burial impact on the Tatra Mts from a rock magnetic and magnetic fabric perspective. Tectonics.

1   **Burial impact on the Tatra Mts from a rock magnetic and magnetic fabric perspective**

2

3   Dorota STANECZEK[1]*, Rafał SZANIAWSKI[2], Leszek MARYNOWSKI[1]

4   [1]Institute of Earth Sciences, University of Silesia in Katowice, Będzińska 60, 41-200 Sosnowiec, Poland;

5   [2]Institute of Geophysics, Polish Academy of Sciences, Księcia Janusza 64, 01-452 Warszawa, Poland.

6   *corresponding author: dorota.staneczek@us.edu.pl

7

8   **Key points**

9   • Variations in magnetite-hematite domain size reflect burial intensity.

10   • Thermal maturity and magnetic mineral trends indicate rising temperatures eastward, peaking at
11   230°C.

12   • Magnetic fabrics document the pre-burial, burial, and post-burial stages of the evolution of the Tatra
13   Mountains.

14

15

16

17

18

19

20

21

22

23

24

25

26   **Abstract**

27   Mountain belts are affected by various processes during their tectonic origin and evolution. One of the

28   most common processes is burial. We investigated the Tatra Mountains in central Europe, as previous

29   works have shown that they are an ideal case study for the impact of burial on the magnetic properties

30   of various rock types. The burial history is elucidated using a interdisciplinary approach that employs

31   analysis of rock magnetic properties and magnetic fabrics, thermal maturity indicators, such as vitrinite

32   reflectance, and biomarker distribution. The paleotemperatures documented by vitrinite reflectance

33   and biomarker ratios show an increasing trend to higher temperature towards the east, with the

34   highest temperature 230°C reached in the eastern Tatra. Similarly, there is a change in both

35   ferromagnetic and paramagnetic magnetic mineralogy towards the east, with an increase in the

36   concentration of the ferrimagnetic minerals. The domain size of the also changes with an increase in

37   the concentration of superparamagnetic grain size. The recorded magnetic fabrics document three

38   main stages of Tatra evolution: pre-, syn-, and post-burial fabrics, especially those affected by the uplift

39   of the Tatra massif. In conclusion, the burial of the youngest parts of the Tatra nappes and their cover

40   are interpreted to have occurred during the Oligocene.

41

42   **Keywords: Carpathians, paleotemperatures, magnetic fabrics, Oligocene**

43

44   1.   Introduction

45   Burial-related processes are known to largely affect the magnetic mineralogy of rocks, causing the

46   formation of new ferromagnetic minerals and, thus remagnetization of rocks (e.g., Aubourg et al.,

47   2012; Banerjee et al., 1997; Elmore et al., 2012; Hirt et al., 1993; Kars et al., 2023). Burial-related

48   remagnetization can enhance or overprint magnetic fabrics as documented in many tectonic studies

49   (e.g., Sun et al., 1992; Grabowski et al., 2009; Calvín et al., 2018a, b). Therefore, a careful examination

50   of the magnetic minerals and their origin is a crucial step when determining the origins of fabrics. In

51   this study, we investigate the Tatra Mts, which constitute the highest part of the Carpathians (Fig. 1)

52   and are affected by various burial events. The most important events are the Turonian burial of the

53   crystalline basement under a thrust nappe system (e.g., Jurewicz, 2005; Králiková et al., 2014; Plašienka

54   & Prokešová, 1996; Plašienka et al., 1997; Prokešová, 1994; Prokešová et al., 2012) and Oligocene

55   burial of the whole massif under the Central Carpathian Paleogene Basin (CCPB) sedimentary rocks

56   (Kováč et al., 2016; Králiková et al., 2014; Soták et al., 2001). The intensity of burial processes was not

57   uniform throughout the massif.

2
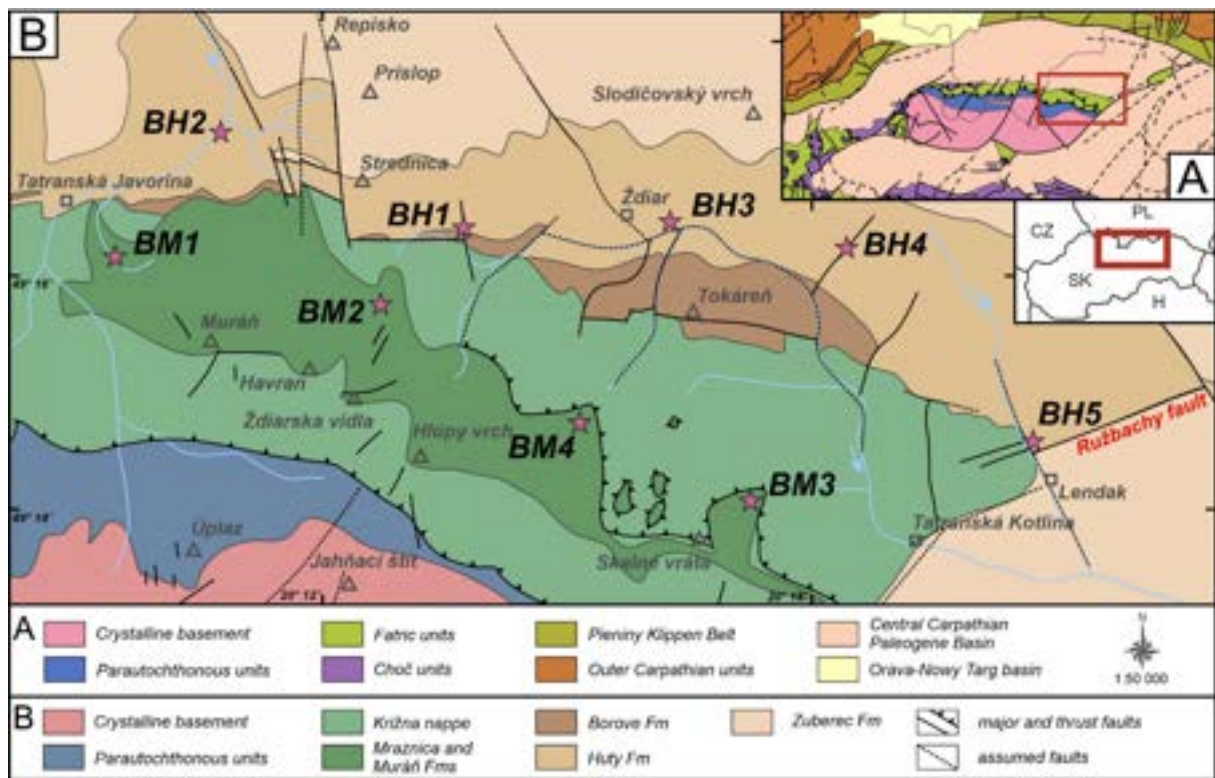
Fig. 1 Simplified geological map of the Belianske Tatry Mts (after Nemčok et al., 1993a) with the sample site locations marked with a star.

Rock magnetic studies have been performed in the Tatra Mts since the 1980s (Grabowski 1996, 1997, 2000; Grabowski & Gawęda, 1999; Hrouda & Kahan 1991; Hrouda et al., 2009; Kruczyk et al., 1992; Kądziałko-Hofmokl & Kruczyk 1987; Márton et al., 2016; Szaniawski et al., 2012, 2020). There have also been an increasing number of studies that have investigated the magnetic fabrics in the Tatra rocks, as a proxy for unraveling the tectonic deformation/processes (Hrouda & Kahan 1991; Staneczek et al., 2022, 2024b). The available magnetic fabric studies have focused mainly on the nappe- and para-autochthonous units of the Western and High Tatra Mts. Only a few sampling/data points are located in the easternmost part of the Tatra block (i.e., the so-called Belianske Tatra Mts), which were studied by Hrouda and Kahan (1991). Hence there is a significant lack of information on the magnetic fabric and rock magnetic properties from this area. In this study, we focus on the Belianske Tatra Mts. From previous studies in this region (Staneczek et al., 2022, 2024b), there is a noticeable trend of increasing paleotemperatures from the west to the east in the larger Tatra region. Therefore, we hypothesize that the Belianske Tatra Mts sedimentary rocks should show the highest thermal alteration in the whole Tatra block, making them suitable for investigating and dating the burial episodes in this area. To achieve this goal, we applied magnetic fabric investigations, including in-phase and out-of-phase anisotropy of magnetic susceptibility, frequency-dependent magnetic susceptibility and anisotropy of anhysteretic remanent magnetization coupled with extensive petromagnetic and paleotemperature

3

78 investigations. In our study, we focus on Cretaceous thrust nappe sedimentary rocks (Mraznica Fm)

79 and on post-thrusting Early Oligocene cover (Huty Fm). Moreover, the thermal maturity picture was

80 expanded to include the Mraznica Fm from the Choč Mts (this study), and Huty Fms (based on

81 Staneczek et al., 2024a).

82   2. Geological setting

83 The Tatra Mts are characterized by a multi-step tectonic evolution from the Late Paleozoic to the

84 Pliocene (Anczkiewicz et al., 2015; Catlos et al., 2022; Jurewicz, 2007; Králiková et al., 2014, 2016; Kováč

85 et al., 1994; Passendorfer, 1952; Plašienka et al., 1997). The oldest known processes are linked to the

86 late Paleozoic Variscan orogeny and resulted in the formation and metamorphism of the crystalline

87 basement rocks (Burchart 1972; Kohút et al. 1999; Kráľ 1977; Petrík & Kohút 1997; Plašienka et al.,

88 1997). The oldest sedimentary rocks in the Tatra region are Upper Permian in age (Nemčok et al.,

89 1993a, b). Rifting events during the Middle Triassic to the Late Jurassic resulted in the opening of wide

90 oceanic domains in the Carpathian region (Csontos & Vörös, 2004). The Cretaceous (Plašienka, 2018)

91 compression resulted in basin inversion and the formation of large thrust nappe systems represented

92 in the Tatra Mts mainly by the Krížna unit. The final emplacement of the thrust nappes on the Tatra

93 crystalline basement with its para-autochthonous cover occurred in the Late Turonian (Prokešová et

94 al. 2012). In the Late Cretaceous-Paleocene, a part of the thrust nappes was eroded, and the

95 autochthonous units were partially exhumed (Králiková et al., 2014). Starting from the Late

96 Eocene/Early Oligocene, a deep-sea basin, i.e., CCPB, developed in the Central Western Carpathian

97 region (Kováč et al., 2016; Soták et al., 2001). The pre-Cenozoic units of the Tatra Mts were buried

98 under a thick pile of Oligocene-Early Miocene clastic sedimentary rocks, which were partially eroded

99 during the final Miocene uplift and exhumation of the Central Western Carpathian horsts. The uplift of

100 the Tatra Mts occurred along the south-bounding Sub-Tatric Fault and was accompanied by a

101 northward tilting of the whole horst (Jurewicz, 2005; Rubinkiewicz & Ludwiniak, 2005; Sperner et al.,

102 2002; Szaniawski et al., 2012).

103 The Mraznica Formation, a member of the allochthonous Fatric unit, and the Huty Formation from the

104 post-thrusting CCPB cover were chosen in this study. The Mraznica Fm comprises Lower Cretaceous

105 variably light to dark grey marls and limestones (Kędzierski & Uchmann, 1997; Lefeld, 1974; Lefeld et

106 al., 1985; Michalík, 2007; Vašíček et al., 1994). The Oligocene Huty Fm consists of dark shales, which

107 are occasionally intercalated with layers of sandstones (Gross et al., 1984). Both chosen formations

108 have proven to be suitable for magnetic investigations in our previous studies (Staneczek et al., 2022,

109 2024b).

110   3. Sample collection and preparation

4

111 Oriented hand samples were collected mostly from outcrops in the streams in the Belianske Tatra Mts

112 and their foreland. No outcrop-scale folds were present at any site; therefore, only the bedding

113 orientation was measured at each site. The Mraznica Fm in the Belianske Tatry Mts comprises mainly

114 marls and marly limestones (sites BM2-4; Nemčok et al., 1993ab). However, the Mraznica Fm is

115 infrequently intercalated by more calcareous layers, which can be difficult to differentiate during

116 fieldwork (site BM1). These differences in the lithology are caused by changes in phyllosilicate supply

117 to the basin (Piotrowska et al., 2013). The main minerals of the Mraznica Fm are calcite, phyllosilicates,

118 and quartz (Lefeld, 1974). Twenty-six hand samples from four sites could be collected during fieldwork.

119 The Huty Fm is located in the Tatra foreland. It comprises mainly dark siltstones, shales, and

120 sandstones. The main minerals are phyllosilicates and quartz (Nemčok et al., 1993b). Five sites were

121 sampled along the northern Tatra margin which include thirty-five oriented hand samples that

122 comprise dark siltstones. Cylindrical specimens (2.54 cm diameter) were drilled from the hand

123 samples. Altogether, 73 specimens for the Mraznica Fm and 113 for the Huty Fm were obtained (BM1:

124 23, BM2: 20, BM3: 18, BM4: 12, BH1: 22, BH2: 25, BH3: 28, BH4: 26, BH5: 12). Not all hand samples

125 could be effectively drilled. Two samples from each site were powdered in preparation for the

126 measurement of temperature-dependent magnetic susceptibility, geochemical studies, and biomarker

127 analyses. Rock chips (average weight 0.15 g) were prepared for hysteresis and isothermal remanent

128 magnetization (IRM) back-field experiments. At least one sample from each site was polished and

129 prepared for vitrinite reflectance measurements.

130 For a regional interpretation of the Belianske Tatra Mts data, additional four samples from the

131 Mraznica Fm in the Choč Mts were prepared for the geochemical, gas chromatography-mass

132 spectrometry (GC-MS) analyses, and vitrinite reflectance measurements. The samples were also used

133 for magnetic susceptibility measurements and the average percentage of the frequency-dependent

134 susceptibility measurements (Dearing et al., 1996) were calculated. Other magnetic parameters are

135 derived from the Staneczek et al. (2022) study.

136   4. Methods

137   a. Organic parameters

138   i. Bulk geochemical data

139 Total organic carbon (TOC; wt.%), total inorganic carbon (TIC; wt.%), and total sulfur (TS; wt.%) values

140 were measured using an Eltra CS-500 IR-analyzer with a TIC module (Faculty of Natural Sciences,

141 University of Silesia in Katowice, Poland). In addition, the carbonate content (CC, wt.%) was calculated

142 from the TIC values (CC = TIC *8.3333; see e.g., Racka et al., 2010).

143   ii. Vitrinite reflectance

144   Freshly polished specimens prepared following the ISO 7404-2 (2009) method were examined in

145   reflected light and immersion oil using an Axio Imager.A2m (Faculty of Natural Sciences, University of

146   Silesia in Katowice, Poland). The standard used was 1.71 % relative reflectance (Rr).

147   iii.   Organic compound analysis

148   The GC–MS analyses were carried out with an Agilent Technologies 7890A gas chromatograph (GC)

149   and an Agilent 5975C Network mass spectrometer with Triple-Axis Detector (MSD) at the Faculty of

150   Natural Sciences, University of Silesia in Katowice, Sosnowiec, Poland. The Agilent J&W HP5-MS (50 m

151   × 0.32 mm i.d., 0.25 µm film thickness) fused silica capillary column coated with a chemically bonded

152   phase (5% phenyl, 95% methylsiloxane) was used. The GC oven temperature was programmed from

153   45 °C (1 min) to 100 °C at 20 °C /min, then to 300 °C (hold 60 min) at 3 °C /min, with a solvent delay of

154   10 min. Helium (6.0 Grade) was used as a carrier gas at a constant flow of 2.6 ml/min. Mass spectra

155   were recorded starting from m/z 45 to 550 (0–40 min) and m/z 50–700 (>40 min). A more detailed

156   description of extraction and fractionation is given in Staneczek et al. (2024a). Three parameters

157   commonly applied for maturity assessment were calculated (for the equations see Table S1). The first

158   parameter is the methylphenanthrene ratio (MPI1) based on the occurrence and distribution of

159   phenanthrene and methylphenanthrene compounds (e.g., Marynowski et al., 2015; Poprawa &

160   Marynowski, 2005; Staneczek et al., 2024a, b). The second parameter, the calculated vitrinite

161   reflectance (Rc), is derived from the MPI1 value and is defined as Rc = 0.6 x MPI1 + 0.4. It is widely used

162   as an equivalent of the measured vitrinite reflectance (Radke & Welte, 1983). These two parameters

163   can be applied effectively to clastic sedimentary rocks, but in limestones, the values are usually not

164   comparable to shales (Radke, 1987). The distribution of methylphenanthrenes, however, can be

165   successfully compared in sites sharing similar lithologies. The third parameter, phenylphenanthrene

166   ratio, is based on the distribution of phenylphenanthrenes and binaphtyls (PhP, Li et al., 2012;

167   Rospondek et al., 2009; Table S1), was calculated to compare the thermal maturity of carbonate and

168   clastic deposits.

169   b.   Rock magnetism

170   i.   Magnetic susceptibility

171   First, we analyzed the in-phase and out-of-phase magnetic susceptibility of prepared samples using

172   the AGICO MFK1-FA multifunction frequency kappabridge in two frequencies (976 Hz and 15616 Hz)

173   and at 200 A/m field intensity in both measurement cycles. The results were volume-normalized (κ, SI

174   units), and the percentage of the frequency-dependent susceptibility (the percentage loss of

175   susceptibility; Kfd = 100*(Kip$_{976Hz}$ − Kip$_{15616Hz}$)/Kip$_{976Hz}$; Dearing et al., 1996) was calculated for each

176   specimen.

177　The changes of in-phase magnetic susceptibility were documented using the AGICO KLY-5A induction

178　bridge with a CS4 unit with temperatures reaching up to 700°C with a 14°C/min heating rate.

179　　　　　　　　　ii.　Magnetic remanence

180　The ferromagnetic mineral type and domain sizes were further investigated by the acquisition of IRM.

181　A direct current (DC) field was applied using a 2G Magnetic Measurements MMPM10 Tesla pulse

182　magnetizer in 29 steps to 3 T and the IRM value was measured using a cryogenic superconducting

183　quantum interference device (SQUID) magnetometer after each field application. This procedure was

184　followed by IRM component analysis which was conducted using the Maxunmix software

185　(https://maxunmix.shinyapps.io/MAX_UnMix_final_version/; Maxbauer et al., 2016). Subsequently,

186　remanent acquisition coercive force (B1/2) and its dispersion (DP) were obtained for each

187　measurement.

188　IRM-back field experiments (25 mT field increment) and hysteresis curves (in 1 T applied field, 50 mT

189　field increment, and 0.1 s averaging time) were performed using a Princeton Measurement

190　Corporation Micro-Mag vibrating sample magnetometer.

191　Finally, high-temperature methods included the thermal demagnetization of a three-component IRM

192　by applying the method of Lowrie (1990). Each analyzed specimen was magnetized along three

193　orthogonal axes using three different field values (z: 3 T, y: 0.5 T, x: 0.15 T), and their IRM values were

194　measured. Afterward, the specimens were demagnetized in a Magnetic Measurements MMTDSC high-

195　precision thermal demagnetizer in 25-50°C steps to 700°C.

196　　　　　　　c.　Magnetic fabrics

197　　　　　　　　　i.　ipAMS and opAMS

198　The anisotropy for each specimen was measured three times in order to obtain the most reproducible

199　results. The ellipsoid parameters were calculated using the Anisoft6 software (AGICO). The in-phase

200　anisotropy of magnetic susceptibility (ipAMS) and out-of-phase anisotropy of magnetic susceptibility

201　(opAMS) for the Mraznica and Huty Fm sites were investigated in 700 A/m field intensity and 1220 Hz

202　field frequency. Measurements were performed using the automated three-dimensional rotator, and

203　the obtained susceptibilities were volume-normalized (κ, SI units). The uncertainty ellipses were

204　calculated using the Anisoft6 software (Agico, Inc.).

205　　　　　　　　　ii.　AARM

206　The Anisotropy of the Anhysteretic Remanent Magnetization (AARM) measurements were conducted

207　in the 0–60 mT coercivity window for at least 9-10 specimens per site (if possible). The Directional

7

208 Anhysteretic Remanent Magnetization (in 60 mT) was applied along six positions, focusing on the

209 diagonal orientation of the specimen's coordinate system axes (B-mode, see:

210 https://www.agico.com/downloads/documents/agicoprints/arm_guide.pdf). Each analyzed sample

211 was demagnetized in a 70 mT alternating field and 0.5 mT direct field after each ARM measurement

212 (AGICO PAM1 demagnetizer,). Remanence subtraction was not needed due to a large difference in

213 intensity between the demagnetized state and ARM. Directional ARM measurements and AARM

214 calculations were conducted using an AGICO JR-6A spinner magnetometer and the Rema6 software

215 using a full-vector approach, respectively. Quantitative ellipsoid parameters were calculated via the

216 Anisoft6 software.

217   5. Results

218   a. Organic parameters

219   i. Bulk geochemical data

220 All samples are generally characterized by low to moderate TOC contents (Table S1). In the Mraznica

221 Fm, the TOC values range from 0.00 wt.% to 0.65 wt.%. The Huty Fm samples display slightly higher

222 TOC values (0.55-1.15 wt.%). The TS content is zero or close to zero in the Mraznica Fm, whereas it

223 reaches 1.04 wt.% in the Huty Fm samples. The measured total inorganic carbon in the Mraznica Fm is

224 relatively high and site-dependent (9-10 wt.% on average). The corresponding CC varies significantly

225 from 97.33% in sample BM1_2 to as low as 27.73% in sample BM2_2 (Table S1), but in most samples

226 CC is >70%. In the Huty Fm, the TIC value is low and does not exceed 3 wt.% and CC reaches a maximum

227 of 22.88 wt.%.

228   ii. Vitrinite reflectance

229 The Mraznica Fm samples show a rather low content of vitrinite grains, which are mostly small in

230 comparison to vitrinite grains in the Huty Fm, and occasionally crushed. The vitrinites are commonly

231 oriented along pressure-solution fissures and are accompanied by partially weathered pyrite grains

232 (Fig. S1). The measured reflectance ranges from 0.79 to 1.70% Rr, with the highest values being

233 measured in the easternmost part of the Tatra Mts (Table S1; Fig. 2). The Huty Fm samples are

234 characterized by a higher content of organic matter. The observed vitrinite grains, which are larger

235 than in the Mraznica Fm, are elongated. In some analyzed samples recrystallized pyrite grains and large

236 pyrite framboids are frequent. The vitrinite reflectance varies from 1.11 % Rr to 1.54 % Rr.

237

238
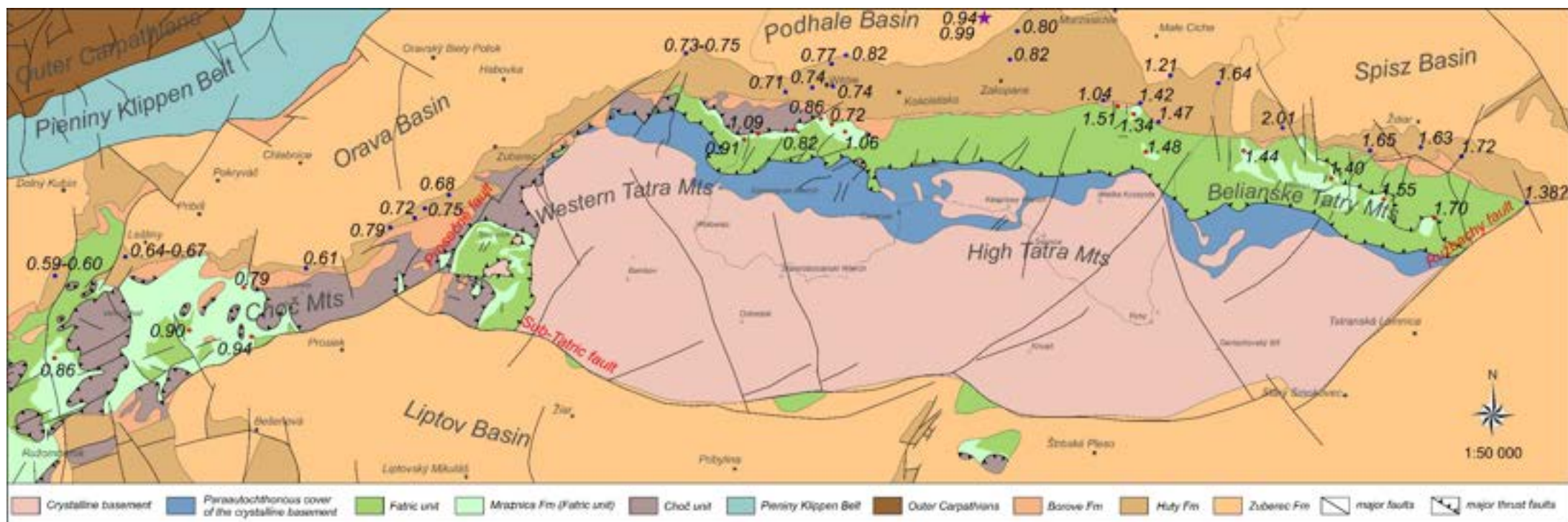
Fig. 2 Simplified geological map of the Tatra Mts and Choč Mts with the marked sampling sites (red and blue for Mraznica and Huty Fms, respectively) and Rr values for Mraznica Fm, and Rc values for the Huty Fm (compiled after Gross et al., 1993; Nemčok et al., 1993a; Piotrowska et al. 2009, 2013). The star depicts the location of the Furmanowa IG-1 well.

242

243   iii.   Organic compound analysis

244 To determine the thermal maturity, analyses of organic compounds were made in addition to the

245 vitrinite reflectance (Table S1). In the case of the Huty Fm the methylphenanthrene index (MPI1) was

246 used (Marynowski et al., 2015; Poprawa & Marynowski, 2005; Staneczek et al., 2024ab), and this

247 parameter can be converted to the calculated vitrinite reflectance (Rc; Radke & Welte, 1983).

248 Methylphenanthrenes show significant changes in distribution. The concentrations of the less stable

249 isomers, i.e., 4-+9-MP and 1-MP, gradually decrease with increasing maturity relative to the more

250 stable 3-MP and 2-MP towards the east (Fig. 3). Moreover, some other group of organic compounds,

251 i.e., phenylphenanthrenes and binaphthyls (Li et al., 2012; Rospondek et al., 2009), also show

252 differences in the thermal maturity across the mountain belt (Fig. 4). Note however, the

253 phenylphenanthrene distribution is similar for the Mraznica Fm and Huty Fm in the case of Western,

254 High, and Belianske Tatra Mts and different for the Choč Mts (Figs. 2, 3 and 4; Table S1; Text S1).
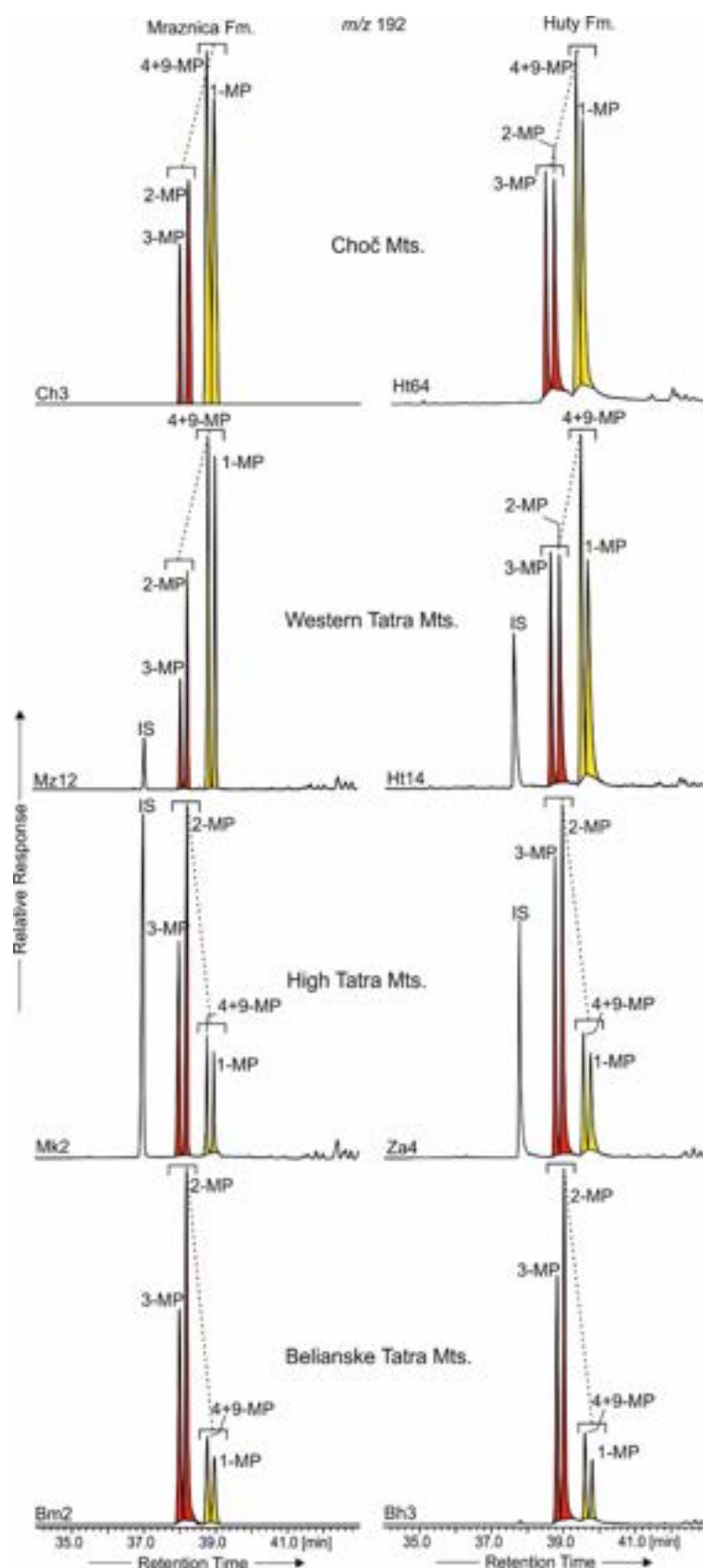
255   Fig. 3 Mass chromatograms (*m/z* 192) showing the similar distribution of methylphenanthrene isomers

256   (MP) for the Huty and Mraznica Fm. samples. The changes in MP isomer distribution between Choč

257   Mts, Western, High and Belianske Tatra Mts are highlighted. IS = internal standard.

11

258
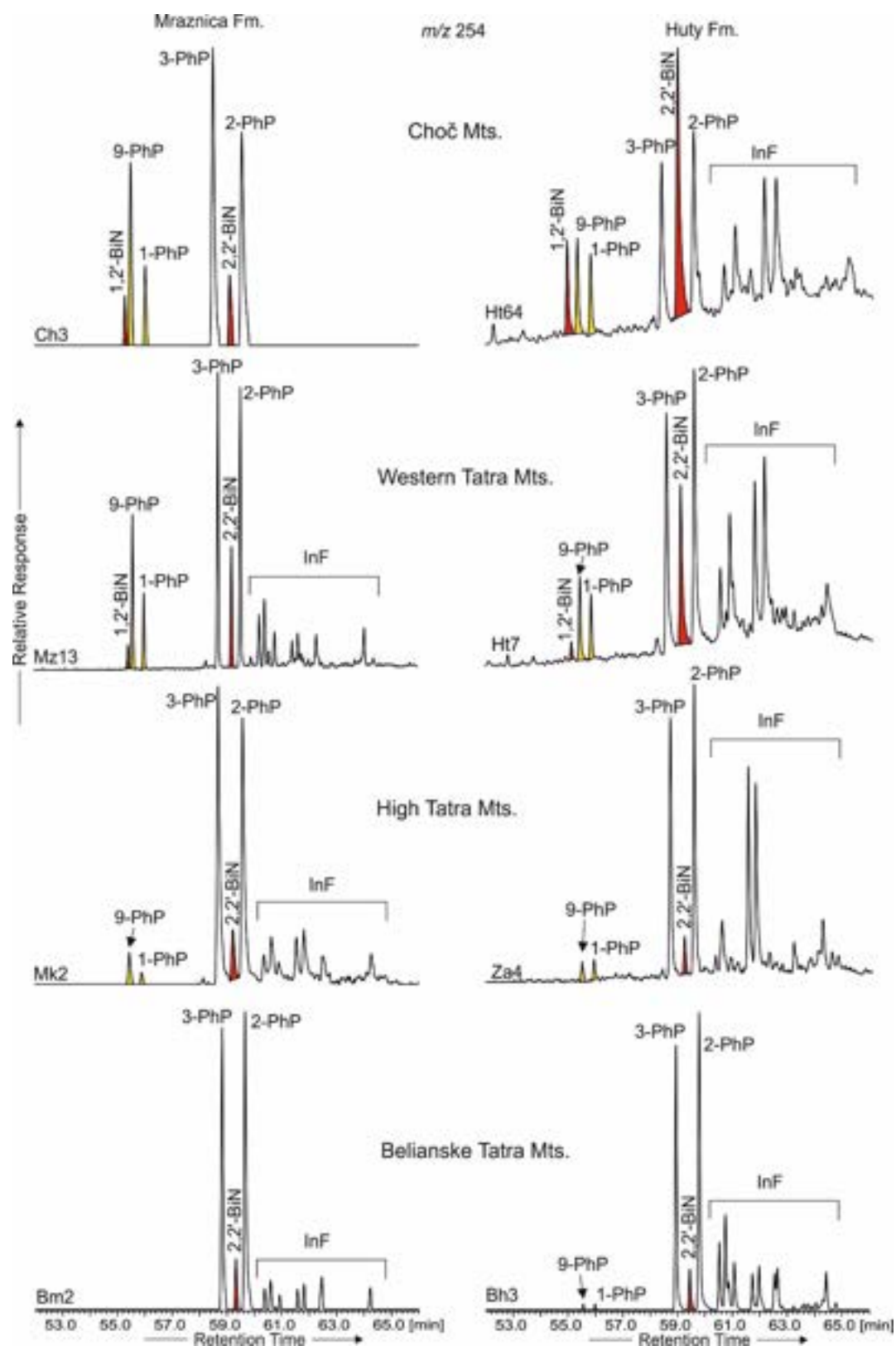
Fig. 4 Mass chromatograms (*m/z* 254) showing changes in the distribution of phenylphenanthrenes

(PhP) and binaphthyls (BiN) in the Choč Mts, and the Western, High and Belianske Tatra Mts and

261 simultaneous similarities between the two formations studied. Note the gradual disappearance of the

262 less thermally stable 1,2'-BiN, 9-PhP and 1-PhP. InF = indenofluorenes.

263   b.   Rock magnetism

264   i.   Magnetic susceptibility

265 The in-phase magnetic susceptibility (Kip) varies considerably in the examined Mraznica Fm specimens

266 (Fig. 5A). The Kip values range from slightly negative (-6.00E-06 [SI]) in the site BM1 to 5.55 x 10^{-4} [SI]

267 in the site BM3. The out-of-phase magnetic susceptibility (Kop) varies from 4.21 x 10^{-7} to 4.58 x 10^{-5}

268 [SI]. The Kip measured in high-frequency is usually a magnitude lower than the low-frequency Kip. The

269 average loss of susceptibility (Kfd) varies from 10 to ~15% in the Belianske Tatry Mts (Fig. 5B). In the

270 Huty Fm, the low-frequency Kip is consistent in all sites with values ranging from 1.30 x 10^{-4} [SI] to 3.82

271 x 10^{-4}[SI]. The Kop is usually two to three magnitudes lower (Fig. 5C). In the higher frequency, the

272 change in Kip is small, hence the Kfd parameter reaches 3.06% at maximum (Fig. 5D).
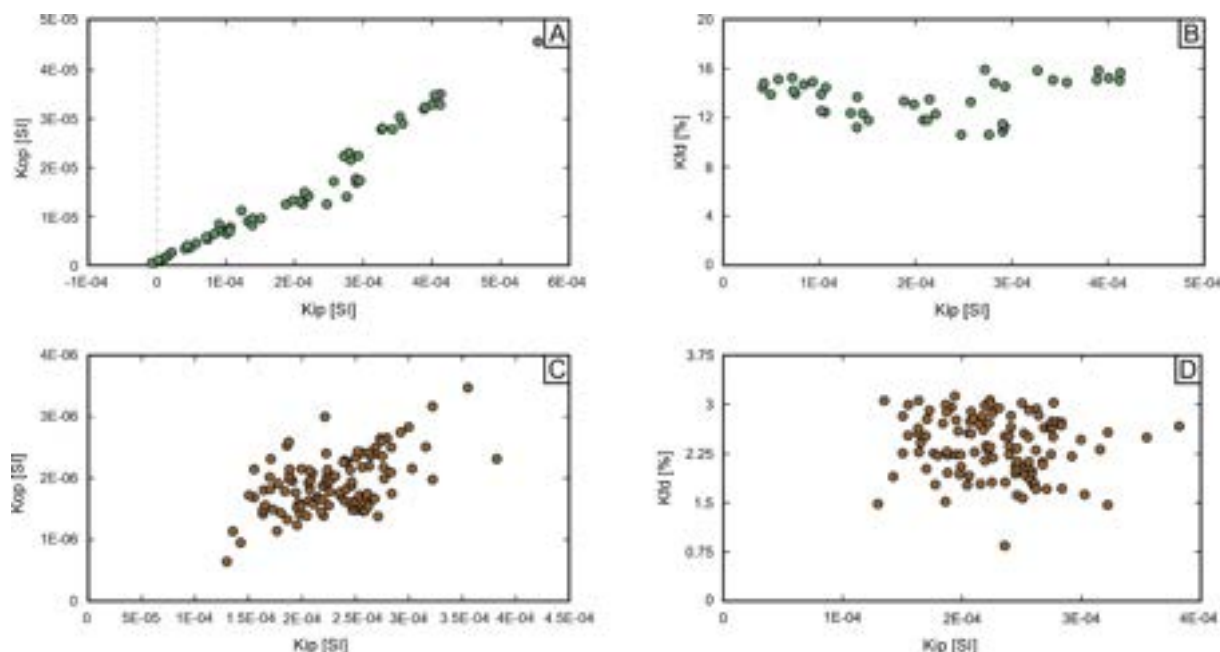
273 Fig. 5 Magnetic susceptibility data: Kip vs Kop in 976 Hz for Mraznica Fm specimens (A); Kip (in 976 Hz)

274 vs Kfd for the Mraznica Fm specimens (B); Kip vs Kop in 976 Hz for Huty Fm specimens (C); Kip (in 976

275 Hz) vs Kfd for the Huty Fm specimens (D). The B and D diagrams show samples where the Kfd parameter

276 could be calculated. Green circles represent Mraznica Fm specimens, and brown are Huty Fm

277 specimens.

13
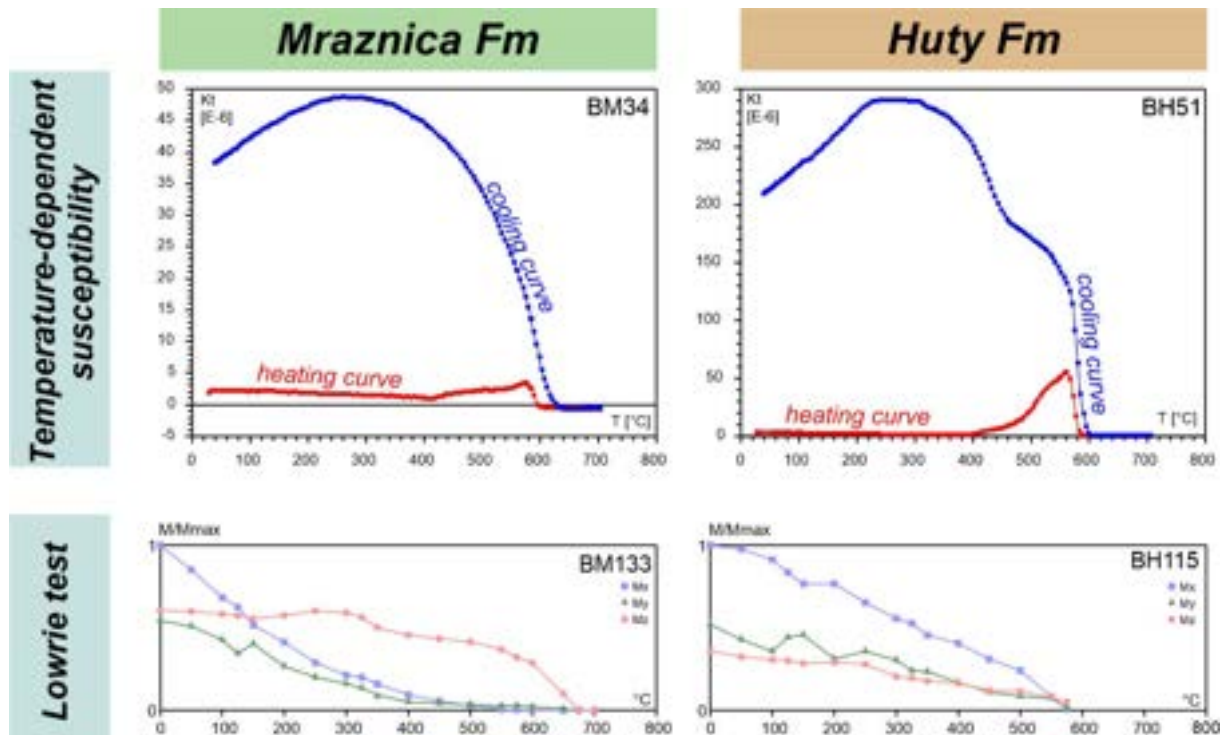
Fig. 6 Temperature-dependent susceptibility and thermal demagnetization of a three-axis IRM (so-called Lowrie test) results for the Mraznica and Huty Fms.

The temperature-dependent susceptibility experiments in the Mraznica Fm samples document two distinct patterns of the thermomagnetic curves. In the samples from sites BM2, BM3, and BM4 the total susceptibility slowly decreases to 400°C, then increases to approximately 580°C and decreases dramatically to 600°C (Fig. 6, S2). The cooling thermomagnetic curves always display substantially higher total susceptibility values. The second pattern, present in the BM1 site, is characterized by a slight increase of the total susceptibility to 300°C followed by a slow decrease to 700°C. The cooling curves are not noticeably different from the heating curves, and the total susceptibility values are very low. In the Huty Fm, the thermomagnetic curves show one consistent pattern in all analyzed samples (Fig. 6, S2). The total susceptibility hyperbolically decreases to 400°C followed by an abrupt increase to 580°C and a final decrease to 590°C. The cooling curves are characterized by much higher values of the total susceptibility.

ii.   Magnetic Remanence

The IRM acquisition curves for the Mraznica Fm are similar in the majority of the analyzed samples (Fig. 7). In the BM133, BM232, and BM353 samples, the magnetization increases rapidly up to an approximately 300 mT applied field, and is followed by a minor increase of magnetization to the maximum applied field. In the BM413 sample, the IRM value increases steadily to a 1 T applied field and displays a smaller increase at higher fields. The SIRM values are significantly different for each

14

298   sample and range from 68.85 mA/m (BM1) to 1062 mA/m (BM3). The Huty Fm samples are

299   characterized by very similar IRM acquisition curves in all sites, except for BH1 (sample BH115; Fig. 7).

300   As in the case of the Mraznica Fm samples, the magnetization values increase rapidly to 300 mT, and

301   then only show a small increase up to 3 T for sites BH2 to BH5. BH115 also acquires an IRM rapidly up

302   to 300 mT, but the IRM continues to grow to 3.0 T in an applied field. The measured SIRM is significantly

303   lower (37-57 mA/m) than the values recorded for the Mraznica samples.
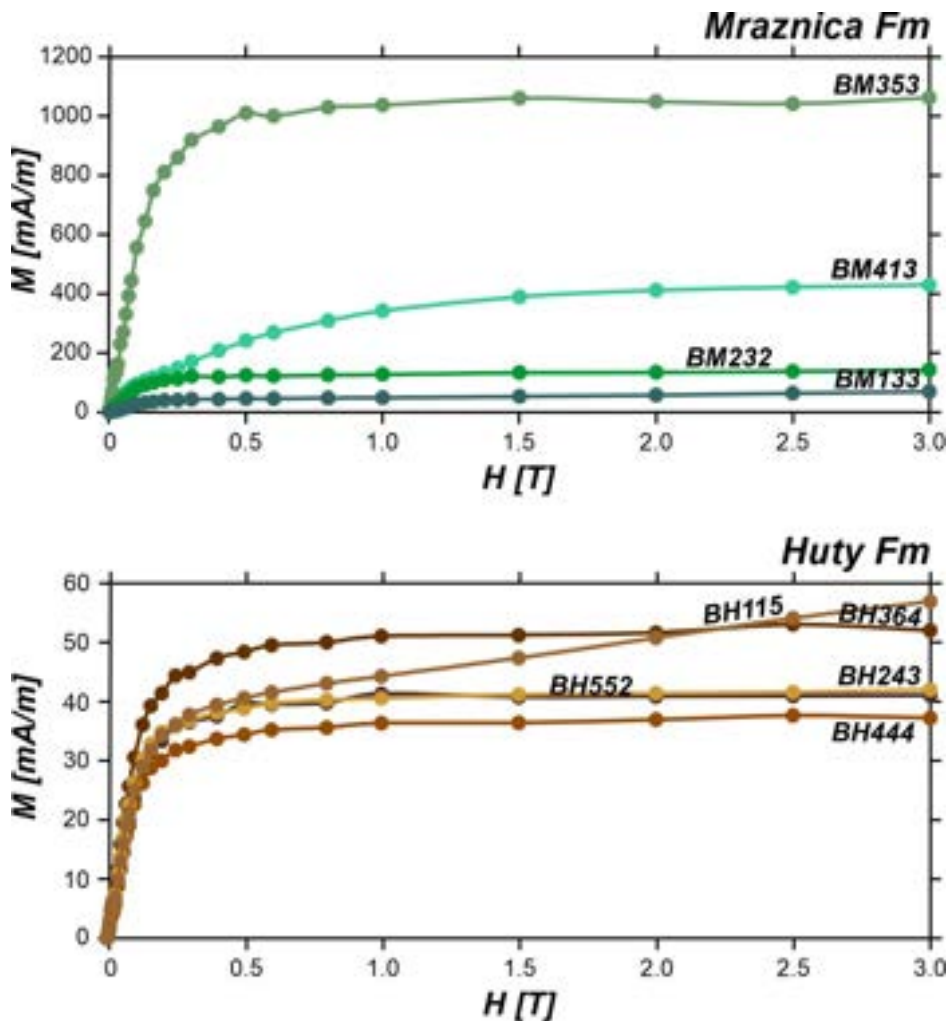
305   Fig. 7 IRM acquisition curves for the Mraznica and Huty Fm.

306   The IRM component analysis documents three different components in the Mraznica samples that

307   contribute to the general IRM (Fig. S3, Table S2). Components 1 and 2 are characterized by very low

308   (8-12 mT) and moderate (90-93 mT for BM133, BM232, BM353 and 55.08 mT for BM413) mean

309   coercivity (B1/2) values. The DP values fall in the range of 0.26-0.44 for the first component, and 0.29-

310   0.35 for the second. The third identified component has high mean coercivity values which vary by site

311   (Table S2). Similarly to the previous unit, the IRM component analysis enabled us to distinguish three

312   main components in the Huty Fm samples. The first component represents the low coercivity fraction

15

with mean coercivity as low as 8-14 mT and DP ranging from 0.34 to 0.40. The second component shows higher mean coercivity values, generally varying from 70 to 85 mT with the exception of BH115, where the mean coercivity value is higher, ~98 mT. The DP values are similar to those for the first component. The last, third component is characterized by the highest mean coercivity values, falling in the 300-420 mT range for the majority of samples. Sample BH115 shows a significantly higher value of this parameter (~1755 mT).

The thermal demagnetization of a three-axis IRM for the Mraznica Fm rocks varies by site (Fig. 6, S4). Samples BM232 and BM353 have a higher initial remanence in the soft component (x-axis), fully demagnetizing by 550-575°C. BM353 shows similar patterns in its intermediate and hard components, while BM232 has a slow y-axis decrease to 675°C and a sharp z-axis drop at this temperature. In BM133, the soft component shows the highest initial remanence, with the x- and y-axes decreasing gradually to 550-575°C, and the z-axis dropping sharply from 600°C. Sample BM413 differs, with all axes demagnetizing fully by 675-700°C and only minor artifacts on the x-axis at 150 and 300°C.

The analyzed Huty Fm documents a much simpler thermal demagnetization pattern characterized by significantly higher initial remanence of the x-axis in comparison to the y- and z-axis remanences in the majority of samples (Fig. 6, S4). The soft component curve shows a smooth decrease of the remanence to 575°C. Similarly, the intermediate component (y-axis) is fully demagnetized at 575°C-600°C, with some artificial drops and highs due to the generally low value of the measured remanence. The hard component curve is too noisy to fully resolve. Therefore, it is negligible in most of the samples due to the close to zero remanence values. Only in samples from the BH1 site (BH115), the z-axis has a higher remanence, which is gradually demagnetized at 700°C.

16
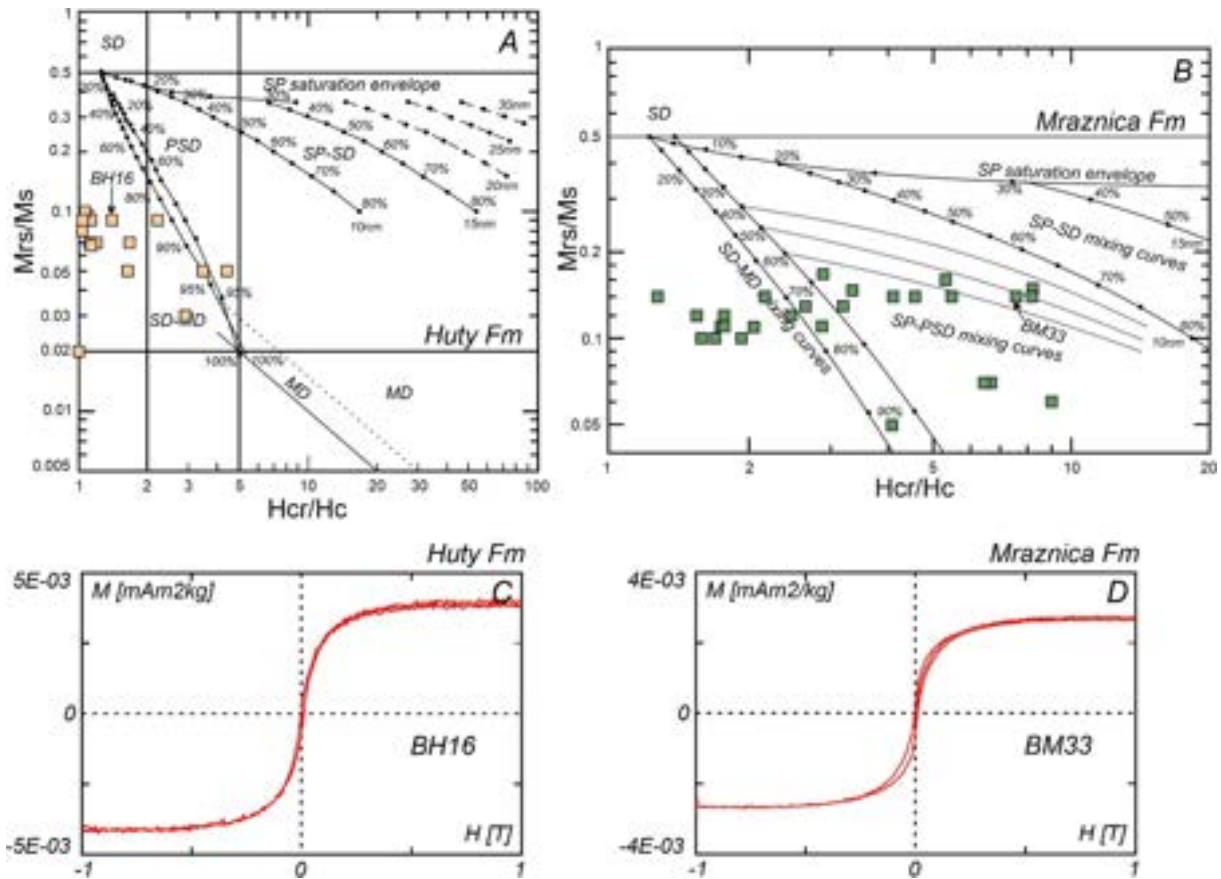
Fig. 8 Day plot for the Huty Fm (A) and Mraznica Fm (B) specimens (after Day et al., 1977 and Dunlop, 2002), and a hysteresis loop after the correction for diamagnetic and paramagnetic minerals for the Huty Fm (C) and Mraznica Fm (D).

In the hysteresis measurements, the dominant linear slope before slope correction in the Mraznica Fm documents the large contribution of paramagnetic minerals in most samples to the induced magnetization (Fig. S5). Site BM1, however, has a prevalent diamagnetic contribution (Fig. S5). The saturation magnetization (Ms) obtained after applying the paramagnetic and diamagnetic correction is site-dependent reaching the highest values in BM3 samples (Table S3). The remanence magnetization (Mr) is also the highest in BM3, and in other samples, it averages 40-200 $\mu Am^2 \cdot kg^{-1}$. The coercivity (Hc) is very low, while the remanence coercivity (Hcr) is much higher. The average calculated ferro/para magnetic mineral content (comparison of the initial slope after the correction for paramagnetic and diamagnetic minerals to the initial slope before the correction times 100 (Table S3); equals 36%, but in some sites it can be higher, reaching even 65% (Table S3). The hysteresis loop after the correction for para- and diamagnetic contribution shows a wasp-waisted shape in some samples (Fig. 8, S5). However, the majority of samples do not show this feature. Similar to the Mraznica Fm, the shape of the hysteresis loop in the Huty Fm samples before the correction for paramagnetic slope is near linear (Fig. S5). The Mr values are usually much lower than those obtained for Mraznica Fm

352 (Table S3). The mean coercivity is very low (3-10 mT) and the coercivity of remanence reaches even 26

353 mT. The calculated ferro/para magnetic mineral content is usually consistent in most samples and

354 averages 9.25% (Table S3).

355 c. Magnetic fabrics

356 i. ipAMS and opAMS

357 In three Mraznica Fm sites, the corrected degree of ipAMS (Pj) is low, with values ranging from 1.02 to

358 1.06 (Fig. 9). Generally, the ellipsoid shape (T) varies from prolate to neutral and oblate (Fig. 9). The

359 ipAMS fabric documents well-defined magnetic lineation (small confidence ellipses), which is slightly

360 inclined from the bedding and a rather dispersed magnetic foliation in all analyzed sites (Fig. 9, S6). At

361 BM1 and BM4, the magnetic lineation is north-trending. The observed magnetic foliation is tilted with

362 respect to the bedding plane. In the two remaining sites, BM2 and BM3, the magnetic lineation trends

363 to the east. As in the previous sites, the magnetic foliation is tilted with respect to bedding. The Huty

364 Fm sites are characterized by predominantly oblate ipAMS ellipsoid shapes and a high degree of

365 alignment (1.10-1.16). The obtained magnetic fabrics are characterized by well-grouped magnetic

366 foliations that are parallel to the bedding planes (Fig. 10, S6). A predominant, well-defined, ENE- to

367 WSW-oriented magnetic lineation is present in the majority of sites. In site BH5, the magnetic lineation

368 has a slightly different WNW to ESE orientation.

369 The opAMS ellipsoid parameters in the sites BM2, BM3, and BM4 appear to be well-defined. The F-

370 test for the site BM1 is low (Staneczek et al., 2024c), which suggests a less precise obtained

371 measurement. The shape parameter documents prolate or neutral ellipsoid shapes in the majority of

372 measured specimens. The Pj values are slightly higher than those obtained for the ipAMS (Fig. 9). In all

373 analyzed sites, the opAMS magnetic fabric traces the orientation of the ipAMS fabric (Fig. 9, Fig. S7).

374 Magnetic lineation and foliation are best defined at the sites BM3-4, where the confidence ellipses are

375 small. The confidence ellipses are the largest at site BM2. Despite the less precise measurement, the

376 BM1 fabric displays a rather well-defined magnetic lineation, which is similar to the lineation in ipAMS.

377 Overall, both the magnetic lineation and the magnetic foliation are more scattered than in their ipAMS

378 equivalents (Fig. 9, Fig. S7).

379 The F-tests obtained from the Huty Fm opAMS measurements are quite low (Staneczek et al., 2024c),

380 yet the majority show values suggesting the anisotropies are significant. However, the Pj and T values

381 are defined poorly. The ellipsoid shape varies from neutral to oblate, and the corrected anisotropy

382 degree reaches a maximum 1.6 (Fig. 10). In sites BH1, BH3 and BH5, the opAMS Huty Fm fabric traces

383 the orientation of the ipAMS fabric (Fig. 10, Fig. S7). In the sites BH2 and BH4, the fabric differs from

384 the ipAMS. Generally, the magnetic foliation in all sites is parallel to the bedding plane and is more

18

385   poorly defined than the ipAMS foliation (large confidence interval ellipses). At sites BH1 and BH3 the

386   magnetic lineation has an approximate ENE- to WSW orientation and is characterized by smaller

387   confidence ellipses in comparison to other Huty Fm sites. At site BH4, the magnetic lineation is NW-

388   orientated and is roughly shifted 90° from the lineation present in other sites. The magnetic foliation

389   deflects slightly from the bedding plane. Two sites (BH2, BH5) show a girdle of maximum-intermediate

390   ellipsoid axes parallel to the magnetic foliation, and no magnetic lineation is present (Fig. 10, Fig. S7).

391   ii.   AARM

392   In the Mraznica Fm sites, the AARM ellipsoid shape varies mainly from triaxial to neutral shapes. The

393   Pj values are higher than for the op- and ipAMS, and range from 1.05 to 1.40. The magnetic fabrics in

394   each site are quite similar to their ipAMS fabrics. The magnetic foliation poles in the Mraznica Fm sites

395   are well grouped and their confidence ellipses are small (Fig. 9, Fig. S8). The magnetic lineation poles

396   are quite well defined in three sites (Fig. 9), and the confidence ellipses are larger than for the magnetic

397   foliation poles. In the site BM4, the magnetic lineation is sub-vertical and N-inclined. The magnetic

398   lineation is trending to the east in BM3, whereas at sites BM1 and BM2, the magnetic lineation

399   orientation is approximately northwest to southeast. The measured Huty Fm specimens display mainly

400   oblate to triaxial ellipsoid shapes and show the lowest values of the Pj parameter in comparison to the

401   ip- and opAMS. The magnetic foliation is generally defined well (small confidence interval ellipses for

402   the magnetic foliation poles). The magnetic foliation poles trace or slightly deflect from the poles to

403   bedding in all sites. The documented magnetic lineation at BH4 and BH2 is similar to the opAMS

404   lineation and is trending from NW-SE to WNW-ESE (Fig. 10, Fig. S8). One site, BH1, displays a NE-SW

405   magnetic lineation orientation, which reoccurs in the ipAMS and opAMS. At BH5, the magnetic

406   lineation poles are more scattered. The magnetic lineation poles in the Huty Fm is characterized by

407   larger confidence ellipses, similar to the Mraznica Fm.

19
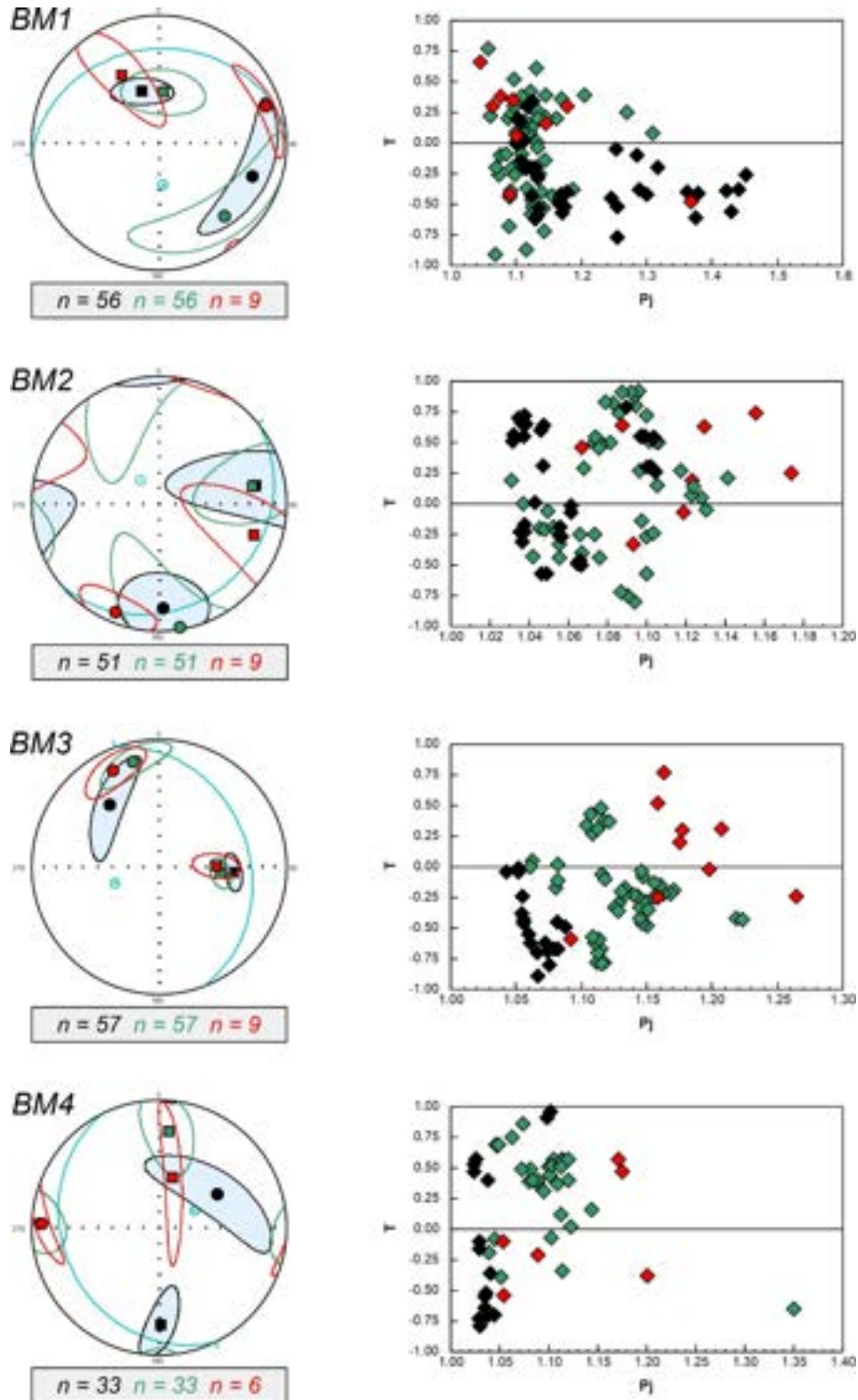
408 Fig. 9 The results of the ipAMS (black), opAMS (green) and AARM (red) measurements for the Mraznica
409 Fm. All fabrics are plotted in lower hemisphere projections in geographic coordinates. Squares and
410 circles represent the maximum and minimum ellipsoid axes derived from the site-mean tensor,
411 respectively. The black color indicates the ipAMS fabric, green indicates the opAMS, and red indicates
412 the AARM fabric. The blue great circle arc indicates the bedding orientation and the blue circles
413 indicate the pole to bedding.

20
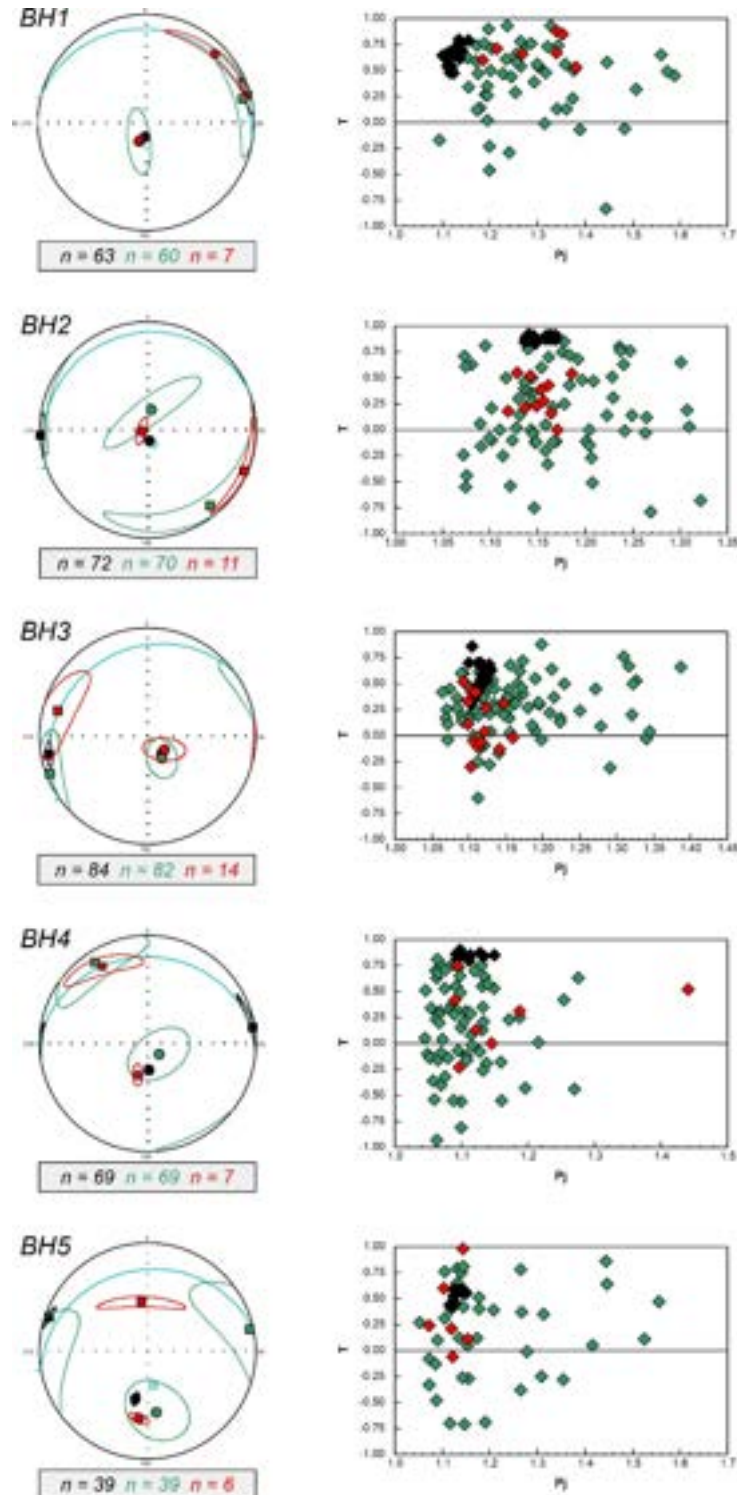
Fig. 10 The results of the ipAMS (black), opAMS (green) and AARM (red) measurements for the Huty Fm. All fabrics are plotted in lower hemisphere projections in geographic coordinates. Squares and circles represent the maximum and minimum ellipsoid axes derived from the site-mean tensor, respectively. The black color indicates the ipAMS fabric, green indicates the opAMS, and red indicates the AARM fabric. The blue great circle indicates the bedding orientation and the blue circles indicate the pole to bedding.

420   6. Discussion

421   a. Paleotemperatures of the eastern Tatra margin

422 To determine the possible paleotemperature range of the Belianske Tatra Mts and their foreland, we

423 measured the Rr and calculated the Rc in the Mraznica and Huty fms. In the Huty Fm the Rc values

424 obtained from MPI1 (methylphenanthrene index 1; Table S1) are more accurate than the measured

425 values (Staneczek et al., 2024a) due to the presence of dark H-rich vitrinites (Fig. S1), which were also

426 detected in the Huty Fm from the Orava basin (a CCPB sub-basin; Staneczek et al., 2024a). In rocks with

427 dark vitrinites, the Rr values are suppressed, and the obtained reflectance may differ from the actual

428 values by up to 0.4% Rr (Goodarzi et al., 1994), therefore, the use of Rc is preferable. The possible

429 paleotemperatures in the Huty Fm of the eastern Tatra Mts were able to reach between 180 to 220°C

430 (based on calculations by Burnham and Sweeney, 1989; Hunt, 1995; Li et al., 2021), and are the highest

431 recorded in the CCPB rocks. However, the Rc values for Mraznica Fm are not realistic due to the

432 occurrence of marine type of organic matter(Staneczek et al., 2024b), and therefore the Rr was used

433 to reconstruct the possible paleotemperature trend. The acquired Rr values in some sites appear lower

434 than those reported in the Huty Fm (Fig. 2), and we interpret this as erroneous measurements. The

435 possible cause is the presence of very small grains of vitrinite in Mraznica Fm (5-10 µm width and

436 smaller than in the Huty Fm), which often leads to a lower accuracy of measurements. Still, the

437 maximum paleotemperatures for the Mraznica Fm must have been higher than those recorded for the

438 Huty Fm, because the thrust units are overlain not only by the Huty Fm, but also by some older beds

439 (like Borove Fm; Gross et al., 1993a, b), creating higher paleotemperatures and prolonged burial. The

440 apparent difference in the temperature rate is also shown in the Kfd parameter values, which are

441 significantly higher (up to 15%) for Mraznica Fm rocks than for Huty Fm (3-4%). Therefore, we infer

442 that the paleotemperatures affecting Mraznica Fm must have been at least in the range of 200-230°C.

443 The phenylphenanthrene ratio (PhP; Rospondek et al., 2009) was used to confirm the temperature

444 trends in the Choč and Tatra Mts. The calculated values of this ratio for the Huty Fm increase from

445 west to east, reaching their maximum in the Belianske Tatra Mts (Table S1). With the Mraznica Fm,

446 this trend is less pronounced, mainly due to possible hydrothermal processes active in the Choč Mts

447 (Bella & Gaal, 2017). However, the highest values are found in the Belianske Tatra Mts and, omitting

448 the Choč Mts, thermal maturity increases from west to east. The calculated vitrinite reflectance results

449 from the Huty Fm correspond well with the vitrinite reflectance values obtained for the Mraznica Fm,

450 and show, that the eastern Tatra Mts margin experienced the highest paleotemperatures in

451 comparison to other parts of the Tatra and Choč Mts, and the Orava-Podhale-Spisz basins (Fig. 2; Table

452 S1; Marynowski et al., 2006; Staneczek et al., 2024a, 2024b; Środoń et al., 2006). Such consistency in

453 the paleotemperature changes towards the southeast indicates one main event that caused the

454 maturation of the studied rocks. We interpret this event to be the Late Oligocene-Early Miocene burial

455 of the Central Western Carpathian (CWC) massifs during CCPB sedimentation. However, we apply this

456 interpretation only to the Krížna nappe units and not to the para-autochthonous cover or the

457 crystalline basement, which may have been more affected during Cretaceous burial (Bac-Moszaszwili

458 & Gąsienica-Szostak, 1990).

459   b.   Main magnetic carriers

460 The first step in investigating the magnetic mineralogy in the Mraznica and Huty fms is establishing the

461 content of dia-, para- and ferromagnetic (*sensu lato*) minerals. Both examined formations show low

462 Kip which falls within a similar range (Fig. 5). Interestingly, the Kip of the Mraznica Fm specimens in

463 the Belianske Tatry Mts are diverse and vary from negative to positive values (Fig. 5A), the latter is not

464 documented in other studied parts of the Tatra Mts and the neighboring Choč Mts (Fig. S9; Staneczek

465 et al., 2022, 2024b). Negative in-phase susceptibilities are documented in the BM1 site, where the CC

466 values are the highest not only from all the analyzed sites in the Belianske Tatra Mts but also in the

467 High and Western Tatra Mts (even 97%; Table 1; Staneczek et al., 2024b). Moreover, the BM1

468 hysteresis loops overall document a diamagnetic behavior (Fig. S5). The CC parameter averages 60-

469 70% in BM3 and BM4 sites (Table S1), but is much lower in BM2, reflecting a change in clastic material

470 supply to the sedimentary basin in the Mraznica Fm previously documented by Piotrowska et al.

471 (2013). However, changes in phyllosilicate content have little effect on Kip and there is no clear

472 correlation with the hysteresis-derived parameters (initial slope and high-field slope comparison; Table

473 S3). Based on these observations, the Kip in the Mraznica Fm sites are predominantly governed by the

474 ferromagnetic fraction, i.e., magnetite and hematite.

475 The Kip measurements of the Huty Fm specimens document consistent values similar to susceptibilities

476 reported from the Western and High Tatra foreland, and the Choč Mts (Fig. S9). Hysteresis curves

477 (before and after correction) and parameters (initial slope and high-field slope comparison) show a

478 predominance of paramagnetic minerals (Fig. S5). Considering the lithology of this unit and the low CC

479 values, the minerals in question are most likely phyllosilicates. The Kop for this unit is controlled by

480 magnetite, which dominates the ferromagnetic fraction in Huty Fm (see next paragraph).

481 The prevalent type of magnetite grains has higher coercivities in the range of 55-95 mT (Table S2) both

482 in Mraznica and Huty fms. Generally, higher coercivities in the magnetite coercivity range correspond

483 to smaller domain sizes (Heider et al., 1996). Since both the Mraznica and Huty fms have lithologies

484 that are characterized by a significant admixture of clay minerals (Gross et al., 1993, Lefeld et al., 1985,

485 Środoń et al., 2006), we interpret the origin of the stable single-domain (SSD) magnetite as a by-

23

486   product of the illite-smectite transformation in the early stages of diagenesis (Hirt et al., 1993) and/or

487   during the first burial episode of the Mraznica Fm (see *Burial impact on the Tatra Mts* paragraph).

488   The next detected magnetite phase/type is characterized by very low coercivity (~8-13 mT, Table S2),

489   indicative of magnetite with larger domain sizes, presumably with a PSD or MD (Fig. 8). Such larger

490   magnetite grains could either be allochthonous minerals or a product of a diagenetic phase. The

491   Mraznica Fm sedimentary environment is reported by Kędzierski and Uchman (1997) to be oxic, which

492   would preserve the large allochthonous MD grains. However, this does not match our observations,

493   since there is a common occurrence of pyrite framboids (Fig. S1) indicative of more oxygen-depleted

494   conditions, which would enable the dissolution of iron oxides during sedimentation and early

495   diagenesis (Canfield et al., 1992; Roberts, 2015). Similarly, the paleoenvironment of the Huty Fm was

496   reported to be dysoxic to euxinic (Marynowski et al., 2006; Soták et al., 2001; Staneczek et al., 2024a),

497   which would also prohibit the preservation of allochthonous magnetite (Canfield & Berner, 1987) and

498   a higher organic matter content (Table 1). We are therefore critical about the detrital origin of

499   magnetite, favoring a diagenetic origin. Primary SD magnetite was formed in the early stages of

500   diagenesis and/or first burial. Next, it grew to PSD domains due to the continuous elevation of

501   temperatures in the Oligocene-Miocene which triggered the final stage of diagenesis (Środoń et al.,

502   2006). Such a PSD population is reported in other parts of the Tatra-Fatra Belt (Grabowski, 2000;

503   Staneczek et al., 2022, 2024b). Considering the thermal and diagenetic history of the studied units we

504   interpret this magnetite population as PSD-grains formed during two stages of diagenesis.

505   The Oligocene burial of the Belianske Tatra Mts induced the formation of superparamagnetic (SP)

506   grains, characterized by notable Kfd parameter values (~15% for Mraznica and 0.75-3% for Huty; Fig.

507   5BD). The Day plot (Fig. 8) indicates the SP magnetite, possibly alongside SP hematite, in the Mraznica

508   Fm sites. SP magnetite generally forms under burial conditions with elevated temperatures (Aubourg

509   & Pozzi, 2010; Kars et al., 2012). During the continuous burial and the temperature increase to 140°C,

510   the formation of new SP-magnetite is faster than the size increase of previously generated grains

511   (Aubourg & Pozzi, 2010; Kars et al., 2012). However, it was not investigated in higher temperatures.

512   The formation of SP hematite, particularly in the Mraznica Fm sites BM1 and BM4, appears also to be

513   linked to burial processes during the Late Oligocene-Early Miocene. The Kfd values in the Belianske

514   Tatra Mts are especially high in comparison to the Western and High Tatra Mts (~2.8% for the Mraznica

515   Fm in High Tatra; Staneczek et al., 2024b) reflecting an intensified phase of SP magnetite and hematite

516   formation. Based on all previous results, the Mraznica Fm in the Belianske Tatra Mts show features

517   indicative of remagnetized limestones (Channel & McCabe, 1994; Dinares-Turell & Garcia-Senz, 2000;

518   Jackson & Swanson-Hysell, 2012; Suk et al., 1993). Remagnetization is documented in limestones

519   across the Central Carpathian region and has been previously attributed to Cretaceous tectonic

24

520 processes (Grabowski et al., 2009). Another possible trigger for SP magnetite formation is the

521 migration of an oxidizing hydrothermal fluid. However, the distribution patterns of Kfd values across

522 the Tatra region suggest that this process was not a primary driver of SP magnetite/hematite

523 formation. Otherwise, it would have had localized rather than regional effects.

524 Petromagnetic measurements reveal the presence of high coercivity minerals interpreted here as

525 hematite. In the Huty Fm, the hematite contribution is very low, even negligible (as in sample BH364,

526 Fig. S4), except the site BH1. There, the rock magnetic results indicate that hematite is the predominant

527 ferromagnetic mineral. We attribute its origin to early weathering processes, as all samples were

528 collected from outcrops characterized by large overgrown pyrite framboids (Fig. S1). The weathering

529 of pyrite likely contributes to iron oxide formation, a mechanism frequently observed in shales (e.g.,

530 Gu et al., 2020). Weathering also affected Mraznica Fm rocks, especially sites BM2 and BM3, where

531 the low coercivity minerals dominate. Sites BM1 and BM4 show a significant hematite contribution,

532 evident from thermomagnetic measurements (Fig. 6, S4) and IRM curves (Fig. 7). Its substantial role in

533 the magnetic mineralogy indicates a different origin than hematite in the Huty Fm. In the Choč Mts,

534 hematite in the Mraznica Fm was interpreted as late diagenetic or resulting from fluid oxidation

535 (Staneczek et al., 2022), facilitated by faults, which is not reported in the Belianske Tatra Mts.

536 Staneczek et al. (2024b) suggest that the formation of hematite and the increase in Hcr/Hc ratios on

537 the Day diagram is linked to elevated burial temperatures, and we support this interpretation.

538   c.   Eo-Alpine to Neogene evolution recorded in the magnetic fabrics of the Tatra region

539   i.   *Pre-CCPB magnetic fabrics*

540 The magnetic fabric of Mraznica Fm sites show two ipAMS lineation patterns: a roughly easterly

541 orientation at BM2 and BM3, and northerly at BM1 and BM4 (Fig. 9, S6). Moreover, the opAMS and

542 AARM fabrics documented in all Mraznica Fm mirror the ipAMS fabric but are more dispersed (Fig. 9,

543 S7, S8). These reflect the alignment of ferromagnetic iron oxides formed on the fixed phyllosilicate

544 matrix, a phenomenon reported in many previous studies (Borradaile & Lagroix, 2000; Calvín et al.,

545 2018a; Hirt et al., 1993; Housen et al., 1993; Li & Kodama, 2005). The first population of these grains

546 is linked with the Cretaceous burial, and the resulting magnetic fabric was strengthened during the

547 Oligocene burial by the formation of new magnetite. An east-oriented ipAMS lineation has been

548 reported across various units in the Tatra Mountains, including nappe structures, para-autochthonous

549 cover layers, and even in the crystalline basement, and was attributed to the Turonian thrust-related

550 shortening(Hrouda & Kahan, 1991; Grabowski, 2000; Szaniawski et al., 2012, 2020; Staneczek et al.,

551 2024b). In the Mraznica Fm, the ipAMS foliation deflects significantly from the bedding plane and is

552 nearly perpendicular in BM2, which resembles patterns seen in the Belianske Tatra's Krížna nappe.

There, Hrouda and Kahan (1991) observed girdles of magnetic foliation poles in the AMS diagrams, indicating combined simple shear and lateral shortening during thrusting, a pattern echoed in other highly deformed nappes (Lamarche & Rochette, 1987). The magnetic lineation generally is perpendicular to the girdle and the shortening direction but can be aligned with the shortening direction under moderate layer-parallel compression (Cifelli et al., 2014; Oliva-Urcia et al., 2009; Parés, 2015; Satolli et al., 2020). Magnetic lineations reflecting Turonian thrusting are widely recognized in both allochthonous and para-autochthonous units and even occur in the crystalline basement (Hrouda & Kahan, 1991; Grabowski & Gawęda, 1999). The primary nappe transport direction in the Central Carpathian region was approximately to the northwest (Jurewicz, 2005; Kováč & Bendík, 2002; Plašienka, 2003; Prokešová et al., 2012), aligning the easterly ipAMS lineation in the Mraznica Fm with Late Cretaceous thrusting. In light of these studies, we interpret the easterly oriented magnetic lineation present in Mraznica Fm as a result of Late Cretaceous complex thrusting mechanisms.

The northerly oriented magnetic lineation pattern in the Mraznica Fm, however, is unique to the Belianske Tatra Mts and has not been documented in other areas of the Tatra Mts and in the whole Huty Fm. This well-grouped lineation with scattered foliation likely also formed during thrusting, albeit through different mechanisms. This N-oriented lineation pattern may reflect simple shear deformation, influenced by the presence of a thick limestone layer (Muraň Fm) overlying the Mraznica marls and marly limestones (Nemčok et al., 1993a, b). In our interpretation, the less competent Mraznica Fm was subjected to simple shear during thrusting, resulting in a magnetic lineation parallel to the shear orientation, similar to findings in the Strážov Mountains (Szaniawski et al., 2020).

ii. Syn-sedimentary and burial-related fabrics

The opAMS lineation in the one Huty Fm site (BH4; Fig. 10, 11, S7) is NW-oriented, and coaxial with extension during the CCPB sedimentation, which was documented by Králiková et al. (2014) in the Tatra region, as well as by other authors in the Orava Basin and Spiš Basin (Pešková et al., 2009; Vojtko et al., 2010). The extension-related orientation of the first diagenetic magnetite population was further strengthened by a second magnetite population formed during the increasing burial rate. This is supported by the similar orientation of the corresponding AARM lineation, which is governed by PSD and SD grains (Fig. 9, 10, S8) Such an NW-oriented lineation is also documented in the Podhale region by Márton et al. (2009), but there it is referred to as sedimentary. However, the well-clustered magnetic lineation points, in our interpretation, points to a tectonic origin. Similarly oriented magnetic lineations were reported in the Western and High Tatra Mts (Staneczek et al., 2024b), and in the Choč Mts (Staneczek et al., 2022). Therefore, we interpret this opAMS and AARM lineations as a result of Oligocene extension.
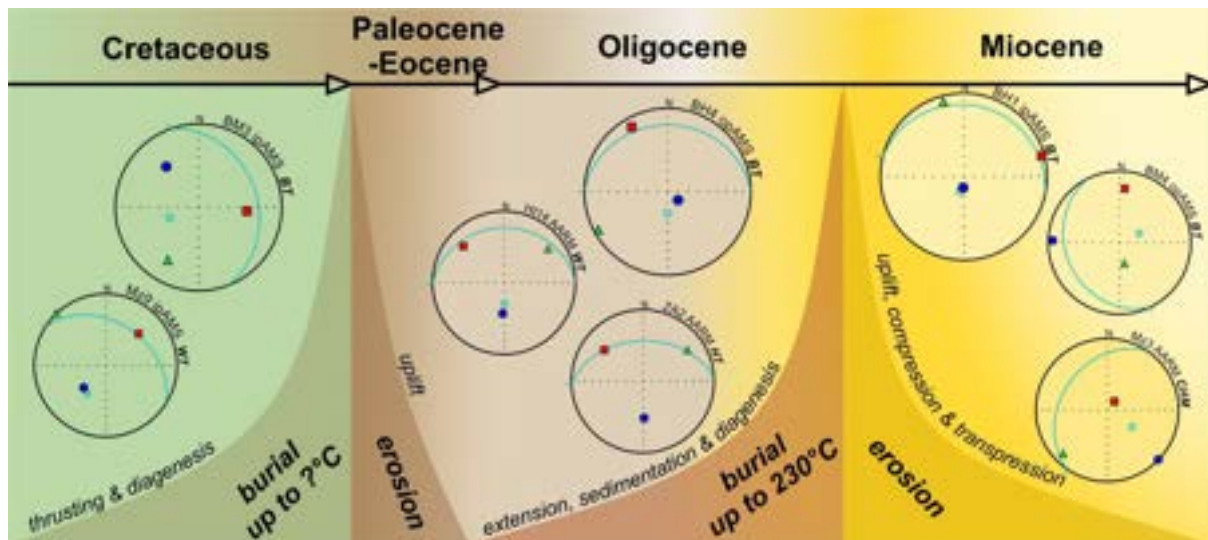
Fig. 11 Tectonic evolution of the Choč-Tatra Belt reflected in magnetic fabrics. All fabrics are plotted in lower hemisphere projections in geographic coordinates. Squares and circles represent the maximum and minimum ellipsoid axes derived from the site-mean tensor, respectively. Abbreviations: WT – Western Tatra Mts, HT – High Tatra Mts, BT – Belianske Tatra Mts, CHM – Choč Mts. Magnetic fabric data were compiled from Staneczek et al. (2022, 2024b).

iii. *Post-CCPB magnetic fabrics*

The ipAMS fabrics of the Huty Fm are consistent and characterized by the presence of a well-defined magnetic foliation and a similarly well-grouped magnetic lineation that is either approximately WNW- to ESE or ENE-to WSW oriented (Fig. 9, 10, 11, S6). In addition, most of the AARM and opAMS fabrics documented in the Huty Fm trace the ipAMS fabric. The good alignment of the magnetic foliation and bedding is the result of both compaction processes during diagenesis and the overall oblate shape of the phyllosilicate matrix. Similar WNW to ESE or ENE to WSW oriented ipAMS lineations are documented widely in the Oligocene foreland of the Tatra-Fatra belt and the Podhale-Spisz region (Madzin et al., 2021; Márton et al., 2009; Staneczek et al., 2022, 2024b). In the latter area, they are interpreted as the effect of turbiditic currents. However, the majority of sites investigated in these studies show coarse-grained rocks more prone to record the paleoflow direction. Moreover, as documented by Staneczek et al. (2024a) in the Orava region, the deposition of the Lower Oligocene (Huty Fm) in the CCPB progressed under dysoxic to intermittently euxinic depositional conditions. Current run-off occurred occasionally and was manifested by a change of fraction to more coarse-grained. The sampled black shales do not show any signs of current flows which may have altered the conditions to aerobic. Under anaerobic conditions, paleocurrent cannot occur as this would involve the supply of oxygen to the bottom waters. The obtained WNW-to ESE to ESE-to WNW orientations correspond reasonably well with the uplift-related Early to Middle Miocene NW- to SE to NNW- to SSE

27

compression documented mainly in the Tatra and their foreland (Králiková et al., 2014; Vojtko et al., 2010), but also in the Orava region (Pešková et al., 2009) and Kozie Chrbty (Sůkalová et al., 2012). The magnetic lineation orientation is therefore parallel to the fold axis of small-scale folds documented in the CCPB sedimentary rocks (Vojtko et al., 2010). In the Western and High Tatras, the ipAMS lineation in Huty sites was attributed to this tectonic stage (Staneczek et al., 2024b). This interpretation concurs also with the Belianske Tatra Mts.

d. Burial impact on the Tatra Mts

i. *Magnetic burial indicators*

The Tatra-Choč Belt, with its eastward trend in increasing paleotemperatures, is an excellent laboratory for studying the burial impact on the magnetic mineralogy (Fig. 2). Compiled magnetic susceptibility (MS) measurements from the Choč Mts and the whole Tatra massif (both Huty and Mraznica; Fig. 12) document changes between different sampling areas which correlate mostly with vitrinite reflectance values. The differences in the burial rate are also highlighted by the Kfd parameter, which is the highest in the Belianske Tatra Mts. Anomalously high Kip values and a shift towards a shift towards the SP-realm in the Day plot (Fig. 13) in the Mraznica Fm from the Choč Mts are linked with the hydrothermal impact on this highly deformed area. Increased fluid circulation has been documented in this area (Bella & Gaal, 2017), and is likely related to the presence of the main Choč-Tatra-Ružbachy Fault (Bella & Bosak, 2012). In contrast, in the Tatra block the MS differences seem to be affected purely by burial because the increase in MS values matches the paleotemperature increase. Moreover, the magnetic susceptibility does not reflect changes in the Mraznica succession type (Zliechov in Western Tatra Mts, and Vysoka in High and Belianske Tatra Mts; Nemčok et al., 1993b). Burial-related changes are also documented by the Day plot compiled for the Mraznica Fm of the Choč-Tatra Belt (Fig. 13), which shows a gradual shift towards the PSD-SP mixing realm/area. The change is related to the increased formation of iron oxides under high temperatures. Such features are not present in the Day plot for Huty Fm (Fig. 13). In the absence of an analysis of the Belianske Tatra samples, it may prove challenging to discern this trend, given that the alteration observed in the burial impact on the Western and High Tatra Mts are comparatively minor and could potentially be confused with other processes.

638
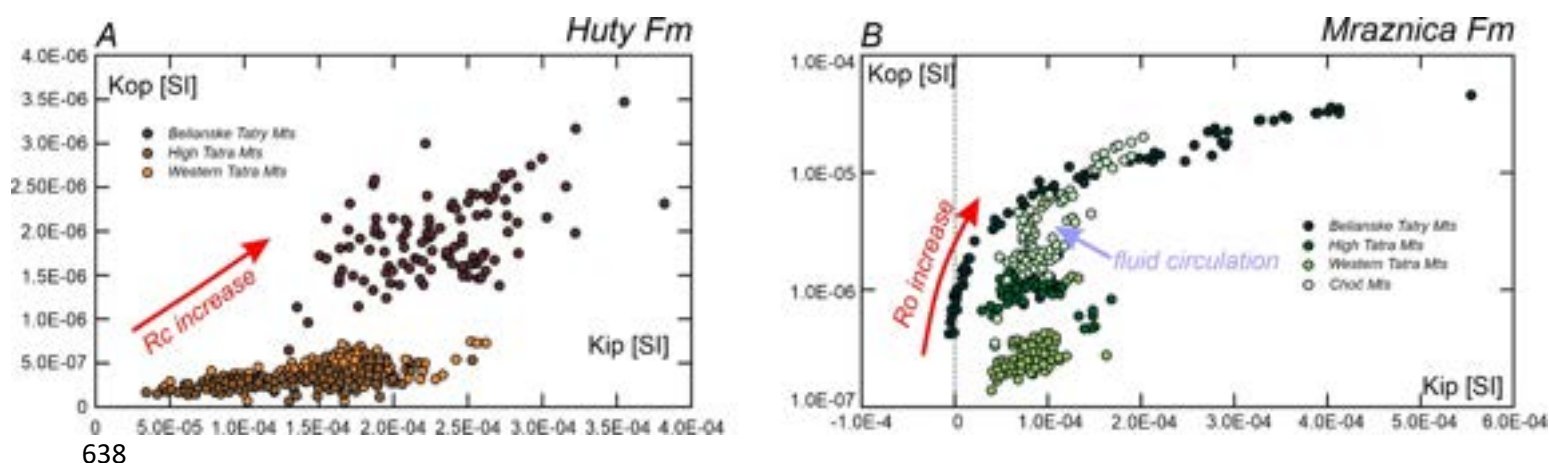
639   Fig. 12 Kip vs Kop plots for samples from the Choč Mts and Tatra Mts (compiled from Staneczek et al.,

640   2024b). The magnetic susceptibility data from the Huty Fm of the Choč Mts could not be plotted due

641   to artificial values of the Kop (Text S1). Rc refers to the calculated vitrinite reflectance, and Rr is the

642   random vitrinite reflectance.

643
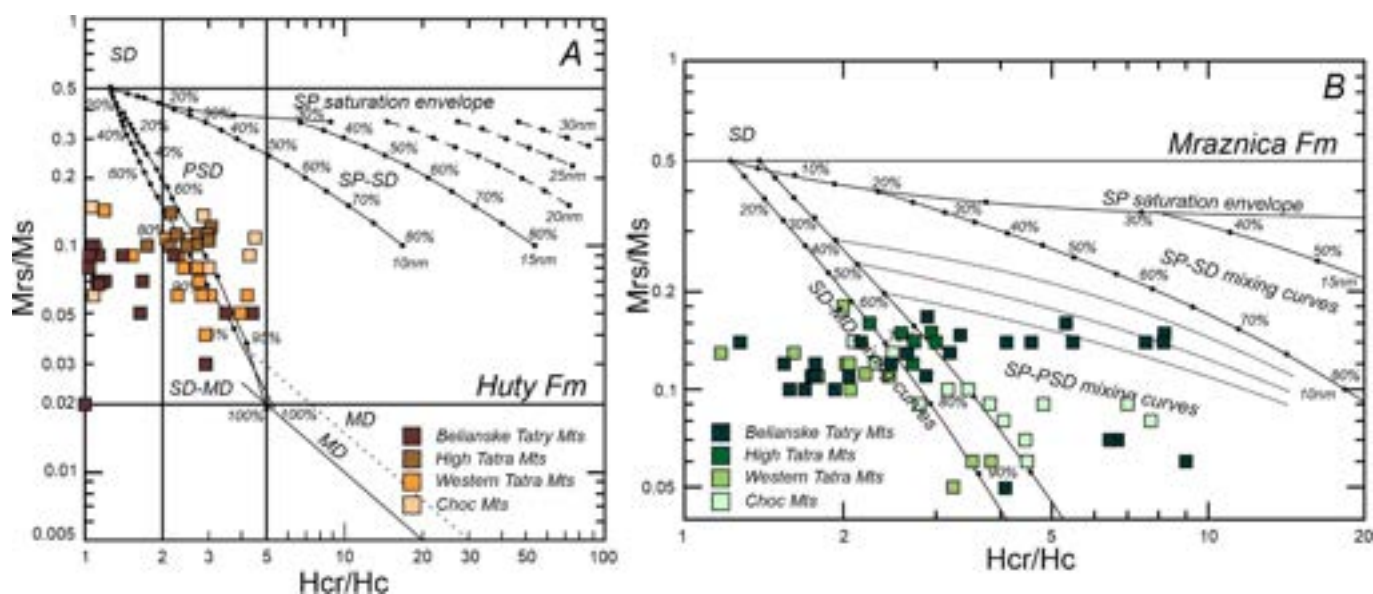
644   Fig. 13 Day plots for samples from the Choč Mts, Western, High, and Belianske Tatry Mts (compiled

645   from Staneczek et al., 2022; Staneczek et al., 2024b).

646   *ii.   The burial age: Turonian or Oligocene?*

647   The age of the most prominent burial of the Tatra massif is the subject of a long-standing discussion.

648   Most of the authors interpret a Late Cretaceous timing related to a nappe thrusting event (e.g.,

649   Anczkiewicz et al., 2015; Campos et al., 2023; Grabowski, 2000; Králiková et al., 2014; Márton et al.,

650   2016; Plašienka et al., 1997; Śmigielski et al., 2016; Środoń et al., 2006). The majority of these studies

29

focus on the crystalline basement. Some thermo-chronometric studies performed in the High Tatra Mts, suggest that the maximum burial of this part occurred approximately in the Late Oligocene (Campos, et al., 2023), which would coincide with the maximum burial reported in this study. On the contrary, Anczkiewicz et al. (2015), Králiková et al. (2014), and Śmigielski et al. (2016) date the maximum burial of the crystalline basement as Late Cretaceous. However, all three studies point to a second burial in the Oligocene followed by a cooling in the Miocene. Such events are caused by the sedimentation of CCPB rocks and the subsequent uplift of the massif. The paleomagnetic studies point towards a Late Cretaceous remagnetization age of the youngest nappe sedimentary rocks (Grabowski, 1997; Márton et al 2016). Although it is generally accepted that the crystalline core of the Tatra Mts was affected by high burial temperatures during Turonian thrusting, the impact of this event on the youngest nappe sedimentary rocks is debatable. Only a few paleomagnetic studies record Paleogene-Neogene pre-tilt remagnetizations in the Tatra Mts (Grabowski, 1997). However, all studies were focused on the Western Tatra nappes, where the crystallization of new magnetite during burial was presumably not as intense as in the Belianske or High Tatra Mts. Therefore, it could retain the Late Cretaceous remagnetization ages due to a low content of magnetite formed during the late Oligocene – early Miocene. The maximum inferred thickness of thrust nappes in the Tatra Mts is presumed not to exceed 4 km (Nemčok et al., 1993b), and the erosion rate is unknown. Assuming that the present-day nappe sedimentary rocks in the Tatra Mts constitute the lower parts of thrust folds and that the Choč nappe was present in all the Tatra region, the eroded part was not thick enough to induce temperatures as high as 200-230°C. The vitrinite reflectance data presented by Poprawa et al. (2002) and Staneczek et al. (2024ab) show an eastward trend in increasing reflectance values. The lowest values for Huty Fm are observed in the Orava basin and increase towards the east (Fig. 2). The Mraznica Fm deposits closely reflect this trend. This is further supported by thermal maturity studies of the Chochołów PIG1 and Bukowina Tatrzańska PIG1 wells (CCPB rocks, including Huty Fm; Poprawa & Marynowski; 2005), and illite crystallinity studies (Środoń et al., 2006). Similar trends in the Rr distribution in both nappe and post-orogenic sedimentary rocks are clear evidence of the Oligocene overburden impact.

Furthermore, the direction of change of various parameters in the Choč-Tatra Belt is noteworthy. The surficial occurrence of Mraznica and Huty Fm is closely related to large faults that cut the Tatra massif (Fig. 2), which could partly contribute to the different thicknesses and erosion rates of the Belianske Tatra and Spisz deposits. However, a significant change in observed magnetic and geochemical parameters is most likely due to different subsidence levels during the sedimentation of CCPB units. Kováč et al. (2016) suggest a migration of depocentres from west to east in the fore-arc basins of the Central Western Carpathians, which most likely caused prolonged and more intensive sedimentation,

30

685 and thus increased overburden of the nappe units in the Belianske Tatra Mts region. Moreover, a
686 thermo-chronometric study performed by Anczkiewicz et al. (2015) described differences in estimated
687 paleotemperatures between sites located in the western and easternmost parts of the Tatra Mts
688 during the Oligocene burial. In addition, the eastern part of the massif experienced a significantly faster
689 uplift than the western part, which, coupled with the maximum paleotemperatures reported in the
690 eastern part, suggests a thicker sedimentary load in the eastern Tatra Mts.

691 7. Conclusions

692 1. In the Belianske Tatra Mts, the Kip of the Mraznica Fm is carried mainly by the
693 ferromagnetic mineral fraction (magnetite, hematite and possibly some iron sulfides),
694 while in Huty Fm it is governed by paramagnetic minerals (i.e., phyllosilicates).

695 2. The Mraznica Fm rocks exhibit features typical for remagnetized limestones, e.g., wasp-
696 waisted hysteresis curves and high content of SP-magnetite and/or SP hematite. The
697 presumed age of this mineral generation is the Late Oligocene/Early Miocene, which
698 coincides with the final stages of the CCPB burial.

699 3. Magnetic fabrics were divided according to their origin as pre-CCPB age, burial-related
700 fabrics, and post-CCPB fabrics. Pre-CCPB fabrics document the shortening during Turonian
701 thrusting. Burial-related fabrics show the Oligocene extension direction. Post-CCPB fabrics
702 are linked with the uplift of the Tatra block.

703 4. In the Choč Mts-Tatra Mts belt, the vitrinite reflectance analysis documents an eastward
704 increase in paleotemperatures. The recorded values in Huty Fm rocks correspond well with
705 the Rr values for Mraznica Fm. This trend is also reflected in the magnetic mineralogy.
706 Overall, the data indicate that Late Oligocene–Early Miocene burial was the most intense
707 along the eastern margin of the Tatra Mts.

708 5. The paleotemperatures that affected the Mraznica Fm during the Oligocene-Miocene
709 burial reached 200-230°C.

710

31

718 Regional Development Fund (ERDF) to the laboratory facilities at the Institute of Geophysics, Polish

719 Academy of Sciences, used in the study.

720

721 Open research

722 Data availability statement

723 The rock magnetic, magnetic fabric, biomarker data and vitrinite reflectance data used for

724 identification of the main magnetic carriers, reconstruction of the stress field by analyzing the

725 magnetic fabrics, and investigating paleotemperatures in the study are available in the ZENODO

726 repository. DOI numbers of the datasets: 10.5281/zenodo.14052269, 10.5281/zenodo.12592033,

727 10.5281/zenodo.12592169,   10.5281/zenodo.12592230,   10.5281/zenodo.12594183,

728 10.5281/zenodo.12594189, 10.5281/zenodo.12594194.

729

730 Literature

731 Anczkiewicz, A.A., Danišík, M., Środoń, J., 2015. Multiple low-temperature thermochronology
732 constraints on exhumation of the Tatra Mountains: New implication for the complex evolution of the
733 Western Carpathians in the Cenozoic. Tectonics 34, 2296–2317.

734 Aubourg, C., Pozzi, J.-P., 2010. Toward a new <250°C pyrrhotite–magnetite geothermometer for
735 claystones.   Earth   and   Planetary   Science   Letters   294,   47–57.
736 https://doi.org/10.1016/j.epsl.2010.02.045

737 Aubourg, C., Pozzi, J.-P., Kars, M., 2012. Burial, claystones remagnetization and some consequences
738 for magnetostratigraphy. Geological Society, London, Special Publications 371, 181–188.
739 https://doi.org/10.1144/SP371.4

740 Bac-Moszaszwili, M., Gąsienica-Szostak, M. 1990. Polish Tatra Mts. Geological guide for tourists. Wyd.
741 Geol., Warszawa, 159 pp. (in Polish)

742 Banerjee, S., Elmore, R.D., Engel, M., 1997. Chemical remagnetization and burial diagenesis: Testing
743 the hypothesis in the Pennsylvanian Belden Formation, Colorado. Journal of Geophysical Research:
744 Solid Earth 102, 24825–24842.

745 Bella, P., Bosak, P., 2012. Speleogenesis along deep regional faults by ascending waters: case studies
746 from Slovakia and Czech Republic. Acta Carsologica 41, 169–192.

747 Bella, P., Gaál, Ľ., 2017. Hypogene Caves in Slovakia, in: Klimchouk, A., N. Palmer, A., De Waele, J., S.
748 Auler, A., Audra, P. (Eds.), Hypogene Karst Regions and Caves of the World, Cave and Karst Systems of
749 the World. Springer International Publishing, Cham, pp. 299–311. https://doi.org/10.1007/978-3-319-
750 53348-3_19

751 Borradaile, G.J., Lagroix, F., 2000. Thermal Enhancement of Magnetic Fabrics in High Grade Gneisses.
752 Geophysical Research Letters 27, 2413–2416. https://doi.org/10.1029/2000GL008522

753 Burchart, J., 1972. Fission-track age determinations of accessory apatite from the Tatra Mountains,
754 Poland. Earth and Planetary Science Letters 15, 418–422.

755 Burnham, A.K., Sweeney, J.J., 1989. A chemical kinetic model of vitrinite reflectance and maturation.
756 Geochim. Cosmochim. Acta 53, 2649–2657.

757 Calvín, P., Villalaín, J.J., Casas-Sainz, A.M., 2018a. Anisotropic magnetite growth in remagnetized
758 limestones: Tectonic constraints and implications for basin history. Geology 46, 751–754.
759 https://doi.org/10.1130/G45158.1

760 Calvín, P., Villalaín, J. J., & Casas-Sainz, A. M., 2018b. The carriers of AMS in remagnetized carbonates.
761 Insights for remagnetization mechanism and basin evolution. Physics of the Earth and Planetary
762 Interiors, 282, 1–20. https://doi.org/10.1016/j.pepi.2018.06.003

763 Campos, D., Catlos, E., Stockli, D., Ketcham, R., Miller, N., Broska, I., Kohut, M., 2023. Exhumation of
764 the High Tatra Mountains and Implications for the Western Carpathians, Slovakia. Geological Society
765 of America Abstracts with Programs. Vol. 55, No. 6. https://doi.org/10.1130/abs/2023AM-393919.

766 Canfield, D. E., & Berner, R. A. (1987). Dissolution and pyritization of magnetite in anoxic marine
767 sediments. Geochimica et Cosmochimica Acta, 51(3), 645–659. https://doi.org/10.1016/0016-
768 7037(87)90076-7

769 Canfield, D. E., Raiswell, R., & Bottrell, S. H. 1992. The reactivity of sedimentary iron minerals toward
770 sulfide. American Journal of Science, 292(9), 659–683. https://doi.org/10.2475/ajs.292.9.659

771 Catlos, E.J., Broska, I., Kohút, M., Etzel, T.M., Kyle, J.R., Stockli, D.F., Miggins, D.P., Campos, D., 2022.
772 Geochronology, geochemistry, and geodynamic evolution of Tatric granites from crystallization to
773 exhumation (Tatra Mountains, Western Carpathians). Geologica Carpathica 73, 517–544.

774 Cifelli, F., Ballato, P., Alimohammadian, H., Sabouri, J., Mattei, M., 2015. Tectonic magnetic lineation
775 and oroclinal bending of the Alborz range: Implications on the Iran-Southern Caspian geodynamics.
776 Tectonics 34, 116–132. https://doi.org/10.1002/2014TC003626

777 Csontos, L., Vörös, A., 2004. Mesozoic plate tectonic reconstruction of the Carpathian region.
778 Palaeogeography, Palaeoclimatology, Palaeoecology 210, 1–56.

779 Day, R., Fuller, M., Schmidt, V., 1977. Hysteresis properties of titanomagnetites: grain-size and
780 compositional dependence. Physics of the Earth and Planetary Interiors 13, 260–267.

781 Dearing, J.A., Dann, R.J.L., Hay, K., Lees, J.A., Loveland, P.J., Maher, B.A., O'grady, K., 1996. Frequency-
782 dependent susceptibility measurements of environmental materials. Geophysical Journal International
783 124, 228–240.

784 Dinarès-Turell, J., Garcia-Senz, J., 2000. Remagnetization of Lower Cretaceous limestones from the
785 southern Pyrenees and relation to the Iberian plate geodynamic evolution. Journal of Geophysical
786 Research105, 19405–19418. https://doi.org/10.1029/2000JB900136

787   Dunlop, D.J., 2002. Theory and application of the Day plot (Mrs / Ms versus Hcr / Hc) 2. Application to
788   data for rocks, sediments, and soils. Journal of Geophysical Research 107.
789   https://doi.org/10.1029/2001JB000487

790   Elmore, R.D., Muxworthy, A.R., Aldana, M., 2012. Remagnetization and chemical alteration of
791   sedimentary rocks. Geological Society, London, Special Publications 371, 1–21.
792   https://doi.org/10.1144/SP371.15

793   Goodarzi, F., Snowdon, L., Gentzis, T., & Pearson, D. 1994. Petrological and chemical characteristics of
794   liptinite-rich coals from Alberta, Canada. Marine and Petroleum Geology, 11(3), 307–319.
795   https://doi.org/10.1016/0264-8172(94)90052-3

796   Grabowski, J., 1996. Magnetic fabric of the Upper Jurassic sediments, Krížna Unit, Tatra Mts., Poland.
797   Geologica Carpathica 47, 331–337.

798   Grabowski, J., 1997. Paleomagnetic results from the cover (High-Tatric) unit and nummulitic Eocene in
799   the Tatra Mts (Central West Carpathians, Poland) and their tectonic implications. Annales Societatis
800   Geologorum Poloniae 67, 13–23.

801   Grabowski, J., 2000. Palaeo- and rock magnetism of Mesozoic carbonate rocks in the Sub-Tatric series
802   (Central West Carpathians) - palaeotectonic implications. In: Polish Geological Institute Special Papers,
803   5, pp. 1–88.

804   Grabowski, J., Gawęda, A., 1999. Preliminary palaeomagnetic study of the High Tatra granites, Central
805   Western Carpathians, Poland. Geological Quarterly 43, 263–276.

806   Grabowski, J., Michalík, J., Szaniawski, R., Grotek, I., 2009. Synthrusting remagnetization of the Krížna
807   nappe: high resolution palaeo-and rock magnetic study in the Strážovce section, Strážovské vrchy Mts,
808   Central West Carpathians (Slovakia). Acta Geologica Polonica 59, 137–155.

809   Gross, P., Köhler, E., Haško, J., Halouzka, R., Mello, J., Nagy, A., 1993. Geology of the southern and
810   eastern Orava. Štátny Geologický Ústav Dionýza Štúra, Bratislava.

811   Gross, P., Köhler, E., Samuel, O., 1984. New lithostratigraphic classification of the Central Carpathians
812   Paleogene. Geologické Práce, Správy 81, 103–17.

813   Gu, X., Heaney, P. J., Reis, F. D. A. A., & Brantley, S. L. (2020). Deep abiotic weathering of pyrite. Science,
814   370(6515), eabb8092. https://doi.org/10.1126/science.abb8092

815   Heider, F., Zitzelsberger, A., & Fabian, K. (1996). Magnetic susceptibility and remanent coercive force
816   in grown magnetite crystals from 0.1 μm to 6 mm. Physics of the Earth and Planetary Interiors, 93(3–
817   4), 239–256.

818   Hirt, A., Banin, A., Gehring, A., 1993. Thermal generation of ferromagnetic minerals from iron-enriched
819   smectites. Geophysical Journal International 115, 1161–1168.

820   Housen, B.A., Richter, C., van der Pluijm, B.A., 1993. Composite magnetic anisotropy fabrics:
821   experiments, numerical models and implications for the quantification of rock fabrics. Tectonophysics
822   220, 1–12. https://doi.org/10.1016/0040-1951(93)90219-A

823   Hrouda, F., 1991. Models of magnetic anisotropy variations in sedimentary thrust sheets.
824   Tectonophysics 185, 203–210. https://doi.org/10.1016/0040-1951(91)90444-W

825 Hrouda, F., Kahan, 1991. The magnetic fabric relationship between sedimentary and basement nappes
826 in the High Tatra Mountains, N. Slovakia. Journal of Structural Geology 13, 431–442.

827 Hrouda, F., Krejčí, O., Potfaj, M., Stráník, Z., 2009. Magnetic fabric and weak deformation in sandstones
828 of accretionary prisms of the Flysch and Klippen Belts of the Western Carpathians: Mostly offscraping
829 indicated. Tectonophysics 479, 254–270.

830 Hunt, J.M., 1995. Petroleum Geochemistry and Geology. W.H. Freeman, New York. 743 pp.

831 ISO 7404-2, 2009. Methods for the Petrographic Analysis of Coals – Part 2: Methods of Preparing Coal
832 Samples. International Organization for Standardization, Switzerland.

833 Jackson, M., Swanson-Hysell, N.L., 2012. Rock magnetism of remagnetized carbonate rocks: another
834 look. Geological Society, London, Special Publications 371, 229–251. https://doi.org/10.1144/SP371.3

835 Jurewicz, E., 2005. Geodynamic evolution of the Tatra Mts. and the Pieniny Klippen Belt (Western
836 Carpathians): problems and comments. Acta Geologica Polonica 55, 295–338.

837 Jurewicz, E., 2007. Multistage evolution of the granitoid core in Tatra Mountains. Granitoids in Poland.
838 Warsaw University, Warsaw 307–317.

839 Kądziałko-Hofmokl, M., Kruczyk, J., 1987. Paleomagnetism of middle-late Jurassic sediments from
840 Poland and implications for the polarity of the geomagnetic field. Tectonophysics, Laurasian
841 Paleomagnetism and Tectonic 139, 53–66. https://doi.org/10.1016/0040-1951(87)90197-1

842 Kars, M., Aubourg, C., Pozzi, J., Janots, D., 2012. Continuous production of nanosized magnetite
843 through low grade burial. Geochemistry, Geophysics, Geosystems 13, 2012GC004104.
844 https://doi.org/10.1029/2012GC004104

845 Kars, M., Aubourg, C., Pozzi, J.-P., 2023. Impact of temperature increase on the formation of magnetic
846 minerals in shales. The example of Tournemire, France. Physics of the Earth and Planetary Interiors
847 338, 107021.

848 Katz, B., Elmore, R., Engel, M., 1998. Authigenesis of magnetite in organic-rich sediment next to a dike:
849 implications for thermoviscous and chemical remagnetizations. Earth and Planetary Science Letters
850 163, 221–234.

851 Kędzierski, M., Uchman, A., 1997. Age and palaeoenvironment of the Koscieliska Marl Formation
852 (Lower Cretaceous) in the Tatra Mountains, Poland: preliminary results. Annales Societatis
853 Geologorum Poloniae 67, 237–247.

854 Kohút, M., Kovach, V.P., Kotov, A.B., Salnikova, E.B., Savatenkov, V.M., 1999. Sr and Nd isotope
855 geochemistry of Hercynian granitic rocks from the Western Carpathians–implications for granite
856 genesis and crustal evolution. Geologica Carpathica 50, 477–487.

857 Kováč, M., Král, J., Márton, E., Plašienka, D., Uher, P., 1994. Alpine uplift history of the Central Western
858 Carpathians: geochronological, paleomagnetic, sedimentary and structural data. Geologica Carpathica
859 45, 83–96.

860 Kováč, M., Plašienka, D., Soták, J., Vojtko, R., Oszczypko, N., Less, G., Ćosović, V., Fügenschuh, B.,
861 Králiková, S., 2016. Paleogene palaeogeography and basin evolution of the Western Carpathians,
862 Northern Pannonian domain and adjoining areas. Global and Planetary Change 140, 9–27.

863 Kováč, P., Bendík, A., 2002. Structural analysis of Adnet limestones at Zvolen-Donovaly. Mineralogica
864 Slovaca 34, 3–4.

865 Král, J. (1977). Fission track ages of apatites from some granitoid rocks in West Carpathians. Geol. Zb.
866 Geol. Carpathica, 28(2), 269–276.

867 Králiková, S., Vojtko, R., Sliva, L., Minar, J., Fuegenschuh, B., Kováč, M., Hok, J., 2014. Cretaceous–
868 Quaternary tectonic evolution of the Tatra Mts (Western Carpathians): constraints from structural,
869 sedimentary, geomorphological, and fission track data. Geologica Carpathica 65, 307–326.

870 Králiková, S., Vojtko, R., Hók, J., Fügenschuh, B., & Kováč, M. (2016). Low-temperature constraints on
871 the Alpine thermal evolution of the Western Carpathian basement rock complexes. Journal of
872 Structural Geology, 91, 144–160.

873 Kruczyk, J., Kadzialko-Hofmokl, M., Lefeld, J., Pagač, P., Túnyi, I., 1992. Paleomagnetism of Jurassic
874 sediments as evidence for oroclinal bending of the Inner West Carpathians. Tectonophysics 206, 315–
875 324.

876 Lamarche, G., & Rochette, P. (1987). Microstructural analysis and origin of lineations in the magnetic
877 fabric of some Alpine slates. Tectonophysics, 139(3–4), 285–293.

878 Lefeld, J., 1974. Middle-Upper Jurassic and Lower Cretaceous biostratigraphy and sedimentology of
879 the sub-Tatric succession in the Tatra Mts (Western Carpathians). Acta Geologica Polonica 24, 227–
880 364.

881 Lefeld, J., Gaździcki, A., Iwanow, A., Krajewski, K., Wójcik, K., 1985. Jurassic and Cretaceous
882 lithostratigraphic units of the Tatra Mountains. Studia Geologica Polonica 84, 1–93.

883 Li, Y.-X., Kodama, K.P., 2005. Assessing thermal effects on magnetic fabrics of sedimentary rocks:
884 Results from synthetic and natural samples. Geophysical Research Letters 32.
885 https://doi.org/10.1029/2004GL022049

886 Li, M., Shi, S., Wang, T-G., Zhong, N., Wang, G., Cui, J., 2012. The occurrence and distribution of
887 phenylphenanthrenes, phenylanthracenes and binaphthyls in Palaeozoic to Cenozoic shales from
888 China. Applied Geochemistry 27, 2560–2569. http://dx.doi.org/10.1016/j.apgeochem.2012.09.002

889 Li, P, Duan, J, Cheng, Z., Zou, H 2021. Using Clumped Isotopes to Reconstruct the Maximum Burial
890 Temperature: A Case Study in the Sichuan Basin. Frontiers in Earth Science 9, 759372. doi:
891 10.3389/feart.2021.759372

892 Lowrie, W. (1990). Identification of ferromagnetic minerals in a rock by coercivity and unblocking
893 temperature properties. Geophysical Research Letters, 17(2), 159–162.
894 https://doi.org/10.1029/GL017i002p00159

895 Madzin, J., Márton, E., Starek, D., Mikuš, T., 2021. Magnetic fabrics in the turbidite deposits of the
896 Central Carpathian Paleogene Basin in relation to sedimentary and tectonic fabric elements. Geologica
897 Carpathica 72, 134–154.

898 Maxbauer, D. P., Feinberg, J. M., & Fox, D. L. 2016. MAX UnMix: A web application for unmixing
899 magnetic coercivity distributions. Computers & Geosciences, 95, 140–145.
900 https://doi.org/10.1016/j.cageo.2016.07.009

901 Márton, E., Gregorová, J., Tokarski, A.K., Túnyi, I., 2016. Palaeomagnetic results from the fold and
902 thrust belt of the Western Carpathians: An overview. Geological Society, London, Special Publications
903 425, 7–36.

904 Márton, E., Jelenska, M., Tokarski, A.K., Soták, J., Kovác, M., Spišiak, J., 2009. Current-independent
905 paleomagnetic declinations in flysch basins: a case study from the Inner Carpathians. Geodinamica
906 Acta 22, 73–82.

907 Marynowski, L., Gawęda, A., Poprawa, P., Żywiecki, M.M., Kępińska, B., Merta, H., 2006. Origin of
908 organic matter from tectonic zones in the Western Tatra Mountains Crystalline Basement, Poland: An
909 example of bitumen – source rock correlation. Marine and Petroleum Geology 23, 261–279.

910 Marynowski, L., Smolarek, J., Hautevelle, Y., 2015. Perylene degradation during gradual onset of
911 organic matter maturation. International Journal of Coal Geology 139, 17–25.

912 Michalík, J., 2007. Sedimentary rock record and microfacies indicators of the latest Triassic to mid-
913 Cretaceous tensional development of the Zliechov Basin (Central Western Carpathians). Geologica
914 Carpathica 58, 443.

915 Nemčok, J., Bezák, V., Biely, A., Gorek, A., Halouzka, R., Janák, M., Kahan, S., Kotański, Z., Lefeld, J.,
916 Mello, J., 1993a. Geological Map of the Tatra Mountains 1: 50 000. Bratislava, Geologickỳ ústav D.
917 Štúra.

918 Nemčok, J., Bezák, V., Janák, M., Kahan, Š., Ryka, W., Kohút, M., Lehotskỳ, I., Wieczorek, J., Zelman, J.,
919 Mello, J., others, 1993b. Explanatory notes to the geological map of the Tatra Mts. at 1: 50,000 scale
920 [Vysvetlivky ku geologickej mape Tatier 1: 50 000]. State Geological Institute of Dionỳz Štúr 1–135.

921 Oliva-Urcia, B., Larrasoaña, J.C., Pueyo, E.L., Gil, A., Mata, P., Parés, J.M., Schleicher, A.M., Pueyo, O.,
922 2009. Disentangling magnetic subfabrics and their link to deformation processes in cleaved
923 sedimentary rocks from the Internal Sierras (west central Pyrenees, Spain). Journal of Structural
924 Geology 31, 163–176.

925 Parés, J.M., 2015. Sixty years of anisotropy of magnetic susceptibility in deformed sedimentary rocks.
926 Frontiers in Earth Science 3, 4. doi: 10.3389/feart.2015.00004

927 Passendorfer, E., 1952. How the Tatras were formed. Państwowe Zakłady Wydawnictw Szkolnych.
928 Warszawa. pp. 286 (in Polish)

929 Pešková, I., Vojtko, R., Starek, D., Sliva, L., 2009. Late Eocene to Quaternary deformation and stress
930 field evolution of the Orava region (Western Carpathians). Acta Geologica Polonica 59, 73–91.

931 Petrík, I., Kohút, M., 1997. The evolution of granitoid magmatism during the Hercynian orogen in the
932 Western Carpathians. In book: Geological evolution of the Western Carpathians, Mineralia Slovaca
933 Grecula P., Hovorka D., Putiš M (Eds). 235–252 pp.

934 Piotrowska, K., Kotański, Z., Gawęda, A., Piotrowski, J., Rączkowski, W., 2009. Detailed Geological Map
935 of Poland. Tatry Zachodnie sheet. Polish Geological Institute.

936 Piotrowska, K., Rączkowski, W., Iwanow, A., Zabielski, R., Derkacz, M., Wójcik, A., Michalik, M., Wasiluk,
937 R., 2013. Detailed Geological Map of Poland. Tatry Wysokie sheet. Szczegółowa Mapa Geologiczna
938 Polski. Arkusz Tatry Wysokie. Polish Geological Institute.

939   Plašienka, D., 2003. Development of basement-involved fold and thrust structures exemplified by the
940   Tatric–Fatric–Veporic nappe system of the Western Carpathians (Slovakia). Geodinamica Acta 16, 21–
941   38.

942   Plašienka, D., 2018. Continuity and episodicity in the early Alpine tectonic evolution of the Western
943   Carpathians: How large-scale processes are expressed by the orogenic architecture and rock record
944   data. Tectonics 37, 2029–2079.

945   Plašienka, D., Grecula, P., Putiš, M., Kováč, M., Hovorka, D., 1997. Evolution and structure of the
946   Western Carpathians: an overview. Geological Evolution of the Western Carpathians, Mineralia Slovaca
947   Corporation - Geocomplex, Bratislava, 1–24 pp.

948   Plašienka, D., Prokešová, R., 1996. Towards an evolutionary tectonic model of the Krížna cover nappe
949   (Western Carpathians, Slovakia). Slovak Geological Magazine 3, 279–286.

950   Poprawa, P., Marynowski, L., 2005. Thermal history of the Podhale Trough (northern part of the Central
951   Carpathian Paleogene Basin)–preliminary results from 1-D maturity modeling. Mineralogical Society of
952   Poland–Special Papers 25, 352–355.

953   Poprawa, P., Grabowski, J., Grotek, I., 2002. Thermal and burial history of the sub-Tatric nappes and
954   the Podhale basin—Constraints from preliminary maturity analysis and modelling. Geologica
955   Carpathica 53.

956   Prokešová, R., 1994. Structural analysis of the Krížna nappe in its near-root and superficial position.
957   Mineralia Slovaca 26, 347–354.

958   Prokešová, R., Plašienka, D., Milovskỳ, R., 2012. Structural pattern and emplacement mechanisms of
959   the Krížna cover nappe (Central Western Carpathians). Geologica Carpathica 63, 13–32.

960   Racka, M., Marynowski, L., Filipiak, P., Sobstel, M., Pisarzowska, A., Bond, D.P.G., 2010. Anoxic
961   Annulata Events in the Late Famennian of the Holy Cross Mountains (Southern Poland): geochemical
962   and palaeontological record. Palaeogeography, Palaeoclimatology, Palaeoecology 297, 549–575.

963   Radke, M., 1987. Organic geochemistry of aromatic hydrocarbons. In: Brooks, J., Welte, D. (Eds.),
964   Advances in Petroleum Geochemistry, Vol. 2. Academic Press, London, pp. 141–207.

965   Radke, M., Welte, D., 1983. The Methylphenanthrene Index (MPI). A maturity parameter based on
966   aromatic hydrocarbons., in: Advances in Organic Geochemistry. J. Wiley and Sons, New York, pp. 504–
967   512.

968   Roberts, A.P., 2015. Magnetic mineral diagenesis. Earth-Science Reviews 151, 1–47.

969   Rochette, P., 1987. Magnetic susceptibility of the rock matrix related to magnetic fabric studies.
970   Journal of Structural Geology 9, 1015–1020.

971   Rospondek, M.J., Marynowski, L., Chachaj, A., Góra, M., 2009. Novel aryl polycyclic aromatic
972   hydrocarbons: phenylphenanthrene and phenylanthracene identification, occurrence and distribution
973   in sedimentary rocks. Organic Geochemistry 40, 986–1004.

974   Rubinkiewicz, J., Ludwiniak, M., 2005. Fracture and fault development in Werfenian quartzitic
975   sandstones–A case study from the autochthonous cover of the Tatra Mts. Annales Societatis
976   Geologorum Poloniae 75, 171–187.

977 Satolli, S., Test, C. R., Staneczek, D., Zanella, E., Calamita, F., & Tema, E. 2020. Magnetic fabric in
978 carbonatic rocks from thrust shear zones: A study from the Northern Apennines (Italy).
979 Tectonophysics, 791, 228573.

980 Śmigielski, M., Sinclair, H., Stuart, F., Persano, C., Krzywiec, P., 2016. Exhumation history of the Tatry
981 Mountains, Western Carpathians, constrained by low temperature thermochronology. Tectonics 35,
982 187–207.

983 Soták, J., Pereszlenyi, M., Marschalko, R., Milicka, J., Starek, D., 2001. Sedimentology and hydrocarbon
984 habitat of the submarine-fan deposits of the Central Carpathian Paleogene Basin (NE Slovakia). Marine
985 and Petroleum Geology 18, 87–114

986 Sperner, B., Ratschbacher, L., Nemčok, M., 2002. Interplay between subduction retreat and lateral
987 extrusion: Tectonics of the Western Carpathians. Tectonics 21, 1051. doi:10.1029/2001TC901028

988 Środoń, J., Kotarba, M., Biroň, A., Such, P., Clauer, N., Wójtowicz, A., 2006. Diagenetic history of the
989 Podhale-Orava Basin and the underlying Tatra sedimentary structural units (Western Carpathians):
990 evidence from XRD and K-Ar of illite-smectite. Clay Minerals 41, 751–774.

991 Staneczek, D., Szaniawski, R., Szczygieł, J., 2022. Transpression-driven deformations of the Chočské
992 vrchy Mountains (Western Carpathians): Insights from magnetic fabric. Geologica Carpathica 73, 451–
993 471.

994 Staneczek, D., Więcław, D., Marynowski, L., 2024a. Depositional conditions, wildfires, maturity, and
995 hydrocarbon potential evaluation of Central Carpathian Paleogene Basin based on integrative
996 approach from Orava Basin. International Journal of Coal Geology 285, 104490.

997 Staneczek, D., Szaniawski, R., Chadima, M., Marynowski, L., 2024b. Multi-stage tectonic evolution of
998 the Tatra Mts recorded in the para- and ferromagnetic fabrics. Tectonophysics 880, 230338.
999 https://doi.org/10.1016/j.tecto.2024.230338

1000 Staneczek, D., Szaniawski, R., Marynowski, L., 2024c. Burial impact on the Tatra Mts from a rock
1001 magnetic and magnetic fabric perspective: magnetic fabric tables and additional rock magnetic
1002 measurements. [Dataset]. Zenodo. 10.5281/zenodo.14052269

1003 Suk, D., Peacor, D.R., der Voo, R.V., 1990. Replacement of pyrite framboids by magnetite in limestone
1004 and implications for palaeomagnetism. Nature 345, 611–613.

1005 Sůkalová, L., Vojtko, R., Pešková, I., 2012. Cenozoic deformation and stress field evolution of the Kozie
1006 chrbty Mountains and the western part of Hornád Depression (Central Western Carpathians). Acta
1007 Geologica Slovaca 4, 53–64.

1008 Sun, W., Jackson, M., & Craddock, J. P. 1993. Relationship between remagnetization, magnetic fabric
1009 and deformation in Paleozoic carbonates. Tectonophysics, 221(3–4), 361–366.
1010 https://doi.org/10.1016/0040-1951(93)90167-I

1011 Szaniawski, R., Ludwiniak, M., Rubinkiewicz, J., 2012. Minor counterclockwise rotation of the Tatra
1012 Mountains (Central Western Carpathians) as derived from paleomagnetic results achieved in hematite-
1013 bearing Lower Triassic sandstones. Tectonophysics 560, 51–61.

1014   Szaniawski, R., Ludwiniak, M., Mazzoli, S., Szczygieł, J., Jankowski, L., 2020. Paleomagnetic and
1015   magnetic fabric data from Lower Triassic redbeds of the Central Western Carpathians: new constraints
1016   on the paleogeographic and tectonic evolution of the Carpathian region. Journal of the Geological
1017   Society 177, 509–522.

1018   Vašíček, Z., Michalík, J., Reháková, D., 1994. Early Cretaceous stratigraphy, palaeogeography and life
1019   in Western Carpathians. Beringeria 10, 3–168.

1020   Vojtko, R., Tokárová, E., Sliva, L., a Pesková, I., 2010. Reconstruction of Cenozoic paleostress fields and
1021   revised tectonic history in the northern part of the Central Western Carpathians (the Spisská Magura
1022   and V̀chodné Tatry Mountains). Geologica Carpathica 61, 211–225.

Supplementary materials to the manuscript 1

Tectonics

Supporting Information for

Burial impact on the Tatra Mts from the rock magnetic and magnetic fabric perspective

Dorota STANECZEK[1]*, Rafał SZANIAWSKI[2], Leszek MARYNOWSKI[1]

[1]Institute of Earth Sciences, University of Silesia in Katowice, Będzińska 60, 41-200 Sosnowiec, Poland;

[2]Institute of Geophysics, Polish Academy of Sciences, Księcia Janusza 64, 01-452 Warszawa, Poland.

*corresponding author: dorota.staneczek@us.edu.pl

Contents of this file

Additional Supporting Information (Files uploaded separately)

Table S1 Bulk geochemical characteristics and measured and calculated vitrinite reflectance values of the sampled rocks.

Introduction

The supporting information contains a description of additional magnetic and geochemical analysis of the Mraznica Fm from the Choč Mts. The figures show visualizations of rock magnetic experiments, petrographic observations, magnetic fabrics and two tables. The rock magnetic figures include temperature-dependent susceptibility measurements, Isothermal Remanent Magnetization curves, hysteresis curves and IRM back-field experiments for Mraznica and Huty Fm samples. The magnetic fabric figures show ip-, opAMS and AARM individual sample directions. The petrographic figure displays the organic matter present the studied units. The table S1 shows the main results of geochemical analysis. Tables S2 and S3 show hysteresis parameters and IRM component analysis, respectively.

1

Text S1.

Additional geochemical and rock magnetic results for the Choč Mts' samples

Four Mraznica Fm samples show a very low TOC content. In three samples the TOC value is <0.02 %, only in one it is higher, approximately 0.66% (Table S1). Except for the last sample, the TOC content is significantly lower than the values obtained for the Belianske Tatry sites. However, it is comparable to Mraznica Fm in the Western and High Tatra Mts. The calculated CC is very consistent in all samples and equals ~75-77%. These values fall in the range of the CC calculated for other Mraznica Fm samples. Random vitrinite reflectance was measured for all samples. The results show intermediate Rr values in the range of 0.79-0.94% that are generally similar to those documented in Western Tatra Mts (Table S1).

The methylphenanthrene ratio (MPI1) and the derived calculated vitrinite reflectance (Rc) were successfully obtained for three Mraznica Fm samples. In samples CH3 and CH4 the MPI1 ranges at 0.44-0.45, whereas in the CH2 sample, it is higher (1.59; Table S1). The Rc in CH3 and CH4 corresponds to the Rr values, and equals 0.78 and 0.81, respectively. In the CH2 sample, the Rc is 1.13. The phenylphenanthrene ratio (PhP) calculated for all samples varies from 0.73 to 0.86, and is similar to PhP values in the Mraznica Fm from the Western Tatra Mts.

The in-phase and out-of-phase magnetic susceptibility (Kip and Kop) was measured for ninety-seven specimens from six sampling sites of the Mraznica Fm in the Choč Mts. The Kip measured in 976 Hz shows values from 2.02×10^{-4} [SI] to 4.32×10^{-5} [SI], and the Kop from 1.18×10^{-5} [SI] to 0.51×10^{-7} [SI] (Fig. S9). These values are quite high in comparison to magnetic susceptibility values from Mraznica Fm specimens in the Tatra Mts. In addition, the Kfd parameter was calculated for all samples and the acquired values range from 1.39% to 11.41% (Fig. S9B). Such dispersion of values is unique for the Mraznica Fm in the Choč -Tatra Belt.

Geochemical data of the Huty Fm samples from the Choč Mts were previously investigated by Staneczek et al. (2024a). Here, we conducted the Kip and Kop measurements for fourty-six specimens from four sampling sites. The Kip values range from 8.6×10^{-5} [SI] to 3.5×10^{-4} [SI] (Fig. S9). The Kop values were negative, which is a measurement error due to a very low content of ferromagnetic minerals. Therefore, the Kfd parameter could not be calculated for these samples.
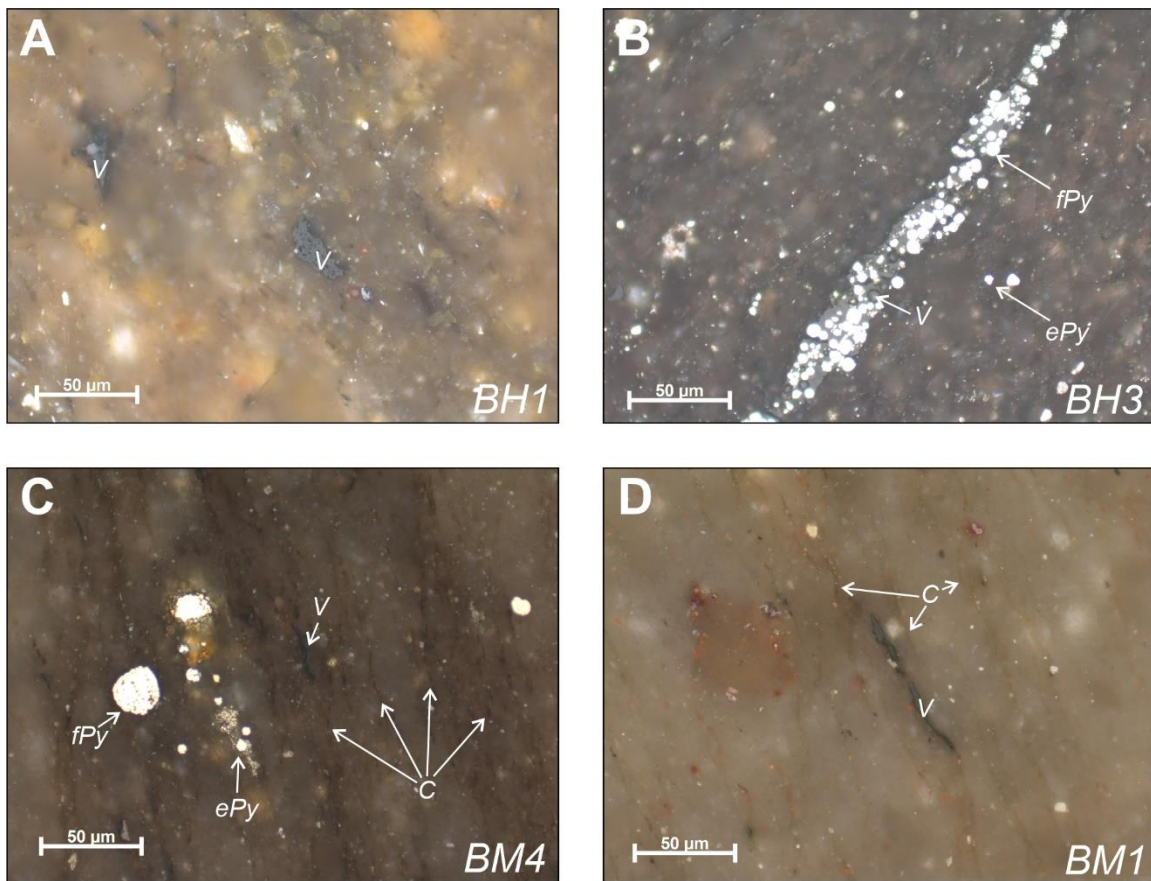
Figure S1. Petrographic analysis of the Mraznica and Huty Fm rocks. Abbreviations: V – vitrinite, ePy – euhedral pyrite, fPy – pyrite framboids; C – crenulation cleavage.

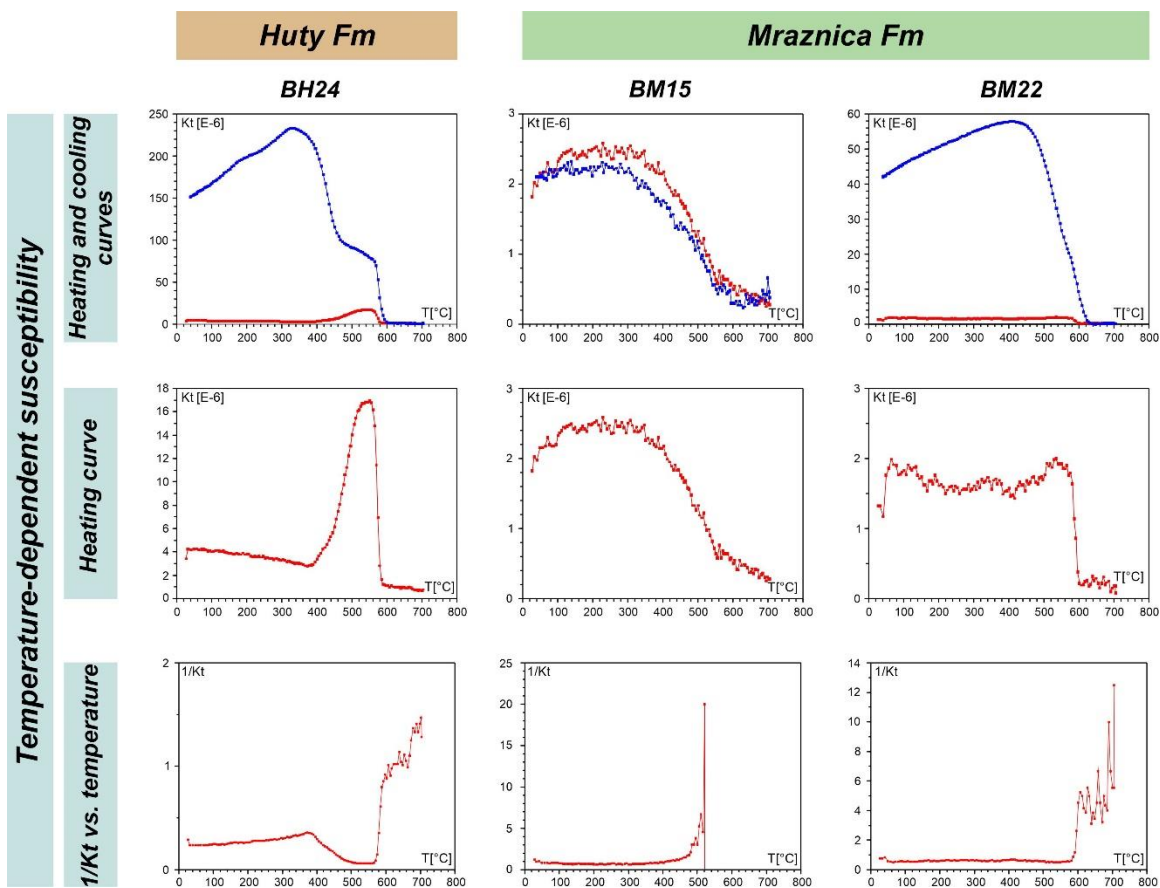**Figure S2.** Temperature-dependent susceptibility experiments for Mraznica and Huty Fm. Red line indicates the heating curve, and blue the cooling curve.
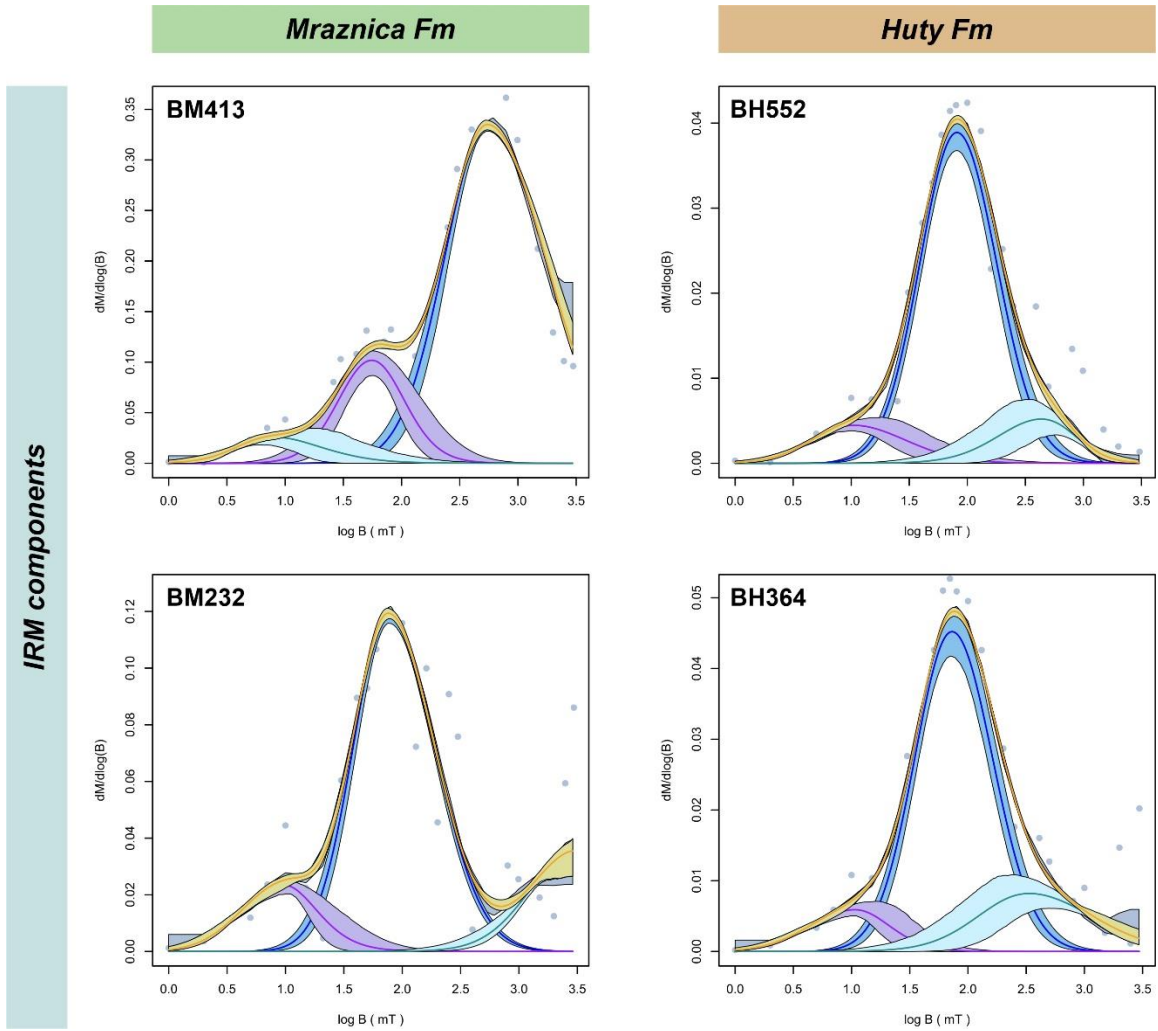
Figure S3. IRM component analysis for Mraznica and Huty Fm.
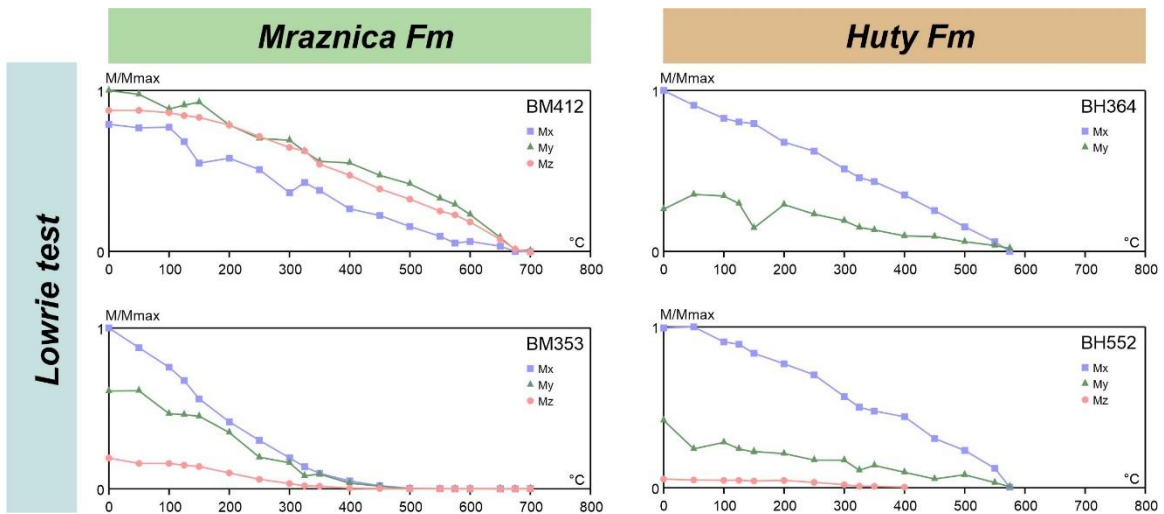
Figure S4. Additional plots of the thermal demagnetization of a three-axis IRM.
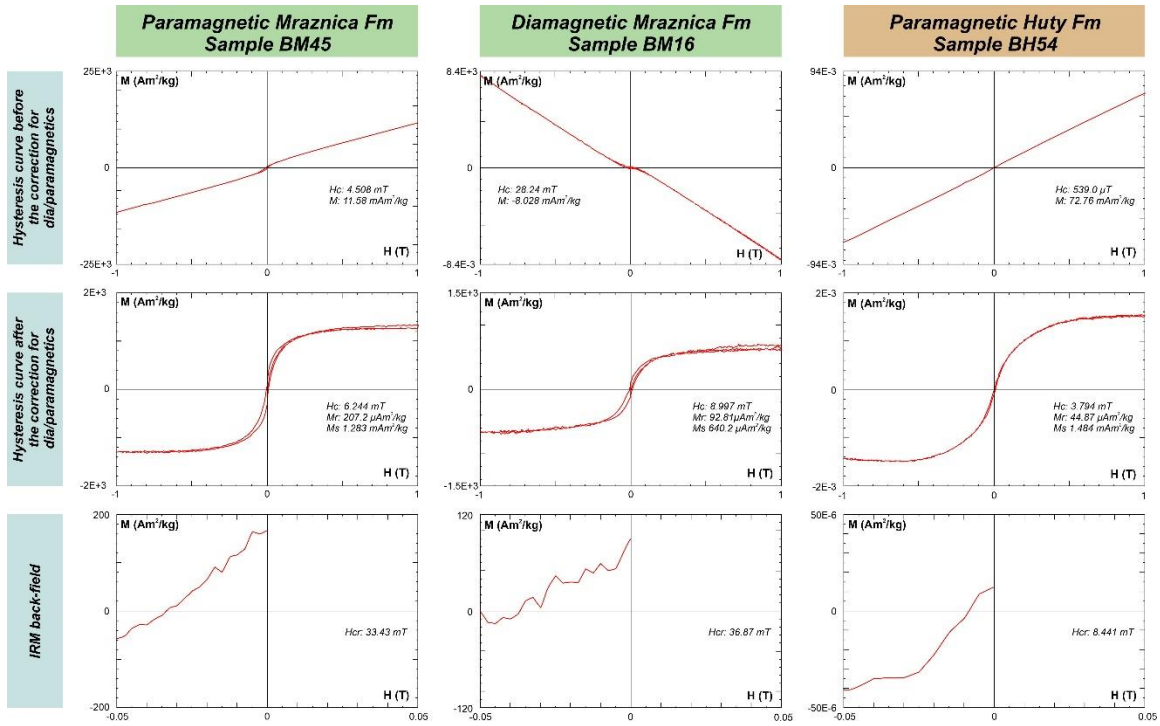
Figure S5. Hysteresis plots before and after para- and diamagnetic corrections with IRM back-field experiments.

Figure S6. The ipAMS diagrams showing individual sample directions. All fabrics are plotted in lower hemisphere projections in geographic coordinates. Squares, triangles and circles represent the maximum, intermediate and minimum ellipsoid axes derived

from the site-mean tensor. The blue great circle shows the bedding plane, and the light blue dot the pole to the bedding.
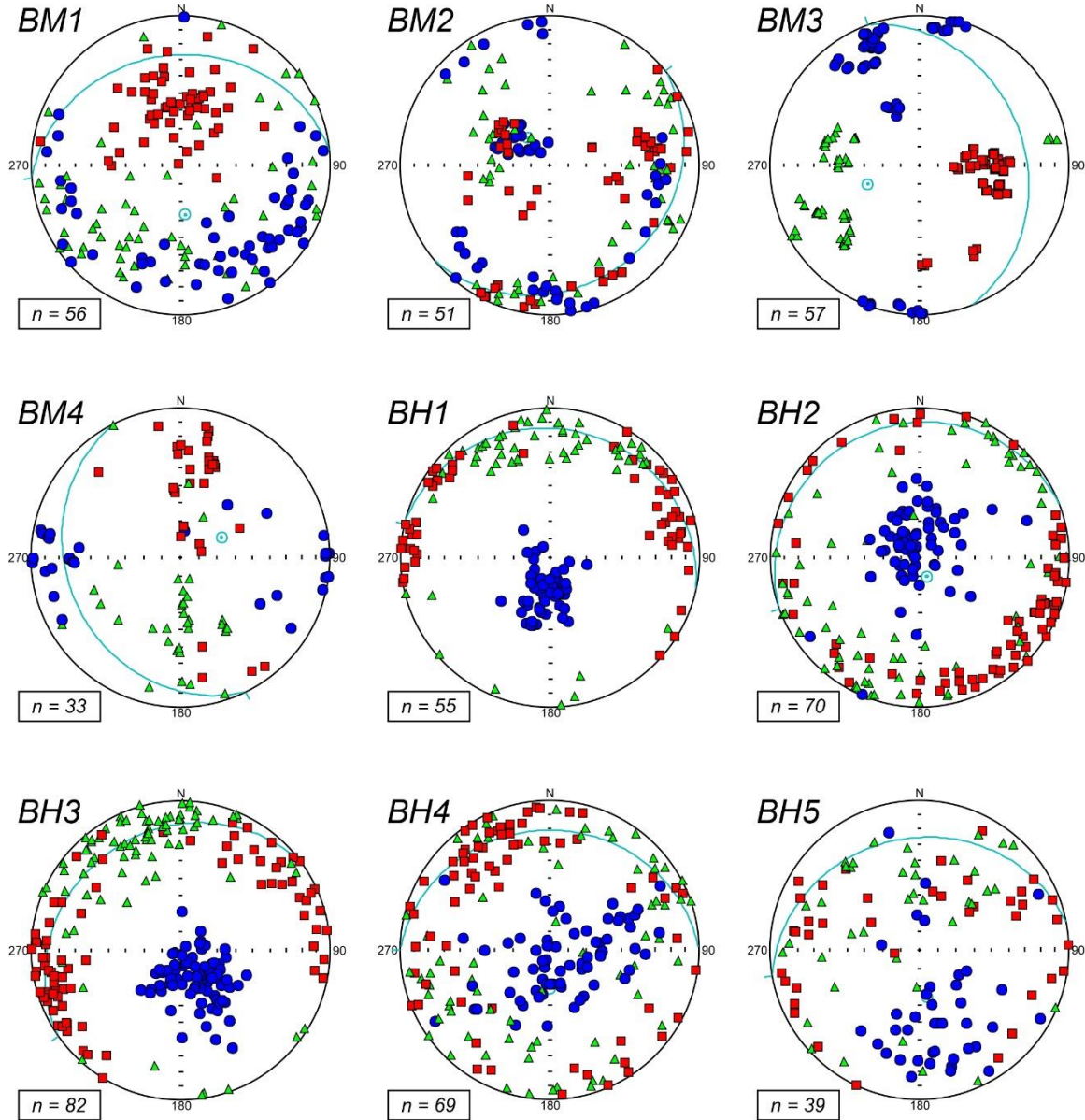
Figure S7. The opAMS diagrams showing individual sample directions. All fabrics are plotted in lower hemisphere projections in geographic coordinates. Squares, triangles and circles represent the maximum, intermediate and minimum ellipsoid axes derived

from the site-mean tensor. The blue great circle shows the bedding plane, and the light blue dot the pole to the bedding.
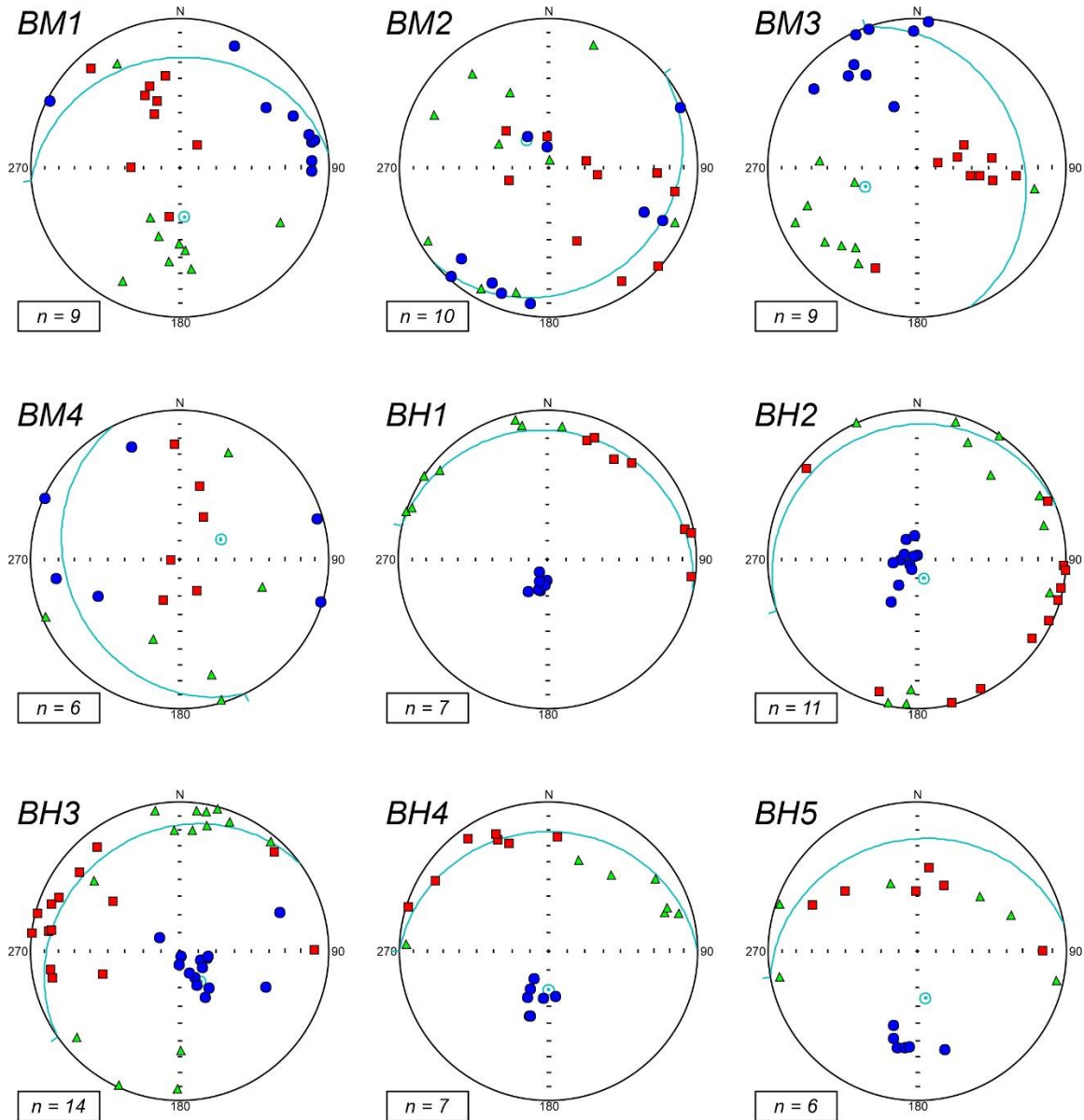
Figure S8. The AARM diagrams showing individual sample directions. All fabrics are plotted in lower hemisphere projections in geographic coordinates. Squares, triangles and circles represent the maximum, intermediate and minimum ellipsoid axes derived

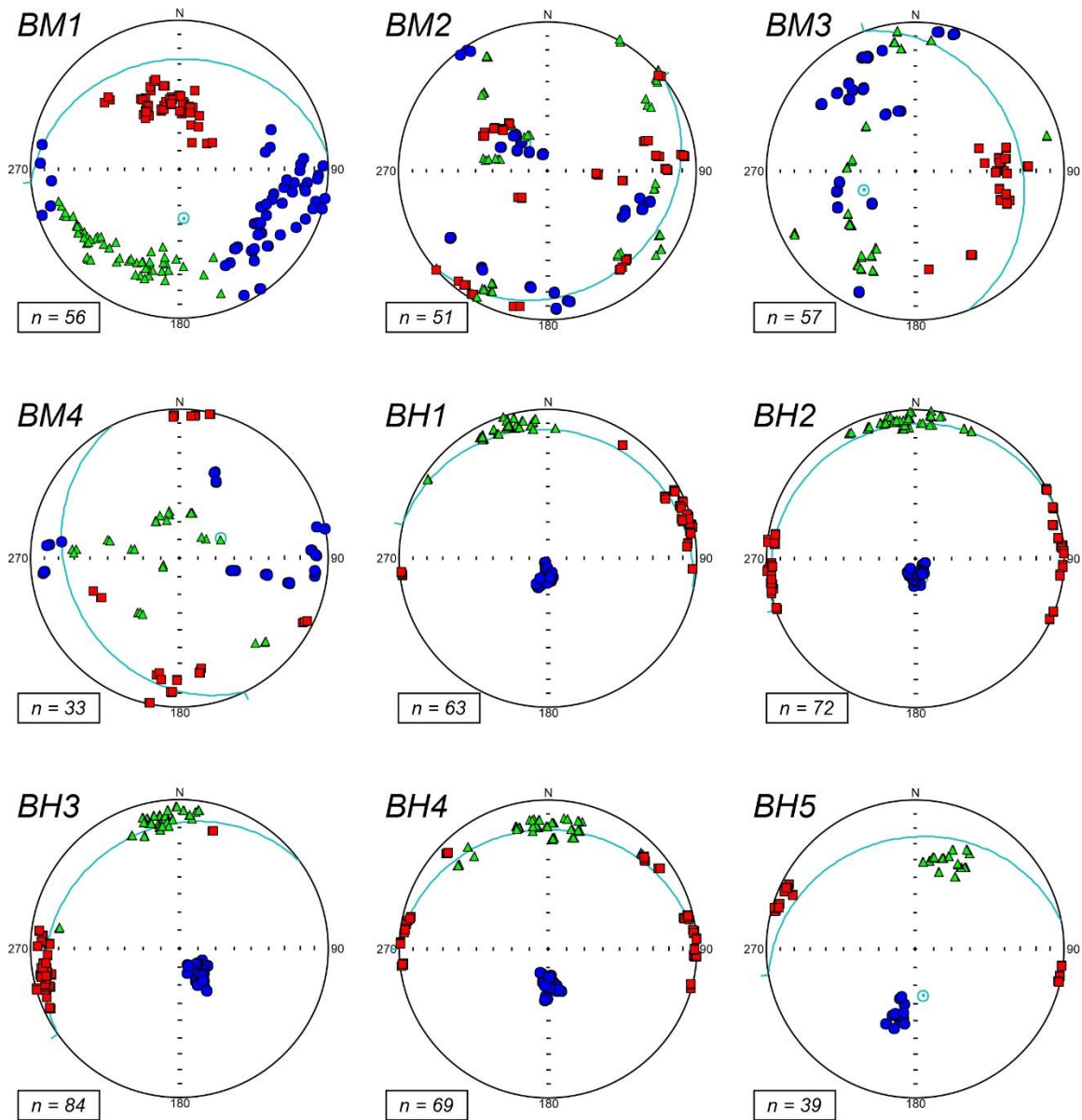from the site-mean tensor. The blue great circle shows the bedding plane, and the light blue dot the pole to the bedding.
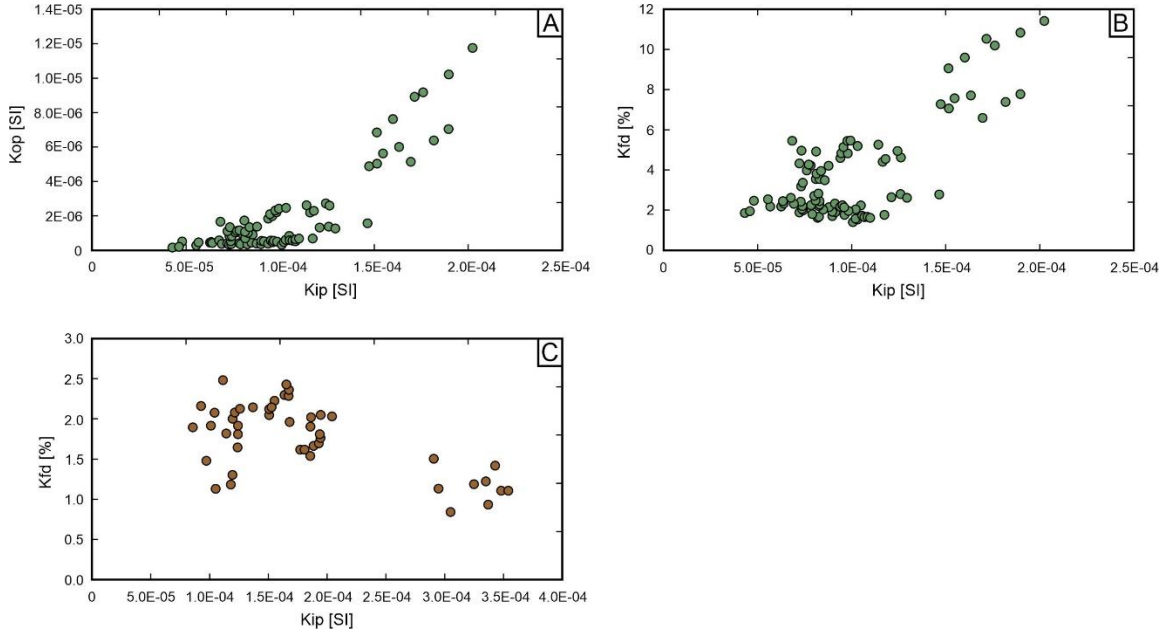

Figure S9. Magnetic susceptibility data for the Mraznica and Huty Fms in the Choč Mts: Kip vs Kop in 976 Hz for the Mraznica Fm (A); Kip (in 976 Hz) vs Kfd for the Mraznica Fm(B), Kip vs Kfd for the Huty Fm (C).

Sample	Unit	Component 1			Component 2			Component 3		
		logB1/2	B1/2 [mT]	DP	logB1/2	B1/2 [mT]	DP	logB1/2	B1/2 [mT]	DP
BM133	Mraznica Fm	0.87	9.43	0.26	1.96	92.99	0.35	3.27	1774.91	0.23
BM232		0.94	8.61	0.34	1.96	90.31	0.35	3.32	2090.53	0.30
BM353		1.07	11.78	0.44	1.96	90.93	0.33	2.49	310.20	0.32
BM413		0.97	9.39	0.37	1.74	55.08	0.29	2.84	693.10	0.44
BH115	Huty Fm	1.13	13.51	0.40	1.99	97.57	0.36	3.24	1755.64	0.31
BH243		0.95	8.82	0.34	1.85	70.75	0.32	2.57	368.38	0.55
BH364		0.95	9.00	0.35	1.89	76.86	0.33	2.62	419.44	0.49
BH444		1.00	9.94	0.36	1.87	74.72	0.32	2.49	309.01	0.65
BH552		1.09	12.32	0.40	1.93	84.96	0.33	2.57	375.69	0.33

Table S2. Results of the IRM component analysis for Mraznica and Huty Fms.

| Site | Sample | Formation | Hysteresis loop (after slope correction) | | | | | IRM back-curve | |
			Ms (µAm²/kg)	Mr (µAm²/kg)	Hc (mT)	Initial slope (mAm²/T*kg)	Slope correction (mAm²/T*kg)	Hcr (mT)	Ferro/para content (%)
BM1	BM13_1		1391	157.4	4.6	17.4	6.0	11.3	_
	BM15		802	106.7	9.3	4.9	9.3	24.5	-
	BM16		640	92.8	9.0	3.6	8.7	36.9	-
BM2	BM21		2093	240.5	6.7	21.4	-18.5	12.1	53.6
	BM21_1		447	47.1	4.5	4.1	-43.0	9.1	8.8
	BM22		969	100.5	6.0	10.6	-11.1	10.2	48.8
	BM22_1		706	98.2	4.5	4.4	-12.0	24.6	26.7
	BM22a		465	65.6	5.3	2.4	-30.1	24.5	7.5
	BM24		1512	84.4	2.6	8.4	-10.1	23.2	45.3
	BM24a		1887	127.4	3.1	10.9	-17.8	21.2	37.8
	BM31	Mraznica Fm	3301	507.0	5.5	19.8	-10.4	45.0	65.6
	BM32		7034	468.3	4.7	53.6	-54.5	30.3	49.6
	BM33		2692	379.8	5.3	16.1	-12.5	40.2	56.3
	BM33		3122	538.0	5.7	40.7	-12.8	16.6	76.1
	BM33_1		3169	468.0	4.7	39.2	-13.1	15.8	74.9
	BM34		1779	251.2	5.2	21.3	-23.3	6.8	47.7
	BM34_1		2597	351.2	5.4	31.9	-24.7	11.7	56.4
BM3	BM35		2319	273.5	5.2	28.4	-9.2	8.7	75.6
	BM35_1		2843	382.9	5.4	34.3	-23.4	17.2	59.4
	BM35_2		2447	338.0	6.5	13.7	-21.1	52.6	39.4
	BM3_2		5928	639.4	5.1	43.7	-35.3	9.1	55.3
	BM36		4803	471.5	4.3	33.6	-22.4	8.3	60.0
	BM36_1		3711	366.2	4.6	25.8	-19.0	7.8	57.6
	BM43_1		5456	643.5	4.8	39.7	-14.7	8.6	73.0
BM4	BM43		1015	46.1	5.2	6.0	-35.7	21.8	14.3
	BM44		777	81.9	6.8	4.5	-30.9	26.7	12.8
	BM45		1283	207.2	6.2	7.8	-10.3	33.4	43.0
	BM45_1		5532	584.1	4.5	39.6	-17.9	8.0	68.9
BH1	BH16		3988	377.2	5.8	27.2	-41.5	8.3	39.6
	BH16_1		3422	295.2	5.5	21.1	-50.8	5.9	29.3
BH2	BH17_1	Huty Fm	2792	266.5	5.8	18.7	-42.5	5.9	30.6
	BH21		1358	69.7	8.6	6.3	-65.8	15.0	8.7
	BH22		1074	76.5	10.5	5.2	-65.7	18.6	7.4
BH3	BH34_1		5273	374.3	4.2	34.3	-65.9	4.8	34.2
	BH35		1218	69.7	5.6	5.2	-65.9	11.0	7.3

	BH35_1	3422	231.4	3.7	21.5	-63.3	4.6	25.4
	BH37	1375	37.1	8.6	5.9	-74.9	25.0	7.3
	BH42	1071	77.5	2.6	6.4	-49.6	8.4	11.4
	BH43	4434	415.7	4.7	27.8	-74.5	4.8	27.2
BH4	BH43	1700	66.3	3.3	7.3	-75.2	6.8	8.8
	BH43_2	4970	410.3	5.7	32.3	-58.7	6.9	35.5
	BH44	1700	66.3	3.3	7.3	-75.2	6.8	9.5
	BH48	1336	114.4	11.5	6.3	-63.0	26.5	9.1
	BH51	1313	59.1	5.4	5.5	-63.7	18.9	7.9
BH5	BH52	1114	57.1	4.4	5.0	-75.1	19.2	6.3
	BH53	1900	63.9	3.7	10.9	-70.0	9.7	13.4

Table S3. Results of hysteresis curve and IRM back-field experiments.

13

Table S1 Bulk geochemical characteristics and measured and calculated vitrinite reflectance values of the sampled rocks.

Sample	Unit	Lithology	TOC [%]	TS [%]	CC [%]	MPI1	Rc [%]	Ro [%]	PhP ratio
Belianske Tatry Mts									
BM1_1		limestone	0.65	0.00	79.10	1.70	1.42	1.44	1.00
BM1_2	*Mraznica Fm*	limestone	0.41	0.00	97.33	1.02	1.01	-	1.00
BM2_1		marly limestone	0.41	0.00	33.45	2.16	1.70	-	1.00
BM2_2		marly limestone	0.48	0.01	27.73	1.00	1.00	-	1.00
BM3_1		marly limestone	0.20	0.00	72.07	0.94	0.96		1.00
BM3_2		marly limestone	0.19	0.07	75.03	-	-	1.70	1.00
BM4_1		marly limestone	0.14	0.00	67.39	-	-	-	1.00
BM4_2		marly limestone	0.01	0.00	63.49	1.18	1.11	1.55	1.00
BH1_1		dark siltstone	0.55	0.94	8.71	2.48	1.89	1.32	1.00
BH1_2		dark siltstone	0.89	0.96	17.17	1.68	1.41	-	0.99
BH2_1		dark siltstone	0.95	0.83	16.53	2.69	2.01	1.04	1.00
BH3_1	*Huty Fm*	dark siltstone	1.15	1.04	8.40	1.72	1.43	1.11	0.99
BH3_2		dark siltstone	0.95	0.91	14.72	2.38	1.83	-	1.00
BH4_1		dark siltstone	0.73	0.92	22.88	2.19	1.72	1.54	1.00
BH4_2		dark siltstone	0.99	0.80	14.46	2.22	1.73	-	-
BH5_1		dark siltstone	0.70	0.57	17.14	1.44	1.26	-	0.97
BH5_2		dark siltstone	0.71	0.61	17.11	1.81	1.49	1.37	0.97
Choč Mts									
CH2		marly limestone	0.02	0.00	77.30	1.59	1.13	0.90	0.86
CH3	*Mraznica Fm*	marly limestone	0.00	0.00	75.70	0.44	0.78	0.94	0.73
CH4		marly limestone	0.00	0.01	77.85	0.45	0.81	0.79	0.83
CH5		marly limestone	0.66	0.00	76.23	-	-	0.86	0.86
64_Ht		mudstone	0.44	0.07	35.67	0.58	0.75	0.35	0.66
65_Ht	*Huty Fm**	sandstone	0.37	0.01	36.27	0.35	0.61	0.44	0.58
66_Ht		mudstone	0.31	0.04	36.81	0.53	0.72	0.41	0.69
67_Ht		mudstone	0.58	0.39	25.13	0.64	0.79	0.55	0.64
Orava*									
77_Ht	*Huty Fm*	black shale	2.72	0.00	7.24	0.33	0.60	-	0.67
78_Ht		black shale	1.98	0.00	14.93	0.32	0.59	0.27	-
82_Ht		black shale	3.19	2.17	5.04	0.46	0.68	0.47	0.67
84_Ht		sandstone	5.39	0.04	11.48	0.41	0.64	0.44	0.65
85_Ht		coal	50.64	0.66	1.62	0.45	0.67	0.45	-
Western and High Tatra Mts**									
Ht5		silty sandstone	0.55	0.54	19.39	0.61	0.77	0.53	-
Ht7		mudstone	0.85	1.09	16.38	0.67	0.8	0.57	0.82
Ht10		mudstone	0.7	0.86	18.45	0.7	0.82	0.41	0.70
Ht11	*Huty Fm*	silty sandstone	0.77	1.25	17.52	0.69	0.82	0.4	-
Ht12		mudstone	0.59	0.59	16.85	0.57	0.74	0.55	0.80
Ht14		black shale	0.66	1.16	17.77	0.57	0.74	0.53	0.58
Ht15		mudstone	1.1	0.25	14.81	0.52	0.71	0.62	0.67
ZA1		black shale	1.59	1.39	34.85	1.07	1.04	0.92	0.91

ZA2		black shale	1.41	0.74	18.41	1.7	1.42	1.3	0.95
ZA3		black shale	0.59	1.04	18.28	2.07	1.64	1.07	0.96
ZA4		black shale	0.65	1.1	21.99	1.78	1.47	1.18	0.95
ZA5		black shale	0.59	1.33	17.9	1.35	1.21	1.1	0.92
PIG_FUR	Well	mudstone	1.92	4.13	5.5	0.74	0.84	-	-
PIG_PR5		mudstone	2.24	0.7	14.76	0.9	0.94	-	-
MZ7		marl	0.12	0	68.17	0.44	0.66	0.72	0.78
MZ8		marl	0.13	0	65.43	0.45	0.67	0.86	0.76
MZ9		marly limestone	0.1	0	74.48	0.41	0.65	1.09	0.75
MZ10		marly limestone	0.1	0.08	73.38	0.35	0.61	0.82	0.78
MZ11		marly limestone	0.1	0.17	49.37	0.44	0.66	0.91	0.76
MZ12	Mraznica Fm	marl	0.1	0	67.2	0.55	0.73	1.06	0.78
MZ13		limestone	0.14	0	81.53	0.46	0.67	0.72	0.71
KRY_MZ_1A		marly limestone	0.41	0	61.32	0.47	0.68	-	0.82
KRY_MZ_2A		marly limestone	0.56	0	57.21	0.41	0.65	-	0.79
MK1		marly limestone	0.1	0.06	69.58	0.64	0.79	1.51	0.84
MK2		limestone	0.1	0	55.76	1.71	1.43	1.48	0.94
MK3		marly limestone	0.1	0	84.15	1.24	1.14	1.34	-
FU_PIG1_1979	Well	conglomerate	0	0.04	61.13	-	-	0.94	-
FU_PIG1_2049		limestone	0.52	0	56.21	-	-	0.99	-

Ro = measured vitrinite reflectance

CC = carbonate content

MPI1 = methylphenanthrene index MPI1 = 1.5 (2-MP + 3-MP)/(P + 1-MP + 9-MP)

Rc [%] = 0.4 + 0.6 x MPI1 (Radke and Welte, 1983); Ph = phenantrene; MP = methylophenantrene

PhP ratio = (2- + 3-PhP)/[(2- + 3-PhP) + (4- + 1- + 9-PhP)] - PhP ratio = phenylphenanthrene ratio (Rospondek et al., 2009)

*data from Staneczek et al. (2024a)

**data from Staneczek et al. (2024b)